SANDIA REPORT

SAND2014-16383
Unlimited Release
Printed July 2014

Analysis of Dust Samples Collected from Spent Nuclear Fuel Interim Storage Containers at Hope Creek, Delaware, and Diablo Canyon, California

Charles R. Bryan and David G. Enos

Prepared by
Sandia National Laboratories
Albuquerque, New Mexico 87185 and Livermore, California 94550

Sandia National Laboratories is a multi-program laboratory managed and operated by Sandia Corporation, a wholly owned subsidiary of Lockheed Martin Corporation, for the U.S. Department of Energy's National Nuclear Security Administration under contract DE-AC04-94AL85000.

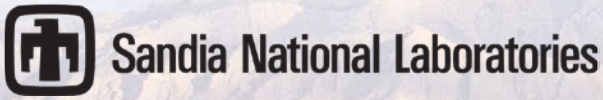

Issued by Sandia National Laboratories, operated for the United States Department of Energy by Sandia Corporation.

Available to DOE and DOE contractors from
U.S. Department of Energy
Office of Scientific and Technical Information
P.O. Box 62
Oak Ridge, TN 37831

Telephone: (865) 576-8401
Facsimile: (865) 576-5728
E-Mail: reports@adonis.osti.gov
Online ordering: http://www.osti.gov/bridge

Available to the public from
U.S. Department of Commerce
National Technical Information Service
5285 Port Royal Rd.
Springfield, VA 22161

Telephone: (800) 553-6847
Facsimile: (703) 605-6900
E-Mail: orders@ntis.fedworld.gov
Online order: http://www.ntis.gov/help/ordermethods.asp?loc=7-4-0#online

SAND2014-16383
Unlimited Release
Printed July 2014

Analysis of Dust Samples Collected from Spent Nuclear Fuel Interim Storage Containers at Hope Creek, Delaware, and Diablo Canyon, California

Charles R. Bryan
Storage and Transportation Technologies Department
Sandia National Laboratories
P.O. Box 5800
Albuquerque, New Mexico 87185-MS0779

David G. Enos
Materials Reliability Department
Sandia National Laboratories
P.O. Box 5800
Albuquerque, New Mexico 87185-MS0888

Abstract

Potentially corrosive environments may form on the surface of spent nuclear fuel dry storage canisters by deliquescence of deposited dusts. To assess this, samples of dust were collected from in-service dry storage canisters at two near-marine sites, the Hope Creek and Diablo Canyon storage installations, and have been characterized with respect to mineralogy, chemistry, and texture. At both sites, terrestrially-derived silicate minerals, including quartz, feldspars, micas, and clays, comprise the largest fraction of the dust. Also significant at both sites were particles of iron and iron-chromium metal and oxides generated by the manufacturing process. Soluble salt phases were minor component of the Hope Creek dusts, and were compositionally similar to inland salt aerosols, rich in calcium, sulfate, and nitrate. At Diablo Canyon, however, sea-salt aerosols, occurring as aggregates of NaCl and Mg-sulfate, were a major component of the dust samples. The sea-salt aerosols commonly occurred as hollow spheres, which may have formed by evaporation of suspended aerosol seawater droplets, possibly while rising through the heated annulus between the canister and the overpack. The differences in salt composition and abundance for the two sites are attributed to differences in proximity to the open ocean and wave action. The Diablo Canyon facility is on the shores of the Pacific Ocean, while the Hope Creek facility is on the shores of the Delaware River, several miles from the open ocean.

ACKNOWLEDGMENTS

This work was carried out as part of a Cooperative Research and Development Agreement with the Electric Power Research Institute. EPRI directed and funded sample collection activities at the fuel storage installations and provided the samples to Sandia for analysis and interpretation. Sampling was performed by Laszlo Zsidai and personnel from Holtec International, with support from personnel of the Hope Creek and Diablo Canyon Nuclear Power Plants. At Sandia, Mark Rodriguez performed XRF and XRD analyses, and Amy Allen provided SEM/EDS support. Kirsten Norman helped with sample preparation.

CONTENTS

FIGURES

TABLES

NOMENCLATURE

DOE	Department of Energy
EDS	energy dispersive [X-ray] spectroscopy
EPRI	Electric Power Research Institute
IC	ion chromatography
ICP-OES	inductively coupled plasma-optical emission spectroscopy
ISFSI	independent spent fuel storage installation
SCC	stress corrosion cracking
SEM	scanning electron microscope
SNF	spent nuclear fuel
SNL	Sandia National Laboratories
XRD	X-ray diffraction
XRF	X-ray fluorescence

1. INTRODUCTION

When spent nuclear fuel (SNF) storage pools at commercial nuclear reactors become filled to capacity, it is necessary to shift SNF to dry storage systems. Modern dry storage systems consist of a stainless steel canister within an overpack that protects the canister from the weather. Decay heat from the waste drives convective airflow through an annulus between the overpack and the canister, cooling the container. Over time, dust, drawn into the overpacks with the circulating air, is deposited on the surfaces of containers within the storage systems. Salts within the dust will deliquesce as heat production declines over time and the packages cool, and it is possible that deliquescence-induced corrosion of the stainless steel waste container could lead to penetration of the container walls by chloride-induced stress corrosion cracking (SCC). To address this concern, the Electrical Power Research Institute (EPRI) has instituted a sampling program for the dust on the surface of in-service SNF storage canisters. The first samples were collected from a NUHOMS horizontal storage system at the Calvert Cliffs Independent Spent Fuel Storage Installation (ISFSI) in June 2012, 15.6 years after waste emplacement (Calvert Cliffs Nuclear Power Plant, 2012). In November 2013, the second set of samples was collected at Hope Creek, from canisters in storage for 6 years; and in January, 2014, a third set was collected from Diablo Canyon, from canisters in storage for 2-4 years. The Calvert Cliffs samples were analyzed in part by an external lab contracted by EPRI, and in part by Sandia and are reported elsewhere (Calvert Cliffs Nuclear Power Plant, 2013; DOE, 2013). The samples from the Hope Creek and Diablo Canyon sites were sent to Sandia National Laboratories (SNL) for characterization.

This report summarizes the results of analyses of dust samples collected from the surface of SNF dry storage containers at the Hope Creek and Diablo Canyon ISFSIs. The dry storage systems that were sampled are Holtec HI-STORM 100S-218, Version B systems, which have a 304 SS storage cask placed into a vertical steel-lined concrete overpack (Figure 1). The system is passively ventilated via four air inlet vents at the base of the unit located 90º from each other, and four outlet vents on the top, offset 45º circumferentially from the inlets.

Both wet and dry samples of the dust/salts were collected at each site, using two different devices:

- The wet samples were collected using SaltSmart™ sensors. These devices are manufactured by Louisville Solutions, Inc., and used in shipyards to quantify the amount of chloride on metal surfaces per unit area. They are designed for use with very low salt loadings. For this study, the sensors were mounted on a remote sampling tool developed by Holtec and lowered into the overpack through one of the outlet vents. Each sensor has a flat wick, which was pressed flat against the metal surface pneumatically; for samples taken from the flat top of the canisters, the sensors were pressed against the surface manually, using a long rod. A small amount of deionized water was then injected into one end of the sensor, and was drawn across the wick by capillary processes to a reservoir pad within the body of the sensor. In the shipyard application, the conductivity of the reservoir pad (a function of the total dissolved salts in the water) is monitored, and is used to estimate the chloride concentration on the metal surface, assuming that the salts are similar in composition to sea salts. For this study, the sensors were placed in sealed

screw-cap polypropylene centrifuge tubes after retrieval from the overpack and shipped overnight to SNL, packed with ice packs to keep them cool. At Sandia, the sensors were disassembled and the soluble salts were rinsed from the internal components and leached out of the wicks and pads for chemical analysis. Rather than estimating chloride concentration from conductivity, the salt compositions were measured directly.

- Dry dust samples were collected using a similar remote sampling tool, equipped a scraper tool instead of the SaltSmart™ sensor. The scraper tool consisted of a rectangular piece of a mildly abrasive Scotch-Brite™ sponge-like pad, backed with a steel plate. As with the SaltSmart™, once the sampling tool was in position, the pad was pneumatically pushed against the canister surface. However, in the case of the dry sampling tool, a second pneumatic valve then moved the pad back and forth across the surface, to dislodge and collect the dust. Once again, canister-top samples were collected by using a long rod to manually brush the over the surface. Following retrieval from the overpack, the dry pad samples were removed from the sampling tool, placed into a screw-cap centrifuge tube, and sent to SNL for characterization of the collected dust.

Figure 1. Holtec HI-STORM Dry Cask Storage Systems at Diablo Canyon.

At SNL, the wet samples were analyzed by chemical analysis to determine the composition and abundance of soluble salts present. The pads containing the dry dust were removed from the steel plate backers and analyzed by X-ray fluorescence to obtain bulk chemical compositions. Then, a small portion of the sponge was removed and retained for scanning electron microscope analysis. The remaining sponge was washed thoroughly with deionized water and the leachate collected, filtered, and analyzed for soluble salts. Original plans were for the remaining

insoluble residue to be digested and analyzed using wet chemical methods. However, because of extensive contamination by talc shed from the pad matrix, it was decided not to determine the bulk chemistry of the insoluble fraction.

Methods used to characterize the samples include:

- X-ray fluorescence (XRF) analysis. This method was implemented as a microbeam technique, allowing chemical mapping of the dry dust samples on the surface of the collection pads, with a resolution of ~100 µm. It provides semi-quantitative chemical analyses; yielding element ratios that can be used in mass balance and normative mineral calculations. However, one limitation is that elements lighter than sodium (e.g. oxygen, nitrogen, carbon) cannot be detected.

- Scanning Electron Microscopy (SEM) imaging and energy dispersive system (EDS) element mapping. SEM/EDS analysis of the dry dust samples provides textural and mineralogical information of dust/dust components, and allows visual identification of organic matter (floral/faunal fragments).

- X-ray diffraction (XRD) analysis of the dry dust on the collection pads. This analysis did not prove useful—the surface of the pads was too rough for effective measurement, and no mineral peaks could be identified.

- Chemical analyses of the dust and soluble salts. The soluble salts were leached form the SaltSmart™ sensors and analyzed. For the dry samples, the pad was washed thoroughly with deionized water and the leachate collected and filtered. The leachate was then analyzed for soluble salts.

As discussed in the following sections, although both the wet and dry sampling methods had limitations, the analyses were effective in identifying the major mineralogy of the dust on the canister surfaces, and the composition of the salts present. The Hope Creek ISFSI is located ~0.25 mile from the Delaware River, about 15 upstream from Delaware Bay. The Delaware River is subject to tides at the site, and is brackish in composition. The Hope Creek canisters had very light salt surface loads, and higher dust and salt concentrations occurred on the canister tops than on the vertical sides. Soluble salts were dominantly calcium, nitrate, sulfate, and carbonate compounds; an assemblage consistent with continental rather than marine aerosol assemblages. Chloride salts, mostly occurring as NaCl, were very rare.

The Diablo Canyon ISFSI is located ~0.35 miles from the Pacific Ocean. In contrast to the Hope Creek samples, dust collected from the surfaces of dry storage canisters at Diablo Canyon were chloride-rich. The chloride was present as sea-salt aggregates consisting dominantly of intergrown NaCl and an Mg-SO_4 phase. The aggregates had characteristic morphologies, occurring as hollow spherical aggregates of halite with interstitial Mg-SO_4 or as euhedral skeletal crystals of halite (NaCl) with sheaf-like bundles of Mg-SO_4. The morphology suggests that the crystals formed by evaporation of droplets of seawater suspended in the atmosphere, drying from the outside inwards. The aggregates were commonly 5-20 microns in diameter. Dust and chloride loads were much heavier on the canister tops than the sides, and the two Diablo Canyon

canisters sampled showed distinct variations in salt chemistry. Dusts on the side of one of the canisters, MPC-123, appeared to contain a significantly larger continental dust component than the other canister.

Detailed sampling and analytical methods, and a list of the samples collected, are provided in Section 2 of this report. Section 3 summarizes the results of the different analyses (complete sets of SEM/EDS and XRF analyses are provided in Appendices A and B), and Section 4 discusses and interprets the data.

2. SAMPLES AND METHODS

2.1. Samples

Sampling at Hope Creek and Diablo Canyon was carried out through one of the upper ventilation openings on each package. After removal of the screen covering the opening, spot welds holding the gamma shield in place were cut, and the gamma shield extracted. Then a guide rail for the sampling device for the side of the package was inserted into the opening by workers on a scissor lift (Figure 2). This rail guided the remote sampling tool down into the narrow (~2 inch) annulus between the canister and the overpack. The sampling tool was forced down the annulus with a steel ribbon, with trailing tubing to operate a pneumatic system on the sampling head. The wet samples were collected using SaltSmart™ sensors, which are used in shipyards to quantify the amount of salts on metal surfaces per unit area. The sensors were mounted on the sampling head in a shallow recess, so that they did not contact the metal surface during the emplacement process. Each sensor has a flat wick, which was pressed flat against the metal surface pneumatically. A small amount of deionized water was then injected into one end of the sensor, and was drawn across the wick by capillary forces to a reservoir pad within the body of the sensor. In the shipyard application, the conductivity of the pad (a function of the total dissolved salts in the water) is monitored, and is used to estimate the chloride concentration on the metal surface, assuming that the salts are similar in composition to sea salts. For this study, the sensors were retained and disassembled at Sandia, where the salts were leached and analyzed to determine composition. Testing has shown that under appropriate conditions, the SaltSmart™ sensors can provide an accurate assessment of the amount and composition of salts on the canister surface (Memo from C. Bryan to L. Zsidai dated Nov. 13, 2013; SAND#2013-9948P).

Dry dust samples were collected using a similar remote sampling tool, equipped a scraper tool instead of the SaltSmart™ sensor. The scraper tool consisted of a rectangular piece of a mildly abrasive Scotch-Brite™ sponge-like pad, backed with a steel plate. Once in position, the pad was pneumatically pushed against the canister surface, and a second pneumatic controller moved the pad back and forth across the surface, to dislodge and collect the dust.

Access to the canister top surfaces was less restricted, so instead of using the pneumatically-powered remote sampling tool, a log rod was used to manually press the SaltSmart™ sensors and dry pads against the metal surface. The dry sampling pads used for the canister tops varied from those used to sample the sides. The pads used to sample the tops of the containers were about 1.5 cm thick (with thinner sides to allow attachment to a steel back-plate), while those used to sample the sides were thinned to ~0.7 cm. Using the thinner pads allowed them to be recessed into the sampling tool, so that they did not contact the surface of the canister until the sampling tool was lowered into position through the narrow annulus and the pads extended pneumatically.

During sampling at Hope Creek and Diablo Canyon, the SaltSmart™ sensors and the abrasive sponges used to the dry dust sampling were always handled with gloves, and once mounted on the sampling tool, were enclosed in a plastic bag until the tool was inserted into the overpack. Upon retrieval from the overpack, a plastic bag was immediately placed over the sampling tool, and not removed until the scissor lift was lowered. At ground level, the plastic bag was removed, and the SaltSmart™ sensor or abrasive sponge was extracted from the sampling tool

and immediately placed into a 50 ml screw-cap polypropylene centrifuge tube. The tubes containing the samples were then placed into a cooler with ice packs to limit degassing and microbial activity. Within a day or two of collection, the samples were shipped to SNL in the cooler, with fresh ice packs to keep them cool. Once at SNL, they were refrigerated until analysis. Table 1 and Table 2 list the samples that were received from Hope Creek and Diablo Canyon, respectively, and provide a short description of each. The SaltSmart™ sensors are referred to as wet samples, because the salts were leached off the storage canister surface by water passing through the wick. The abrasive pads collected dust without the aid of water, and are referred to as dry samples.

Figure 2. Sampling dust from the surface of interim storage canisters within their overpacks.

The samples were collected from two canisters at each site. At Hope Creek, these canisters were designated MPC-144 and MPC-145; at Diablo Canyon, they were MPC-123 and MPC-170. Upon delivery to Sandia, the samples were examined and a description was recorded. Additionally, when the SaltSmart™ samples were disassembled to extract the soluble salts, the condition of the wick and the reservoir pad was noted. Table 1 and Table 2 also list the sampling location and the canister surface temperature at the sampling location for each sample. Initially, all samples were given to Sandia without location information to ensure that the analyses were not biased, but during data interpretation, the canister surface locations and temperatures were provided. Samples were also collected from the gamma shields after removal, and a few blanks were included as unknowns. SNL was not informed of the identity of each sample until most of the analyses had been completed.

Photographs of the samples as received at Sandia are provided in Figures 3-10. Figure 3 and Figure 4 show the SaltSmart™ and dry pad samples, respectively, from Hope Creek storage canister MPC-144; Figure 5 and Figure 6, for Hope Creek canister MPC-145; Figure 7 and Figure 8 for Diablo Canyon canister MPC-123; and Figure 9 and Figure 10, for Diablo Canyon canister MPC-170. A few general observations can be made. First, for both the wet and dry samples, those collected from the flat tops of the canisters are more heavily coated with dust than those collected from the sides. This suggests that more dust was present on the tops of the canisters, but it should be remembered that the different collection method and the thicker pads used to collect the dry samples from the canister tops may have contributed to this. Also, for the Hope Creek samples, the SaltSmart™ wicks are generally more lightly coated along the upstream (inlet) edge of the wick (to the right in Figure 3 and Figure 5); sometimes, a clear dividing line is visible. This suggests that the sensors were not flat against the surface. This is consistent with the field observation that the water tube attached to the sensor inlet was thicker than the SaltSmart™ sensor, and when the sample holder was pneumatically extended to press the sample against the canister surface, the water line was pinched between the sample holder and the surface, preventing the SaltSmart™ from lying flat against the surface. In general, most of the wick surface (80-90%) appears to have contacted the canister (e.g., Figure 3, samples 144-013, 144-014; Figure 5, sample 145-013); however, for one sample (Figure 5, sample 145-006), only about 1/3 of the wick appears to have contacted the surface. When estimating the salt load per unit area, it is important to remember that the surface area sampled may be slightly less than the area of the SaltSmart™ wick. It is not clear that the Diablo Canyon SaltSmart™ samples had the same issue, as the dust coatings on these samples were generally too light to see. Finally, it is worth noting that windblown seeds of the marsh grass *Phragmites,* which is abundant around the site, were observed on the canister tops at Hope Creek, apparently having been blown in through the outlet vents. One of these was captured by the dry sampler, and is visible on the upper edge of sample 145-012 in Figure 6.

Table 1. Hope Creek Samples

Sample #	Sample Type	T (ºC)	Sample location	Description
Canister MPC-144				
144-001	Dry pad		Gamma shield, bottom of top section	Thin pad, slight brown discoloration on the surface.
144-002	Dry pad		Gamma shield, side of top section	Thin pad, no visible discoloration.
144-003	SaltSmart		Gamma shield, side of bottom section	No visible discoloration. During collection, appeared to be unsaturated.
144-004	SaltSmart		Gamma shield, side of bottom section	No visible discoloration.
144-005	Dry pad	28.9	Canister side. Insertion depth: 13.5 ft from upper edge	Thin pad, little or no discoloration.
144-006	Dry pad	32.0	Canister side. Insertion depth: 8.5 ft from upper edge	Thin pad, little or no discoloration.
144-007	Dry pad	52.4	Canister side. Insertion depth: 1.0 ft from upper edge	Thin pad, little or no discoloration.
144-008	SaltSmart	34	Canister side. Insertion depth: 13.0 ft from upper edge	No visible discoloration.
144-009	SaltSmart	46.9	Canister side. Insertion depth: 7.5 ft from upper edge	Slight brown discoloration on the wick; one large (a few mm) brown stain.
144-010	SaltSmart	56.6	Canister side. Insertion depth: 1.0 ft from upper edge	No visible discoloration.
144-011	Dry pad	55.9	Canister top. Insertion (horiz.): 40.5 in.	Thick pad, strongly discolored.
144-012	Dry pad	60.7	Canister top. Insertion (horiz.): 64.5 in.	Thick pad, slightly discolored.
144-013	SaltSmart	58.9	Canister top. Insertion (horiz.): 42.5 in.	Wick heavily coated with brown dust; upon disassembly, the absorbent pad was also discolored
144-014	SaltSmart	60.7	Canister top. Insertion (horiz.): 58.5 in.	Wick discolored—some grains coarse enough to be seen by eye.
Canister MPC-145				
145-001	Dry pad		Gamma shield	Thin pad, no visible discoloration.
145-002	SaltSmart		Gamma shield	No visible discoloration.
145-003	Dry pad	21.6	Canister side. Insertion depth: 13.5 ft from upper edge	Thin pad, no visible discoloration.
145-004	Dry pad	34.1	Canister side Insertion depth: 8.5 ft from upper edge	Thin pad, no visible discoloration.
145-005	Dry pad	50.3	Canister side Insertion depth: 1.5 ft from upper edge	Thin pad, slight brown discoloration.
145-006	SaltSmart	21.4	Canister side. Insertion depth: 13 ft from upper edge	Wick shows slight discoloration in a band at one end (~1/3 of the pad). It appears that the sensor was tilted, and the wick was only partially in contact with the surface. Pad was nearly dry upon disassembly.
145-007	SaltSmart	38.2	Canister side. Insertion depth: 7.5 ft from upper edge	Wick shows no discoloration.
145-011	SaltSmart		Blank	Wick shows no discoloration. Upon disassembly, pad was not saturated.
145-012	Dry pad	77.8	Canister top. Insertion (horiz.): 64.5 in.	Thick pad, heavy discoloration, a small seed was adhering to one edge of the pad.
145-013	SaltSmart	78.9	Canister top. Insertion (horiz.): 58.5 in.	Wick heavily discolored with brown dust. Upon disassembly, the pad was not saturated.
145-014	SaltSmart	54.6	Canister side. Insertion depth: 1.0 ft from upper edge	No visible discoloration.

Table 2. Diablo Canyon Samples

Sample #	Sample Type	T (ºC)	Sample location	Description
Canister MPC-123				
123-001	Dry pad		Gamma shield	Thin pad, no visible discoloration.
123-002	SaltSmart		Gamma shield	No visible discoloration.
123-003	SaltSmart	48.7	Canister side. Insertion depth: 14 ft from upper edge	No visible discoloration. One black speck visible with hand lens.
123-004	SaltSmart	78.6	Canister side. Insertion depth: 11.5 ft from upper edge	No visible discoloration. A few black specks visible with hand lens.
123-005	SaltSmart	86.1	Canister side. Insertion depth: 10.5 ft from upper edge	No visible discoloration. A few black specks visible with hand lens. Note: Wick adhered to silicone pressure pad, reservoir pad only partially wetted.
123-006	Dry pad	80.7	Canister side. Insertion depth: 11 ft from upper edge	Thin pad, minor discoloration along two edges of pad.
123-007	Dry pad		Blank (removed form tool after failed attempt to enter annulus).	Thin pad, no visible discoloration.
123-008	Dry pad	99.8	Canister side. Insertion depth: 7.5 ft from upper edge	Thin pad, moderately discolored.
123-009	Dry pad	118.6	Canister side. Insertion depth: 3.0 ft from upper edge	Thin pad, slight discoloration in one corner.
123-010	SaltSmart		Blank	No visible discoloration.
123-011	Dry pad	97.1	Canister top (center). Insertion (horiz.): 64.5 in.	Thick pad, slightly discolored, with visible black specks.
123-012	Dry pad	95.6	Canister top (7” from closure ring). Insertion (horiz.): 7 in.	Thick pad, moderately discolored, with visible black specks.
Canister MPC-170				
170-001	Dry pad		Gamma shield	Thick pad, no visible discoloration.
170-002	SaltSmart		Gamma shield	No visible discoloration.
170-003	Dry pad	86.4	Canister top (center). Insertion (horiz.): 64.5 in.	Thick pad, somewhat discolored
170-004	Dry pad	67.7	Canister side. Insertion depth: 11 ft from upper edge	Thin pad, slightly discolored.
170-005	Dry pad	89.9	Canister side. Insertion depth: 7.5 ft from upper edge	Thin pad, discolored along one edge.
170-006	Dry pad	82.6	Canister side. Insertion depth: 3.0 ft from upper edge	Thin pad, slightly discolored along two edges.
170-007	SaltSmart	80.8	Canister side. Insertion depth: 10.5 ft from upper edge	No visible discoloration. A few black specks visible with hand lens. Note: Wick adhered to silicone pressure pad, reservoir pad only slightly damp.
170-008	SaltSmart	83.8	Canister side. Insertion depth: 9.5 ft from upper edge	No visible discoloration. Black specks visible to naked eye and with hand lens. Note: Wick adhered to silicone pressure pad, reservoir pad only partially wetted.
170-009	SaltSmart	86.8	Canister side. Insertion depth: 9.0 ft from upper edge	No visible discoloration. Black specks visible to naked eye and with hand lens. Note: Wick adhered badly to silicone pressure pad, but reservoir pad well wetted.

Complete SaltSmart™ sensor. During sample collection, the SaltSmart™ sensor was placed against the canister angled so that the water source (right) was higher than the pad. Flow is from right to left. In each of the following images, the orientation is the same as shown above.

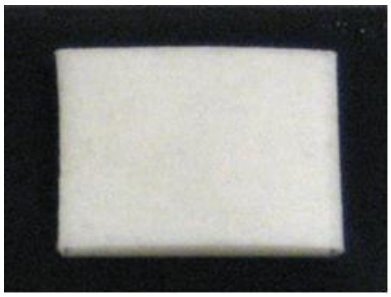

144-003

144-004

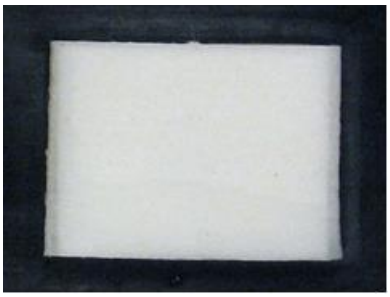

144-008

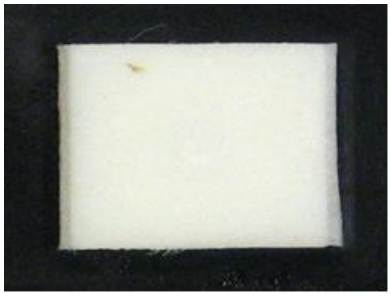

144-009

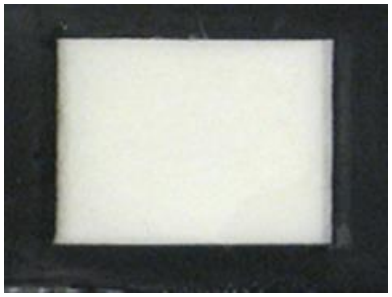

144-010

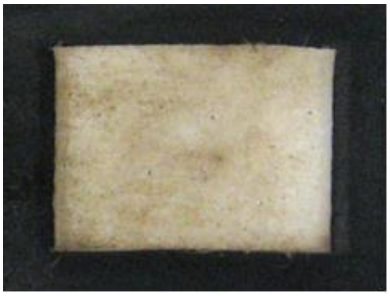

144-013

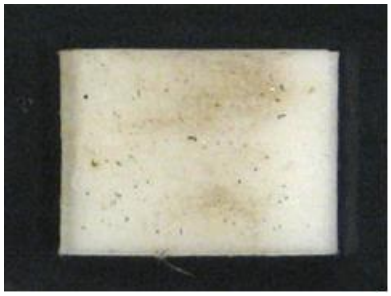

144-014

Figure 3. SaltSmart™ samples collected from canister MPC-144, Hope Creek.

Figure 4. Dry pad samples collected from canister MPC-144, Hope Creek.

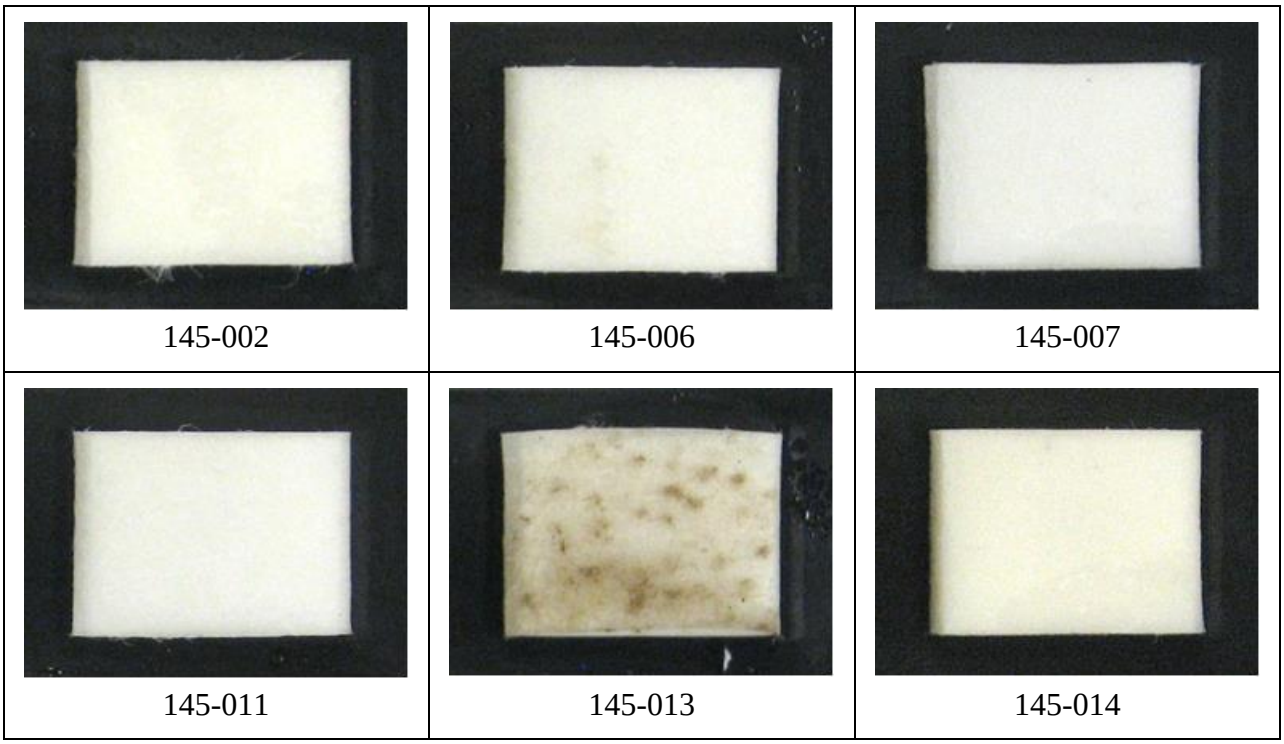

Figure 5. SaltSmart™ Samples collected from canister MPC-145, Hope Creek. (Note: sample 145-001 was inadvertently not photographed)

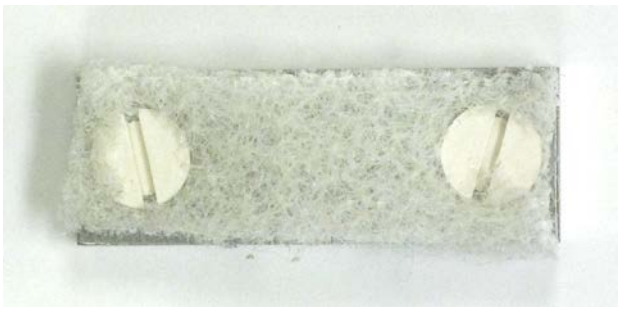

145-003

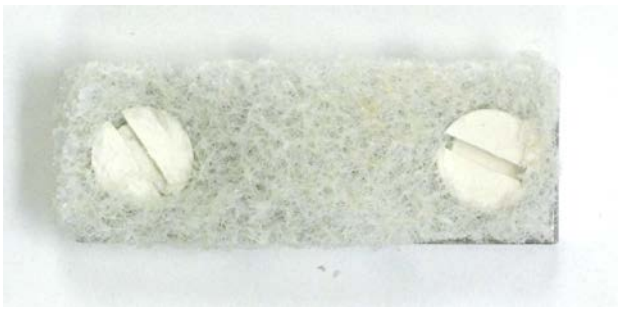

145-004

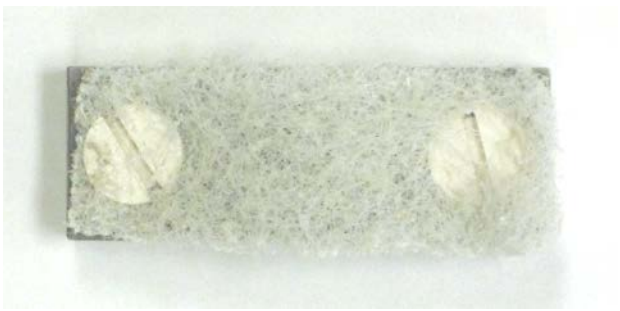

145-005

145-012

Figure 6. Dry pad samples collected from canister MPC-145, Hope Creek. Note the small seed adhering to the upper edge of sample 145-012.

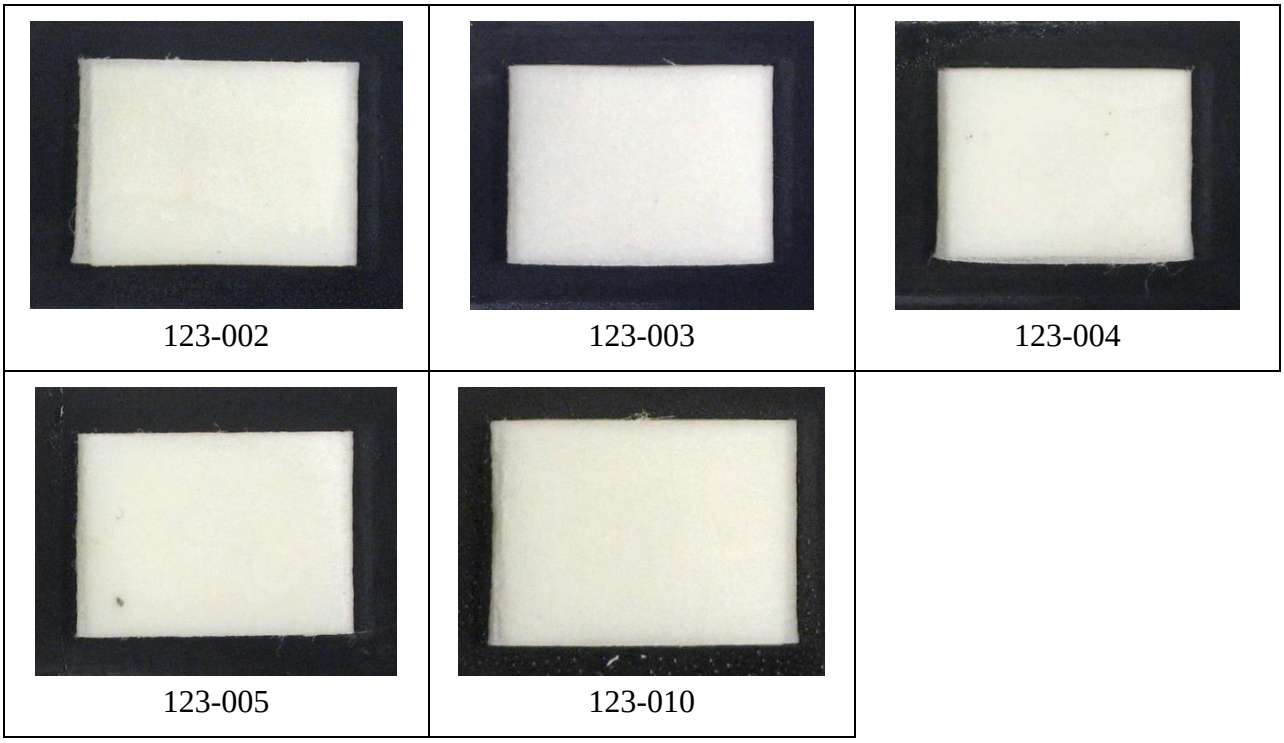

Figure 7. SaltSmart™ samples collected from canister MPC-123, Diablo Canyon.

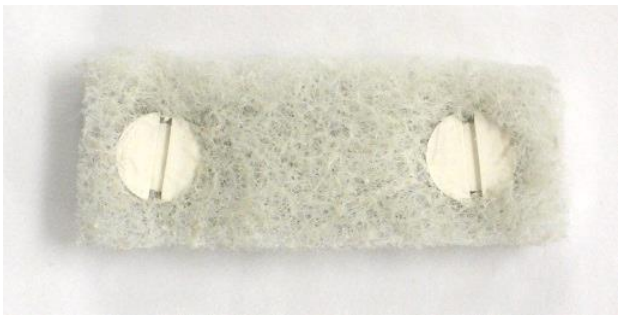

123-001

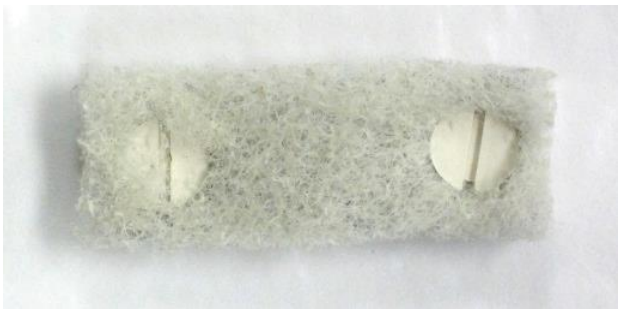

123-006

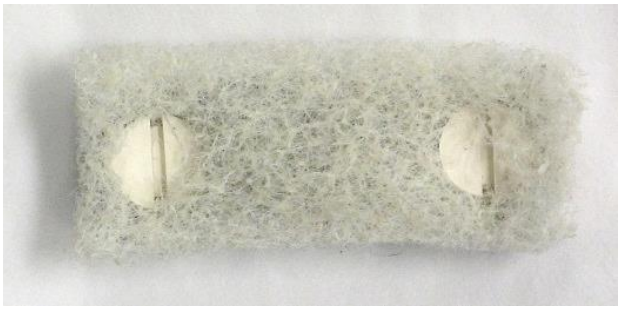

123-007

123--008

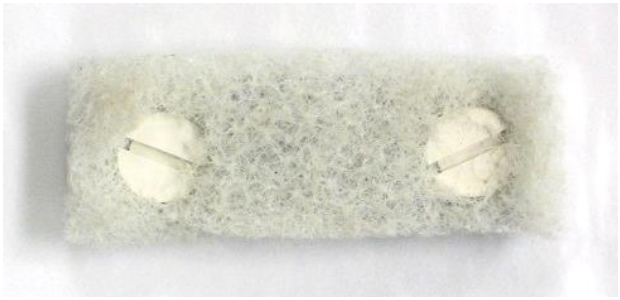

123--009

123-011

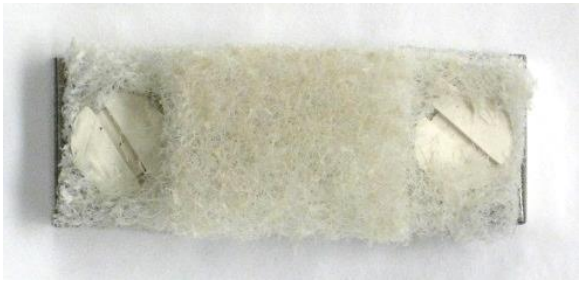

123-012

Figure 8. Dry pad samples collected from canister MPC-123, Diablo Canyon.

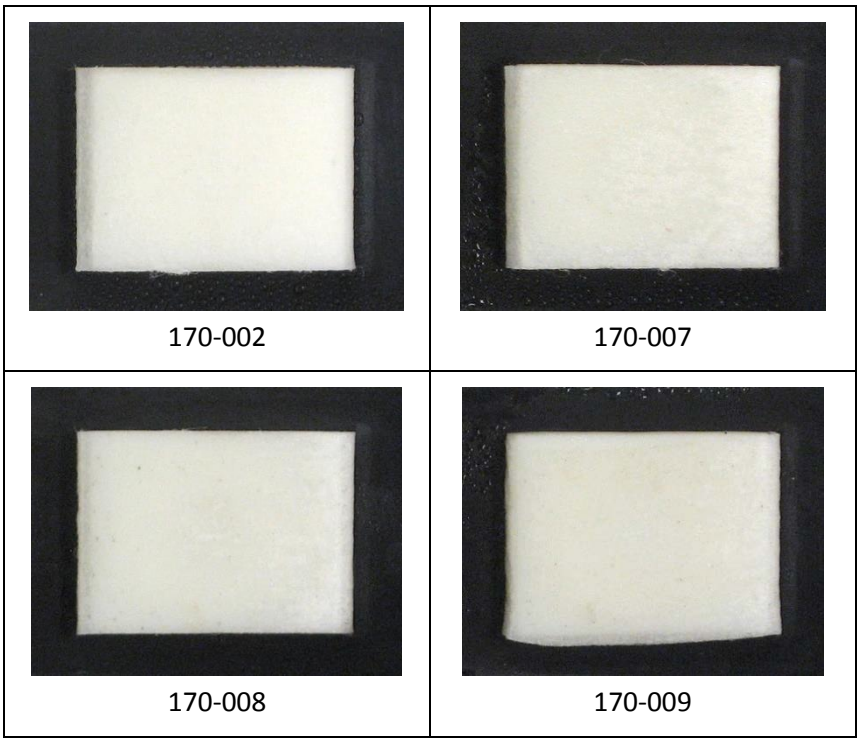

Figure 9. SaltSmart™ samples collected from canister MPC-170, Diablo Canyon.

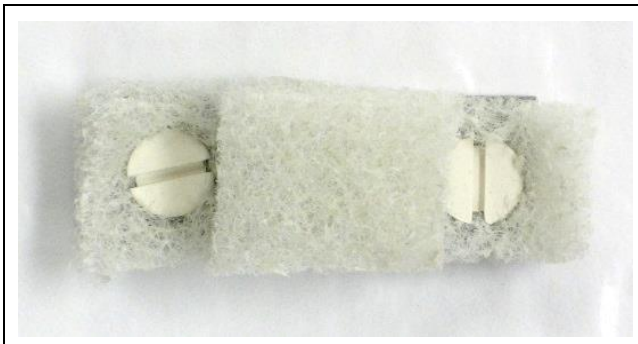

170-001

170-003

170-004

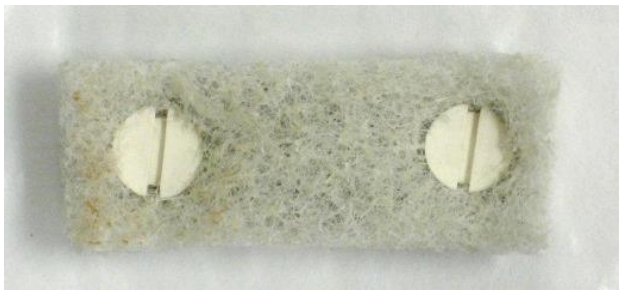

170--005

170--006

Figure 10. Dry pad samples collected from canister MPC-170, Diablo Canyon.

The surface temperatures at each sampling location are provided in Table 1 and Table 2, and are plotted versus sample location in Figure 11 and Figure 12 for the Hope Creek and Diablo Canyon canisters, respectively. It should be noted that in the case of Hope Creek MPC-144 and Diablo Canyon MPC-170, temperatures were not consistent over the course of the sampling effort, with measured temperatures for the wet and dry sampling forming two different trends as a function of depth. The observed temperature differences are too large to be due to variations in the external air temperature, and it is assumed that readings from one or more of the thermocouples are inaccurate; possibly, poor contact was achieved with the canister surface.

Testing by the manufacturer indicated that the maximum operating temperature for the SaltSmart™ sensors was 90ºC. The dry pads had a much higher maximum operating temperature. For this reason, thermocouple readings or dry pad samples were taken first, and the recorded temperatures used to determine what parts of the canisters could be sampled using the SaltSmart™ sensors. The Hope Creek canisters were sufficiently cool that the entire surface of each canister could be sampled, but the Diablo Canyon canisters were much hotter, and only the lower portion of the canister sides was sampled with the SaltSmart™ devices. The SaltSmart™ sensors actually began to operate poorly at temperatures ≥~80ºC; the wick would adhere to the silicone pressure pad backing it, and the reservoir pad would not be fully wetted, suggesting that water flow through the sensor may have been limited, and salt recovery may not have been complete. SaltSmart™ samples where the wick adhered to the pressure pad, or which did not have fully wetted reservoir pads, are also shown in Figure 11 and Figure 12.

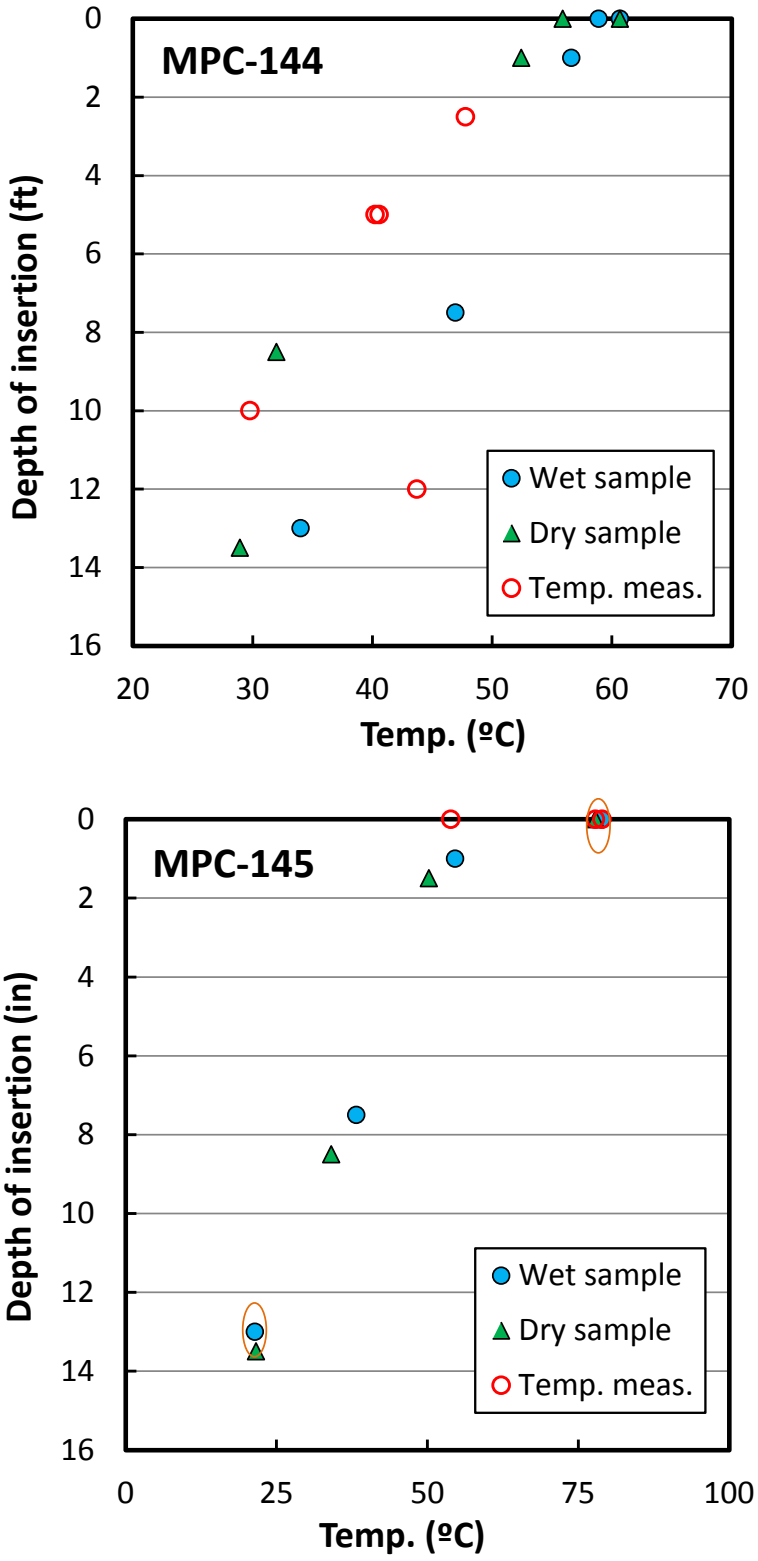

Figure 11. Hope Creek sample locations and temperatures. Orange ovals mark SaltSmart™ samples with heat-damaged wicks or unsaturated reservoir pads.

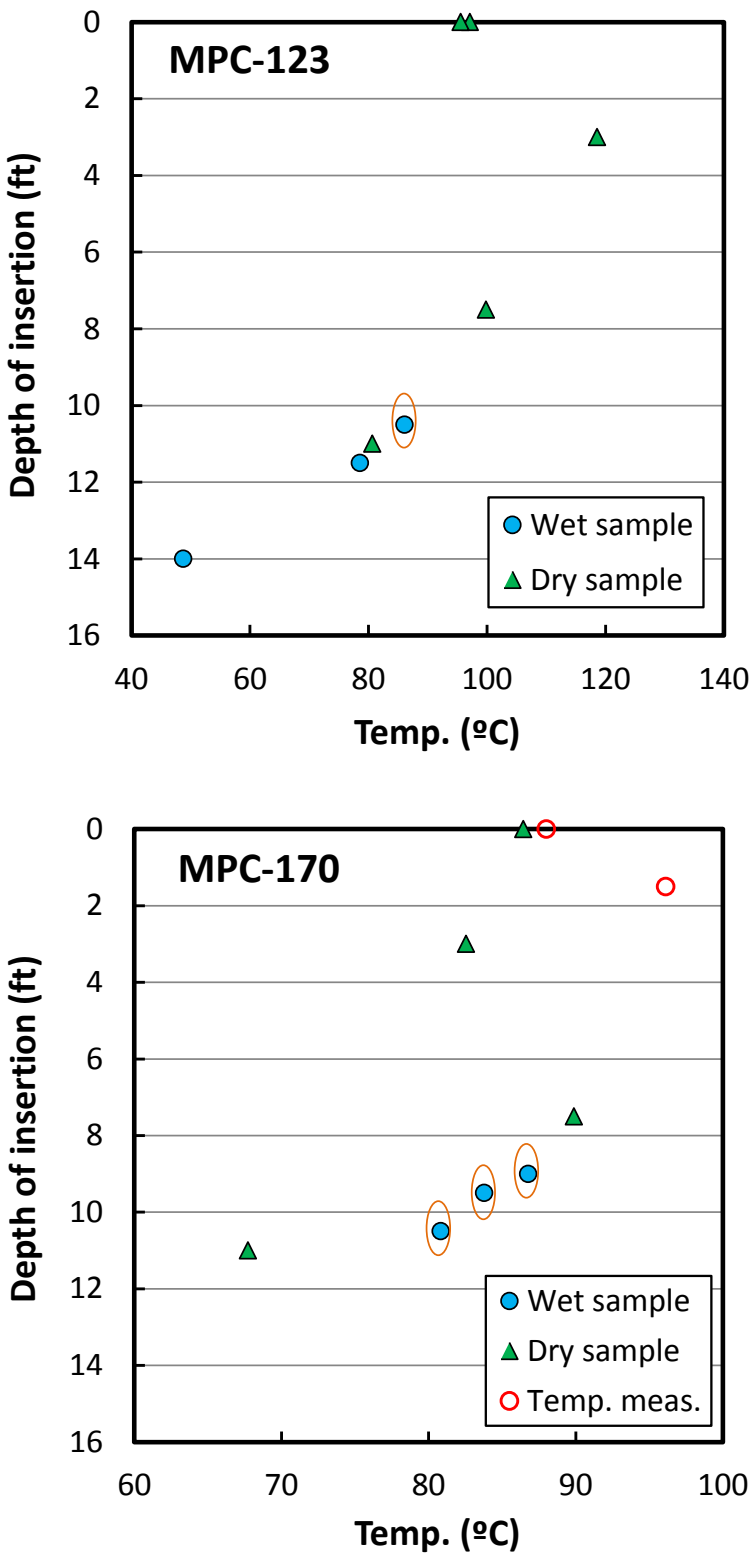

Figure 12. Diablo Canyon sample locations and temperatures. Orange ovals mark SaltSmart™ samples with heat-damaged wicks or unsaturated reservoir pads.

2.2. Methods

2.2.1 SEM Imaging and EDS Analysis

SEM/EDS analysis of the dry dust samples provides textural and mineralogical information of dust/dust components, and allows visual identification of organic matter (floral/faunal fragments). Sample fractions retained for SEM analysis were plasma-coated with gold to reduce sample charging during analysis. Imaging and element mapping was done with a Carl Zeiss Supra^{Tm} 55VP SEM, equipped with an Oxford X-Max EDS detector and Aztec$^{©}$ software. An accelerating voltage of 15 keV was used, and working distances of 7.1 to 9.4 mm, with varying degrees of magnification. Images were obtained using both secondary and backscattered electron imaging. A relatively high beam current was used to produce a high count rate and facilitate rapid element mapping. However, the elevated beam current did enhance sample charging for the fibrous pad samples, resulting lower image quality in some cases.

2.2.2 XRF Analysis

Due to an equipment failure at Sandia, the XRF mapping was accomplished at Los Alamos National Laboratories, using an EDAX Eagle Micro-XRF system, instead of the Bruker M4 Tornado micro-XRF system used for analysis of Calvert Cliffs samples. This energy dispersive system was equipped with a micro-focus Rhodium X-ray source operated at 40 keV and 200 µA. The spatial resolution was ~100 µm. Mapping was performed via an XY translation stage. Samples were run under vacuum atmosphere ($5x10^{-3}$ Torr). The summed X-ray spectrum was processed to produce a semi-quantitative chemical analysis for the abrasive pad and the dust on the sample surface. The XRF analysis provides element ratios which, in combination with the wet chemical analysis, can be used in mass balance and normative mineral calculations. However, one limitation is that elements lighter than sodium (e.g. oxygen, nitrogen, carbon) cannot be detected, and detection limits for sodium are poor.

2.2.3 XRD Analysis

XRD analysis was performed using a Bruker D2 Phaser diffractometer with a Cu Kα X-ray source, and a LynxEye solid-state energy discriminating X-ray detector. Samples were analyzed "as-received," with minimal preparation, directly on the abrasive pads. However, the abrasive pads were too coarsely porous to allow in-situ XRD analysis, and no mineral peaks were identified. An additional attempt was made to analyze the insoluble residue remaining after washing the soluble salts from the dry pads and filtering the residue onto Whatman 541 paper filters. This, too, was largely unsuccessful—only a single peak, the most prominent peak for quartz, and a few small possibly corresponding to talc were identifiable. The XRD analysis will not be discussed further here.

2.2.4 Chemical Analysis

2.2.4.1. SaltSmart™ sensors — soluble salts

Once at Sandia, the SaltSmart™ sensors were disassembled and the soluble salts were extracted with DI water for chemical analysis. Then the salt compositions, including chloride concentration, were measured directly by inductively-coupled plasma optical emission spectroscopy (ICP-OES), and cation/anion ion chromatography (IC).

For analysis, the SaltSmart™ sensors were removed from the 50 ml centrifuge tubes and split open along the seam with a small chisel. The component parts of each sensor are shown in Figure 13. The wick and the reservoir pad inside the SaltSmart™ device were removed and transferred to a pre-weighed 50 ml polypropylene screw-cap sample tube. Moisture was observed on other plastic internal pieces of the sensors and on the inside surfaces of the two halves of the shell. The internal pieces, and the inside surfaces of the shells, were rinsed with deionized water (>18MΩ) and the water transferred to the polypropylene sample tubes containing the wicks and pads. The original centrifuge tubes used for shipping the samples commonly contained condensate, and these were also rinsed into the polypropylene sample tubes. Additional DI water was added, to achieve a total water volume of ~15 ml per sample; the exact volume was determined by the weight difference between the empty and filled vials; the weights of a dry wick and reservoir pad were also considered. The samples were placed on a shaker table overnight to leach the salts in the wick and pad into the solution.

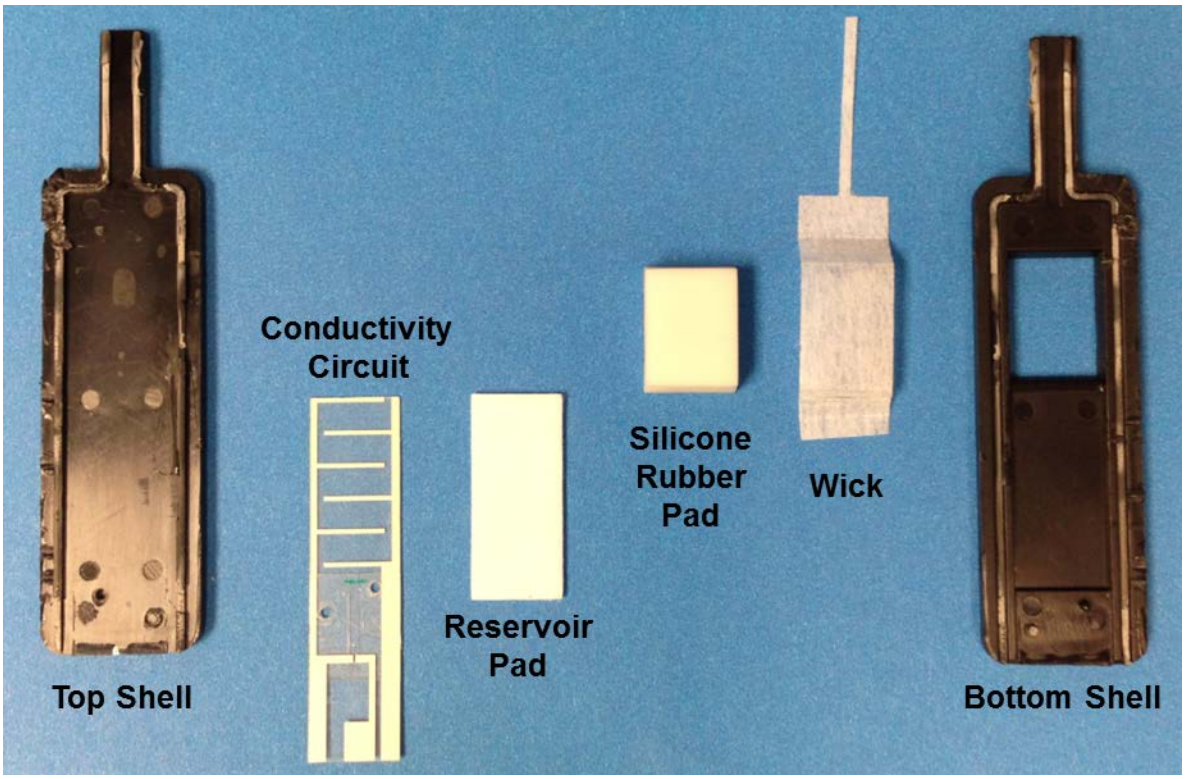

Figure 13. Disassembled SaltSmart™ Device.

Also during disassembly, the condition of the wick and the saturation state of the reservoir pad were recorded. During normal operation of the sensor, the reservoir pads inside the sensors are completely saturated after use, indicating that water flow was adequate through the sensor. This was confirmed by ambient-temperature testing of SaltSmart™ sensors at Sandia. Testing at Sandia using metal coupons with known deposited salt loadings showed that SaltSmart™ sensors are efficient at removing soluble salts from metal surfaces, and that the disassembly and leaching procedure used on the Hope Creek and Diablo Canyon samples is effective (Memo from C. Bryan to L. Zsidai dated Nov. 13, 2013; SAND#2013-9948P); experimental salt recoveries were in the 80-100% range.

Although testing by the SaltSmart™ company suggested that the sensors performed adequately to ~90ºC, the condition of the Hope Creek and Diablo Canyon samples indicated that the operational limit for SaltSmart™ sensors is lower. During sample disassembly, it was observed that the reservoir pad was saturated in most of the relatively low-temperature Hope Creek samples, but that that the wicks adhered strongly to the silicon pressure pad for samples collected at temperatures of ~80ºC and above; in nearly all of those cases, the reservoir pad was not saturated. Wick adherence and/or poor reservoir pad saturation was observed for three of the Hope Creek samples and for most of the Diablo Canyon samples (See Figure 11 and Figure 12). In only one instance was poor wetting associated with a lower-temperature sample (sample 145-006); in this case, it appears to be associated with poor contact between the wick and canister surface. It is possible, perhaps likely, that salt removal was incomplete for SaltSmart™ samples that were poorly wetted, as the adherence of the wick to the silicone pressure pad and the incomplete saturation of the reservoir pad suggest that water transport through the wick was limited.

Following equilibration, aliquots of each sample were separated for analysis. Approximately 8 ml of the solution (the actual amount was determined by weight) was extracted from the sample tubes and retained for cation analysis. This fluid was spiked to contain 2% Optima-grade HNO_3 and 1 mg/L Sc as an internal standard, and brought to a volume of 12 ml for analysis by inductively coupled plasma optical emission spectroscopy (ICP-OES). ICP-OES analyses were done using a sequential Perkin-Elmer Optima 8000 ICP-OES, in both axial and radial viewing modes. Analytes examined were Ca^{2+}, Mg^{2+}, Na^{+}, and K^{+}. A minimum of two wavelengths were evaluated for each element; collected spectra were evaluated for interfering peaks, and for each element, the wavelength was chosen that best reproduced known standard concentrations when the standards were analyzed as unknowns. Concentrations were estimated using integrated peak areas. Because the range of concentrations in the samples was unknown, five to six standards were made by diluting Spex Certiprep™ Assurance and Claritas-Grade ICP stock solutions and were run with the samples. Sample concentrations were estimated using a subset of the standards (never less than three and a blank), excluding those which were higher than necessary to constrain the sample concentration. This was done because the calibration curves were based on the least squares method, which over-weights higher-concentration standards and results in larger errors for values in the lower part of the range.

Three ml of the solution was extracted from the sample tubes and retained for anion analysis by ion chromatography (IC). Anionic analytes were F^{-}, Cl^{-}, Br^{-}, NO_2^{-}, NO_3^{-}, SO_4^{-2}, and PO_4^{-3}. IC analyses were done with a Dionex ICS-1100 RFIC Ion chromatograph with a Dionex Ionpac AS-

23 RFIC column and AG-23 guard column, and a Dionex AERS 500 suppressor. Blanks were run every two-three samples to assess carryover, but little was observed. As with the cation analyses, five to six standards and a blank were made by dilution of stock Dionex IC anion standards, but only a bounding subset was used to estimate sample concentrations.

Finally, three ml of the solution was acidified to 0.1% HNO_3 and retained for analysis of ammonium, $(NH)_4^+$. Unlike other cationic components of the salts, ammonium cannot be measured by ICP-OES. The analyses were done with a Dionex ICS-1100 RFIC Ion chromatograph with a Dionex Ionpac CS-12A column and CG-12A guard column, and a CSRS 300 suppressor, all 4 mm in diameter. The standards were made by dilution of stock Dionex IC cation standards.

2.2.4.2. Dry pads — soluble salts

Following analysis of the whole pad by Micro-XRF, the pad samples were removed from the steel plates and sectioned. About ¼ of each pad was retained for SEM/EDS analysis, while the rest was used for chemical analysis of soluble salts. The remainder of each sample was placed in a pre-weighed polypropylene sample vial, and the vials were reweighed to determine the pad weight (to allow for accurate blank correction later). Then, 10 ml of cold deionized water was added to each vial, and each vial was reweighed to determine the exact liquid mass present. The samples were agitated for two hours on a shaker table, and the pads were removed from the vials and transferred to filter funnels containing pre-rinsed Whatman #541 paper. The leachate containing the soluble salts transferred to a syringe, filtered through 0.2 µm polyethersulfone syringe filters, and split into three aliquots for chemical analysis (ICP-OES cations, IC anions, and IC ammonia) as described previously for the SaltSmart™ samples. Any sediment remaining in the vials after transferring the leachate was added to the pad samples in the filter funnels.

The pads and sediment in the filter funnels were rinsed thoroughly with ~40 ml DI water, making an effort to dislodge any particles on the pads. Then, then the pads were extracted from the filters and discarded. The paper filters with the remaining insoluble residues were then dried. An attempt was made to analyze them by XRD, but little was observed—the X-ray pattern from the nylon in the pad dominated the spectrum. A very small peak was tentatively identified as the dominant peak for quartz was present in the patterns of the more heavily loaded canister top samples. In one sample, a few small peaks that may represent talc, used as filler in the resin in the pads, were also observed. Because of the very light dust load on most pads, and the high degree of contamination by talc, a decision was made not to perform bulk analyses of the dry pad insoluble residues.

3. RESULTS

3.1. SEM/EDS Analysis

SEM/EDS analysis of the dry pad samples was carried out to determine dust and salt mineralogy, to identify organic materials present, and to determine dust particle size and morphology. Analyzed samples include a blank pad and pads from both Hope Creek and Diablo Canyon (Table 1 and Table 2). SEM images were taken of characteristic features, and EDS element mapping was done to assess mineralogy. Results are summarized here with typical images from some samples; a complete suite of analyses is provided in Appendix A, and allows the reader to better assess the representativeness of the results provided here.

3.1.1. Blanks

The sponge-like pads used to collect the dry dust samples were 3M Scotch-Brite™ light-duty scrubbing pads (part # 3M-05683). The pad consists of nylon fibers bound together with a resin. The pads were purchased after consultation with 3M, and were intended not to contain any mineral components. However, after using the pads, it was determined that talc (Mg-silicate) is present as filler in the resin binding the pads together. The pads are easily abraded, and when this occurs, the talc, which has perfect basal cleavage, flakes apart, generating particulate material, which interfered with analysis of dust collected from the storage canisters. Although this was a problem, the simple chemical composition of talc ($Mg_3Si_4O_{10}(OH)_2$) meant that it was in general possible to distinguish it from the dust adhering to the canisters, and to identify the dust species.

Figure 14 is a low-magnification image of the blank pad. The fibers form a network, and the resin-filler binds the mass together, forming broad bridges at fiber intersections. The talc is generally embedded within the resin, and does not penetrate the exposed surface, except where the resin has been abraded. The bridges are ideal locations for analysis of adhering dust, because the talc is embedded within the resin, particulate talc contamination is commonly minimal, and the broad flat surface is ideal for SEM analysis. However, in cases where the sampled dust load is light, the adhering dust may be mostly on the exposed uppermost surfaces of the pads, where abrasion has revealed the talc. In these cases, much of the particulate matter on the pads may be talc flakes. In addition to Mg, Si, and O in the talc, the nylon is an amide, containing carbon (C), nitrogen (N), and oxygen (O), and these species are reflected in the EDS spectrum and the element maps. The dominant chemical components in the pad, as identified by EDS, are C, Si, and Mg; N is obscured by proximity to the C peak, but shows up in the element maps. Other chemical components that leach from the pad during chemical analysis include sodium (Na), phosphate (containing phosphorous, P), and sulfate (containing sulfur, S); however, these contribute too little to the bulk composition to be identified by SEM/EDS analysis.

Figure 15 is a higher resolution image of the bad blank, showing the texture of the pad and the embedded talc. In general, the blank pad had little adhering particulate matter, other than talc particles freed by abrasion during cutting and handling of the pad for SEM analysis.

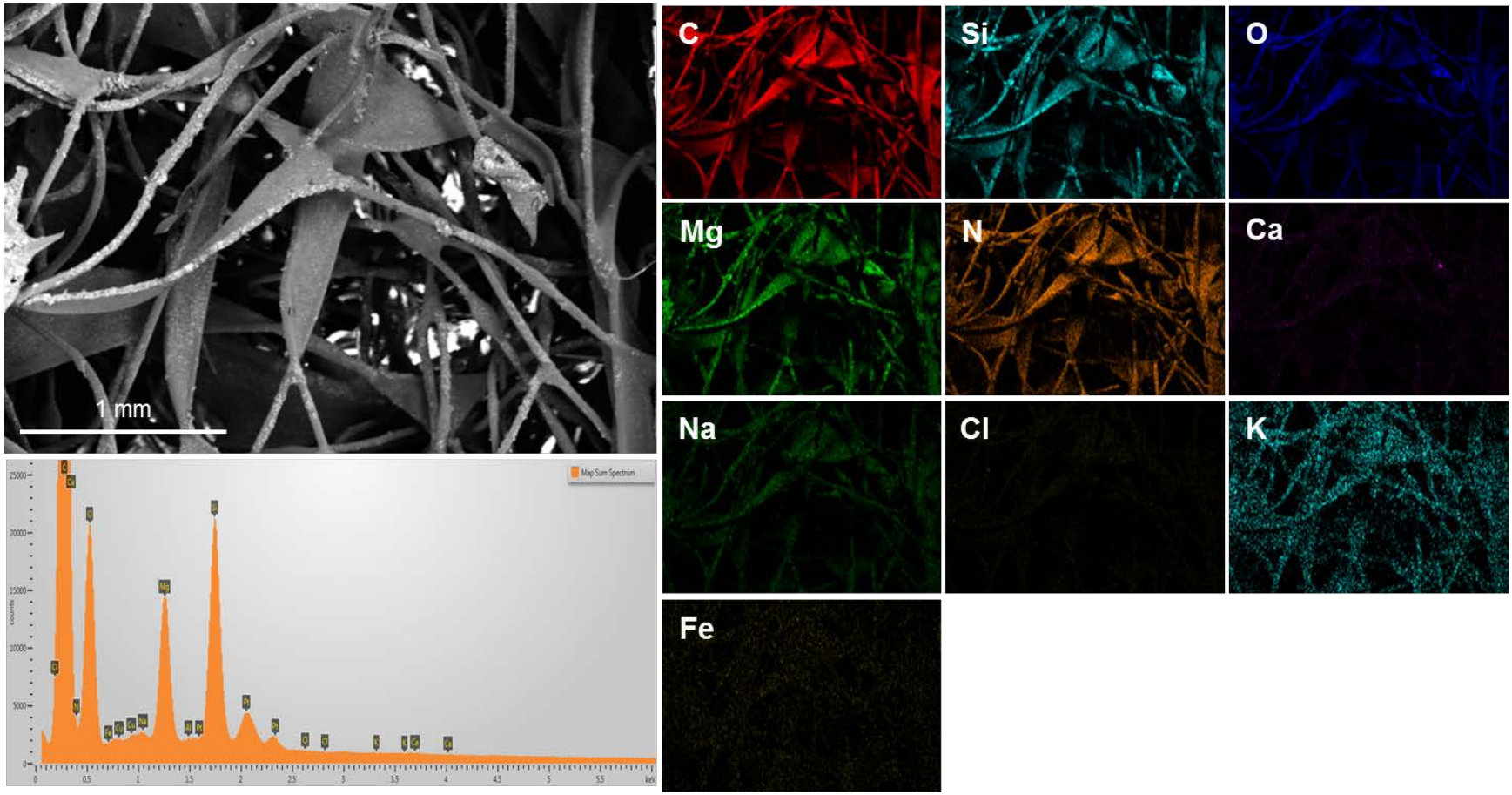

Figure 14. Low magnification SEM image/EDS map of Scotch-Brite™ pad blank.

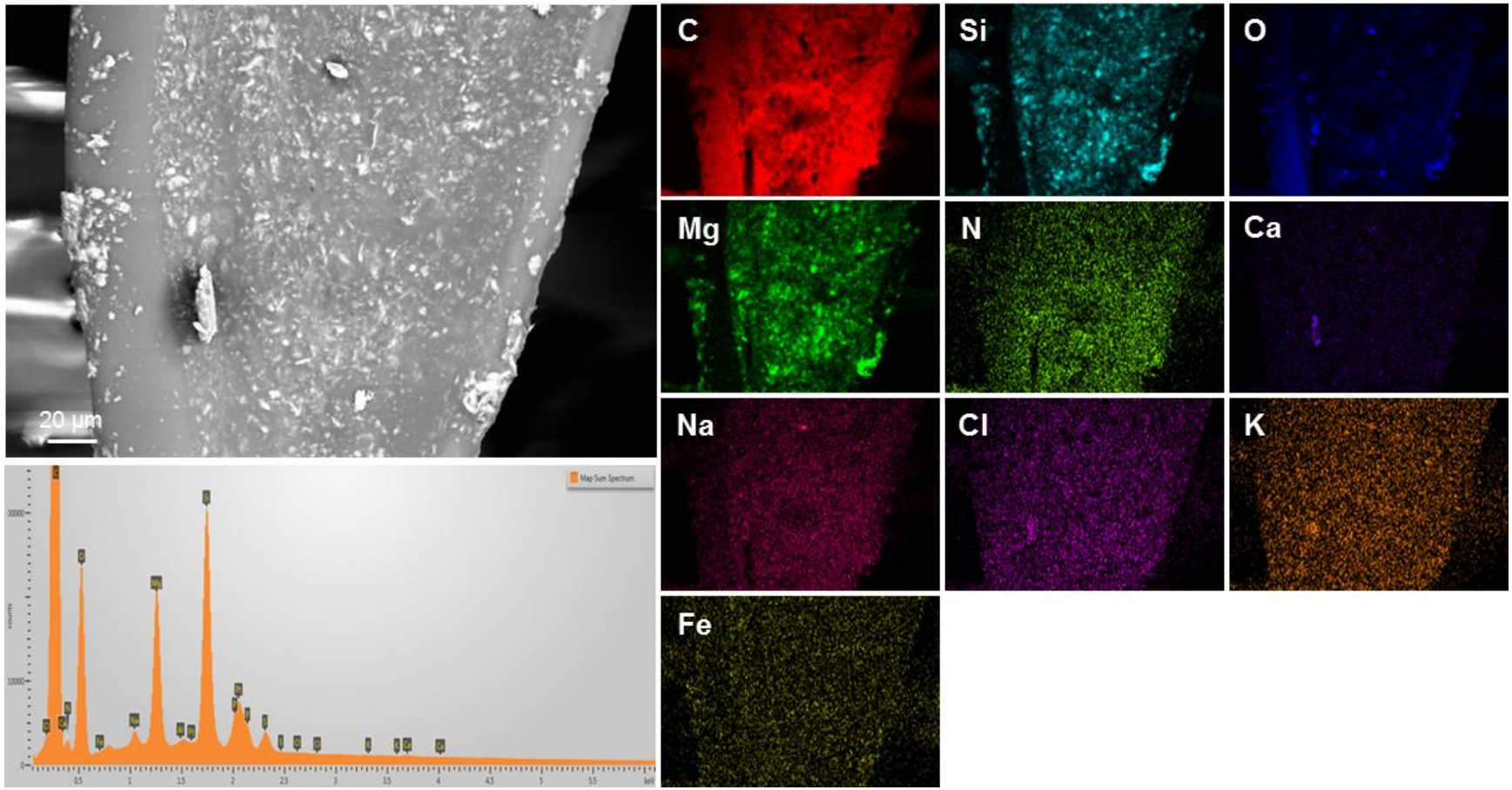

Figure 15. High magnification SEM image/EDS map of Scotch-Brite™ pad blank.

3.1.2. Hope Creek Samples

Two canisters were sampled at the Hope Creek ISFSI. These were designated MPC-144 and MPC-145. For this study, the complete suite of samples was analyzed only for canister MPC-145. To verify that mineralogy did not vary significantly from canister to canister, two samples from MPC-144 were analyzed—the lowermost sample collected from the canister side, and a sample from the canister top. For each canister, a few representative SEM image/EDS element map combinations are discussed here; a complete suite of analyses is provided in Appendix A. It should be noted that for some of the samples from the canister sides, dust was so sparse that only a few sites on each pad had any adhering dust at all. For very lightly loaded samples, the SEM images are not typical of the pad surface; the images represent locations where concentrations of dust particles are present, and hence provide an overestimation of the total dust loading.

MPC-145. Sample #MPC-145, for which a complete suite of samples were analyzed, will be discussed first. Samples 145-003, 145-004, and 145-005 were collected from the canister side at distances, respectively, of 13.5, 8.5, and 1.5 feet below the upper edge of the canister. Sample #145-012 was collected from the top of the canister, near the center. Dust and salt loads on pads used to sample the sides of the canister were extremely light. However, the flat top of the canister had large amounts of dust, and much adhered to the sampling pad. There is no significant variation in the mineralogy present from place to place on the canister surface. The phases observed on all of the samples from MPC-145 are listed in Table 3. Most of the dust consists of terrestrially-derived detrital mineral grains, including quartz (Si-O), and several different aluminosilicates. The aluminosilicates include blocky, angular Na, K, and Ca bearing phases that appear to be feldspars, platy biotite flakes, and aggregate grains of finer particles that are likely to be clays. Angular Fe and Fe-Cr particles in various stages of oxidation are steel and stainless steel particles generated during manufacturing of the canisters; spherical particles of the same compositions may be welding spatter. The only common soluble salt is a Ca-SO_4 phase (gypsum or anhydrite); chloride occurs mostly as rare small particles of NaCl.

SEM/EDS data for Sample 145-003, collected at a distance of 13.5 feet below the upper edge of the canister, are shown in Figure 16. Figure 16 shows an accumulation of dust, mostly aluminosilicates and Fe-Cr particles, near an abraded edge—note that many of the particles in the image are talc released from the pad by abrasion. On very lightly loaded pads, dust is commonly only present on or near abraded areas. Also, on lightly loaded pads, Fe-Cr particles form a larger proportion of the total, because the amount of environmentally-derived dust (as opposed to manufacturing-derived), is low.

Sample #145-004 (Figure 17) was collected 8.5 feet below the top of the canister. Most of the particles visible in Figure 17 are talc, freed by abrasion of the pad. Adhering particles are sparse, and are generally small, less than 5 microns in diameter. The dominant dust phases include quartz, aluminosilicates, 304SS particles, and Ca-sulfate.

Sample 145-005 was collected 1.5 feet below the upper edge of the canister, and once again, the pad was very lightly loaded; adhering dust was largely restricted to topographically high regions on the pad, which had been abraded by contact with the canister surface. Figure 18 shows the only region of the pad with identifiable dust. Fine particles of stainless steel are embedded in the resin, and two large dust grains are present. The two larger grains are biotite, and a Na-Zn phase,

apparently from the corrosion-inhibiting Zn-rich paint on the outer surface of the canister overpack. Similar Zn-Na rich grains were seen on the other cask from Hope Creek, and on a canister at Diablo Canyon.

Samples from the tops of the canisters at Hope Creek, such as 145-012, were heavily coated with dust (Figure 19). Canister top samples are invariably more heavily coated than canister side samples, and it is likely that this reflects a higher salt load on the canister top. However, it is important to remember that a different sampling technique was used for the canister tops—sampling by hand using a long rod, rather than the remote, pneumatically-operated sampler used for the canister sides. A larger area was probably sampled, and the pressure on the pad certainly varied for the two methods. It is likely that the dust removal efficiency varies between the two methods, and this may be responsible for some of the differences in dust loading on the sample pads.

A typical SEM/EDS map for sample 145-012 is shown in Figure 20. In this map, and in other SEM/EDS maps in Appendix A, quartz and aluminosilicates are the dominant phases in this sample. The aluminosilicates are mostly blocky mineral fragments that are probably feldspars, and biotite. Ca and Ca-Mg carbonates are also common. Soluble salts include sparse NaCl and Ca-SO_4.

Table 3. Minerals Observed in Dry Pad Samples from MPC-145

Elemental analysis	Morphology	Interpretation	Abundance
Si-O	Angular grains	Quartz fragments	Common to abundant
K-Al-Si-O	Blocky, angular fragments	Potassium feldspar	Common
Na(±Ca)-Al-Si-O	Blocky, angular fragments	Sodic plagioclase	Common
Ca(±Na)-Al-Si-O	Blocky, angular fragments	Calcic plagioclase	Rare
Na-K-Al-Si-O	Blocky, angular fragments	Volcanic alkali feldspar or zeolite?	Rare
Ca-K-Na-Al-Si-O	Blocky, angular fragments	Zeolite?	Sparse
K-Fe-Mg-Al-Si-O	Large planar flakes	Biotite	Rare-common
Al-Si-O	Aggregate grains	Kaolinite	Rare
Fe-Cr	Striated flakes and fragments	Stainless steel particles generated by machining	Abundant
(K,Na,Ca)-Fe-Al-Si-O	Aggregate grains	Clays?	Common
Ca-Al-Si-O	Aggregate grains	Clays?	Rare
Ca-O-(C?)	Angular grains	Calcium carbonate	Common
Mg-O-(C?)	Angular grains	Magnesium carbonate	Rare
Mg-Ca-O-(C?)	Angular grains	Magnesium-calcium carbonate	Common
Na-Zn-O	Rounded particles	Particles from Zr-rich paint on the outside of the overpack?	Rare
C	Oval to spherical grains	Pollen	Rare to common
Fe-O	Angular particles	Iron oxides	Rare
Ca-S-O	Very fine particles	Gypsum	Rare to common
Na-Cl	Cubes and aggregates, commonly etched or corroded	Halite	Sparse
Na-K-Cl	Aggregate grains	Sylvite/halite aggregate?	Rare
C-Cl	Aggregate grains	Chloride-rich organic material?	Rare
Na-K-S-O	Aggregate grains	Aggregate of sulfates?	Rare

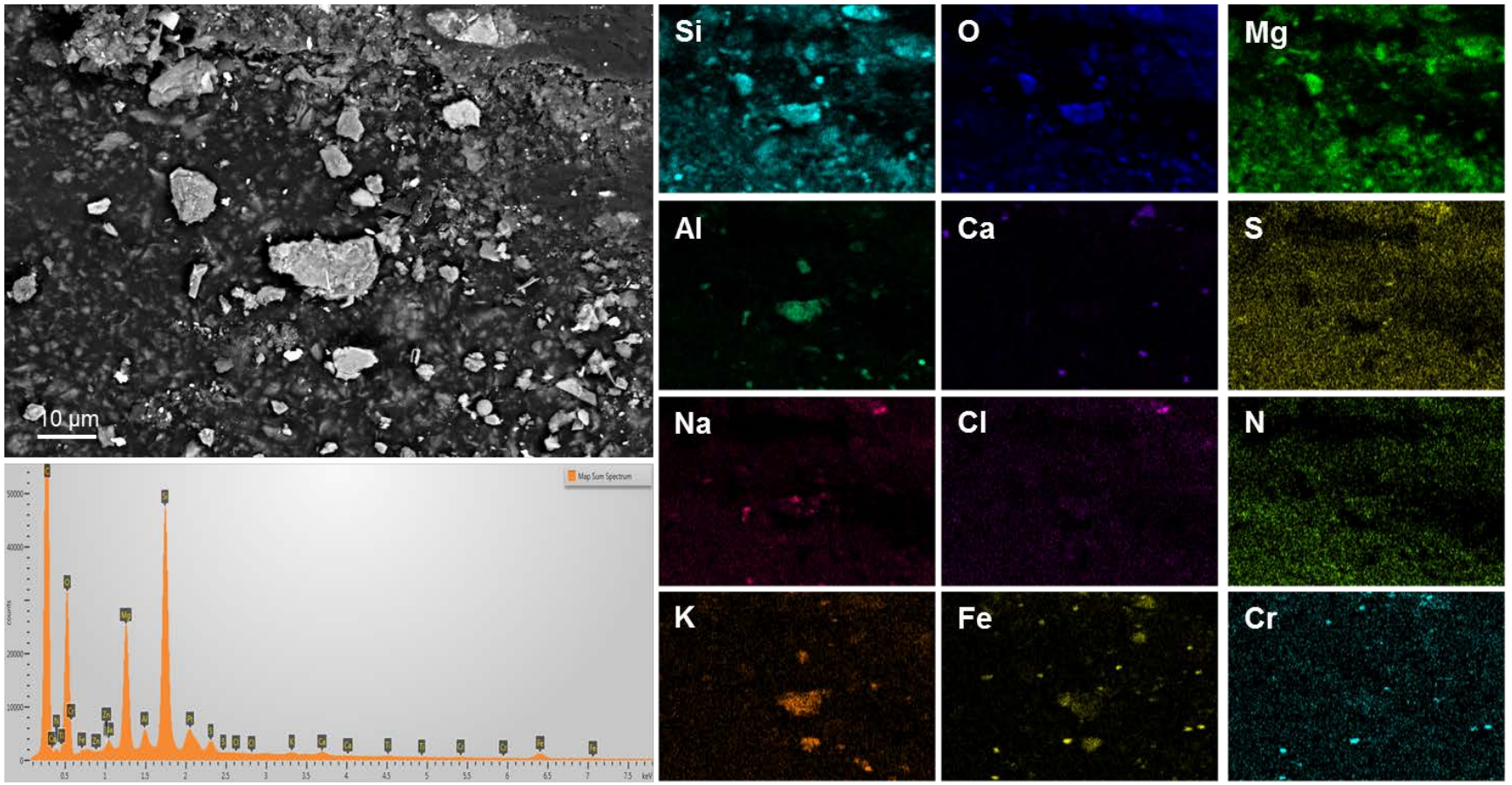

Figure 16. SEM image/EDS map (#2) of Sample 145-003, collected from the canister side, 13.5 feet below the upper edge.

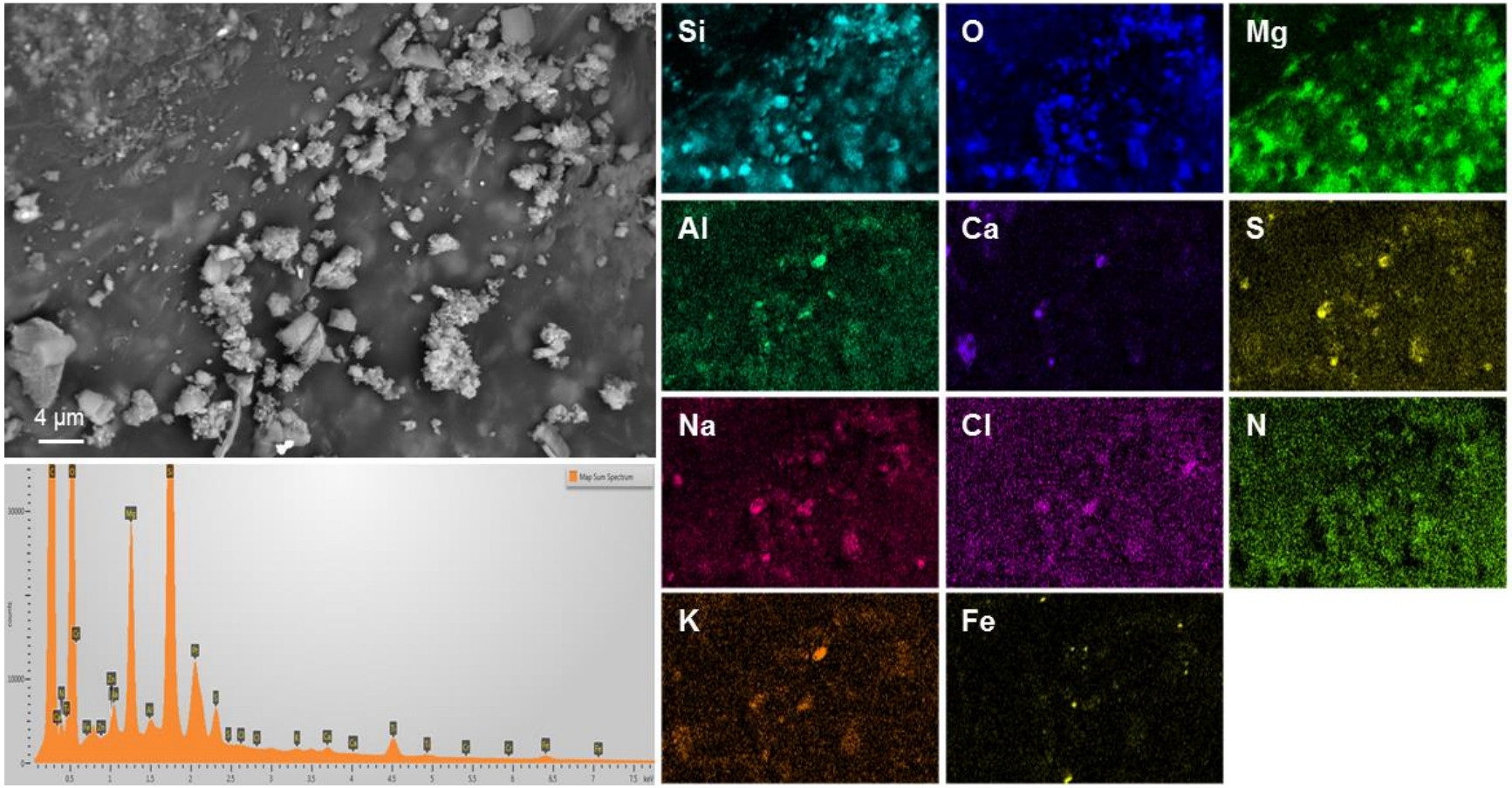

Figure 17. SEM image/EDS map of Sample 145-004, collected from the canister side, 8.5 feet below the upper edge.

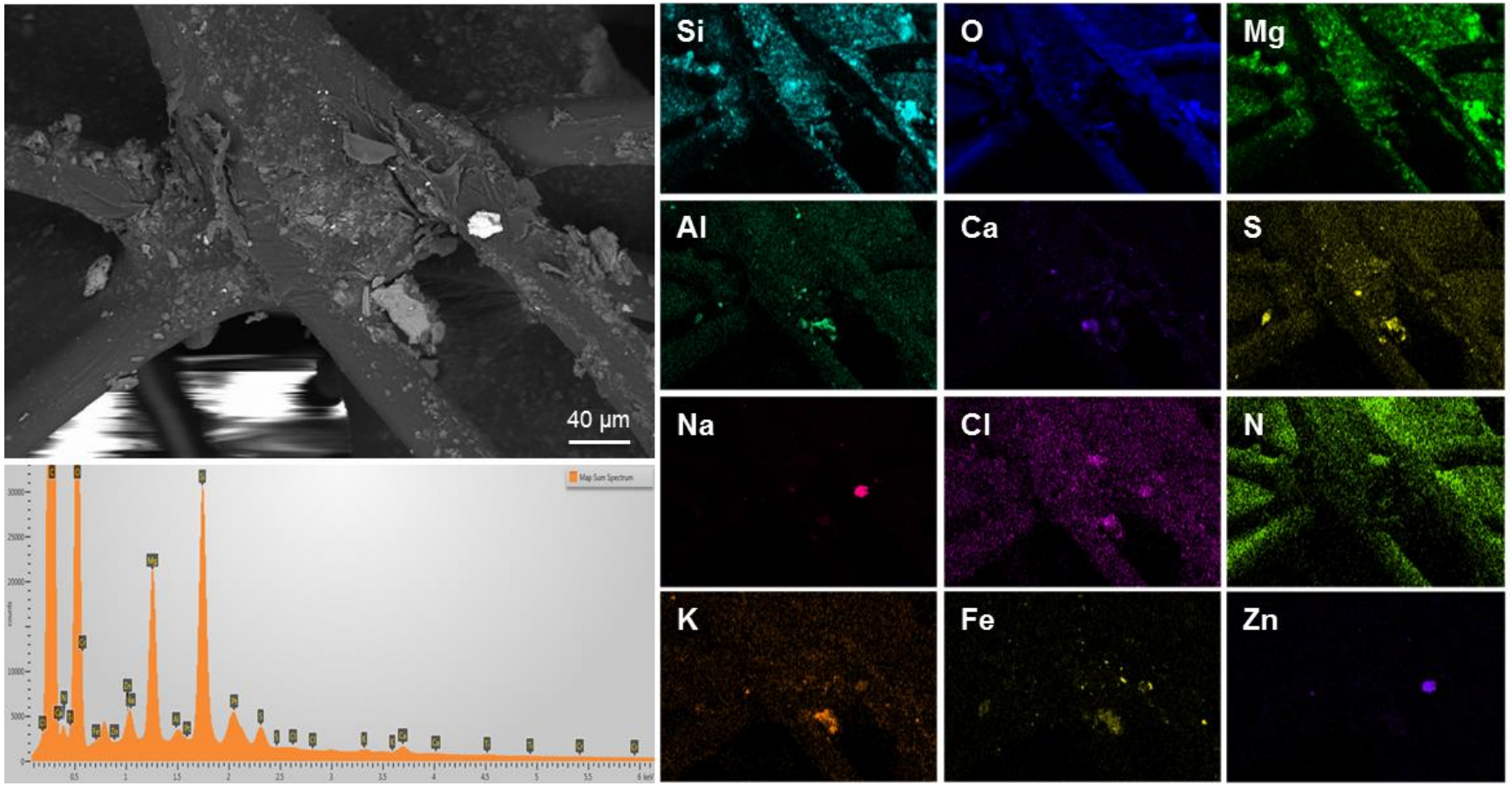

Figure 18. SEM image/EDS map of Sample 145-005, collected from the canister side, 1.5 feet below the upper edge.

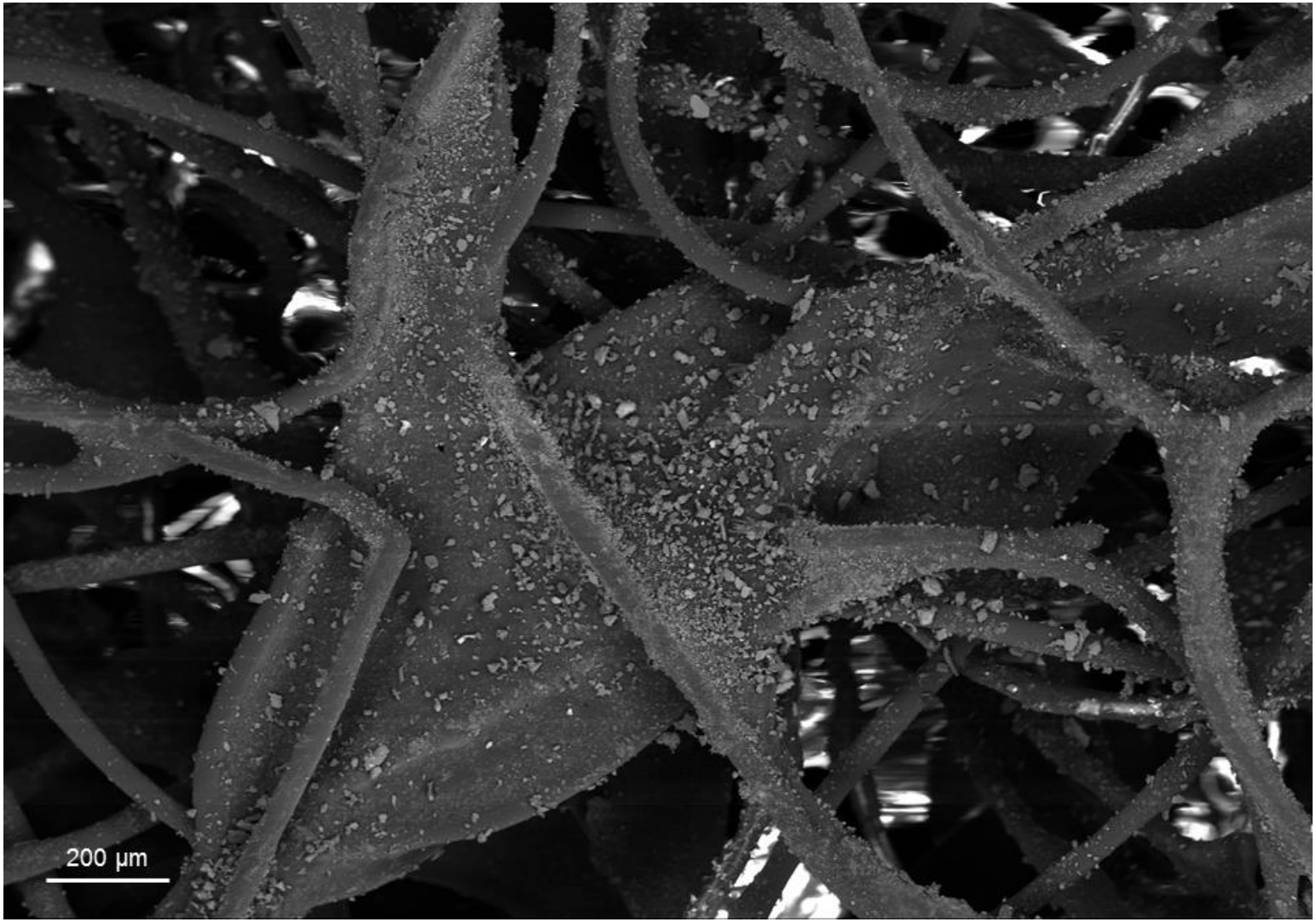

Figure 19. SEM image of sample 145-012, collected from the canister top, showing the heavy dust load.

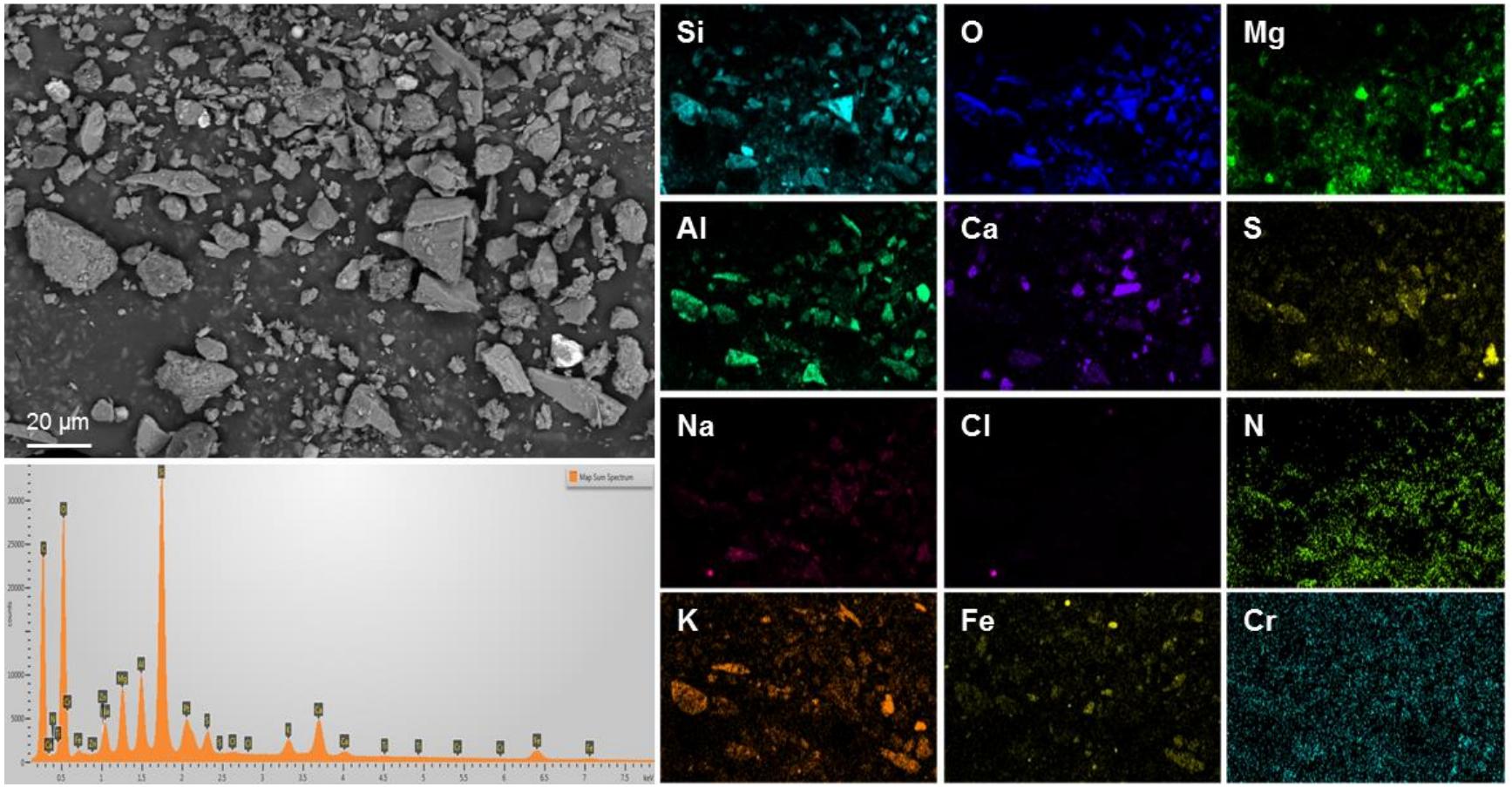

Figure 20. SEM image/EDS map of sample 145-012, collected from the canister top.

MPC-144. Results for MPC-144 were very similar to those for MPC-143. Phases observed during SEM analysis of samples from MPC-144 are listed in Table 4. Sample 144-005 was collected near the base of the canister, at a depth of 13.5 feet from the upper edge. The dust load on the pad was very light, and dust was largely restricted to areas where clear abrasion of the pad was present. SEM/EDS data for Sample 144-005 are shown in Figure 21 and Figure 22. Observed phases in sample 144-005 include coarse blocky grains K and Na feldspars, quartz grains, particles of 304SS; and sparse NaCl particles (note that a shadow partially obscures the element maps in Figure 22, strongly affecting the maps the lighter elements such as Na). Ca-carbonate was also commonly observed. Sample 144-011 was collected from the canister top, and copious amounts of dust adhered to the pad. An SEM/EDS map is shown in Figure 23. The dominant dust phases are identical to those in 144-005. In other images of this sample (Appendix A), pollen grains were common, and rare salt particles of NaCl and Ca-SO4 were observed. A single Zn-Na grain was present; again, this is attributed to the Zn-rich anticorrosive paint on the exterior of the overpack.

Table 4. Minerals Observed in Dry Pad Samples from MPC-144

Elemental analysis	Morphology	Interpretation	Abundance
Si-O	Angular grains	Quartz fragments	Abundant
K-Al-Si-O	Blocky, angular fragments	Potassium feldspar	Abundant
Na-Al-Si-O-Ca	Blocky, angular fragments	Sodic plagioclase	Abundant
Ca-Al-Si-O	Blocky, angular fragments	Calcic plagioclase (?)	Rare
K-(Mg?)-Al-Si-O	Large flat flakes	Muscovite	Abundant
K-Fe-Mg-Al-Si-O	Large planar flakes	Biotite	Common-Abundant
Fe-Cr	Striated flakes and fragments	Stainless steel particles generated by machining	Abundant
Fe-Mg-Al-Si-O	Aggregate grains	Clays?	Common
Ca-Al-Si-O	Aggregate grains	Clays?	Rare-common
Mg-Al-Si-O	Aggregate grains	Clays?	Rare-common
Ca-O-(C?)	Angular grains	Calcium carbonate	Common
Na-Zn-O	Rounded particles	Particles of Zn-rich paint from the outside of the overpack?	Rare
C	Oval to spherical grains	Pollen	Rare-common
Fe-O	Isolated spheres, some hollow	Fly ash?	Rare-common
Ca-S-O	Very fine particles	Gypsum	Rare
Na-Cl	Cubes and aggregates, commonly etched or corroded	Halite	Sparse

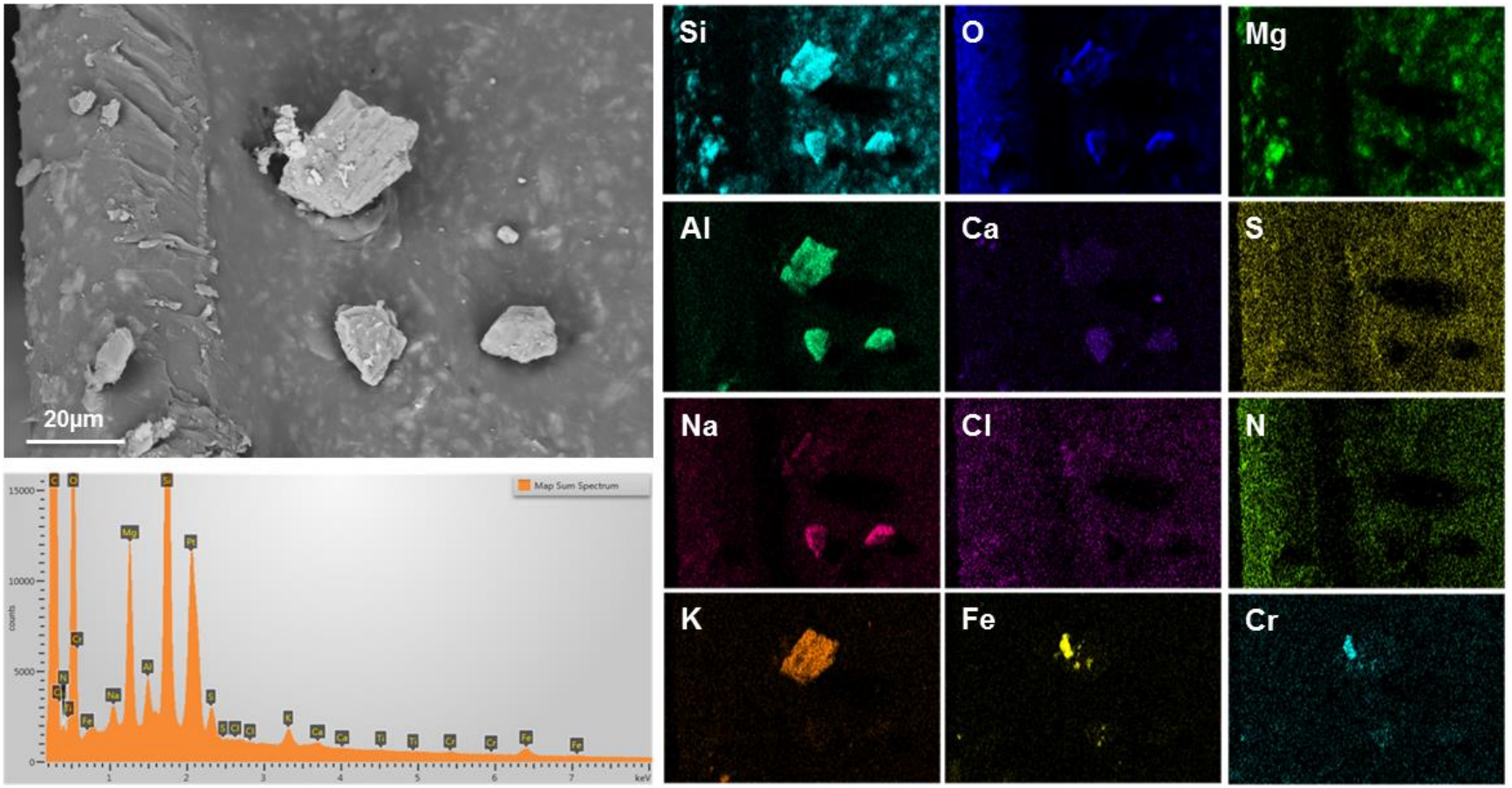

Figure 21. SEM image/EDS map (#1) of sample 144-005, collected from the canister side, 13.5 feet below the upper edge.

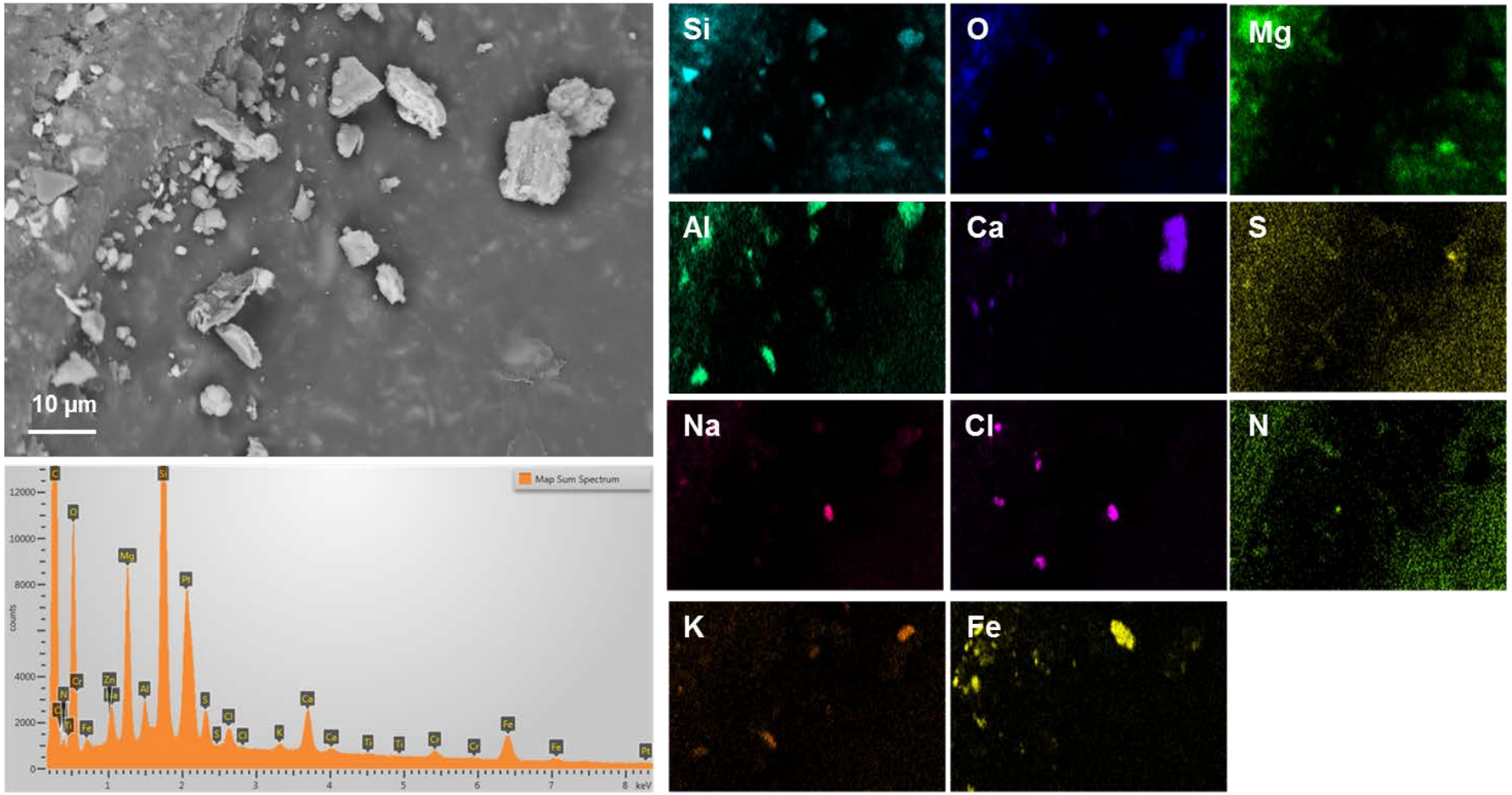

Figure 22. SEM image/EDS map (#2) of sample 144-005, collected from the canister side, 13.5 feet below the upper edge.

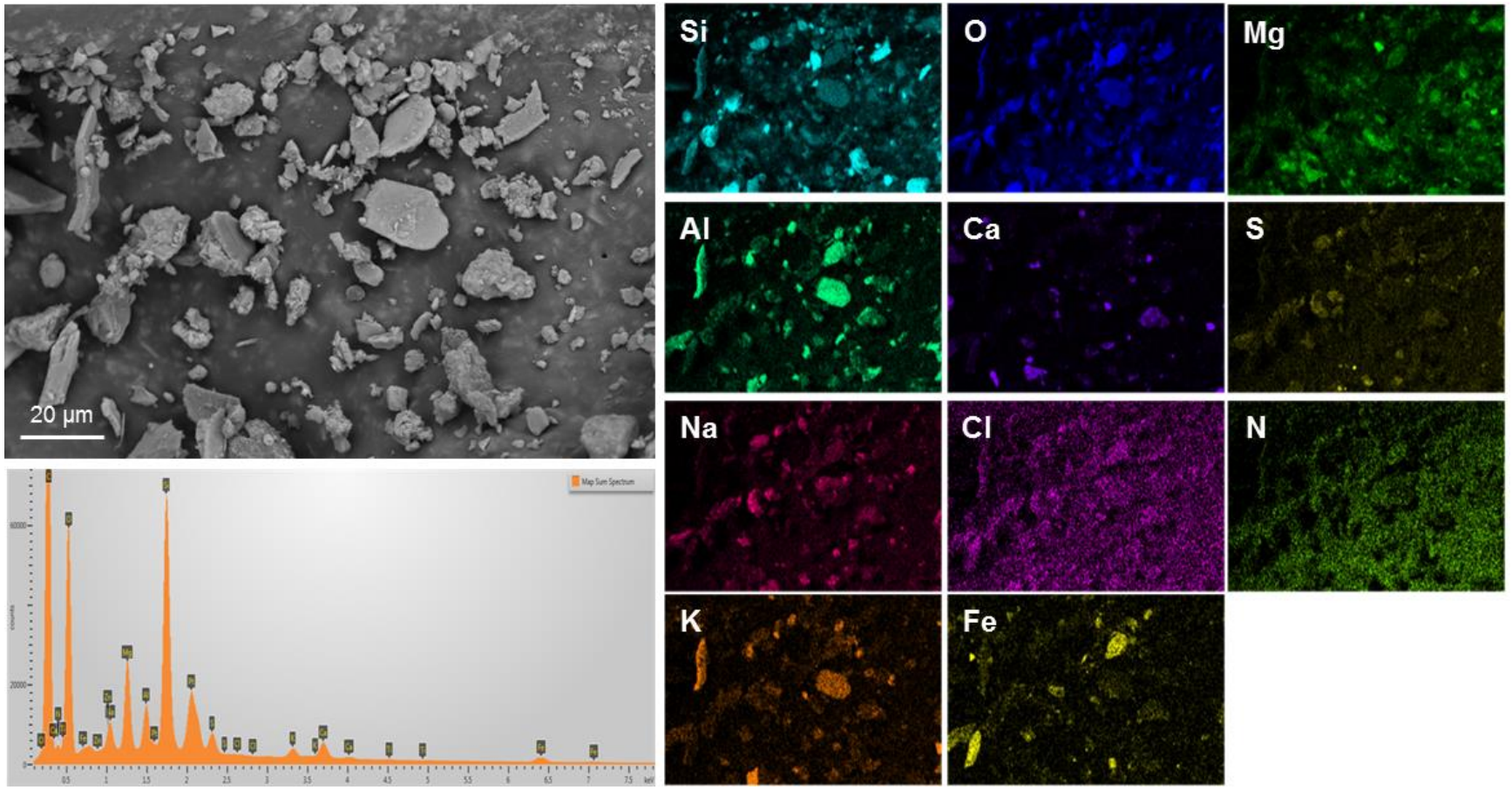

Figure 23. SEM image/EDS map (#2) of sample #144-011, collected from the canister top.

Summary of Hope Creek SEM/EDS results. To summarize, dust loads on the dry pad samples from the Hope Creek storage canisters were very light on the pads from the canister sides and heavy on the pads used to sample the upper surface. The mineralogy is similar over the entire surface of each canister, and on both canisters. The dust consists largely of terrestrially-derived detrital grains of quartz and aluminosilicates, including larger grains of feldspars and the micas, and sparser grains or aggregates of possible clay phases such as kaolinite and illite. Other common phases are particles of 304SS, sparse iron oxides, and Ca-carbonate. Salts were rarely observed in the dust, and consist largely of Ca-sulfate and rare grains of NaCl. Other materials present include pollen and iron oxide spherules (possibly representing oxidized fly ash or welding spatter).

The salts in the Hope Creek samples occur as heavily etched individual grains of NaCl, often only a few microns across, although a single spherical aggregate was seen in one image (see lower left center, Figure 22). It is not clear that the NaCl grains observed at Hope Creek are sea-salts in origin. The NaCl grains observed at Hope Creek may source to mist and fog being emitted from the nearby onsite cooling tower, which uses brackish river water. These do not resemble the sea-salt aerosols on the Diablo Canyon canisters, described below.

3.1.3. Diablo Canyon Samples

Two canisters were sampled at the Diablo Canyon ISFSI. These were designated MPC-123 and MPC-170. Because salt minerals comprised a large fraction of the dusts on these packages, a suite of samples was analyzed from each canister, including 3 samples from the side of each canister, and one from the top. For each sample, representative SEM image/EDS element map combinations are discussed here and additional analyses are provided in Appendix A.

MPC-123. For canister MPC-123, samples 123-006, 123-008, and 123-009 were collected from the canister side at distances, respectively, of 11, 7.5, and 3.0 feet below the upper edge of the canister MPC-123. For all of these samples from the vertical side of the cask, dust and salt loads were extremely light. Sample 123-012 was taken from the flat top of the canister, and was heavily loaded with dust. Low magnification images of the pads in Appendix A provide an understanding of the relative dust loads on the canister side and top samples.

The minerals observed on all of the samples from MPC-123 are listed in Table 5. Insoluble species vary little from canister to canister, or between canister top and side. Aluminosilicates are abundant, including feldspars and biotite, and fine particles or aggregate grains of clay minerals. Quartz is common. Fe-bearing phases are very abundant, and have variable compositions and morphologies. Fe-rich and Fe-Cr-rich particles are common, and occur in both metallic and oxidized form; they are generally angular, and probably represent variably oxidized particulates generated by machining during construction of the canister. But they can also be spherical, and apparently formed by welding or torch cutting of steel and stainless steel. However, the salt phases on different samples do vary, and these differences will be discussed below.

SEM/EDS data for sample 123-006 collected 11.0 feet below the upper edge of the canister, are shown in Figure 24 and Figure 25. Dust was sparse on this sample, but in Figure 24, several

phases can be recognized, including quartz, K-feldspar, and a Ca-O phase which is probably calcium carbonate. This image also illustrates the variability in the Fe-bearing phases present in the dust. In addition to Fe-oxides, there is a large particle of Fe-Cr (stainless steel) and a sphere of Fe-Cr oxide, apparently an oxidized melt droplet formed by welding or cutting stainless steel. Figure 25 shows a few grains of NaCl; interestingly, the associated sulfate appears to be Ca-SO_4 rather than Mg-SO_4.

Table 5. Minerals Observed in Dry Pad Samples from MPC-123

Elemental analysis	Morphology	Interpretation	Abundance
Si-O	Angular grains	Quartz fragments	Common
K-Al-Si-O	Blocky, angular fragments	K-feldspar	Abundant
Ca(±Na)-Al-Si-O	Blocky, angular fragments	Calcic plagioclase	Rare
Ca-Fe-Al-Si-O	Large angular grains	Mafic aluminosilicate?	Rare to common
Ca-Mg-Fe-Al-Si-O	Large flakes	Biotite	Rare
K-Fe-Al-Si-O	Aggregate grains	Clays?	Sparse
Al-Si-O	Angular grains and aggregates	Kaolinite?	
Al-O-(H?)	Angular fragment	Gibbsite or brucite?	Rare
Fe±Cr±O	Striated flakes and fragments, spheres	Steel particles, of varying oxidation, generated by machining, Spheres generated by cutting and welding?	Abundant
Ca-S-O	Aggregate grains	Gypsum or anhydrite	Sparse
Ca-K-S-O	Aggregate grains	Aggregate of sulfates?	Rare
Na-Cl + Mg-S-O + Ca + K	Sea salt aggregates, commonly spherical. Cubes of NaCl associated with sheaf-like clusters of Mg-sulfate. Minor Ca and K, commonly associated with the sulfate.	Sea-salt aggregates	Abundant
Na-Cl-N-O	Anhedral grains	Nitrate was on the grain surface and rapidly burned off in the beam; interpreted as NaCl, partially converted to $NaNO_3$ via particle-gas conversion reactions.	Sparse (Common in sample 123-009)
Na-N-O	Fine grains	Sodium nitrate, possibly representing NaCl converted to NaNO3 via particle-gas conversion reactions	Sparse (Common in sample 123-009)
Ca-O-(C?)	Cylindrical needle	Calcium carbonate-biogenic	Single Feature
Ca-O-(C?)	Toothed blade	Biogenic calcium carbonate structure	Single feature

Dust on sample 123-008, somewhat higher on the package, has a similar mineralogy (Figure 26) in that Fe-bearing phases seem to dominate. Steel particles of varying degrees of oxidation, including Fe-Cr (stainless steel), Fe-Cr oxide, Fe metal and Fe oxide are common. Also present is a single grain of pyrite (Fe-S), and a grain of an Al-O-(H?) phase. A few tiny grains of NaCl are present, but also a particle of $NaNO_3$; a third grain appears to be mixture of the two salts.

SEM/EDS data for 123-009 are shown in Figure 27 and Figure 28. This sample represents the canister side just below the upper edge, and it was the hottest sample collected. As with the other canister side samples, dust was very sparse. Figure 27 shows little but Fe-Cr particles and salts. The salts are mostly $NaNO_3$ particles, with only a few NaCl grains. Other maps from sample 123-009 in Appendix A show composite NaCl-$NaNO_3$ particles. For these composite grains; it was observed that the X-ray beam caused the grains to shrink. The relative amount of nitrogen present decreased the longer the grain was in the beam. For these composite grains, it appears that the nitrate is mostly present on the surface of the NaCl grains. A 20 µm Ca-carbonate rod of probable biogenic origin is also present in Figure 27. Figure 28 shows another part of the pad. In this area, NaCl is more common, although$NaNO_3$ is still present. The NaCl grains are co-located and apparently intergrown with a Ca-S-O phase (calcium sulfate).

Sample 123-012 is from the top of the canister, and is heavily loaded with dust. Moreover, the dust compositions vary significantly from the samples collected from the sides of the canister. Figure 29 and Figure 30 show SEM/EDS maps of the sample. The mineralogy is similar in both cases. Salt aggregates, consisting of NaCl + Mg-SO_4 (referred to as Mg-SO_4 rather than $MgSO_4$, because the hydration state is unknown), with minor associated Ca and K, are abundant in the dust. These aggregates are commonly hollow spherical aggregates of halite crystals with intergrown Mg-sulfate, but euhedral halite crystals with associated Mg-sulfate also occur. As Na, Cl, Mg, and SO_4 are the most abundant ionic species in seawater, these are certainly sea-salt aggregates. The hollow spheres formed when droplets of seawater, suspended in the air by breaking waves, evaporated from the outside inwards. They commonly have an aperture, apparently where the last fluid escaped. As morning fogs are common at Diablo Canyon, it is likely that this evaporation occurred, in many cases, within the overpack as the deliquesced sea-salt droplets were drawn in and moved upwards through the heated annulus. Figure 29 illustrates the abundance of salts in the dust, and Figure 30 is a close-up of three salt aggregates, showing the size and morphology. Figure 31 magnifies a single sea-salt aggregate, showing the structure of the aggregate, and the relationship between the NaCl crystals and the interstitial Mg-SO_4. Several examples of the sea-salt aggregates from sample 123-012 are shown in Figure 32. While salt particles of all sizes are present on the canister surfaces, the aggregates are commonly quite coarse, in the 5-20 µm size range, and it is likely that these large grains account for most of the chloride deposited on the canister surfaces.

Samples from the side of canister MPC-123 differ from samples collected from the top of the canister in several ways. First, particles associated with manufacturing (i.e., Fe-Cr particles) are proportionally more common on the pad samples from the canister side. It is likely that this is mostly because the environmentally-derived proportion of the dust is much smaller on the side than on the top. Second, salt aggregates are mixed NaCl/Ca-SO_4 minerals rather than the NaCl and Mg-SO_4 aggregates found on the canister top (and on all samples from MPC-170). Finally, nitrates particles and nitrate-chloride mixed grains are present only on the side of MPC-123, not

on the top, and not on MPC-170. Salt particles on the sides of the canister are generally smaller than those on the top—perhaps the compositional difference is a function of particle size. Temperature may also play a role—the greatest abundance of nitrate-containing particles is on the sample from the hottest location (sample # 123-009) on the package. We speculate that the nitrate represents particle-gas conversion reactions that occurred prior to the salts entering the overpack—reactions with HNO_3 in the air that convert chloride particles to nitrates. This process is more efficient for small particles, and results in a NaCl mineral partially converted to $NaNO_3$. At high canister surface temperatures, nitrate and mixed chloride-nitrate particles were preserved on the canister surface, because deliquescence and acid degassing could not occur. At lower temperatures, deliquescence occurred and both HCl and HNO_3 degassed; however, chloride was replenished by dissolution of the abundant chloride minerals. Replenishment of nitrate did not occur, so the nitrate was eventually depleted. This also explains the corroded surface of many of the NaCl crystals on the canister surfaces (see, for instance, Figure 32).

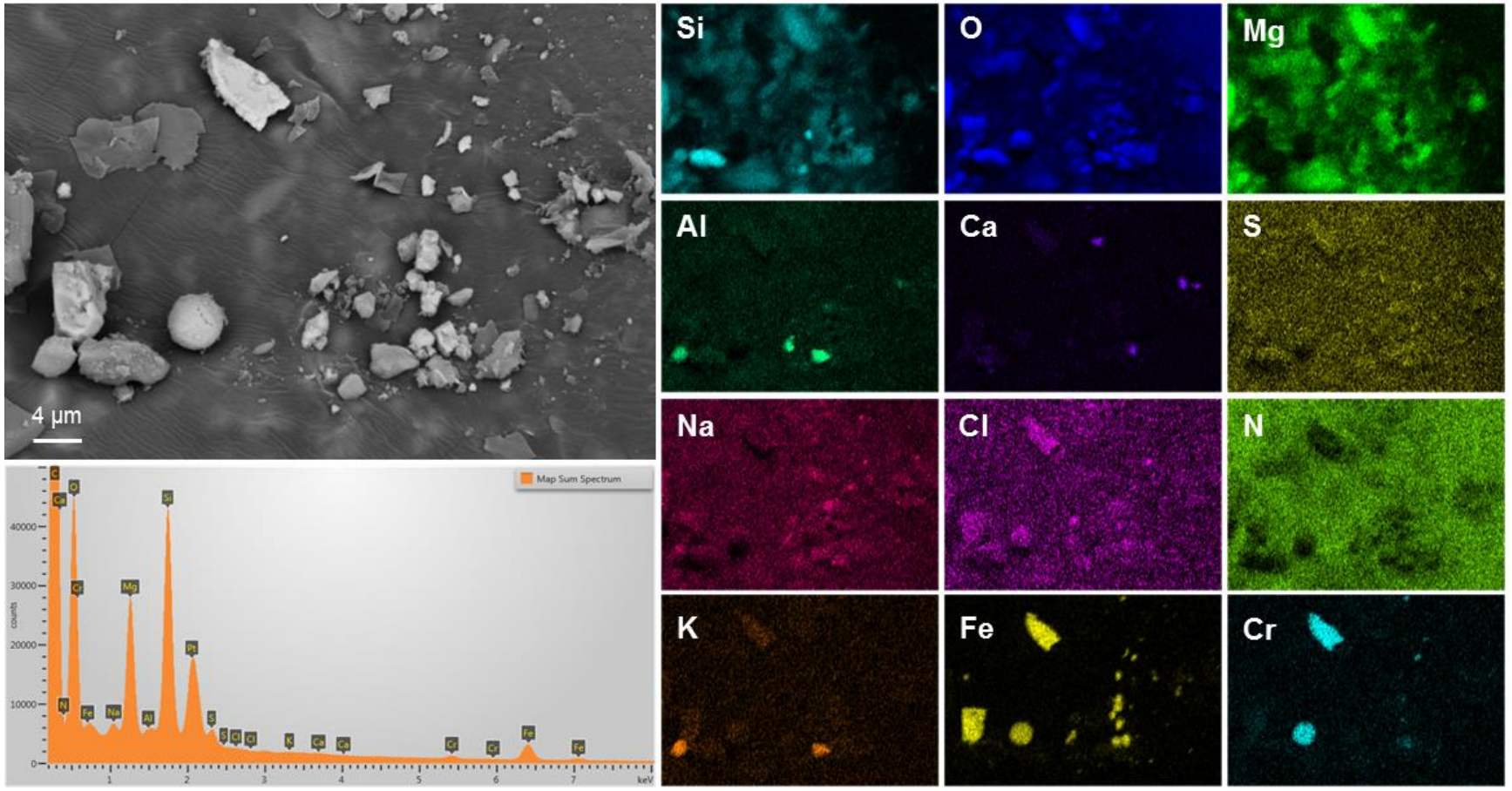

Figure 24. SEM image/EDS map (#1) of sample 123-006, collected from the canister side, 11.0 feet below the upper edge.

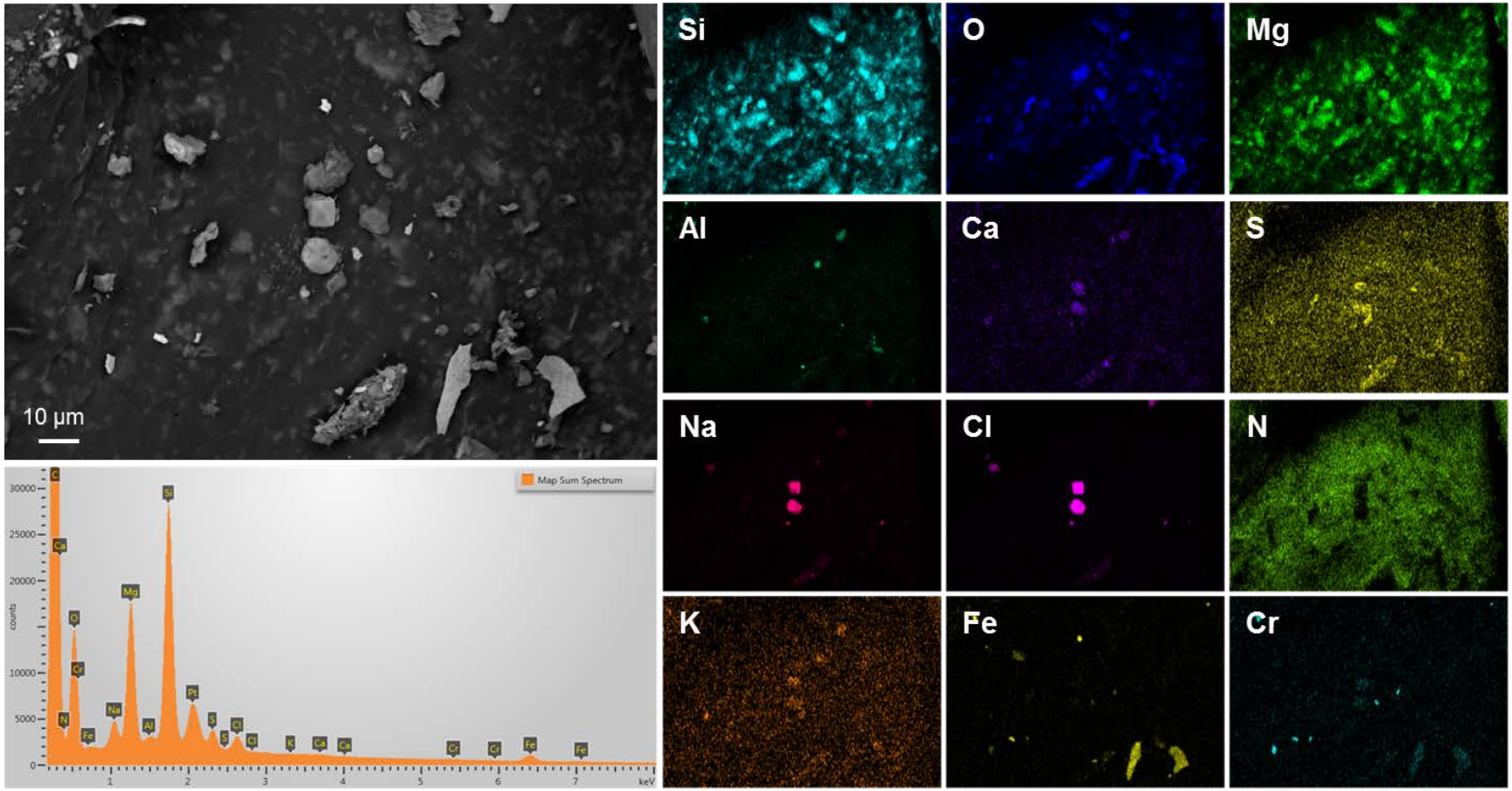

Figure 25. SEM image/EDS map (#2) of sample 123-006, collected from the canister side, 11.0 feet below the upper edge.

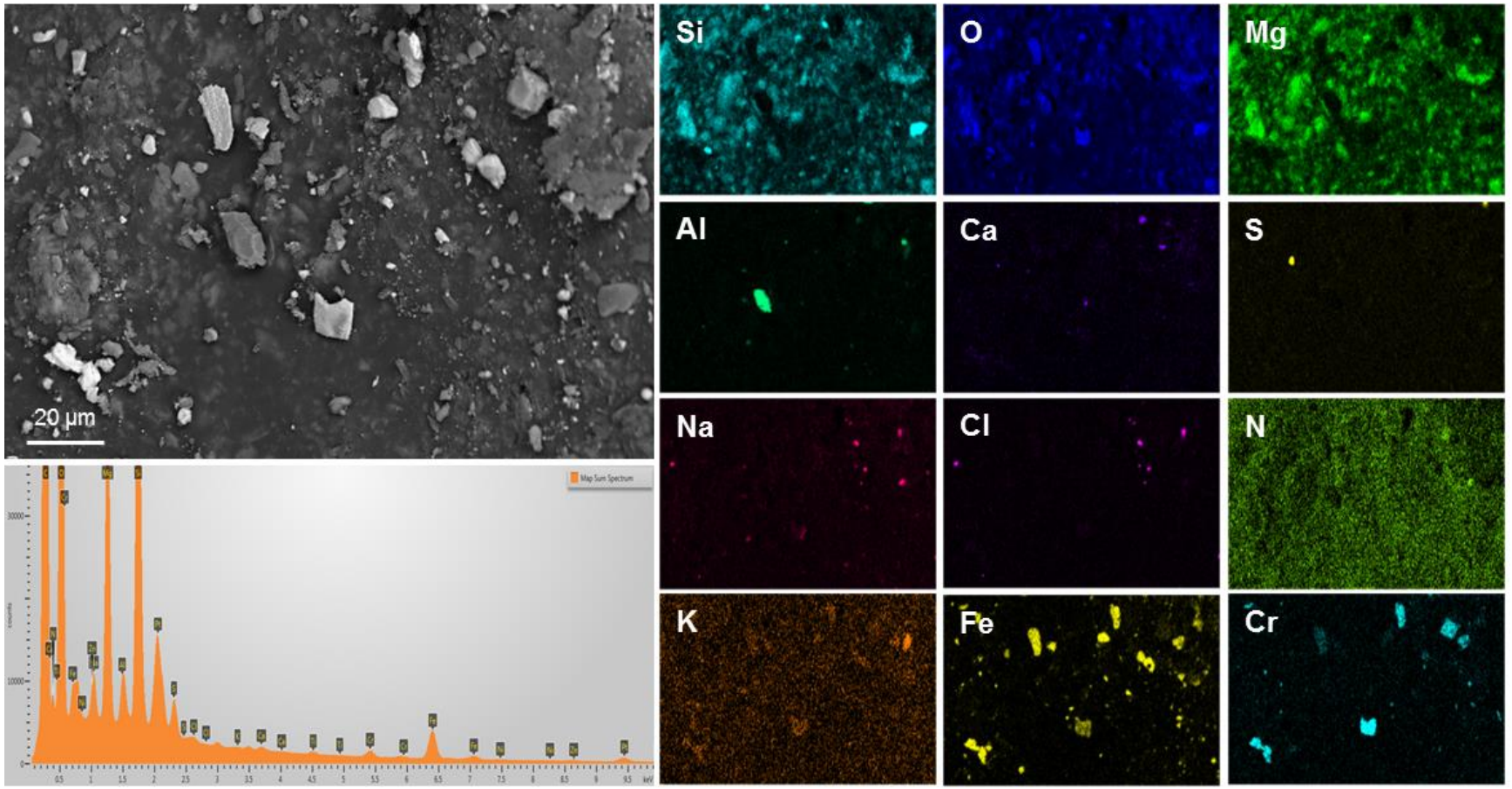

Figure 26. SEM image/EDS map (#1) of sample 123-008, collected from the canister side, 7.5 feet below the upper edge.

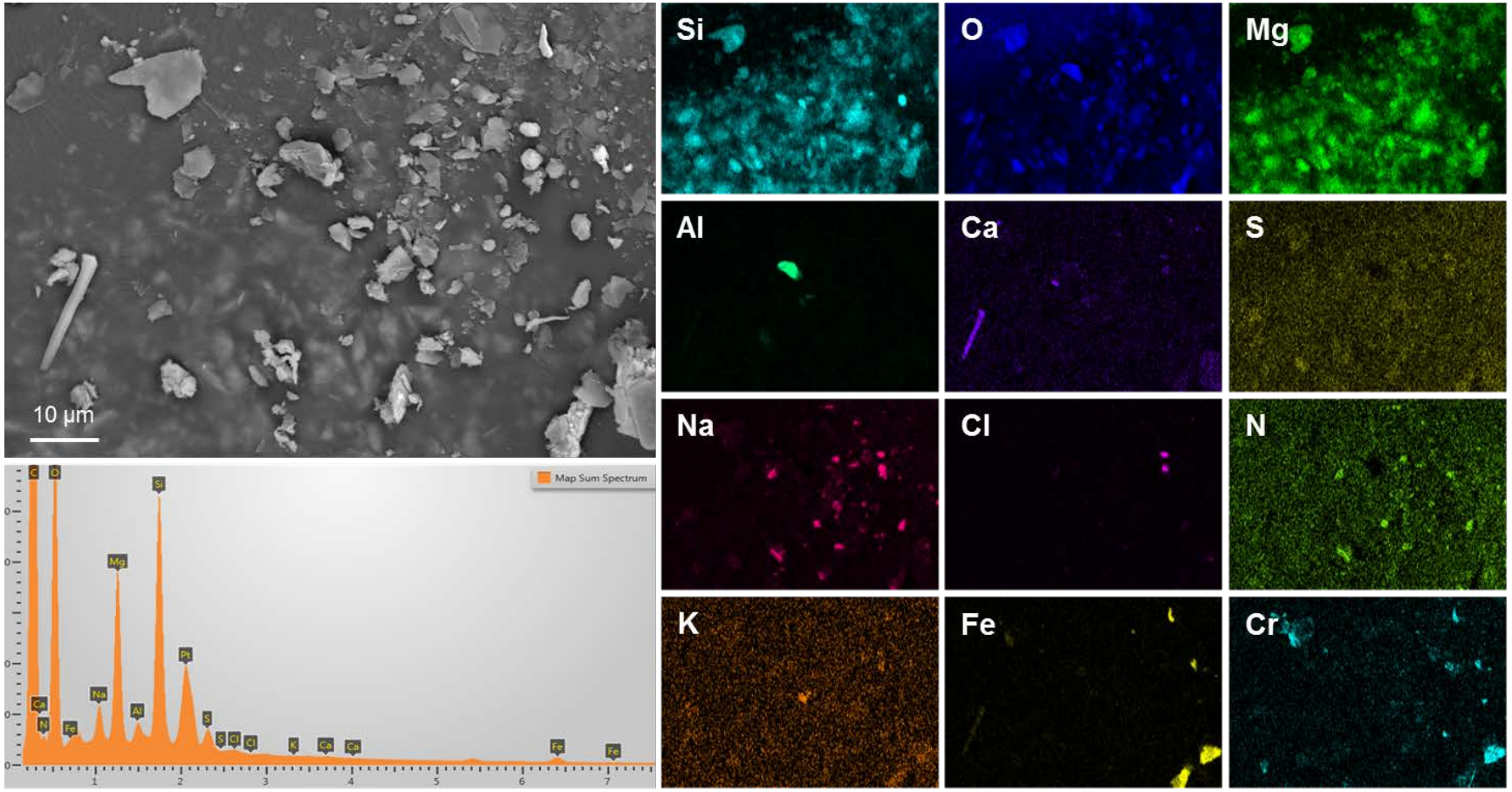

Figure 27. SEM image/EDS map (#1) of sample 123-009, collected from the canister side, 3.0 feet below the upper edge.

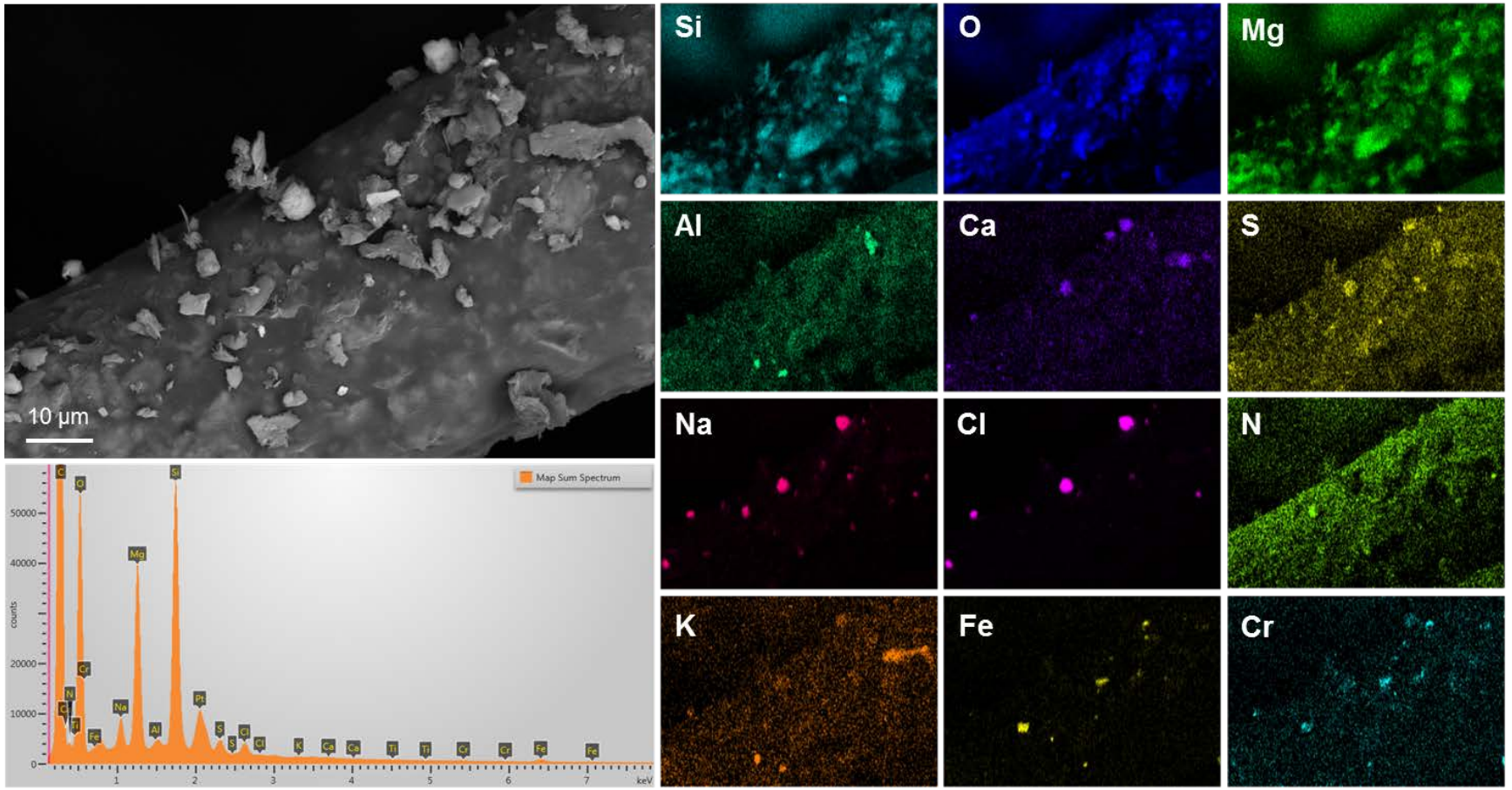

Figure 28. SEM image/EDS map (#2) of sample 123-009, collected from the canister side, 3.0 feet below the upper edge.

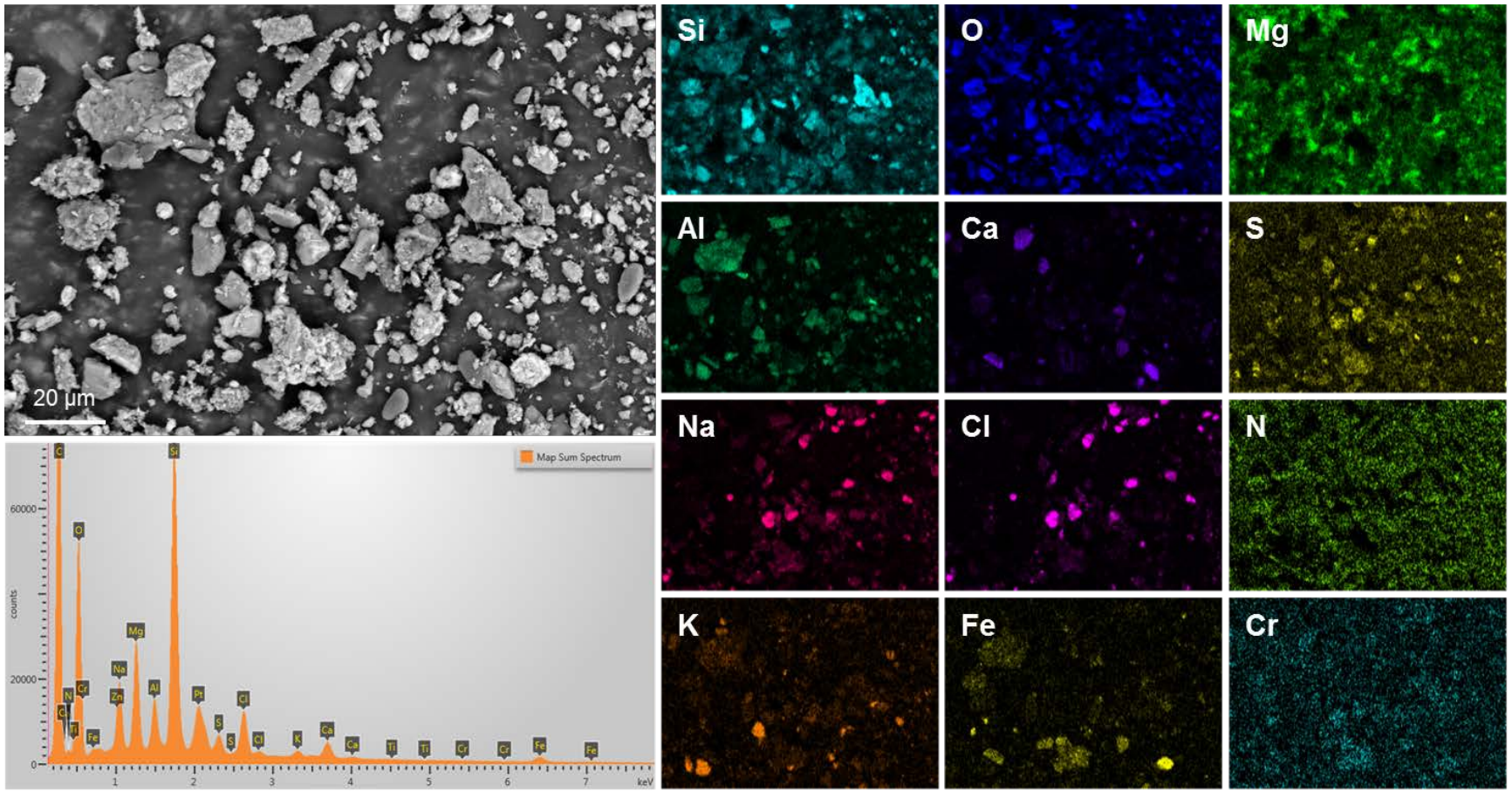

Figure 29. SEM image/EDS map (#1) of sample 123-012, collected from the canister top.

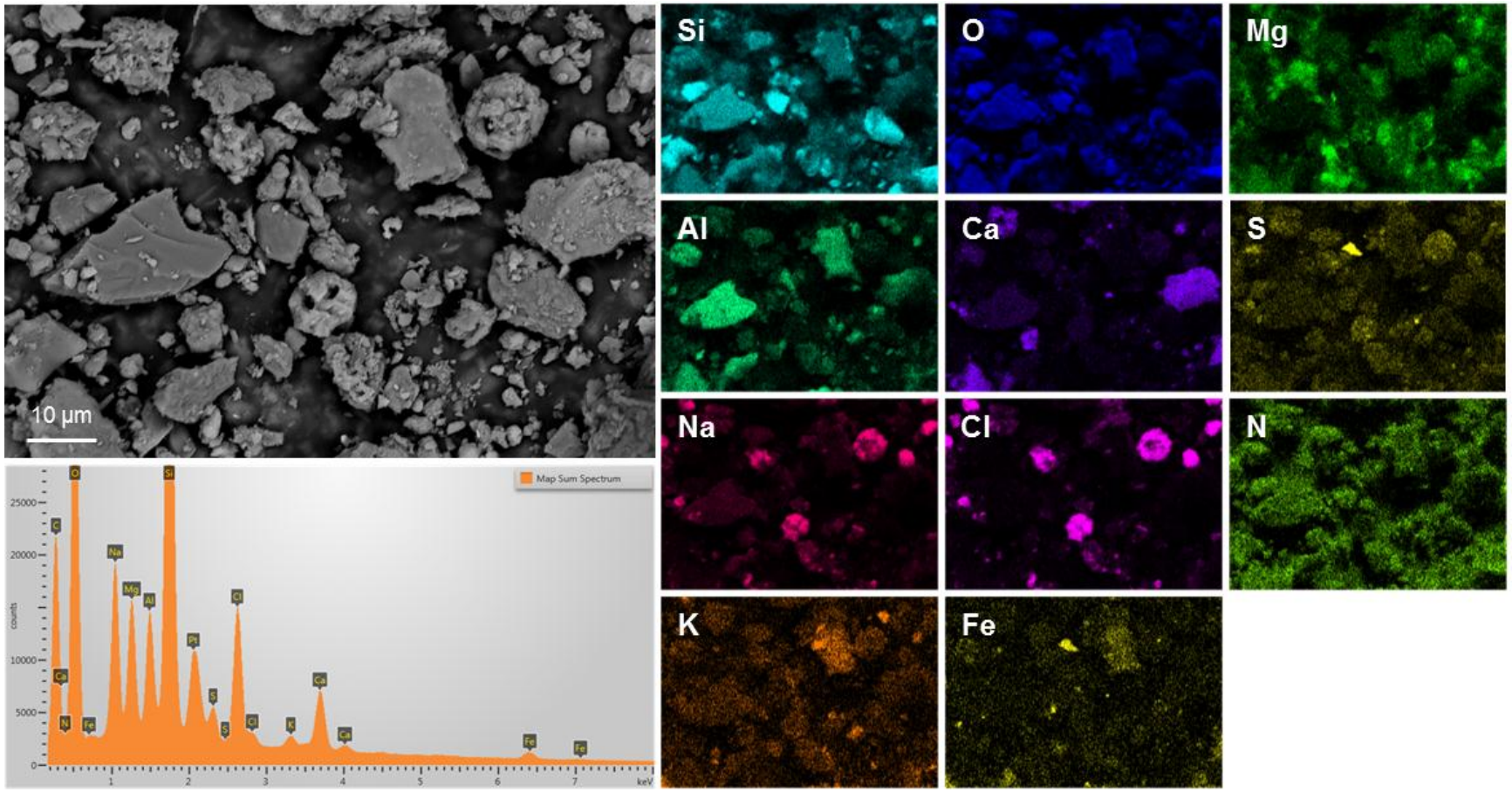

Figure 30. SEM image/EDS map (#2) of sample 123-012, collected from the canister top.

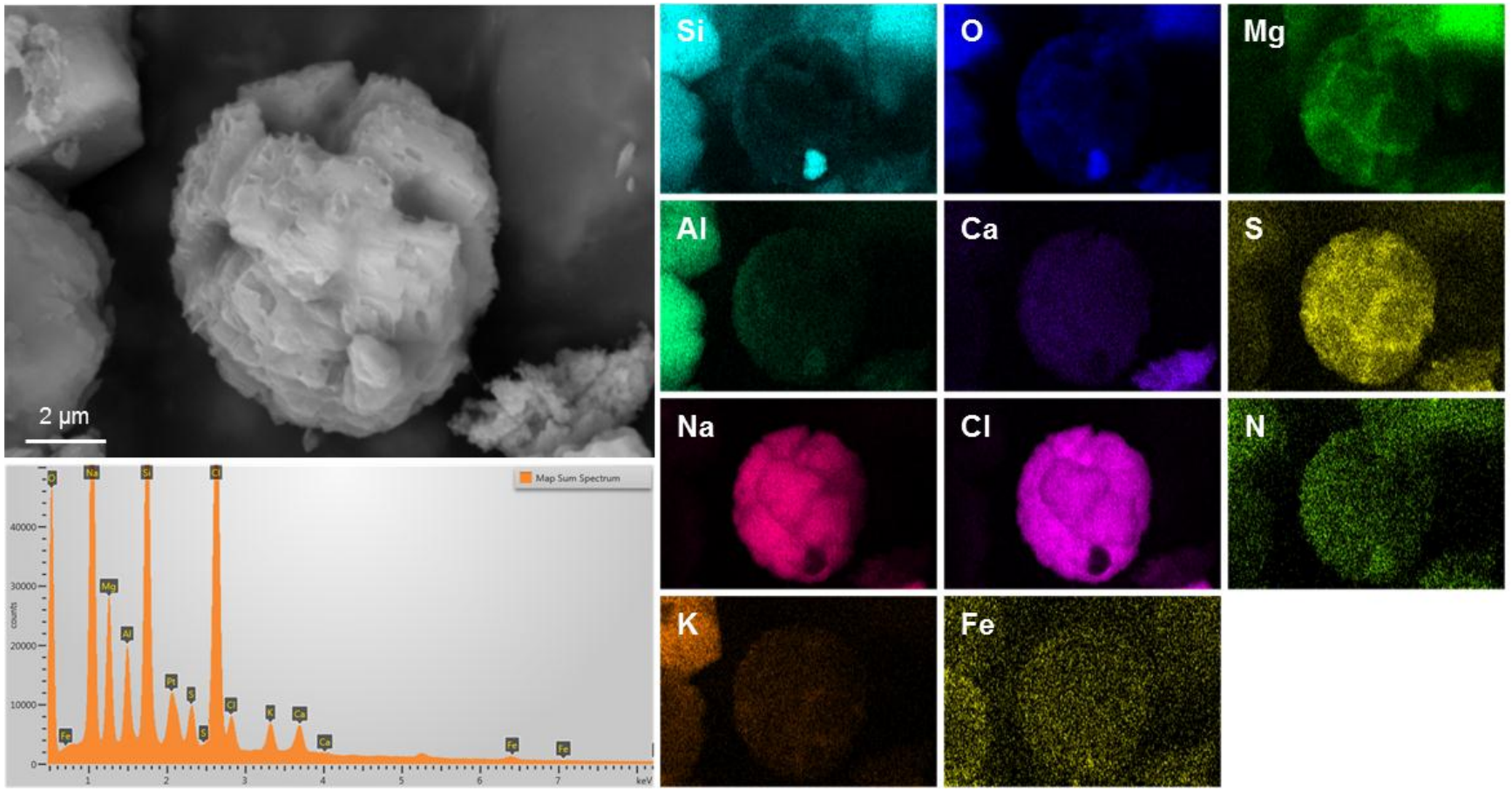

Figure 31. SEM image/EDS map of a sea-salt cluster in sample 123-012, collected from the canister top.

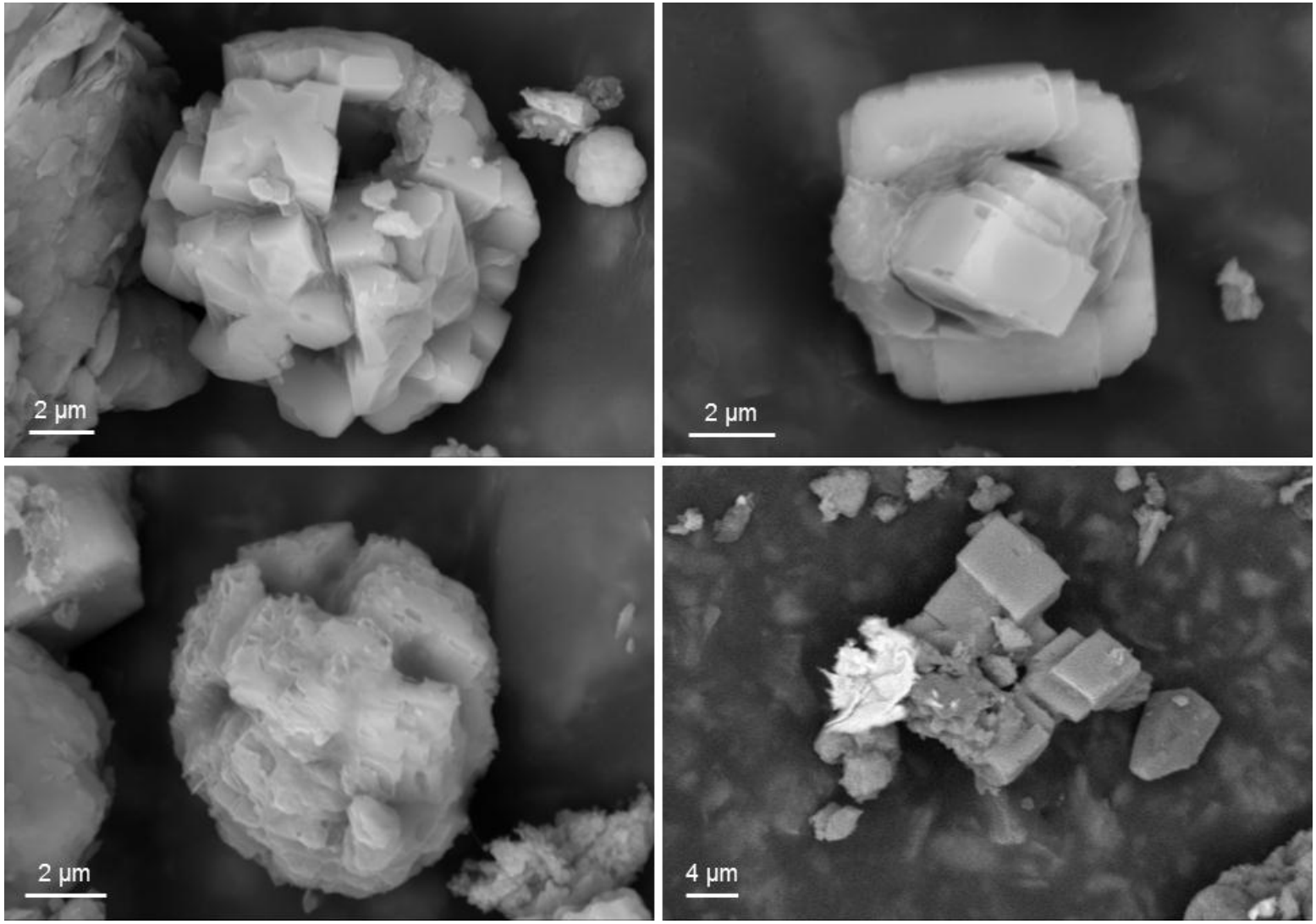

Figure 32. SEM images of sea-salt (intergrown NaCl cubes with interstitial Mg-SO_4) aggregates in sample 123-012, collected from the canister top.

MPC-170: Four samples were also analyzed from canister MPC-170. Samples 170-004, 170-005, and 170-006 were collected from the canister side at distances, respectively, of 11, 7.5, and 3.0 feet below the upper edge of the canister. As with MPC-123, all of the dust and salt loads were extremely light for samples collected from the vertical side of the canister; in many cases, only a few spots on the sample pad had any visible dust. Sample 170-003 was taken from the flat top of the canister, and was heavily loaded with dust. The minerals observed in the samples from MPC-170 are listed in Table 6. Unlike MPC-123, the mineralogy varied little across the surface of MPC-170.

Table 6. Minerals Observed in Dry Pad Samples from MPC-170

Elemental analysis	Morphology	Interpretation	Abundance
Si-O	Angular grains	Quartz	Abundant
K-Al-Si-O	Blocky, angular fragments	K-feldspar	Common
Na-Al-Si-O	Medium to fine particles	Sodic plagioclase?	Common
Al-Si-O	Aggregates of grains	aluminum oxide/hydroxide	Sparse
K-Mg-Fe-Al-Si-O	Large flakes	Biotite	Abundant
K-Al-Si-O	Fine particles and aggregate grains	Illite?	Sparse
Ca-Al-Si-O	Blocky, angular fragments and fine grains	Calcic plagioclase (?)	Rare
Fe-Cr	Striated flakes and fragments	Stainless steel particles generated by machining	Abundant
Fe	long striated grain	Fe metal	Rare
Fe-O	Angular grains	Iron oxides	Common
Fe-O	Isolated spheres, some hollow	Fly ash or welding spatter (oxidized)	Rare
Ca-S-O	Very fine particles	Gypsum or anhydrite	Common
Ca-O-(C?)	Fine particles and aggregates	Calcium carbonate	Rare to common
Na-Cl + Mg-S-O + (Ca + K)	Sea salt aggregates, commonly spherical, of euhedral NaCl associated with sheaf-like clusters of Mg-sulfate. Minor Ca and K. Sometimes, isolated NaCl crystals. In 170-001, Na-Cl + Ca-SO_4 aggregates common.	Sea-salt aggregates	Abundant
Na-Zn-O	Rounded particles	Zr-rich paint particles from the outside of the overpack(?)	Rare
C	Oval to spherical particles	Pollen	Rare to common
C	Fibers	Plant matter	Rare

Sample 170-004 was collected from the canister side, 11 feet below the upper edge. Figure 33 and Figure 34 show dust on the pad, which was very lightly loaded. Dust in Figure 33 consists of a few coarse (<20 μm) grains of quartz and aluminosilicate, with some finer sea-salt aggregates. Figure 34 shows an accumulation of dust on an abraded edge on the pad. The dust is almost entirely sea-salt particles, with a few aluminosilicates. Many of the sea-salt particles are very fine, and may have formed by comminution of coarser sea-salt grains as the pad was rubbed over the canister surface. The sea-salt aggregates are mixtures of NaCl and Mg-SO_4, with smaller amounts of Ca and K, generally associated with the sulfate.

Sample 170-005 was collected 7.5 feet below the upper edge of the canister. The dust load on the pad was very sparse. Figure 35 shows a large sea-salt grain, of NaCl and Mg-sulfate. Figure 36 shows an accumulation of dust near an abraded edge. Most of the particles in the image are talc, freed by abrasion of the pad, but aluminosilicates and sea-salt particles are also present. Sample 170-006 was collected 3.0 feet below the upper edge of the canister, and was practically dust-free. Figure 37 shows an abraded fiber, heavily coated with talc particles freed by abrasion of the pad. But a few dust particles are present, and they are mostly stainless steel particles. A few grains of NaCl are also present.

Sample 170-003 was collected from the flat top of the canister, and the pad was heavily loaded with dust. Figure 38 shows a typical region on the pad. The dust consists largely of aluminosilicate minerals, with common sea-salt aggregates of intergrown NaCl and Mg-SO_4; Ca-SO_4 is also common as a separate phase. Figure 39 shows a similar region, with similar mineralogy, but somewhat coarser dust and sea-salt particles. A magnified view on one of the sea-salt particles is shown in Figure 40; this particular grain consists of intergrown halite and Mg-sulfate, and does not appear to be hollow.

The typical morphology and size of the sea-salt grains is shown in Figure 41. All of these images are from sample 170-003, but they are similar to the sea-salt aggregates on canister MPC-123 (Figure 32). These large aggregates, which formed by evaporation of aerosolized seawater droplets, generally range in size from 5-20 μm. Although sea-salt grains occur in the finer size fractions (e.g., <2.5 μm), the majority of the salts on the tops of the Diablo Canyon packages, in terms of mass, are present as coarse aggregates such as these.

Summary for Diablo Canyon canisters. The soluble salts collected from the tops of the canisters MPC-123 and MPC-170 have similar mineral and salt compositions, the salts being dominated by large sea-salt aggregates of NaCl and Mg-SO_4. However, the samples taken from the sides of the two canisters differ significantly. The salts on the sides of the packages are mostly finer grained, with a significant fraction being in the <2.5μm range. The dry pad samples from the sides of MPC-170 have higher loads of dust and sea-salts, and the sea-salt aggregates consist of NaCl and Mg-SO_4, while those on MPC-123 seem to be mixtures of NaCl and Ca-SO_4. Moreover, Ca-SO_4 is common as an individual mineral phase on the MPC-170 samples, while it is quite rare in samples from MPC-0123.

Finally, no nitrate minerals were observed on samples collected from the surface of MPC-170, although they were common in the samples collected from the sides of MPC-123. Nitrate salts *were* seen on sample 170-001, from the overpack gamma shield (see Appendix A, Sample 170-

001, Map B; however. It is not clear why the samples from the canisters show such differences, but it is noted that the outlet vents that were used for sampling faced in opposite directions. The vent for MPC-123 faced SSE, while that for MPC170 faced NNW. The nearest inlet vents to these outlets also faced in opposite directions. Perhaps the observed differences in salt composition are due to variations in the proportion of continentally-derived versus ocean-derived salts with vent direction. An additional difference between the two Diablo Canyon canisters is temperature. The surface of MPC-123 was somewhat hotter (Figure 12), potentially limiting deliquescence and acid degassing, and preserving the nitrate salts.

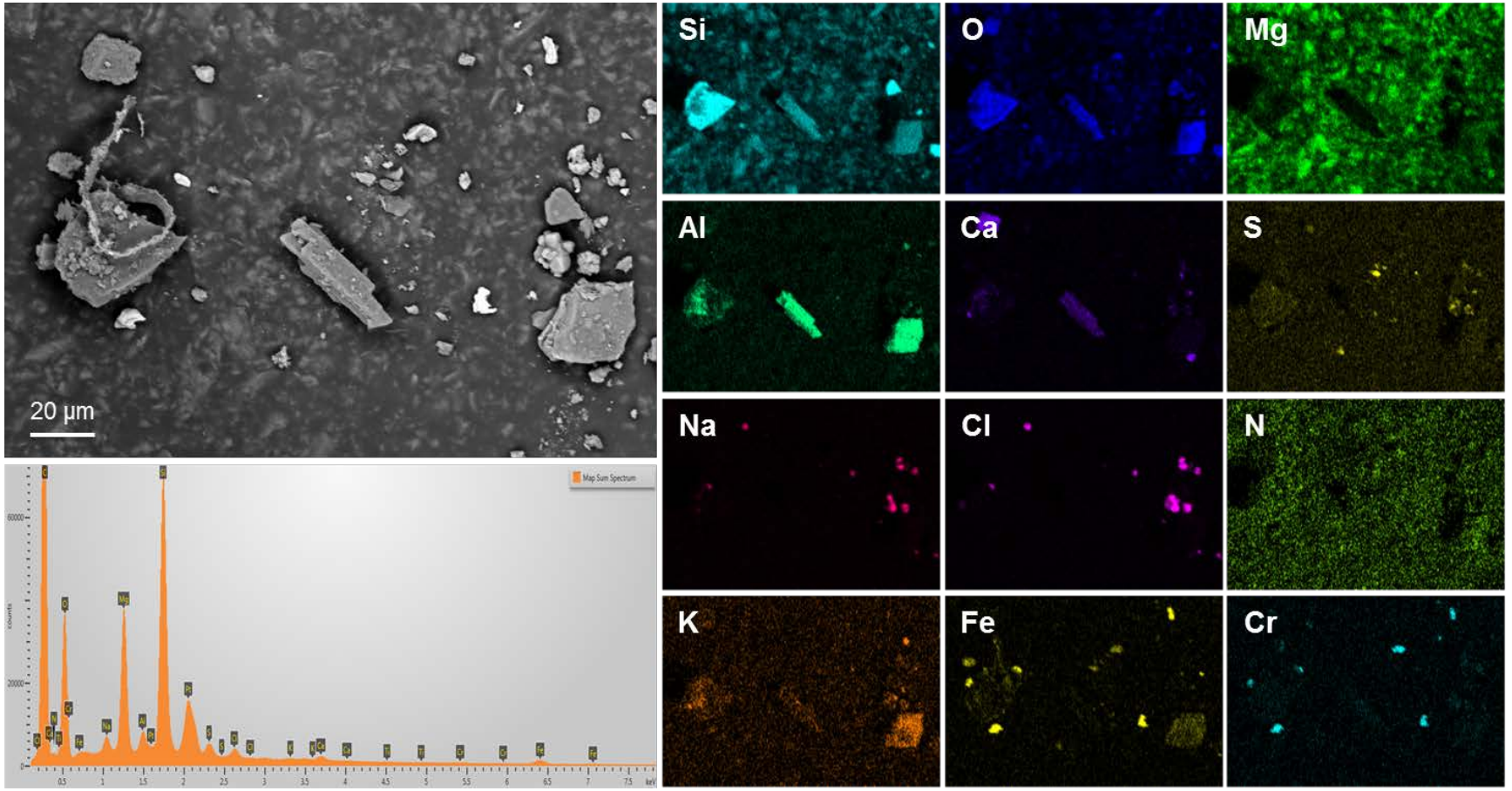

Figure 33. SEM image/EDS map (#1) of sample 170-004, collected from the canister side, 11.0 feet from the upper edge.

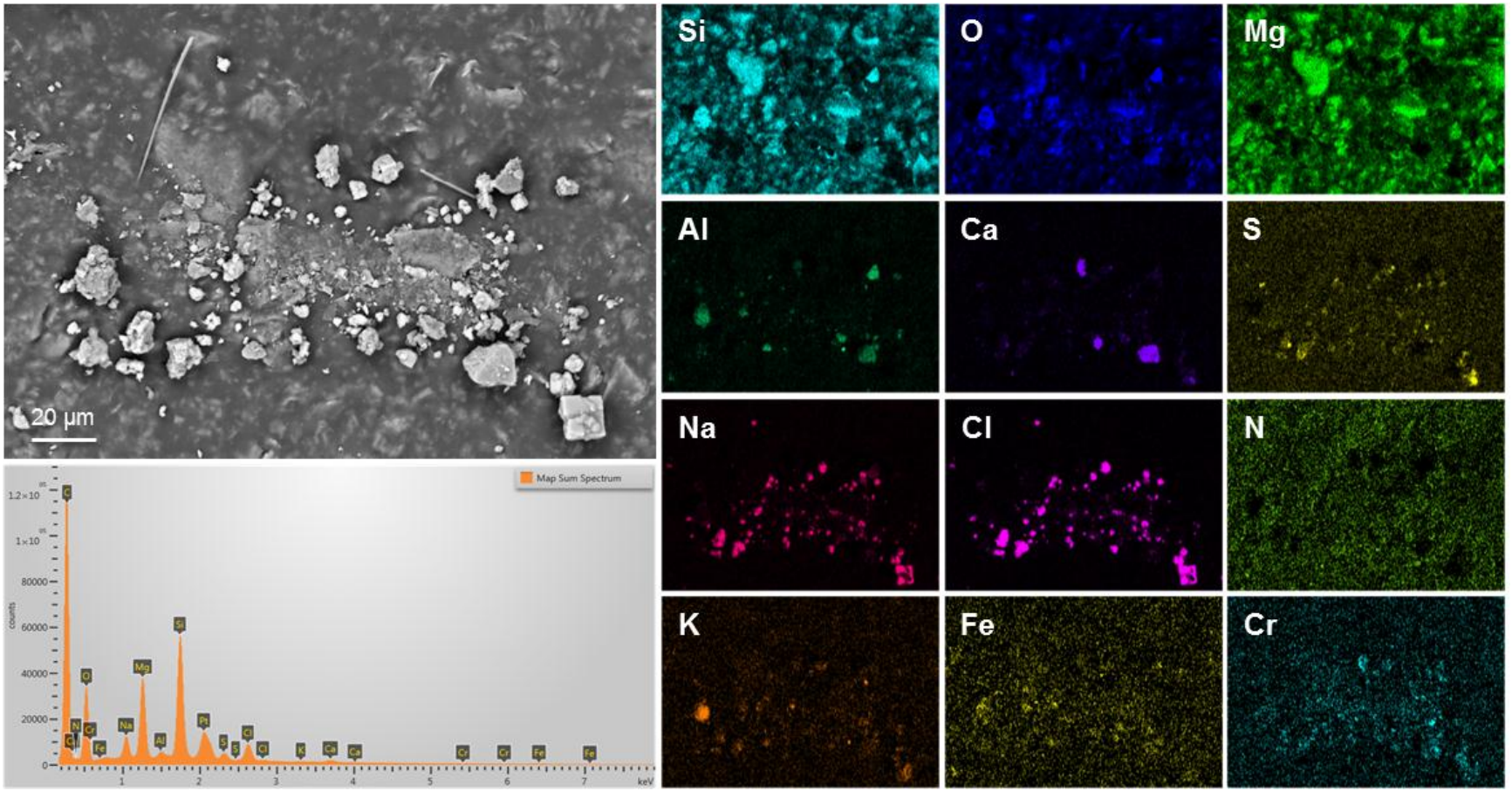

Figure 34. SEM image/EDS map (#2) of sample 170-004, collected from the canister side, 11.0 feet from the upper edge.

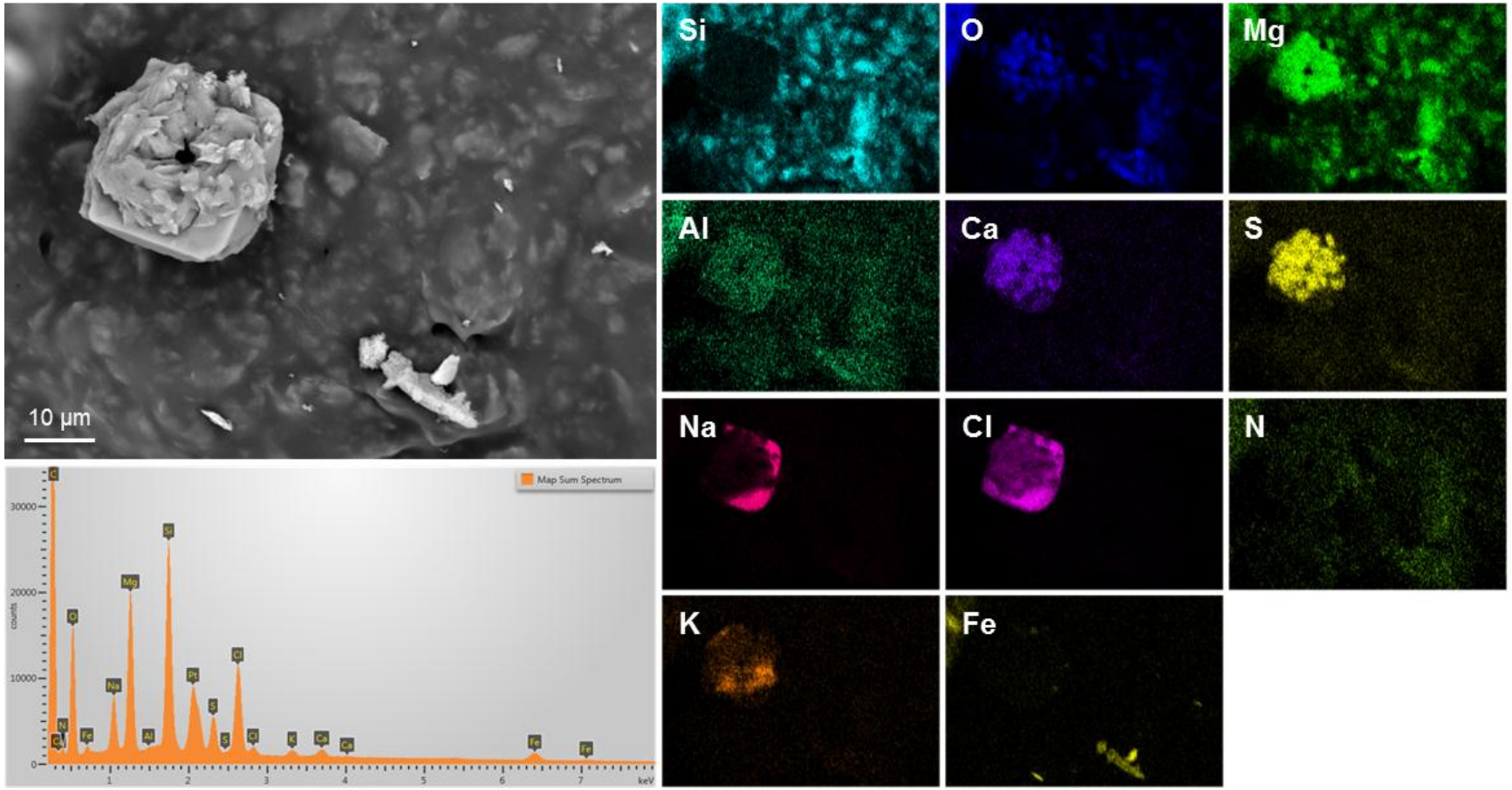

Figure 35. SEM image/EDS map (#1) of sample 170-005, collected from the canister side, 7.5 feet from the upper edge.

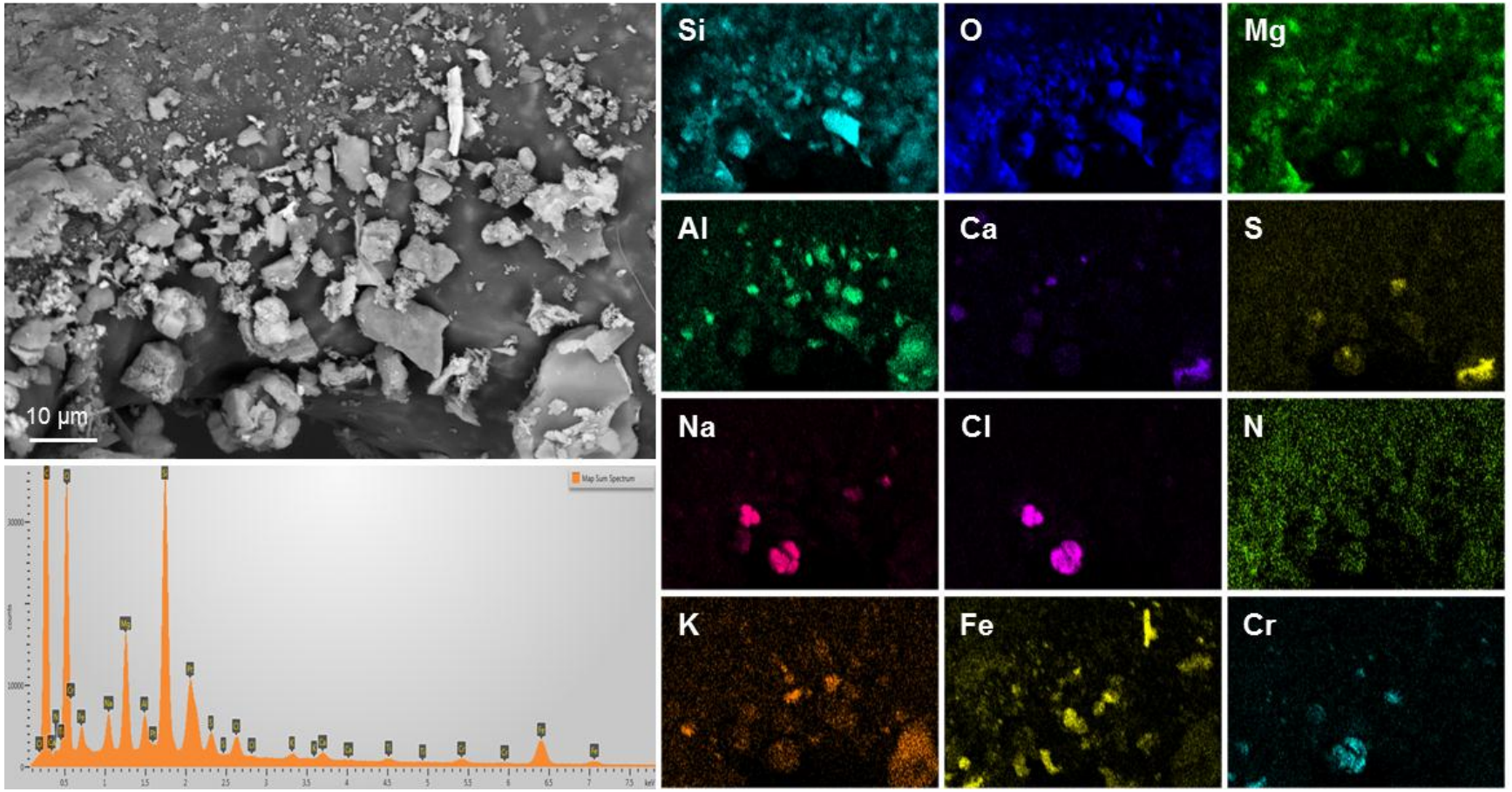

Figure 36. SEM image/EDS map (#2) of sample 170-005, collected from the canister side, 7.5 feet from the upper edge.

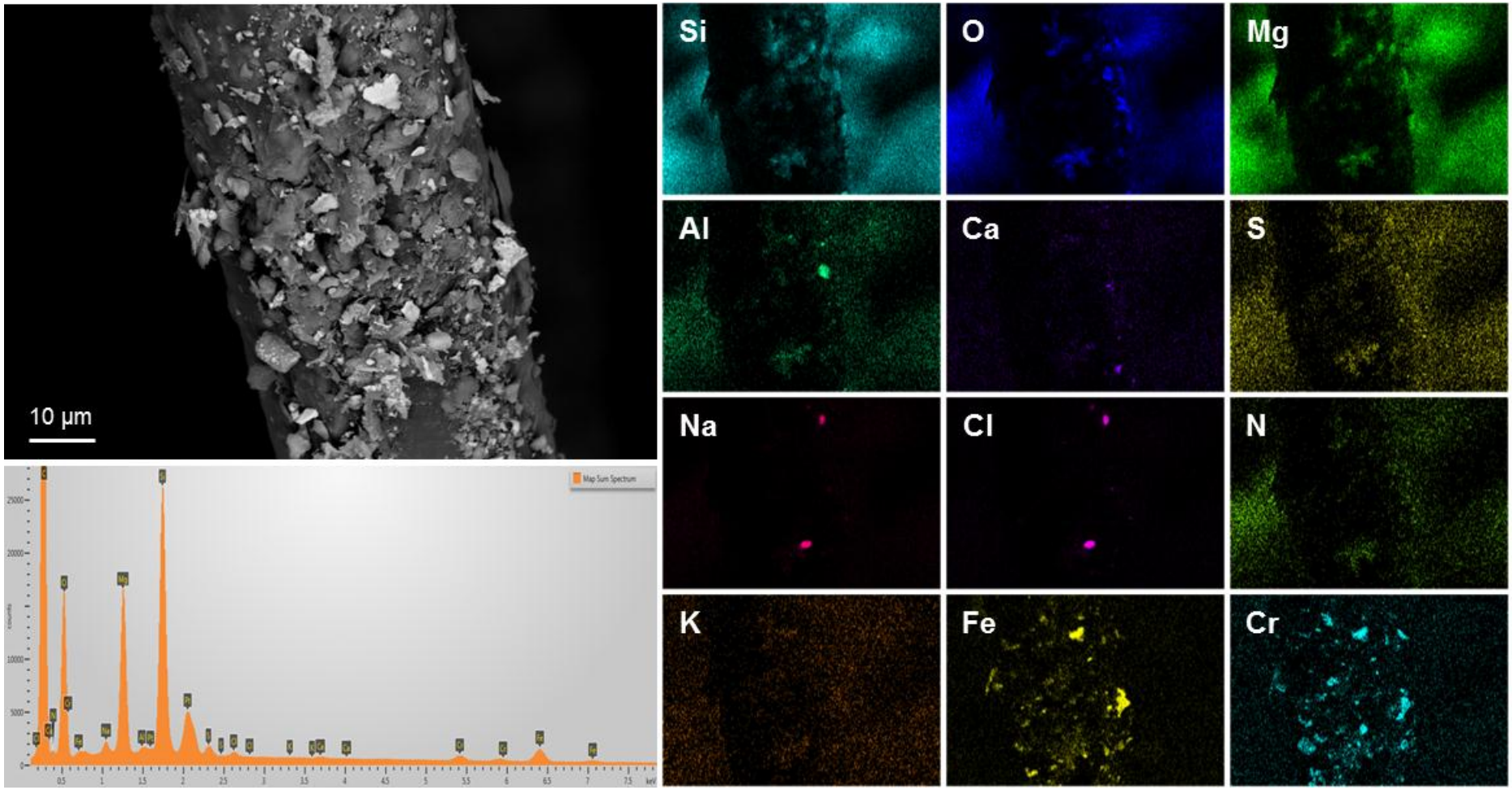

Figure 37. SEM image/EDS map of sample 170-006, collected from the canister side, 3.0 feet from the upper edge.

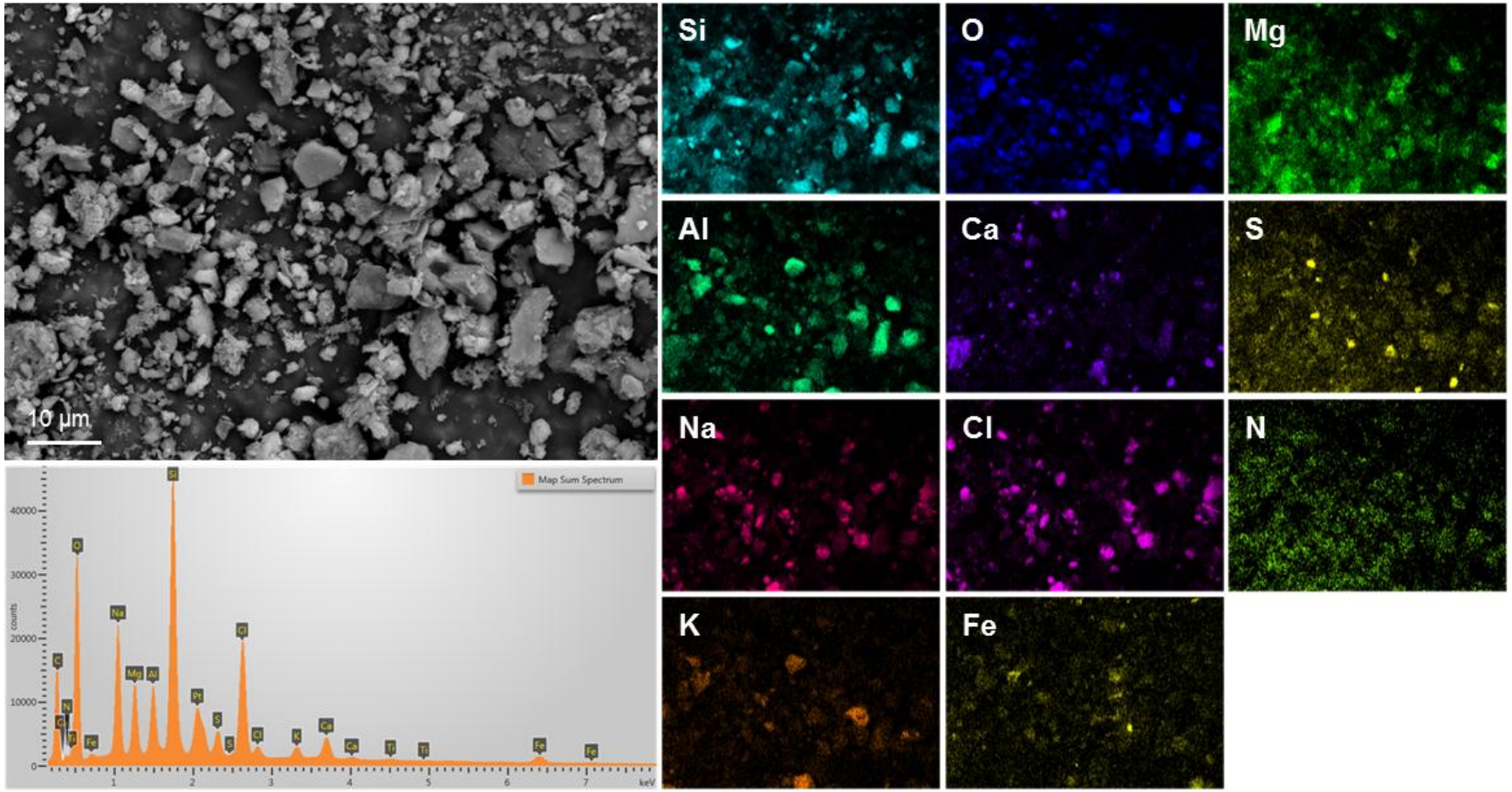

Figure 38. SEM image/EDS map (#1) of sample 170-003, collected from the canister top.

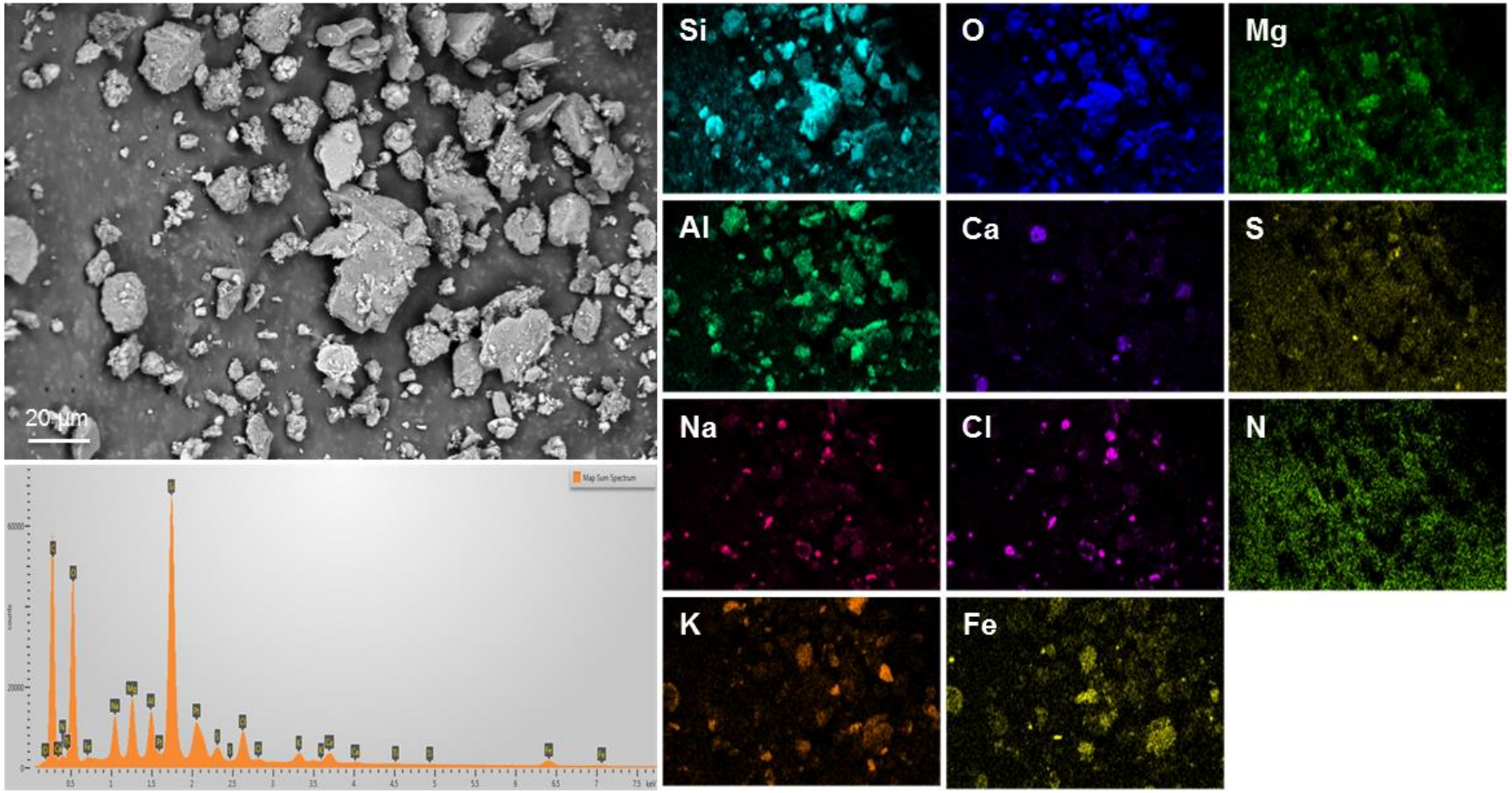

Figure 39. SEM image/EDS map (#2) of sample 170-003, collected from the canister top.

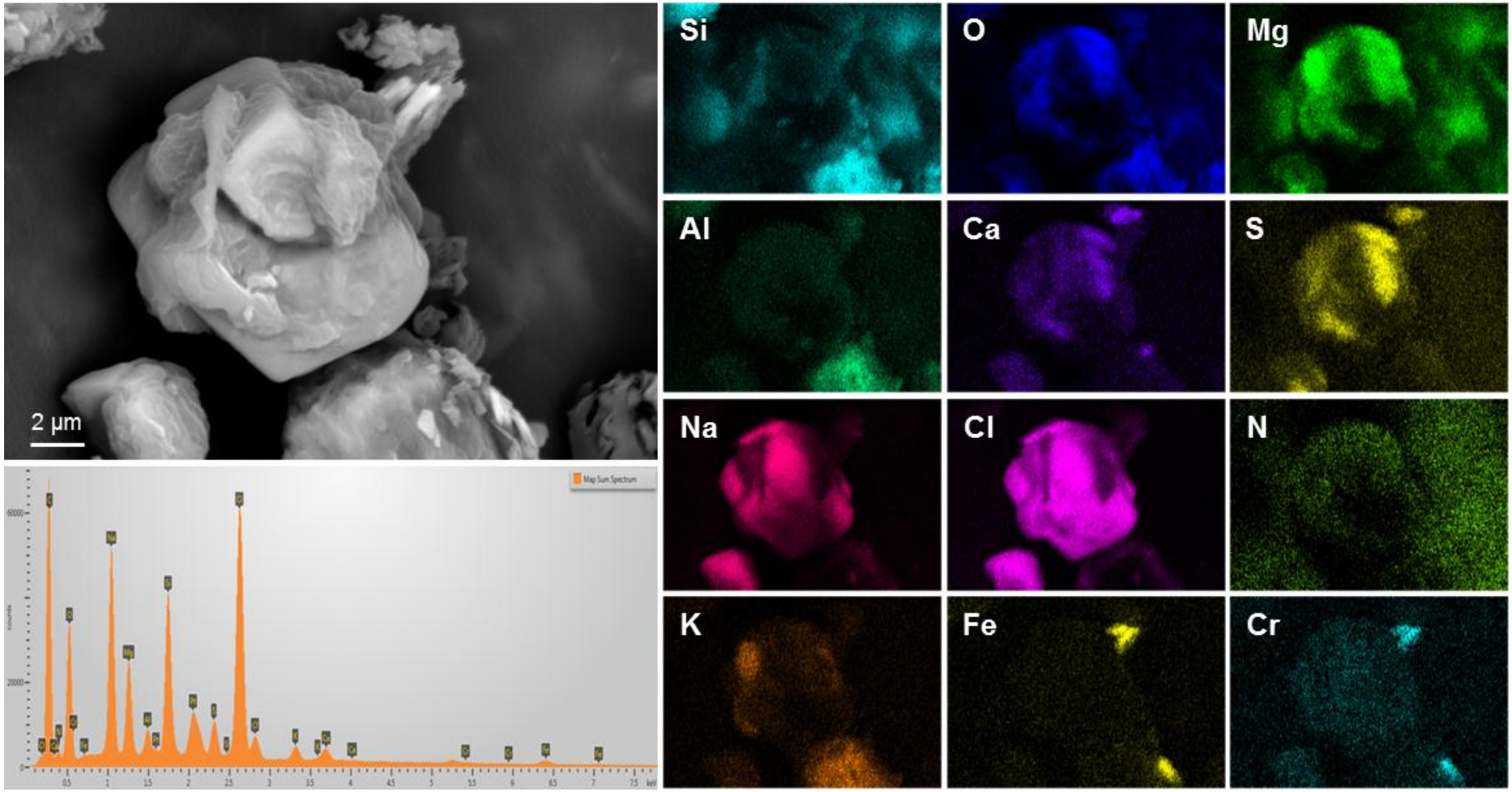

Figure 40. Magnified view of a sea-salt particle in Figure 39, showing intergrown halite and Mg-SO_4.

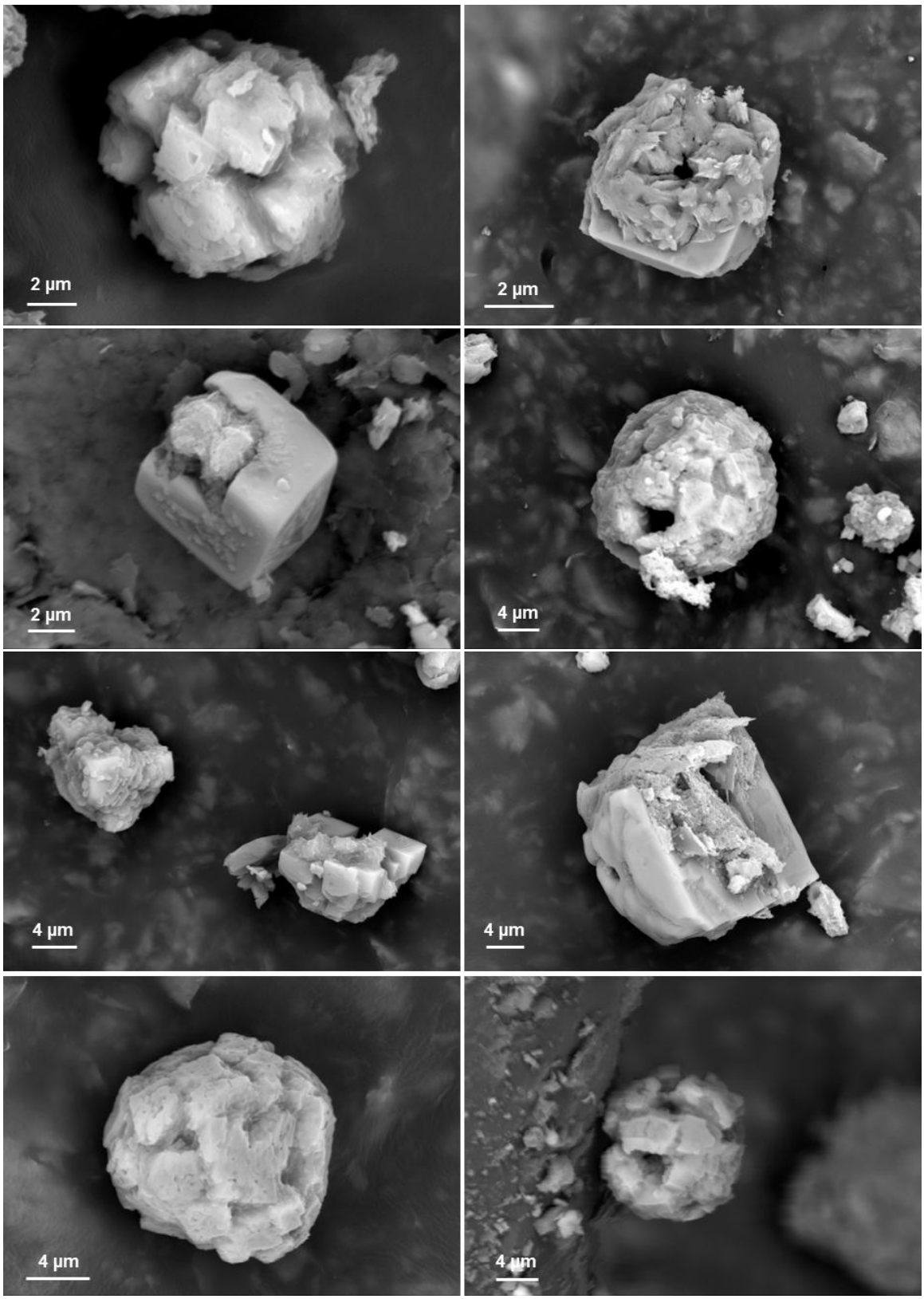

Figure 41. SEM images of sea-salt aggregates (intergrown NaCl cubes with interstitial Mg-SO_4) on sample 170-003, collected from the canister top.

3.1.4. Summary of SEM/EDS analyses

To summarize, dust loads on the dry pad samples from the Hope Creek and Diablo Canyon storage canisters were very light on the pads from the canister sides and heavy on the pads used to sample the upper surface. In both cases, the dust consists largely of terrestrially-derived detrital grains of quartz and aluminosilicates, including larger grains of feldspars and the micas, and sparser grains or aggregates of possible clay phases such as kaolinite and illite. Carbonates of Ca and Ca-Mg were also common. Particles of 304SS, Fe-Cr oxides, iron, and iron oxide are common, and were generated during the canister manufacturing process. At Hope Creek, pollen was abundant in many samples, while at Diablo Canyon, pollen was rare, but fragments of diatoms and biologically derived carbonate structures were occasionally observed.

The composition and abundance of salt phases differed greatly at Hope Creek and Diablo Canyon. At Hope Creek, salts were rarely observed in the dust, and consist largely of Ca-sulfate and small (<5 μm), heavily etched grains of NaCl. At Diablo Canyon, salts were abundant, and occurred primarily as sea-salt aggregates of NaCl and Mg-SO_4. The morphology of these grains suggests they formed largely though evaporation of aerosol droplets of seawater, possibly after entering the heated overpack.

The SEM observations of dust from the surface of canisters MPC-123 and MPC-170 are critical to understanding the deposition, accumulation, and distribution of salts, and chloride, on the canister surfaces. If efforts are undertaken to characterize aerosols at the ISFSI sites using air samplers, a sufficient size range of particles must be sampled. Using PM10 sampling techniques is inadequate, as many of the sea salt grains that are deposited on the canister surfaces are larger than 10 μm. A method for sampling total suspended particulates (TSP) might be required. Also, the morphology of the sea-salt particles indicates that they formed by evaporation of seawater droplets suspended in the atmosphere. It is not clear when this evaporation occurred, but seems likely that on humid days, the sea-salts may be transported into the overpack dominantly as deliquesced or partially deliquesced droplets; the common occurrence of sea fogs in the Diablo Canyon area supports this conclusion. Therefore, the transported particles would be even larger and heavier than the observed sea-salt grains; again, this suggests that a TSP sampling method might be more accurate for determining the relevant atmospheric aerosol load than a PM10 instrument.

While the vast majority of the salt mass in the air is undoubtedly in large sea-salt particles, dust deposited on the sides of the canisters (the most critical location with respect to SCC), seems to have a relatively large fraction of finer sized (<2.5 μm) materials. Hence it is important to characterize the PM2.5 aerosol fraction as well. Moreover, the relative proportion of continental versus ocean-derived salts in air entering the overpack may vary with inlet direction, resulting in variations in the composition of deposited dusts. Many aerosol samplers use omnidirectional sampling heads, and yield only averaged values for dust composition.

The same caveats hold true for developing models for dust and chloride deposition. Any particle deposition model must consider a large range of particle sizes, as well as potential variations in dust composition with particle size (e.g. proportion of continentally-derived versus marine-derived particles). It might be necessary to consider the effects of inlet vent direction and

dominant wind direction as well. Finally, an aerosol transport and deposition model would have to consider that the salts may frequently be entering the package as deliquesced or partially deliquesced droplets. An aerosol transport model must therefore capture the changes in mass and aerodynamic properties as the particles rise and dry out in the heated annulus of the overpack. The deposition model should consider the changes in the sticking properties of the particles, as they transition from brine droplets to dry salts. Aerosol particles impacting the canister near the inlet vent may still be partially deliquesced, resulting in build-up of salts at that location.

Any deposition model must also explain the greater rates of deposition on the canister tops. It should be noted that during sampling at Hope Creek, *Phragmites* grass seeds were observed in large amounts on the canister top. Surface stains and variations in the amount of accumulated dust (dunes) were also observed, suggesting that materials and rainwater may be regularly blown onto the canister tops through the outlet vents, an additional complicating factor.

It is important to remember that the canisters at Hope Creek and at Diablo Canyon are of the same type and geometry. In both cases, there are four outlet air vents at 90º from each other around the top of the overpack. These vents are offset 45º degrees from the inlet vents at the base of the units. Because the dust sampling was performed in a vertical line extending downward from the outlet vents, regions near the inlet vent were not sampled. It seems likely that there is preferential deposition of salts near the inlet vents, especially if the salts enter the inlet vents as deliquesced droplets. We have no information on the surface deposits near the inlet vents.

A limited set of analyses were presented in this section to save space. It is recommended that the reader review images and EDS maps of samples from the Hope Creek and Diablo Canyon canisters in Appendix A to obtain a better understanding of the observed dust loads and the morphology and composition of dust phases.

3.2. XRF Analysis

XRF analysis was used to quantify element concentrations on the pads. The XRF was capable of mapping the filters and pads with a resolution of 100 µm, providing spatial information on the scale of the filters. This information provides a link between the SEM data, which is confined to small areas on the sample surface, and the chemical analysis, which does not discriminate spatially, but rather provides an averaged composition for all the phases present. Moreover, the analysis provides element ratios which may be useful in estimating concentrations of some insoluble elements.

Relative to previous work with samples from Calvert Cliffs, the XRF instrument used here had lower sensitivity. This meant needing to count longer for each spatial position in the XRF map, selecting smaller map regions and increasing the step width (to ~100 mm) which decreased resolution for the measurement. Also, the samples did not appear to have as much residue on them as the previous samples from Calvert Cliffs, so the detection of material posed further difficulties. Finally, the pads used this time contained many elements that are commonly found in potential dust minerals, namely silicon, magnesium and, iron. The low signal issue was addressed by comparing the full spectrum obtained on each sample to that of a clean, unused pad. Blank subtraction was performed to look for residual intensity that possibly could be assigned to residue on the sample. This method appears to work somewhat reasonably for qualitative assessment of material present on these pads. For each XRD pattern, a qualitative analysis is provided. It is important to note, when evaluating the XRF patterns provided in this report, that peak heights do not correspond to elemental abundances, but rather are a function of varying detection efficiencies as a function of wavelength.

The XRF results for a few representative samples are shown here; the complete suite of analyses is provided in Appendix B. In each case, the raw XRF pattern is shown, as well as a blank-subtracted XRF pattern, to emphasize the differences between the samples and the blank.

Blanks. The XRF pattern and qualitative analysis results for the pad blank are shown in Figure 42. Although the pad was intended to be mineral-free, it actually contained talc ($Mg_3Si_4O_{10}(OH)_2$ as a filler material. This resulted in large Mg and Si peaks in the blank, and large estimated concentrations of Mg and Si in the blank pad (red boxes in Figure 42). Other compounds present in the pad include Ti, which is probably present in the oxide form as a white pigment, Ca, P, and S. All of these elements contribute to the measured XRD signal, but not all can be leached from the pad. The Mg, Si, Fe, Ti, and Ca appear to be sequestered in insoluble compounds in the pad. However, PO_4, SO_4, and Na leach from the pad in large concentrations and interfere with measurement of these elements in the dust soluble fractions leached from the pads. Note that Na does not appear in the X-ray spectrum because of the low sensitivity of the method for this element.

Canister side samples. For both Hope Creek and Diablo Canyon, the dust loads on samples from the sides of the canisters were very light, and the XRF patterns and analyses varied little from the blank (see Appendix B). Typically only Fe and Si were enriched relative to the blank. An example pattern for the lightly-coated canister side samples is represented by Hope Creek sample 144-005 (collected 13.5 feet below the upper edge of the canister) in Figure 43. The initial X-ray

spectrum was similar to the blank spectrum. Following blank subtraction, only Fe was detected in the sample.

Canister top samples. For samples from the tops of the canisters, where the salt loads are higher, there is a clear X-ray contribution from the dust on the filters. Results for Hope Creek sample 144-011 are shown in Figure 44. Relative to the blank, several elements are significantly enriched, including Fe, Si, Zn, Ca, K, and S. The enrichment in Fe is consistent with the SEM observations of abundant stainless steel particles and Fe-oxides in the dust; and that of Si is consistent with the observations of abundant quartz and aluminosilicate minerals. Although Zn-rich particles, apparently from the paint on the outside of the overpacks, were only rarely observed, they are apparently the source of the Zn X-ray peak shown here. Minerals containing Ca, K, and S (as sulfate) were observed by SEM, and these elements comprise a large fraction of the soluble salts extracted from the pads (Section 3.3). These results are typical for the Hope Creek canister top samples.

XRF analysis results for sample #123-011, a representative canister top sample from Diablo Canyon, are shown in Figure 45. Relative to the blank, the Diablo Canyon sample is enriched in Fe, Si, Zn, Ca, K, S, and Cl. In some other Diablo Canyon samples, peaks for Cr were also present. As with the Hope Creek samples, this is largely consistent with the phases identified in the dust by SEM. Given the prevalence of sea-salt aggregates, one might expect to see peaks for Mg and Na as well; however, the method sensitivity for Mg is low, and for Na, very low. The detection of Cl and Zn, and of Cr in some other samples from Diablo Canyon (Appendix B), is convincing, because these elements do not occur in the blank.

Because many of the elements that were detected in the canister top samples from Hope Creek and Diablo canyon are present in relatively high amounts in the blank, caution must be taken in interpreting these results. False positive detections may occur because of variations in sample geometry, and the canister top collection sponges are thicker than the ones used for the canister sides—the additional compression (and concomitant densification) of the canister top sample sponges required during loading into the XRF may be responsible for the observed enrichments in the elements that are present pad matrix. Also, there are variations in the amount of resin/filler through the thickness of the original Scotch-Brite™ abrasive pads that were cut apart and thinned to make the sample pads. The pads used in the remote tool sample vary slightly in thickness from pad to pad, and the pads used on the canister tops were full thickness. Moreover, it is unlikely that the same side of the original pad was used to make all of the sampling pads and the blanks, or that the same face of each trimmed sampling pad was used during sampling and analysis. Hence, some of the variation in the contribution of the pads is almost certainly due to variations in the amount of binder/filler present. As will be discussed in Section 3.3, this conclusion is supported by the compositions of soluble salts leached from the dry pads samples.

The results of the XRF analysis of the sponges are summarized in Table 7 for Hope Creek, and in Table 8 for Diablo Canyon. The enrichment in Fe relative to the blank in all samples from the canister surface may be real, as the SEM analyses show that steel particles were abundant components of the dust in almost all cases. Moreover, the detection of Cr is some samples from Diablo Canyon is strong evidence that that the stainless steel particles in the dust are contributing to the X-ray signal. Similarly, the enrichment of Si in most samples may reflect a contribution

from the dust. However, given the variability in the pad matrices, it is not possible to clearly attribute a portion of the signal for any component to the dust unless it is not present at all in the blank.

To conclude, XRF analysis of the dry pad samples was complicated by the presence of several elements in the blank, and by differences in pad resin/filler content. It is clear that some elements, however, represent dust collected from the canister surfaces. Detection of Zn on the Hope Creek pads, and Zn, Cl, and Cr on the Diablo Canyon pads, must represent components in the dust, as these are not present in the blank. It is likely that at least some of the enrichments observed in other elements, such as Fe and Si, are also at least in part due to dust on the pads.

Table 7. XRF Analysis of Hope Creek Dry Pad Samples—Elemental Enrichments Relative to the Blank Sample.

Sample	Location	Fe	Si	Ca	K	S	Zn
144-001	Unknown	minor	–	–	–	–	–
144-002	Unknown	–	–	–	–	–	–
144-005	Canister side	minor	–	–	–	–	–
144-006	Canister side	minor	trace	–	–	–	–
144-007	Canister side	trace	–	–	–	–	–
144-011	Canister top	major	minor	trace	trace	trace	trace
144-012	Canister top	major	minor	trace	trace	–	trace
145-001	Unknown	trace	–	–	–	–	–
145-003	Canister side	major	minor	–	–	–	–
145-004	Canister side	minor	minor	–	–	–	–
145-005	Canister side	minor	minor	–	–	–	–
145-012	Canister top	minor	trace	trace	trace	–	trace

Table 8. XRF Analysis of Diablo Canyon Dry Pad Samples—Elemental Enrichments Relative to the Blank Sample.

Sample	Location	Fe	Si	Ca	K	S	Zn	Cl	Cr	Ti
123-001	Unknown	major	minor	–	–	trace	–	–	–	–
123-006	Canister side	minor	minor	–	–	trace	–	–	–	–
123-007	Unknown	minor	minor	–	–	trace	–	–	–	–
123-008	Canister side	minor	trace	–	–	–	–	–	–	–
123-009	Canister side	major	minor	–	–	trace	–	–	–	–
123-011	Canister top	major	minor	trace	trace	trace	trace	–	–	minor
123-012	Canister top	minor	trace	–	minor	trace	trace	minor	minor	–
170-001	Unknown	major	trace	–	–	–	–	–	–	–
170-003	Canister top	major	minor	–	trace	trace	trace	minor	–	–
170-004	Canister side	major	minor	–	–	trace	trace	–	trace	–
170-005	Canister side	minor	minor	–	–	trace	trace	–	–	–
170-006	Canister side	major	minor	–	–	trace	trace	–	–	–

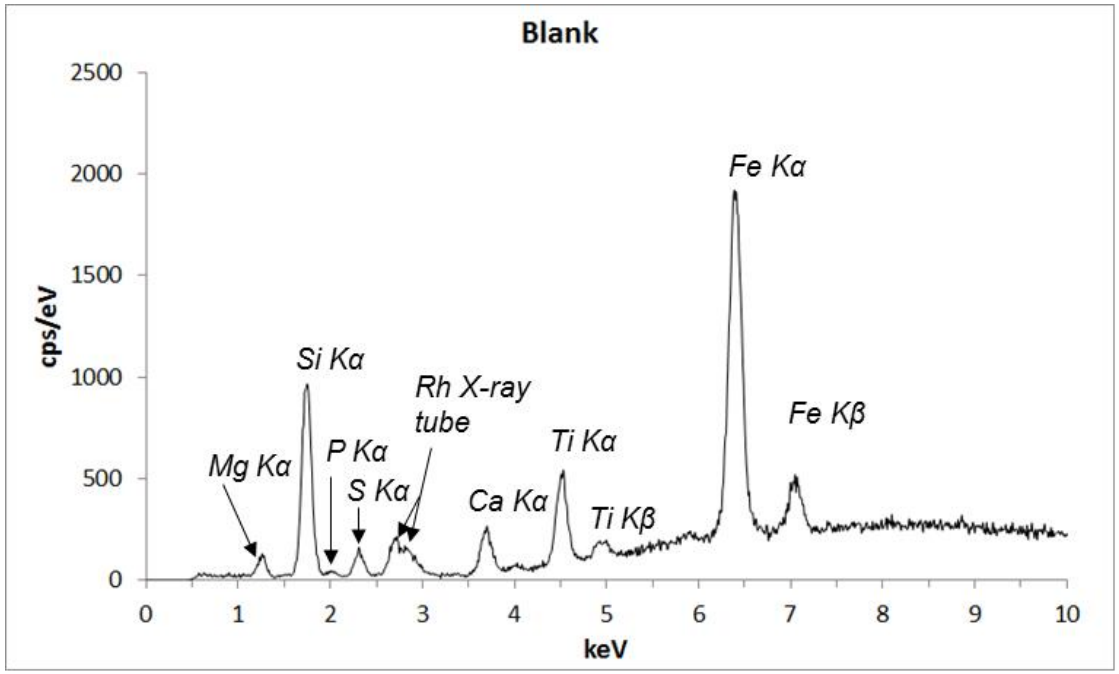

Vision Quant Results: **Blank**				
Total Area Spc from ROI Map		12:53 PM		10-Feb-14
Elem:	Net	Wt%	At%	I-Error%
MgK	1.57	29.42	35.12	3.79
AlK	0.2	1.2	1.29	18.91
SiK	15.88	47	48.58	1.02
P K	0.45	1.77	1.66	10.07
S K	2.06	4.06	3.68	3.32
K K	0.18	0.22	0.17	25.03
CaK	4.25	3.5	2.54	2.25
TiK	8.81	3.67	2.23	1.62
CrK	0.27	0.08	0.04	43.76
MnK	1.12	0.28	0.15	12.39
FeK	38.9	8.46	4.4	0.73
NiK	0.53	0.11	0.06	30.79
ZnK	0.81	0.17	0.07	21.53
ZrK	0.23	0.05	0.02	36.82

Elemental map for Fe

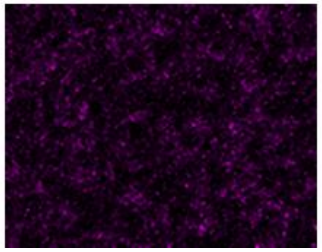

Figure 42. XRF pattern and XRF qualitative analysis results for the pad blank.

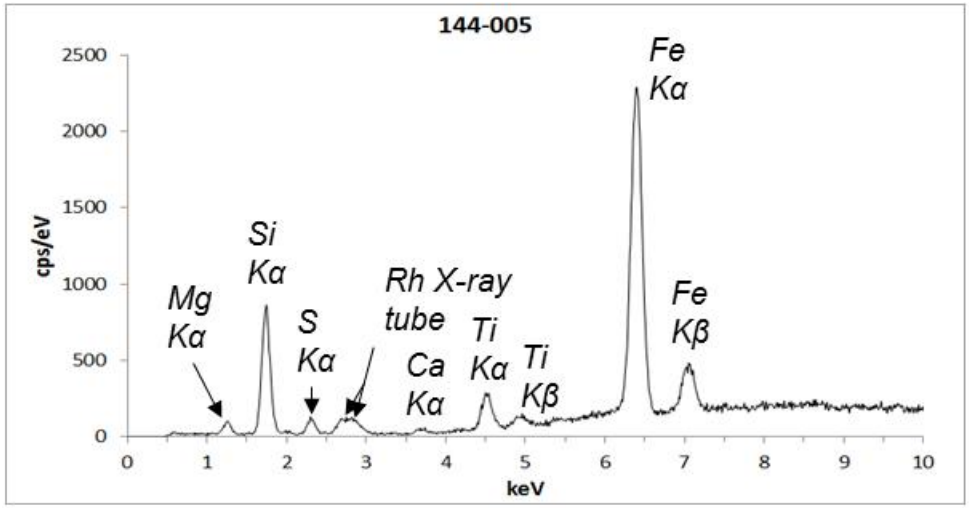

Vision Quant Results: 144-005				
Total Area Spc from ROI Map		2:04 PM		11-Feb-14
Elem:	Net	Wt%	At%	I-Error%
MgK	1.27	29	34.98	4.35
AlK	0.1	0.72	0.79	34.75
SiK	13.4	46.39	48.44	1.11
P K	0.32	1.46	1.39	12.82
S K	1.71	3.9	3.57	3.66
ClK	1.14	2.57	2.13	4.88
K K	0.17	0.25	0.19	23.98
CaK	0.62	0.6	0.44	8.46
TiK	4.8	2.2	1.35	2.26
CrK	0.54	0.17	0.09	18.27
MnK	0.64	0.17	0.09	17.98
FeK	49.14	12	6.3	0.61
NiK	0.56	0.15	0.07	24.74
ZnK	1.26	0.32	0.14	12.11
ZrK	0.3	0.08	0.03	26.5

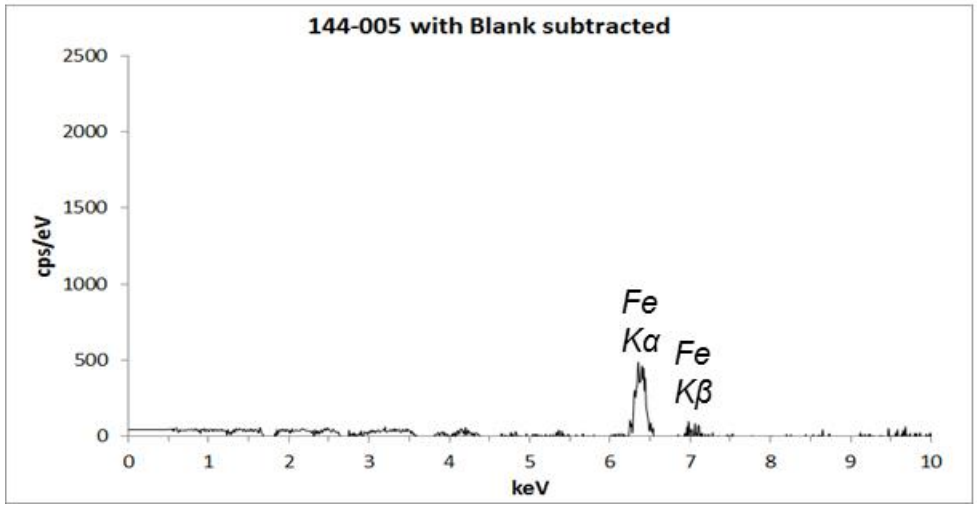

Vision Quant Results: **Blank**				
Total Area Spc from ROI Map		12:53 PM		10-Feb-14
Elem:	Net	Wt%	At%	I-Error%
MgK	1.57	29.42	35.12	3.79
AlK	0.2	1.2	1.29	18.91
SiK	15.88	47	48.58	1.02
P K	0.45	1.77	1.66	10.07
S K	2.06	4.06	3.68	3.32
K K	0.18	0.22	0.17	25.03
CaK	4.25	3.5	2.54	2.25
TiK	8.81	3.67	2.23	1.62
CrK	0.27	0.08	0.04	43.76
MnK	1.12	0.28	0.15	12.39
FeK	38.9	8.46	4.4	0.73
NiK	0.53	0.11	0.06	30.79
ZnK	0.81	0.17	0.07	21.53
ZrK	0.23	0.05	0.02	36.82

Figure 43. XRF pattern and XRF qualitative analysis results for Hope Creek sample 144-005, from the side of the canister.

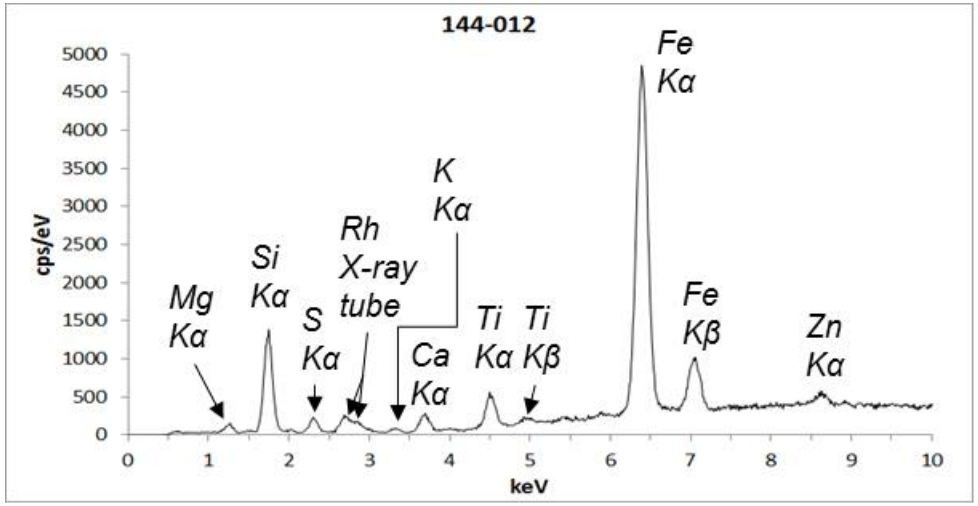

Vision Quant Results: 144-005				
Total Area Spc from ROI Map		2:04 PM		11-Feb-14
Elem:	Net	Wt%	At%	I-Error%
MgK	1.27	29	34.98	4.35
AlK	0.1	0.72	0.79	34.75
SiK	13.4	46.39	48.44	1.11
P K	0.32	1.46	1.39	12.82
S K	1.71	3.9	3.57	3.66
ClK	1.14	2.57	2.13	4.88
K K	0.17	0.25	0.19	23.98
CaK	0.62	0.6	0.44	8.46
TiK	4.8	2.2	1.35	2.26
CrK	0.54	0.17	0.09	18.27
MnK	0.64	0.17	0.09	17.98
FeK	49.14	12	6.3	0.61
NiK	0.56	0.15	0.07	24.74
ZnK	1.26	0.32	0.14	12.11
ZrK	0.3	0.08	0.03	26.5

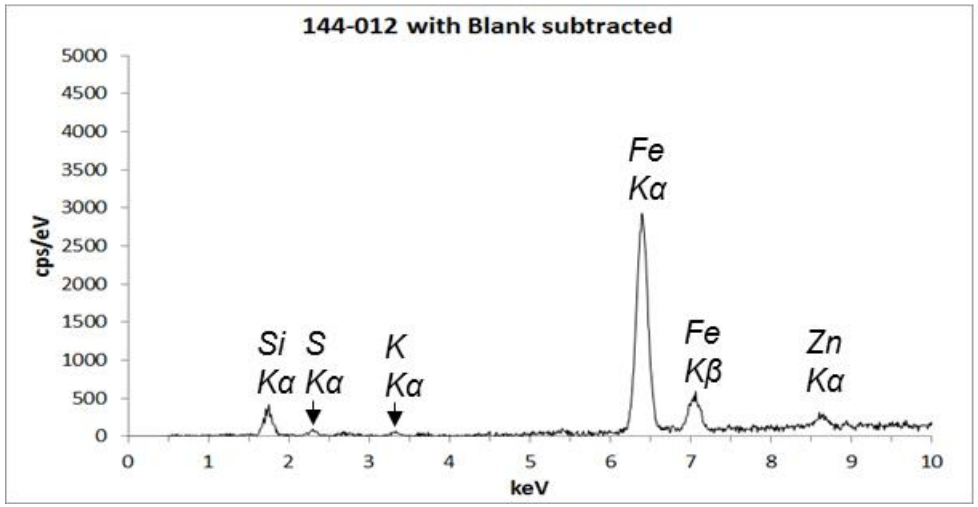

Vision Quant Results: **Blank**				
Total Area Spc from ROI Map		12:53 PM		10-Feb-14
Elem:	Net	Wt%	At%	I-Error%
MgK	1.57	29.42	35.12	3.79
AlK	0.2	1.2	1.29	18.91
SiK	15.88	47	48.58	1.02
P K	0.45	1.77	1.66	10.07
S K	2.06	4.06	3.68	3.32
K K	0.18	0.22	0.17	25.03
CaK	4.25	3.5	2.54	2.25
TiK	8.81	3.67	2.23	1.62
CrK	0.27	0.08	0.04	43.76
MnK	1.12	0.28	0.15	12.39
FeK	38.9	8.46	4.4	0.73
NiK	0.53	0.11	0.06	30.79
ZnK	0.81	0.17	0.07	21.53
ZrK	0.23	0.05	0.02	36.82

Figure 44. XRF pattern and XRF qualitative analysis results for Hope Creek sample 144-011, from the top of the canister.

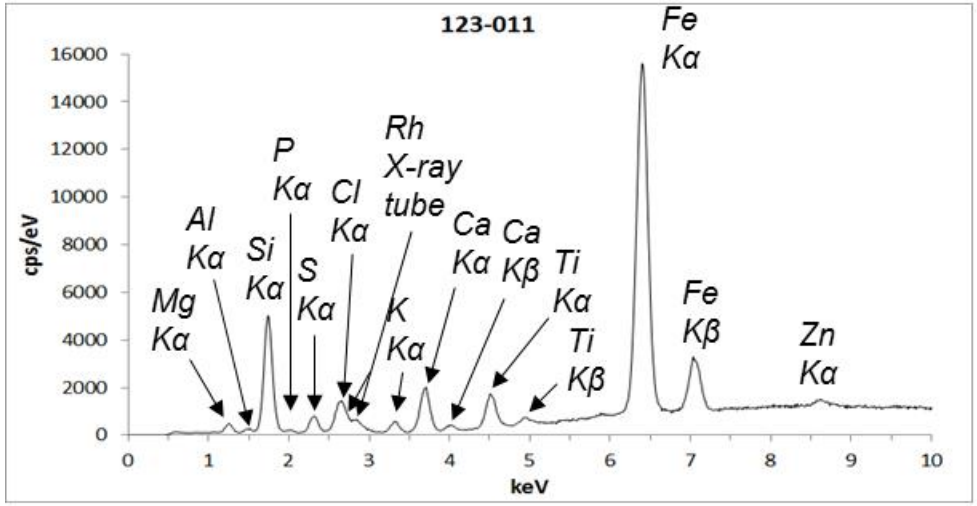

Vision Quant Results: 123-011				
Total Area Spc from ROI Map		5:57 PM		12-Feb-14
Elem:	Net	Wt%	At%	I-Error%
MgK	1.44	21.30	27.08	2.16
AlK	0.68	2.71	3.11	3.85
SiK	19.89	39.33	43.29	0.46
P K	0.47	1.18	1.18	5.41
S K	3.04	3.77	3.64	1.34
ClK	6.1	7.60	6.62	0.88
K K	1.97	1.77	1.40	1.86
CaK	8.68	5.26	4.05	0.74
TiK	7.18	2.24	1.45	0.92
CrK	0.43	0.09	0.05	13.57
MnK	1.14	0.21	0.12	5.97
FeK	83.69	13.94	7.72	0.23
NiK	0.63	0.11	0.06	13.5
ZnK	2.6	0.45	0.21	3.7
ZrK	0.21	0.04	0.01	24.84

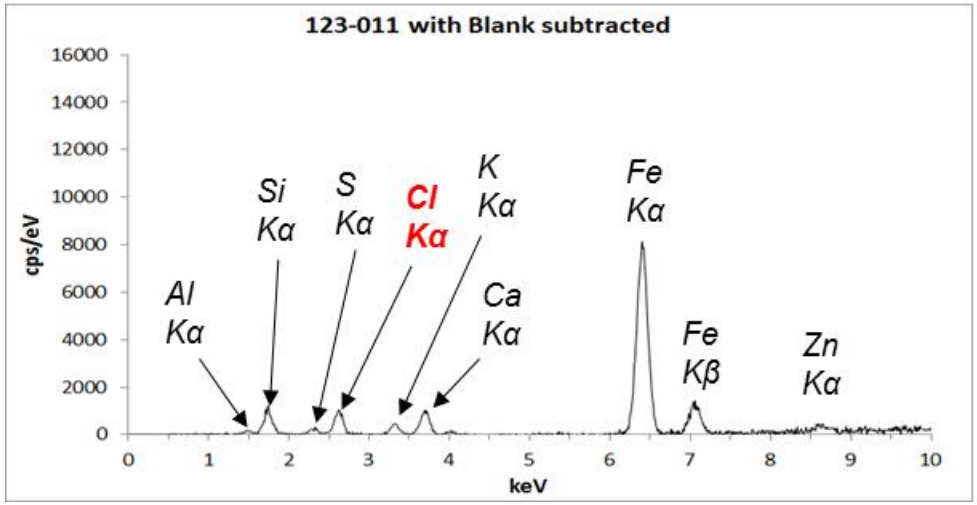

Vision Quant Results: **Blank**				
Total Area Spc from ROI Map		12:53 PM		10-Feb-14
Elem:	Net	Wt%	At%	I-Error%
MgK	1.57	29.42	35.12	3.79
AlK	0.2	1.2	1.29	18.91
SiK	15.88	47	48.58	1.02
P K	0.45	1.77	1.66	10.07
S K	2.06	4.06	3.68	3.32
K K	0.18	0.22	0.17	25.03
CaK	4.25	3.5	2.54	2.25
TiK	8.81	3.67	2.23	1.62
CrK	0.27	0.08	0.04	43.76
MnK	1.12	0.28	0.15	12.39
FeK	38.9	8.46	4.4	0.73
NiK	0.53	0.11	0.06	30.79
ZnK	0.81	0.17	0.07	21.53
ZrK	0.23	0.05	0.02	36.82

Figure 45. XRF pattern and XRF qualitative analysis results for Diablo Canyon sample 123-011, from the top of the canister.

3.3. Chemical Analysis

The methods used for chemical analysis of the SaltSmart™ and dry pad samples from Hope Creek and Diablo Canyon are described in Section 2.2. As discussed in that section, the soluble salts extracted from the SaltSmart™ sensors and from the dry pads were analyzed. Because of the very light dust load on most pads, and the high degree of contamination by talc, a decision was made not to perform bulk analyses of the insoluble residues from the dry pads. The results of the analyses are presented and discussed below.

3.3.1. Hope Creek Samples

3.3.1.1 SaltSmart™ Sensors

Thirteen SaltSmart™ sensors were analyzed from the Hope Creek site, representing three samples from the side of each of the two containers sampled, and one or two from the top of each. Concentrations of soluble salts were generally quite low. Two samples of unknown origin were also analyzed from each canister. The amounts of each ionic species present in µg per sample are given in Table 9. Values in micro-equivalents (µEq) are provided in Table 10, along with the calculated charge balance errors. Also shown in these tables are three SaltSmart™ blanks run at Sandia, two with contact times of 8 minutes, and one with a contact time of 15 minutes. In addition, the 15 minute sample was stored approximately one week prior to analysis, to assess whether anything leached out of the SaltSmart™ components over time. There are several notable points. First, the salt loads are generally very light (≤25 µg/sample) for the sensors used on the sides of the storage container. Only the three samples from the canister tops (144-013, 144-014, and 145-013) have significant amounts of salt. The dominant cation in all cases was Ca, but Mg and Na are also abundant in the higher-concentration samples. Sulfate was the dominant anion in all samples, and nitrate was the second most abundant in all samples except for 144-014, for which chloride was the second most abundant.

Many of the charge balances are poor, and consistently indicate an anion deficiency. There are three possible reasons for this:

- Analytical uncertainties are high because of the very low salt concentrations. However, the consistent anion deficiency would suggest an analytical bias, not just analytical scatter.

- The ammonium data are suspect. Ammonium concentrations are low in terms of µg/sample, but ammonium has a low atomic mass, and the low values correspond to a significant fraction of the measured µEq of cations in most samples. Ammonium concentrations in the Hope Creek samples are similar to the concentrations observed in the blanks; in fact, they are always lower than the value for the 15 minute blank. During disassembly of the sensors, it was noted that silicone cement is used to seal the back of the sensors, where the flat film containing the electrodes exits the sensor. Since many silicone cements degas ammonia during curing, this material may be a source of the observed ammonium in the blanks. Reaction of ammonia with water in the sensor would produce ammonium and hydroxyl, and would contribute to the poor charge balances, because hydroxyl was not measured.

- Carbonate, a potentially important contributor to the anion total, was not analyzed. Since carbonate minerals were commonly observed in the dust samples by SEM, it is likely that at least a fraction of the charge balance error is due to the lack of data for carbonate.

The charge balance error correlates with the amount of calcium and magnesium present, and is actually largest for the two samples with the highest amounts of salts, for which the effect of ammonium is minimal, and analytical errors should be smallest. Thus, it is likely that the charge balance error is largely due to the presence of carbonate/bicarbonate minerals in the dust, and carbonate accounts for the missing unanalyzed anionic species in the leachate.

The chloride loads per unit surface area are given in Table 11. They are generally less than 10 mg/m^2, but the two highest samples, 144-013 and 144-014, get up to 14 and 60 mg/m^2, respectively. It should be noted that the concentrations listed here may in some cases underestimate the amount of salt and chloride present. For three samples, the reservoir pad was only partially saturated and it is not clear that sufficient water passed through the wick and across the canister surface to leach off all the soluble salts present. Also, for sample number 145-006, the SaltSmart™ wick apparently did not completely contact the surface; the discoloration on the wick covered only about 1/3 of the total area, so the listed chloride concentration probably underestimates the actual value on the package.

Table 9. Ion Concentrations in the Hope Creek SaltSmart™ Samples (µg/sample).

Sample #	Loc.	Depth, ft	Temp., ºF	Na	K	Ca	Mg	NH_4^+	F^-	Cl^-	NO_3^-	PO_4^{3-}	SO_4^{2-}	SUM
144-008	Side	13.0	93.2	*0.1*	*0.8*	3.4	0.6	2.7	nd	0.9	2.7	nd	4.1	15.4
144-009	Side	7.5	116.5	*0.1*	1.7	4.5	0.5	2.7	nd	0.9	6.4	*1.1*	6.5	24.3
144-010	Side	1.0	133.9	*0.4*	1.4	4.2	0.4	2.4	nd	1.2	5.0	nd	4.4	19.4
144-013	Top	0.0	138	42	18	102	33	2.8	0.4	4.2	19	4.8	91	317
144-014	Top	0.0	141.2	13	6.4	29	8.0	2.7	0.4	18	7.3	1.3	55	142
144-003	G.S.	—	—	nd	*0.6*	2.2	0.4	1.4	nd	*0.5*	3.3	1.2	2.1	11.6
144-004	G.S.	—	—	nd	*0.3*	3.2	0.6	2.9	nd	0.8	1.8	*0.5*	1.7	11.8
145-006*#	Side	13.0	70.6	*0.5*	2.2	4.4	0.6	2.3	nd	2.2	8.1	nd	4.7	25.1
145-007	Side	7.5	100.8	*0.7*	1.0	2.4	0.6	2.9	nd	2.1	2.2	*0.7*	5.3	17.9
145-014	Side	1.0	130.3	*0.6*	*0.9*	3.2	0.8	3.2	nd	1.2	2.5	nd	9.1	21.5
145-013**	Top	0.0	174.1	32	15	91	30	2.8	nd	2.2	15	3.5	82	273
145-011*	Blank	—	—	nd	*0.2*	2.3	0.3	3.0	nd	*0.7*	1.3	nd	1.7	9.6
145-002	G.S.	—	—	nd	1.2	4.8	0.5	2.7	nd	*0.7*	5.9	*0.8*	2.0	18.5
SS-Bl-8 min-1	—	—	—	nd	nd	1.3	0.2	1.1	nd	*0.4*	1.6	nd	*0.6*	5.1
SS-Bl-8 min-2	—	—	—	nd	nd	1.2	0.2	1.5	nd	*0.7*	*0.9*	*0.5*	*0.2*	5.2
SS-Bl-15 min	—	—	—	nd	nd	1.5	0.5	5.7	0.2	*0.7*	1.1	1.6	1.7	12.9

Notes: Italicized values in gray were above blank values, but too low to quantify accurately. nd = not detected.

* Reservoir pad only damp
** Reservoir pad only partially saturated
# SaltSmart™ wick appears to have only partially contacted the canister surface (~1/3 of the pad).

Table 10. Ion Concentrations in the Hope Creek SaltSmart™ Samples (µEq/sample).

Sample #	Na	K	Ca	Mg	NH_4^+	F^-	Cl^-	NO_3^-	PO_4^{3-}	SO_4^{2-}	Sum, Cation	Sum Anion	Chrg. Bal. Error, %†
144-008	*5.7E-03*	*2.1E-02*	1.7E-01	5.3E-02	1.5E-01	nd	2.6E-02	4.4E-02	nd	8.5E-02	4.0E-01	1.5E-01	44.4
144-009	*4.2E-03*	4.3E-02	2.2E-01	3.8E-02	1.5E-01	nd	2.5E-02	1.0E-01	*3.3E-02*	1.4E-01	4.6E-01	3.0E-01	21.5
144-010	*1.7E-02*	3.7E-02	2.1E-01	3.2E-02	1.3E-01	nd	3.3E-02	8.1E-02	nd	9.2E-02	4.3E-01	2.1E-01	35.1
144-013	1.8E+00	4.6E-01	5.1E+00	2.7E+00	1.5E-01	2.0E-02	1.2E-01	3.1E-01	1.5E-01	1.9E+00	1.0E+01	2.5E+00	61.0
144-014	5.8E-01	1.6E-01	1.4E+00	6.6E-01	1.5E-01	2.1E-02	5.1E-01	1.2E-01	4.0E-02	1.2E+00	3.0E+00	1.8E+00	24.1
144-003	nd	*1.6E-02*	1.1E-01	3.1E-02	7.7E-02	nd	*1.4E-02*	5.4E-02	3.8E-02	4.3E-02	2.3E-01	1.5E-01	22.3
144-004	nd	*8.1E-03*	1.6E-01	5.0E-02	1.6E-01	nd	2.1E-02	2.9E-02	*1.6E-02*	3.6E-02	3.8E-01	1.0E-01	57.7
145-006*#	*2.3E-02*	5.6E-02	2.2E-01	5.3E-02	1.3E-01	nd	6.2E-02	1.3E-01	nd	9.8E-02	4.8E-01	2.9E-01	24.3
145-007	*3.0E-02*	2.7E-02	1.2E-01	4.9E-02	1.6E-01	nd	6.0E-02	3.5E-02	*2.2E-02*	1.1E-01	3.8E-01	2.3E-01	25.5
145-014	*2.6E-02*	*2.3E-02*	1.6E-01	6.2E-02	1.8E-01	nd	3.5E-02	4.0E-02	nd	1.9E-01	4.5E-01	2.6E-01	25.7
145-013**	1.4E+00	3.8E-01	4.5E+00	2.5E+00	1.5E-01	nd	6.3E-02	2.3E-01	1.1E-01	1.7E+00	8.9E+00	2.1E+00	61.8
145-011*	nd	*6.1E-03*	1.1E-01	2.9E-02	1.7E-01	nd	*2.1E-02*	2.1E-02	nd	3.5E-02	3.2E-01	7.6E-02	61.2
145-002	nd	3.0E-02	2.4E-01	4.3E-02	1.5E-01	nd	*1.9E-02*	9.5E-02	*2.4E-02*	4.1E-02	4.6E-01	1.8E-01	44.3
SS-BI-8 min-1	nd	nd	6.3E-02	1.6E-02	6.2E-02	nd	*1.0E-02*	2.6E-02	nd	*1.2E-02*	1.4E-01	4.9E-02	48.9
SS-BI-8 min-2	nd	nd	5.9E-02	1.5E-02	8.3E-02	nd	*2.0E-02*	*1.5E-02*	*1.5E-02*	*5.1E-03*	1.6E-01	5.5E-02	48.4
SS-BI-15 min	nd	nd	7.4E-02	4.0E-02	3.2E-01	1.2E-02	*1.9E-02*	1.8E-02	4.9E-02	3.5E-02	4.3E-01	1.3E-01	52.7

Notes: Italicized values in gray were above blank values, but too low to quantify accurately. nd = not detected.

† Charge balance calculated as ((Cations-Anions)/(Cations + Anions)) × 100

* Reservoir pad only damp

** Reservoir pad only partially saturated

SaltSmart™ wick appears to have only partially contacted the canister surface (~1/3 of the pad).

Table 11. Measured Chloride concentrations, in mg/m^2, on the Hope Creek Canister Surfaces.

Sample #	Loc.	Depth, ft	Temp., ºF	Cl^-, mg/m^2
144-008	Side	13.0	93.2	3.0
144-009	Side	7.5	116.5	2.9
144-010	Side	1.0	133.9	3.9
144-013	Top	0.0	138	14
144-014	Top	0.0	141.2	60
144-003	G.S.	—	—	*1.6*
144-004	G.S.	—	—	2.5
145-006*#	Side	13.0	70.6	7.3
145-007	Side	7.5	100.8	7.1
145-014	Side	1.0	130.3	4.1
145-013**	Top	0.0	174.1	7.5
145-011*	Blank	—	—	*2.5*
145-002	G.S.	—	—	*2.2*
SS-Bl-8 min-1	—	—	—	*1.2*
SS-Bl-8 min-2	—	—	—	*2.3*
SS-Bl-15 min	—	—	—	*2.2*

Notes: Italicized values in gray were above blank values, but too low to quantify accurately.

* Reservoir pad only damp
** Reservoir pad only partially saturated
# SaltSmart™ wick appears to have only partially contacted the canister surface (~1/3 of the pad).

3.3.1.2 Dry Pad Samples

Twelve dry pad samples were delivered to Sandia from the two canisters at Hope Creek, and three pad blanks. Two empty sample vials were also supplied as blanks. The amounts of each ionic species present in µg per sample are given in Table 12. Values in micro-equivalents (µEq) are provided in Table 13, along with the calculated charge balance errors.

As shown in Table 12, large quantities of Na^+, SO_4^{2-}, and PO_4^{3-} leach from the pad matrix, making quantification of these elements in any adhering dust impossible. Leachable amounts of each of these species are in the hundreds of micrograms per sample. If the concentrations of these species are entirely due to leaching from the pads, then the concentration of each should vary with the mass of the pad sample. While each of these species shows a strong trend with pad mass, there is significant scatter. The scatter could be due to contributions from dust, but is more likely due to variations in the pad matrix as discussed in Section 3.2. To address this, rather than plotting species concentrations against mass, it is more useful to plot them against PO_4^{3-}, a species that is unlikely to be present in the dust in any significant quantities (unlike Na^+ and SO_4^{2-}). These plots are shown in Figure 46. If the species is dominantly from the pad, then the blanks and samples should form a linear trend versus PO_4^{3-}, intersecting the origin of the plot. If the species is in the dust, or has a significant contribution from the dust, then it will not show a clear linear trend. There will still be a general increase in species concentration with PO_4^{3-}, however, because the larger sample pads were used on the canister tops and were more heavily loaded with dust. Examining the graphs, it is clear that, in addition to Na^+, SO_4^{2-}, and PO_4^{3-}, NH_4^+ is also leaching from the pads, and for all four of these, any contribution from the dust is negligible. K^+ and Mg^{2+} display weak trends, and may be partially derived from the pad. Other species such as Ca^{2+}, Cl^-, and NO_3^-, show no trend; these must be largely sourced to the dust.

Charge balance errors for the dry pad soluble salt analyses are generally less than a few percent, reflecting the high concentrations of the pad leachates, which reduce analytical uncertainty. Moreover, carbonate in the dust cannot contribute significantly to the total, so the lack of carbonate analyses has no effect on the charge balance.

Given the limitation in the data, the dry pad samples offer little additional information than the SaltSmart™ sensors. The soluble components from the pads appear to be less Ca-rich and NO_3-rich than the material extracted from the SaltSmart™ sensors, and possibly contain slightly more Cl^-. However, given the small amounts of dust-derived material extracted from the pads, and the large amount of material leaching from the pads, even these qualitative statements must be viewed with caution.

Table 12. Ion Concentrations in the Hope Creek Dry Pad Samples (µg/sample).

Sample #	Loc.	Depth, ft	Temp., ºF	Pad wt., g	Na	K	Ca	Mg	NH_4^+	F^-	Cl^-	NO_3^-	PO_4^{3-}	SO_4^{2-}	SUM
144-005	Side	13.0	84.1	0.2879	339	6.5	0.20	0.80	12.7	*0.08*	5.3	5.5	384	111	865
144-006	Side	8.5	89.6	0.2990	302	5.5	0.27	0.76	12.3	*0.04*	5.3	4.8	304	89	723
144-007	Side	1.0	126.4	0.3373	316	5.1	*0.18*	0.71	12.0	*0.03*	5.0	5.5	365	107	816
144-011	Top	0.0	132.6	0.5146	544	11.8	1.6	2.3	20.9	*0.06*	8.7	10.9	573	178	1352
144-012	Top	0.0	141.2	0.4086	422	7.0	1.5	1.9	16.2	*0.09*	6.5	4.2	503	145	1107
144-001	G.S.	—	—	0.3083	317	6.7	0.54	0.99	13.2	*0.05*	8.6	12.2	400	121	880
144-002	G.S.	—	—	0.3419	324	5.7	0.72	0.80	11.8	—	—	—	—	—	—
145-003	Side	13.5	70.9	0.3349	344	5.8	0.22	0.87	14.2	*0.03*	4.3	5.7	429	124	927
145-004	Side	8.5	93.3	0.3454	356	5.9	0.22	1.05	14.3	*0.04*	7.8	6.7	435	123	950
145-005	Side	1.5	122.5	0.2985	332	6.3	0.24	0.87	12.9	*0.05*	5.1	9.3	379	116	861
145-012	Top	0.0	172.1	0.5769	582	11.4	1.1	2.5	23.2	*0.09*	7.8	8.4	712	221	1569
145-001	G.S.	—	—	0.3847	360	7.5	*0.17*	0.91	13.6	nd	6.0	5.8	448	129	971
Pad-Blank-1		—	—	0.3060	241	3.0	*0.12*	0.43	8.9	*0.04*	2.1	2.5	303	89	650
Pad-Blank-2	—	—	—	0.3447	269	2.7	*0.14*	0.62	9.9	*0.09*	2.3	1.3	355	103	744
Pad-Blank-3	—	—	—	0.3047	235	2.4	*0.07*	0.35	8.3	*0.06*	1.9	1.5	299	89	638
Vial-Blank-1	—	—	—	—	nd	nd	0.39	nd	0.26	*0.01*	0.29	0.65	nd	nd	1.6
Vial-Blank-2	—	—	—	—	nd	nd	0.24	nd	0.20	nd	0.44	1.3	nd	nd	2.2

Notes: Italicized values in gray were above blank values, but too low to quantify accurately. nd = not detected.

Table 13. Ion Concentrations in the Hope Creek Dry Pad Samples (µEq/sample).

Sample #	Na	K	Ca	Mg	NH_4^+	F^-	Cl^-	NO_3^-	PO_4^{3-}	SO_4^{2-}	SUM Cations	SUM Anions	Ch. Bal Error, %
144-005	1.5E+01	1.7E-01	1.0E-02	6.6E-02	7.0E-01	*4.0E-03*	1.5E-01	8.9E-02	1.2E+01	2.3E+00	1.6E+01	1.5E+01	3.3
144-006	1.3E+01	1.4E-01	1.3E-02	6.2E-02	6.8E-01	*1.9E-03*	1.5E-01	7.7E-02	9.6E+00	1.8E+00	1.4E+01	1.2E+01	9.1
144-007	1.4E+01	1.3E-01	*8.9E-03*	5.8E-02	6.7E-01	*1.8E-03*	1.4E-01	8.9E-02	1.2E+01	2.2E+00	1.5E+01	1.4E+01	2.1
144-011	2.4E+01	3.0E-01	7.8E-02	1.9E-01	1.2E+00	*3.2E-03*	2.5E-01	1.8E-01	1.8E+01	3.7E+00	2.5E+01	2.2E+01	6.6
144-012	1.8E+01	1.8E-01	7.4E-02	1.6E-01	9.0E-01	*4.6E-03*	1.8E-01	6.8E-02	1.6E+01	3.0E+00	2.0E+01	1.9E+01	1.2
144-001	1.4E+01	1.7E-01	2.7E-02	8.1E-02	7.3E-01	*2.6E-03*	2.4E-01	2.0E-01	1.3E+01	2.5E+00	1.5E+01	1.6E+01	-2.6
144-002	1.4E+01	1.4E-01	3.6E-02	6.6E-02	6.5E-01	nd	nd	nd	nd	nd	1.5E+01	—	—
145-003	1.5E+01	1.5E-01	1.1E-02	7.1E-02	7.9E-01	*1.6E-03*	1.2E-01	9.3E-02	1.4E+01	2.6E+00	1.6E+01	1.6E+01	-1.2
145-004	1.5E+01	1.5E-01	1.1E-02	8.6E-02	7.9E-01	*2.4E-03*	2.2E-01	1.1E-01	1.4E+01	2.6E+00	1.7E+01	1.7E+01	-0.4
145-005	1.4E+01	1.6E-01	1.2E-02	7.1E-02	7.2E-01	*2.7E-03*	1.4E-01	1.5E-01	1.2E+01	2.4E+00	1.5E+01	1.5E+01	2.4
145-012	2.5E+01	2.9E-01	5.7E-02	2.1E-01	1.3E+00	*4.7E-03*	2.2E-01	1.3E-01	2.2E+01	4.6E+00	2.7E+01	2.7E+01	-0.6
145-001	1.6E+01	1.9E-01	*8.3E-03*	7.5E-02	7.5E-01	nd	1.7E-01	9.4E-02	1.4E+01	2.7E+00	1.7E+01	1.7E+01	-1.1
Pad-Blank-1	1.0E+01	7.7E-02	*6.0E-03*	3.6E-02	4.9E-01	*1.9E-03*	6.0E-02	4.1E-02	9.6E+00	1.8E+00	1.1E+01	1.2E+01	-1.9
Pad-Blank-2	1.2E+01	6.9E-02	*6.7E-03*	5.1E-02	5.5E-01	*4.5E-03*	6.4E-02	2.1E-02	1.1E+01	2.1E+00	1.2E+01	1.3E+01	-4.1
Pad-Blank-3	1.0E+01	6.1E-02	*3.6E-03*	2.9E-02	4.6E-01	*3.1E-03*	5.4E-02	2.4E-02	9.4E+00	1.9E+00	1.1E+01	1.1E+01	-2.7

Notes: Italicized values in gray were above blank values, but too low to quantify accurately. nd = not detected.

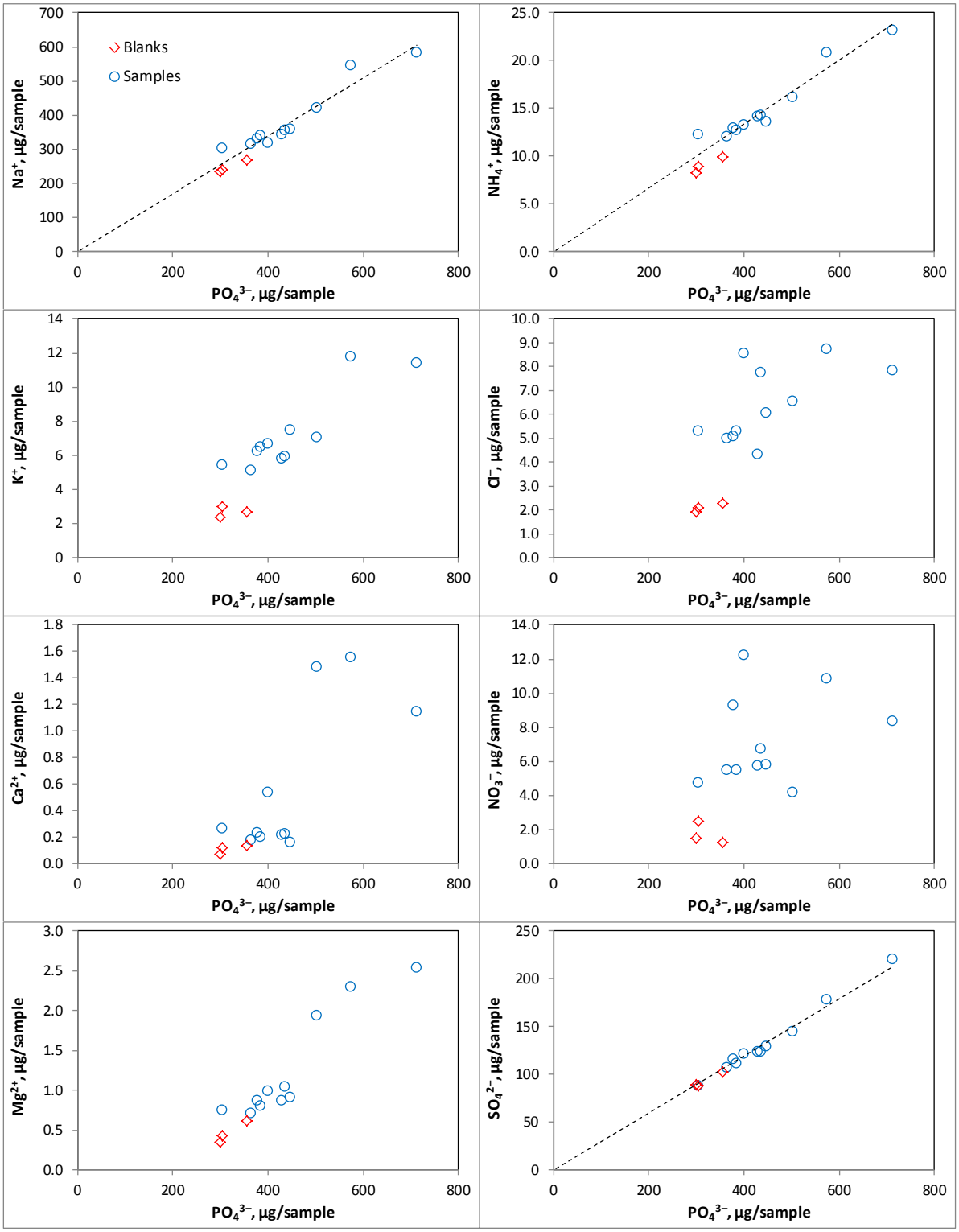

Figure 46. Plots of soluble species concentration versus PO_4^{3-} concentration for the Hope Creek dry pad samples.

3.3.2. Diablo Canyon Samples

3.3.2.1 SaltSmarts™

Nine SaltSmart™ sensors were analyzed from the Diablo Canyon site, representing three samples each from the sides of the two containers sampled, and three samples of unknown provenance. These canisters were much hotter than the Hope Creek canisters, exceeding the stated operating temperature of the SaltSmart™ sensors (90ºC) in many areas. For this reason, no SaltSmart™ samples were taken from the canister tops, and only a limited portion of the canister sides was sampled. However, as noted previously (Section 2.1), the actual temperature limit for the SaltSmart™ sensors is ~80ºC. Above that temperature, the wicks adhered to the silicone pressure pads behind them, and the reservoir pads inside the sensors were only moist, instead of saturated. It is not clear that the sensors extracted all of the salts from the waste package surface at temperatures above 80ºC, and the results shown here may be underestimates of the salt load on the canister surface.

The amounts of each ionic species present in µg per sample are given in Table 14. Values in micro-equivalents (µEq) are provided in Table 15, along with the calculated charge balance errors. For the samples from the canister sides, the total salt loads were extremely light (<25 µg), in some cases within the range of the blanks. This is not inconsistent with the SEM observations of the pads used for side sampling, but it may also be in part due to poor extraction efficiency at elevated temperatures, as discussed above.

For all of the canister samples, the mass of NO_3^- present exceeded that of Cl^-, and in most cases, Ca^{2+} was more abundant than Na^+. This seems inconsistent with the SEM data, which show abundant sea salt aggregates on the packages (Section 3.2.3); however, for the samples from MPC-123, at least, nitrate was commonly observed on the canister sides, and chloride salts were relatively rare.

For the two samples collected from the gamma shields of the Diablo Canyon canisters, Na^+ was the most abundant cation by mass. Chloride was the most abundant anion on the gamma shield from storage system MPC-123, while nitrate was the most abundant on the gamma shield from system MPC-170. Both gamma shield samples are Ca-rich. This suggests that the dust on the gamma shields contains both sea salts (rich in Na^+, Cl^-, Mg^{2+}, and SO_4^{2-}), and continental salts (rich in NH_4^+, Ca^{2+}, NO_3^-, and SO_4^{2-}).

Also shown in Table 14 and Table 15 are six SaltSmart™ blanks produced at Sandia and run with the Diablo Canyon samples to assess if contact time has any effect on the blanks. The SaltSmart™ blanks were run at contact times of 6, 8, 10, 12, and 14 minutes, and one sample (Blank-8(2)) was aged for 1 week after use and prior to disassembly and analysis, to see if additional materials would leach from the SaltSmart™ components over time. The blanks were all low and showed no compositional trends with contact time or with aging.

As with the Hope Creek SaltSmart™ data, the charge balances for the Diablo Canyon SaltSmart™ samples are poor, and consistently show a deficiency of anions. Once again, this is likely due to the presence of carbonate in the dust, since it was a common phase observed by

SEM. As noted for the Hope Creek samples, another potential contributing factor might be ammonia.

Table 16 shows the measured chloride surface loads, in mg/m^2. In most cases, the measured chloride loads were $<5\ mg/m^2$, in the range of the blanks. Only the samples from the gamma shields, which were collected at ambient temperatures after removal of the shield, showed a significant chloride load. The SEM analyses indicated that the dust loads on the dry pads from the Diablo Canyon canister sides were very light, so it is possible that these low values are correct. However, sea-salt aggregates were abundant in the small amount of dust that was present (Section 3.2.3), and it such a small chloride load seems unreasonable. Given the potential issues with the SaltSmart™ sensors at the elevated temperatures of the canister surface (generally >80ºC), the measured salt and chloride loads for the Diablo Canyon samples must be considered questionable.

Table 14. Ion Concentrations in the Diablo Canyon SaltSmart™ Samples (µg/sample).

Sample #	Loc.	Depth, ft	Temp., ºF	Na	K	Ca	Mg	NH_4^+	F^-	Cl^-	NO_3^-	PO_4^{3-}	SO_4^{2-}	SUM, µg
123-003	Side	14.0	119.7	0.30	0.76	2.9	0.73	2.5	0.40	1.4	1.8	*0.51*	5.1	16.4
123-004	Side	11.5	173.4	0.29	1.4	3.2	0.46	1.9	*0.17*	1.1	4.5	*0.15*	2.6	15.8
123-005*	Side	10.5	187.0	nd	0.33	4.5	0.30	1.7	0.35	0.59	0.7	*0.58*	1.7	10.7
123-002	G.S.	—	—	17.7	1.1	7.4	1.1	2.4	1.2	17.4	13.9	nd	12.8	75
123-010	Blank	—	—	4.0	2.3	2.7	0.59	2.8	1.2	7.5	1.6	1.03	2.0	26
170-007*	Side	10.5	177.5	1.2	0.43	2.5	0.31	1.4	0.32	1.3	2.4	nd	1.7	11.6
170-008*	Side	9.5	182.8	0.23	0.62	2.9	0.26	1.8	0.40	0.87	2.8	0.77	0.70	11.4
170-009*	Side	9.0	188.2	0.33	2.8	4.0	0.25	1.3	0.30	0.76	11.5	0.72	1.1	23
170-002	G.S..	—	—	9.0	1.6	7.3	1.6	2.6	*0.27*	4.0	26	0.98	7.6	61
Blank-6	—	—	—	0.88	1.2	2.2	0.23	1.4	*0.10*	1.3	3.9	0.87	0.45	12.5
Blank-8(1)	—	—	—	nd	0.23	1.2	0.15	1.4	0.53	0.42	*0.29*	*0.34*	*0.26*	4.8
Blank-10	—	—	—	*0.01*	0.35	1.5	0.21	1.1	0.38	0.68	2.3	0.97	0.35	7.8
Blank-12	—	—	—	0.33	1.0	1.3	0.19	1.2	*0.26*	1.2	2.2	0.91	0.33	8.9
Blank-14	—	—	—	nd	*0.14*	1.1	0.16	1.2	0.32	0.44	0.92	1.29	*0.23*	5.8
Blank-8(2)	—	—	—	nd	0.26	1.4	0.27	1.0	0.38	0.39	1.3	nd	0.52	5.5

Notes: Italicized values in gray were above blank values, but too low to quantify accurately. nd = not detected.

* Wick adhered to the silicone pressure pad, and reservoir pad only partially saturated

Table 15. Ion Concentrations in the Diablo Canyon SaltSmart™ Samples (µEq/sample).

Sample #	Na	K	Ca	Mg	NH_4^+	F^-	Cl^-	NO_3^-	PO_4^{3-}	SO_4^{2-}	Sum, Cation	Sum Anion	Chrg. Bal. Error, %†
123-003	1.3E-02	2.0E-02	1.4E-01	6.0E-02	1.4E-01	2.1E-02	4.0E-02	2.9E-02	*1.6E-02*	1.1E-01	3.7E-01	2.1E-01	27.3
123-004	1.3E-02	3.6E-02	1.6E-01	3.8E-02	1.1E-01	*9.2E-03*	3.1E-02	7.3E-02	*4.7E-03*	5.3E-02	3.5E-01	1.7E-01	34.8
123-005*	nd	8.4E-03	2.2E-01	2.5E-02	9.5E-02	1.9E-02	1.7E-02	1.1E-02	*1.8E-02*	3.5E-02	3.5E-01	1.0E-01	55.6
123-002	7.7E-01	2.7E-02	3.7E-01	8.6E-02	1.3E-01	6.1E-02	4.9E-01	2.2E-01	nd	2.7E-01	1.4E+00	1.0E+00	14.1
123-010	1.8E-01	5.9E-02	1.4E-01	4.9E-02	1.5E-01	6.1E-02	2.1E-01	2.5E-02	3.3E-02	4.2E-02	5.7E-01	3.7E-01	21.1
170-007*	5.3E-02	1.1E-02	1.2E-01	2.6E-02	8.0E-02	1.7E-02	3.6E-02	3.8E-02	nd	3.6E-02	2.9E-01	1.3E-01	39.6
170-008*	9.8E-03	1.6E-02	1.4E-01	2.1E-02	1.0E-01	2.1E-02	2.4E-02	4.5E-02	2.4E-02	1.5E-02	2.9E-01	1.3E-01	38.8
170-009*	1.5E-02	7.1E-02	2.0E-01	2.1E-02	7.0E-02	1.6E-02	2.2E-02	1.9E-01	2.3E-02	2.3E-02	3.8E-01	2.7E-01	16.6
170-002	3.9E-01	4.2E-02	3.6E-01	1.3E-01	1.4E-01	*1.4E-02*	1.1E-01	4.2E-01	3.1E-02	1.6E-01	1.1E+00	7.3E-01	18.9
Blank-6	3.8E-02	3.0E-02	1.1E-01	1.9E-02	7.8E-02	*5.2E-03*	3.5E-02	6.3E-02	2.8E-02	9.3E-03	2.8E-01	1.4E-01	32.4
Blank-8(1)	nd	5.9E-03	5.8E-02	1.2E-02	7.8E-02	2.8E-02	1.2E-02	*4.7E-03*	*1.1E-02*	*5.4E-03*	1.5E-01	6.1E-02	43.6
Blank-10	*5.6E-04*	8.9E-03	7.6E-02	1.7E-02	6.1E-02	2.0E-02	1.9E-02	3.6E-02	3.1E-02	7.3E-03	1.6E-01	1.1E-01	18.0
Blank-12	1.4E-02	2.6E-02	6.6E-02	1.6E-02	6.9E-02	*1.4E-02*	3.3E-02	3.5E-02	2.9E-02	6.8E-03	1.9E-01	1.2E-01	24.2
Blank-14	nd	*3.6E-03*	5.5E-02	1.3E-02	6.6E-02	1.7E-02	1.3E-02	1.5E-02	4.1E-02	*4.8E-03*	1.4E-01	9.0E-02	21.1
Blank-8(2)	nd	6.6E-03	7.2E-02	2.2E-02	5.7E-02	2.0E-02	1.1E-02	2.0E-02	nd	1.1E-02	1.6E-01	6.2E-02	43.7

Notes: Italicized values in gray were above blank values, but too low to quantify accurately. nd = not detected.

* Wick adhered to the silicone pressure pad, and reservoir pad only partially saturated

Table 16. Measured Chloride concentrations, in mg/m^2, on the Diablo Canyon Canister Surfaces.

Sample #	Loc.	Depth, ft	Temp., ºF	Cl^-, mg/m^2
123-003	Side	14.0	119.7	4.8
123-004	Side	11.5	173.4	3.6
123-005*	Side	10.5	187.0	2.0
123-002	G.S.	—	—	58
123-010	Blank	—	—	25
170-007*	Side	10.5	177.5	4.2
170-008*	Side	9.5	182.8	2.9
170-009*	Side	9.0	188.2	2.5
170-002	G.S.	—	—	13
Blank-6	—	—	—	4.2
Blank-8(1)	—	—	—	1.4
Blank-10	—	—	—	2.3
Blank-12	—	—	—	3.8
Blank-14	—	—	—	1.5
Blank-8(2)	—	—	—	1.3

Notes: Italicized values in gray were above blank values, but too low to quantify accurately.

* Wick adhered to the silicone pressure pad, and reservoir pad only partially saturated

3.3.2.1 Dry Pad Samples

Twelve dry pad samples were delivered to Sandia from the two canisters at Diablo Canyon. While the SaltSmart™ sampling was limited by high canister surface temperatures, the dry pads are not temperature-sensitive. Therefore, the entire vertical extents of the canister sides were sampled, and samples were taken from the canister tops as well. The compositions of the leachates for each sample, in µg per sample are given in Table 17. Values in µEq are provided in Table 18, along with the calculated charge balance errors.

As with the Hope Creek samples, the Diablo Canyon dry pad samples were affected by large quantities of Na^+, SO_4^{2-}, and PO_4^{3-} leaching from the pad matrix, making quantification of these elements in any adhering dust impossible. Once again, we can plot each species against the concentration of PO_4^{3-} to assess whether there is any significant contribution from the dust (Figure 47). The species Na^+, SO_4^{2-}, and PO_4^{3-}, and NH_4^+ are clearly derived from the pad matrix, while K^+ and Mg^{2+} appear to be partially derived from the pad, but also to have a dust

contribution, especially at the higher concentrations; Cl^- and NO_3^- do not appear to have a contribution from the pads.

Although the soluble salts are strongly affected by the effect of leaching from the pads, it is clear that both Cl and NO_3^- are enriched in all the samples relative to the blanks, and must be present in significant amounts in the dust. Moreover, samples from the tops of the canisters (the three points falling well above the trends in Figure 47) show the greatest enrichment in these species, reflecting the higher dust load on these samples. Ca, Mg, and K are also significantly enriched in the canister top samples, falling above the trends in Figure 47. Because sea-salts were commonly observed in the SEM analyses, we can infer that some fraction of the Na and SO_4 concentrations is also from the dust; however, any dust contribution to these species is insignificant relative to that of the pads, and these samples do not deviate significantly from the trend defined by the pad releases.

The soluble salt data from the pads confirm that chloride-rich salts are present on the canister surfaces, but cannot be used to quantify the amount of chloride present, because the efficiency of the pads with respect to dust collection is not known.

As with the Hope Creek samples, charge balance errors for the leachate analyses from the dry pad samples are generally less than a few percent, reflecting the high concentrations of the pad leachates, which reduce analytical uncertainty. Moreover, dust components comprise too small a fraction of the total ion load to affect the charge balance, even if unmeasured species such as carbonate are present in the dust.

Table 17. Ion Concentrations in the Diablo Canyon Dry Pad Samples (µg/sample).

Sample #	Loc.	Depth, ft	Temp., ºF	Pad wt., g	Na	K	Ca	Mg	NH_4^+	F^-	Cl^-	NO_3^-	PO_4^{3-}	SO_4^{2-}	SUM, µg
123-006	Side	11.0	177.2	0.4151	439	7.7	0.2	1.3	18.2	0.19	9.4	9.3	535	158	1179
123-008	Side	7.5	211.7	0.4837	519	8.8	0.3	1.4	22	0.18	10.4	9.1	619	171	1362
123-009	Side	3.0	245.5	0.5119	518	8.6	0.7	1.8	22	0.18	12.9	9.4	656	172	1401
123-011	Top	0.0	206.8	0.6222	676	13.7	1.9	4.0	24	0.18	74	21.5	732	236	1784
123-012	Top	0.0	204.0	0.5798	638	15.3	1.3	3.3	24	0.16	79	17.4	693	217	1690
123-001	G.S.	—	—	0.4765	485	7.5	0.2	1.3	19.5	0.14	16.7	11.3	579	173	1294
123-007	Blank	—	—	0.4518	478	9.0	0.2	1.4	20	0.16	11.4	9.1	581	168	1278
170-004	Side	11.0	153.9	0.4497	492	8.5	*0.2*	1.1	21	0.22	10.3	6.1	583	168	1291
170-005	Side	7.5	193.8	0.5594	616	9.9	0.5	2.2	26	0.26	8.2	7.9	754	225	1651
170-006	Side	3.0	180.6	0.5305	596	9.2	0.3	2.1	26	0.23	5.7	6.3	nd	202	849
170-003	Top	0.0	187.6	0.6155	710	12.7	0.8	3.5	29	0.22	67	11.5	818	253	1907
170-001	G.S.	—	—	0.5760	597	10.2	0.4	2.1	24	0.15	9.1	29.1	716	205	1594
Pad-Blank-1	—	—	—	0.3060	241	3.0	*0.12*	0.43	8.9	*0.04*	2.1	2.5	303	89	650
Pad-Blank-2	—	—	—	0.3447	269	2.7	*0.14*	0.62	9.9	*0.09*	2.3	1.3	355	103	744
Pad-Blank-3	—	—	—	0.3047	235	2.4	*0.07*	0.35	8.3	*0.06*	1.9	1.5	299	89	638

Notes: Italicized values in gray were above blank values, but too low to quantify accurately. nd = not detected.

Table 18. Ion Concentrations in the Diablo Canyon Dry Pad Samples (µEq/sample).

Sample #	Na	K	Ca	Mg	NH_4^+	F^-	Cl^-	NO_3^-	PO_4^{3-}	SO_4^{2-}	SUM Cations	SUM Anions	Ch. Bal Error, %
123-006	1.9E+01	2.0E-01	1.0E-02	1.1E-01	1.0E+00	1.0E-02	2.6E-01	1.5E-01	1.7E+01	3.3E+00	2.0E+01	2.1E+01	-0.4
123-008	2.3E+01	2.3E-01	1.3E-02	1.2E-01	1.2E+00	9.3E-03	2.9E-01	1.5E-01	2.0E+01	3.6E+00	2.4E+01	2.4E+01	1.1
123-009	2.3E+01	2.2E-01	3.5E-02	1.5E-01	1.2E+00	9.5E-03	3.6E-01	1.5E-01	2.1E+01	3.6E+00	2.4E+01	2.5E+01	-1.3
123-011	2.9E+01	3.5E-01	9.7E-02	3.3E-01	1.3E+00	9.2E-03	2.1E+00	3.5E-01	2.3E+01	4.9E+00	3.2E+01	3.0E+01	1.8
123-012	2.8E+01	3.9E-01	6.5E-02	2.7E-01	1.4E+00	8.5E-03	2.2E+00	2.8E-01	2.2E+01	4.5E+00	3.0E+01	2.9E+01	1.5
123-001	2.1E+01	1.9E-01	1.1E-02	1.0E-01	1.1E+00	7.4E-03	4.7E-01	1.8E-01	1.8E+01	3.6E+00	2.2E+01	2.3E+01	-0.2
123-007	2.1E+01	2.3E-01	1.1E-02	1.1E-01	1.1E+00	8.5E-03	3.2E-01	1.5E-01	1.8E+01	3.5E+00	2.2E+01	2.2E+01	-0.2
170-004	2.1E+01	2.2E-01	*7.5E-03*	9.1E-02	1.2E+00	1.2E-02	2.9E-01	9.9E-02	1.8E+01	3.5E+00	2.3E+01	2.2E+01	1.2
170-005	2.7E+01	2.5E-01	*2.3E-02*	1.8E-01	1.5E+00	1.3E-02	2.3E-01	1.3E-01	2.4E+01	4.7E+00	2.9E+01	2.9E+01	-0.3
170-006	2.6E+01	2.4E-01	*1.4E-02*	1.7E-01	1.4E+00	1.2E-02	1.6E-01	1.0E-01	na	4.2E+00	2.8E+01	—	—
170-003	3.1E+01	3.3E-01	3.9E-02	2.9E-01	1.6E+00	1.1E-02	1.9E+00	1.9E-01	2.6E+01	5.3E+00	3.3E+01	3.3E+01	0.0
170-001	2.6E+01	2.6E-01	1.9E-02	1.7E-01	1.3E+00	8.0E-03	2.6E-01	4.7E-01	2.3E+01	4.3E+00	2.8E+01	2.8E+01	0.2
Pad-Blank-1	1.0E+01	7.7E-02	*6.0E-03*	3.6E-02	4.9E-01	1.9E-03	6.0E-02	4.1E-02	9.6E+00	1.8E+00	1.1E+01	1.2E+01	-1.9
Pad-Blank-2	1.2E+01	6.9E-02	*6.7E-03*	5.1E-02	5.5E-01	4.5E-03	6.4E-02	2.1E-02	1.1E+01	2.1E+00	1.2E+01	1.3E+01	-4.1
Pad-Blank-3	1.0E+01	6.1E-02	*3.6E-03*	2.9E-02	4.6E-01	3.1E-03	5.4E-02	2.4E-02	9.4E+00	1.9E+00	1.1E+01	1.1E+01	-2.7

Notes: Italicized values in gray were above blank values, but too low to quantify accurately. na = not analyzed.

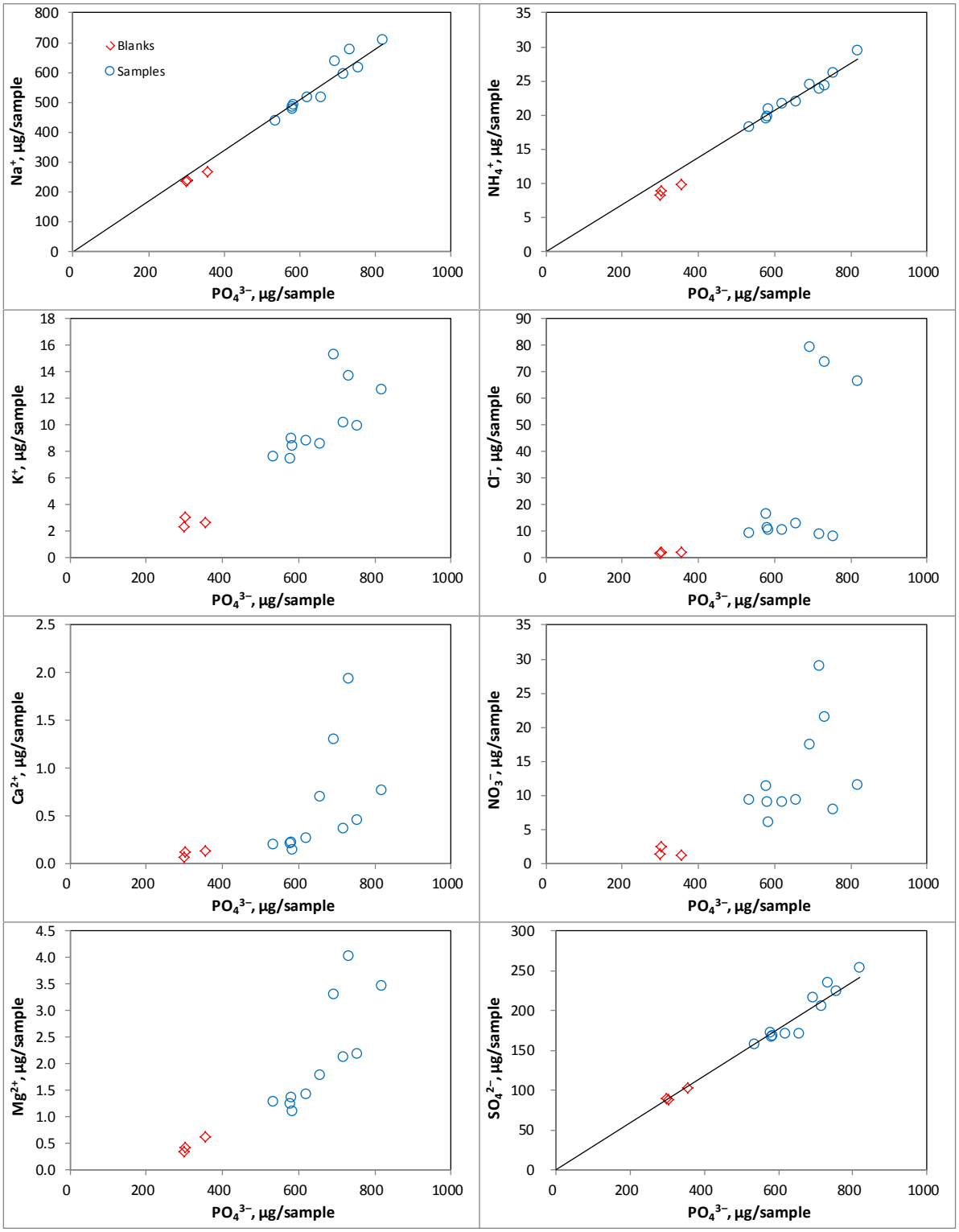

Figure 47. Plots of soluble species concentration versus PO_4^{3-} concentration for the Diablo Canyon dry pad samples.

4. CONCLUSIONS

As part of a program to characterize possible environments on the surface of spent nuclear fuel dry storage canisters, the Electric Power Research Institute has sampled dust on the surface of in-service storage canisters at three different near-marine Independent Spent Fuel Storage Installations. Following collection, the samples from the final two sites, the Hope Creek and Diablo Canyon ISFSIs, were sent to Sandia National Laboratories for chemical and mineralogical characterization.

Two canisters were sampled at each site, and two different types of samples were collected. First, SaltSmart™ sensors were used to sample the soluble salts on the canister surface. Ideally, the SaltSmart™ sensor samples provide, upon analysis, salt and chloride loads per unit surface area. Second, an abrasive sponge was brushed across the metal surface, dislodging and collecting dust. Although the dry pad samples do not allow quantification of the salt load per unit area, the collected dust was analyzed by SEM/EDS to provide mineralogy and textural information. Additional compositional information was gained by XRF analysis of the dust on the dry pads, and by leaching and analysis of soluble salts on the pads. These data complement that collected by the SaltSmart™ sensors.

Both methods had limitations. The SaltSmart™ wicks are widely used in industry, and quantitatively leach salts from the contacted surface at room temperature (Memo from C. Bryan to L. Zsidai dated Nov. 13, 2013; SAND#2013-9948P). However, their stated operational temperature limit of 90ºC limited their use on the hot Diablo Canyon canisters; moreover, their performance actually degraded at temperatures greater than ~80ºC, affecting most of the samples collected from the Diablo Canyon canisters. The dry sponge pads had no temperature limitations, and were used sample the entire surfaces of the canisters at both Hope Creek and Diablo Canyon. Although the dry pad samples were effective for providing dust mineralogical and textural information, the matrix of the pads leached many chemical species that are potentially in the dust (especially Na^+, SO_4^{2-}, PO_4^{3-}, and NH_4^+), limiting their use for determining soluble salt compositions.

Despite the limitations of the methods utilized, samples from the two sites were successfully characterized. At both sites, canister tops were much more heavily loaded with dust than canister sides, and terrestrially-derived silicate minerals, including quartz, feldspars, micas, and clays, comprise the largest fraction of the dust. Also significant at both sites were particles of iron and iron-chromium metals and oxides generated by the manufacturing process. Soluble salt phases were a minor component of the Hope Creek dusts, and were compositionally similar to inland salt aerosols, rich in calcium, sulfate, and nitrate. Chloride surface loads were very low, <8 mg/m^2 on the canister sides and ≤ 60 mg/m^2 on the canister tops. At Diablo Canyon, however, sea-salt aerosols, occurring as aggregates of NaCl and Mg-sulfate with trace amounts of K and Ca, were a major component of the dust samples. The sea-salt aerosols were 5-20 μm in diameter, and commonly occurred as hollow spheres, which may have formed by evaporation of suspended aerosol seawater droplets, possibly while rising through the heated annulus between the canister and the overpack. Although sea-salt aggregates were a significant component of the dusts on the Diablo Canyon canisters, measured chloride loads on the canister sides were very low (<5 mg/m^2). Damage to the sensors at the elevated sampling temperatures suggests that salt

recovery from the surface may not have been complete, so these results should be treated with caution; they may underestimate the actual salt loads at the areas sampled. Even if the measured salt loads at Diablo Canyon are accurate, they may not be bounding, because the heavily-loaded canister tops at Diablo Canyon were too hot to sample using the SaltSmart™ sensors.

An additional reason why the salt and chloride loads measured at both Hope Creek and Diablo Canyon may not be bounding is that the sampling was done through outlet vents; the sampled locations, extending downward for the outlet vents, were not proximal to inlet vents, where salts may preferentially be deposited.

The differences in salt composition and abundance for the two sites are attributed to differences in proximity to the open ocean and to wave action. The Diablo Canyon facility is on the shores of the Pacific Ocean, while the Hope Creek facility is on the shores of the Delaware River, several miles from the open ocean. Hence, the Hope Creek dusts have a much small component of coarse, wave-derived sea salt aerosols.

Finally, at Diablo Canyon, nitrate salts were found in the finest fraction of the surface dust, but on only one of the two sampled canisters. The nitrates occurred on the canister with the hottest surface temperatures. We conjecture that the hot surface temperatures prevented deliquescence of the salts and degassing of the nitrate as nitric acid. Alternatively, perhaps the presence of nitrates is tied to vent and wind directions, and differences in source direction; sampling was carried out on opposite sides of the two canisters evaluated at Diablo Canyon.

5. REFERENCES

Bryan C. and Enos D., 2013, *Memo to Laszlo Zsidai of Holtec International entitled: Analysis of SaltSmart™ Samples from Holtec Test Run"*, SAND2013-9948P, Sandia National Laboratories, Albuquerque, NM, November 2013.

Calvert Cliffs Nuclear Power Plant, 2012, *Response to Request for Additional Information, RE: Calvert Cliffs Independent Spent Fuel Storage Installation License Renewal Application (TAC No. L24475)*, ADAMS ML12212A216.

Calvert Cliffs Nuclear Power Plant, 2013, *Response to Request for Additional Information, RE: Calvert Cliffs Independent Spent Fuel Storage Installation License Renewal Application (TAC No. L24475)*, ADAMS ML13170A574.

Department of Energy (DOE), 2013, *Data Report on Corrosion Testing of Stainless Steel SNF Storage Canisters.* FCRD-UFD-2013-000324. Sandia National Laboratories, Albuquerque, NM.

APPENDIX A: SEM/EDS DATA

SEM/EDS data for the Hope Creek and Diablo Canyon dust samples are discussed in Section 3.0, and a subset of the results is presented. This appendix contains the complete suite of SEM/EDS analyses collected for these samples, allowing the reader to better evaluate the representativeness of the results provided in Section 3.0.

Blank

Map A

Notes: Low magnification SEM image/EDS map of the dry pad blank.

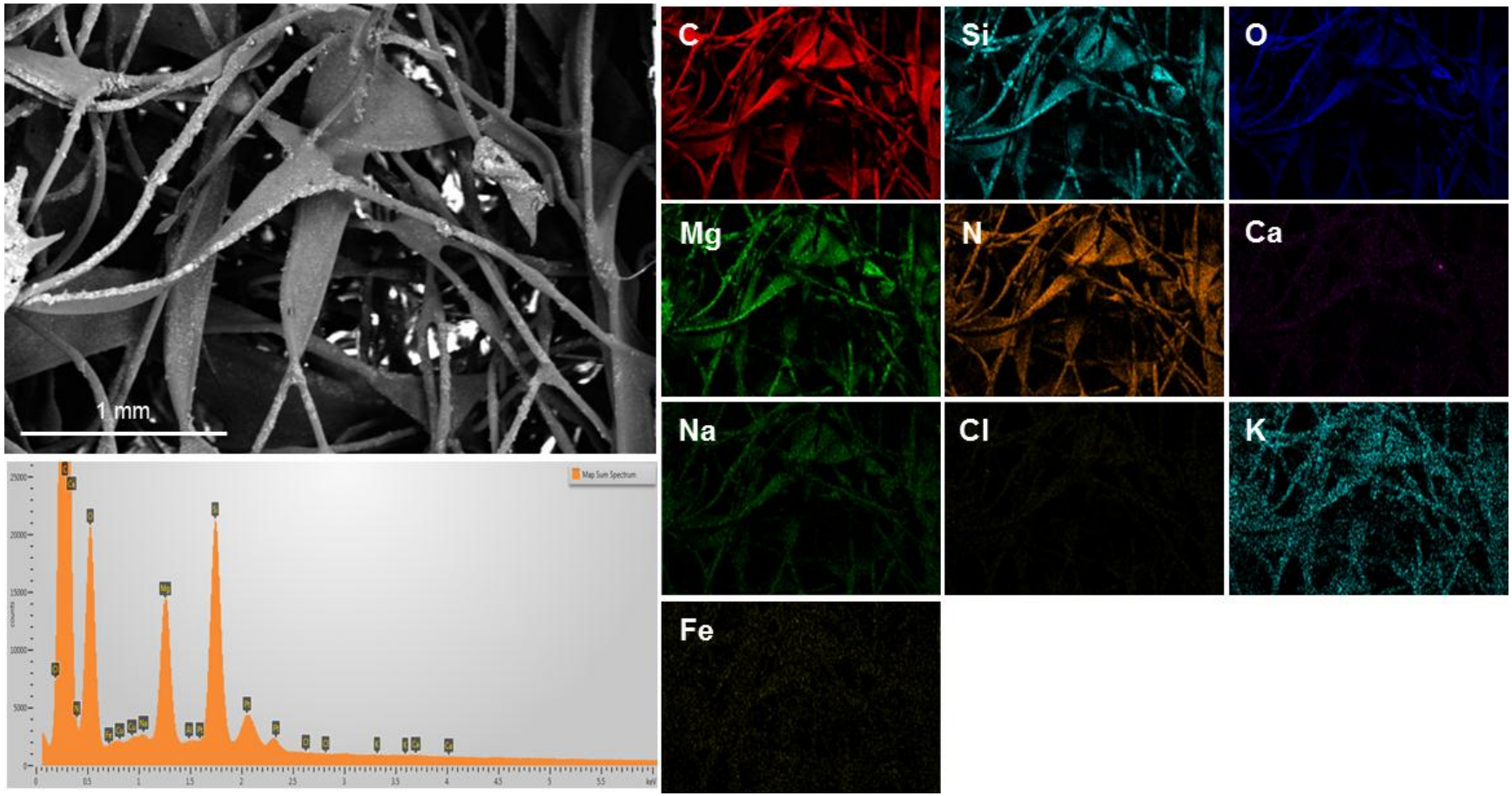

Blank

Map B

Notes: Magnified view of the blank pad, showing the matrix and the talc (magnesium silicate) filler.

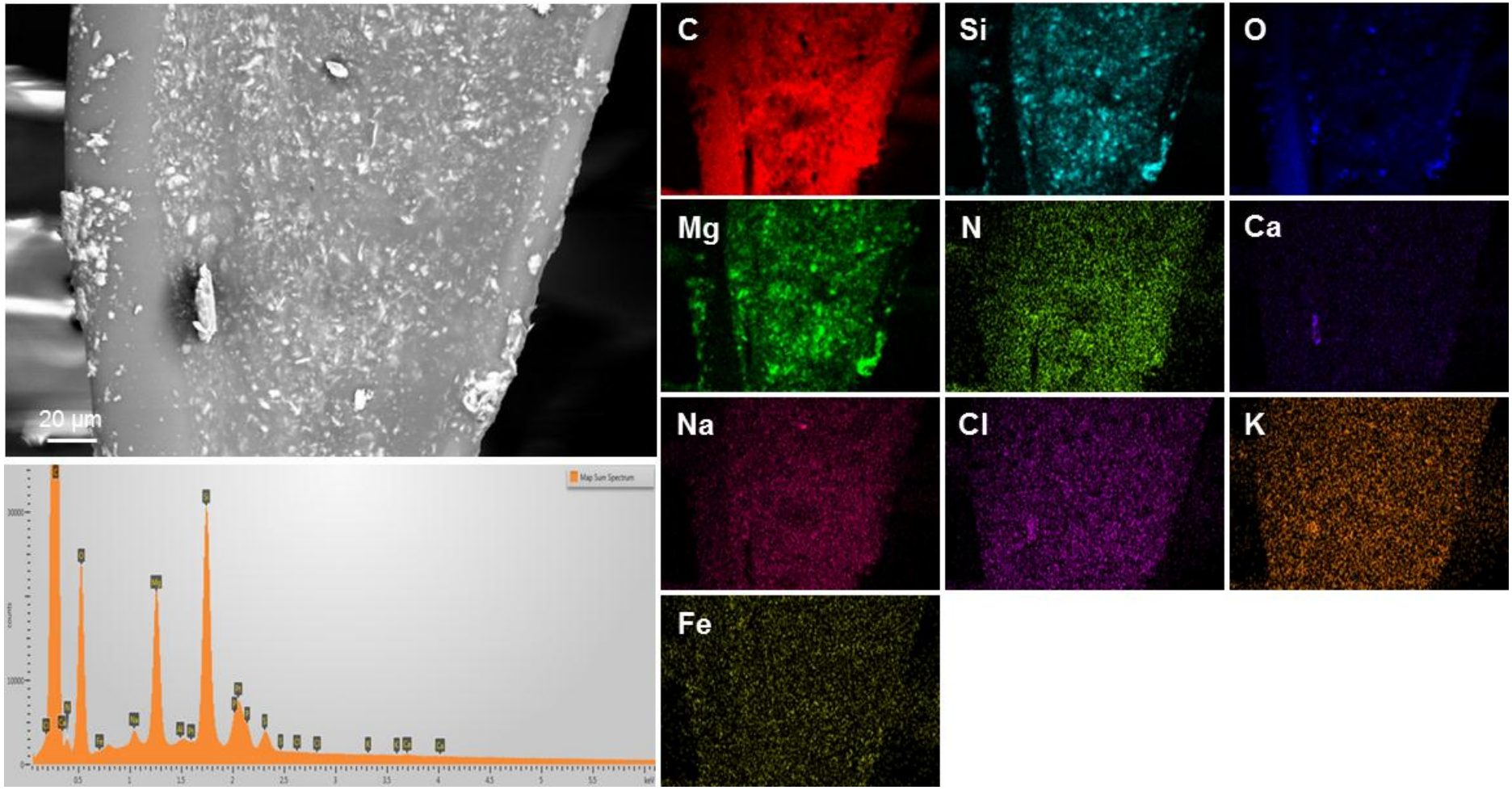

Sample: 144-005

Notes: Overview image of dry pad sample 144-005, showing the very light dust load.

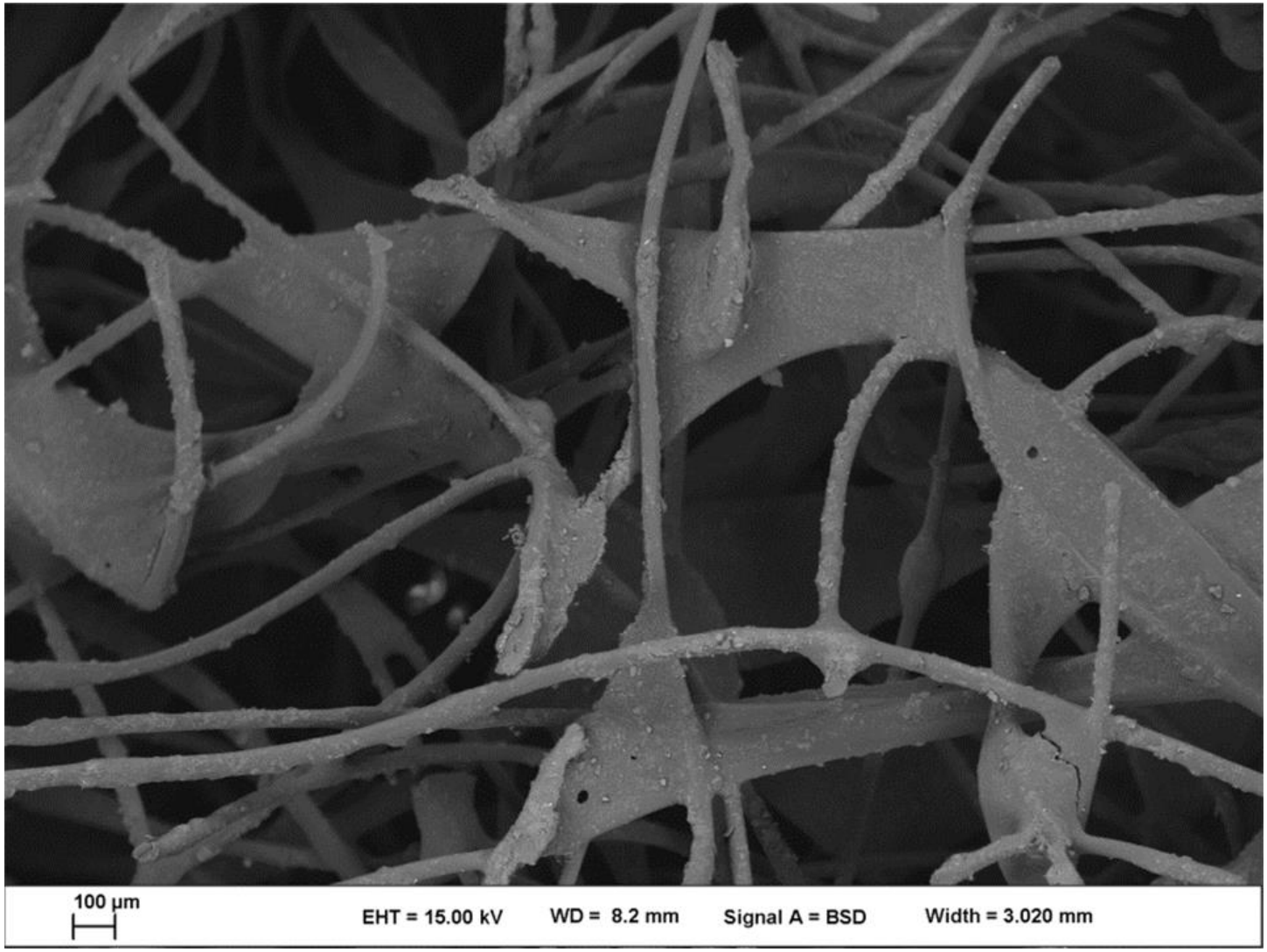

Sample: 144-005
Map A

Notes: Large aluminosilicate mineral grains.

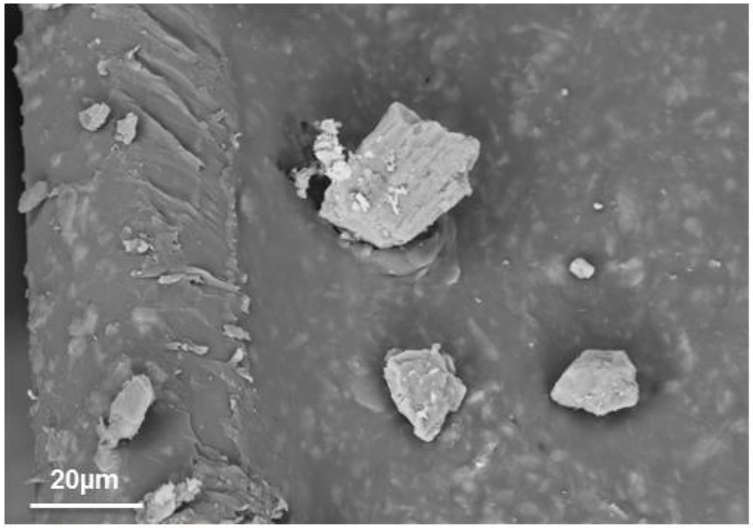

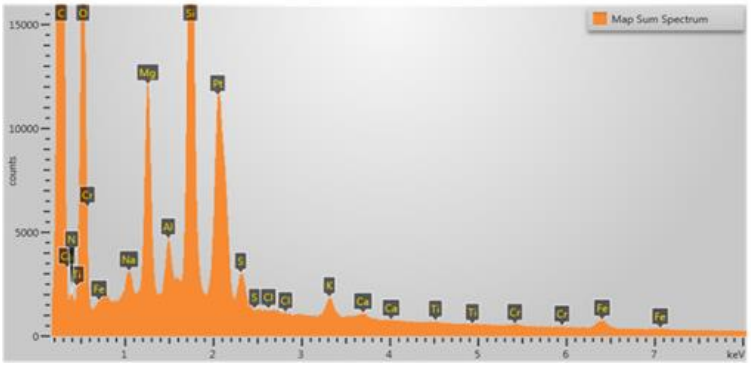

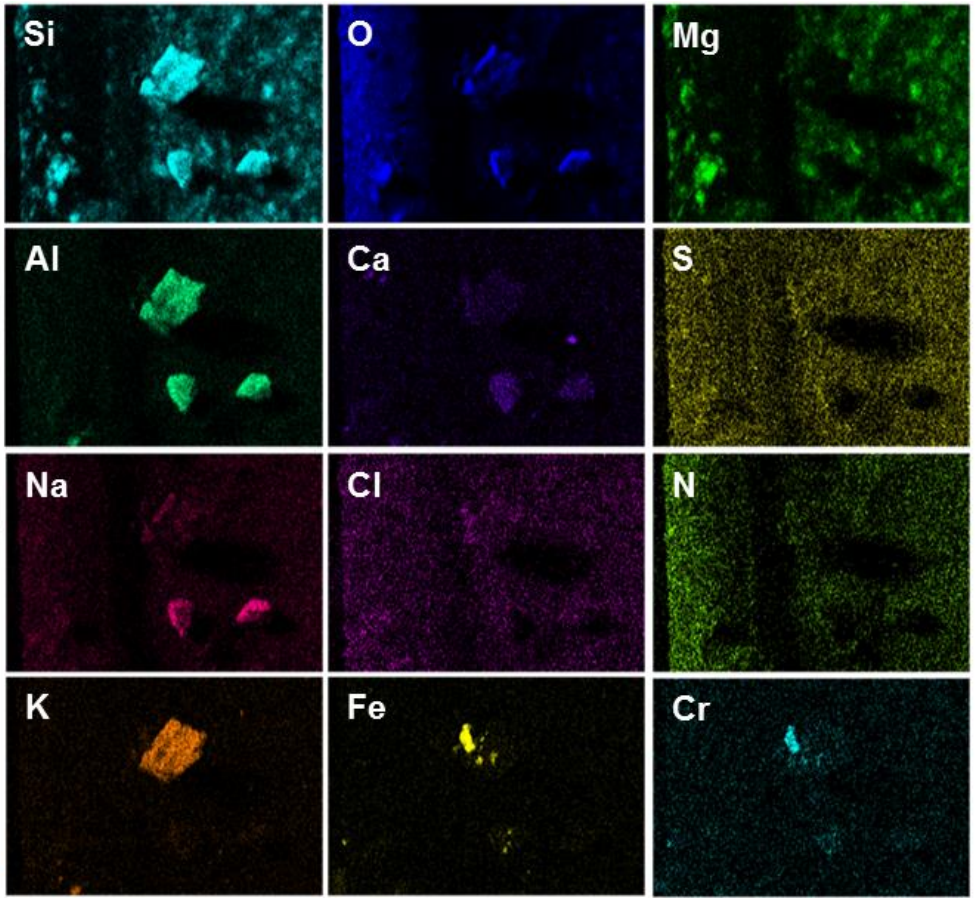

Sample: 144-005
Map B

Notes: This sample has a shadow across the middle of the image; light elements do not show up in this area. Despite this, it was used here because several chloride grains are visible in this image. Most fall within the shadow and do not appear on the Na map, but they appear to be NaCl. The lowermost chloride grain appears to be a spherical cluster of NaCl crystals.

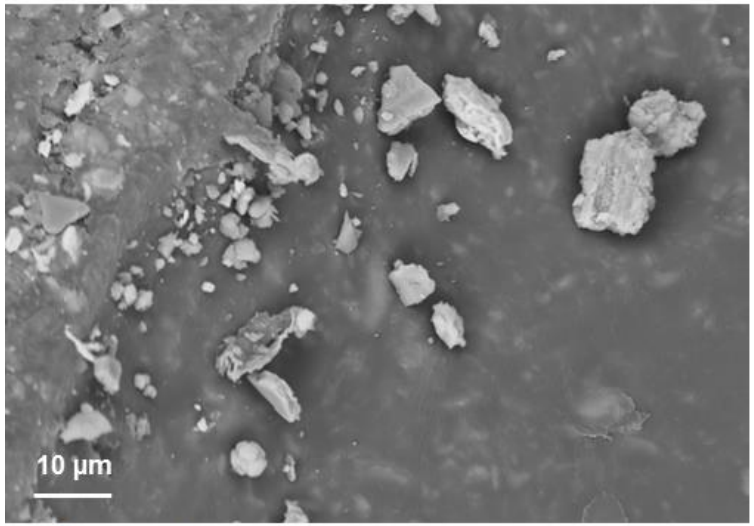

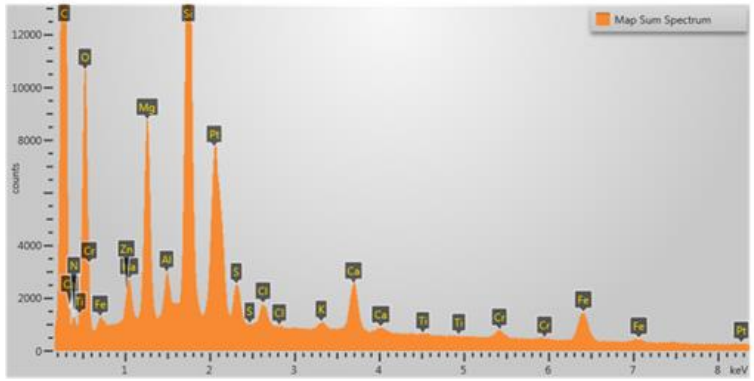

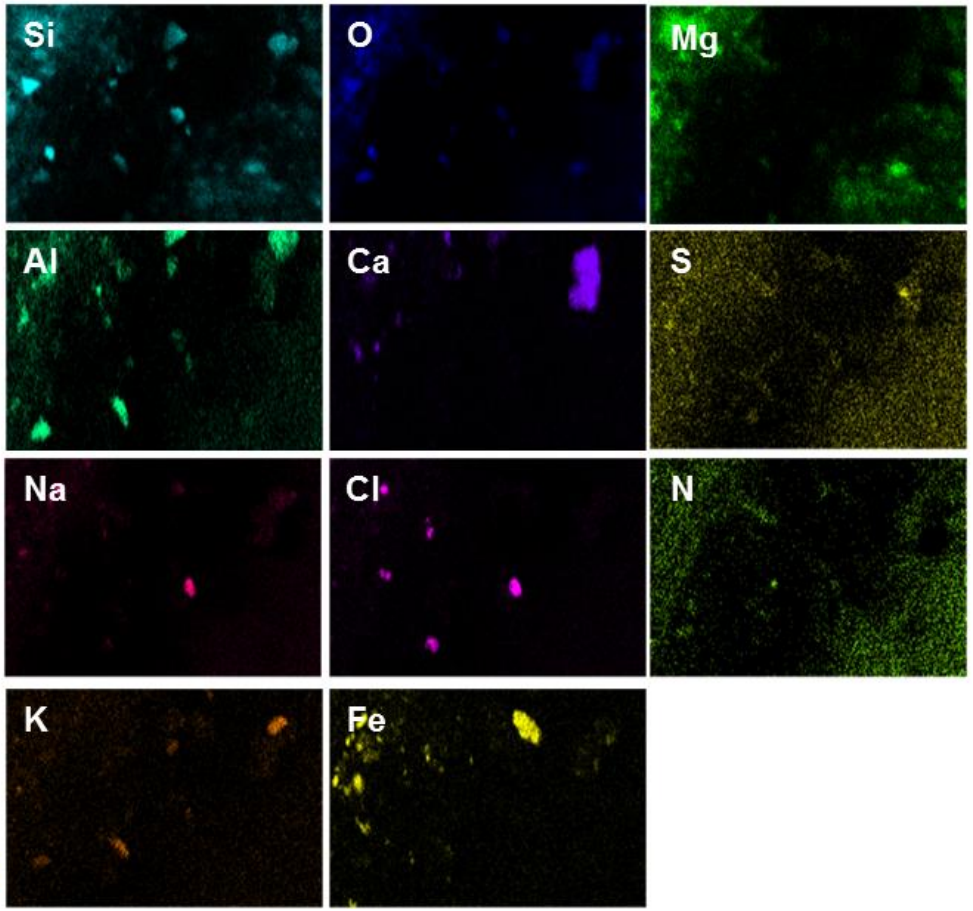

Sample: 144-005
Map C

Notes: Close-up of NaCl grain. The surface of the grain is heavily etched.

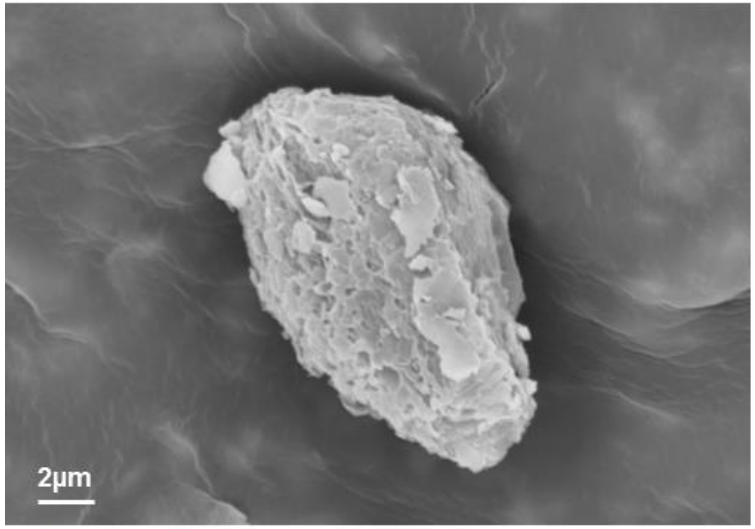

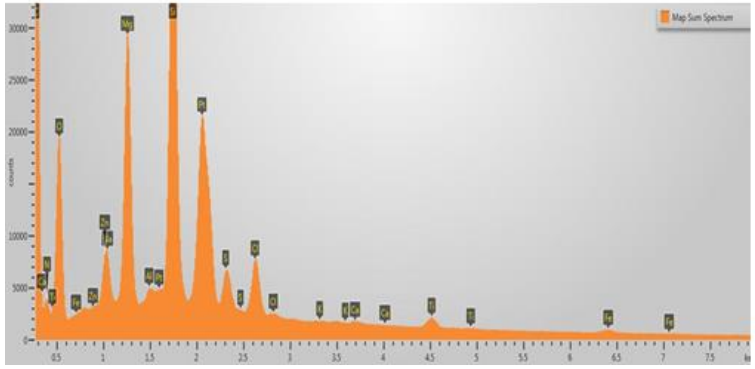

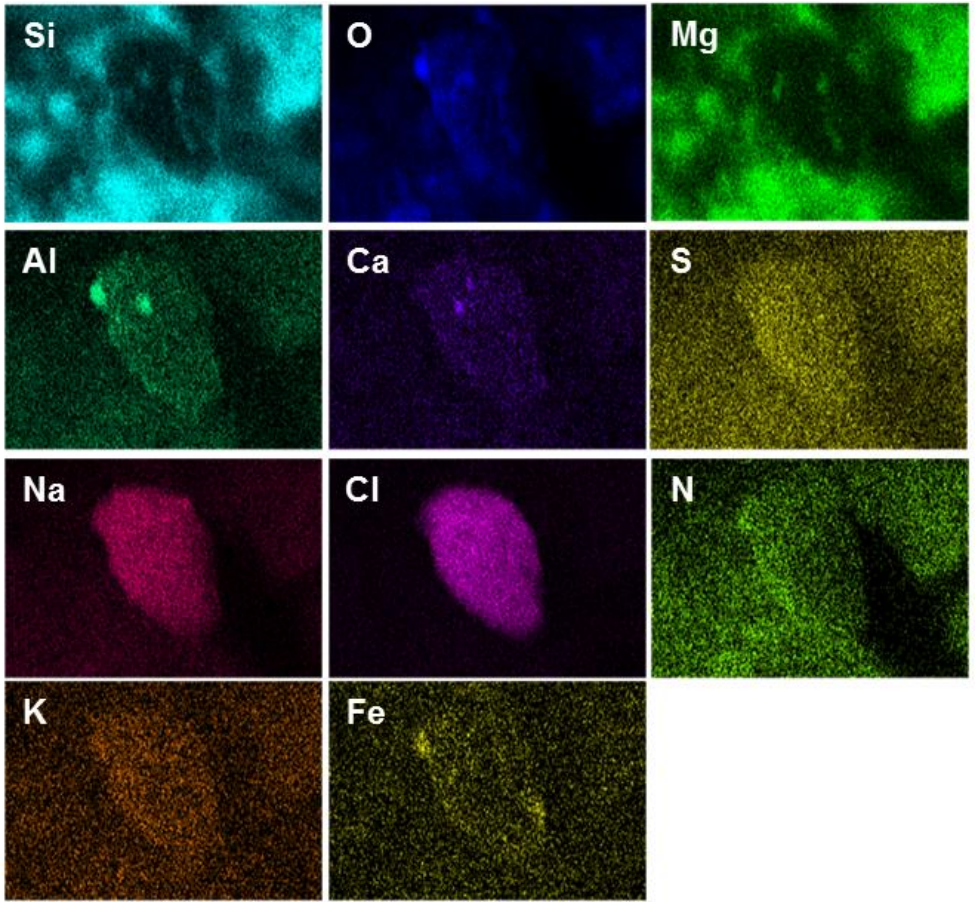

Sample: 144-011

Notes: Overview image of pad sample 144-011, showing the heavy dust load.

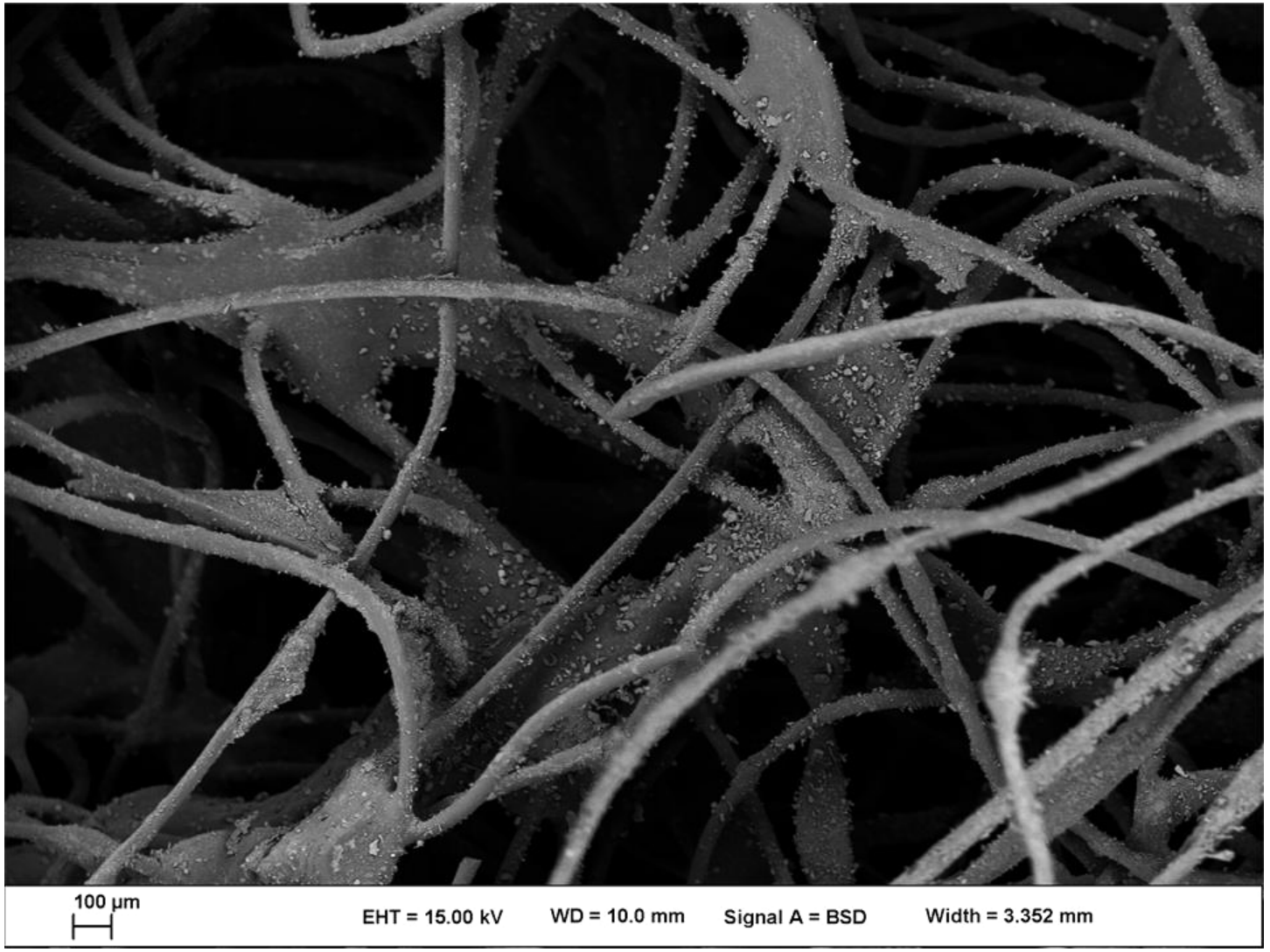

Sample: 144-011
Map A

Notes: Minerals are dominantly aluminosilicates, but note the Fe-oxide sphere in the center of the image, and the Na-Zn rich phase (carbonate?) in the lower center.

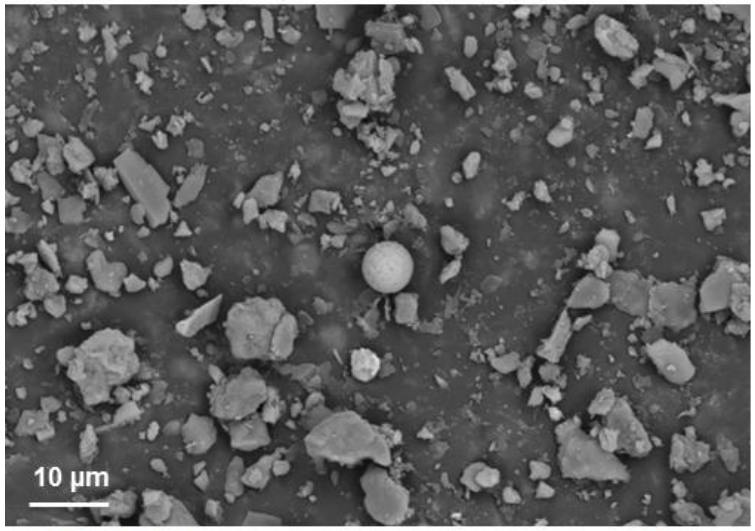

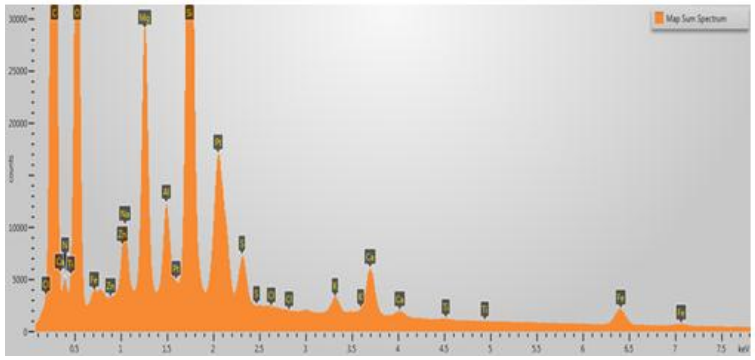

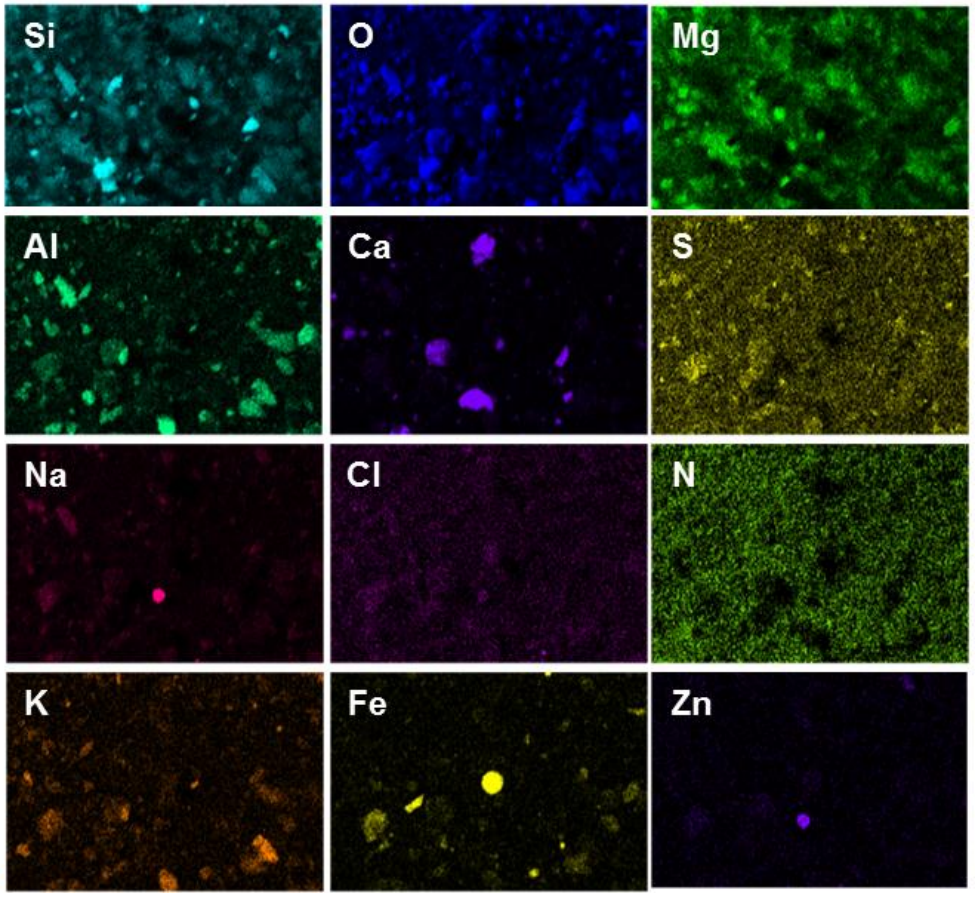

Sample: 144-011
Map B

Notes: Minerals are largely aluminosilicates.

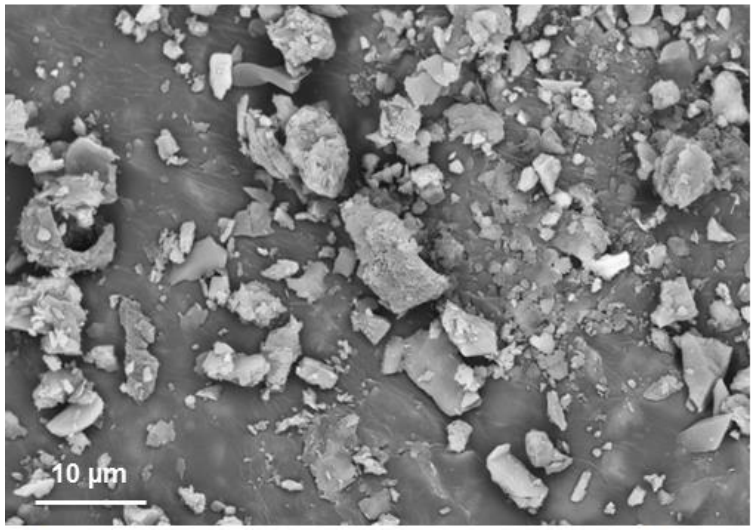

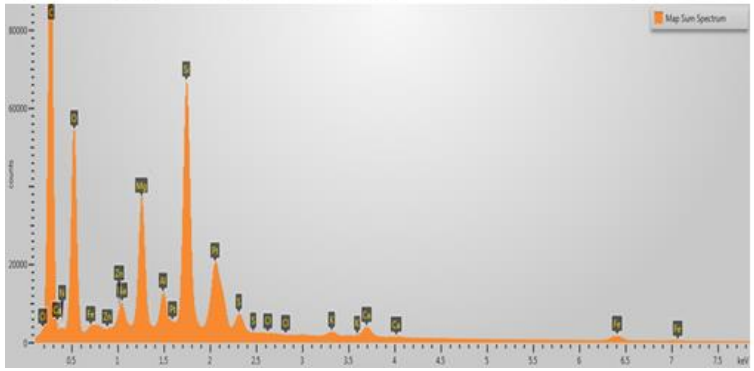

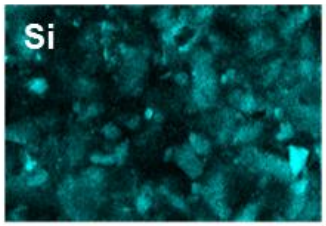

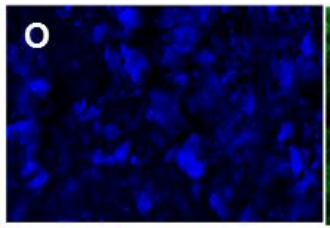

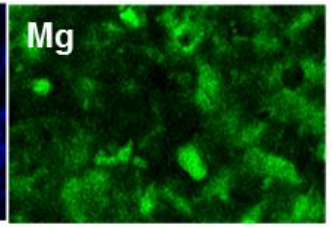

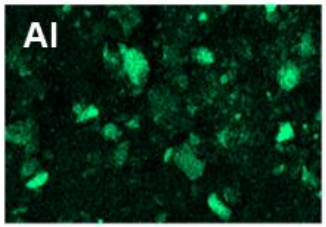

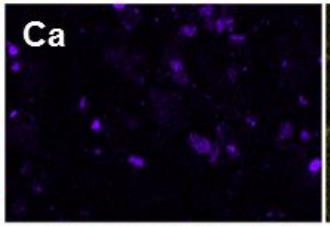

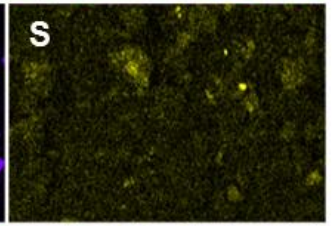

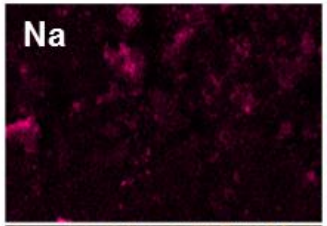

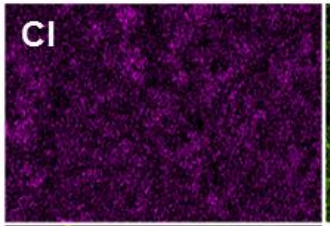

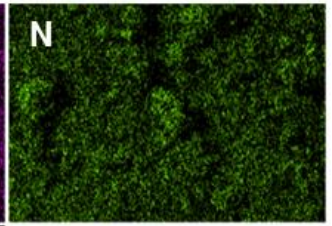

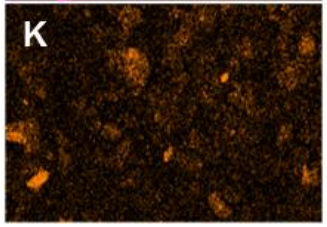

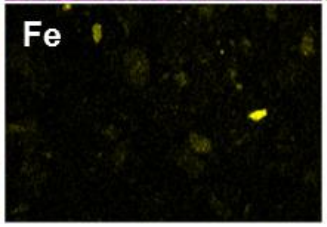

Sample: 144-011
Map C

Notes: Minerals are largely aluminosilicates.

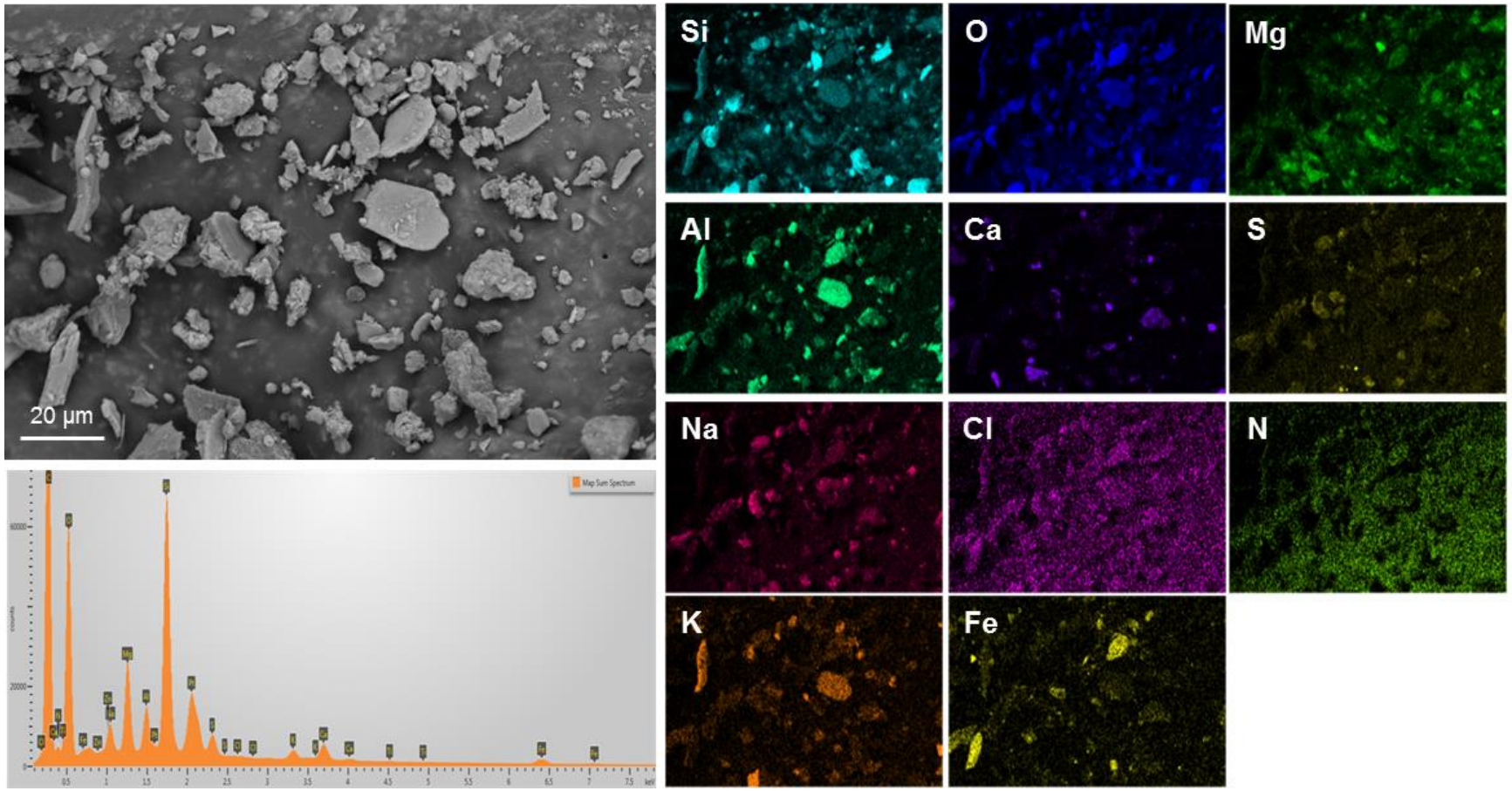

Sample: 144-011
Map D

Notes: Minerals are largely aluminosilicates.

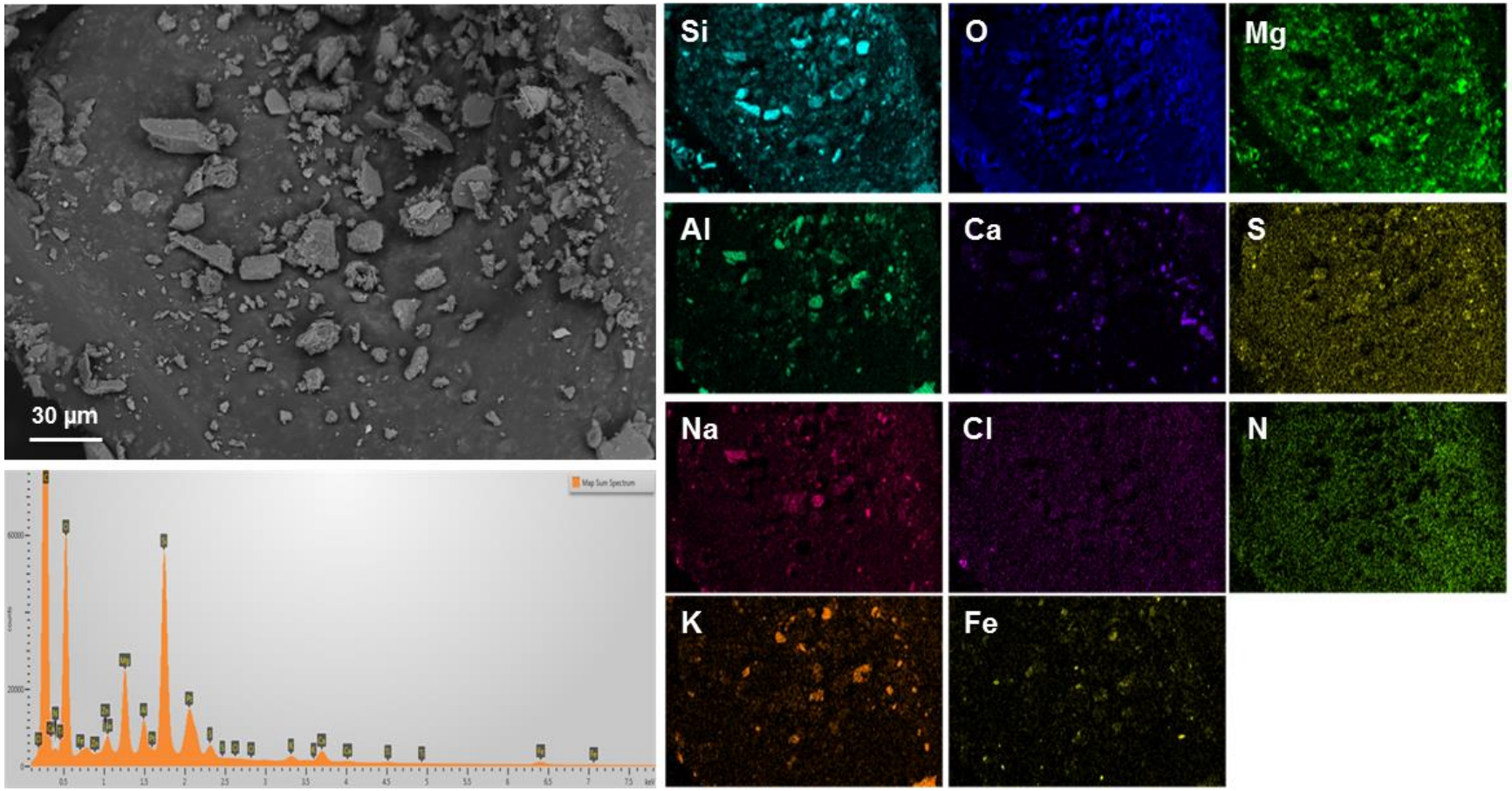

Sample: 144-011
Map E

Notes: Close-up of the lower left corner of Map D, showing the chloride-rich phase.

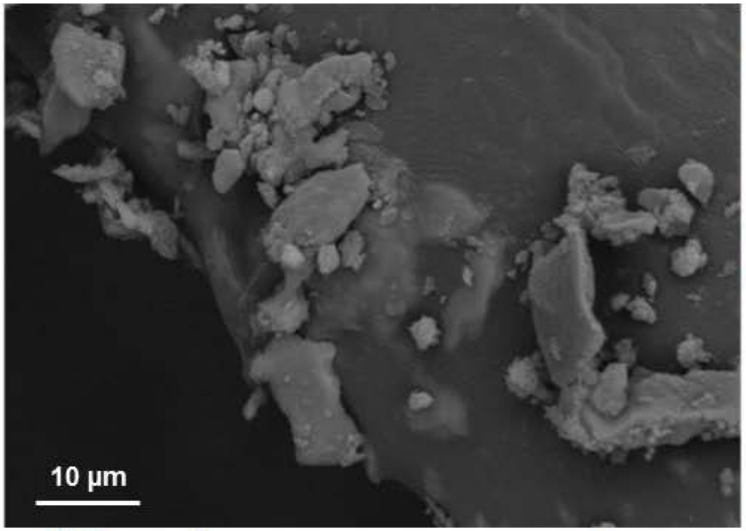

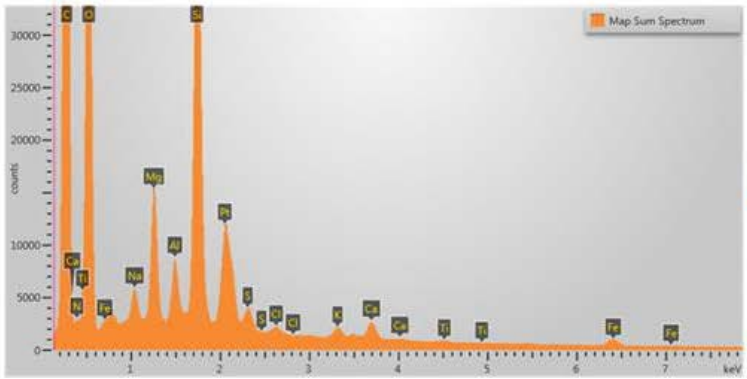

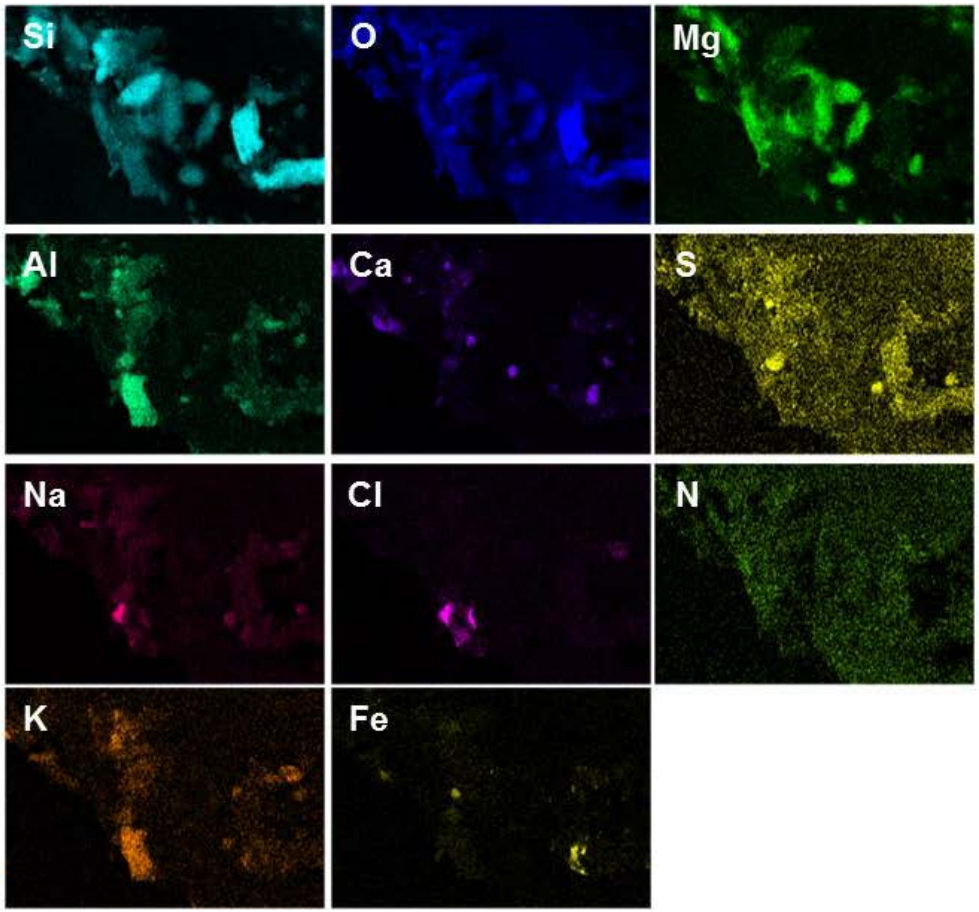

Sample: 144-011
Map F

Notes: Minerals are largely aluminosilicates.

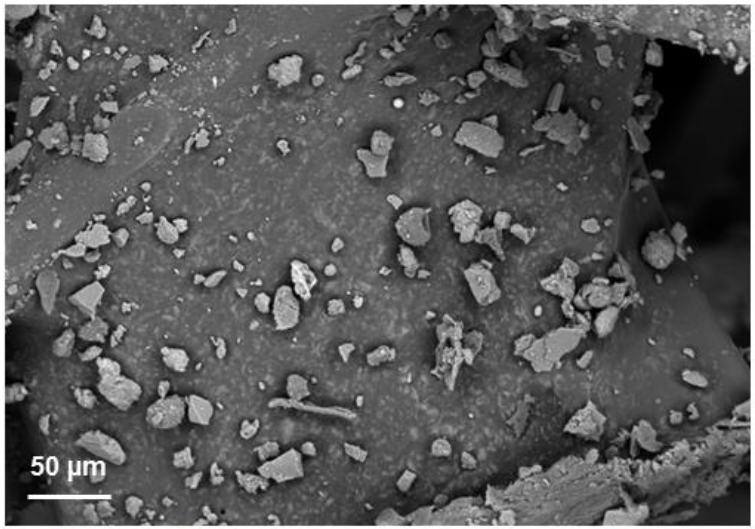

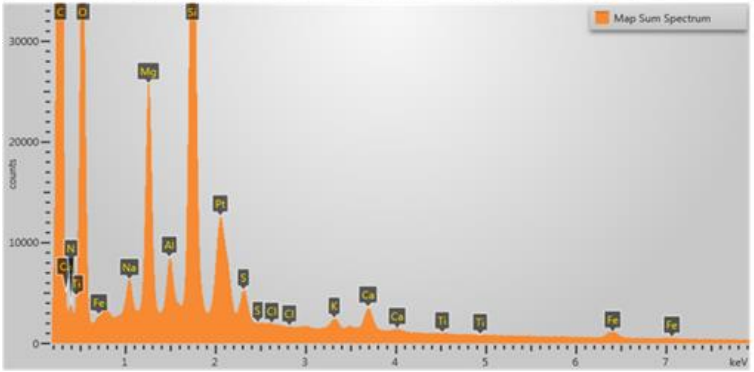

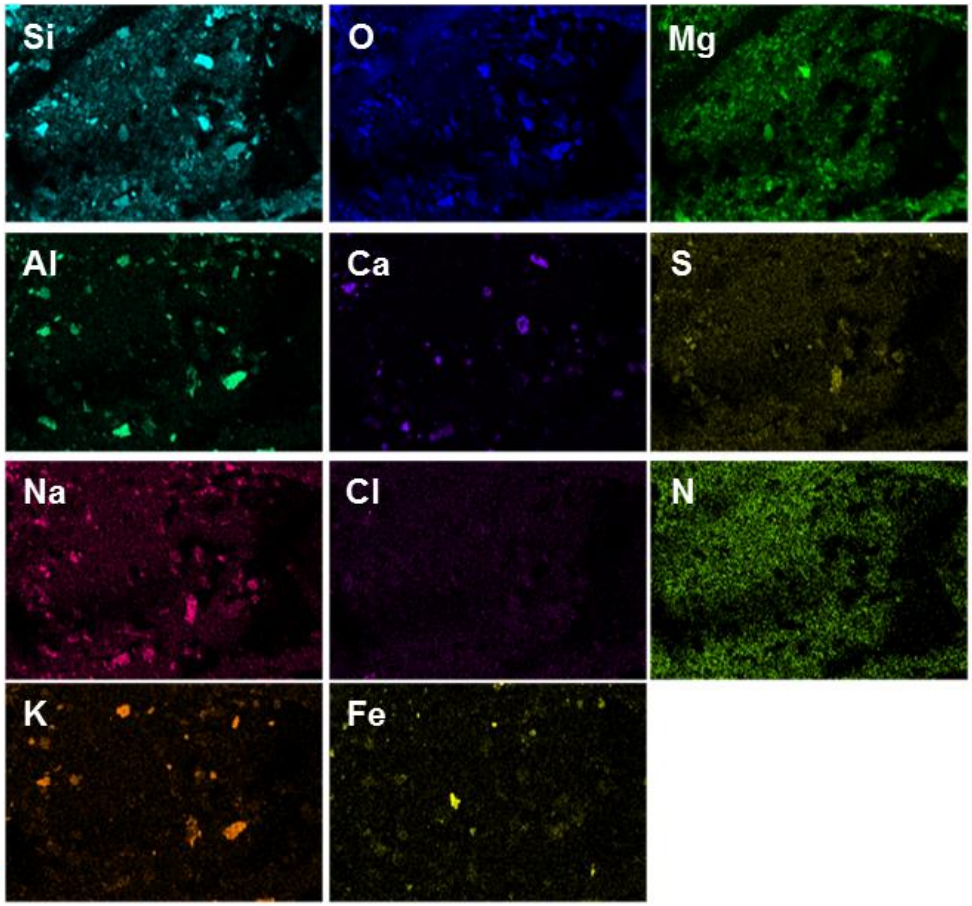

Sample: 145-001
Map A

Notes: Dust accumulation at an abraded edge. Dust phases are largely aluminosilicates and stainless steel particles.

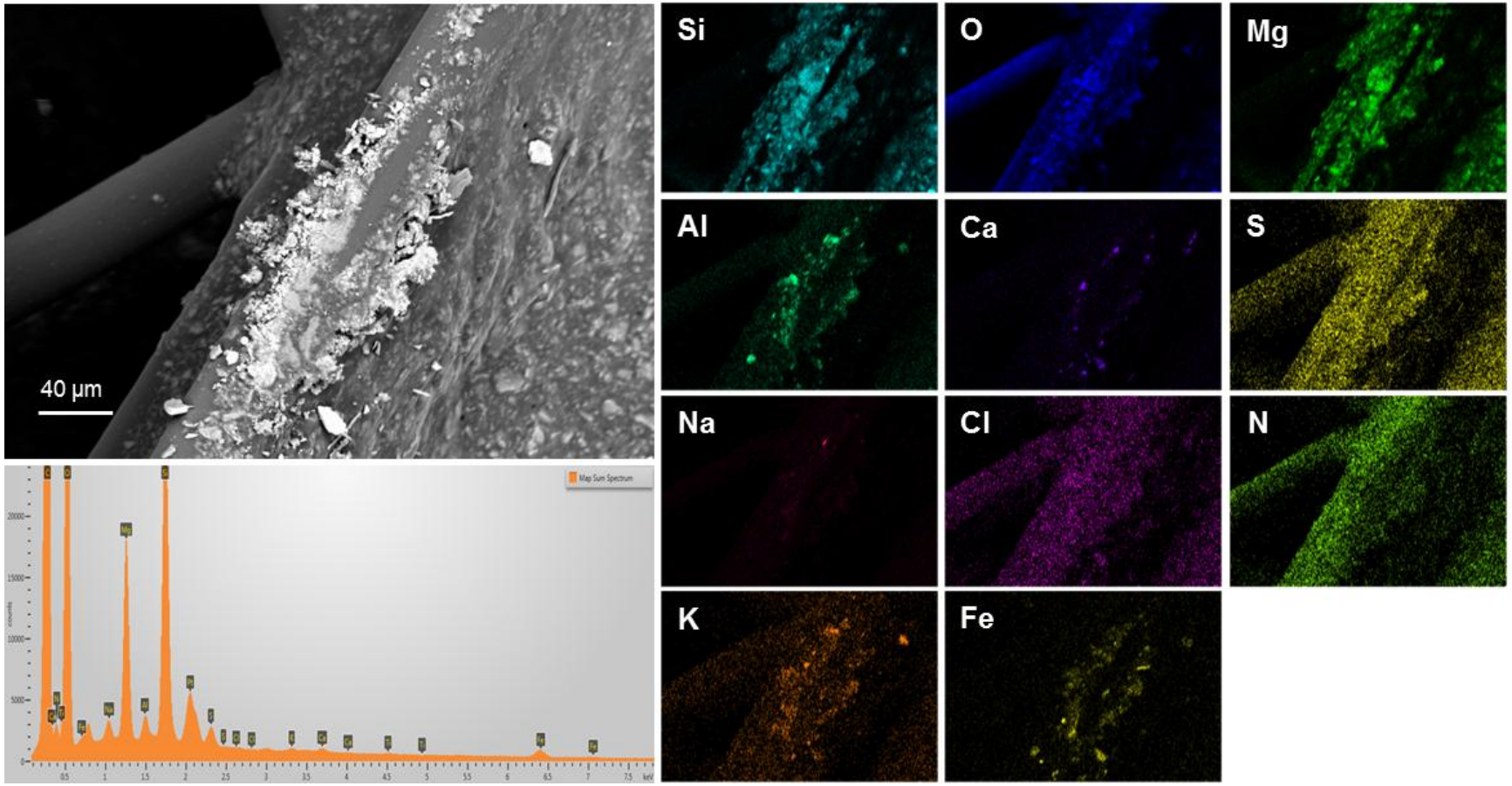

Sample: 145-001
Map B

Notes: Dust accumulation on an abraded edge. Minerals are largely aluminosilicates, with some stainless steel particles.

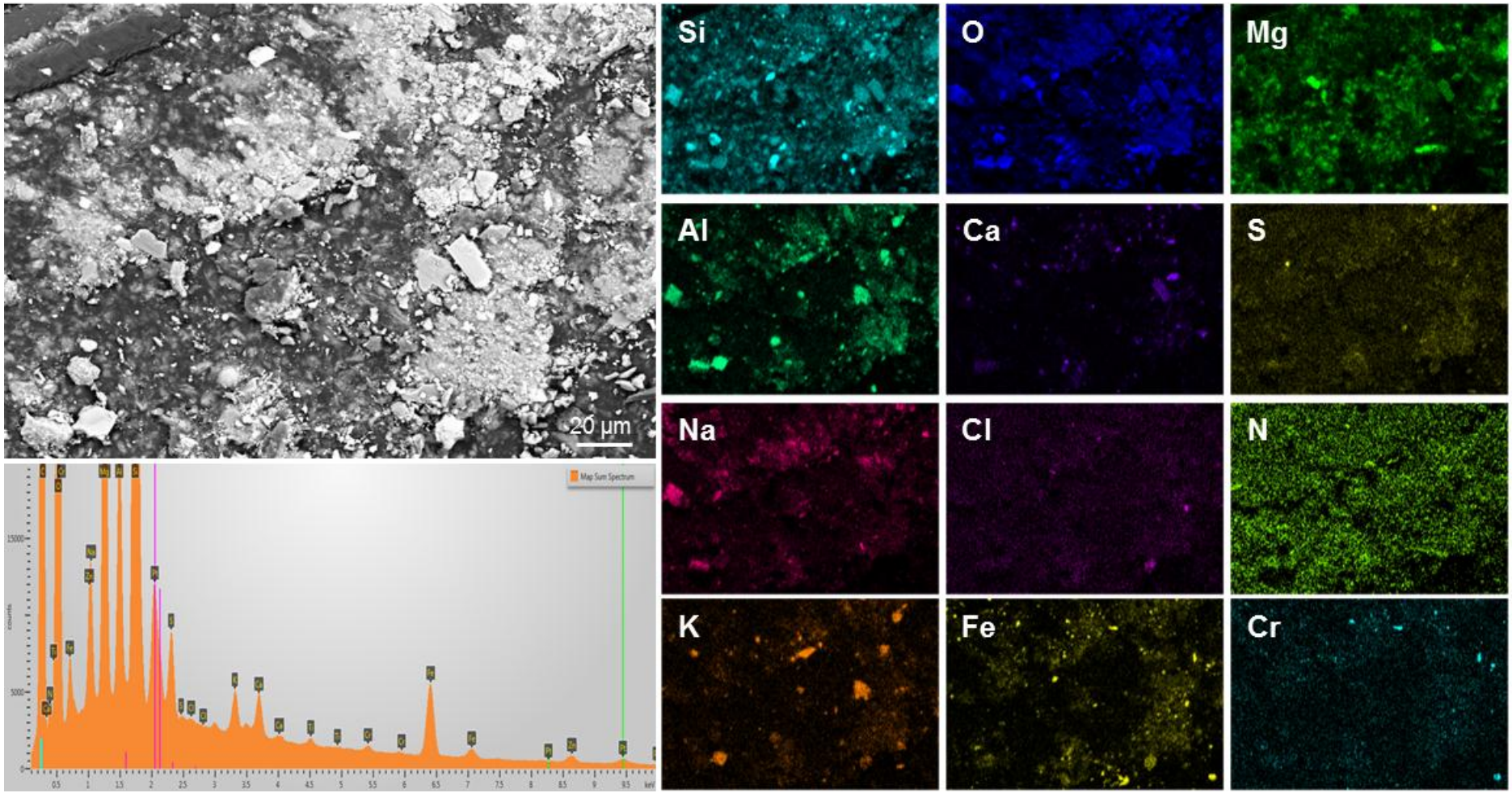

Sample: 145-001
Map C

Notes: Dust particles on an abraded surface. Particles are mostly stainless steel.

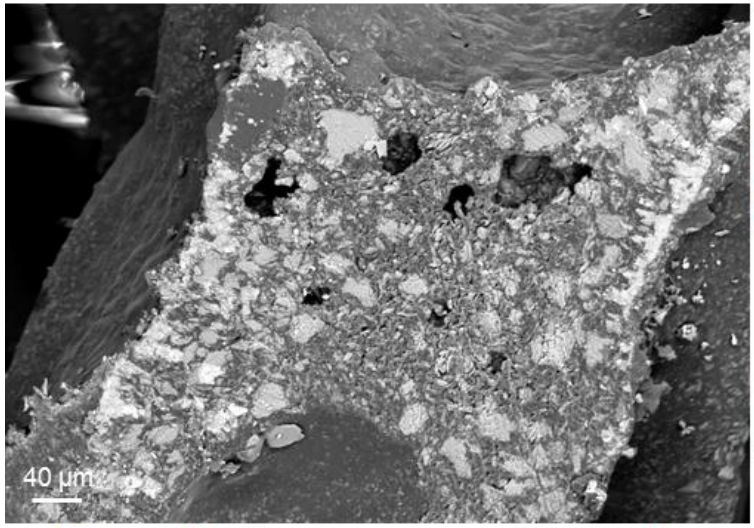

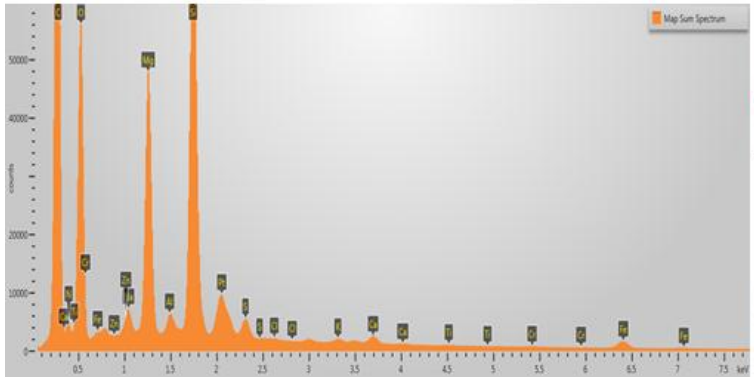

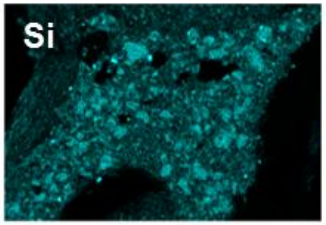

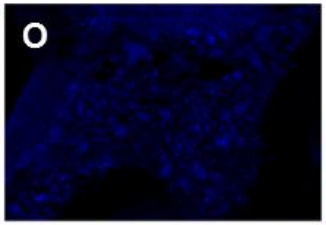

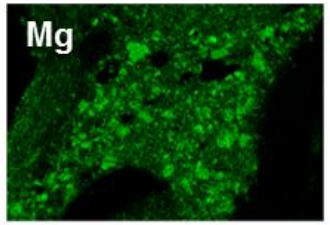

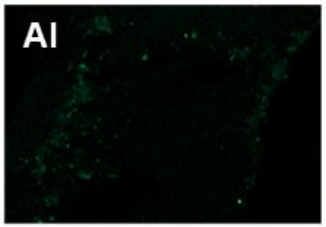

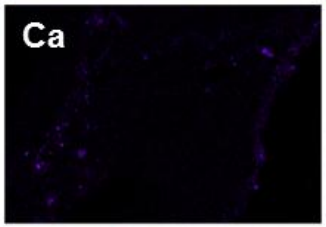

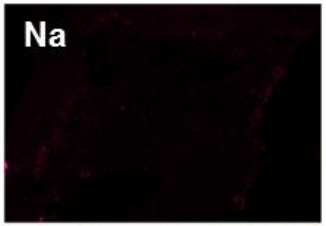

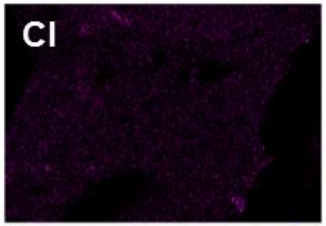

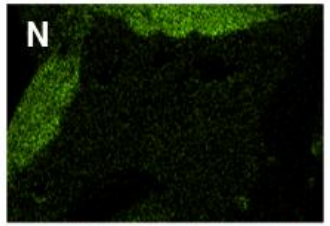

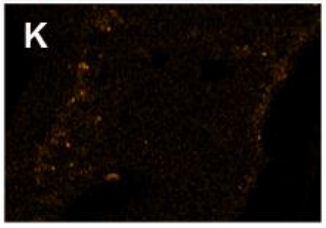

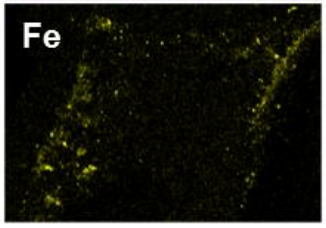

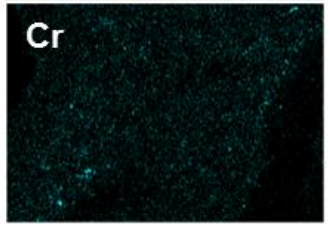

Sample: 145-001
Map D

Notes: Dust accumulation on an abraded edge. Embedded particles are mostly aluminosilicates and stainless steel.

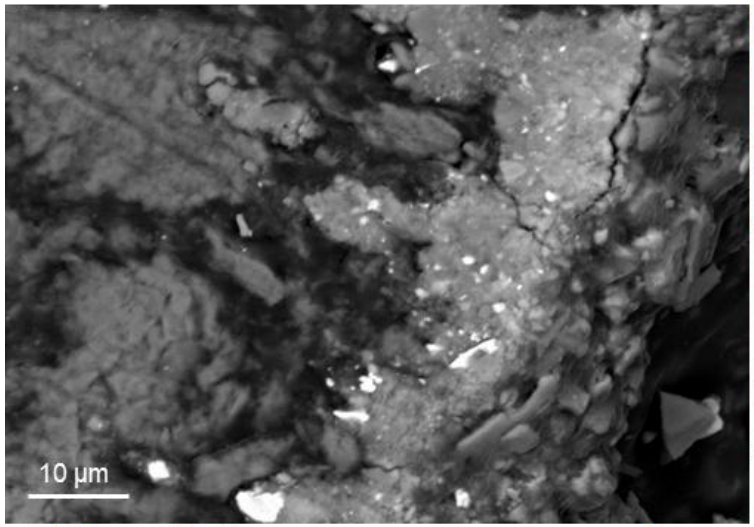

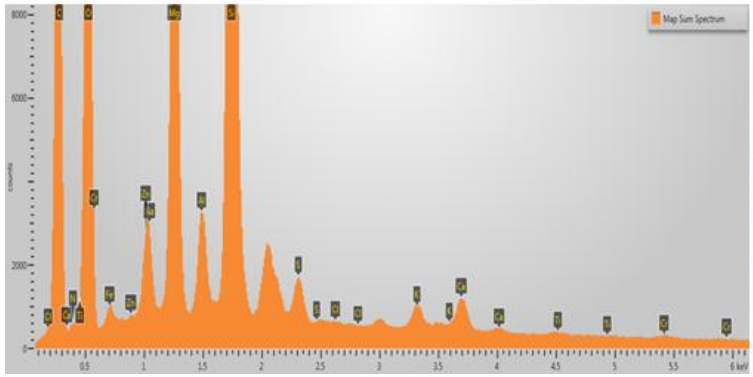

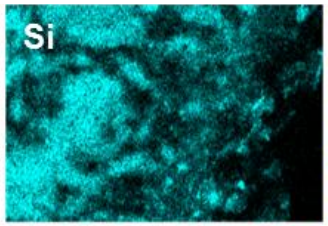

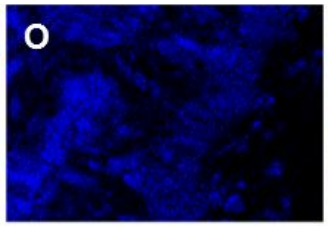

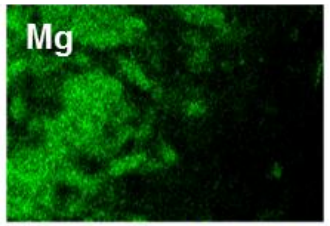

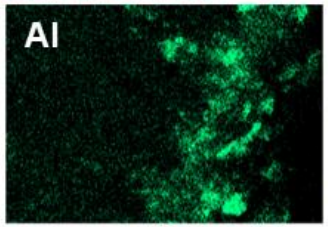

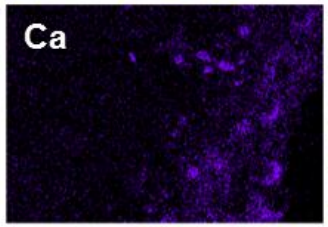

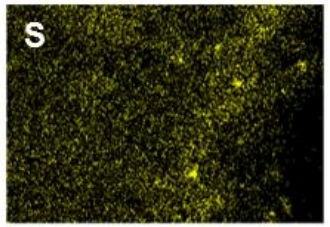

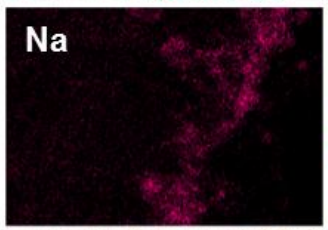

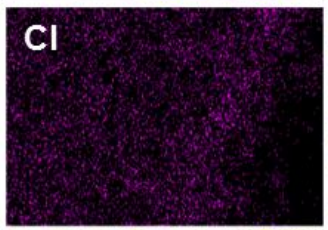

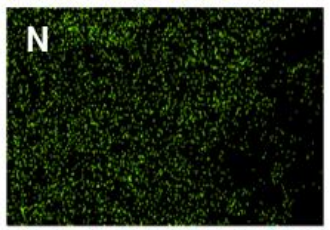

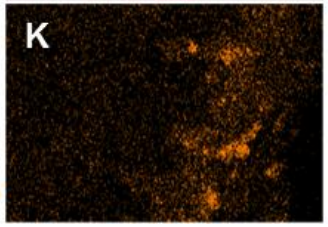

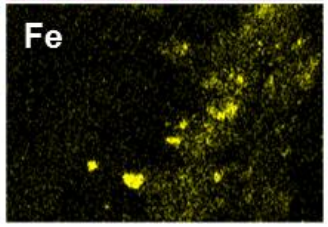

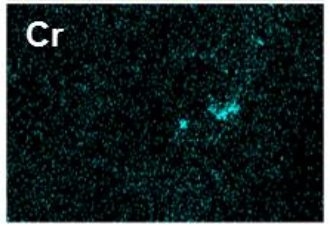

Sample: 145-001
Map E

Notes: Particles are mostly aluminosilicates.

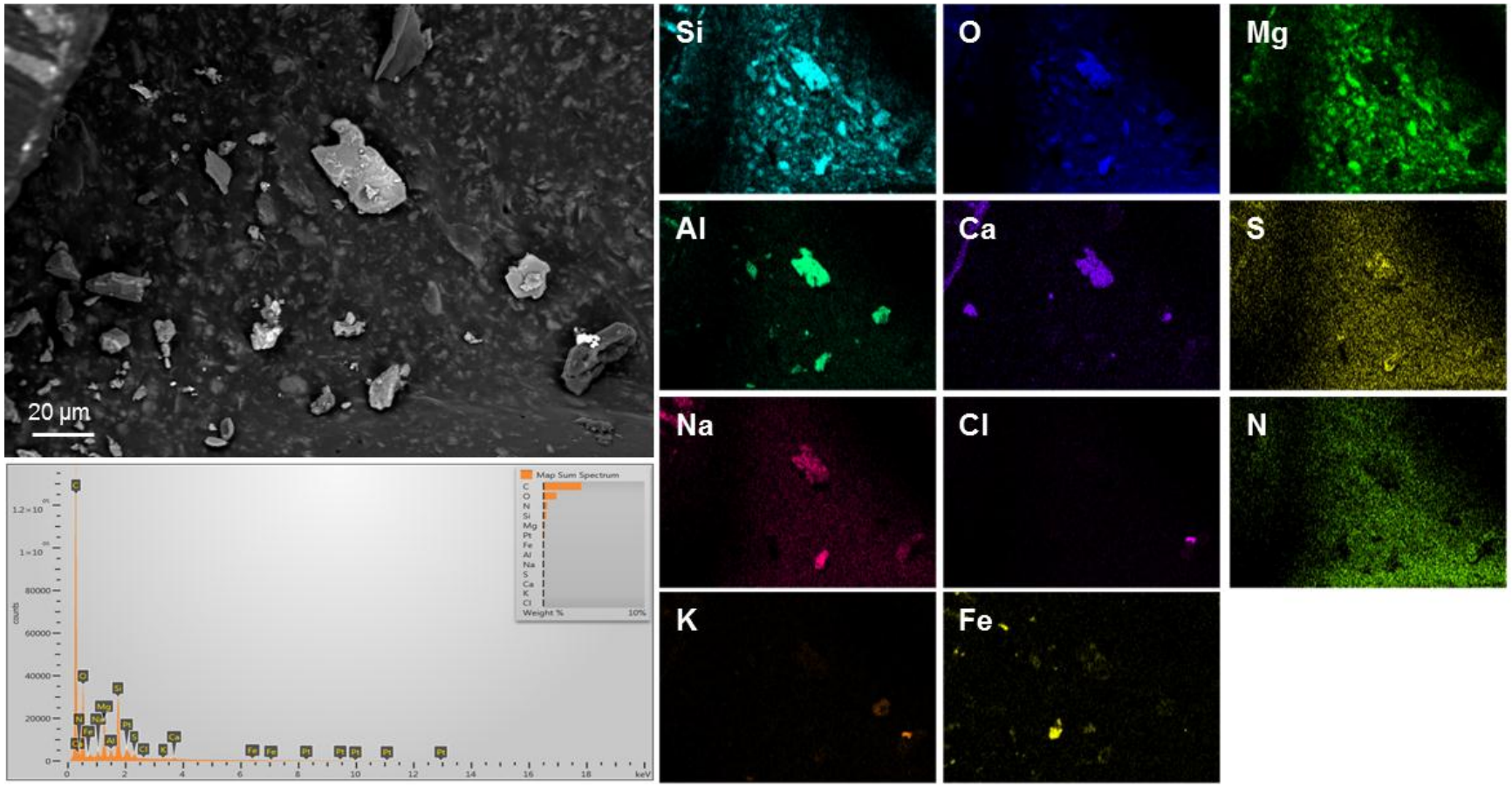

Sample: 145-001
Map F

Notes: Dust particles on an abraded edge of sample 145-001. Particles are mostly aluminosilicates and stainless steel particles. A Zn-Na-rich particle is in the lower center.

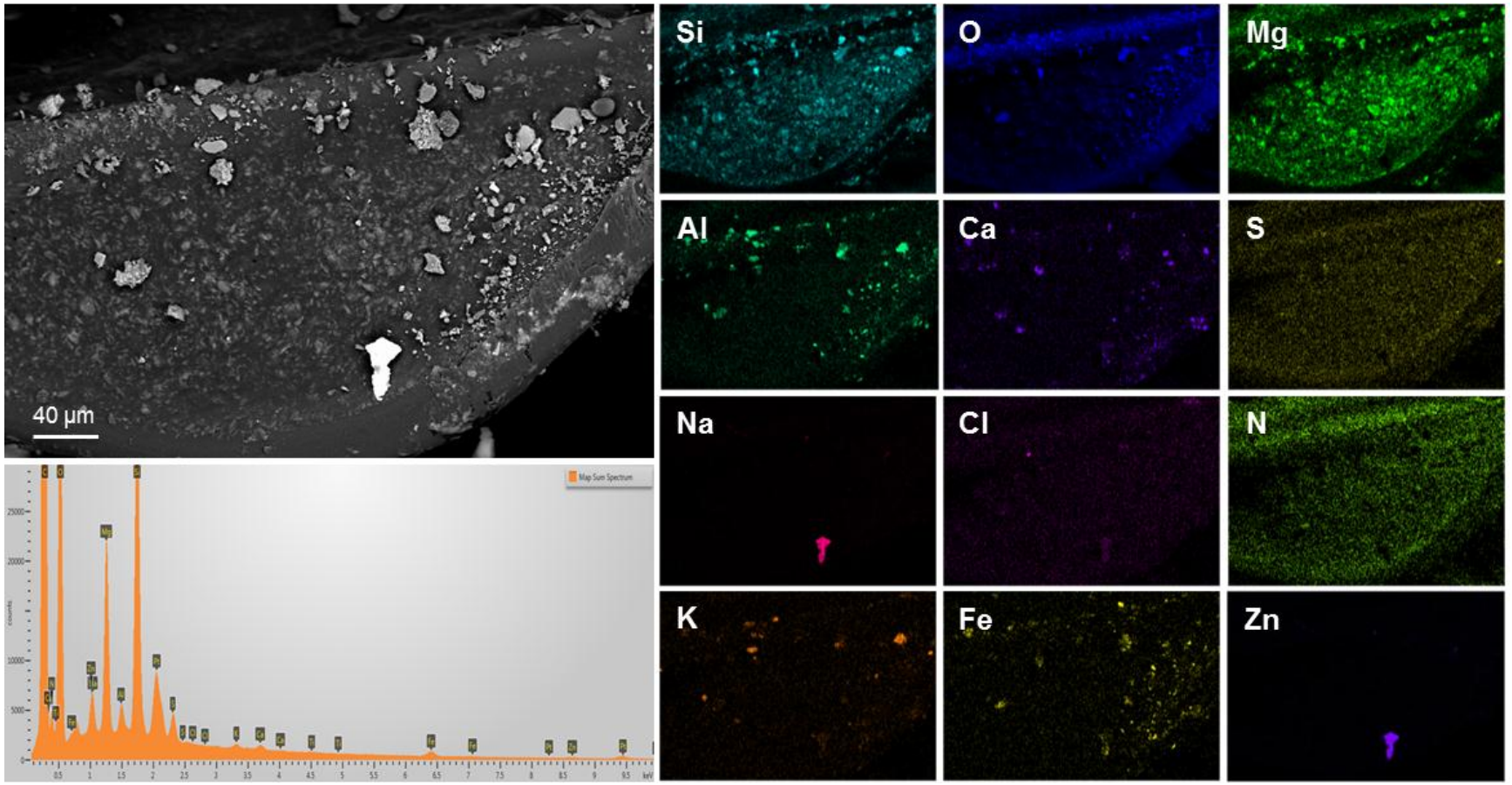

Sample: 145-001
Map G

Notes: A composite Fe-oxide and aluminosilicate grain.

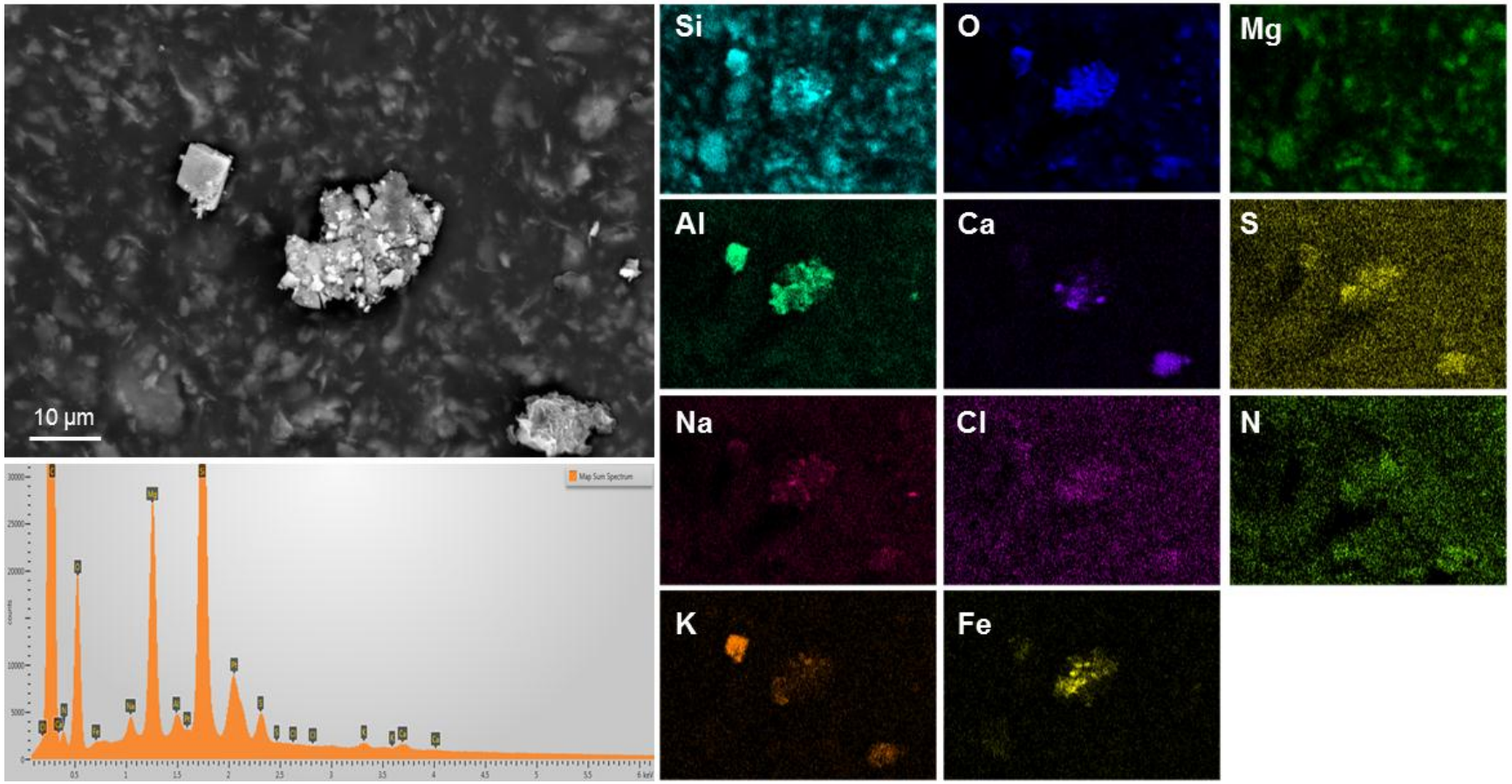

Sample: 145-001
Map H

Notes: Dominantly aluminosilicates, with some Ca-carbonate. A pollen grain is visible in the upper left corner of the image.

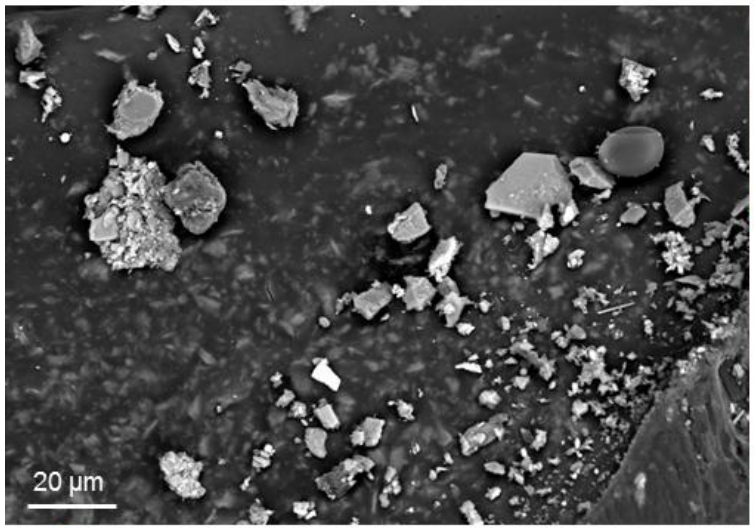

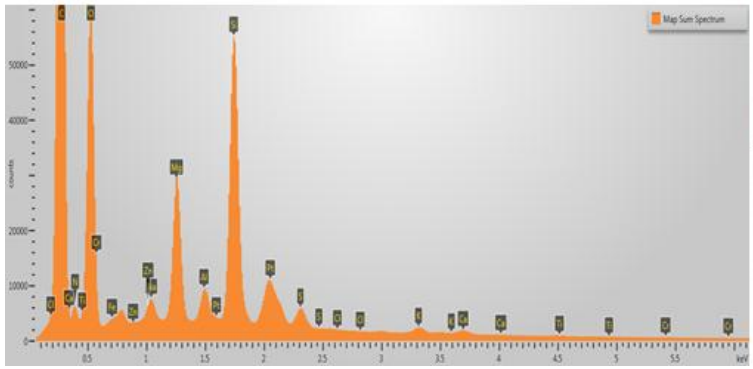

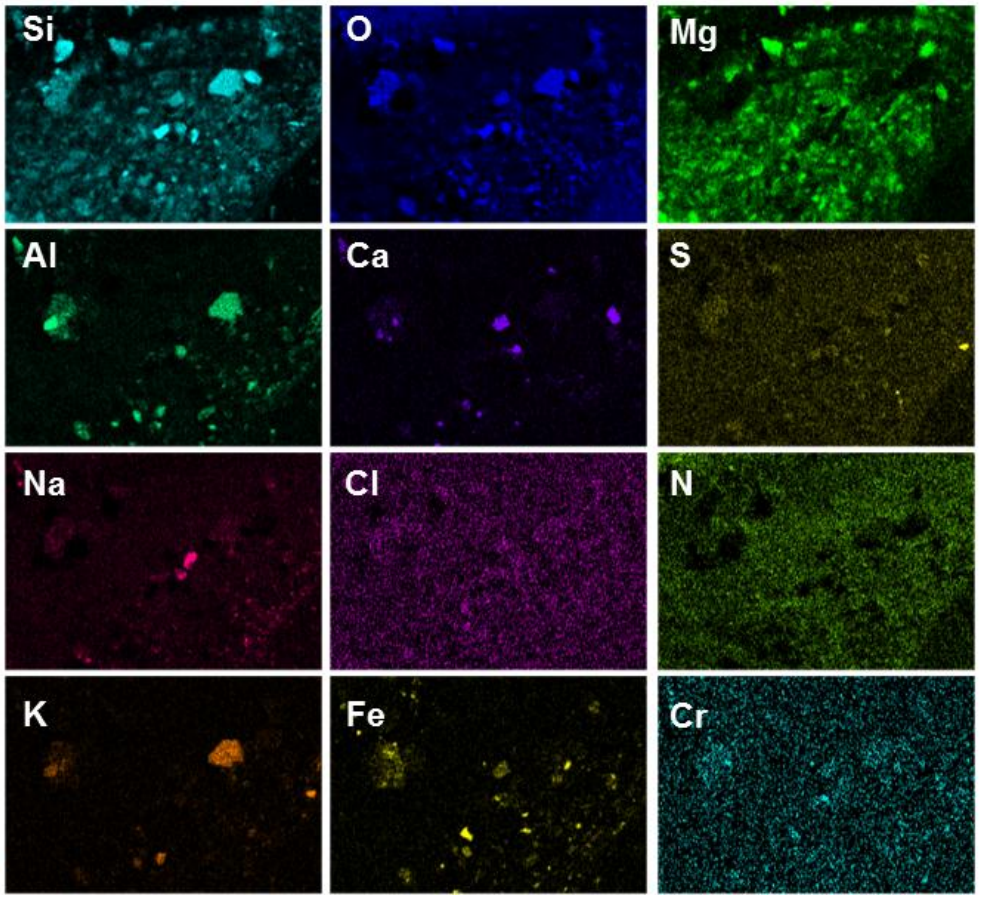

Sample: 145-003

Map A

Notes: An abraded edge on the pad. Embedded dust grains are mostly stainless steel particles.

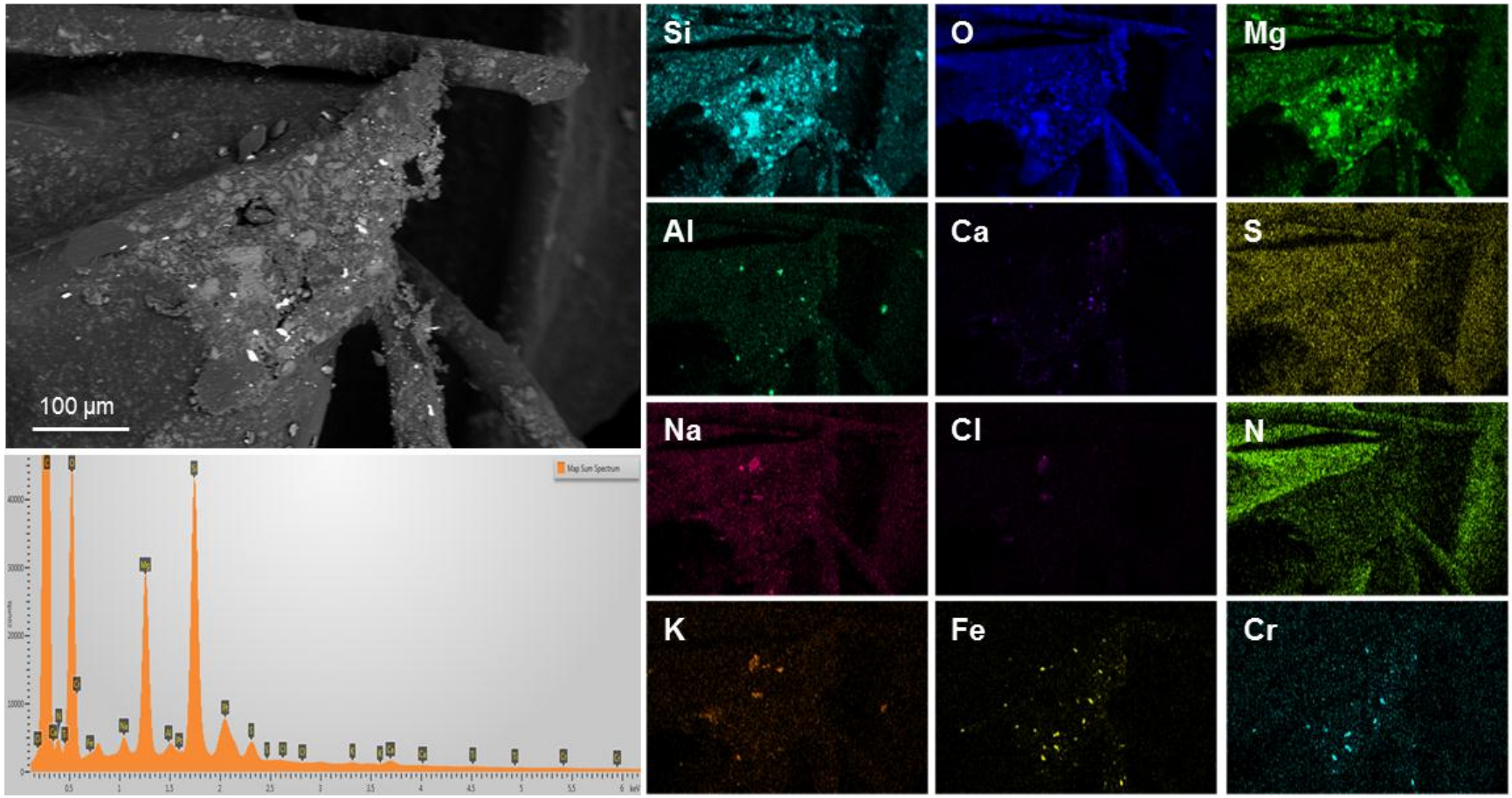

Sample: 145-003

Map B

Notes: Dust particles are mostly aluminosilicates and stainless steel particles.

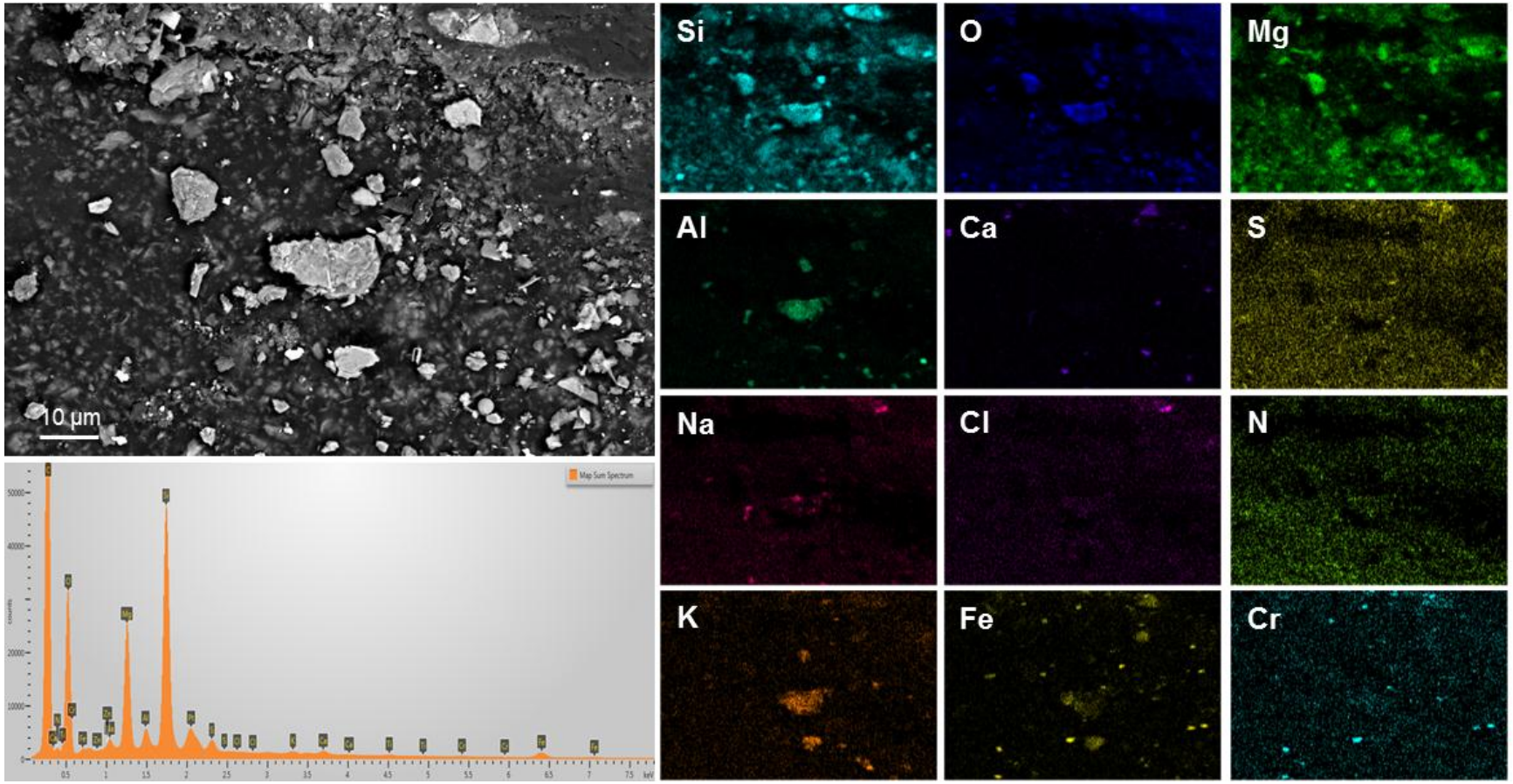

Sample: 145-003

Map C

Notes: Particles mostly talc, liberated by abrasion of the pad. Calcium carbonate is also present, and particles of stainless steel.

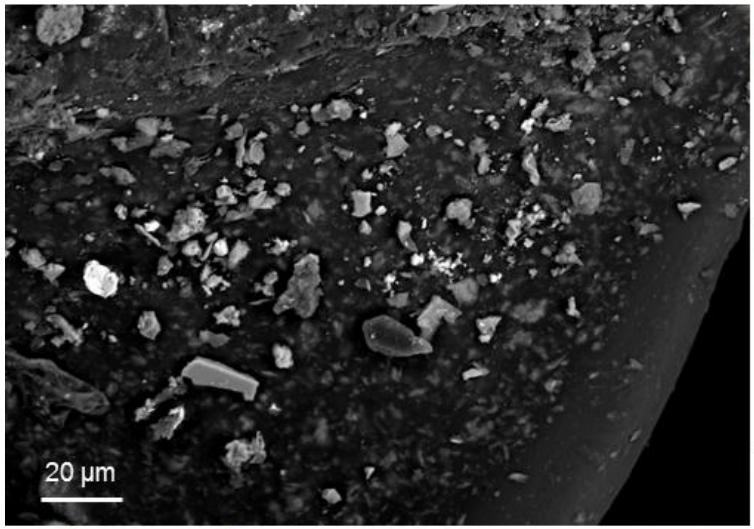

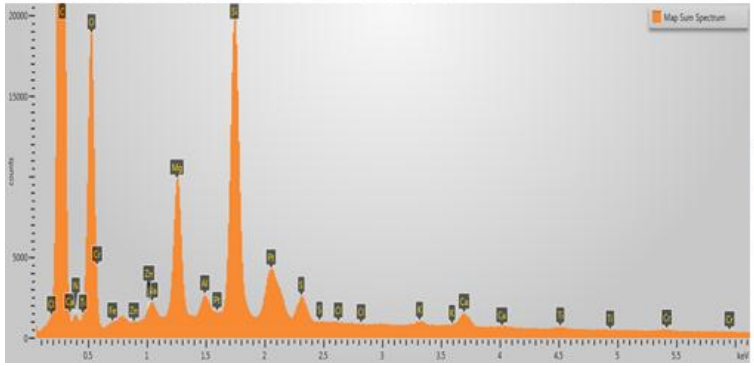

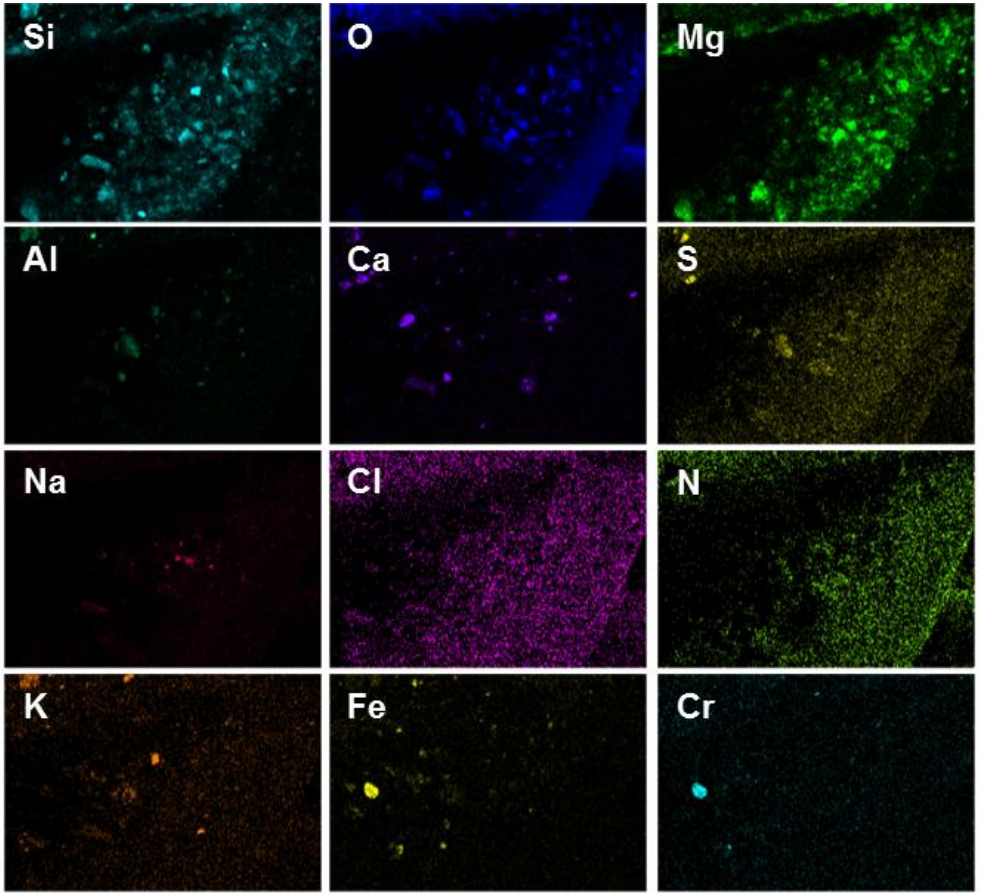

Sample: 145-004
Map A

Notes: Particles mostly talc, liberated by abrasion of the pad. Several grains of Ca-SO_4 are also present.

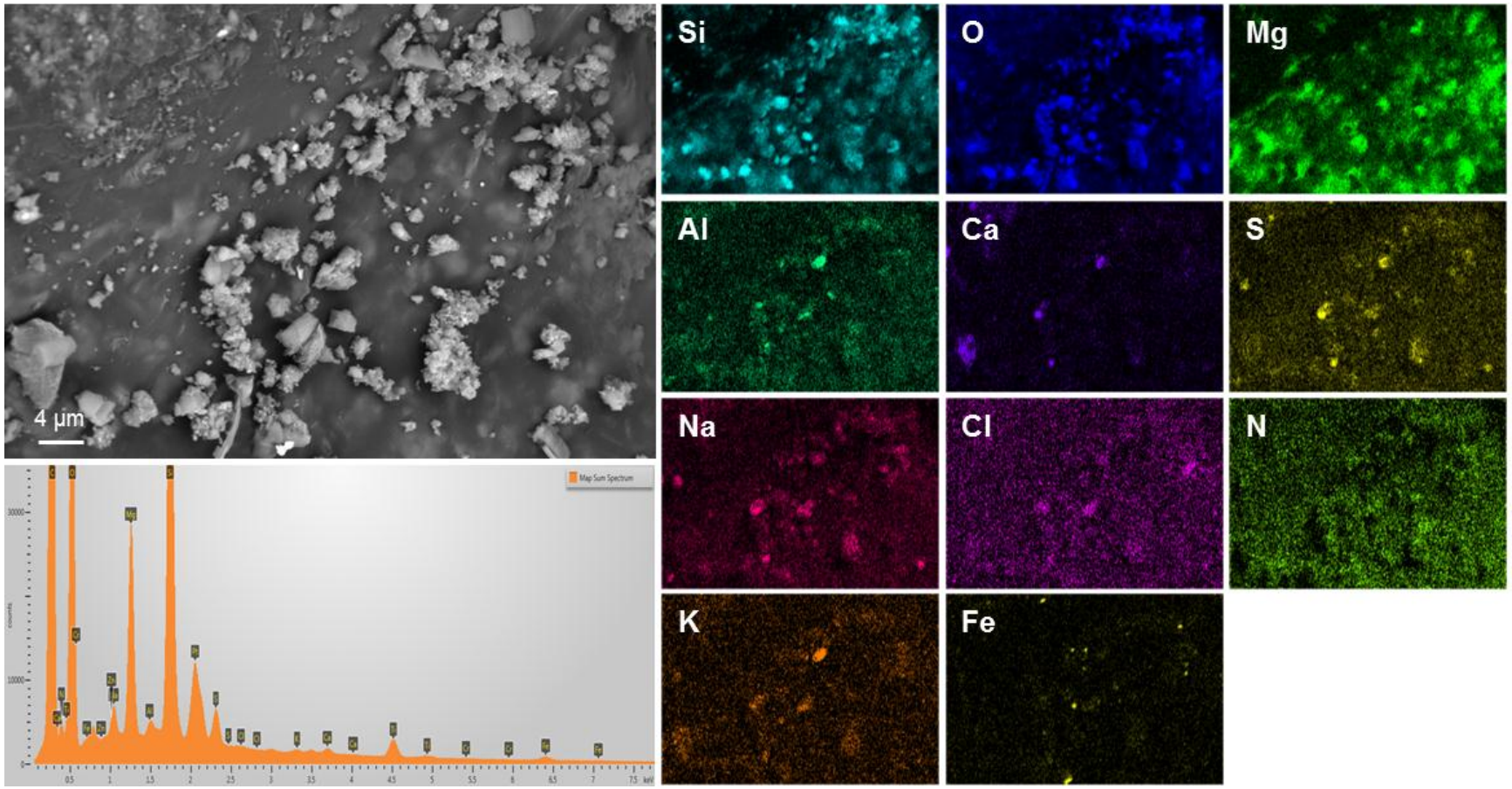

Sample: 145-004

Map B

Notes: Accumulated dust on an abraded edge. Embedded grains are dominantly stainless steel.

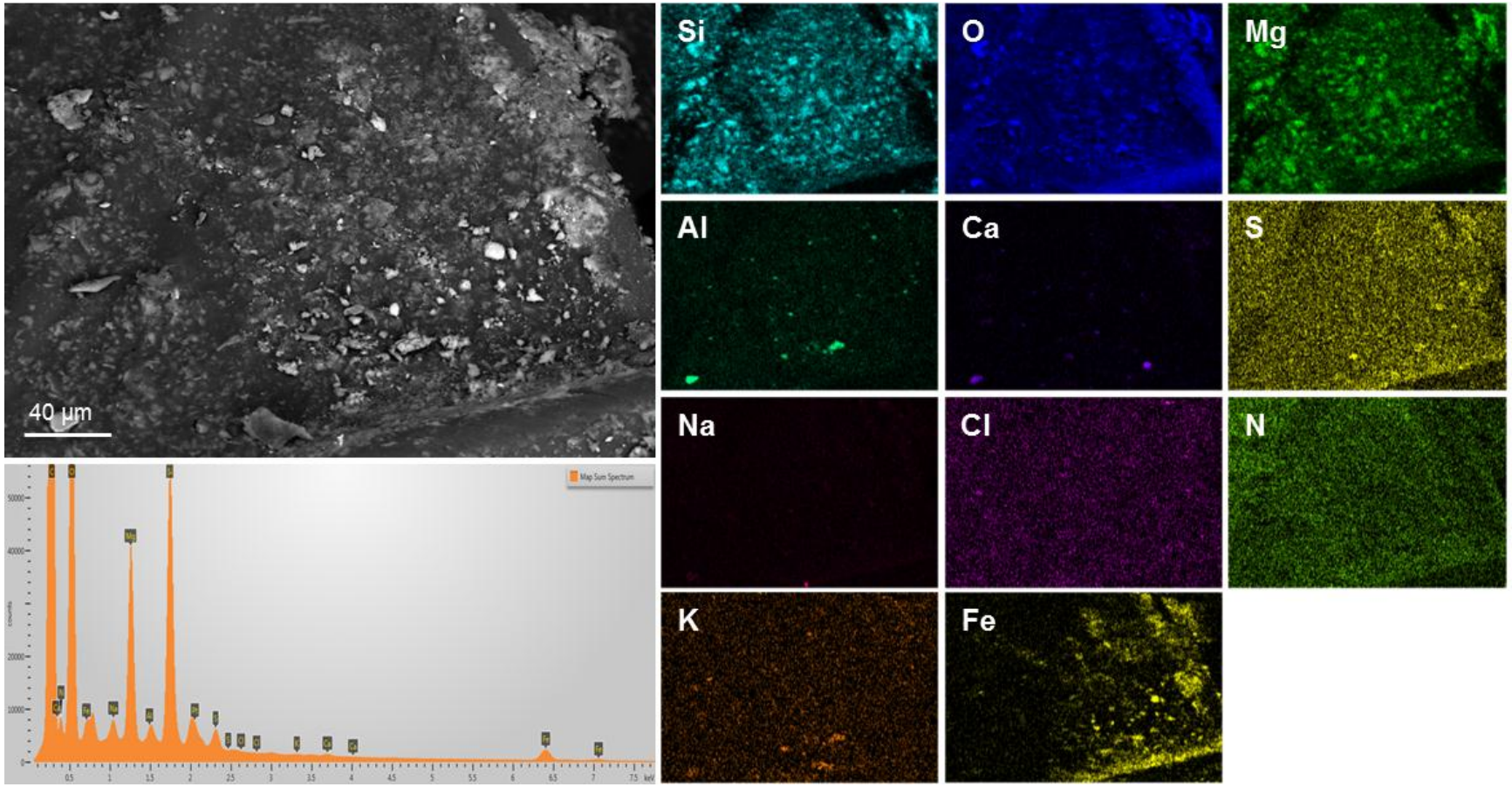

Sample: 145-005
Map A

Notes: Accumulation of trace dust on an abraded edge.

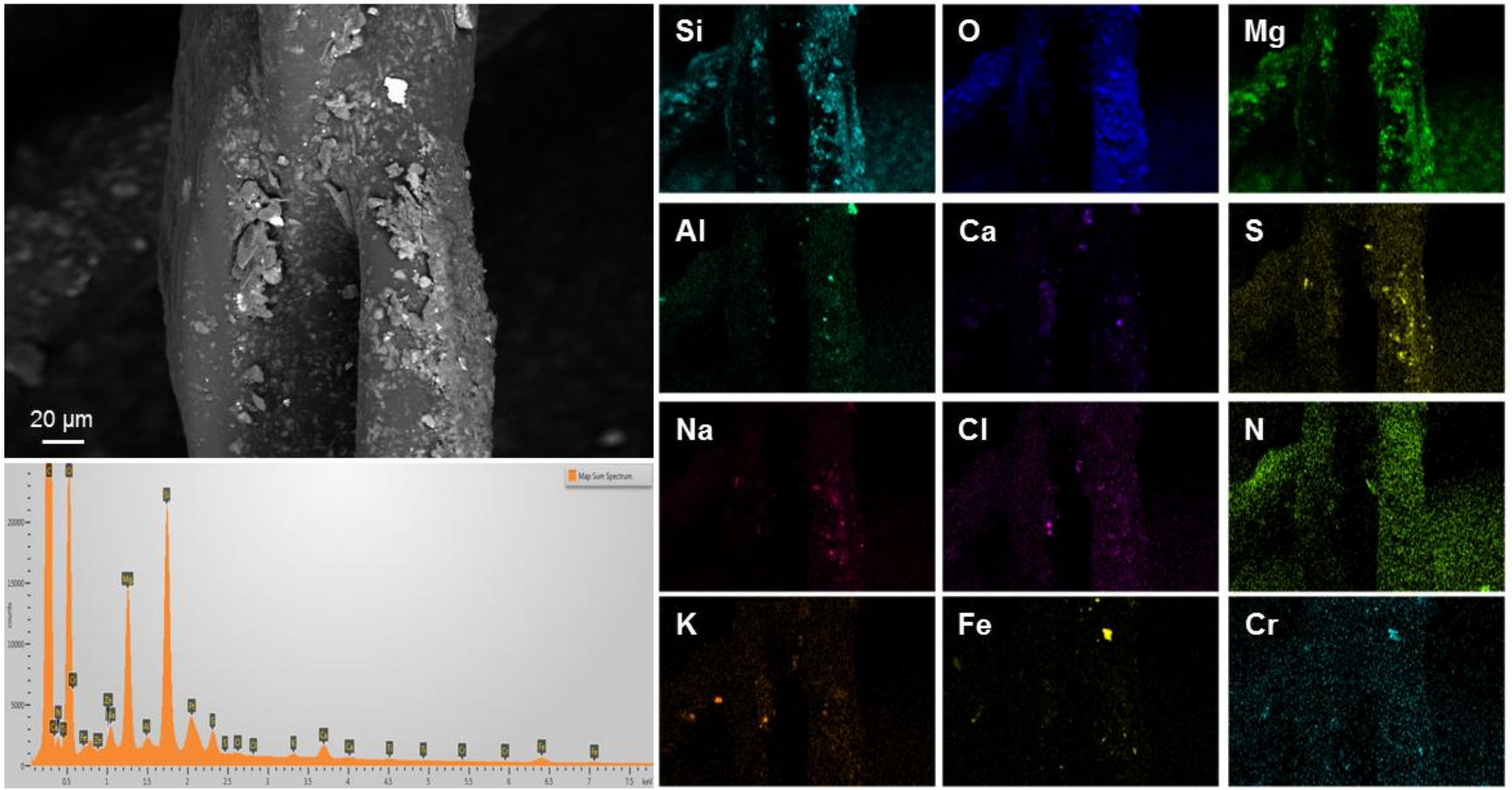

Sample: 145-005
Map B

Notes: Trace dust on an abraded edge. Note the large Na-Zn carbonate (?) grain at left center.

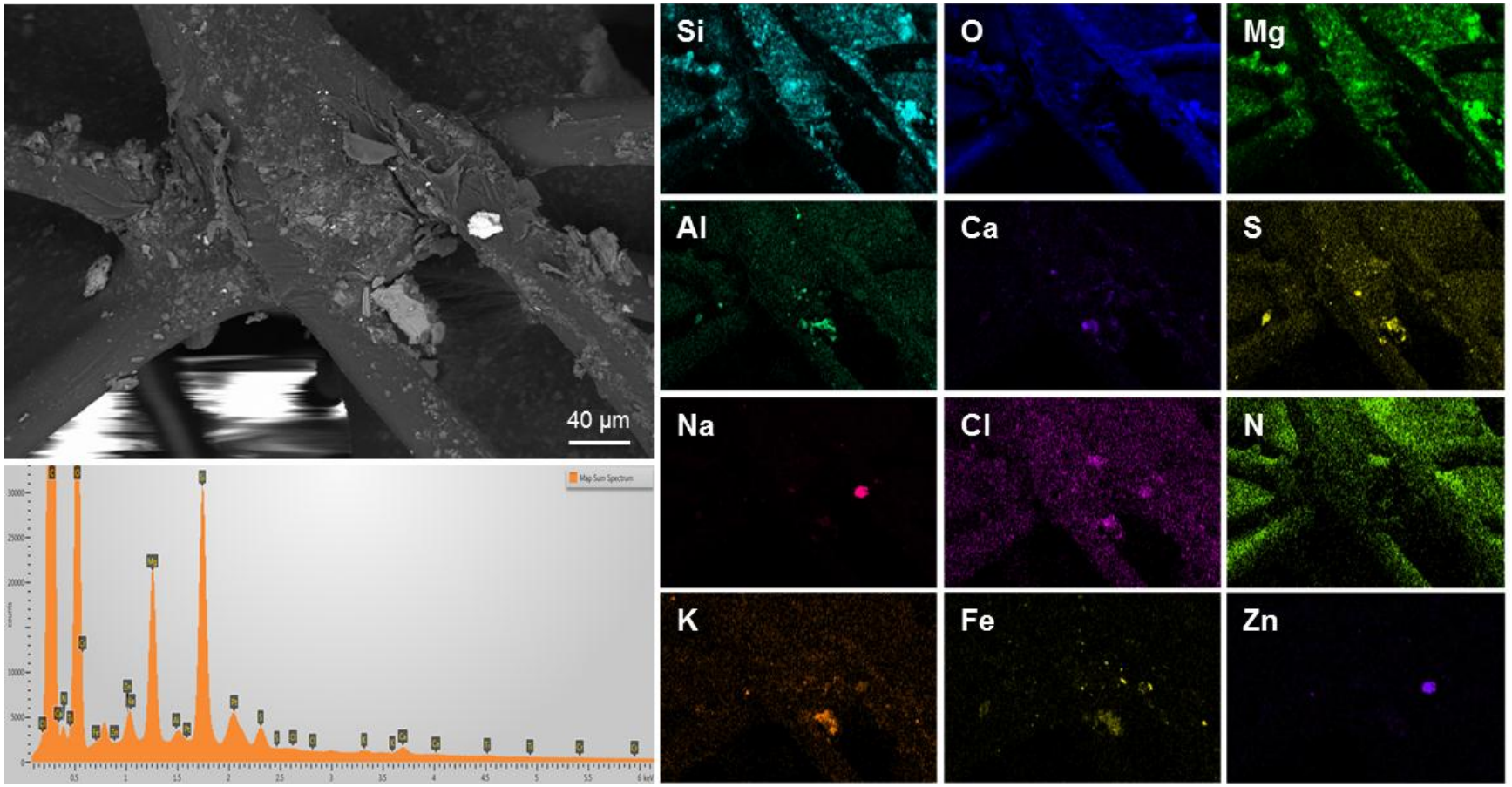

Sample: 145-012

Notes: Overview image of pad sample 145-012, showing the heavy dust load.

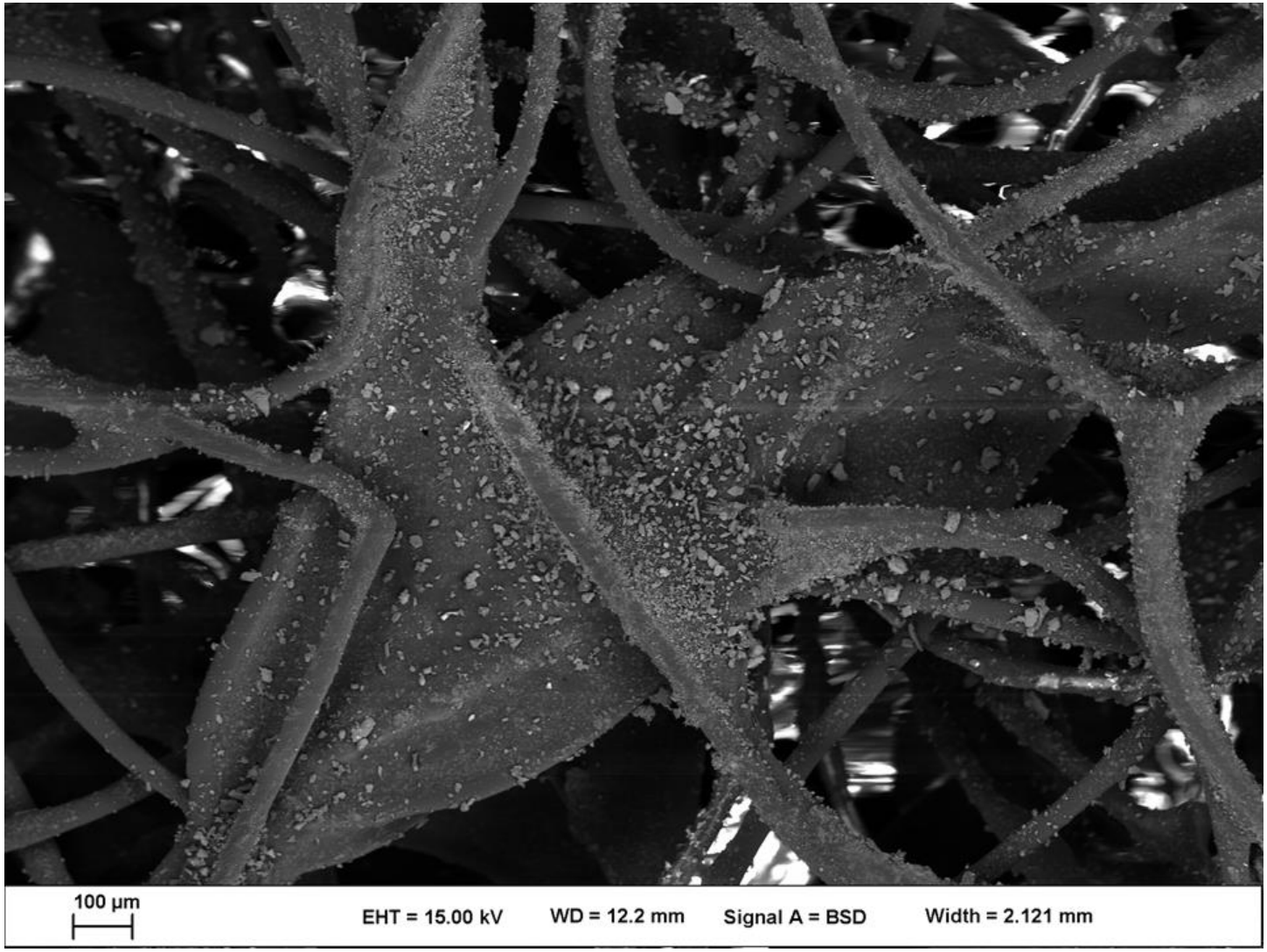

Sample: 145-012
Map A

Notes: Aluminosilicate and Ca-SO_4 grains.

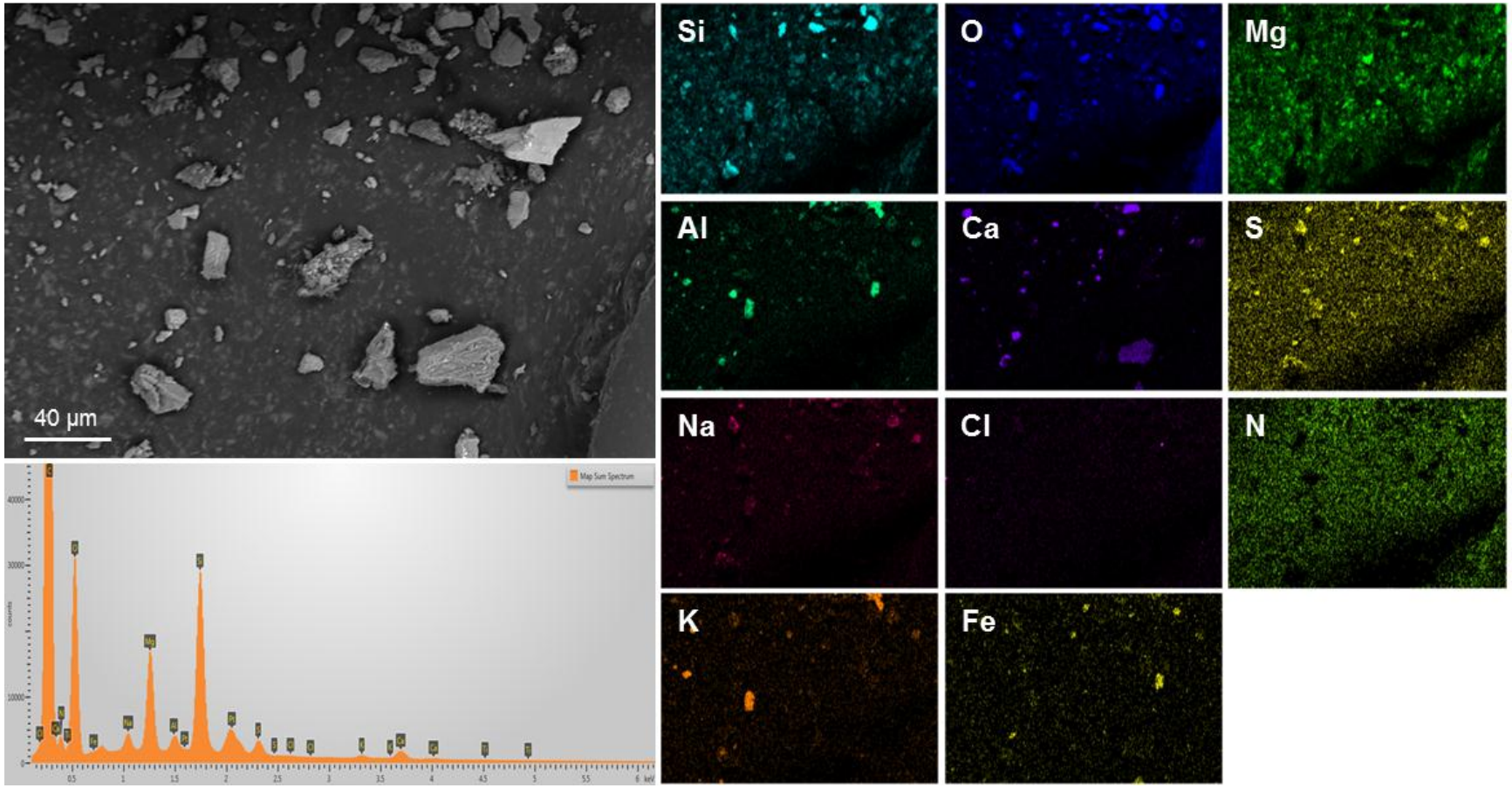

Sample: 145-012
Map B

Notes: Rare NaCl particle.

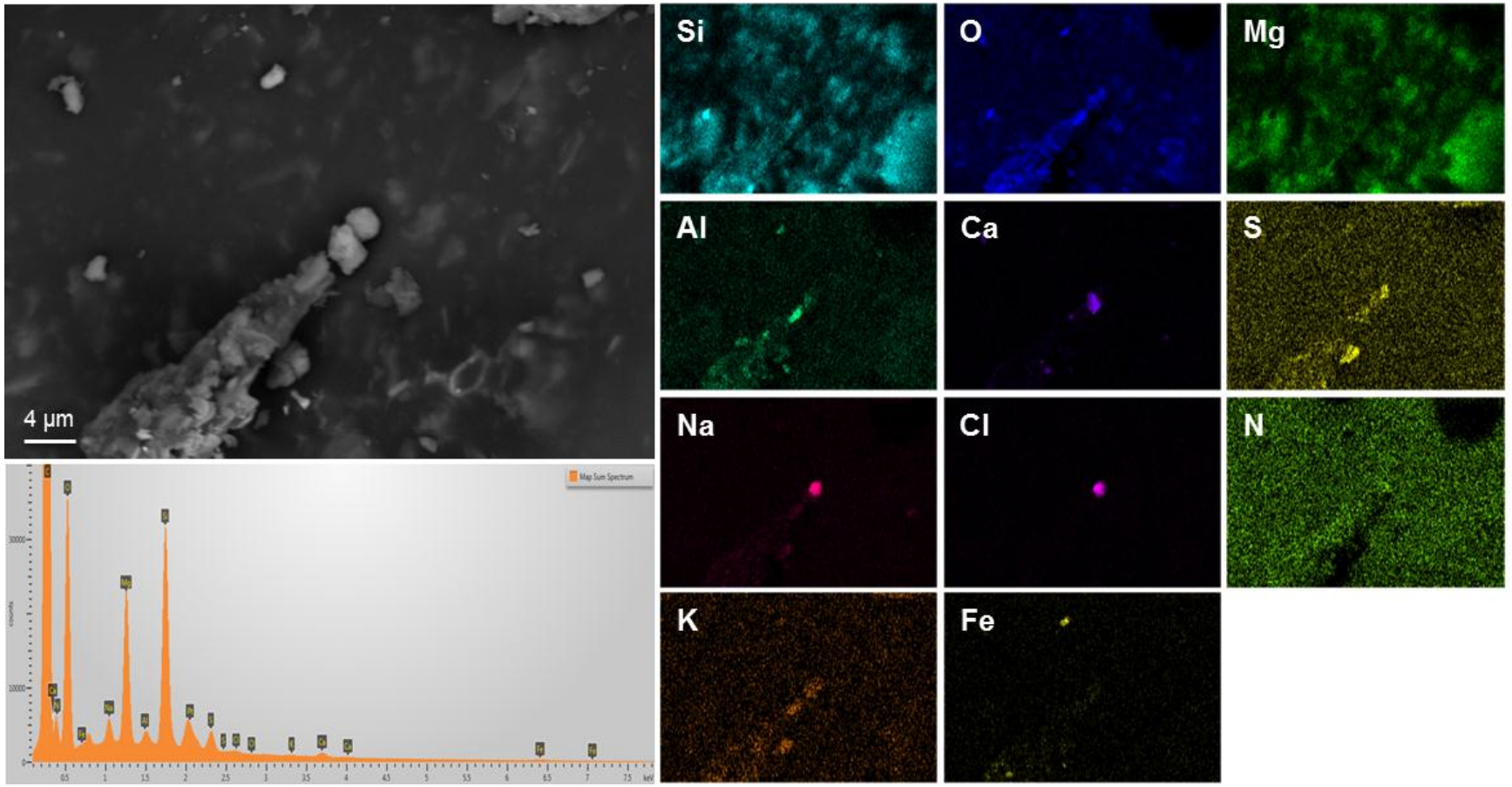

Sample: 145-012
Map C

Notes: Aluminosilicate grains and stainless steel particles.

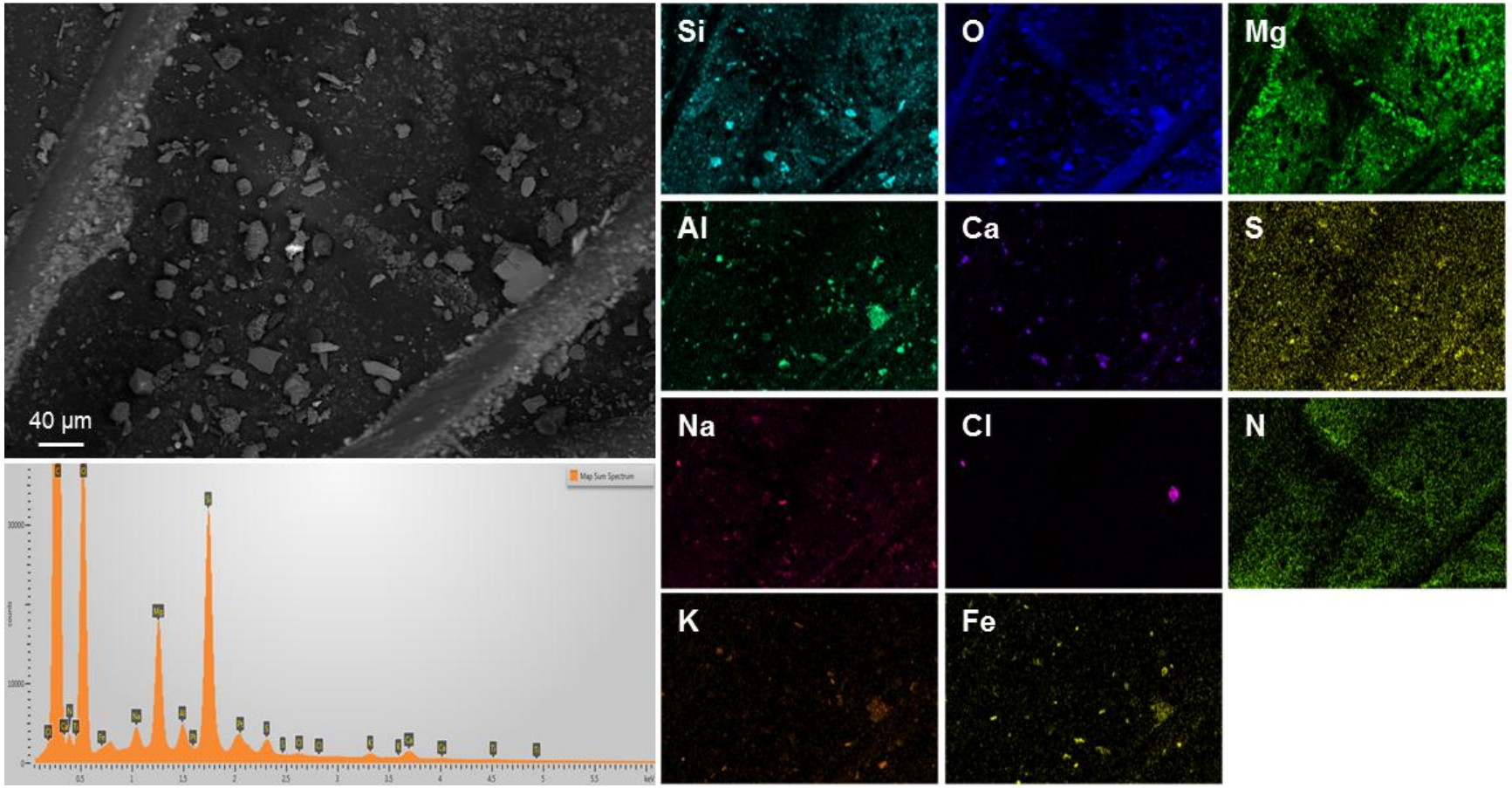

Sample: 145-012
Map D

Notes: Chloride-rich organic particle.

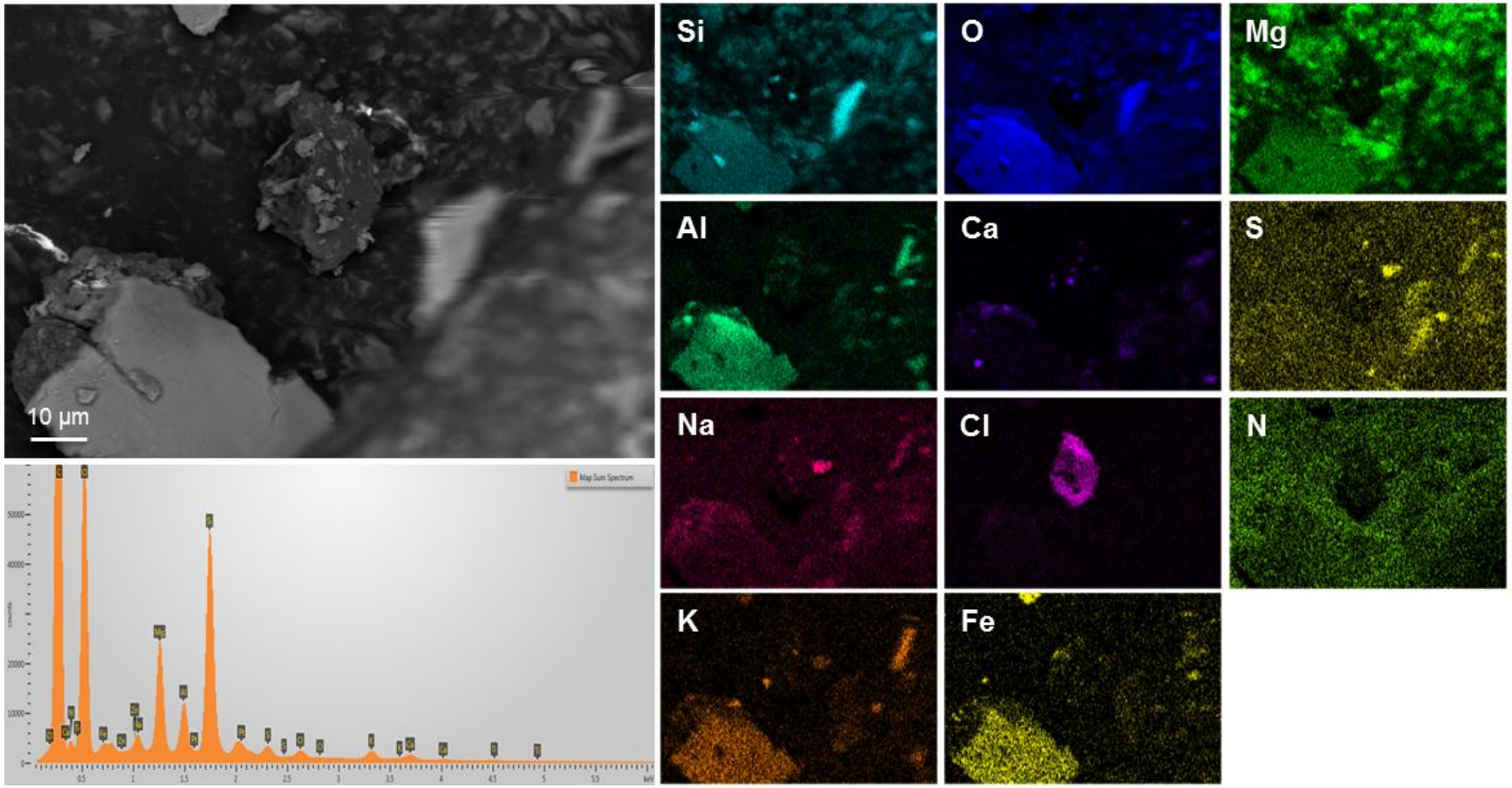

Sample: 145-012
Map E

Notes: Heavy dust load, dominantly aluminosilicates.

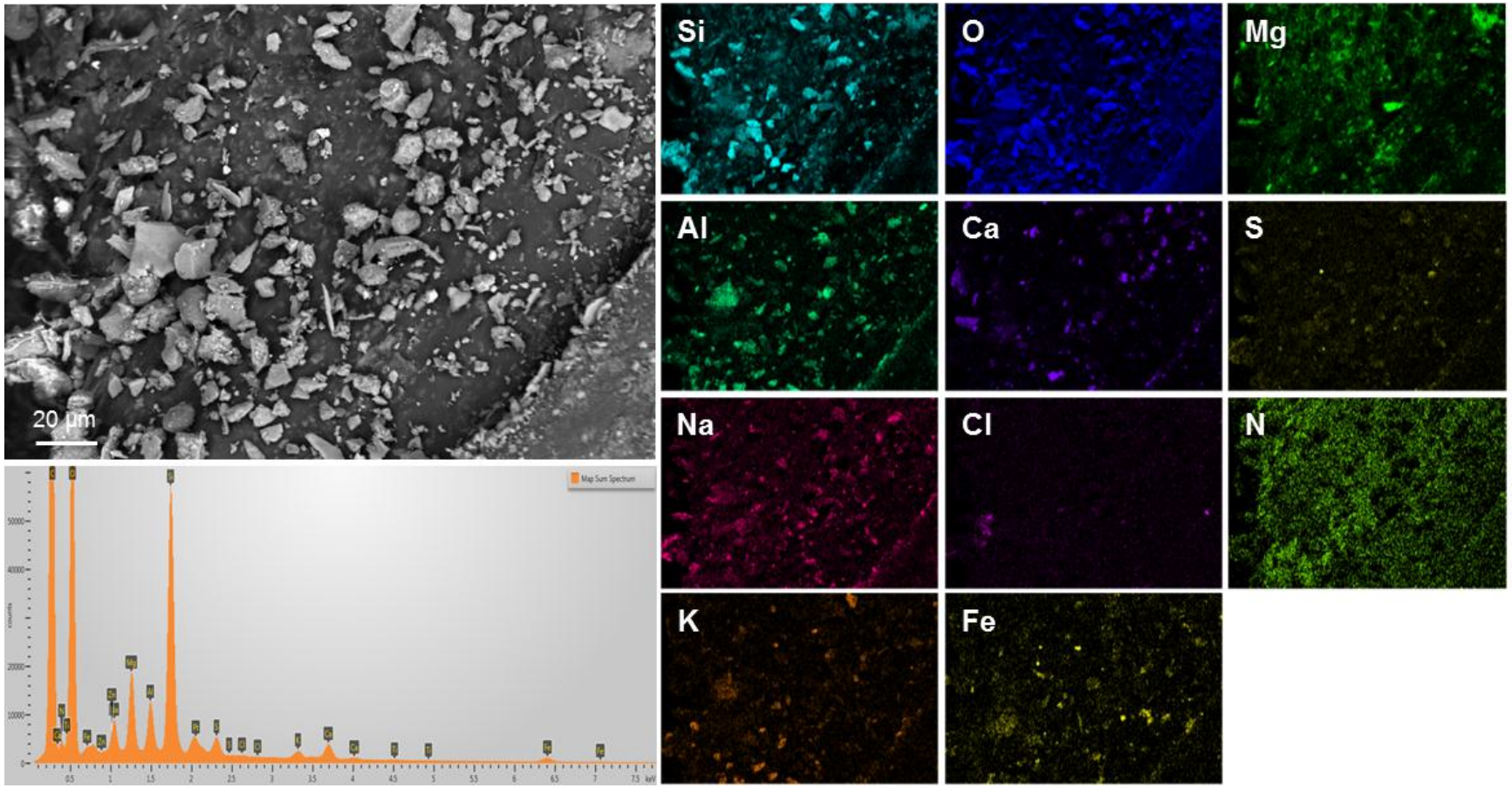

Sample: 145-012
Map F

Notes: heavy dust load, dominantly aluminosilicates, calcium carbonate, and Fe-oxides.

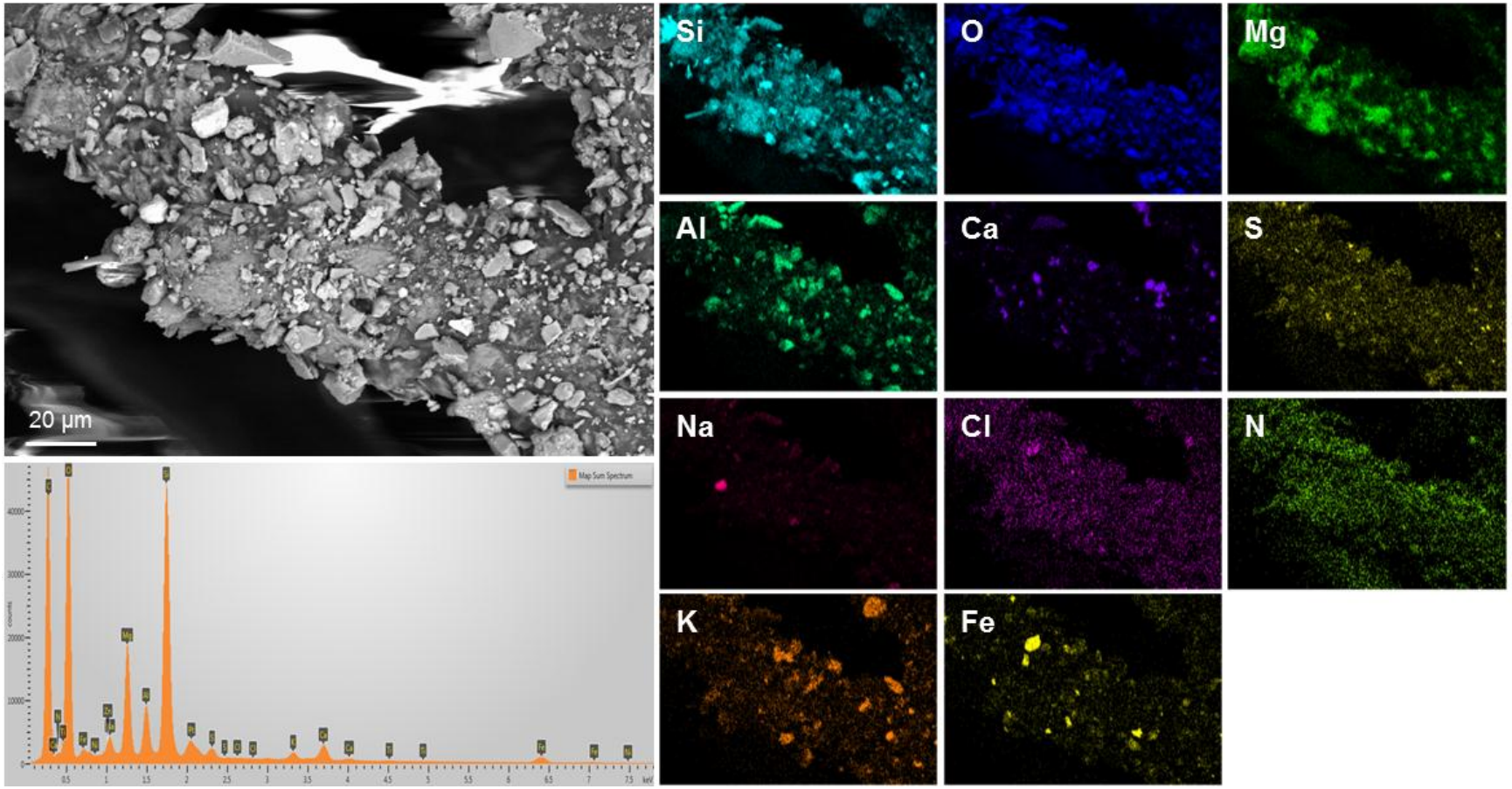

Sample: 145-012
Map G

Notes: Heavy dust load, dominantly aluminosilicates and calcium carbonate.

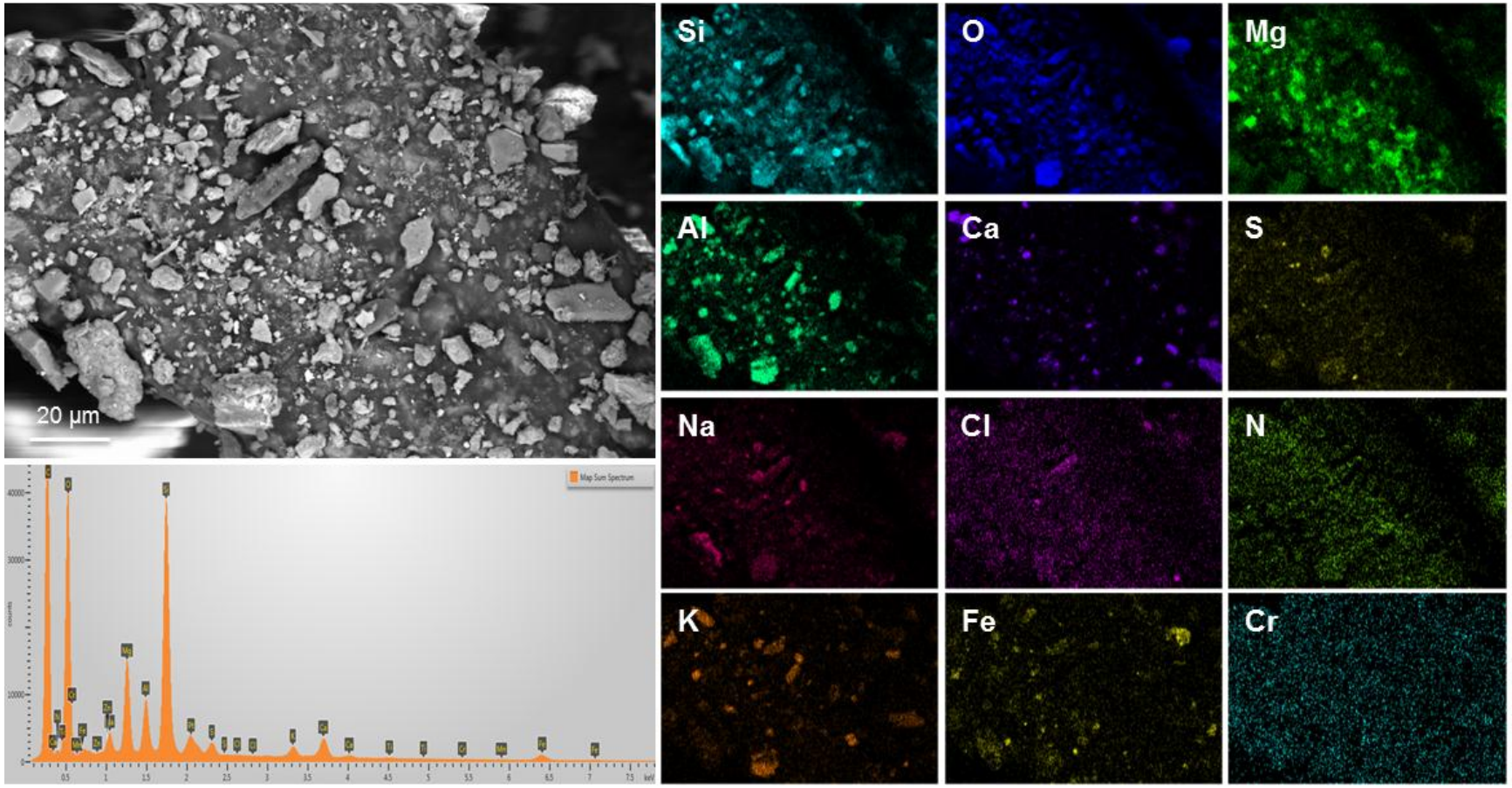

Sample: 145-012
Map H

Notes: Heavy dust load, dominantly aluminosilicates and calcium carbonate.

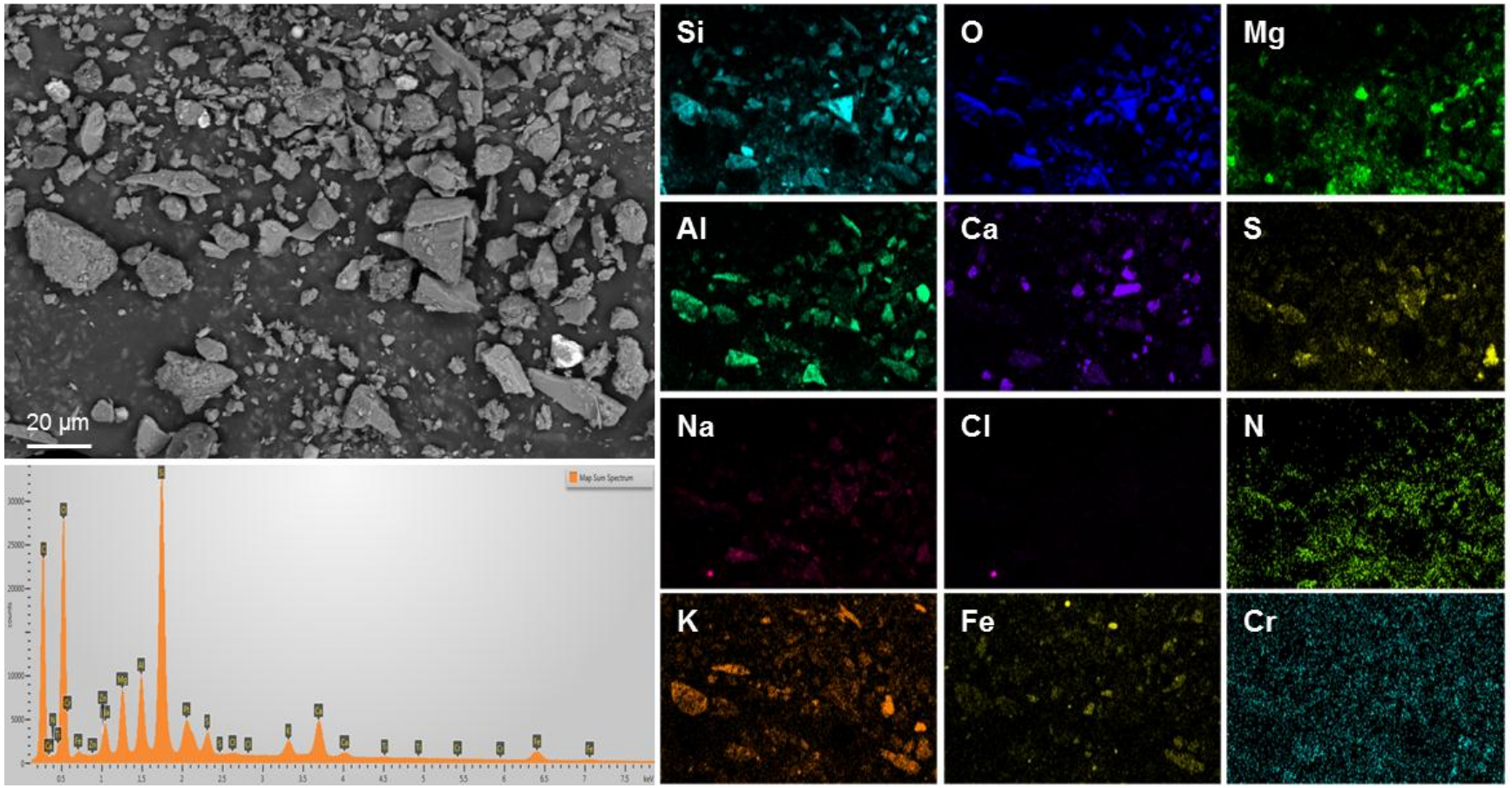

Sample: 145-012
Map I

Notes: Close-up of chloride-rich grain, lower left corner of Map H.

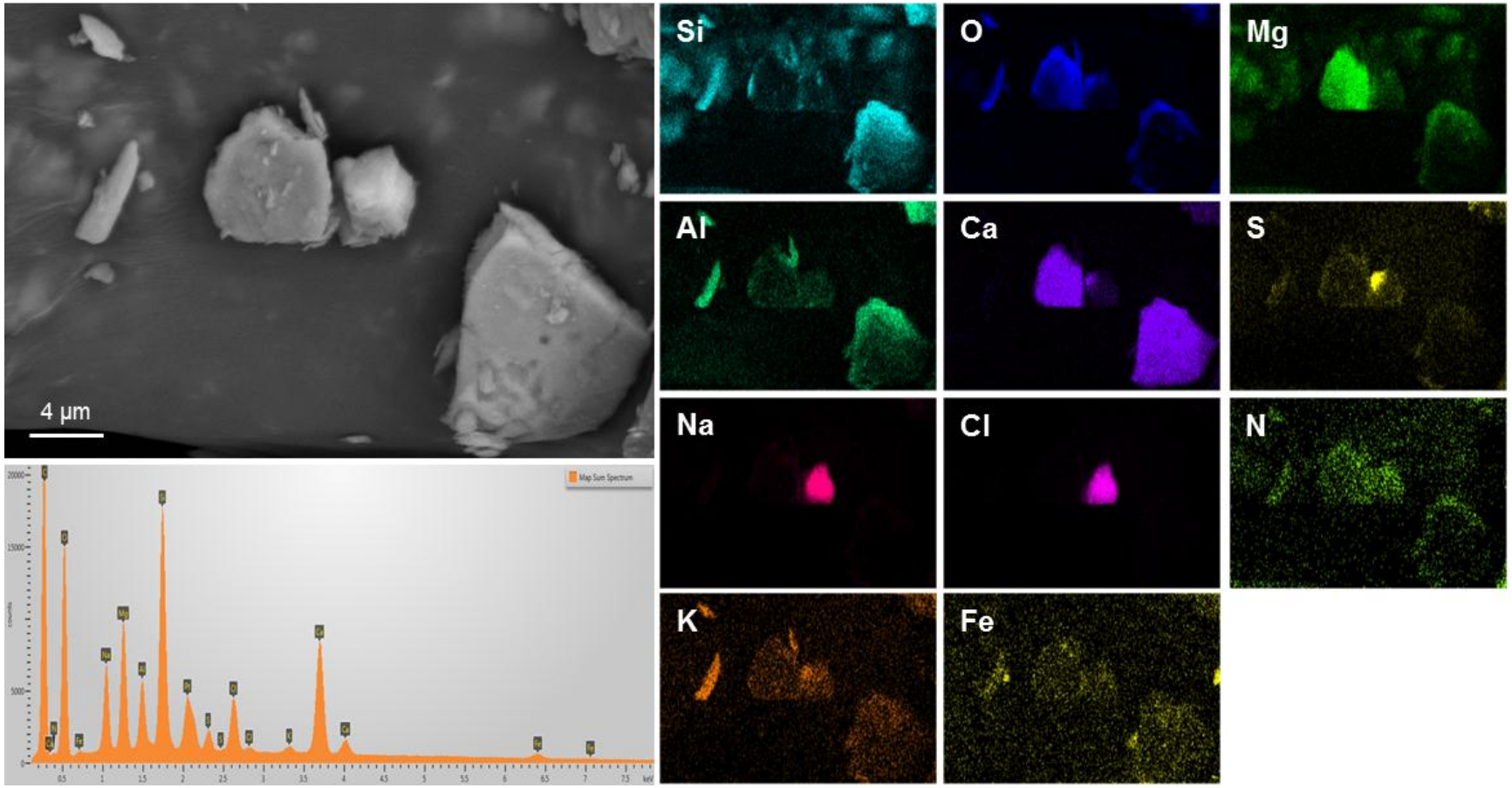

Sample: 145-012
Map J

Notes Heavy dust load, mostly aluminosilicates and calcium carbonate.

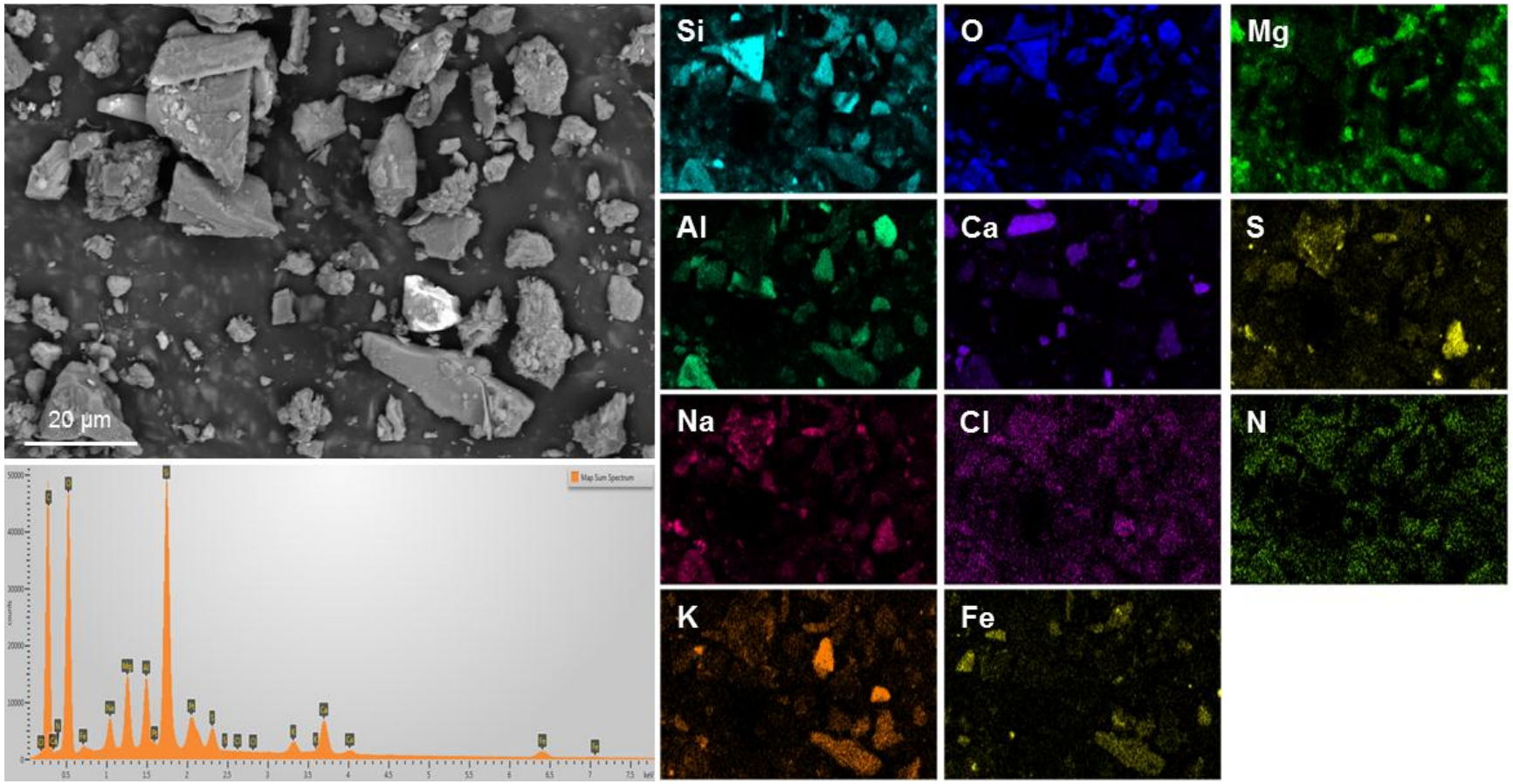

Sample: 123-001

Notes: Overview image of pad sample 123-001, showing the light load of fine dust particles.

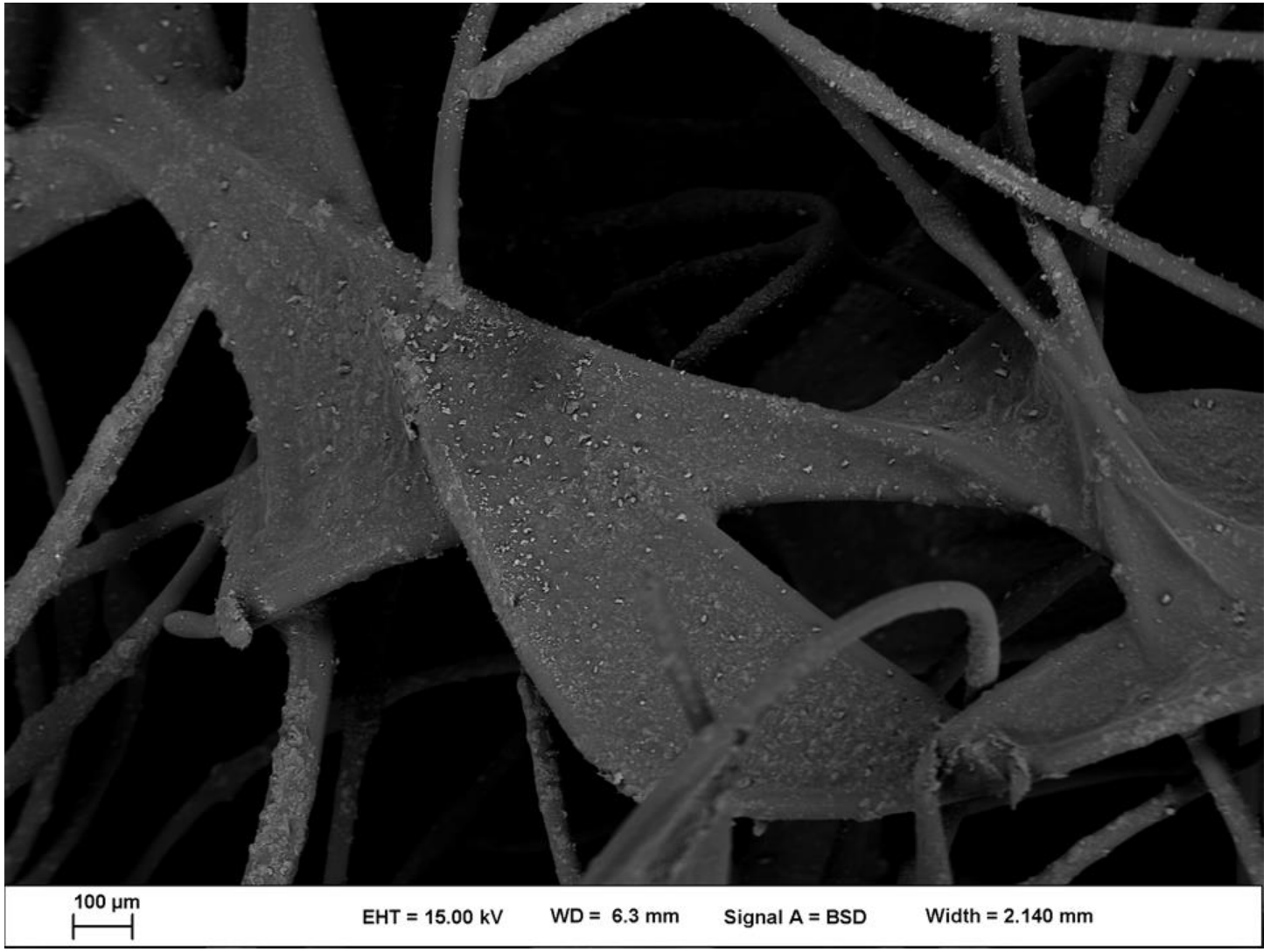

Sample: 123-001
Map A

Notes: Sparse mineral grains, dominantly NaCl with associated Ca-SO_4.

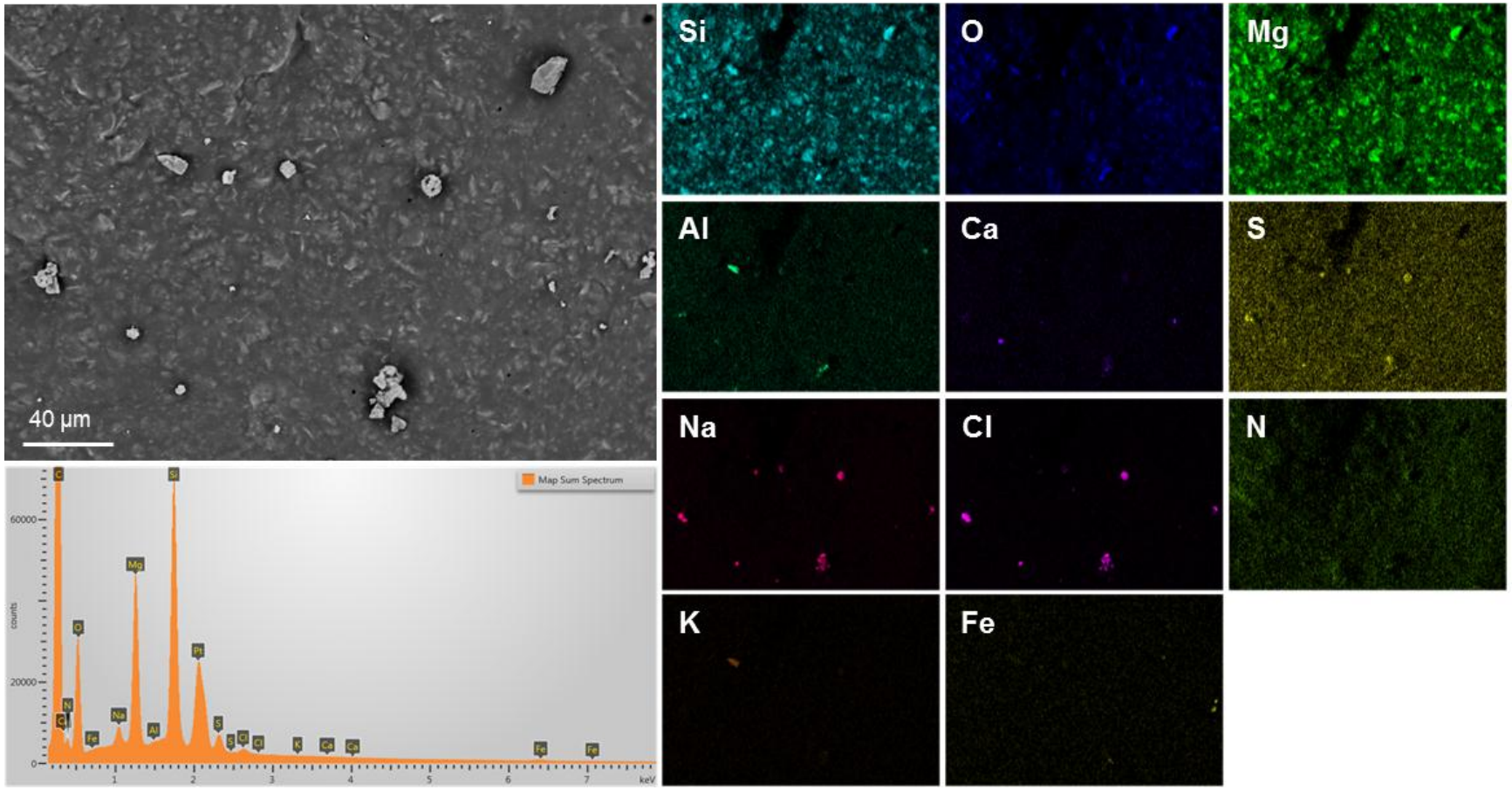

Sample: 123-001

Map B

Composite mineral grain, with NaCl and aluminosilicates.

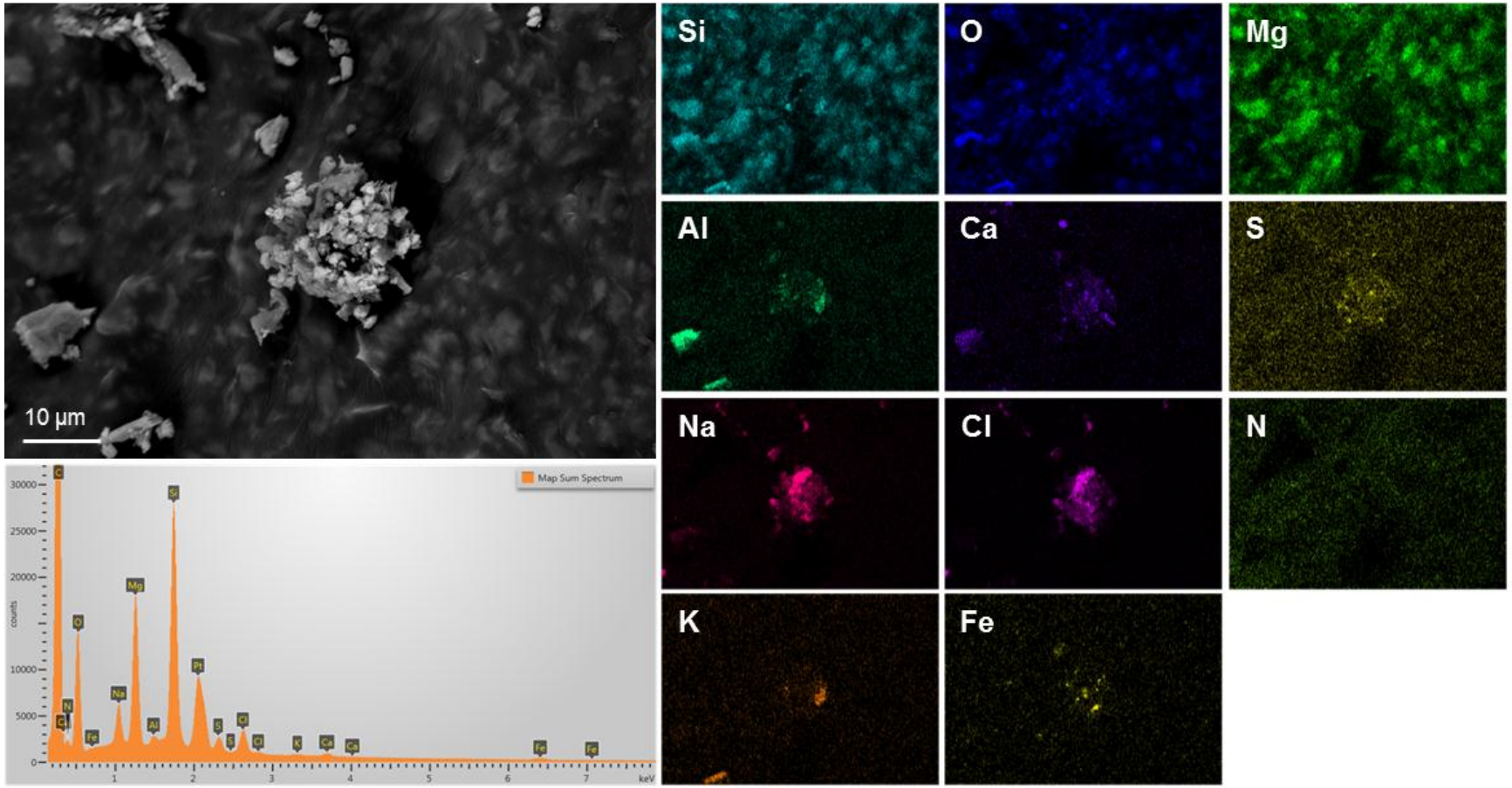

Sample: 123-006

Notes: Overview image of pad sample 123-006, showing the light dust load around an abraded region on the pad.

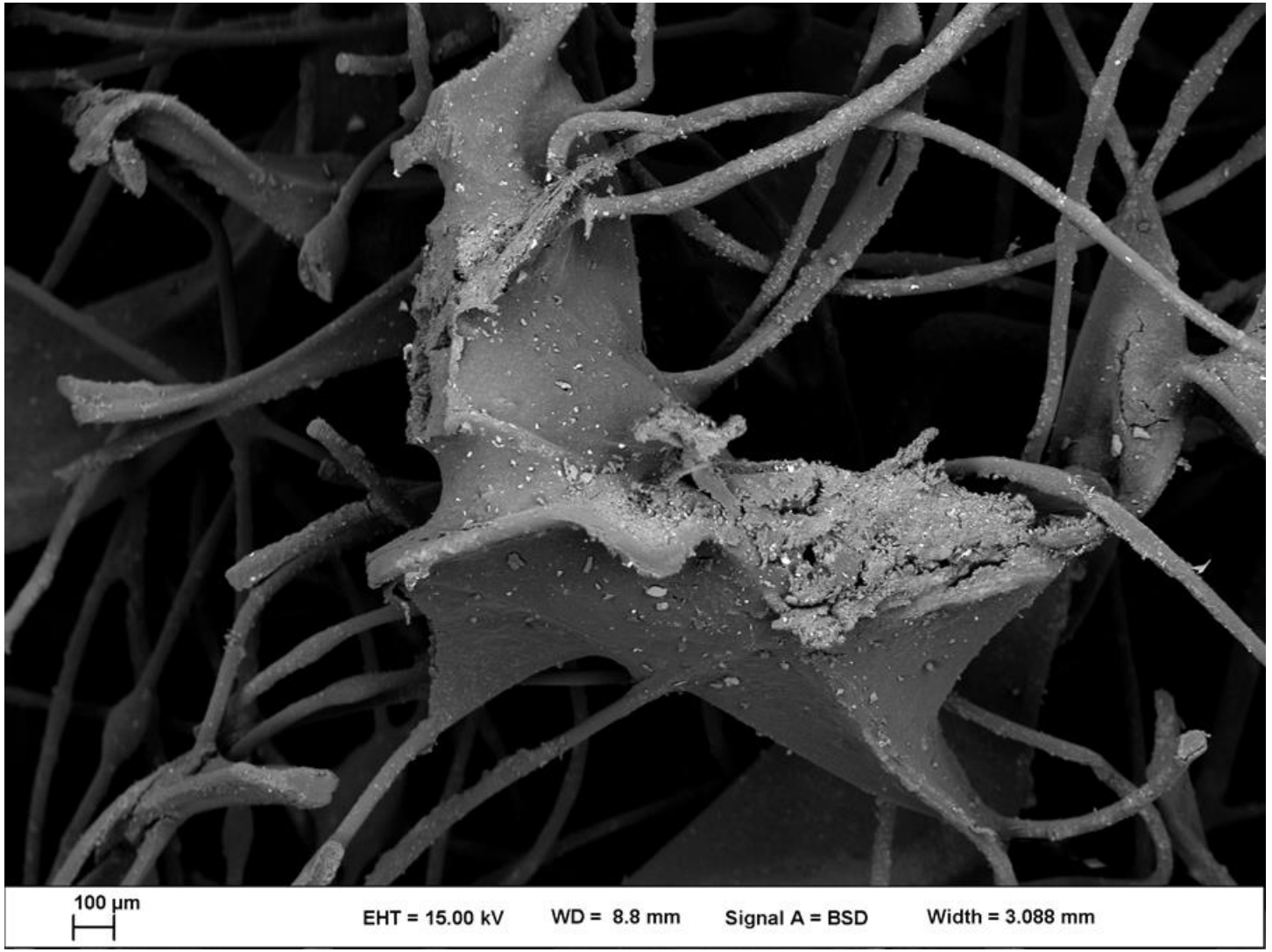

Sample: 123-006
Map A

Notes: Particles mostly talc, liberated by abrasion of the pad. Dust phases include NaCl.

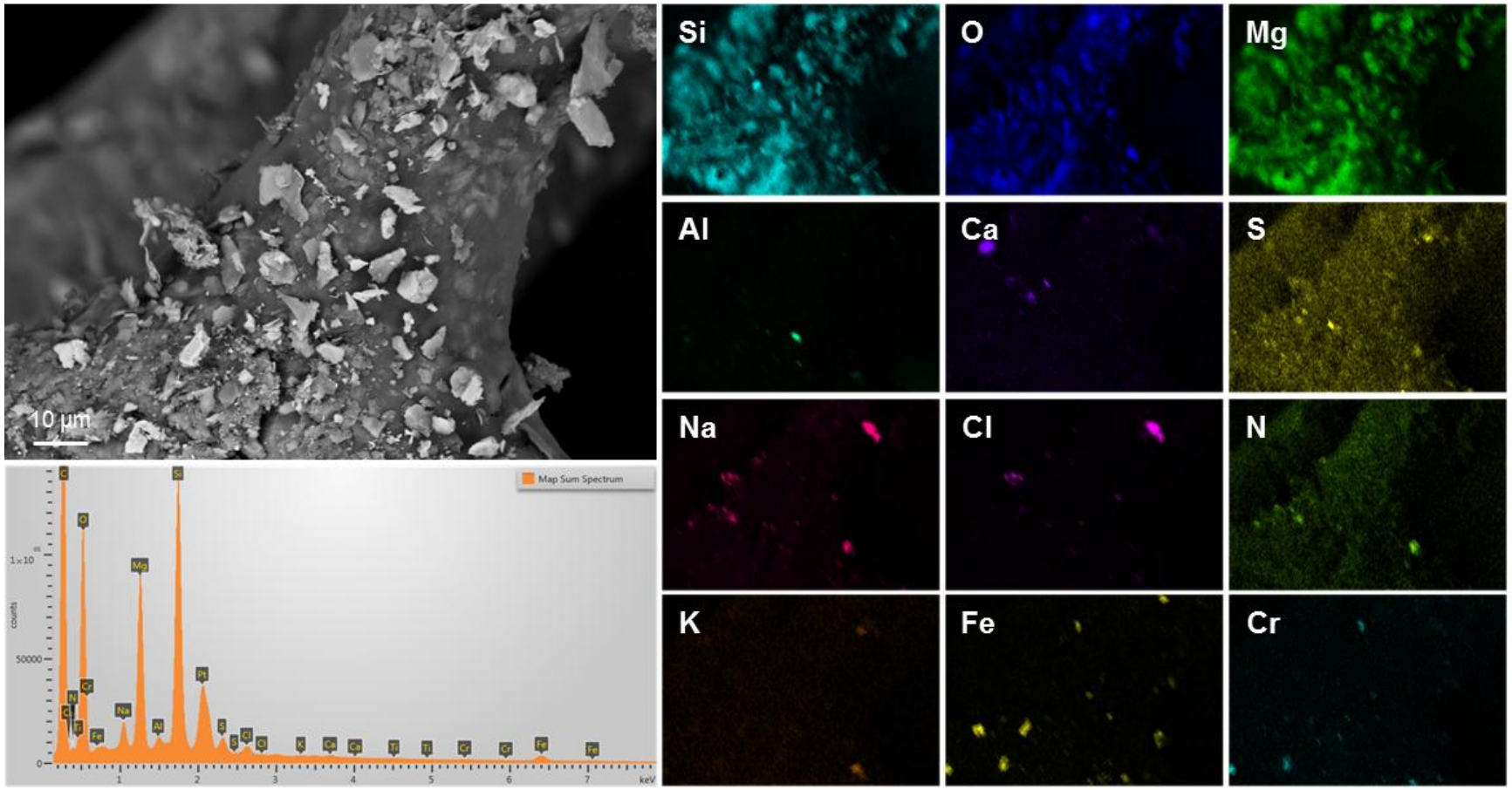

Sample: 123-006
Map B

Notes: Particles mostly talc, liberated by abrasion of the pad. Sparse dust particles, dominantly stainless steel (Fe-Cr) and Fe.

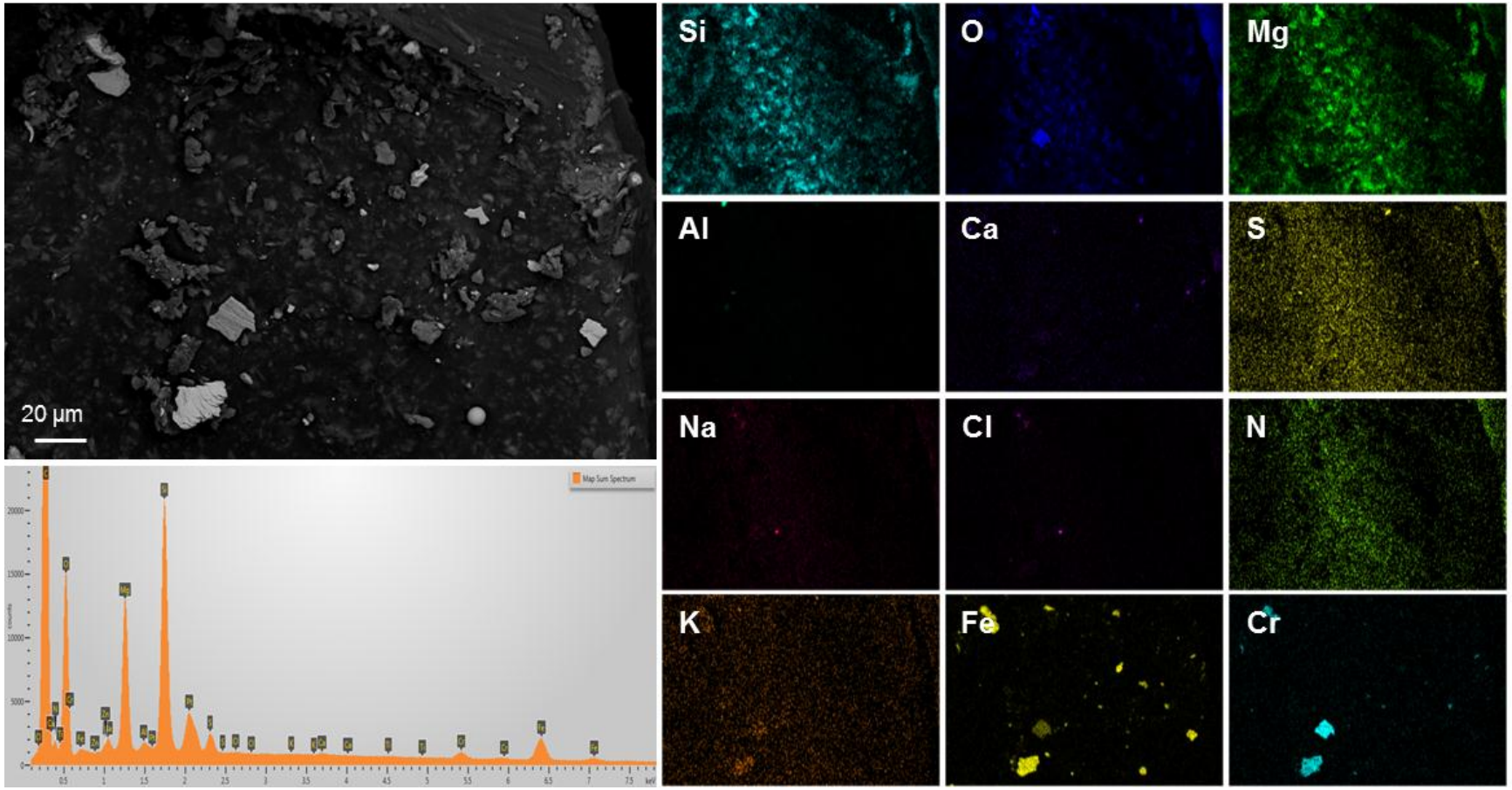

Sample: 123-006
Map C

Notes: Large NaCl grains. Stainless steel and Fe-oxide particles are also present.

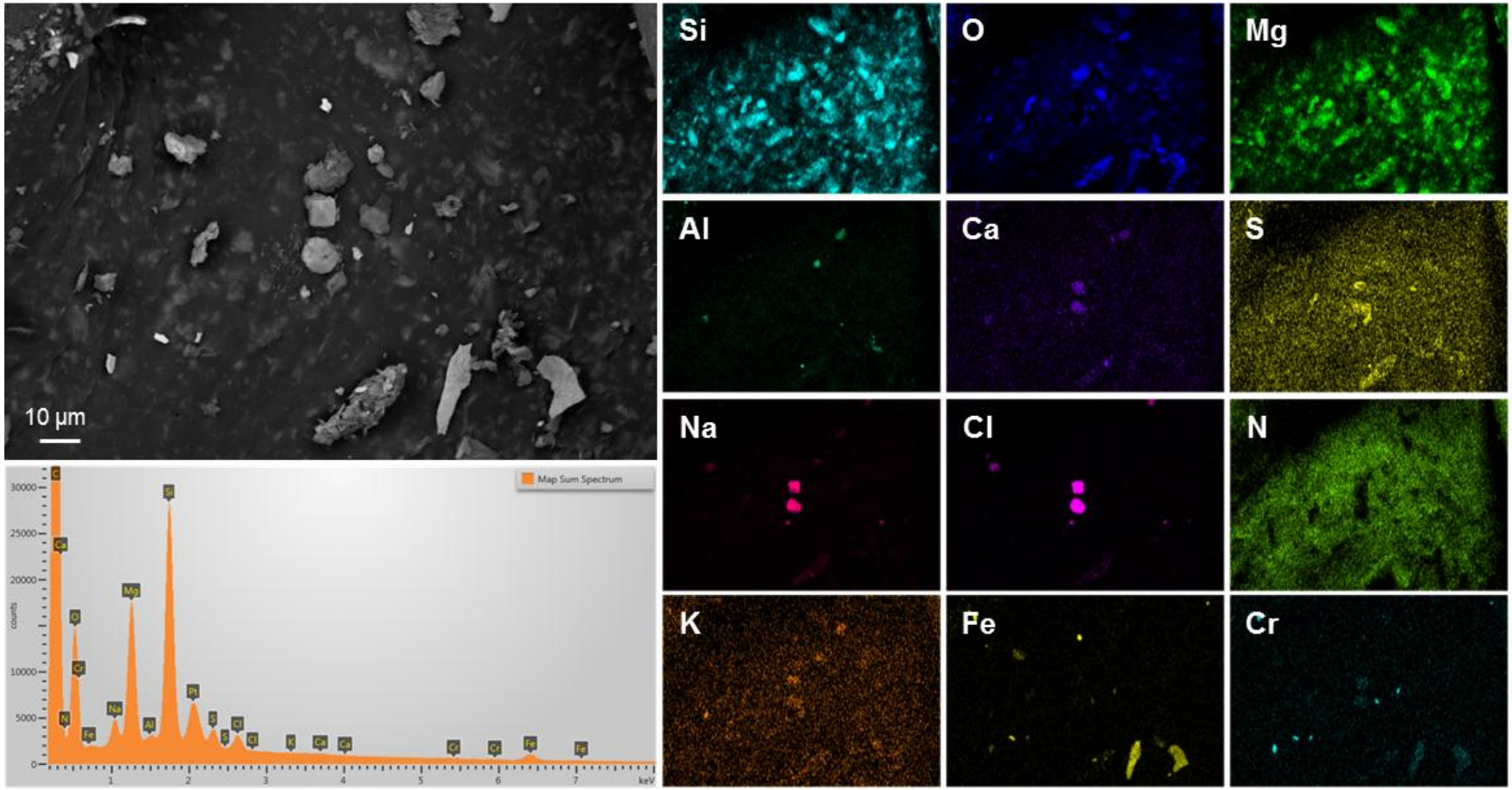

Sample: 123-006
Map D

Notes: Particles mostly talc, liberated by abrasion of the pad. Some stainless steel and iron particles, and aluminosilicates.

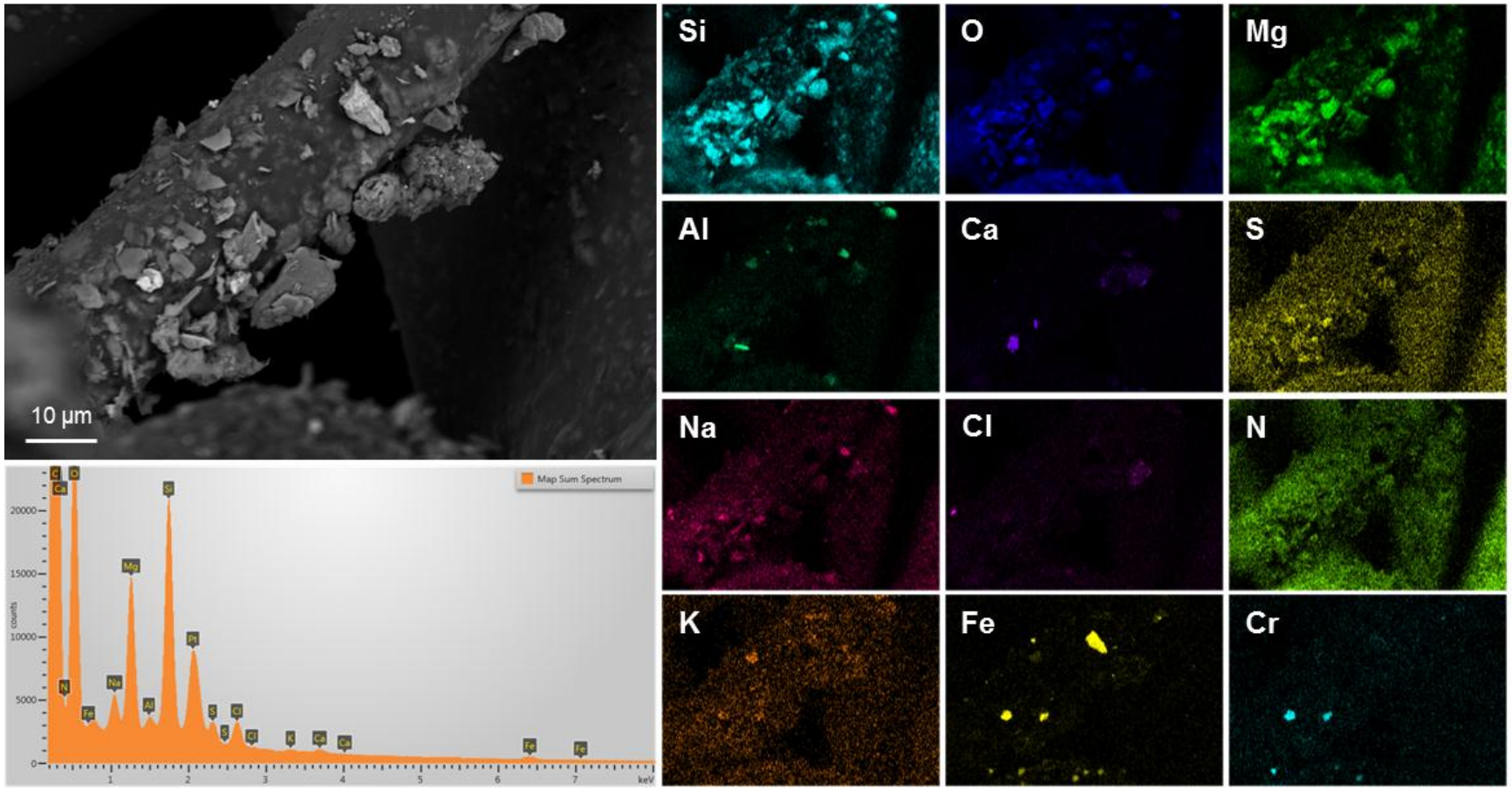

Sample: 123-008

Notes: Overview image of pad sample 123-008, showing the light dust load.

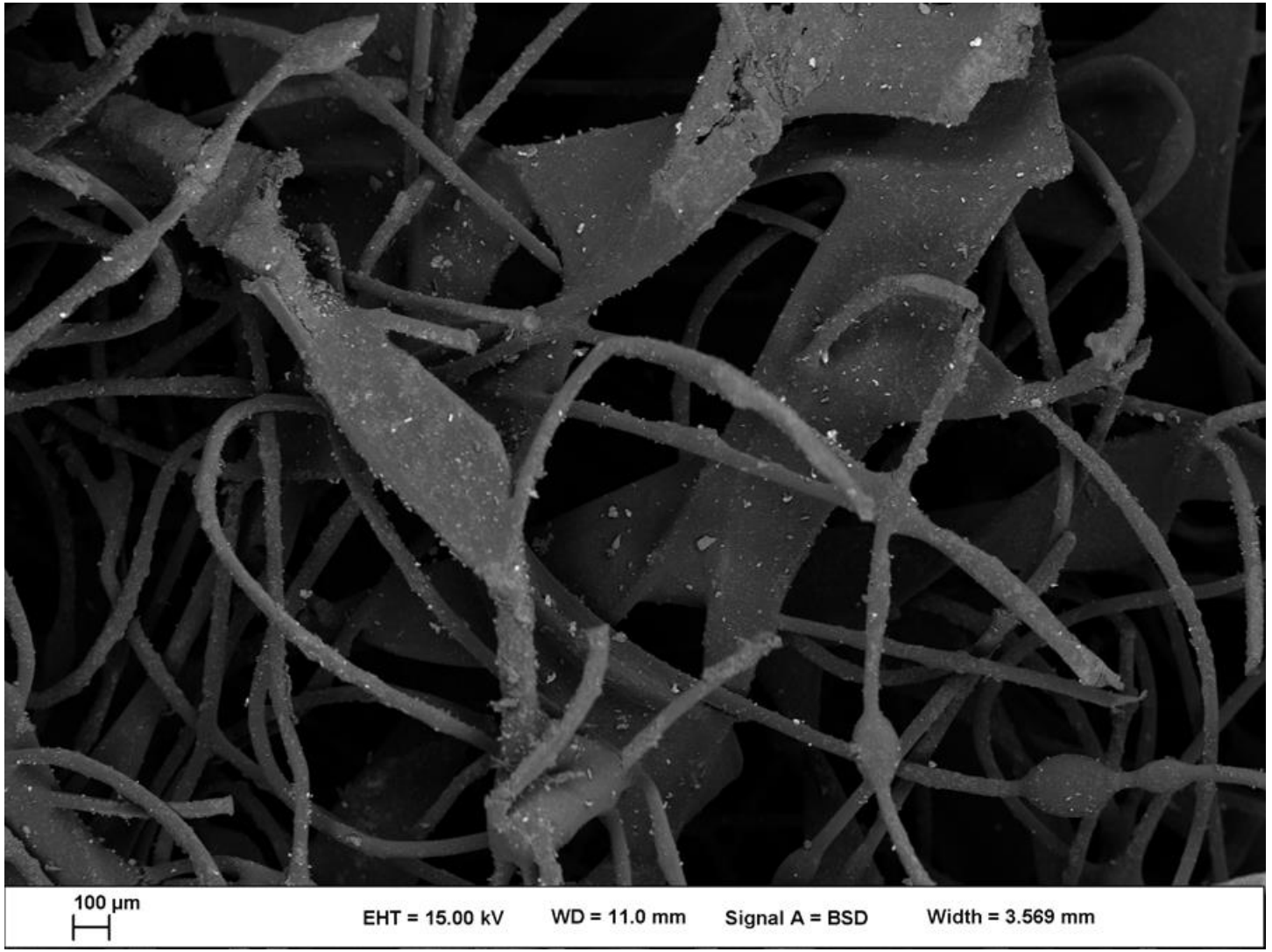

Sample: 123-008
Map A

Notes. Sparse dust particles, dominantly phases rich in Fe and Fe-Cr; some are oxidized. Probably products of canister manufacturing.

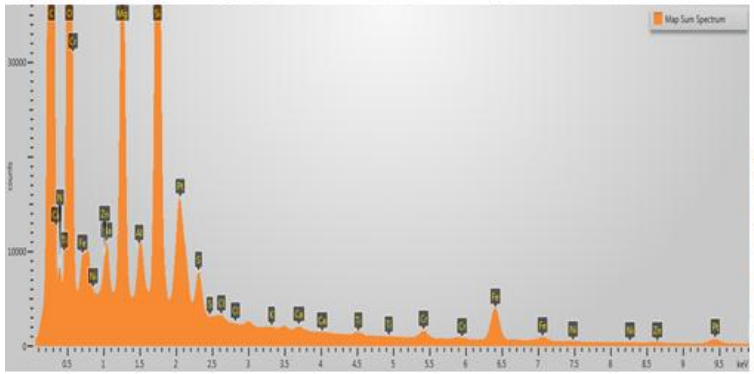

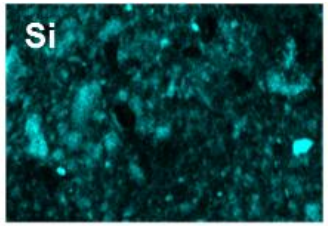

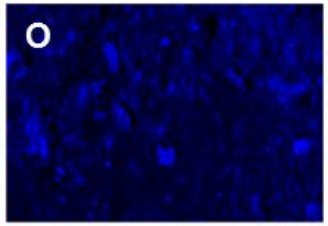

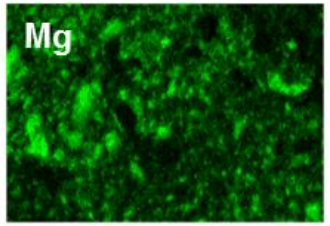

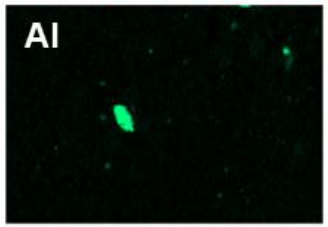

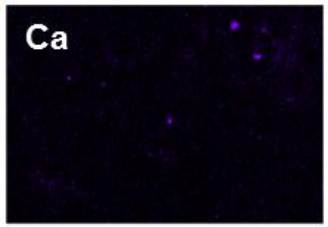

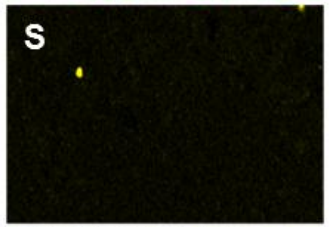

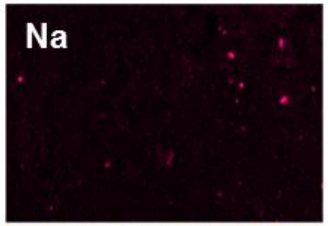

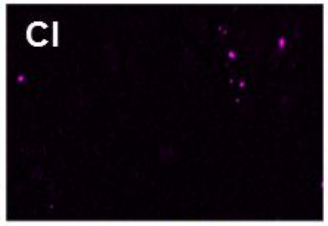

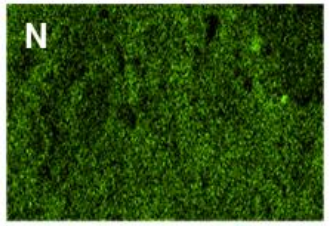

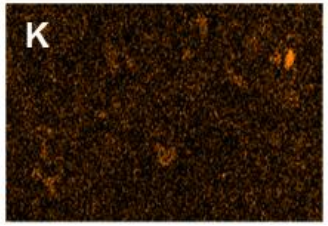

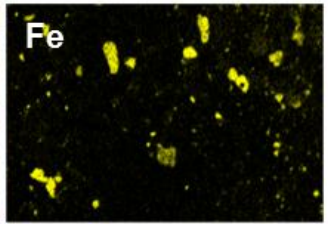

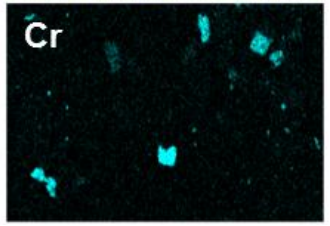

Sample: 123-008
Map B

Notes: Sparse dust particles, dominantly phases rich in Fe and Fe-Cr; some are oxidized.

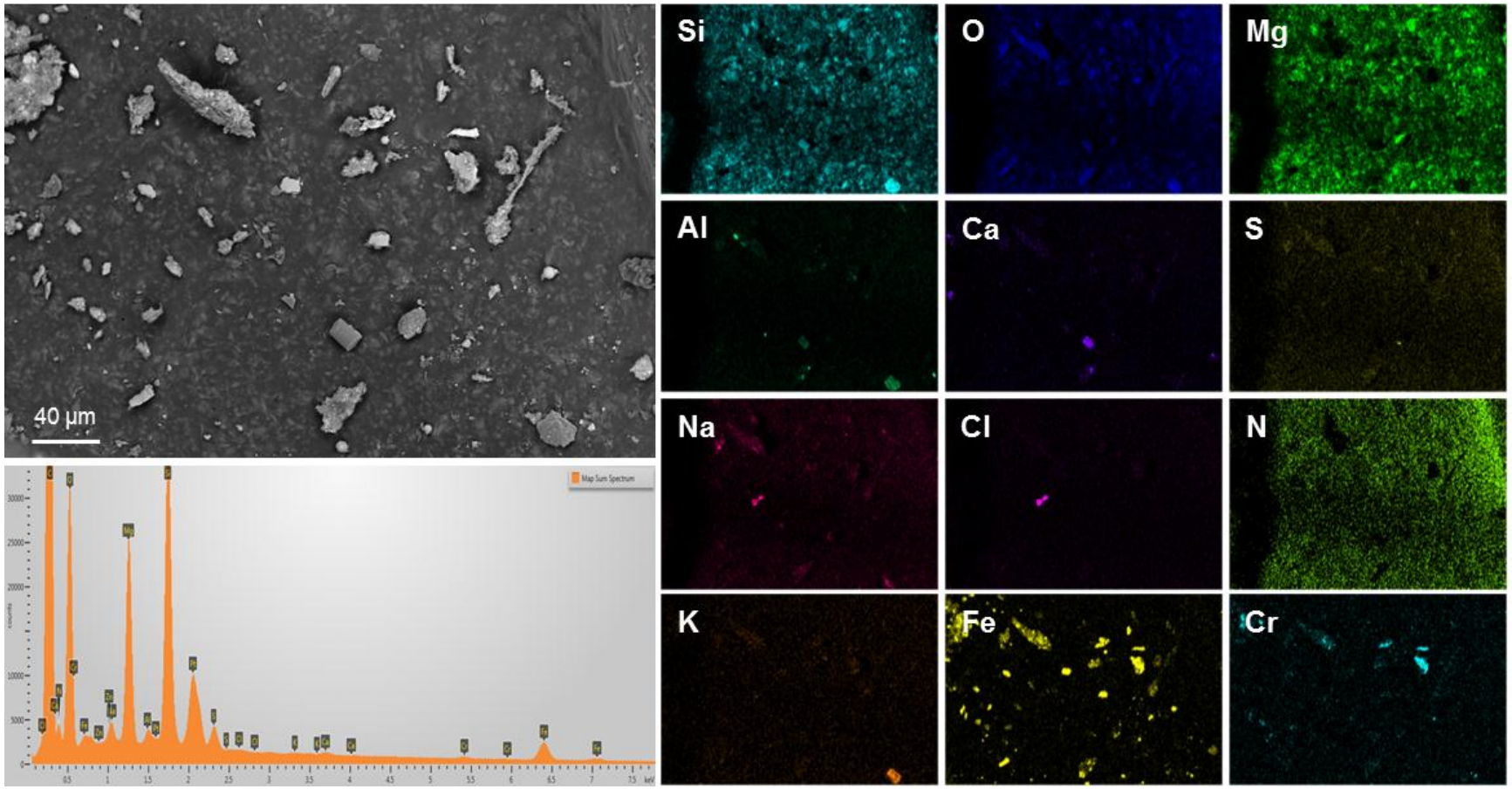

Sample: 123-008
Map C

Notes: Sparse dust particles, dominantly phases rich in Fe and Fe-Cr (Cr map not collected).

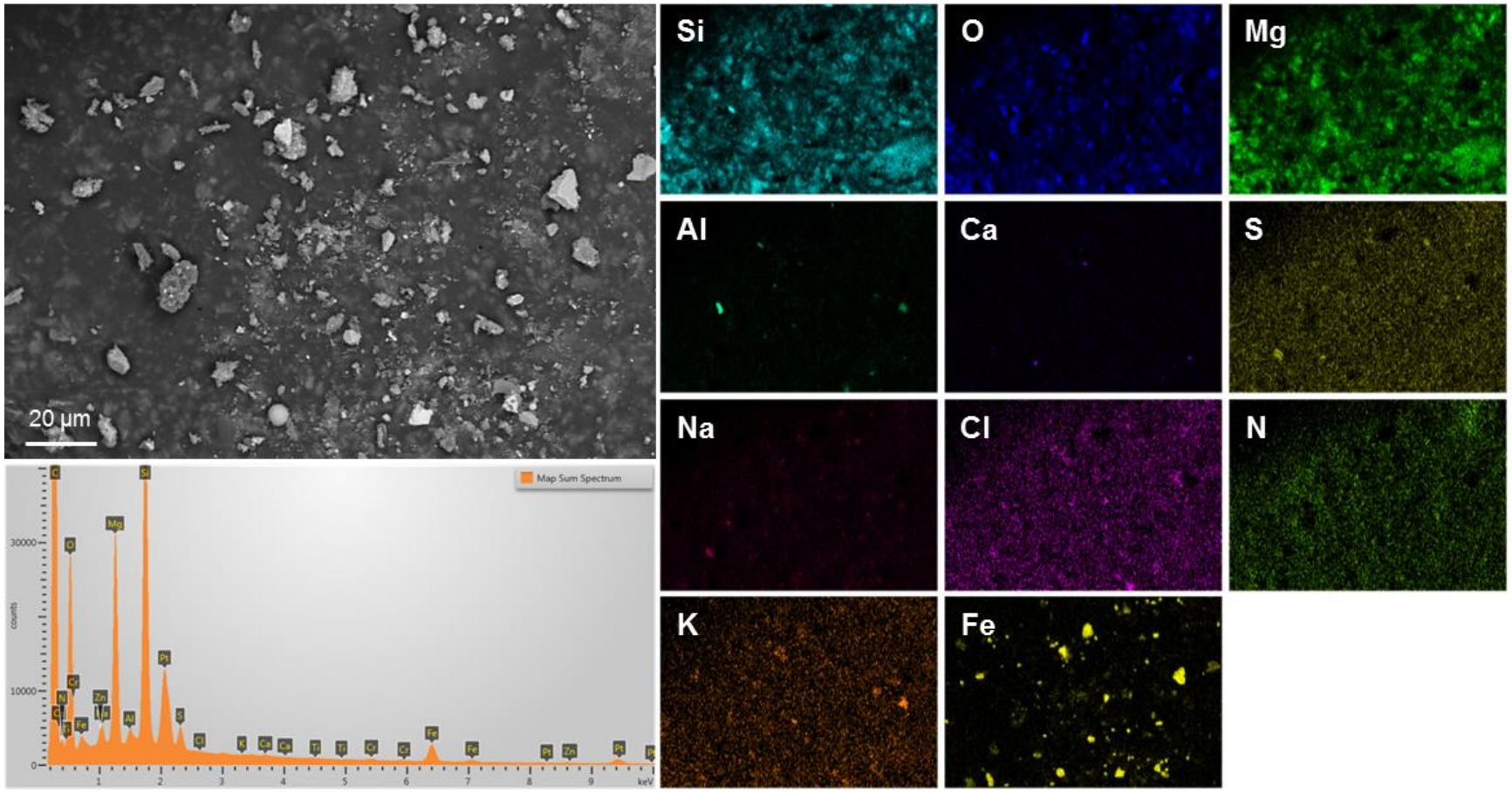

Sample: 123-009

Notes: Overview image of pad sample 123-009, showing the light dust load.

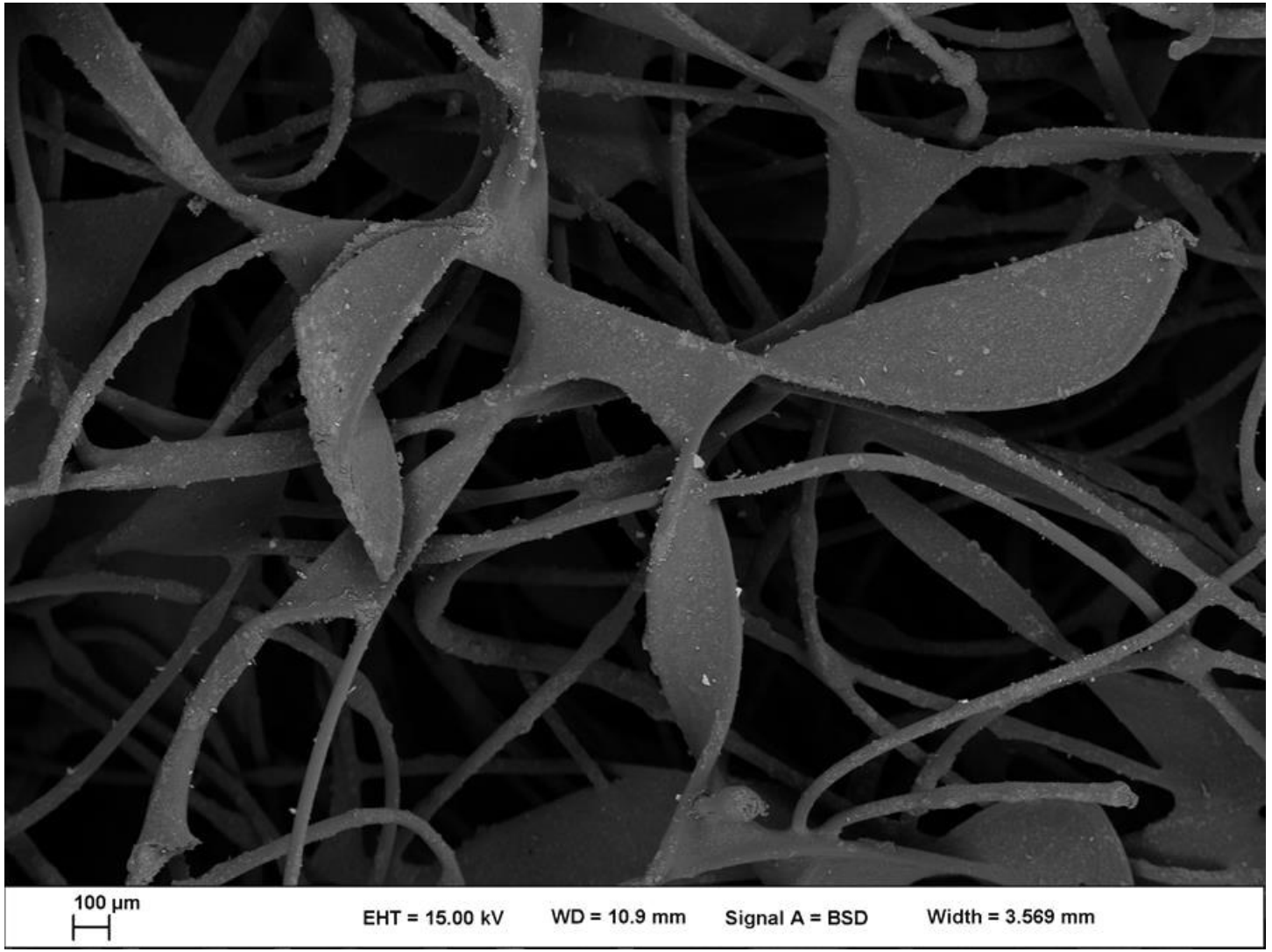

Sample: 123-009
Map A

Notes: Sparse dust particles, dominantly stainless steel.

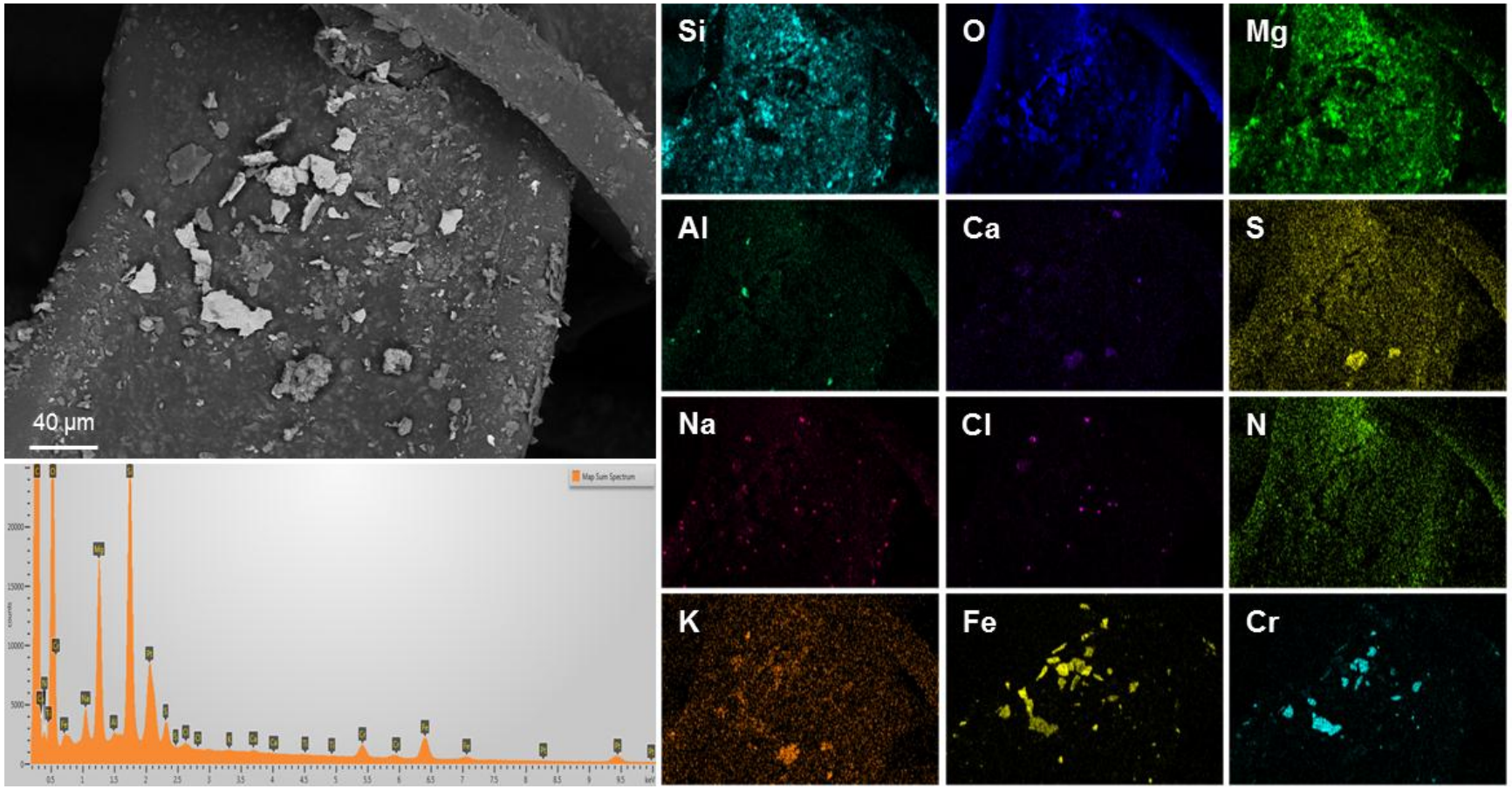

Sample: 123-009
Map B

Notes: Organic-rich composite grain showing possible biostructures?

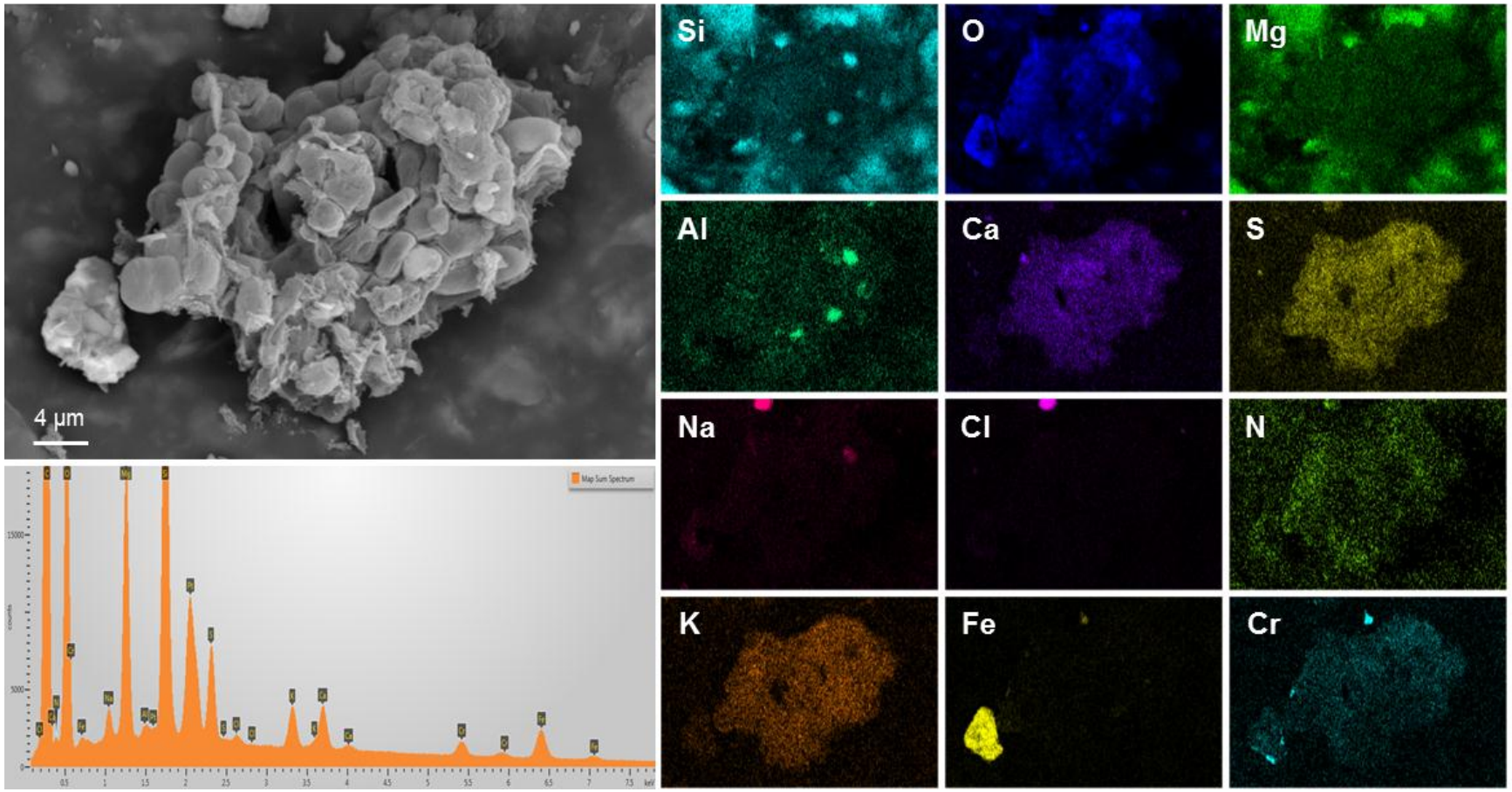

Sample: 123-009
Map C

Notes: $NaNO_3$ and NaCl salt particles. Stainless steel particles common. Ca-carbonate rod of biological origin in lower left.

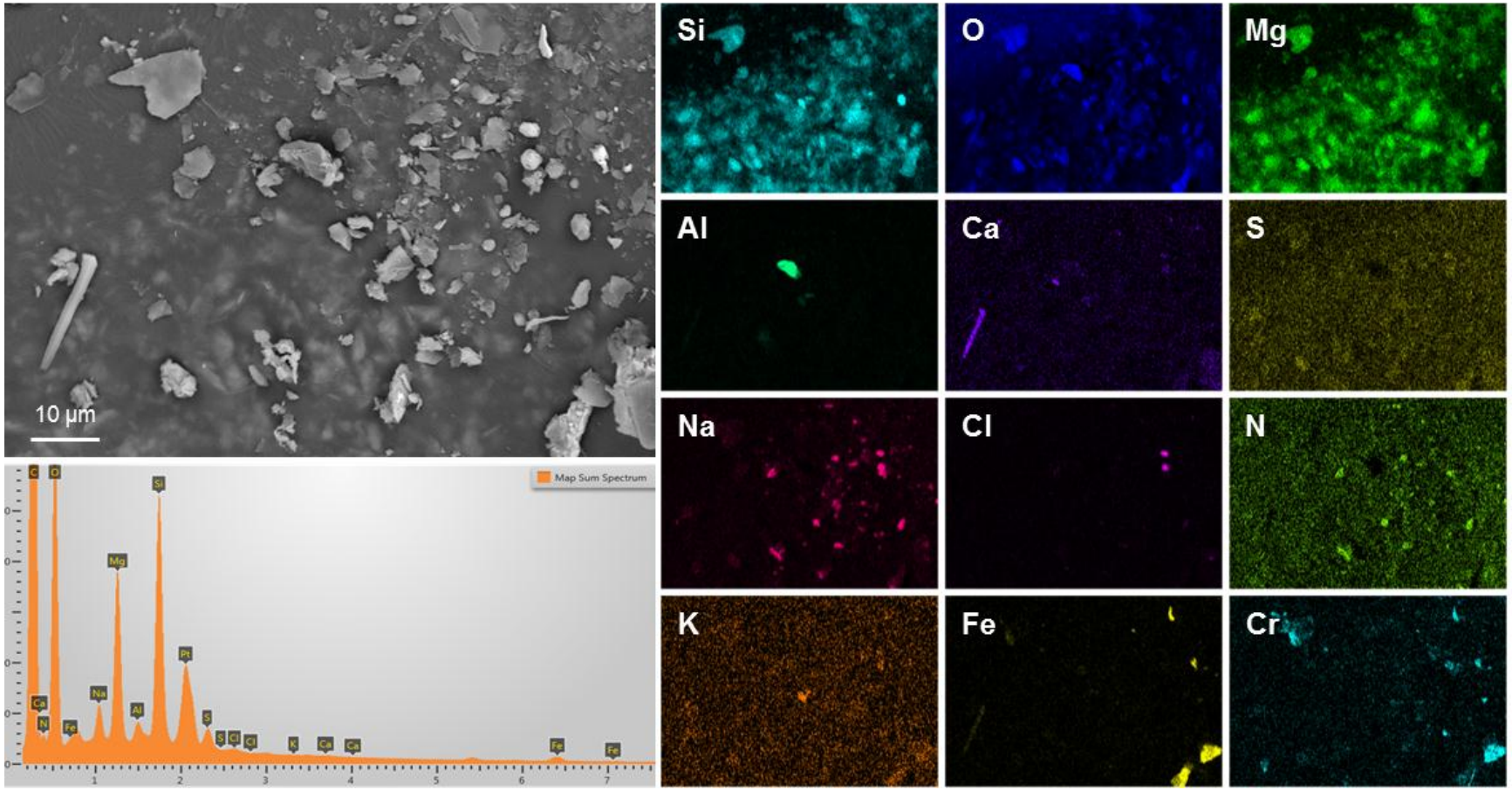

Sample: 123-009
Map D

Notes: Close-up of Na-NO_3 phase in the lower left corner of image C. Nitrogen content decreased as the sample was heated in the beam, and chloride signal increased, suggesting that the nitrogen phase was decomposing in the beam.

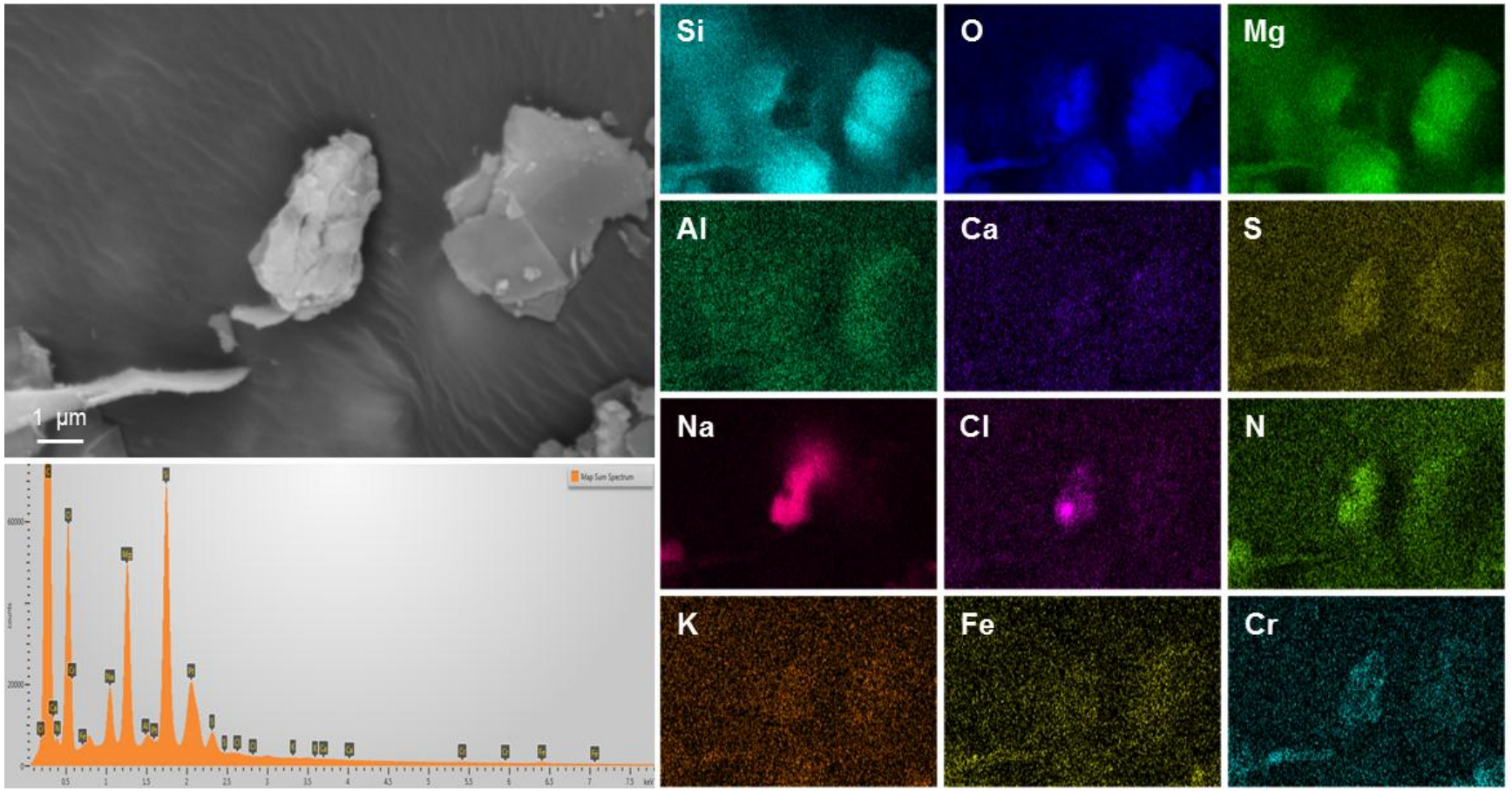

Sample: 123-009
Map E

Notes: Composite grain of NaCl and $NaNO_3$ salts.

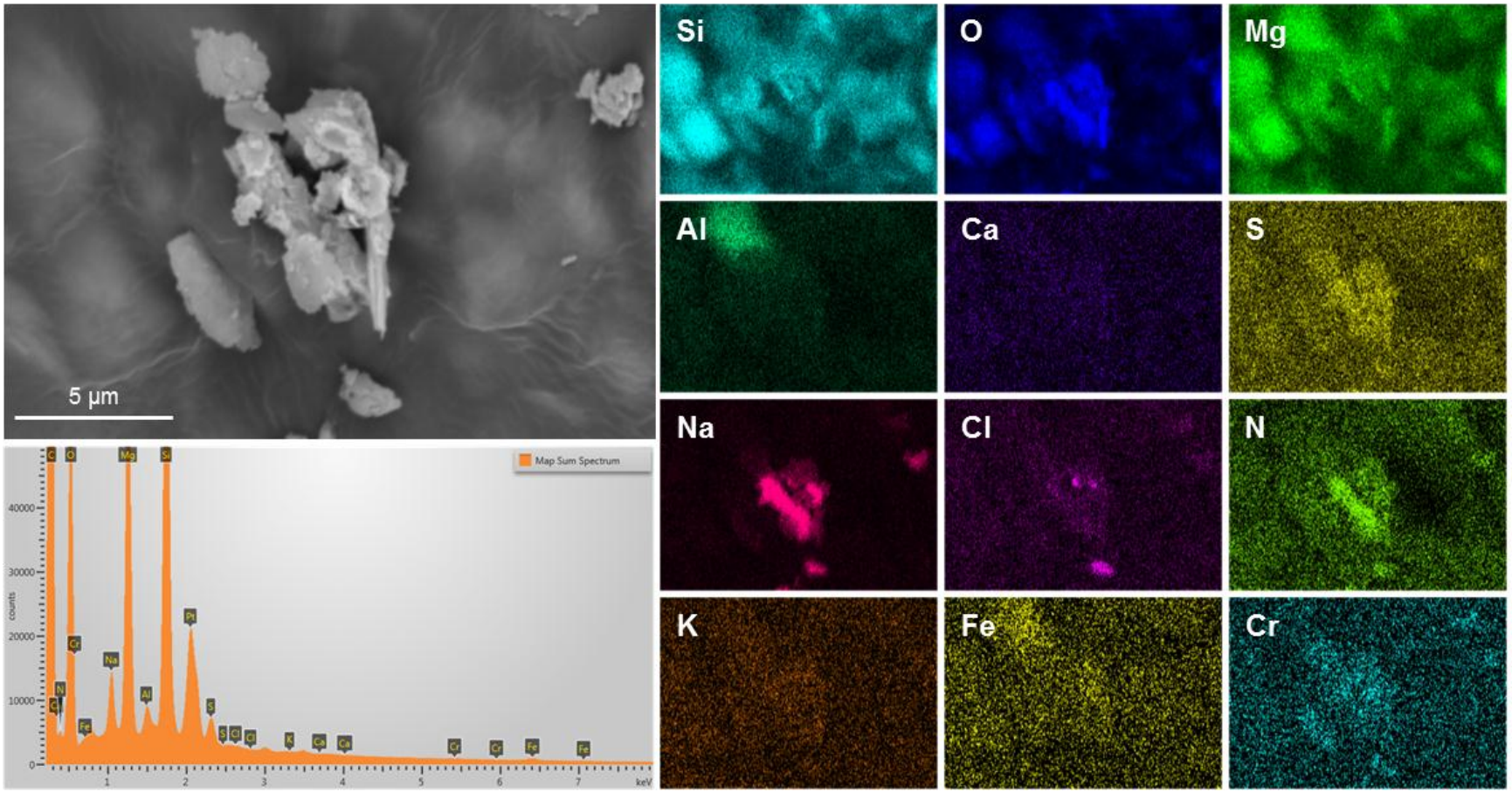

Sample: 123-009
Map F

Notes: Most particles are talc, liberated by abrasion of the pad. Sparse dust, including $NaNO_3$ and stainless steel particles.

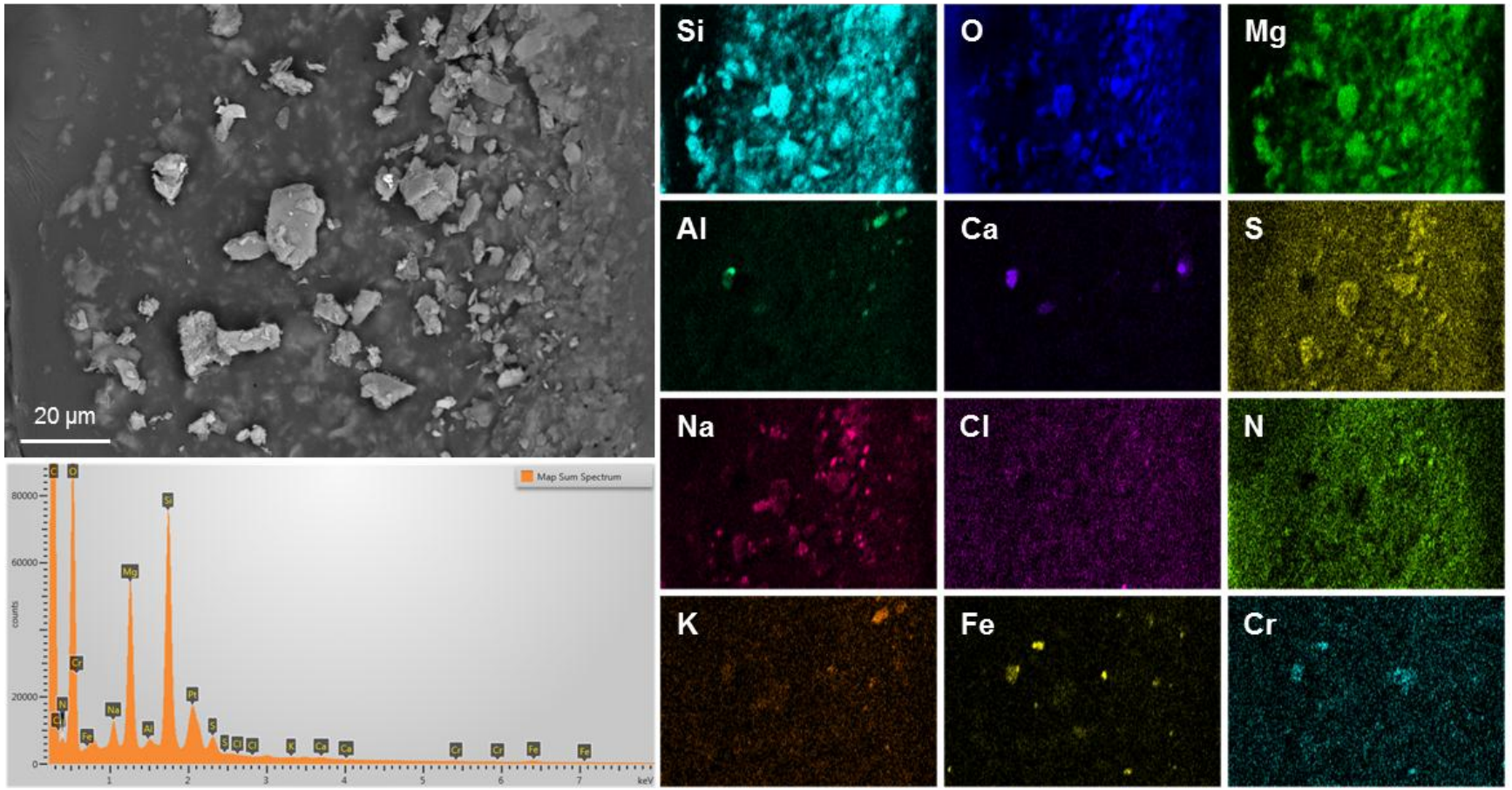

Sample: 123-009
Map G

Notes: Most particles are talc, liberated by abrasion of the pad. Sparse dust, including $NaNO_3$.

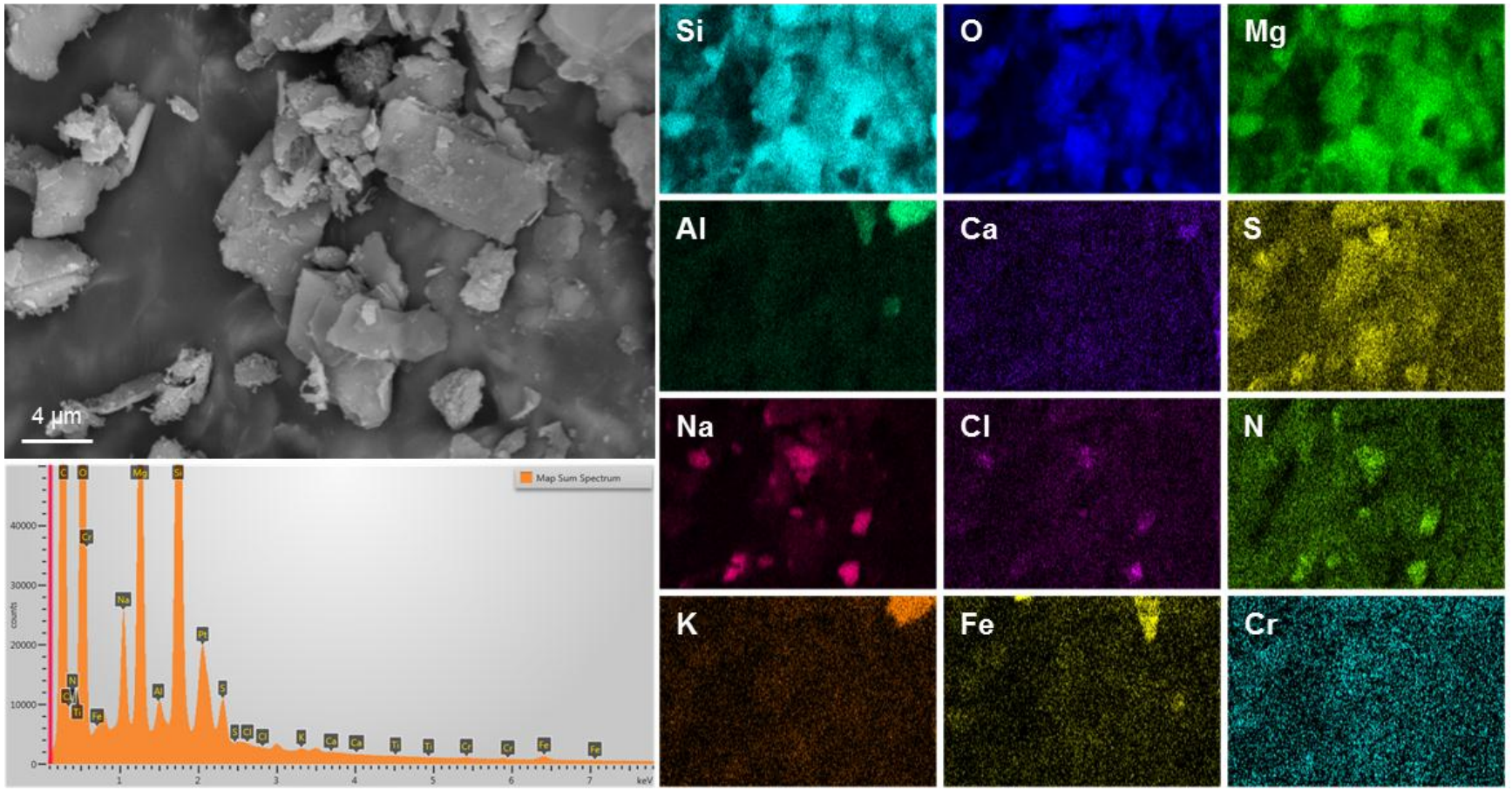

Sample: 123-009
Map H

Notes: Most particles are talc, liberated by abrasion of the pad. Sparse dust, including NaCl and $NaNO_3$, and stainless steel particles. Note association of Ca-SO_4 with NaCl.

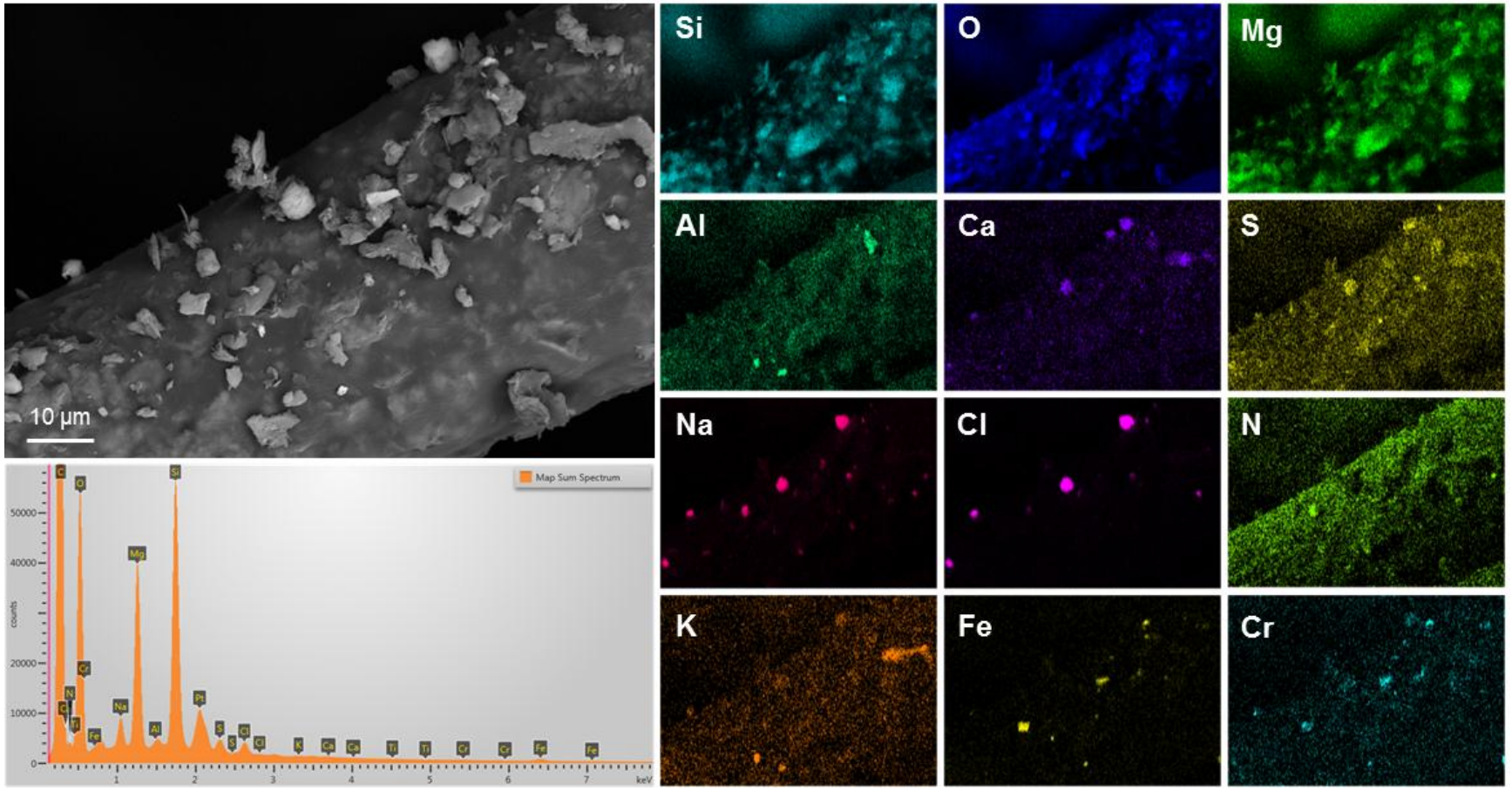

Sample: 123-009
Map I

Notes: Close-up of NO_3-rich grain in left center of Map H. Nitrogen content dropped as the beam heated the grain, and the chloride content increased, suggesting that the grain was decomposing and releasing nitrate, leaving behind a core of chloride.

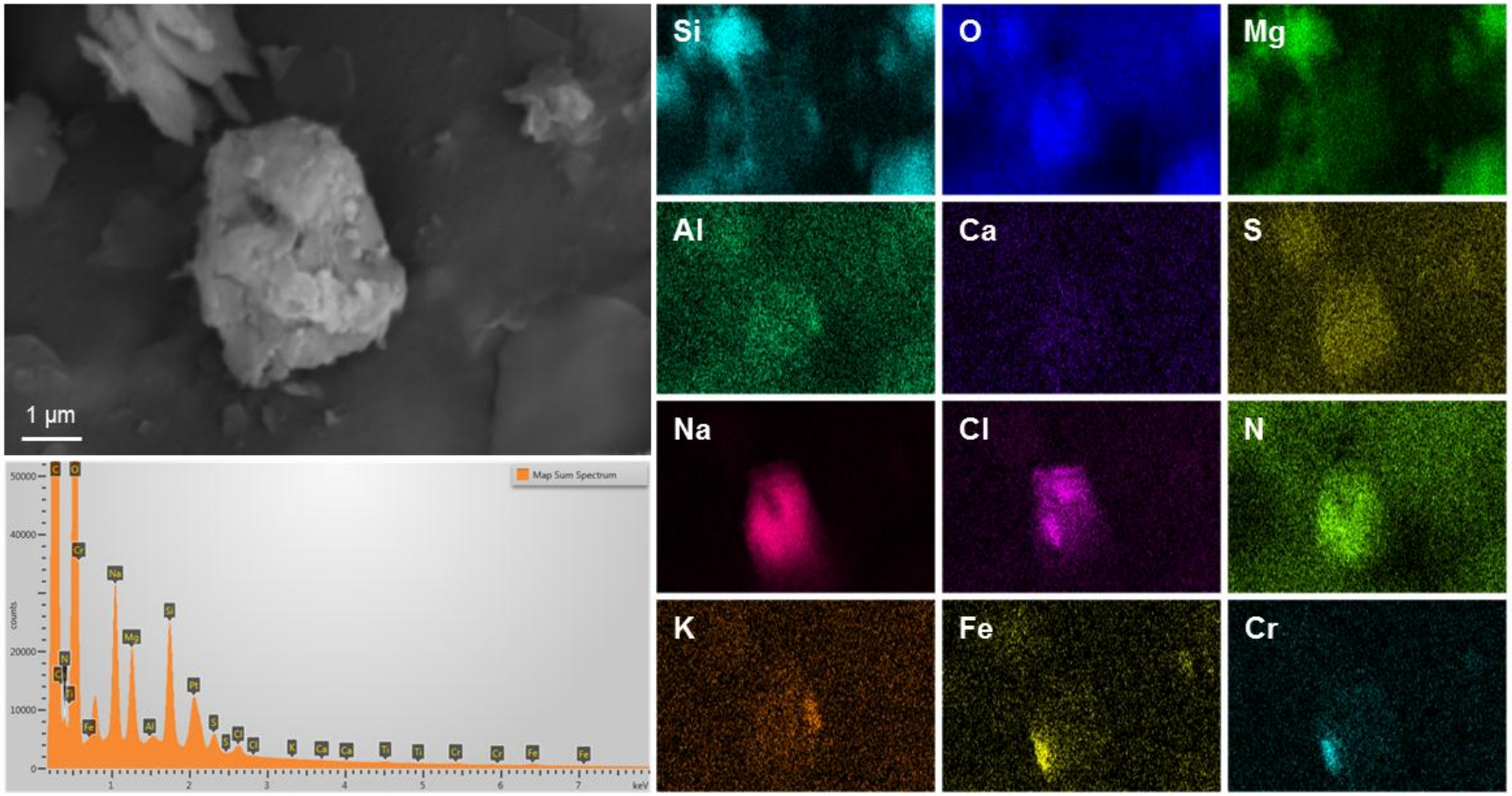

Sample: 123-009
Image of grain in Map I, before and after element mapping

Notes: Grain was originally Na-NO_3 rich, but decomposed due to heating during element mapping; nitrogen signal decreased, while the Chlorine signal increased. Interpreted as loss of $NaNO_3$ from the grain surface, revealing a NaCl core.

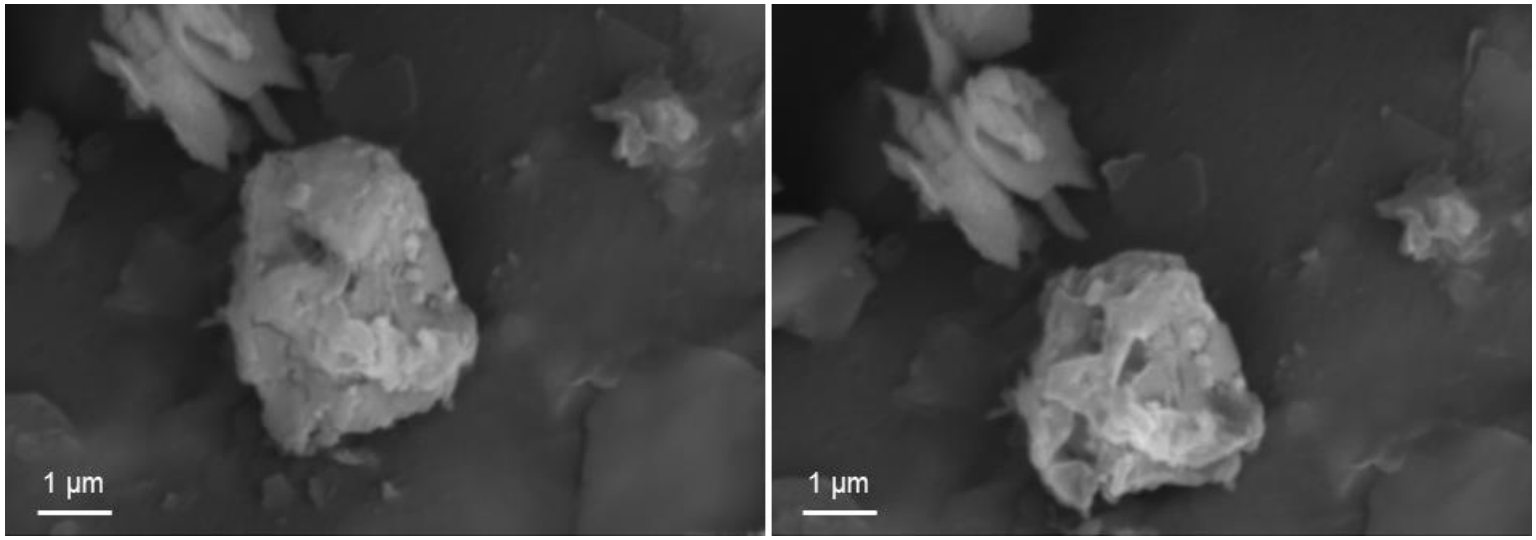

Sample: 123-012

Notes: Overview image of pad sample 123-012, showing the heavy dust load.

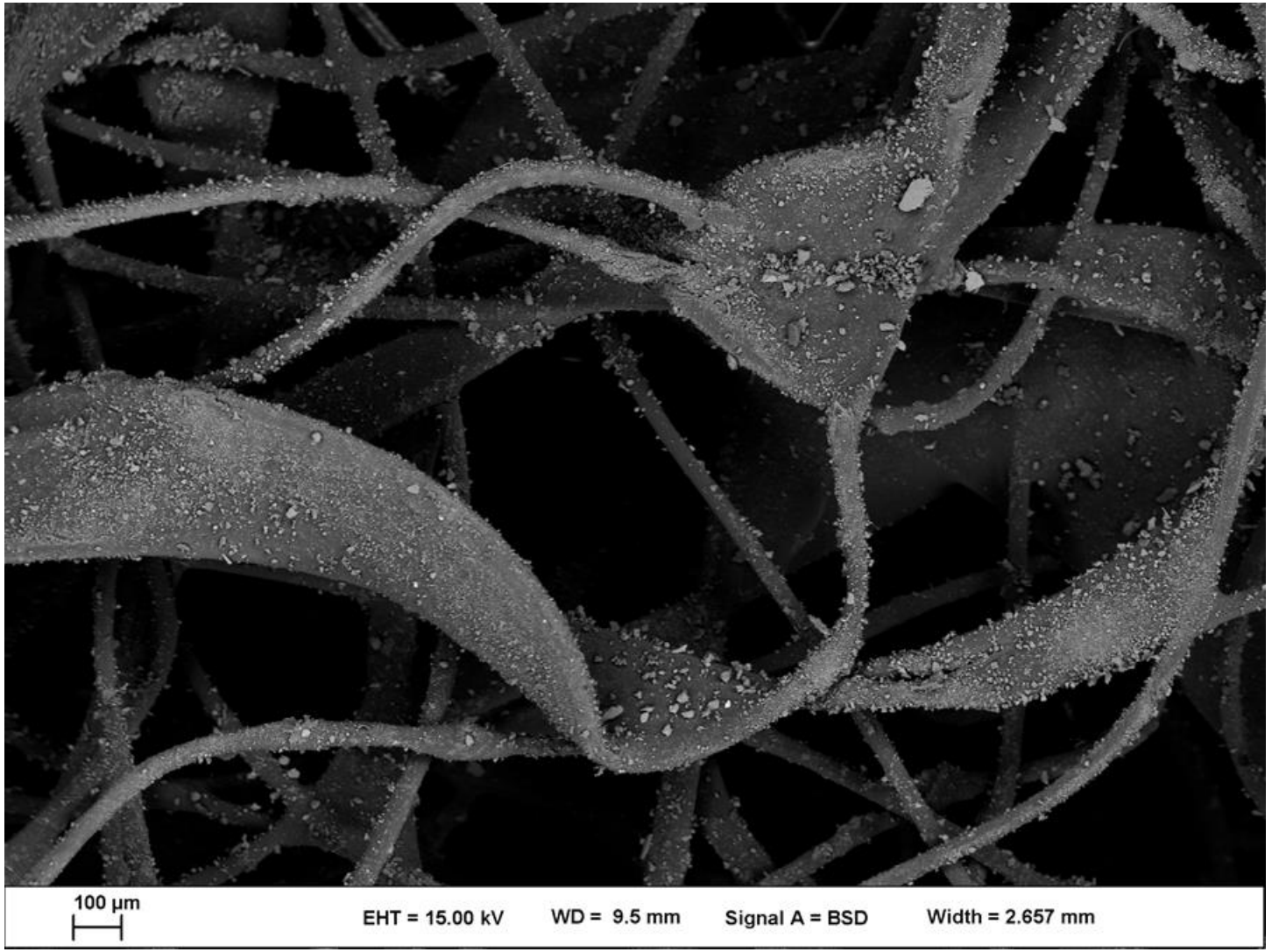

Sample: 123-012
Map A

Notes: Heavy dust load, dominantly aluminosilicates and Sea-salts (aggregates of NaCl and Mg-SO_4).

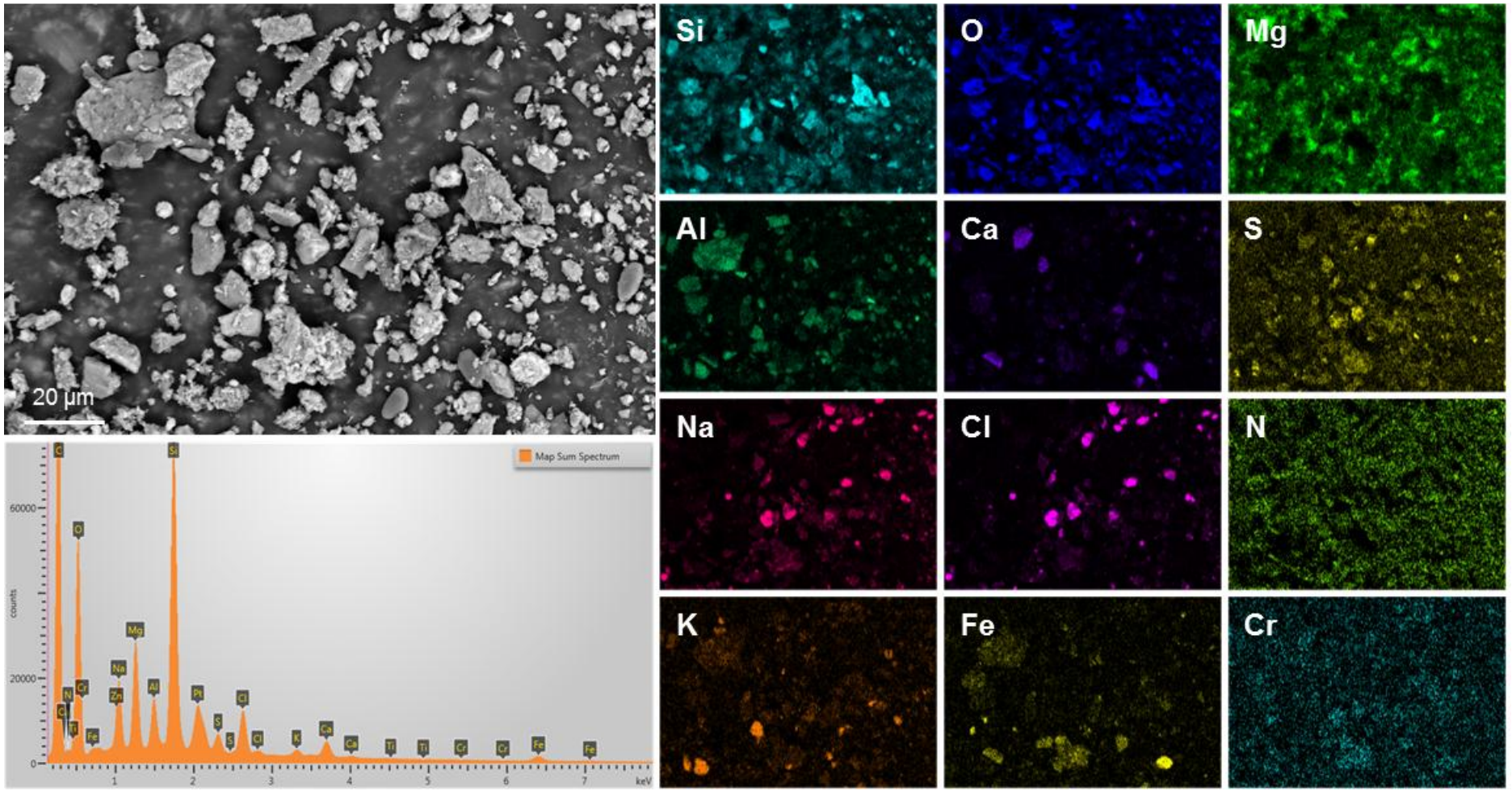

Sample: 123-012
Map B

Notes: Close-up of two large sea-salt aggregates near the center of Map A.

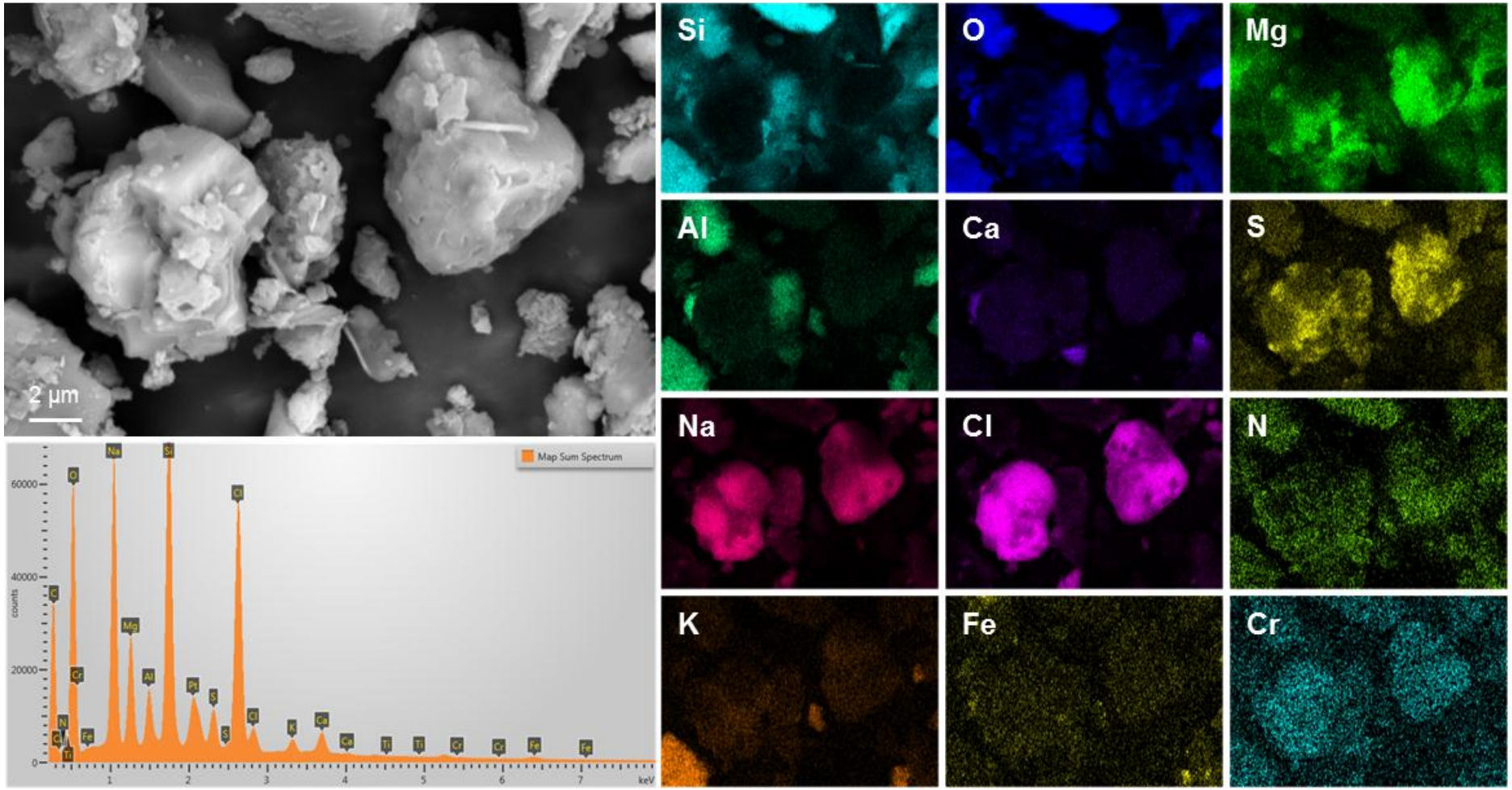

Sample: 123-012
Map C

Notes: Dust is dominantly aluminosilicates.

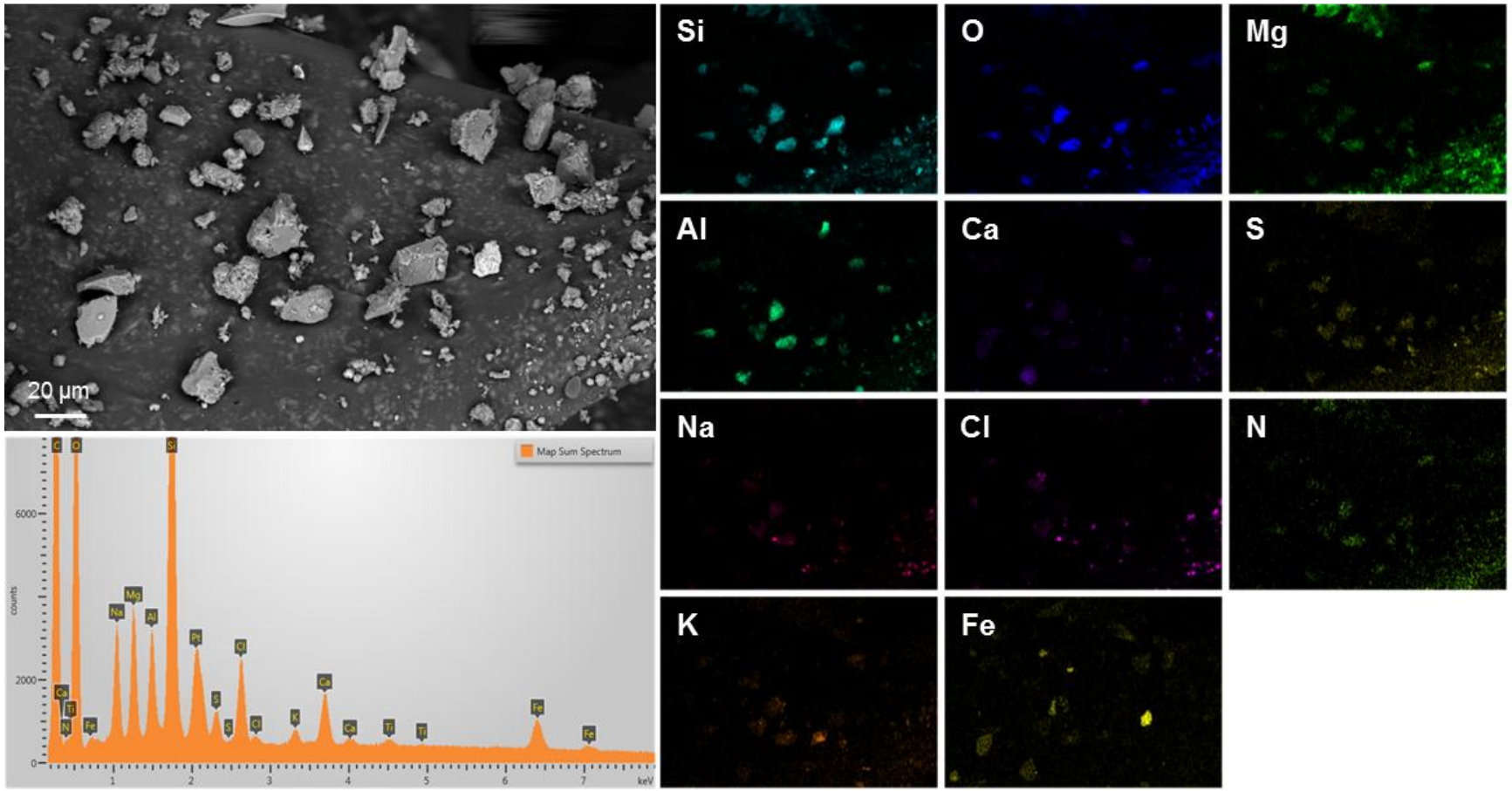

Sample: 123-012
Map D

Notes: Coarse dust grains are dominantly aluminosilicates and sea-salts.

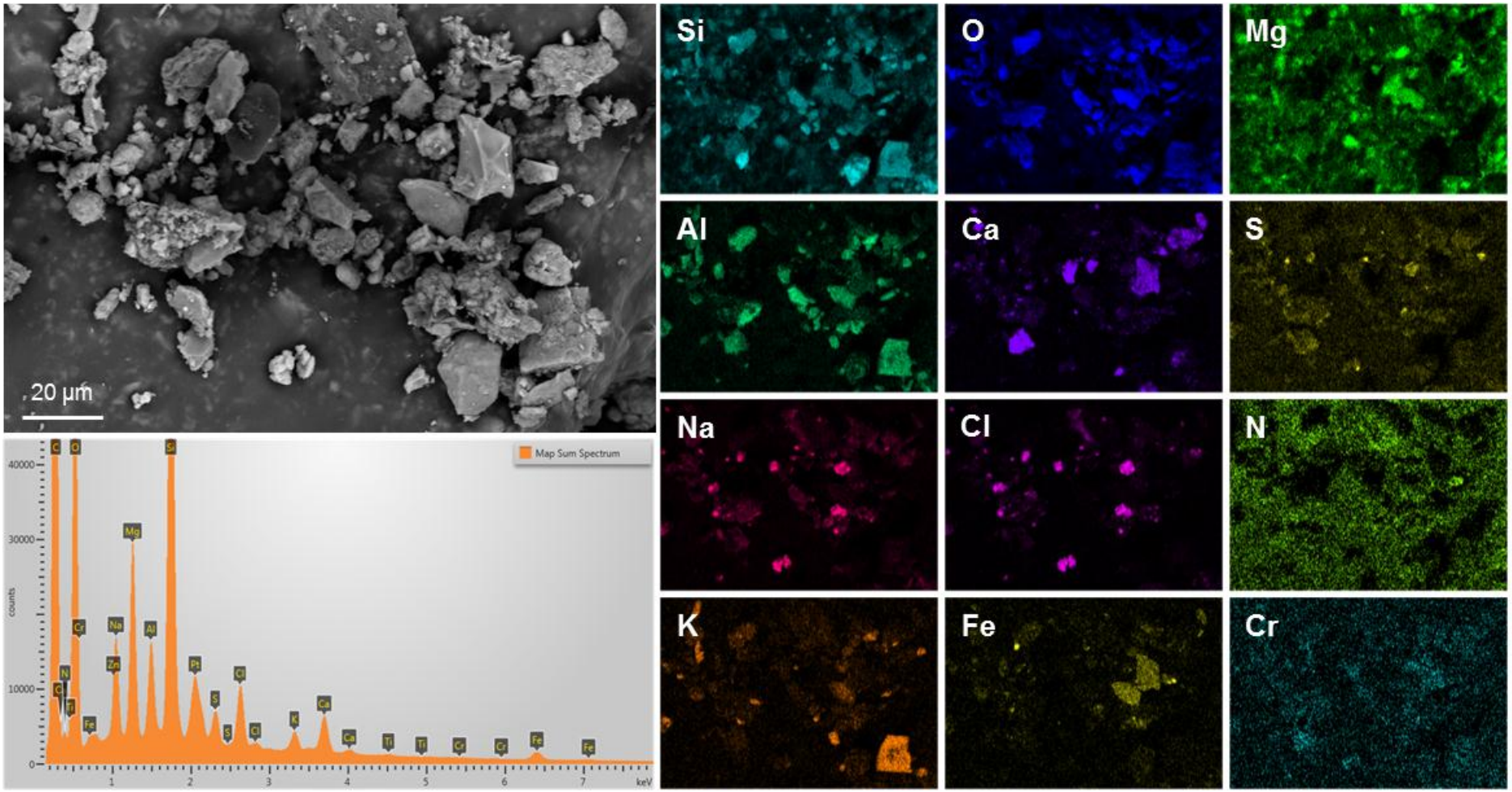

Sample: 123-012
Map E

Notes: Coarse dust grains are dominantly aluminosilicates and sea-salts.

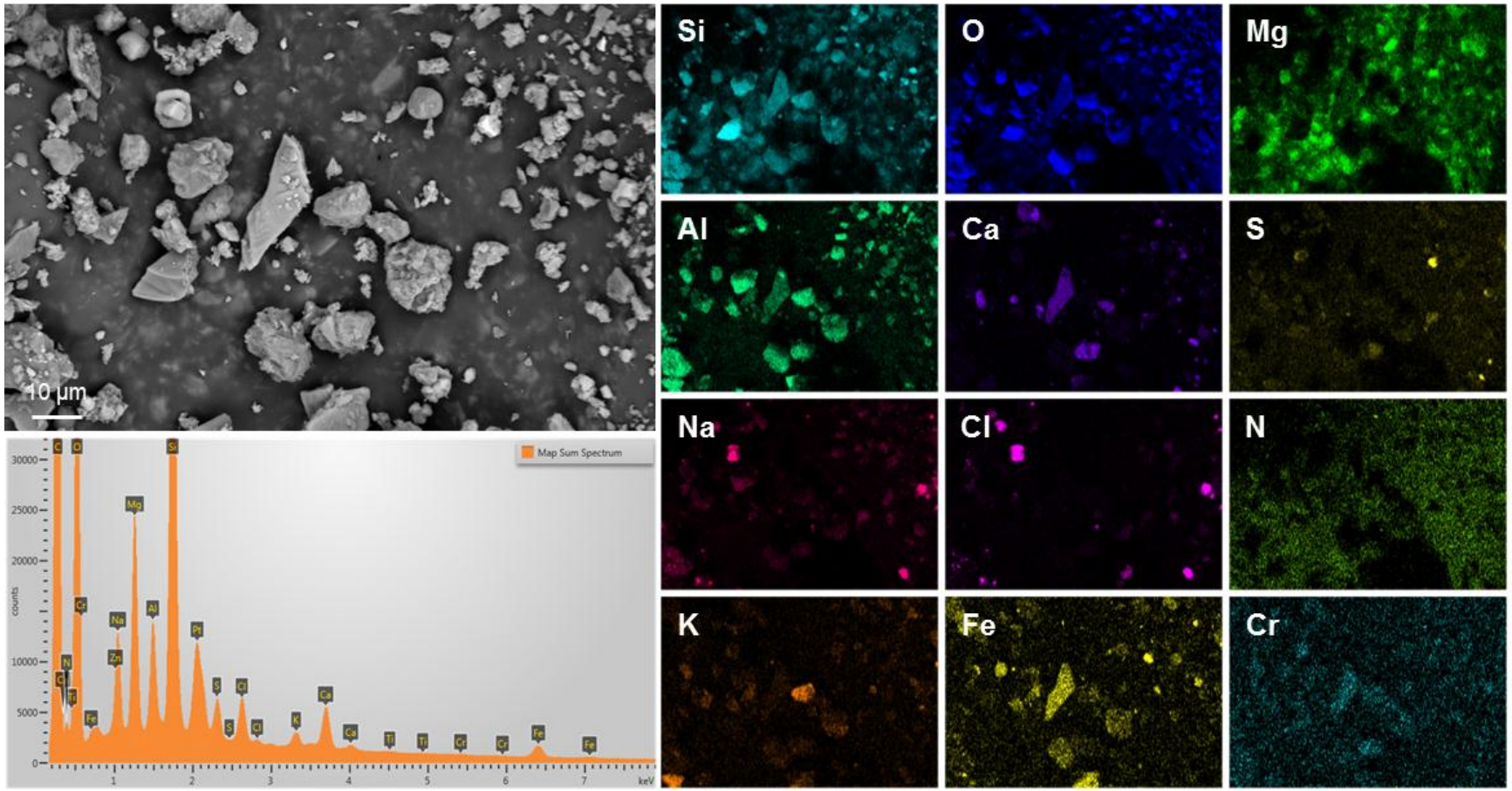

Sample: 123-012
Map F

Notes: Close-up of sea-salt aggregate, in upper left of Map E. Intergrown NaCl and Mg-SO_4. Note that K appears to be associated with the sulfate.

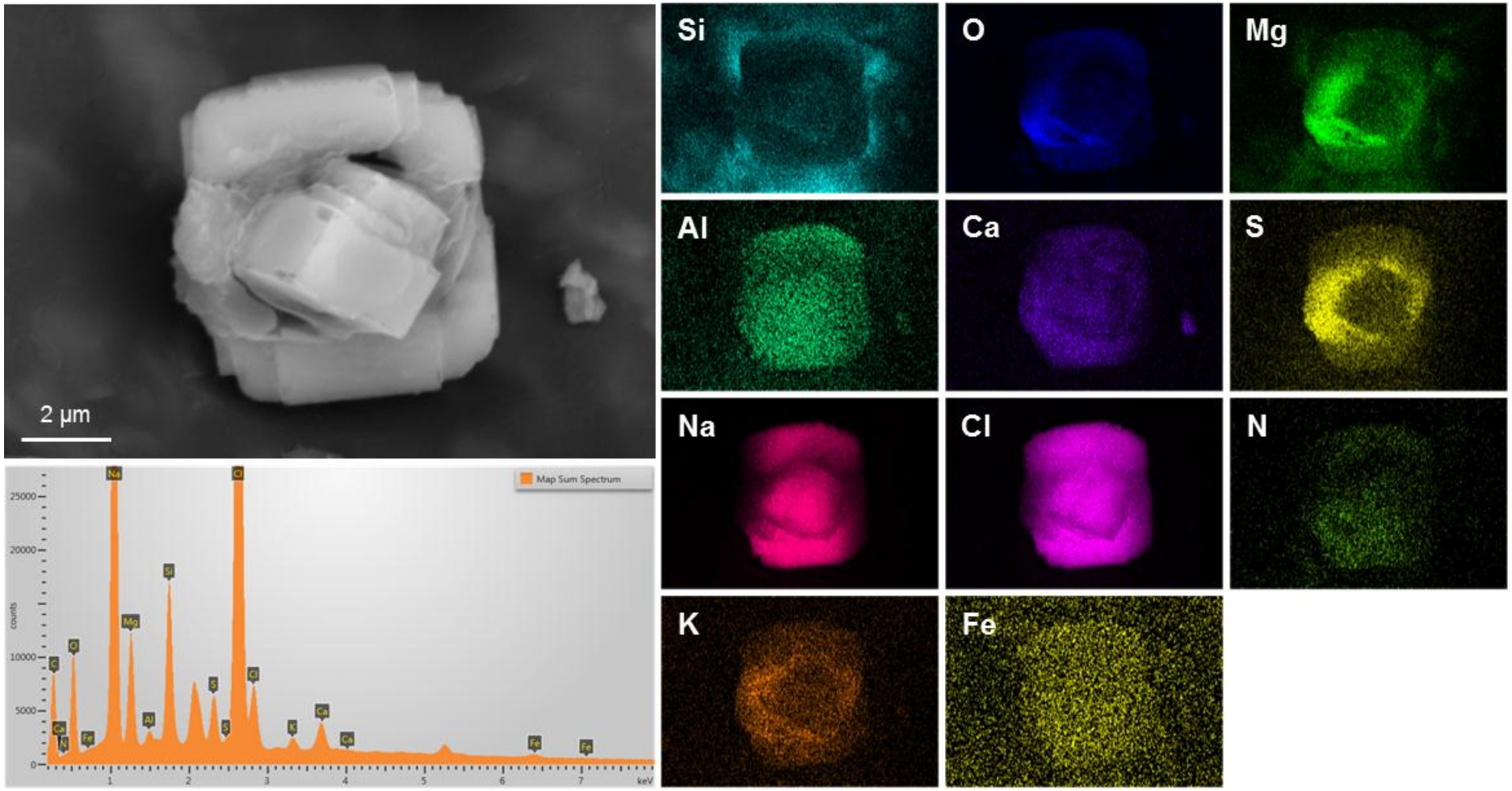

Sample: 123-012
Map G

Notes: Coarse dust grains are dominantly aluminosilicates and sea-salts.

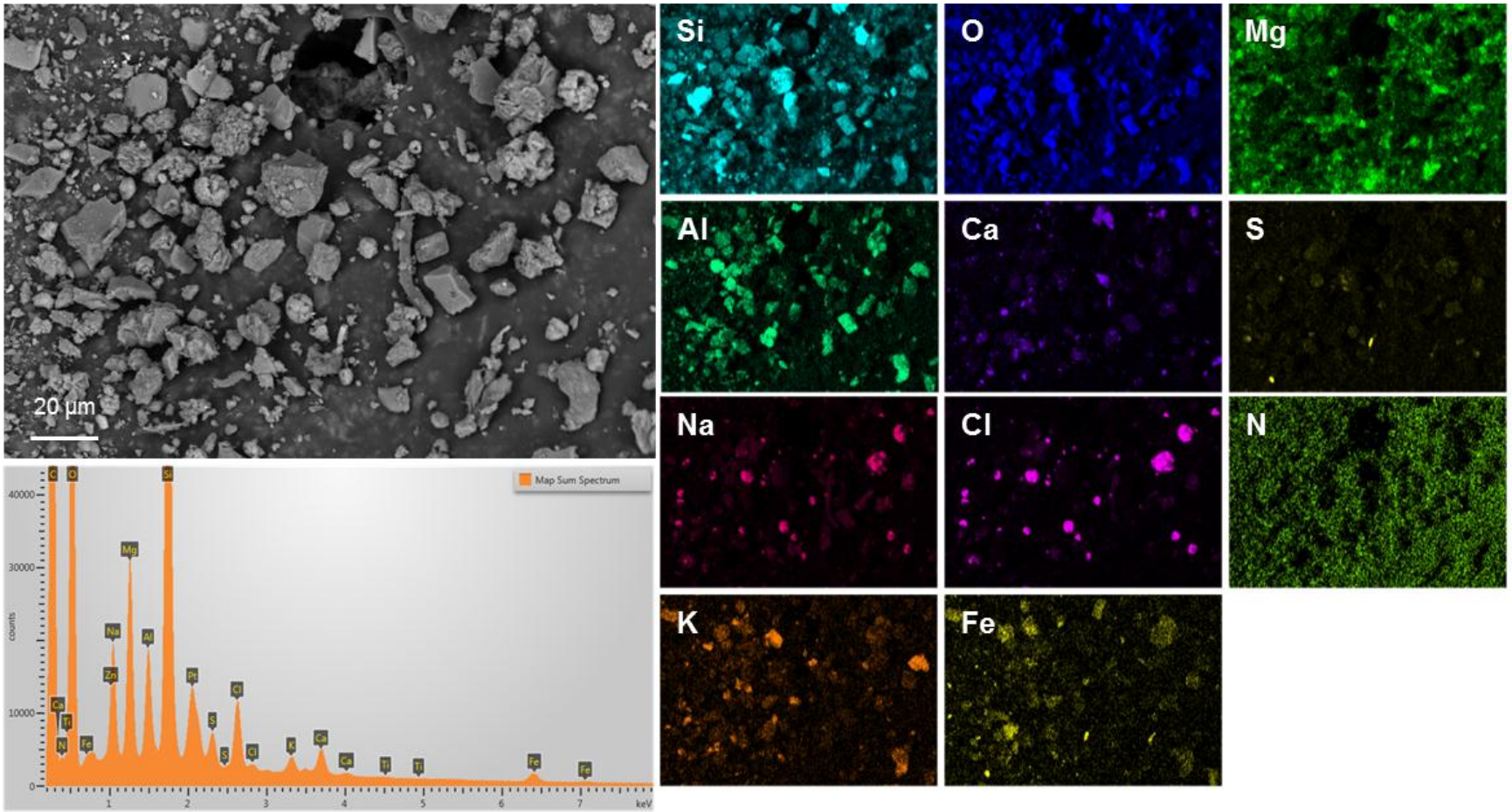

Sample: 123-012
Map H

Notes: Close-up of two spherical aggregates of sea-salts, from the upper right corner of Map G.

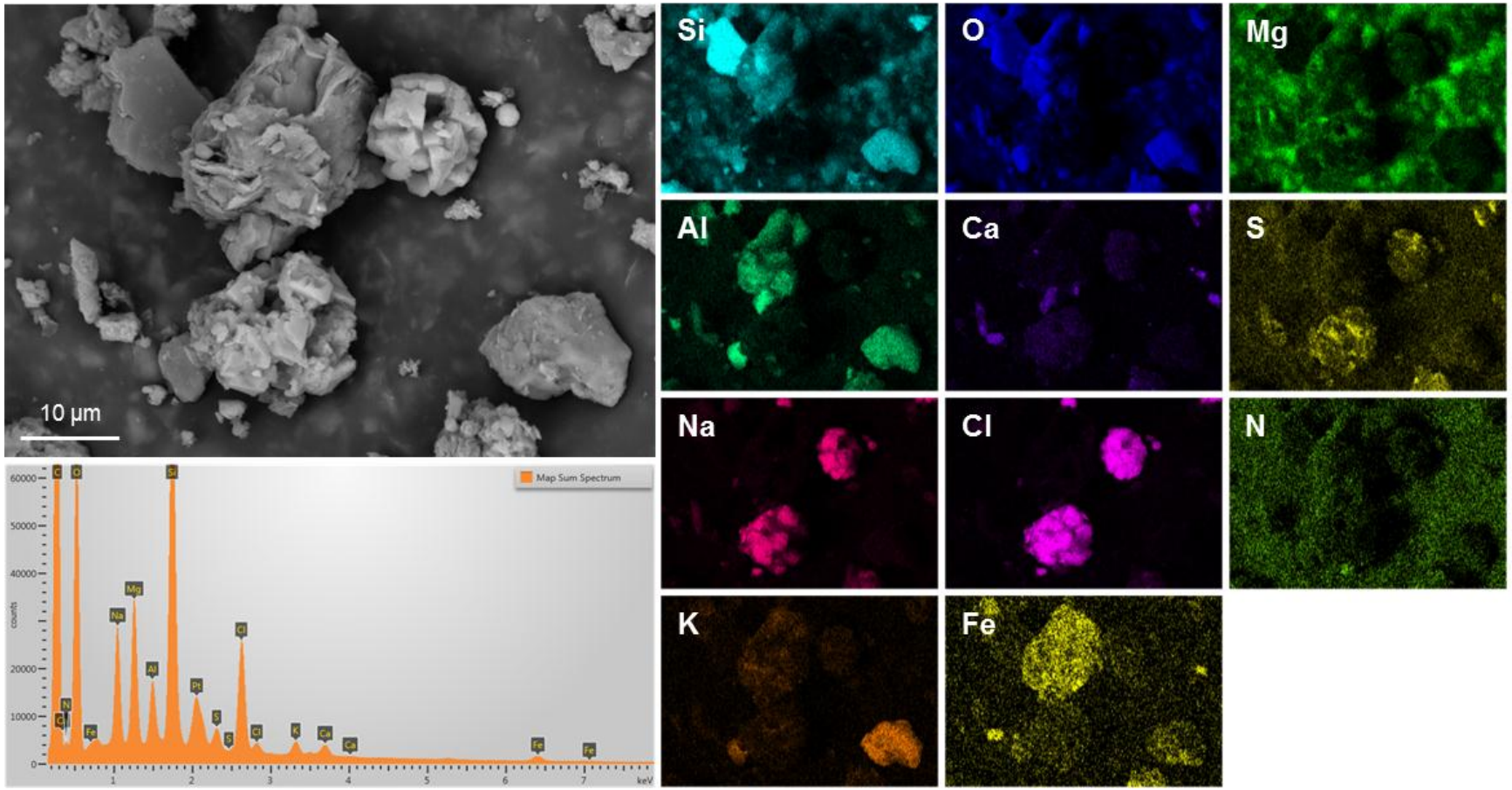

Sample: 123-012
Map I

Notes: Close-up of spherical sea-salt aggregate consisting of etched NaCl cubes and interstitial Mg-SO_4.

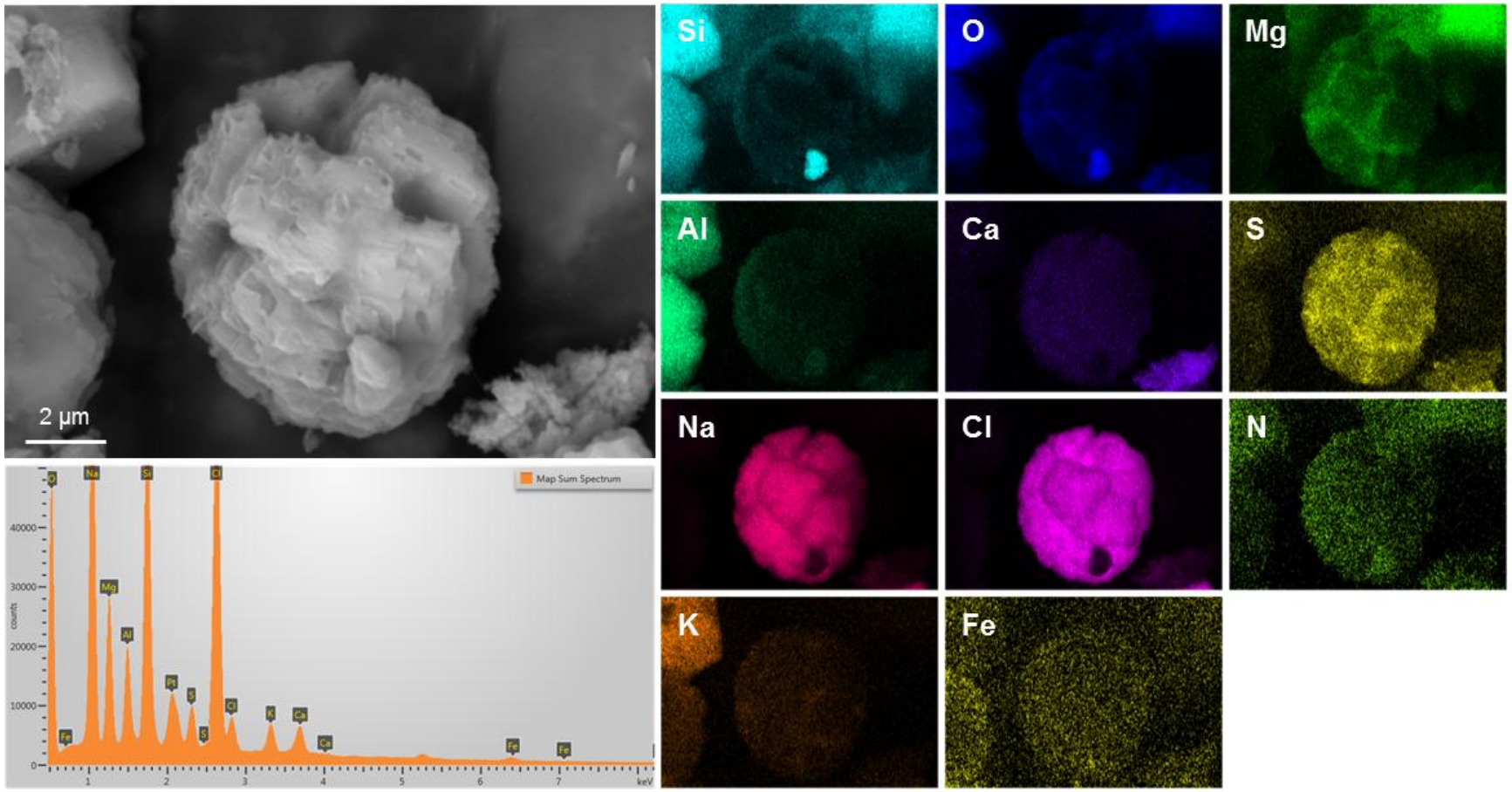

Sample: 123-012
Map J

Notes: Heavy dust load, dominantly aluminosilicates and sea-salts.

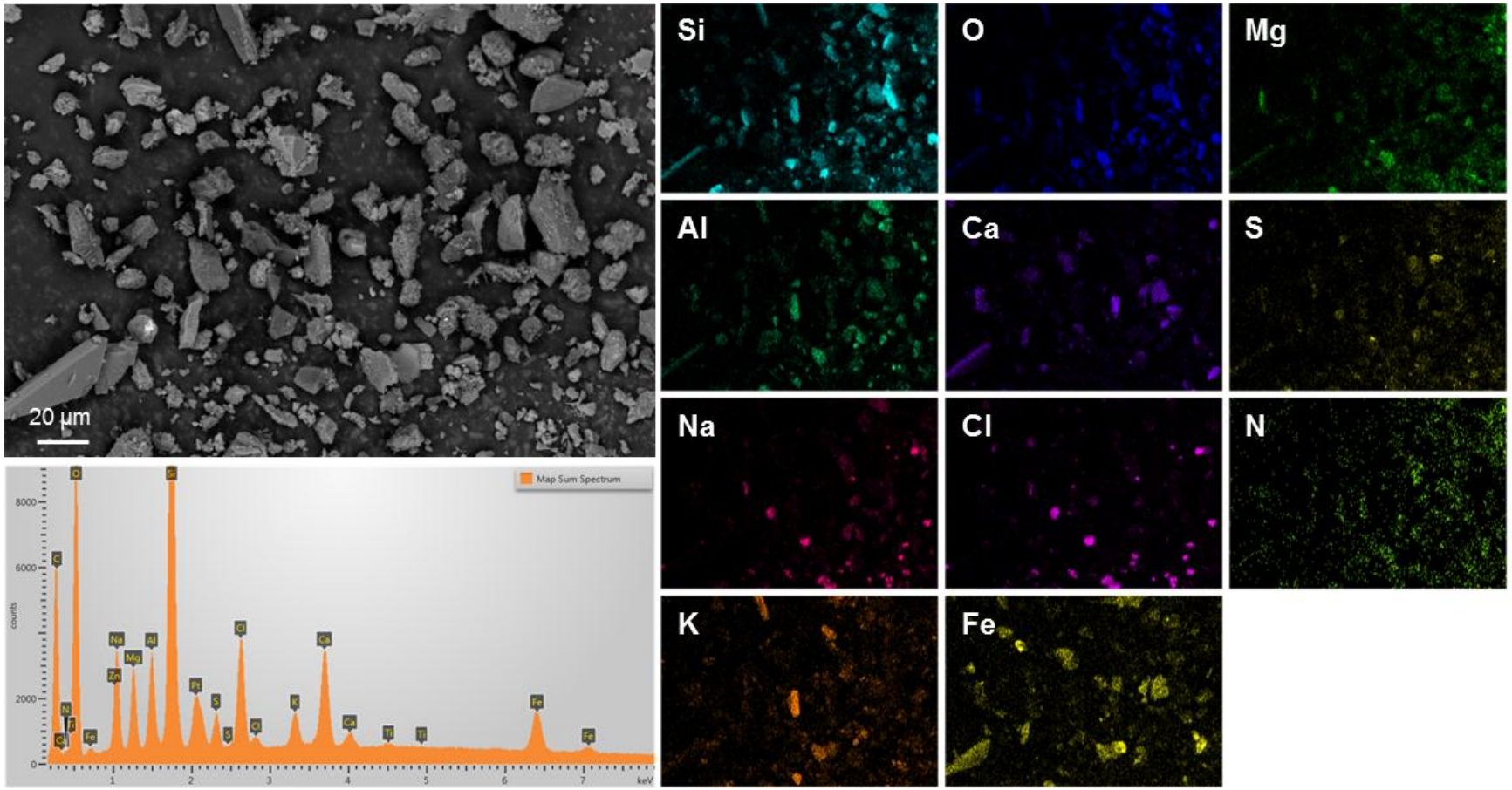

Sample: 123-012
Map K

Notes: Heavy dust load, dominantly aluminosilicates and sea-salts.

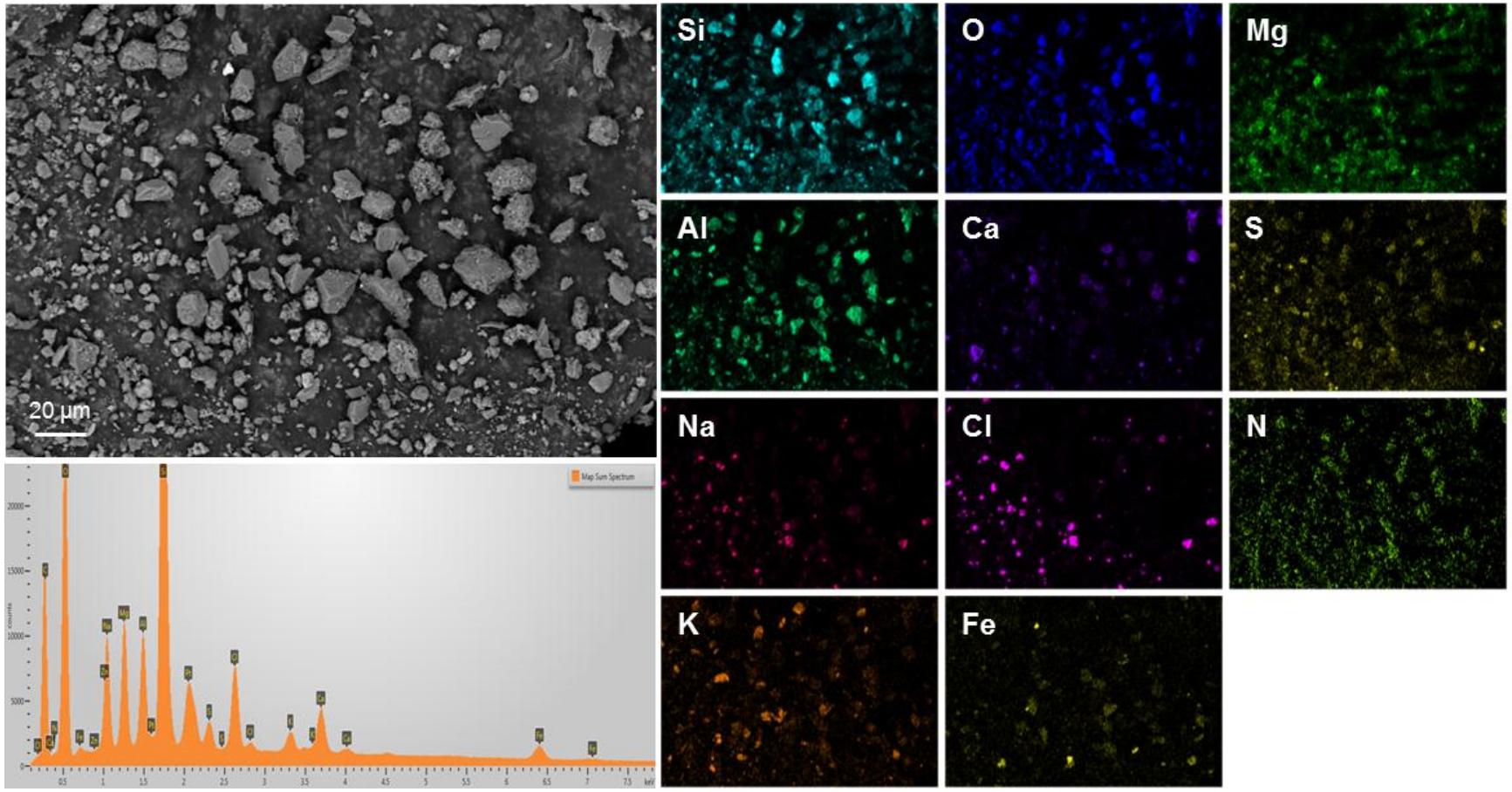

Sample: 123-012
Map L

Notes: Heavy dust load, dominantly aluminosilicates and sea-salts, commonly occurring as spherical aggregates.

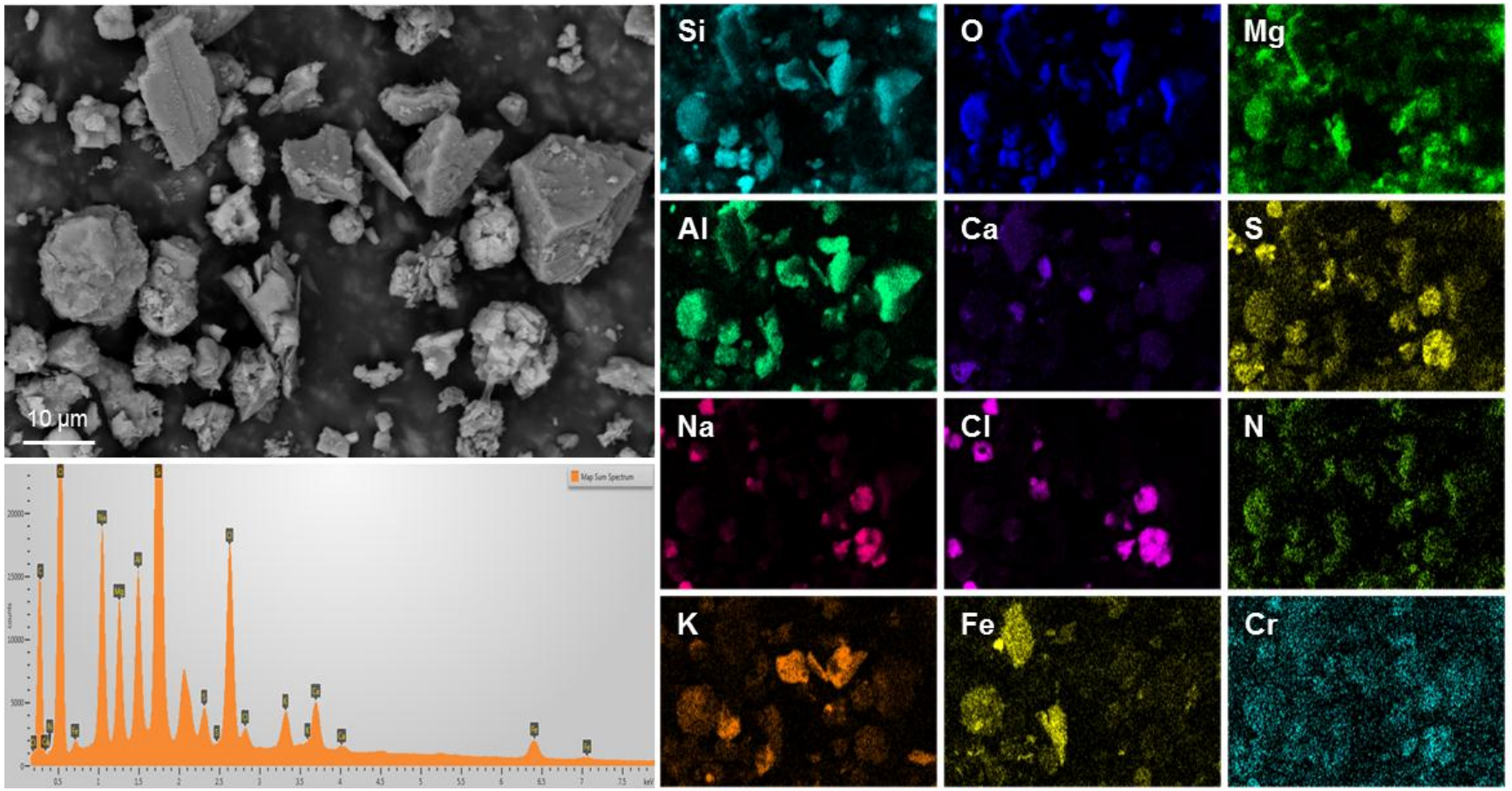

Sample: 123-012
Map M

Notes: Heavy dust load, dominantly aluminosilicates and sea-salts, commonly occurring as spherical aggregates.

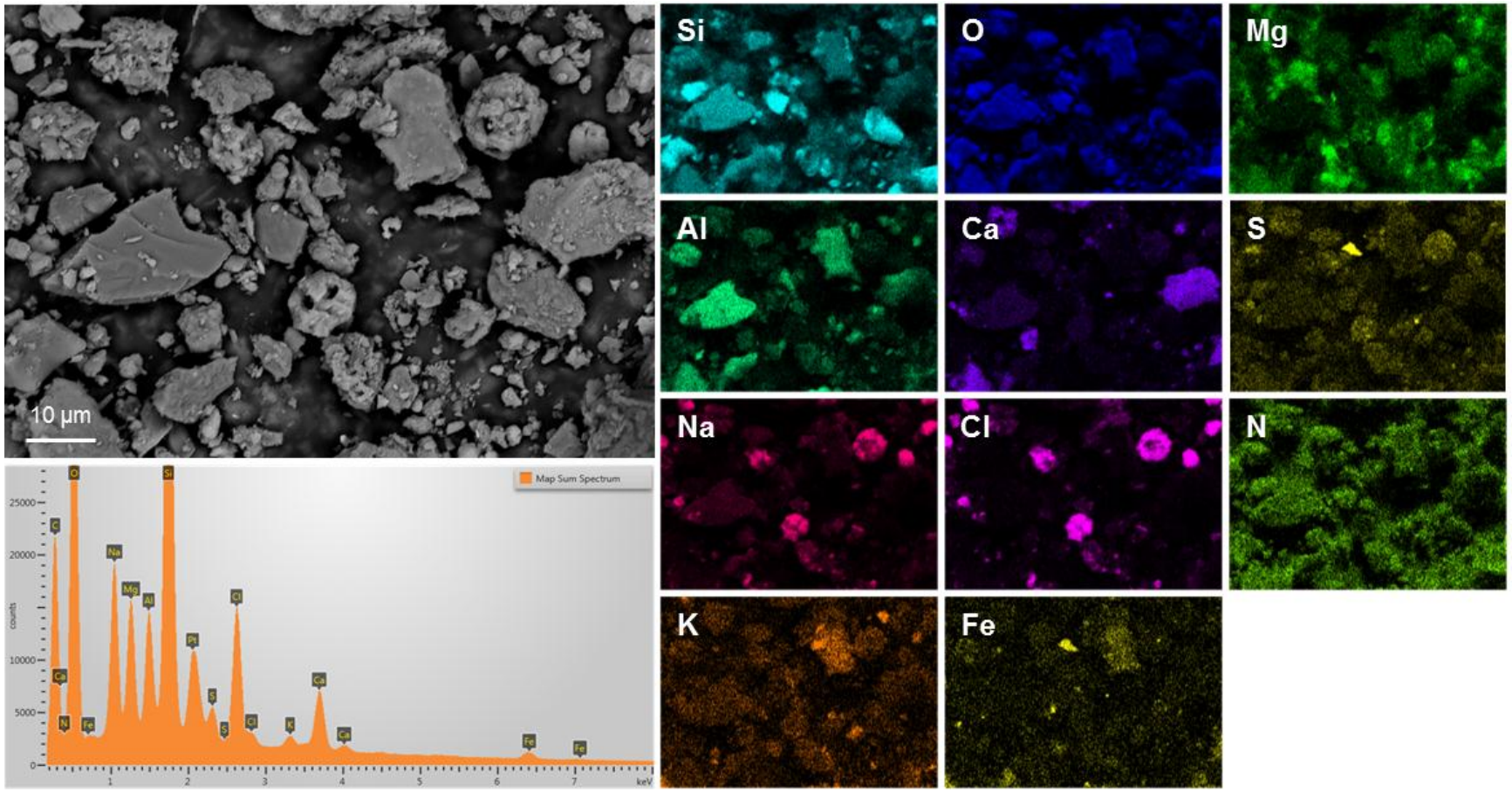

Sample: 123-012
Map N

Notes: Heavy dust load, dominantly aluminosilicates and aggregates of sea-salts.

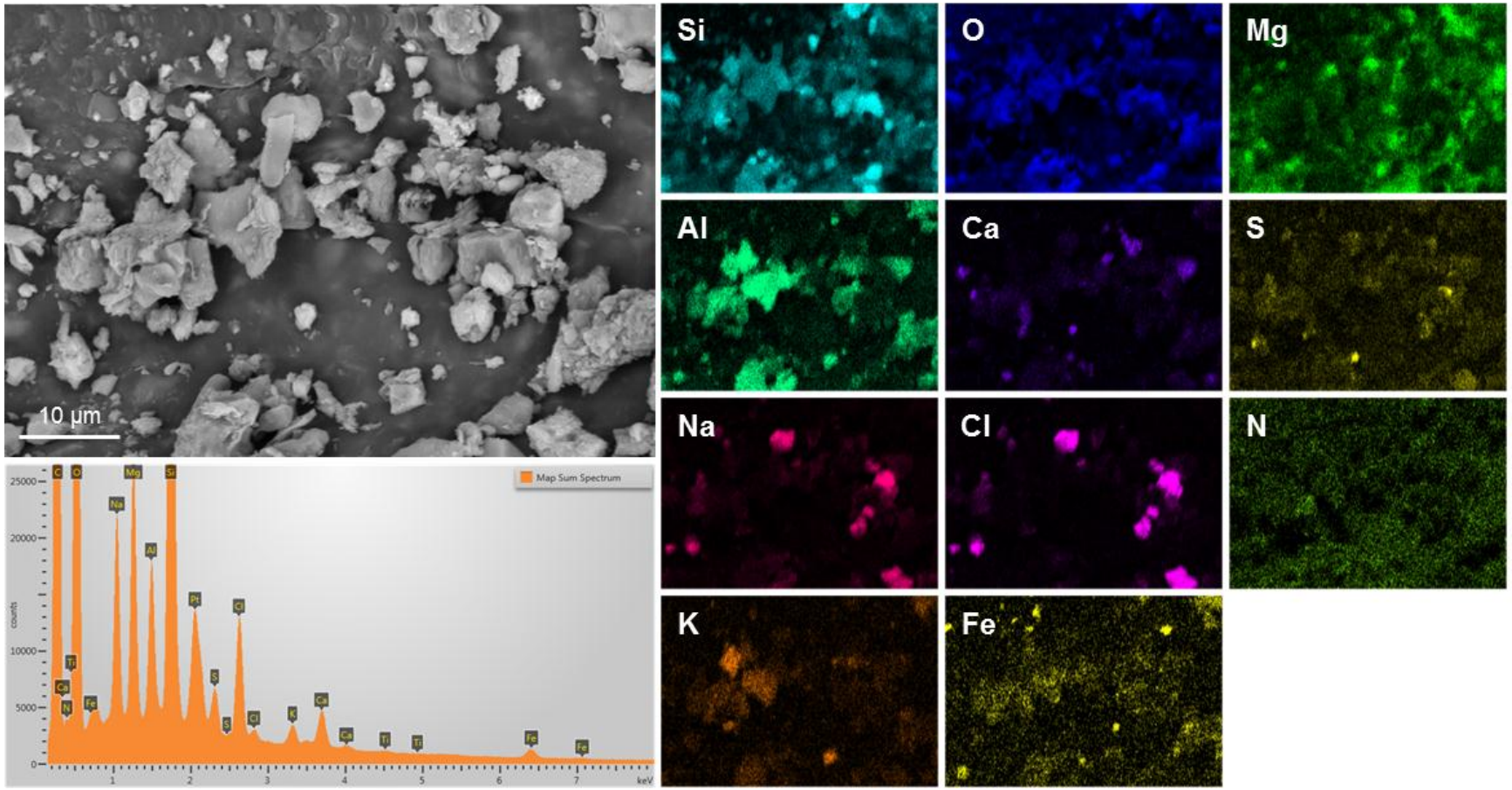

Sample: 170-001

Notes: Overview image of pad sample 170-001, showing the moderate dust load.

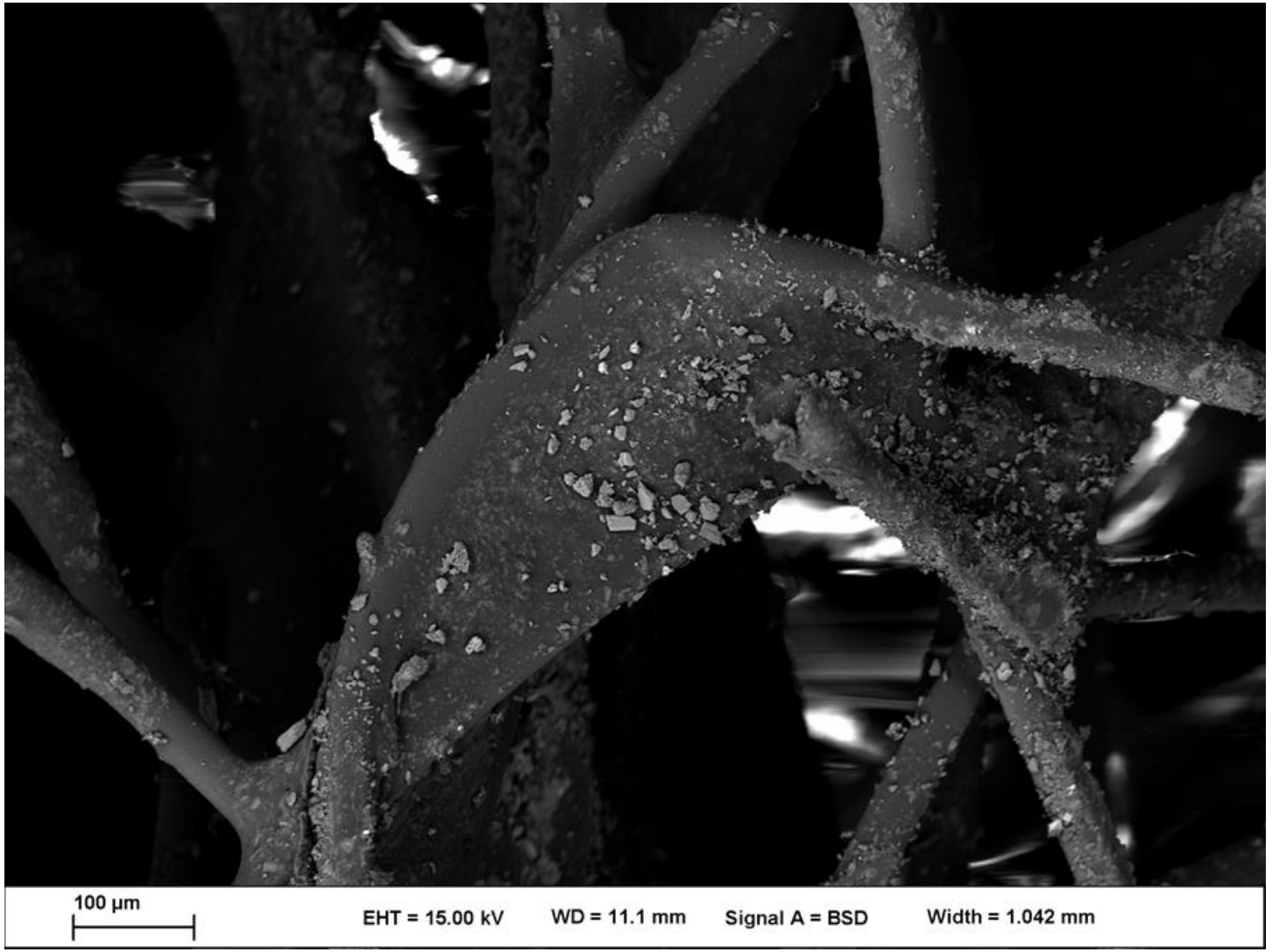

Sample: 170-001
Map A

Notes: Sparse dust load, mostly aluminosilicates. A single grain of NaCl.

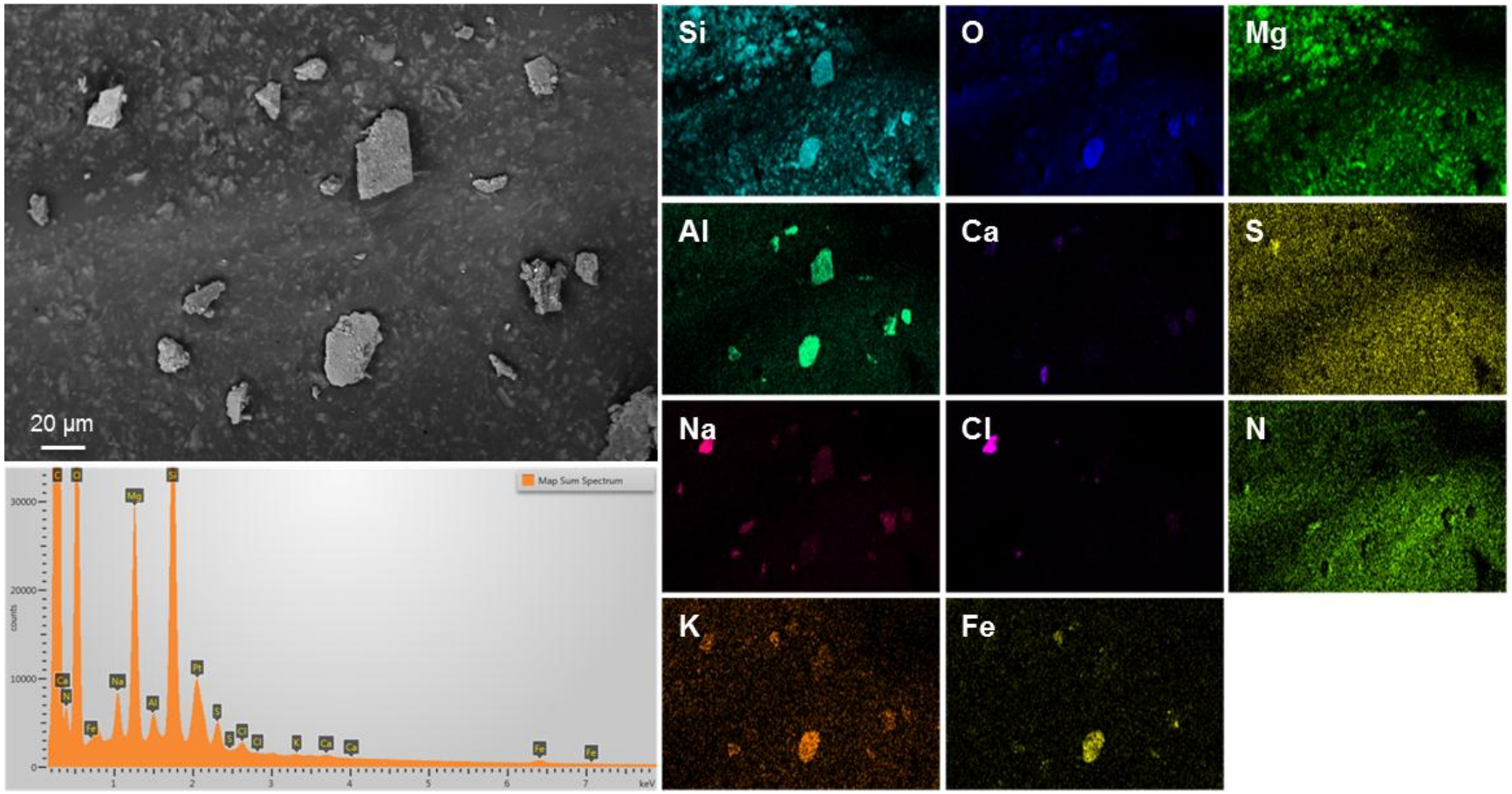

Sample: 170-001
Map B

Notes: Abundant fine dust particles along an abraded edge. Dominantly aluminosilicates and sea-salts; some Ca-sulfate.

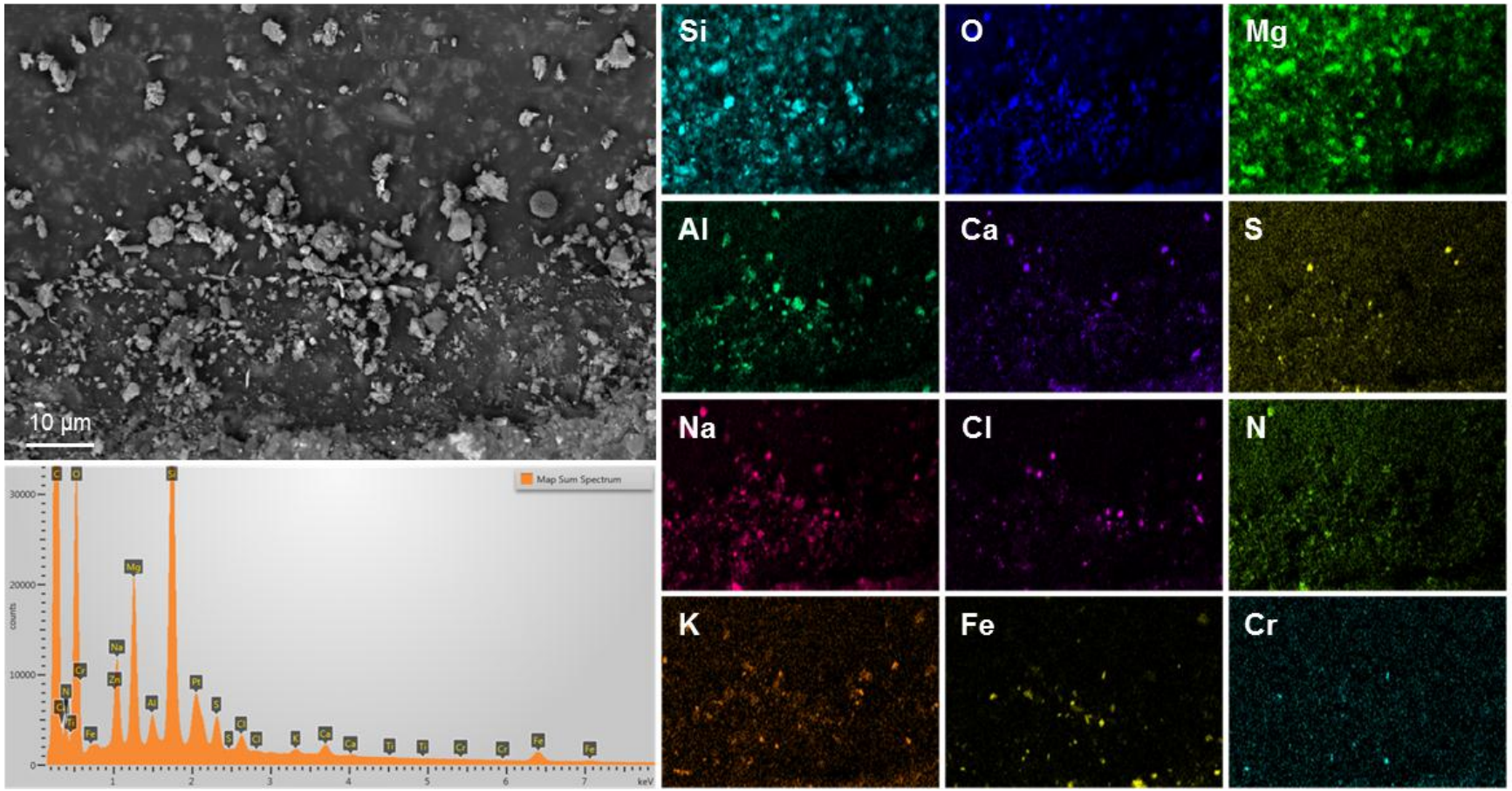

Sample: 170-001
Map C

Notes: Dust particles along an abraded edge. Dominantly aluminosilicates.

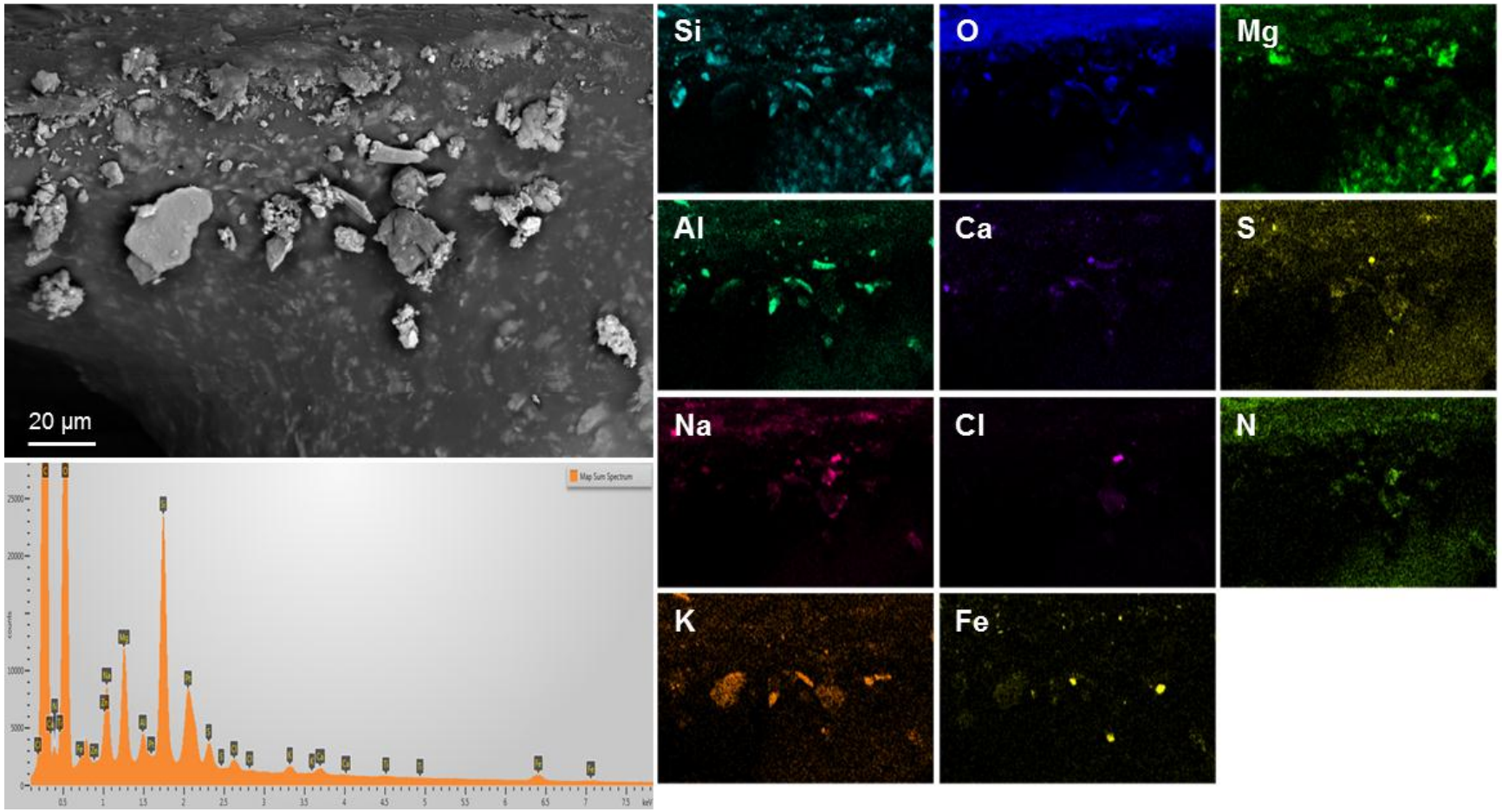

Sample: 170-001
Map D

Notes: Sparse dust particles, dominantly aluminosilicates.

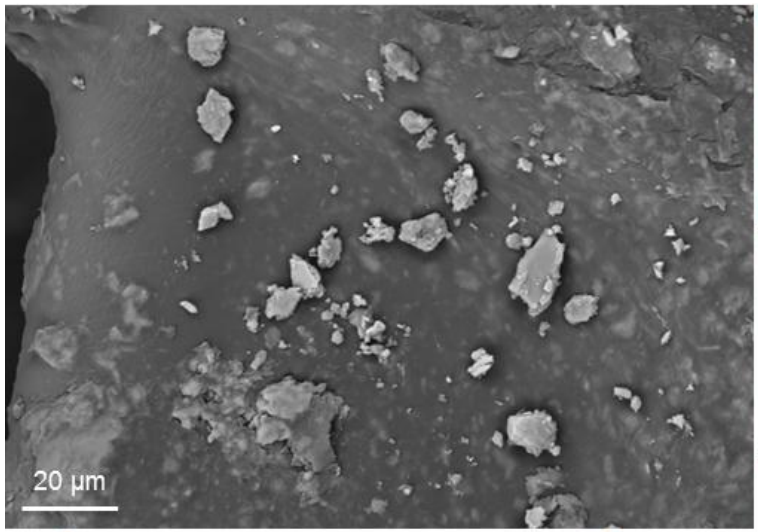

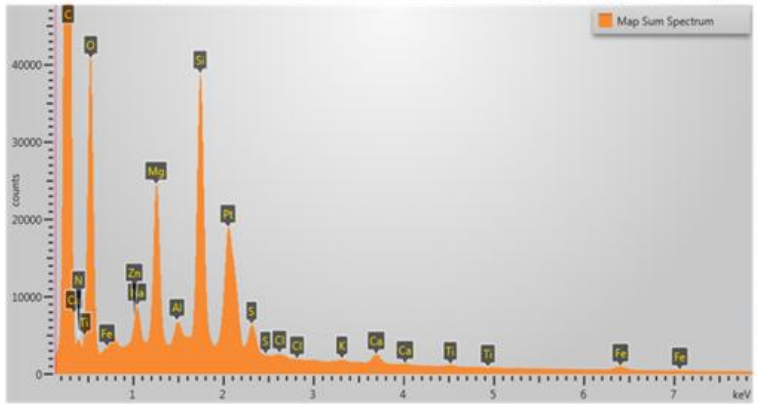

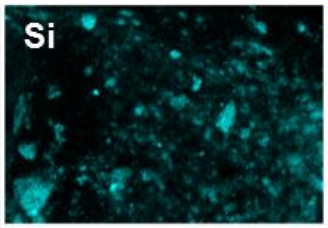

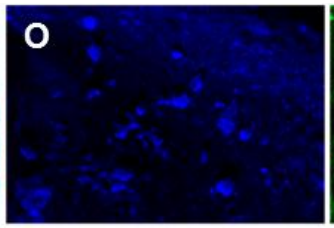

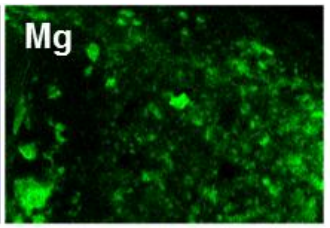

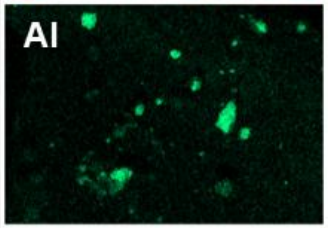

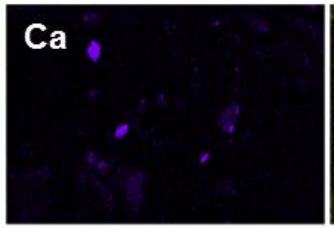

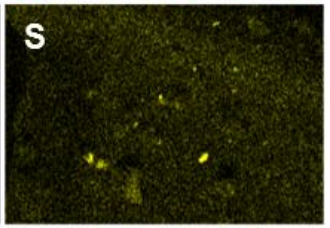

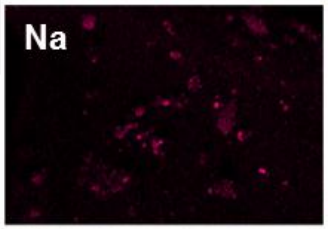

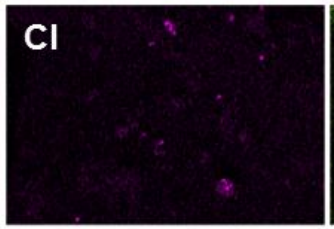

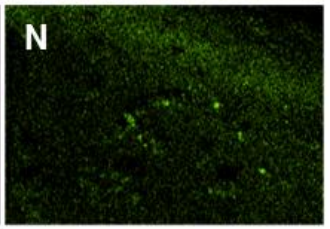

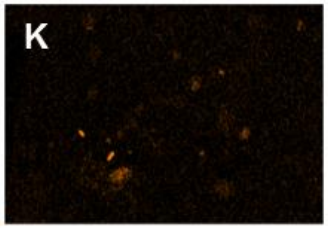

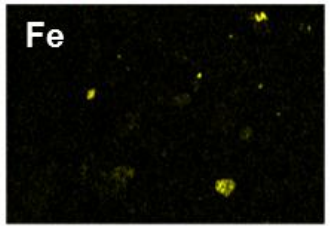

Sample: 170-001
Map E

Notes: Close-up of grain in lower right corner of Map D.

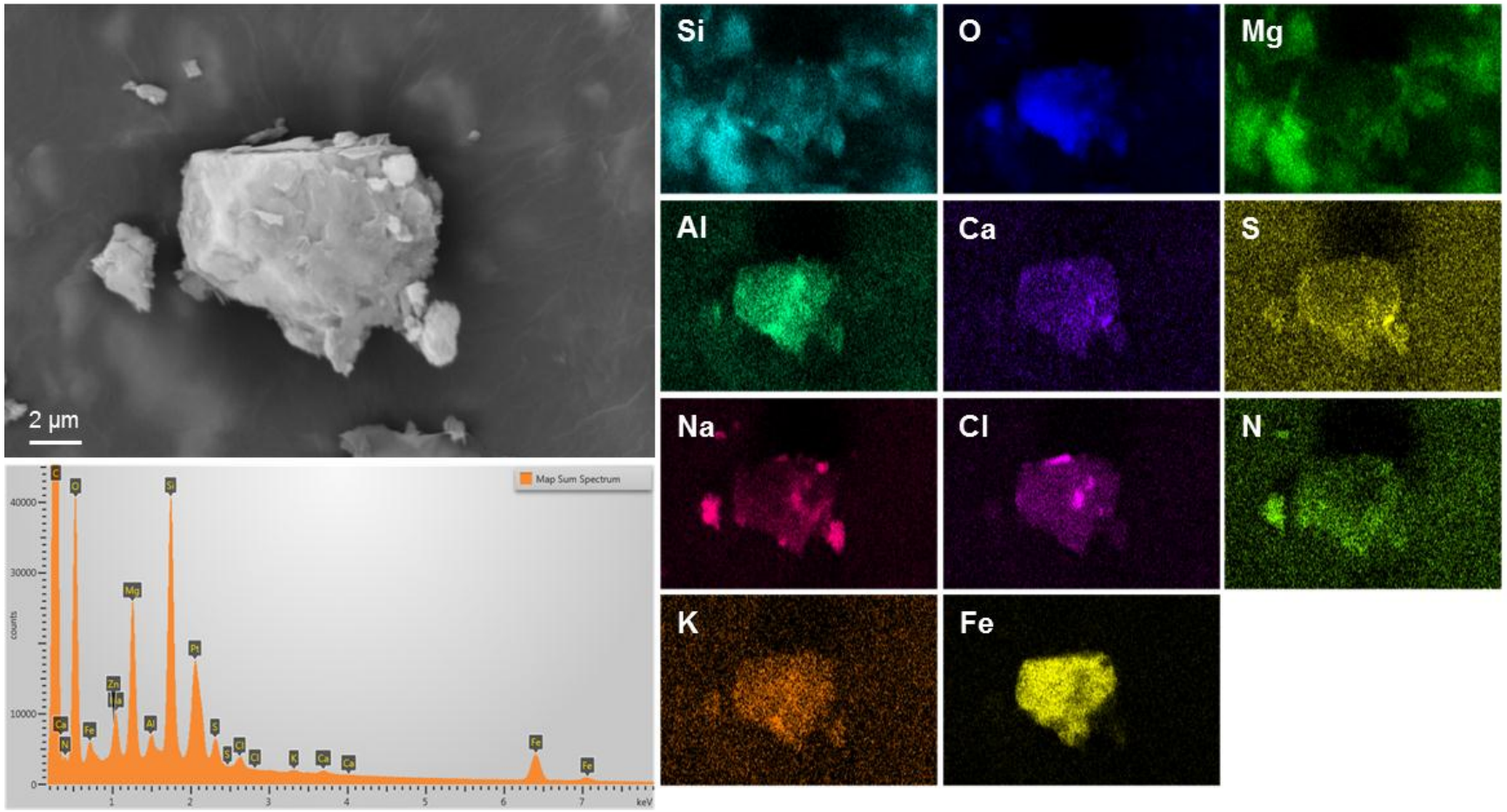

Sample: 170-001
Map F

Notes: Particles along an abraded edge. Most particles are talc, liberated by abrasion of the pad. Dust is dominantly aluminosilicates, Ca-sulfate.

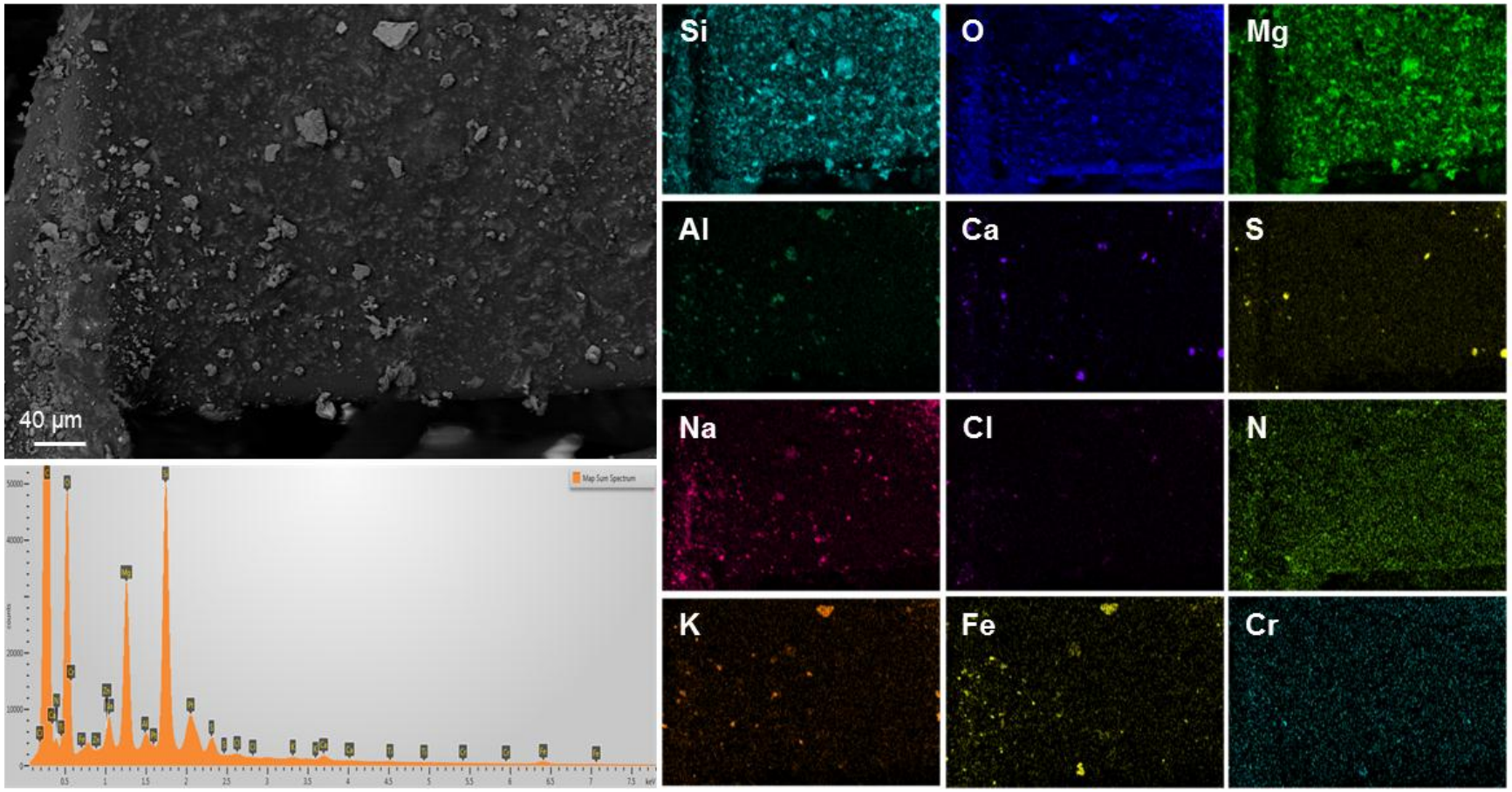

Sample: 170-003

Notes: Overview image of pad sample 170-003, showing the heavy dust load.

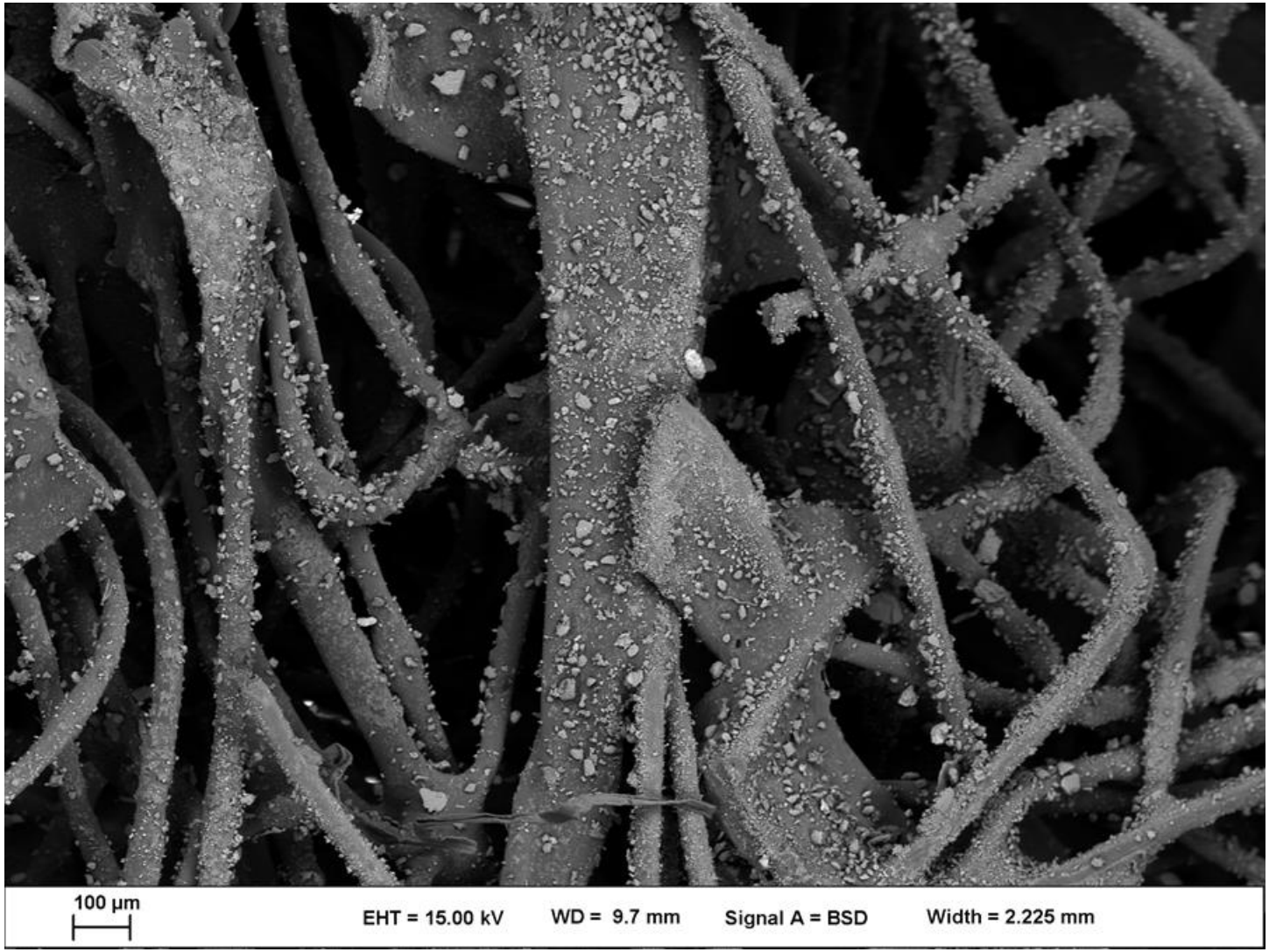

Sample: 170-003
Map A

Notes: Heavy dust load, dominantly aluminosilicates and sea-salt aggregates.

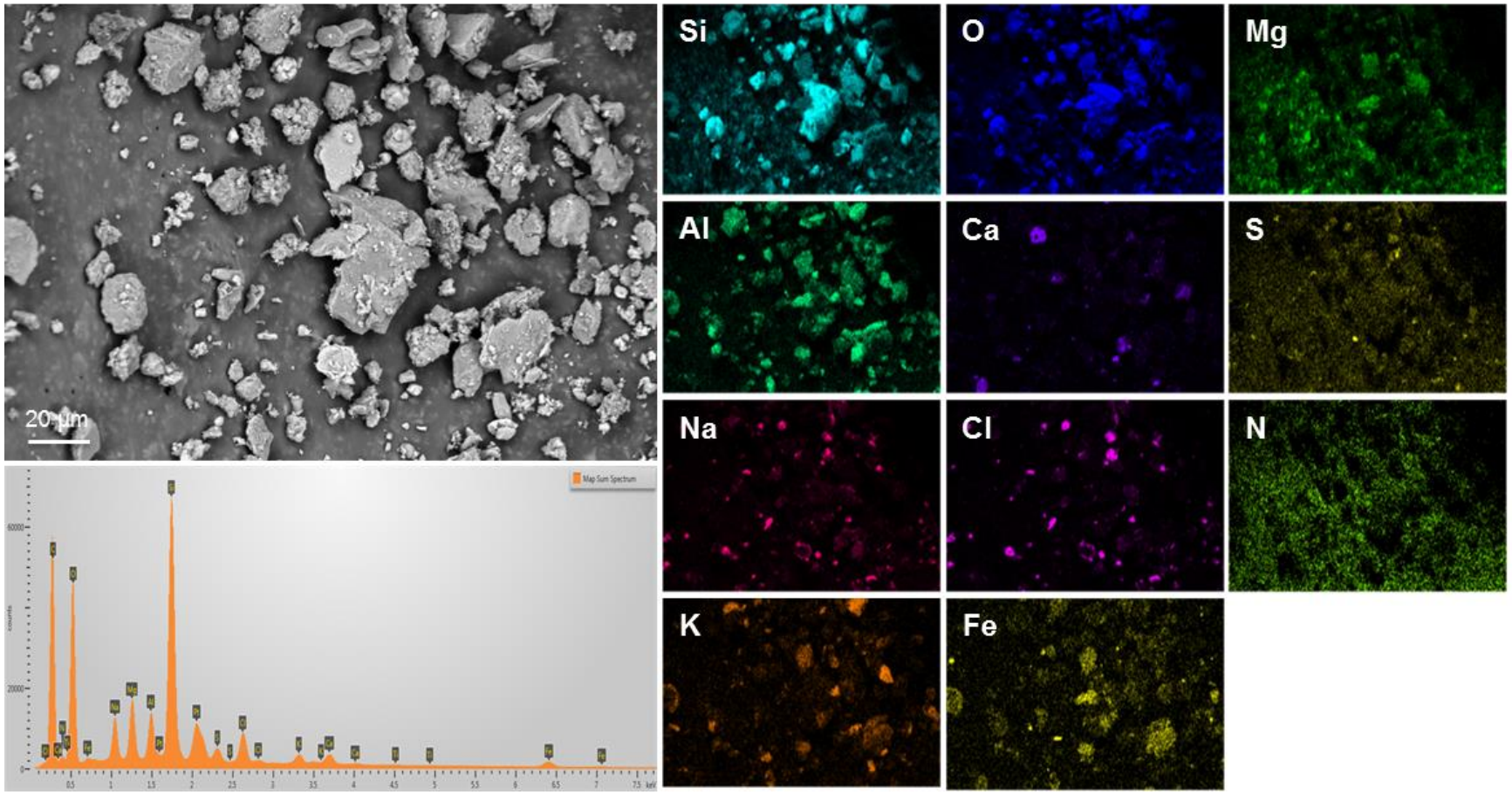

Sample: 170-003

Map B

Notes: Close-up of area in upper center of Map A. Area contains three large sea-salt aggregates among aluminosilicates grains.

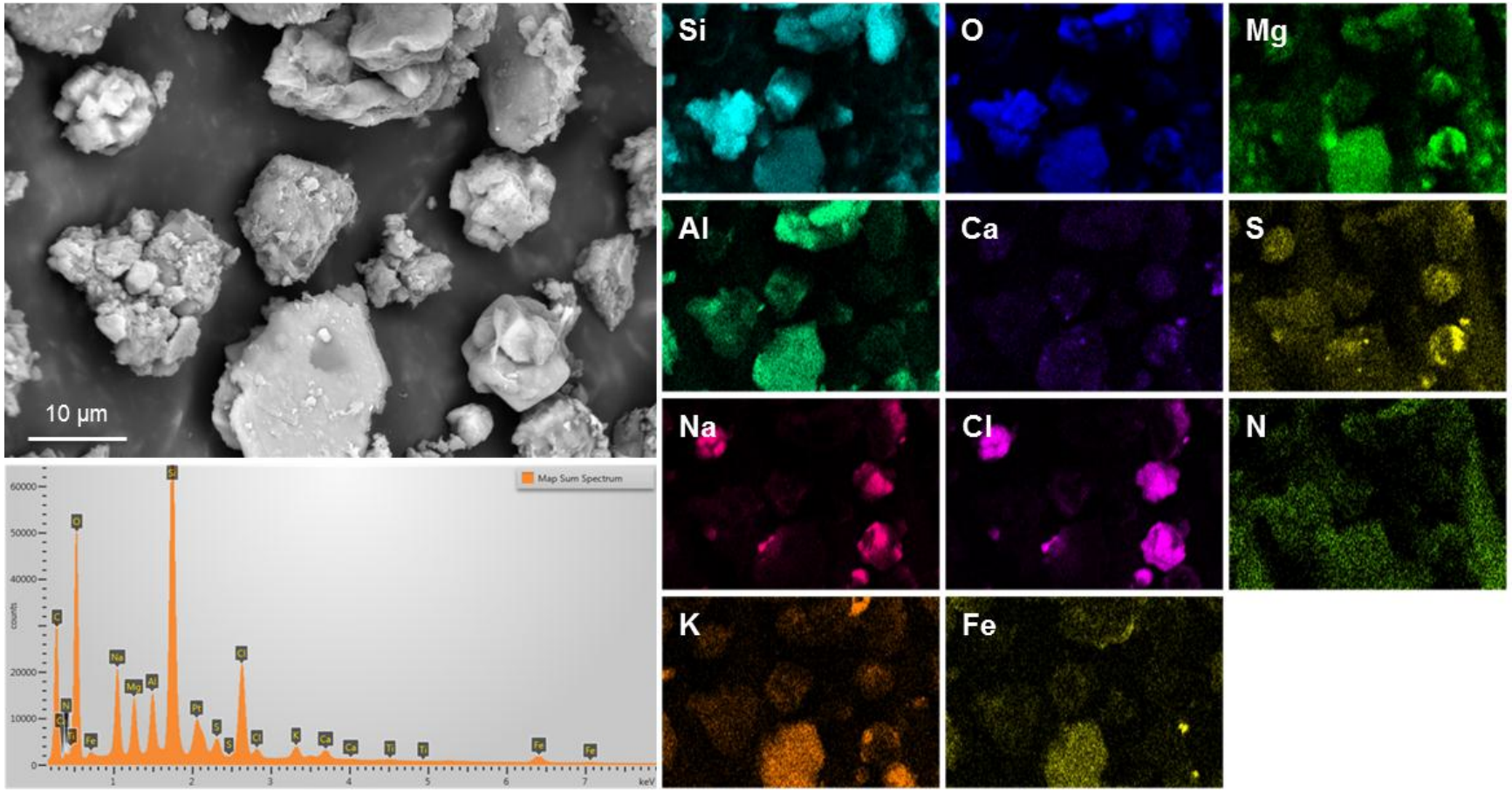

Sample: 170-003
Map C

Notes: Close-up of sea-salt aggregate in upper left corner of Map B, showing intergrown NaCl cubes with interstitial Mg-SO_4, and trace Ca, K.

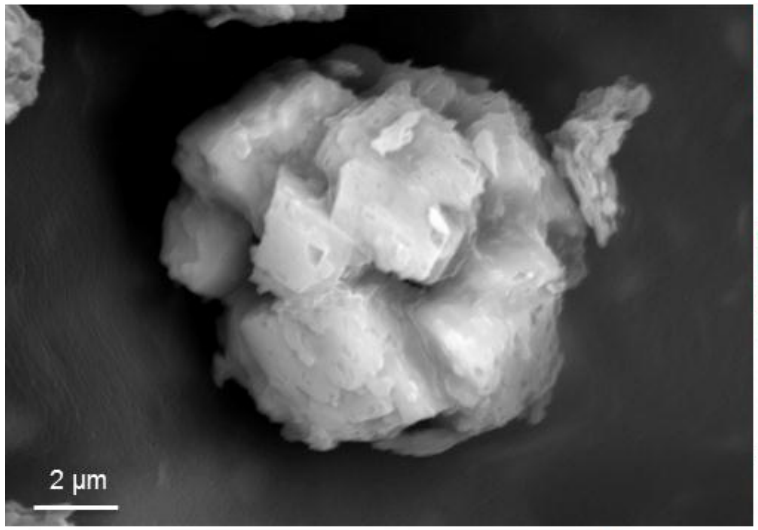

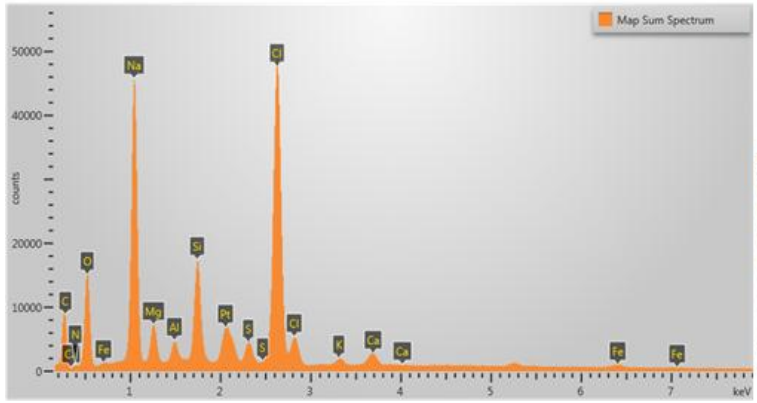

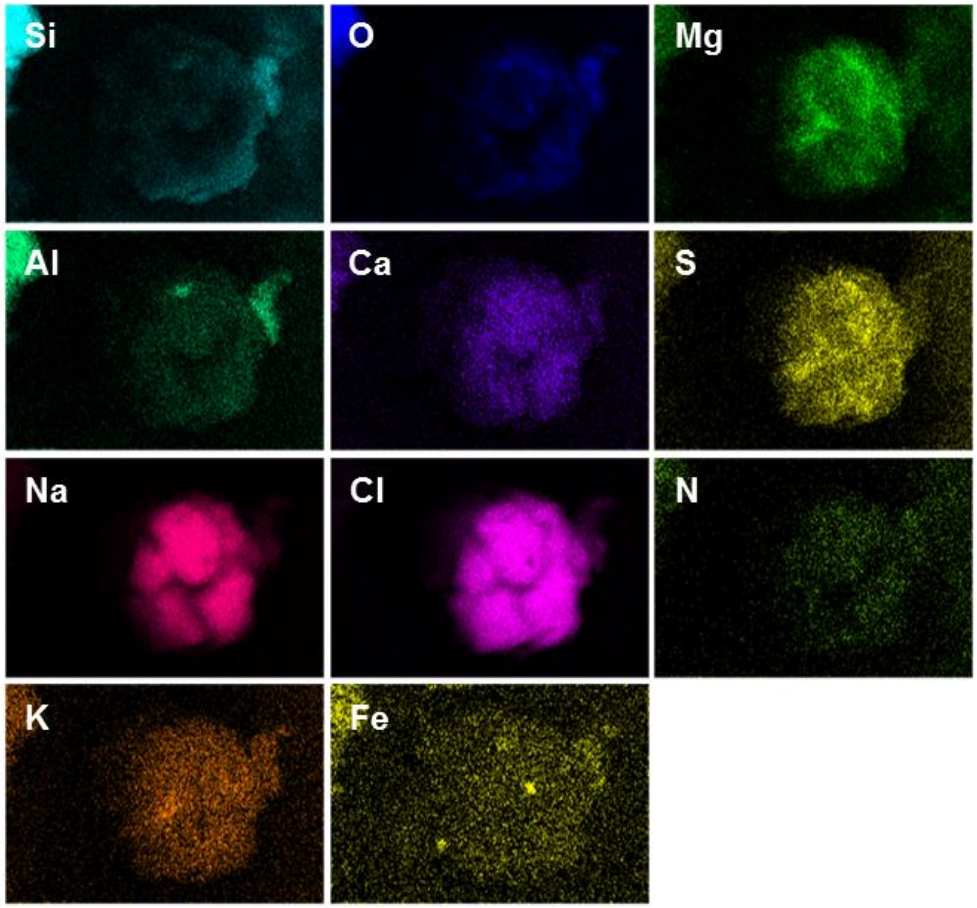

Sample: 170-003
Map D

Notes: Close-up of sea-salt aggregate in lower right corner of Map B, showing intergrown NaCl cubes with interstitial Mg-SO_4, and trace Ca, K.

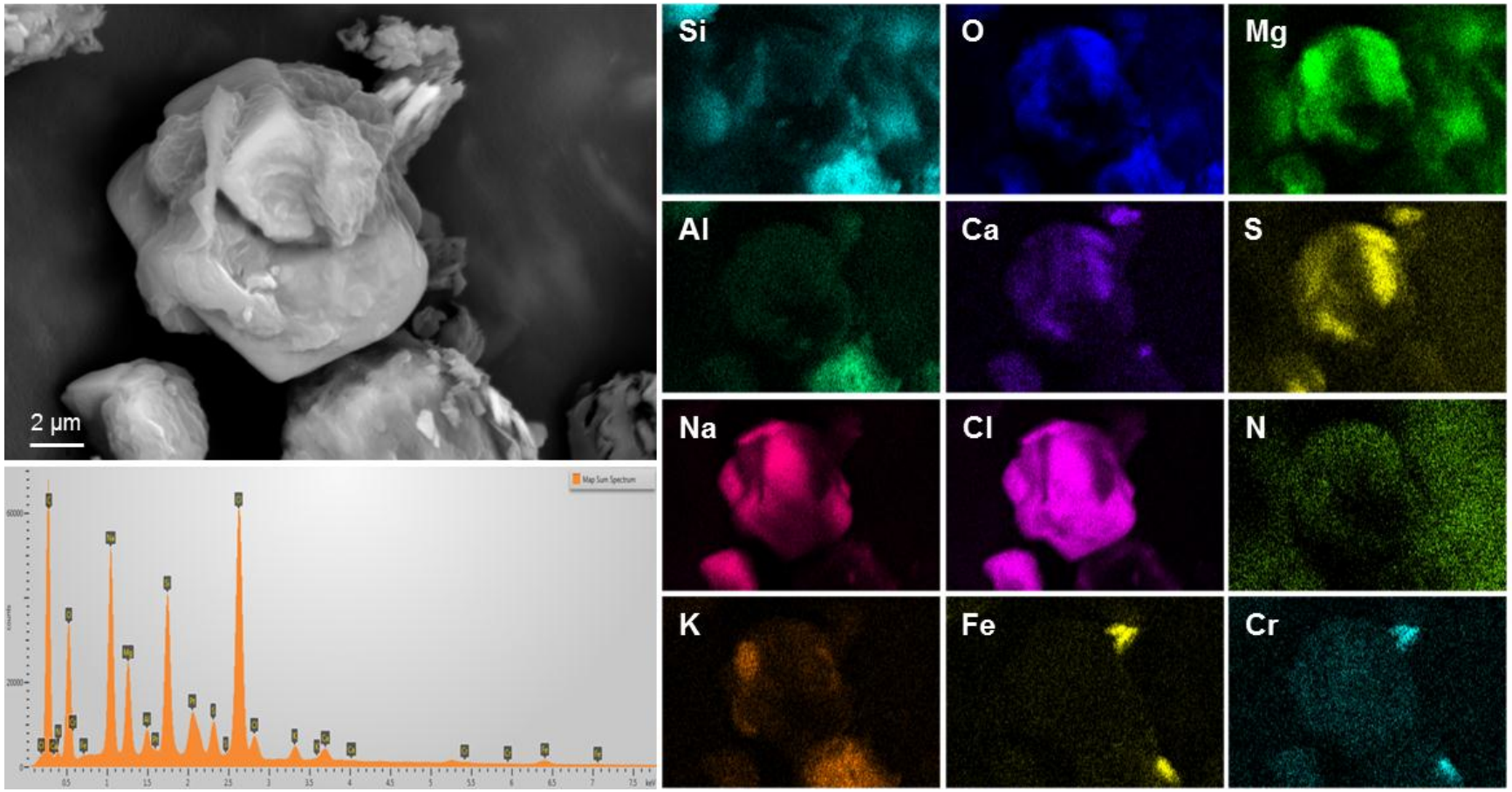

Sample: 170-003
Map E

Notes: Close-up of sea-salt aggregate in upper right corner of Map B, showing intergrown NaCl cubes with interstitial Mg-SO_4, and trace Ca, K.

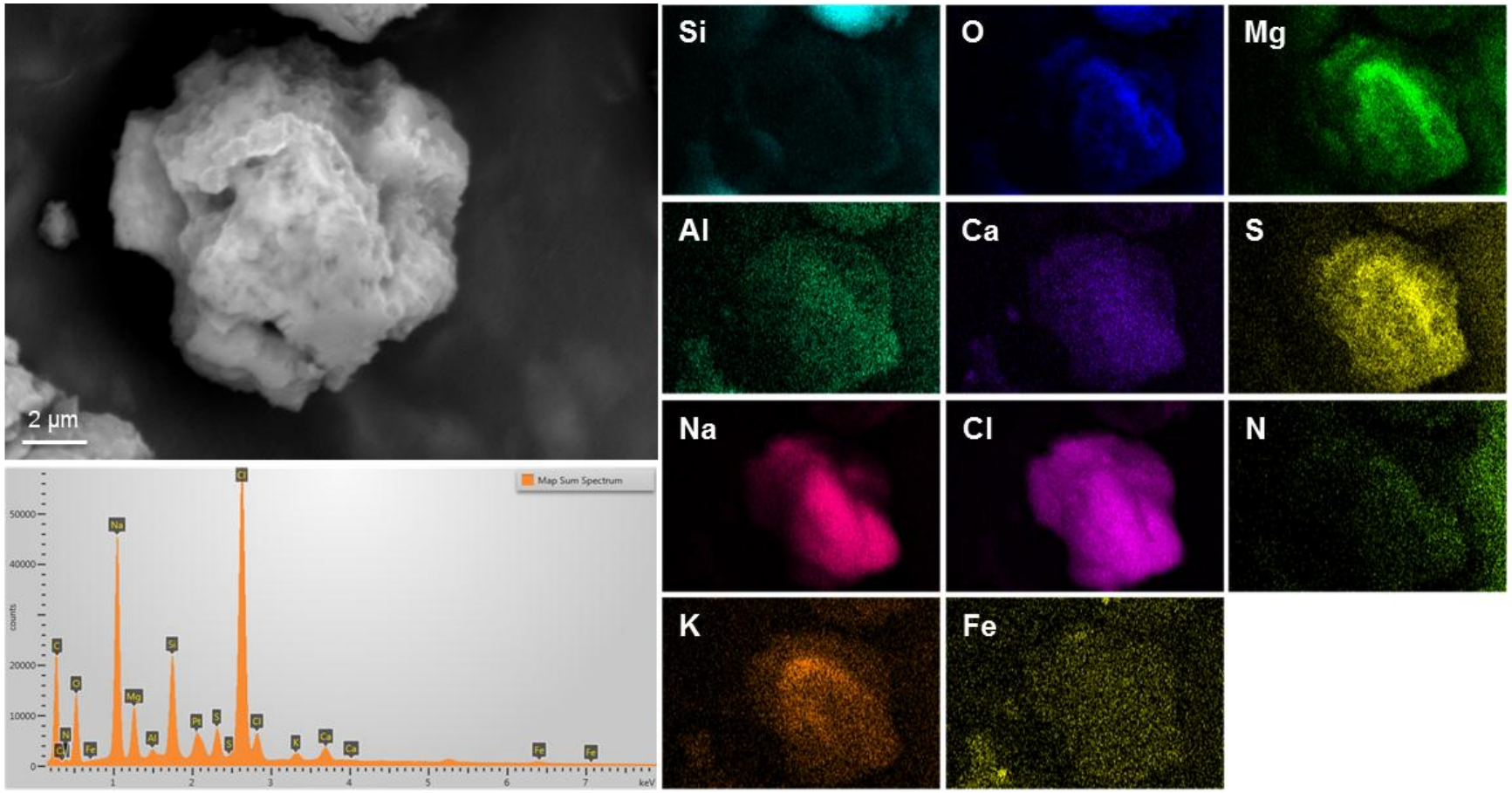

Sample: 170-003
Map F

Notes: This Map is largely in a shadow, making the element maps nearly useless. But the image does show a degraded pollen grain.

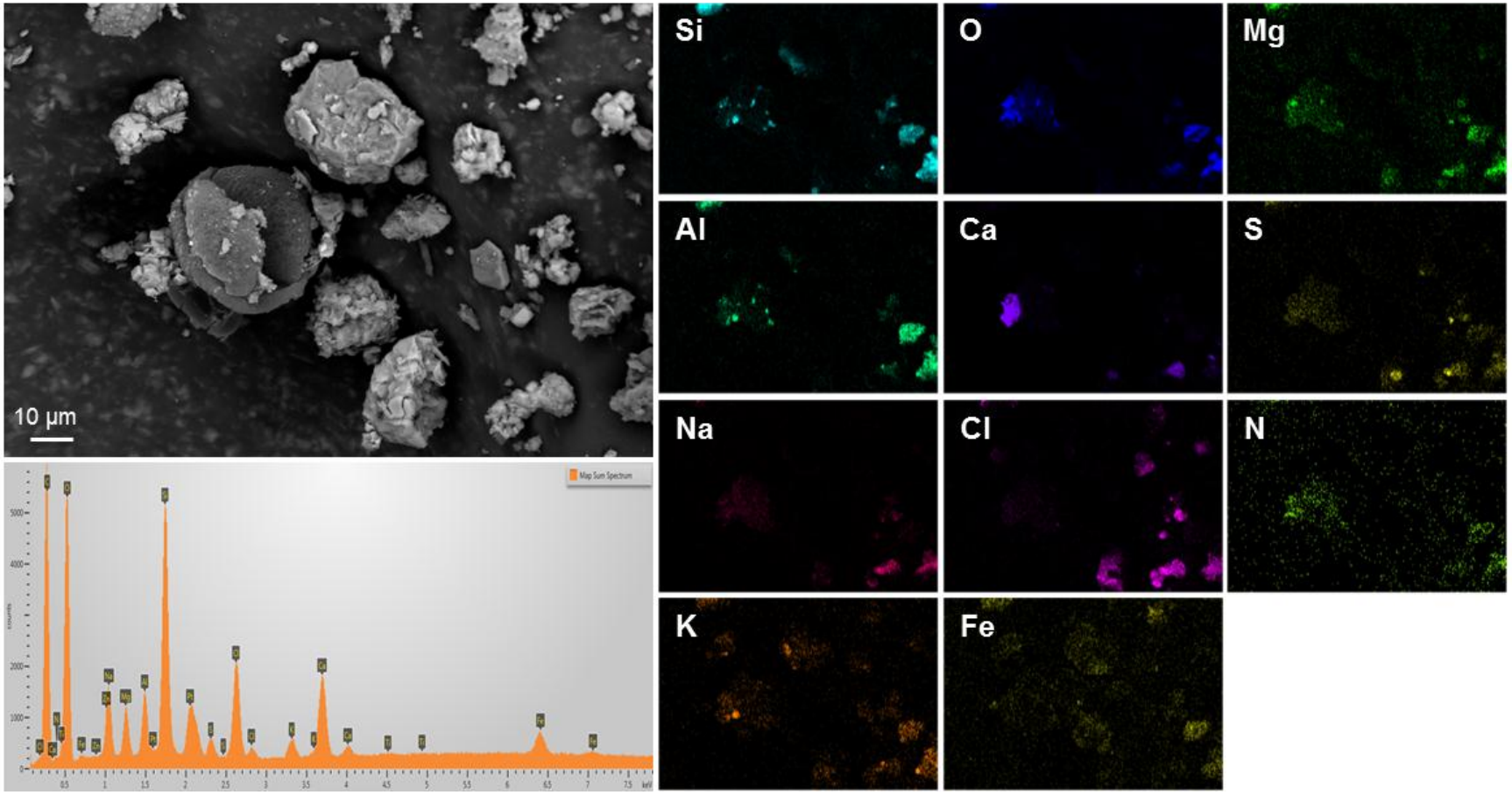

Sample: 170-003
Map G

Notes: Abundant dust on an abraded edge, consisting dominantly of aluminosilicates and sea-salt aggregates.

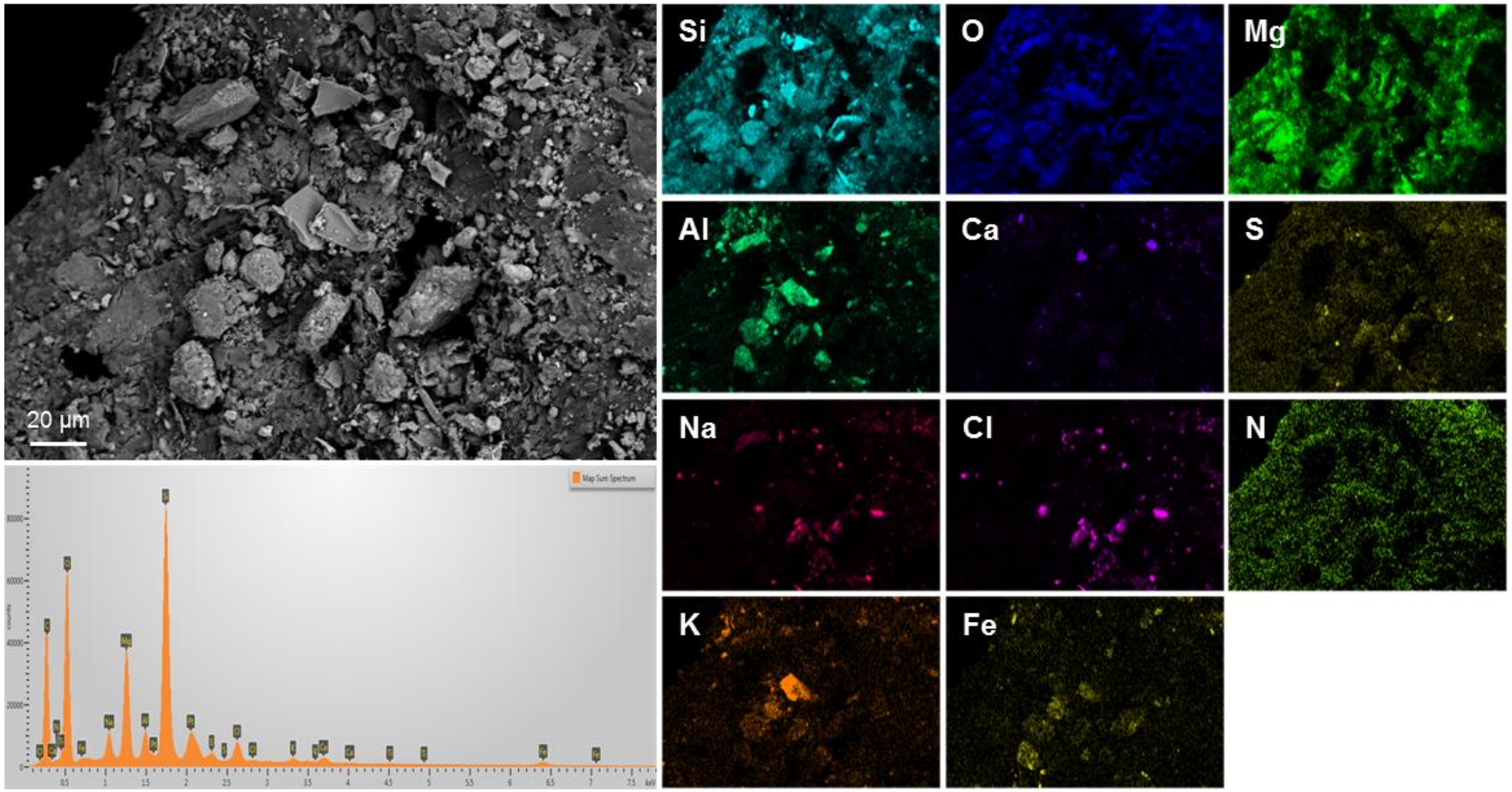

Sample: 170-003
Map H

Notes: Dust consisting dominantly of aluminosilicates and sea-salt aggregates.

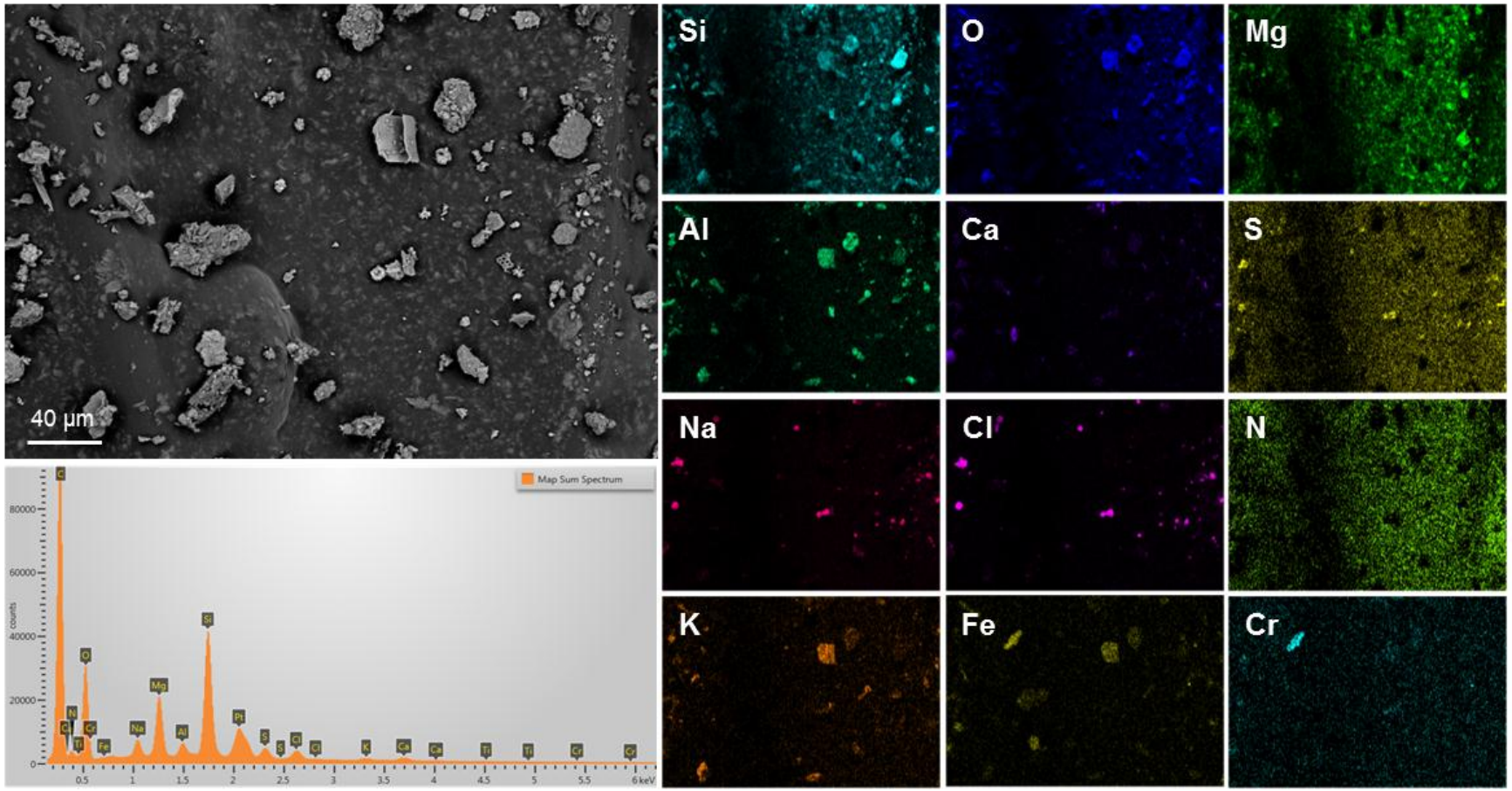

Sample: 170-003
Map I

Notes: Close-up of sea-salt aggregates, consisting of skeletal NaCl crystals and Mg-SO_4, with trace Ca and K. The third grain is an unidentified aluminosilicate.

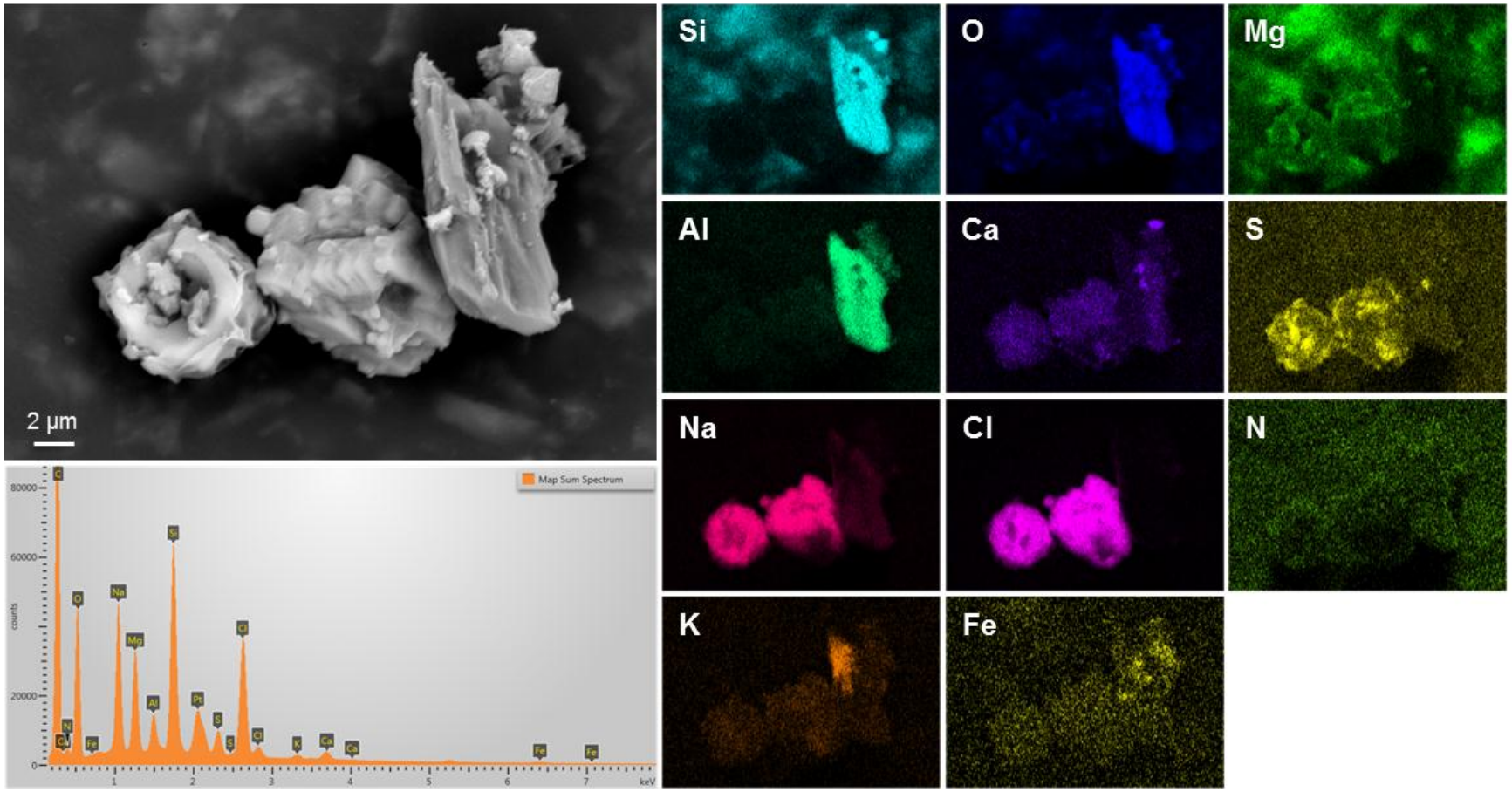

Sample: 170-003
Map J

Notes: Dust consisting dominantly of aluminosilicates and sea-salt aggregates.

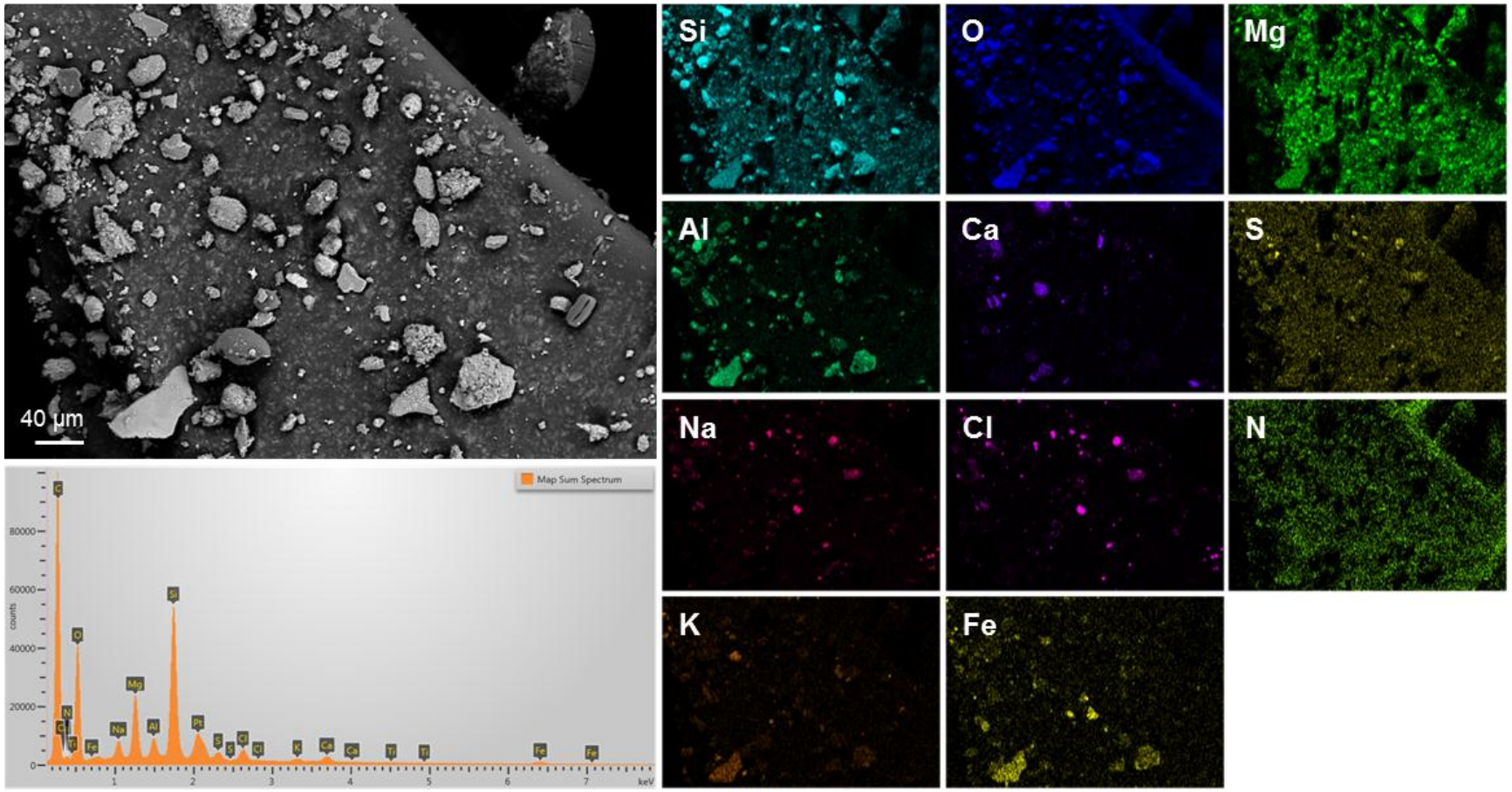

Sample: 170-003
Map K

Notes: Dust consisting dominantly of aluminosilicates and sea-salt aggregates (NaCl and Mg-SO_4). Ca-carbonate is also present.

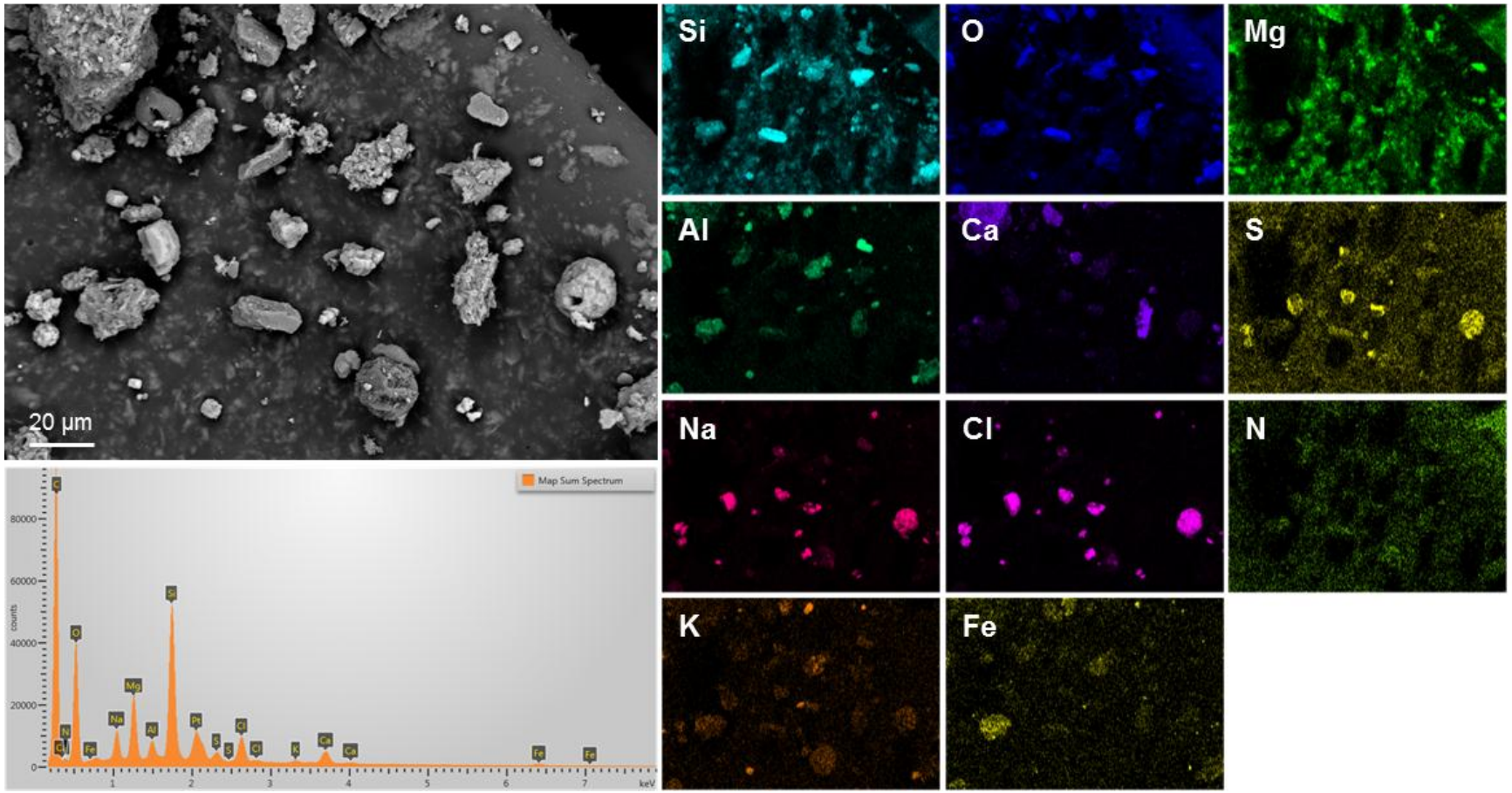

Sample: 170-003
Map L

Notes: Close-up of two sea-salt aggregates, consisting of skeletal NaCl crystals and interstitial Mg-SO_4, with trace Ca and K.

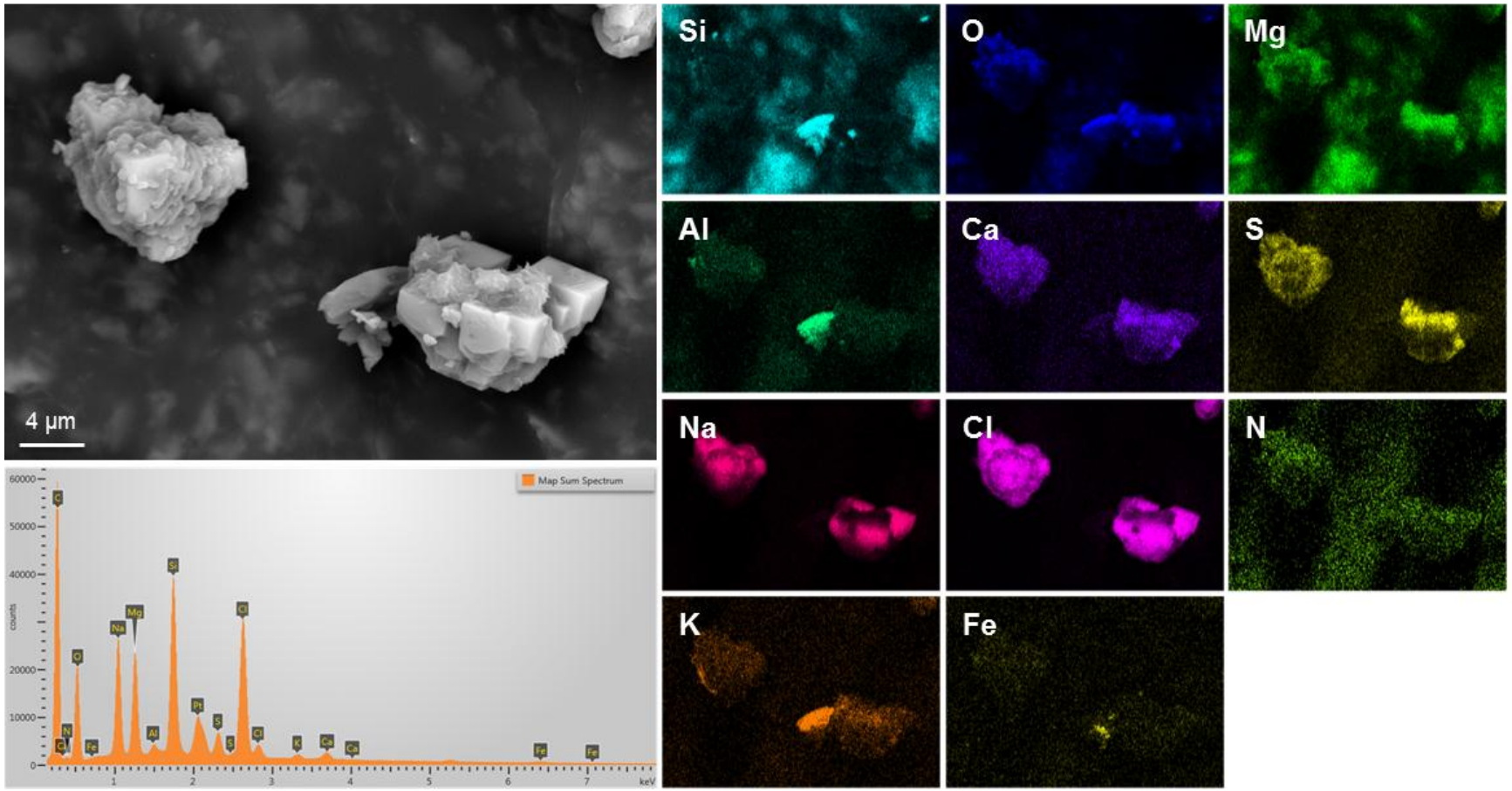

Sample: 170-003
Map M

Notes: Dust consisting dominantly of aluminosilicates and sea-salt aggregates (NaCl and Mg-SO_4).

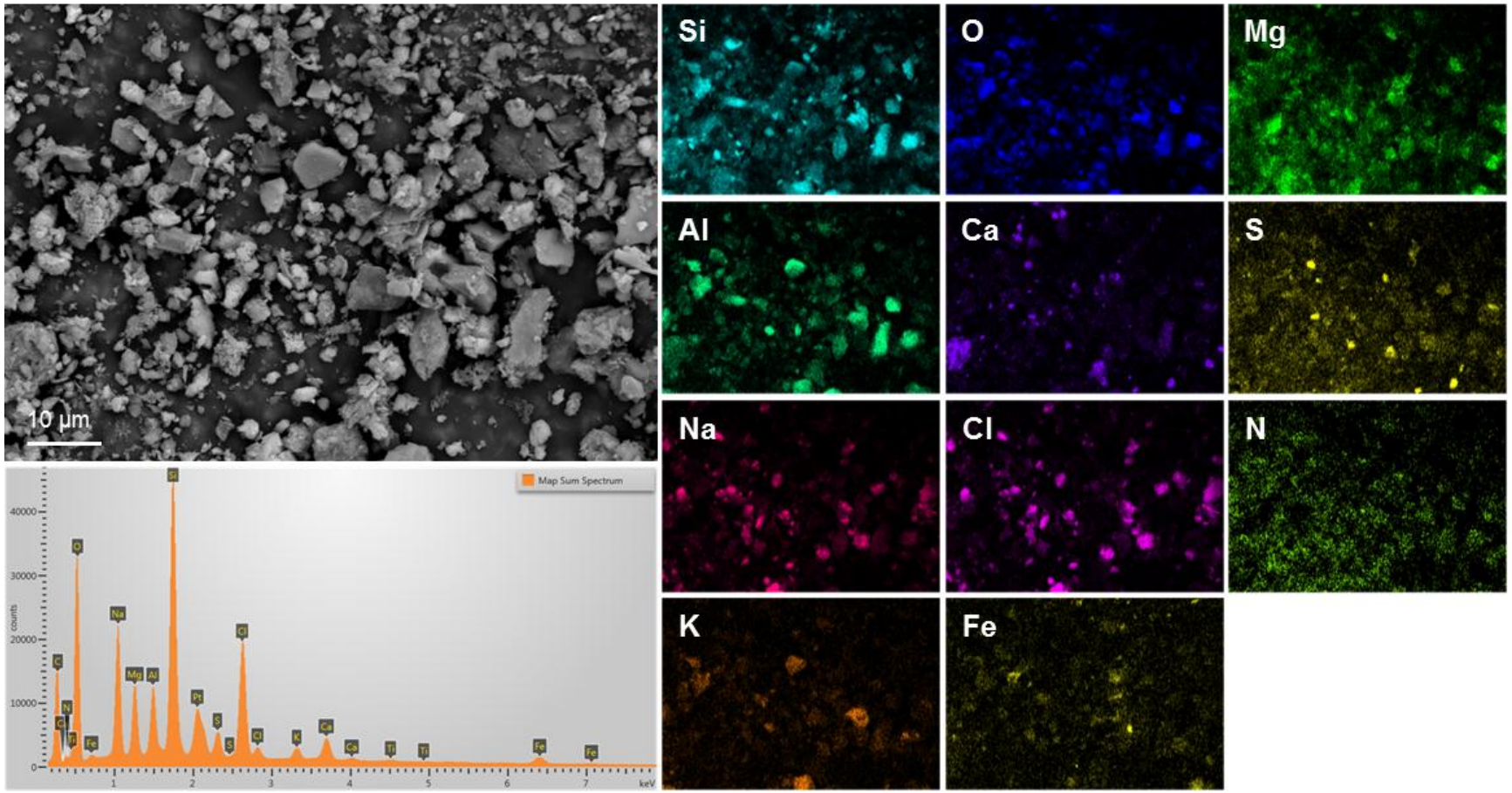

Sample: 170-003
Map N

Notes: Dust consisting dominantly of aluminosilicates and sea-salt aggregates (NaCl and Mg-SO_4). Ca-sulfate is also present.

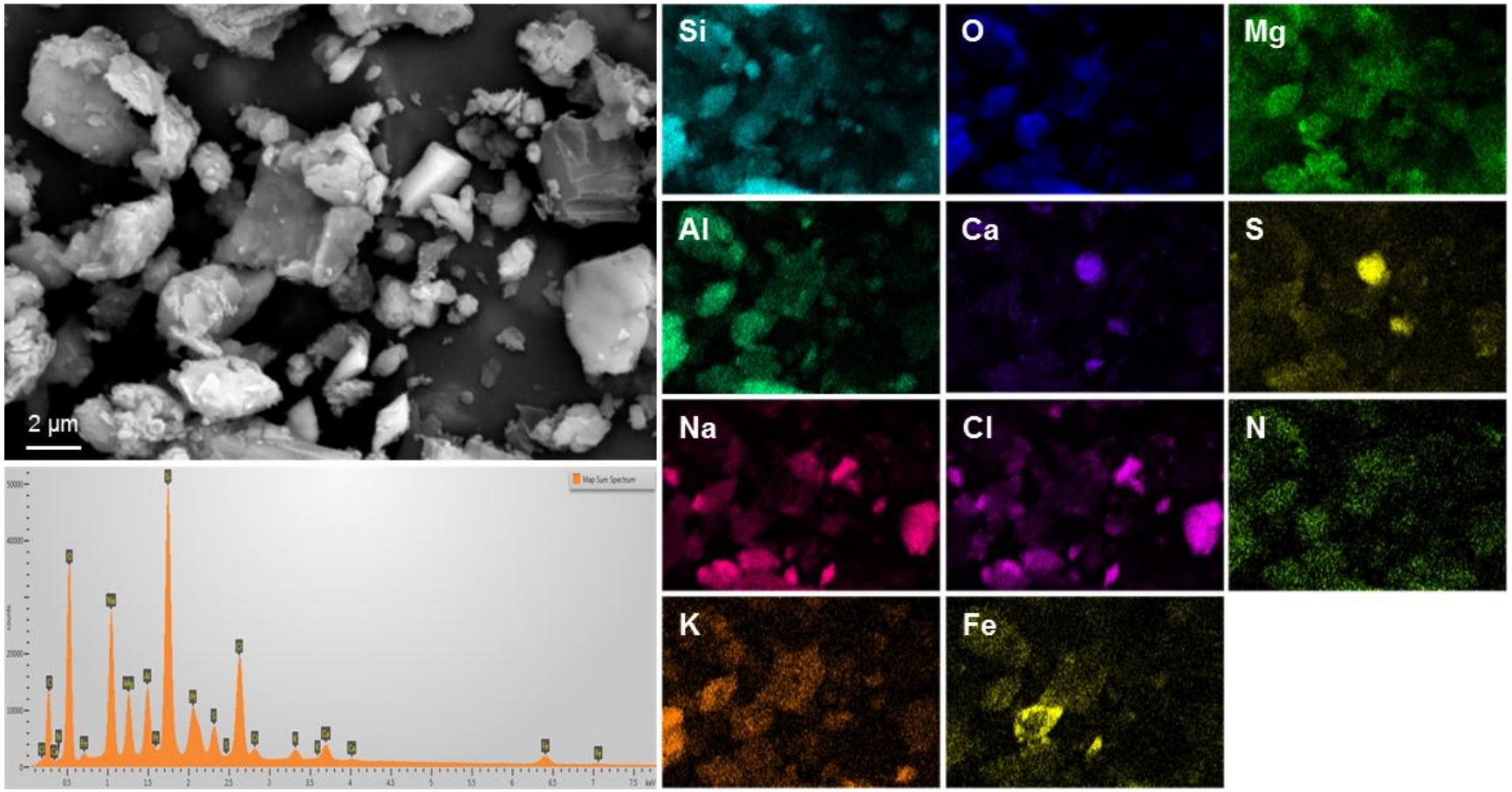

Sample: 170-003
Map O

Notes: Dust consisting dominantly of aluminosilicates and sea-salt aggregates (NaCl and Mg-SO_4).

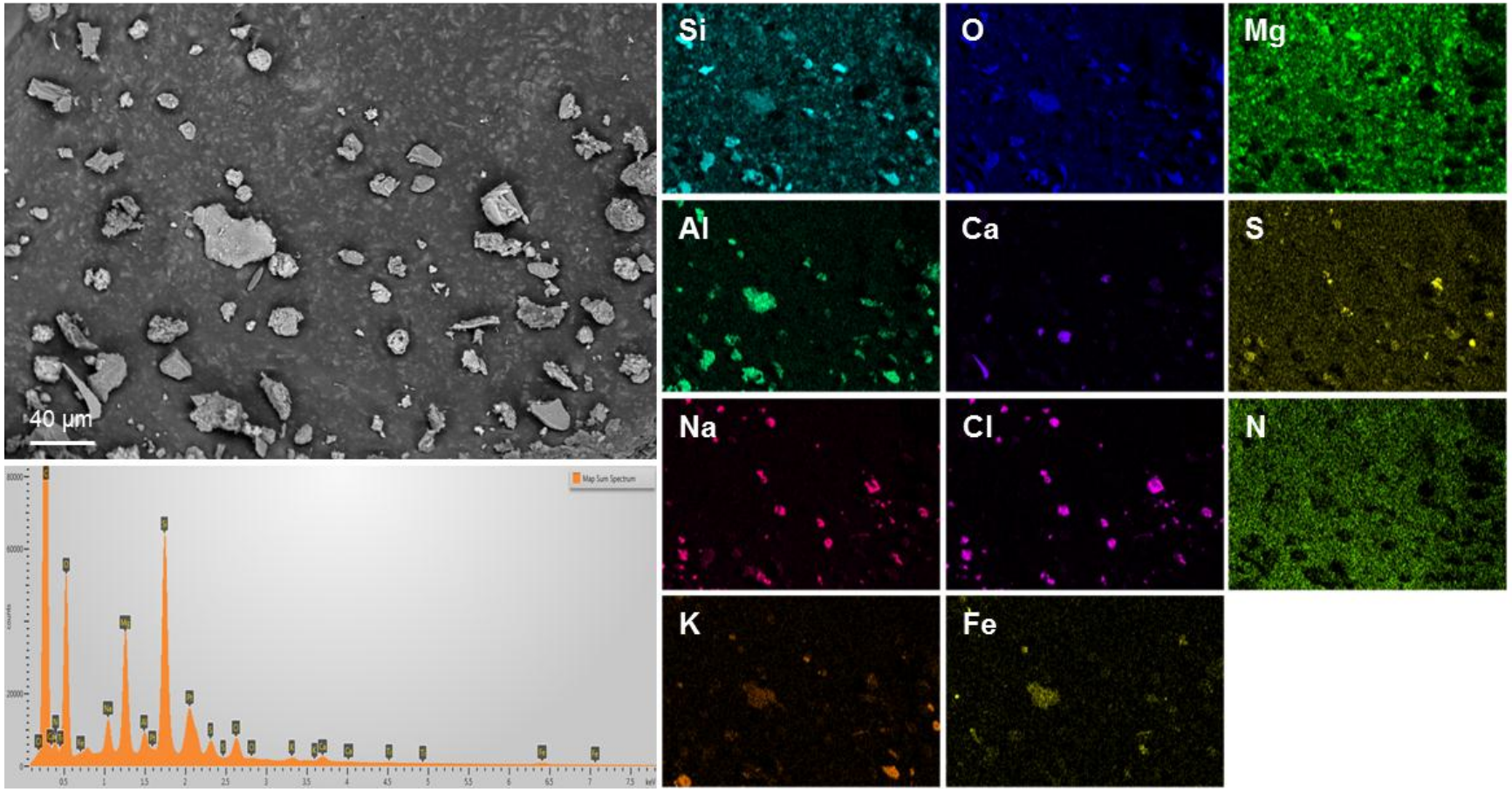

Sample: 170-003
Map P

Notes: Close-up of sea-salt aggregate in left center of Map O, showing intergrown NaCl cubes and sheaf-like Mg-SO_4, and trace Ca and K, both mostly associated with the sulfate.

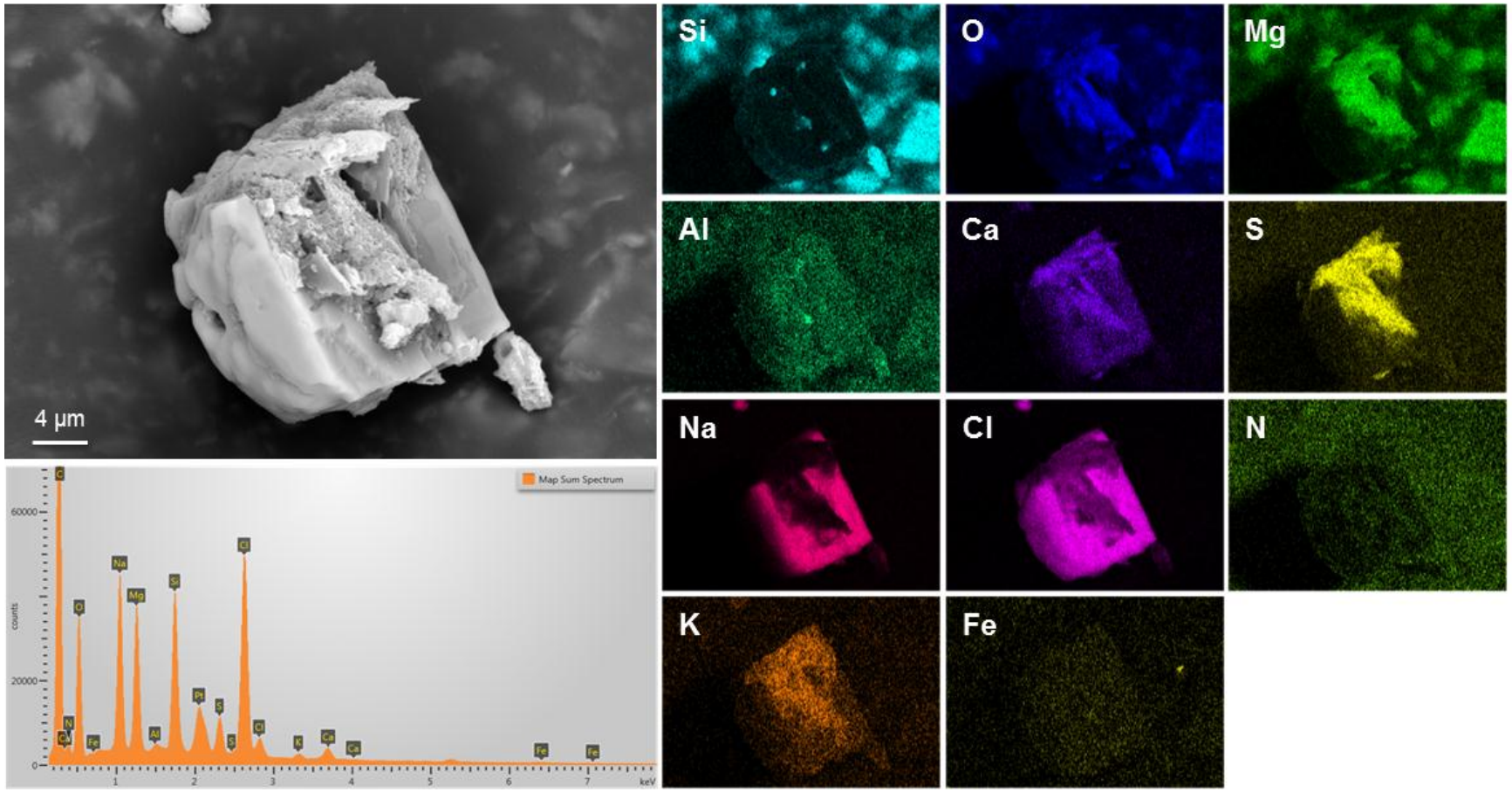

Sample: 170-003
Map Q

Notes: Dust consisting dominantly of aluminosilicates and sea-salt aggregates (NaCl and Mg-SO_4). A large grain of Ca-sulfate is present.

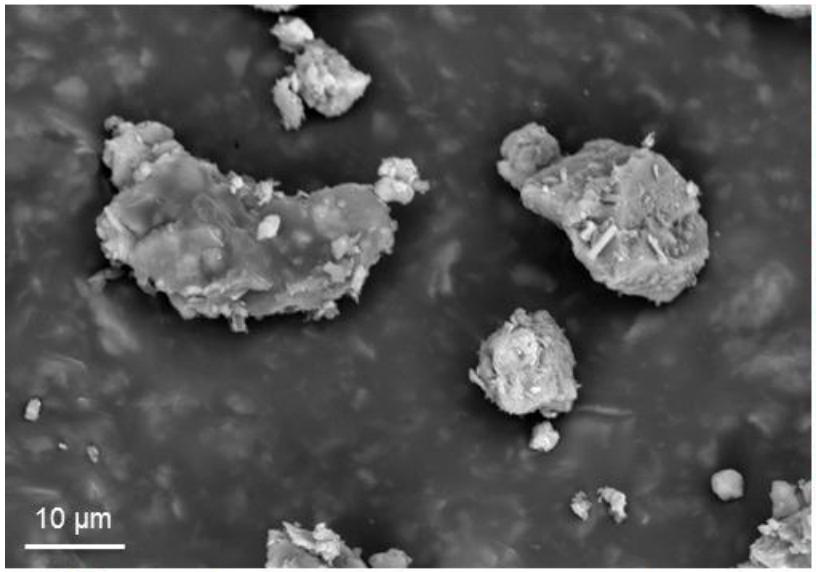

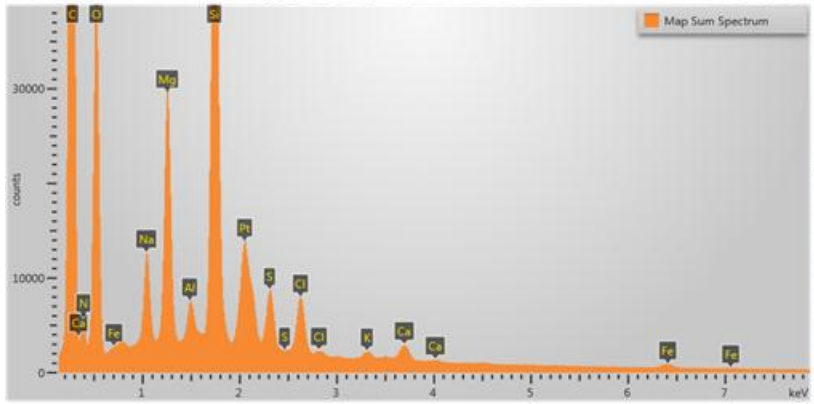

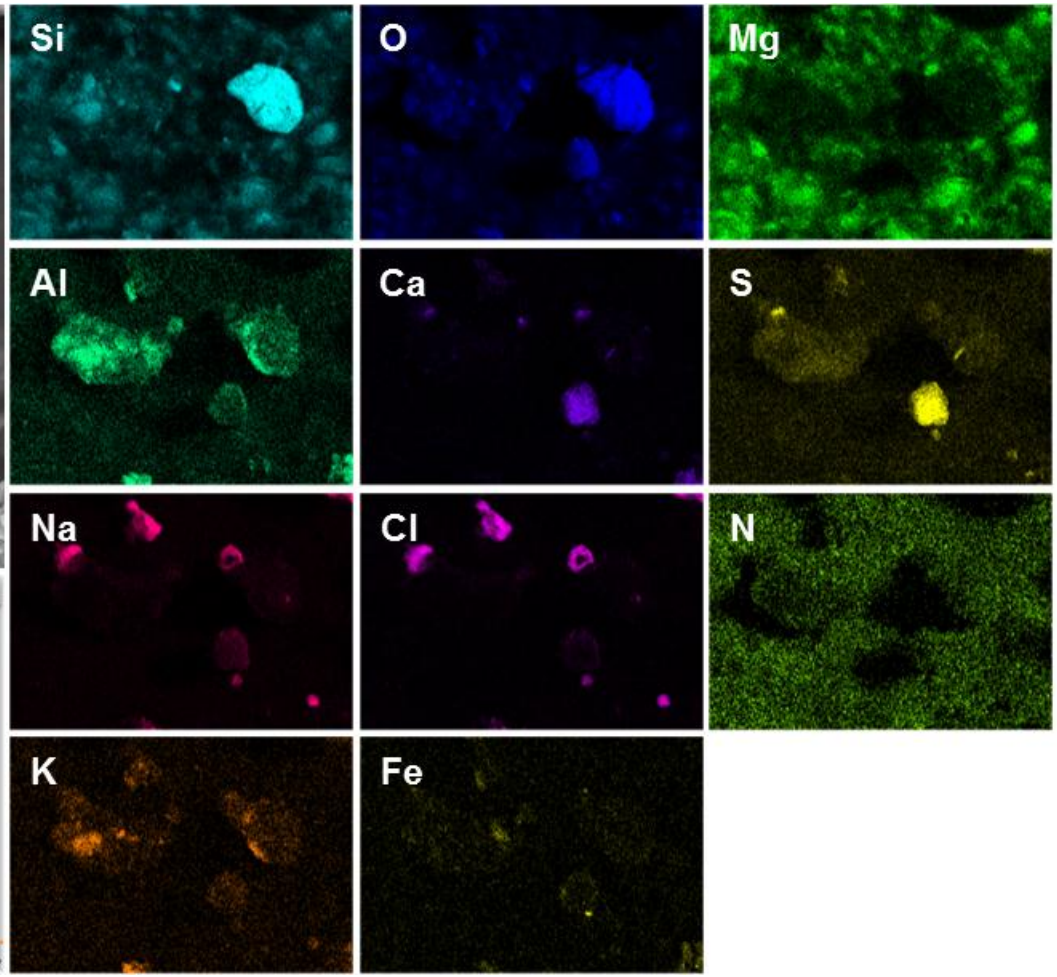

Sample: 170-003
Map R

Notes: Close-up of sea-salt aggregate, showing intergrown NaCl cubes and interstitial Mg-SO_4, and trace Ca and K.

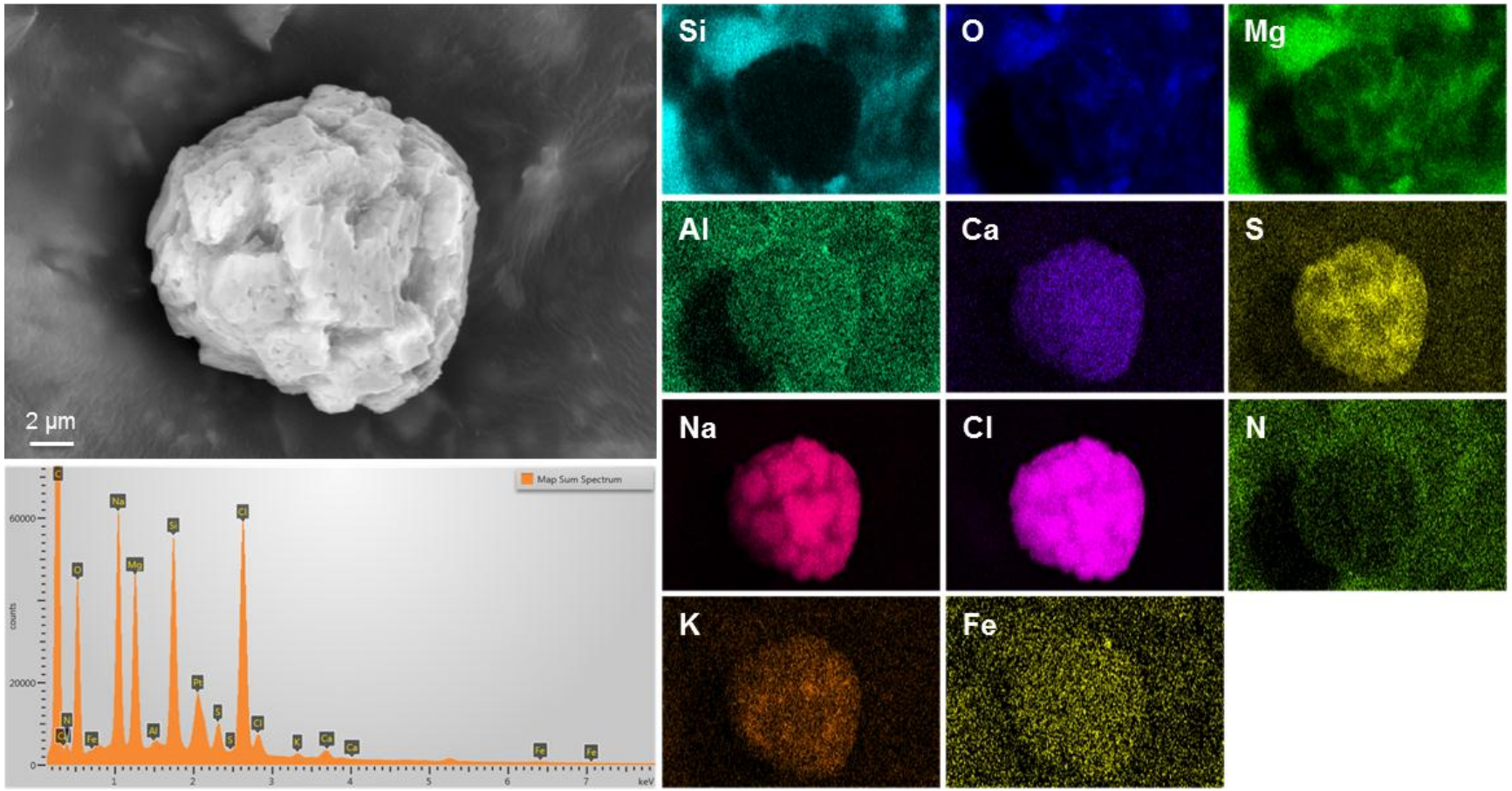

Sample: 170-004

Notes: Overview image of pad sample 170-004, showing the light dust load.

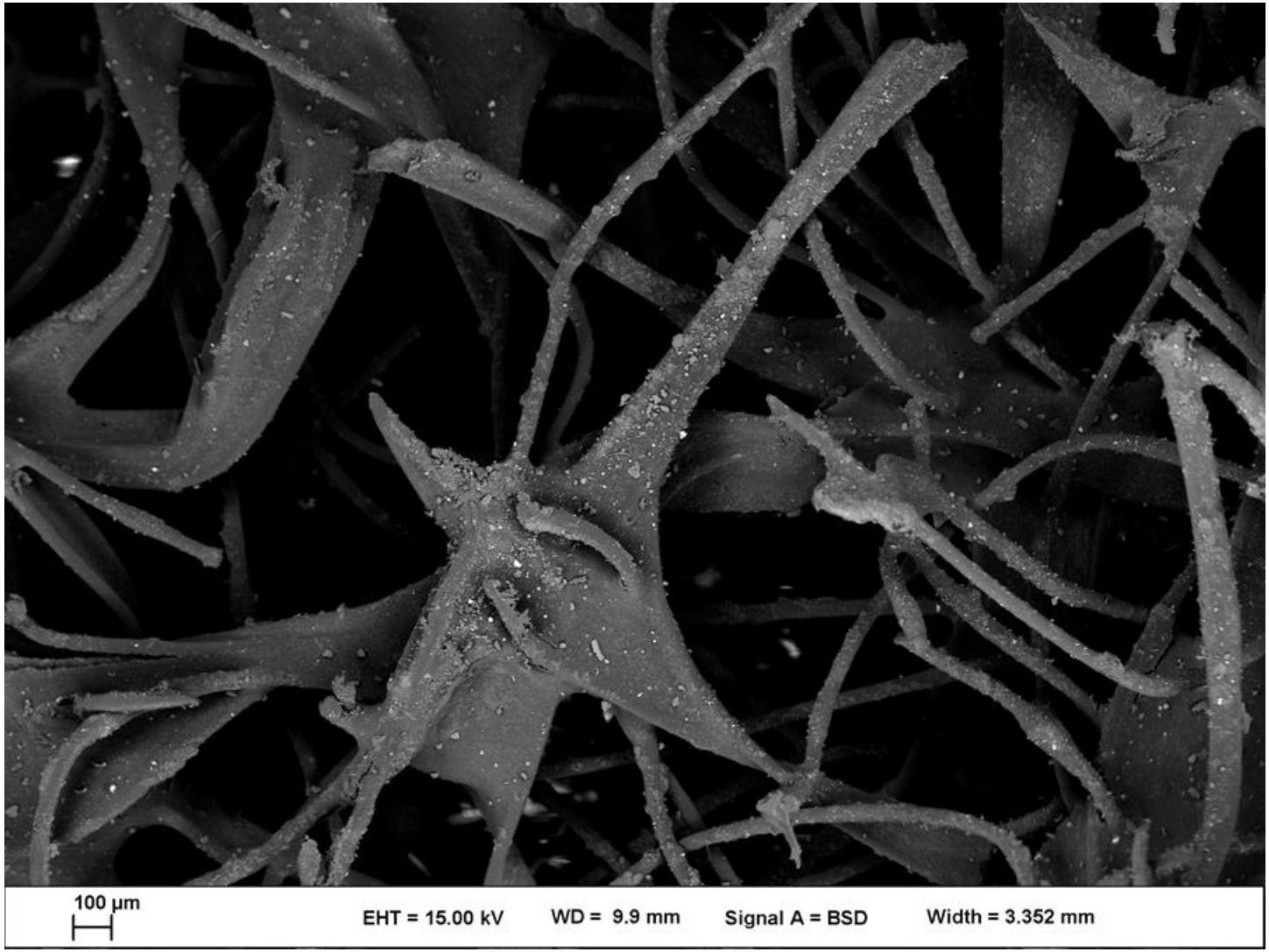

Sample: 170-004
Map A

Notes: Dust consisting of aluminosilicates, sea-salt particles, and stainless steel particles.

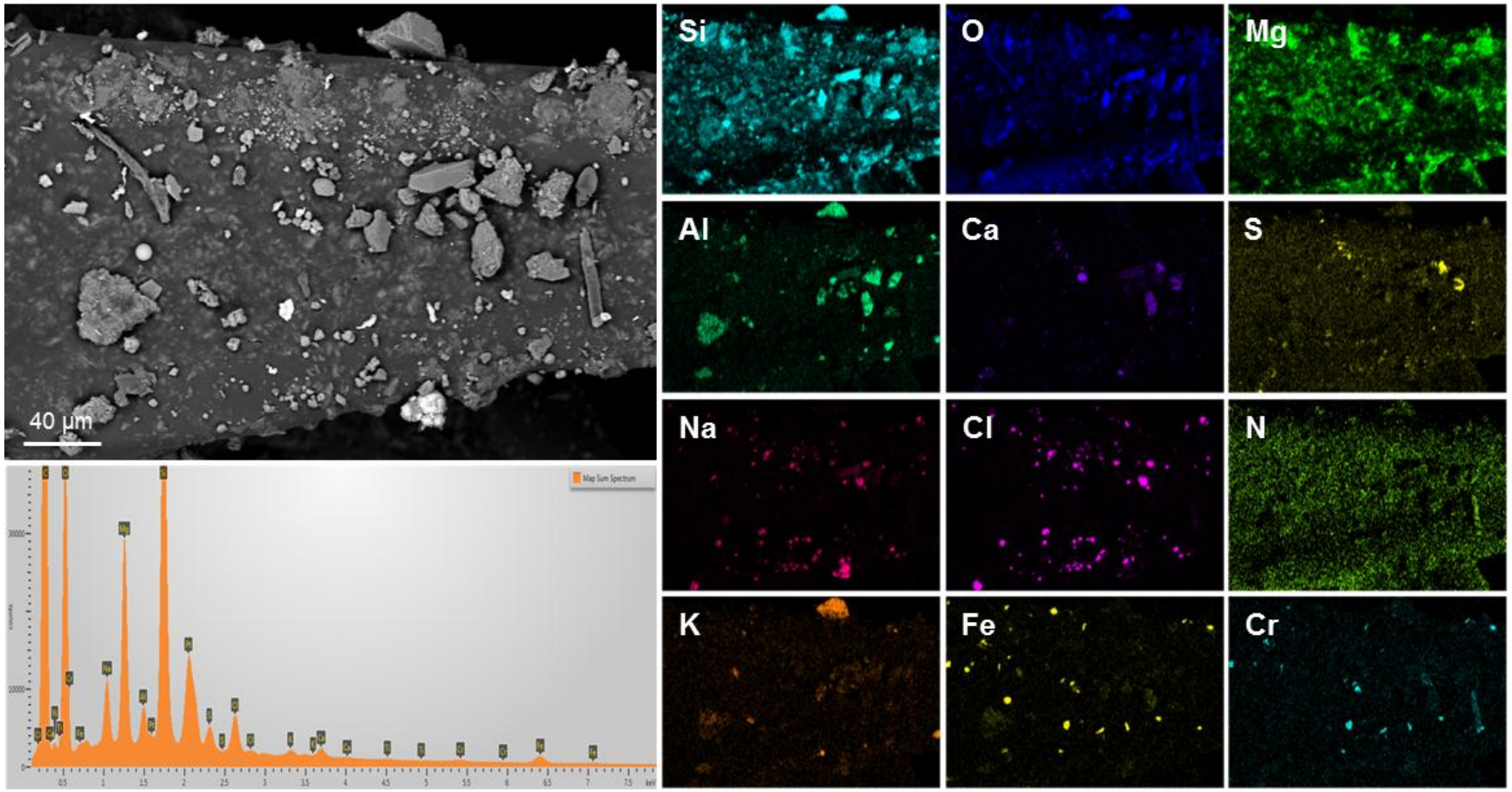

Sample: 170-004
Map B

Notes: Close-up of upper left quadrant of Map A, showing aluminosilicates, sea-salt aggregates, and Ca-sulfate. A pollen grain is present on the far right side of the image.

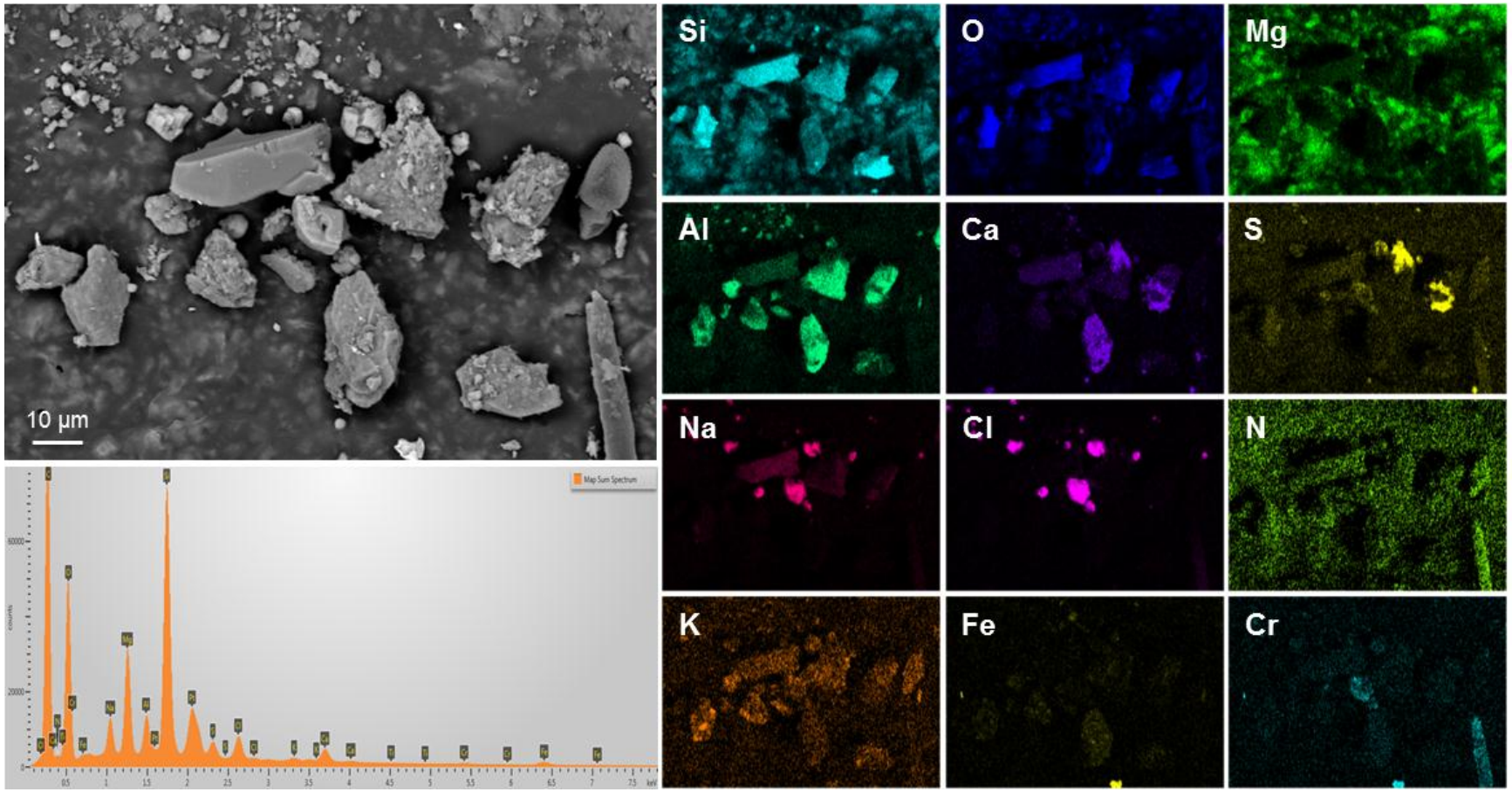

Sample: 170-004
Map C

Notes: Close-up of bright Na- and Zn-rich feature along the bottom edge of Map A.

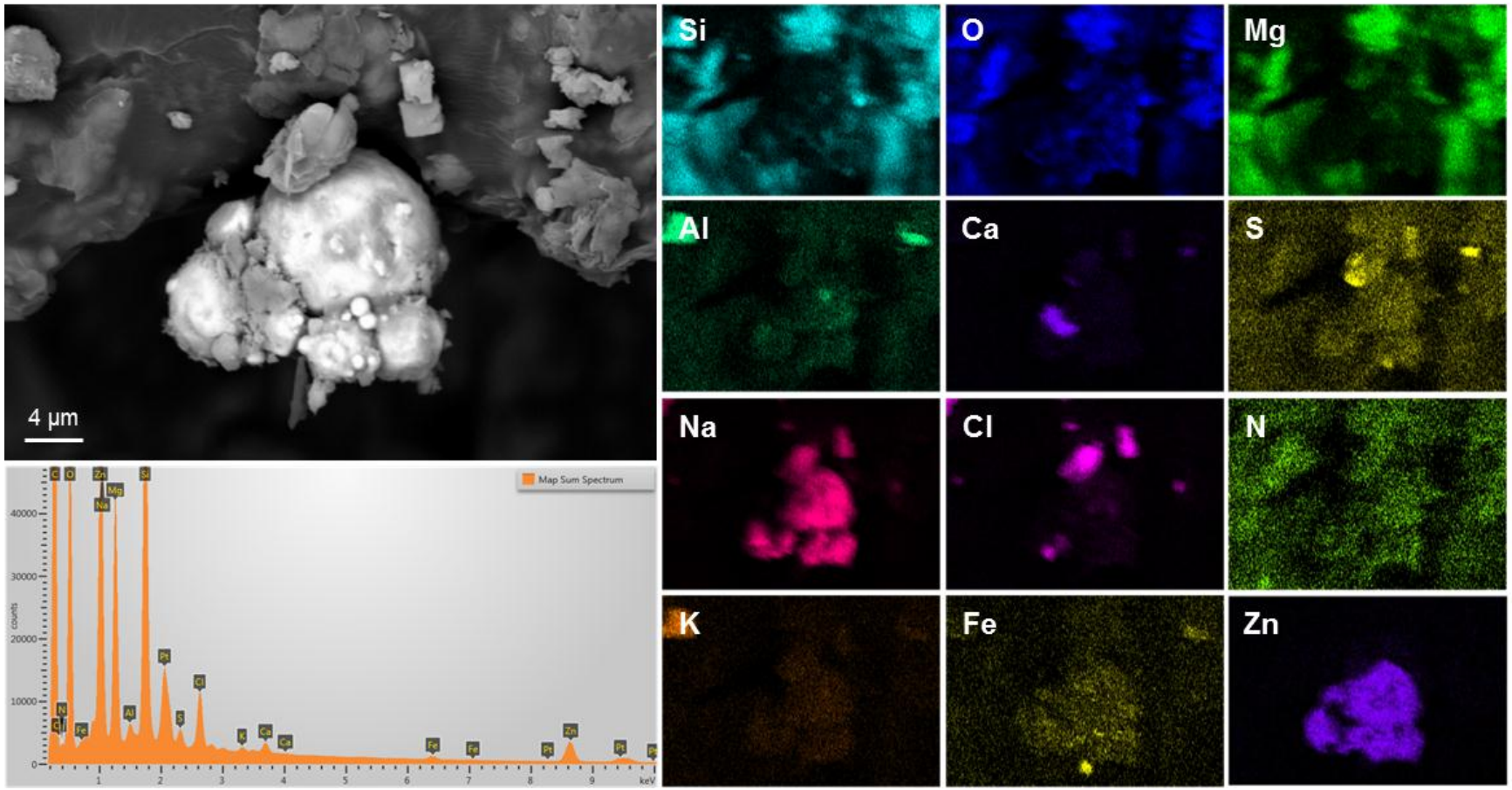

Sample: 170-004
Map D

Notes: Dust containing aluminosilicates, sea-salt aggregates, and stainless steel particles.

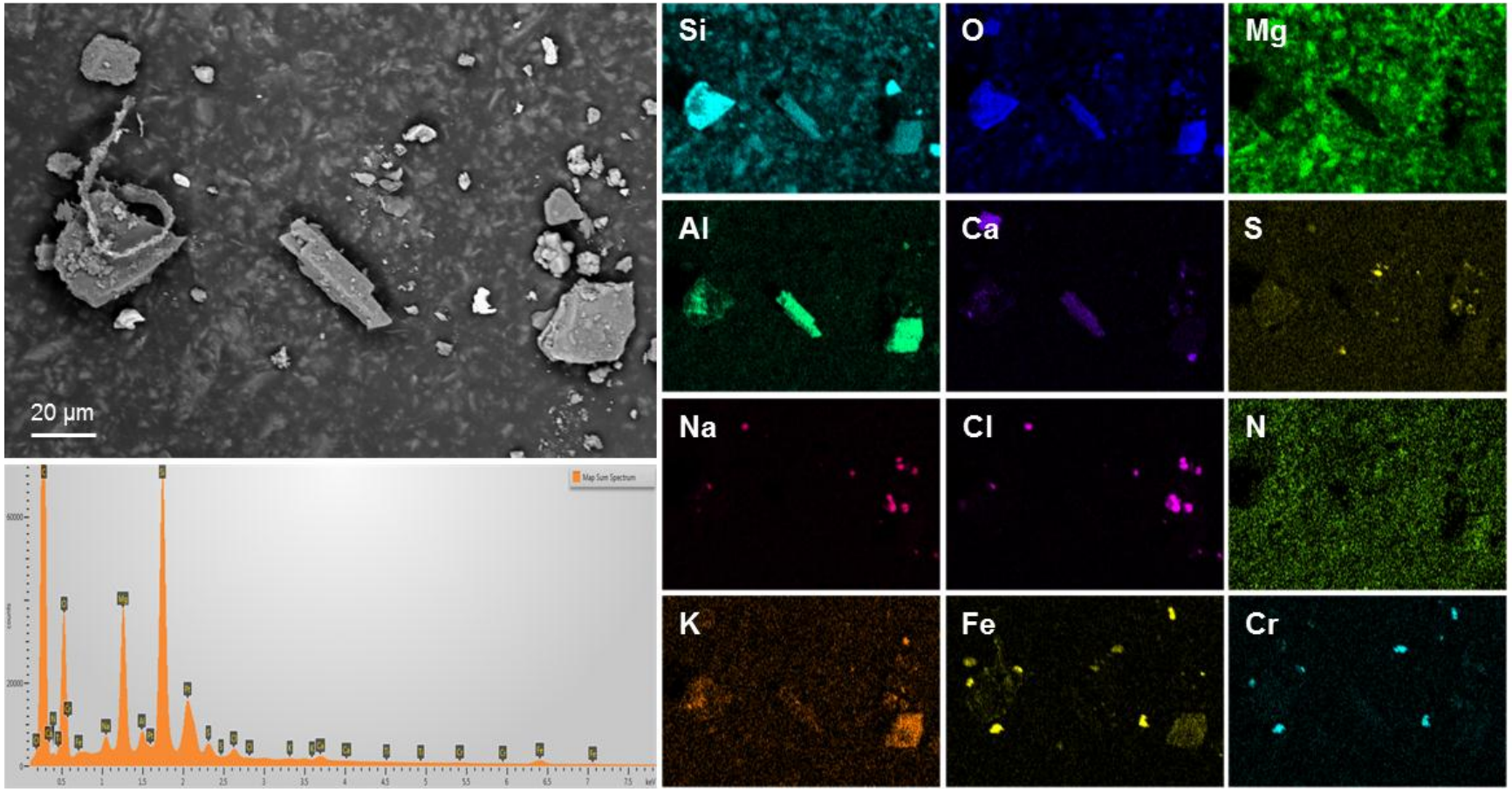

Sample: 170-004
Map E

Notes: Dust consisting mostly of aluminosilicates and sea-salt aggregates. The large platy grain is probably biotite.

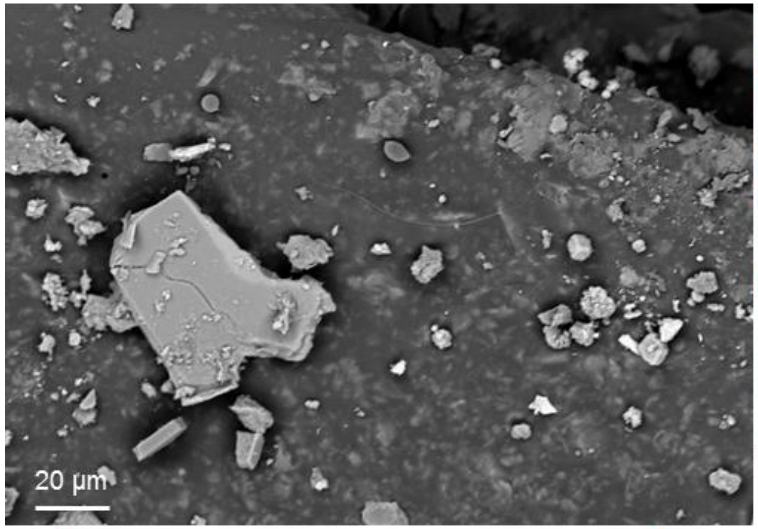

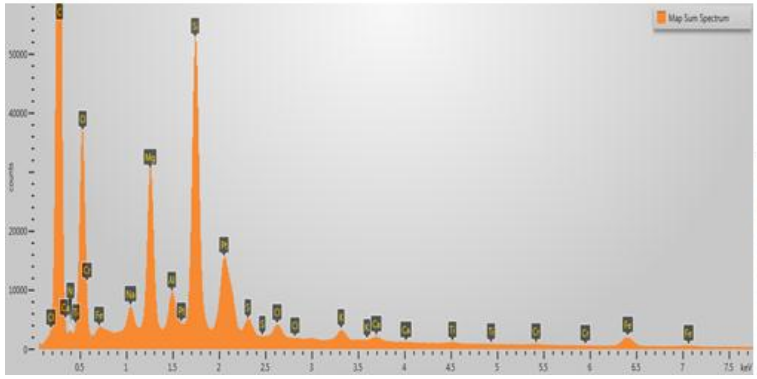

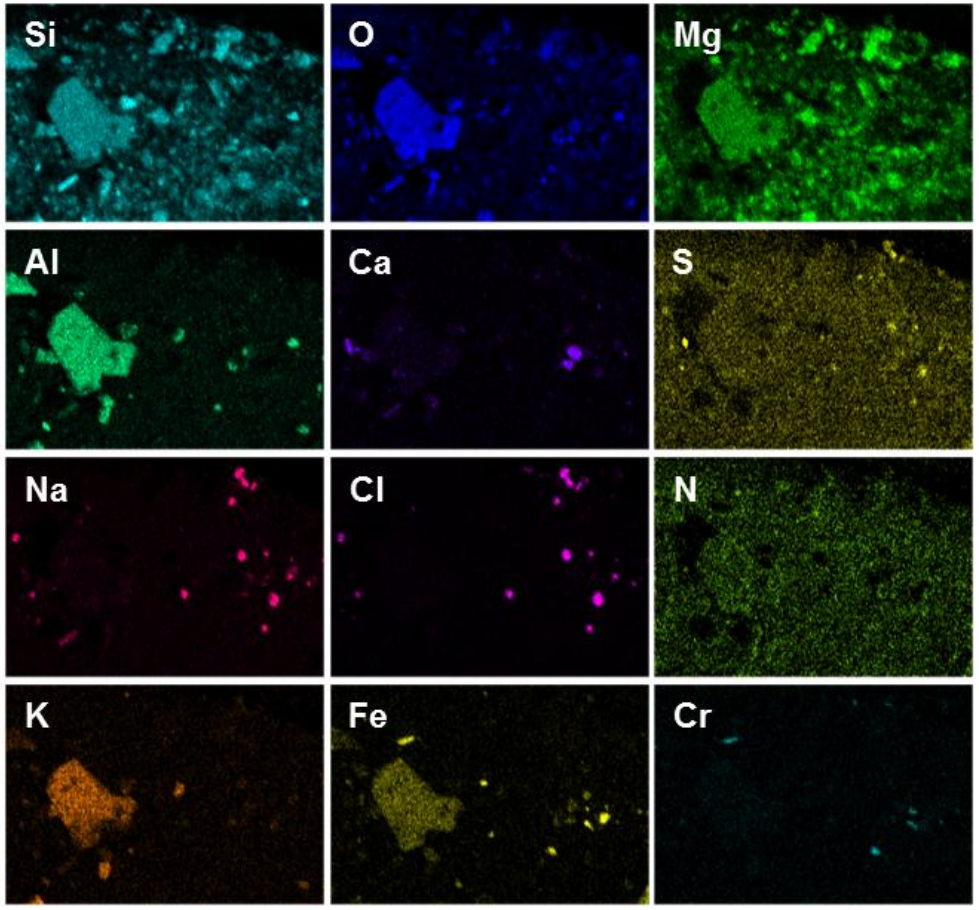

Sample: 170-004
Map F

Notes: Dust containing aluminosilicates, sea-salt aggregates, and Ca-carbonate.

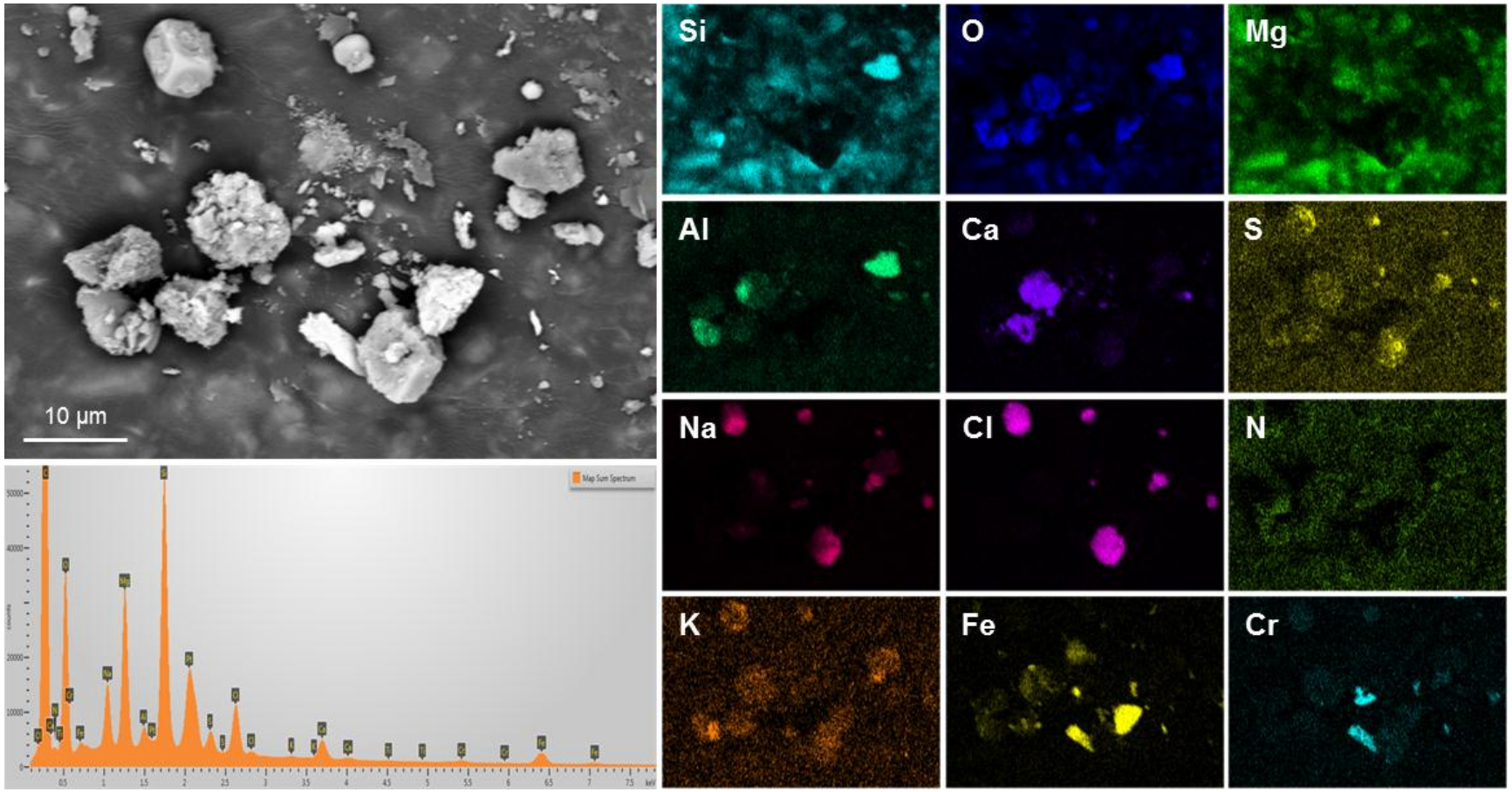

Sample: 170-004
Map G

Notes: Dust adhering to an abraded edge. Possibly comminuted during collection. Consists mostly of sea-salts.

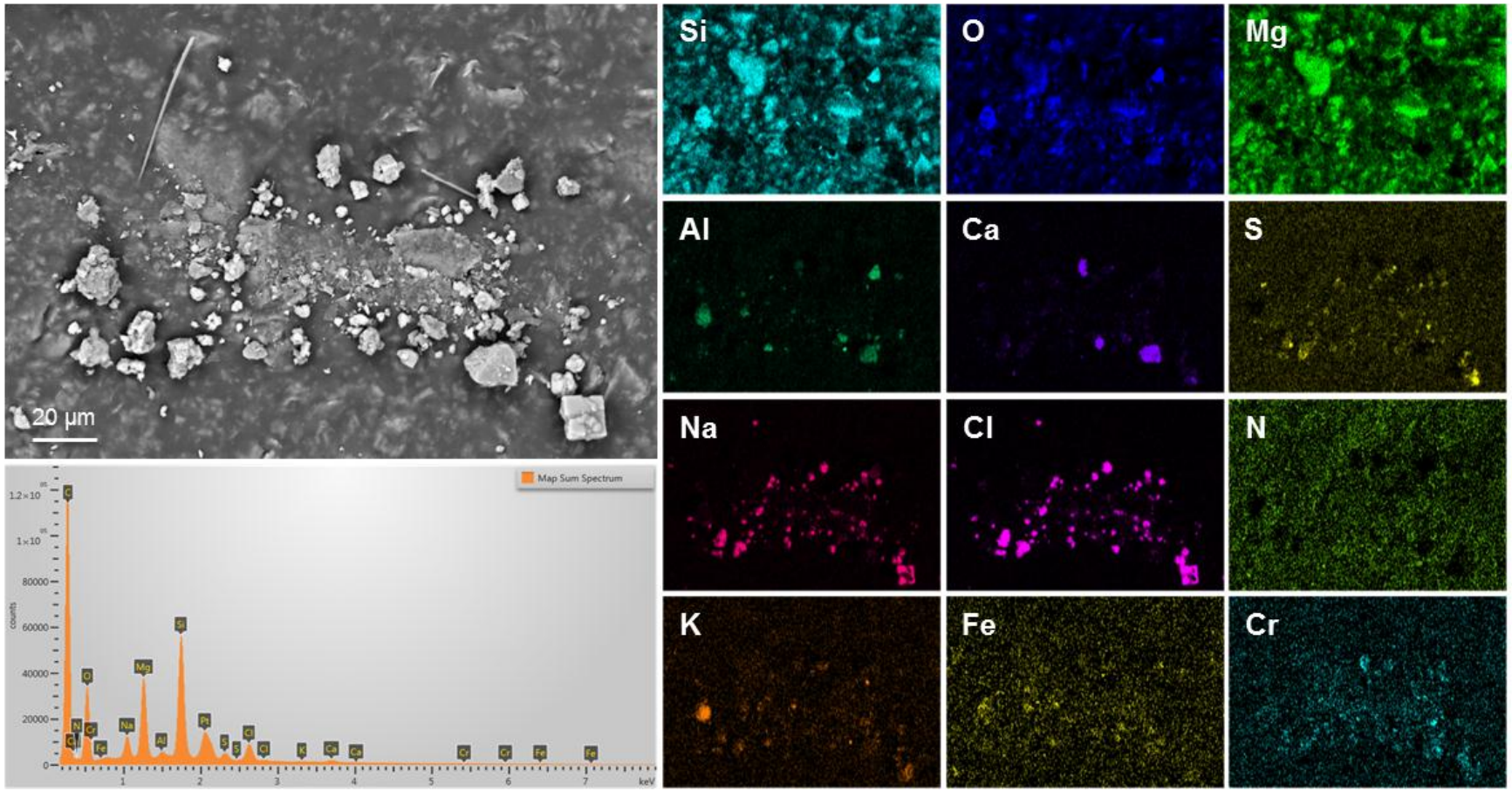

Sample: 170-004
Map H

Notes: Close-up of sea-salt aggregate in lower right corner of Map G, consisting of skeletal or intergrown NaCl cubes, and Mg-SO_4, and trace Ca and K.

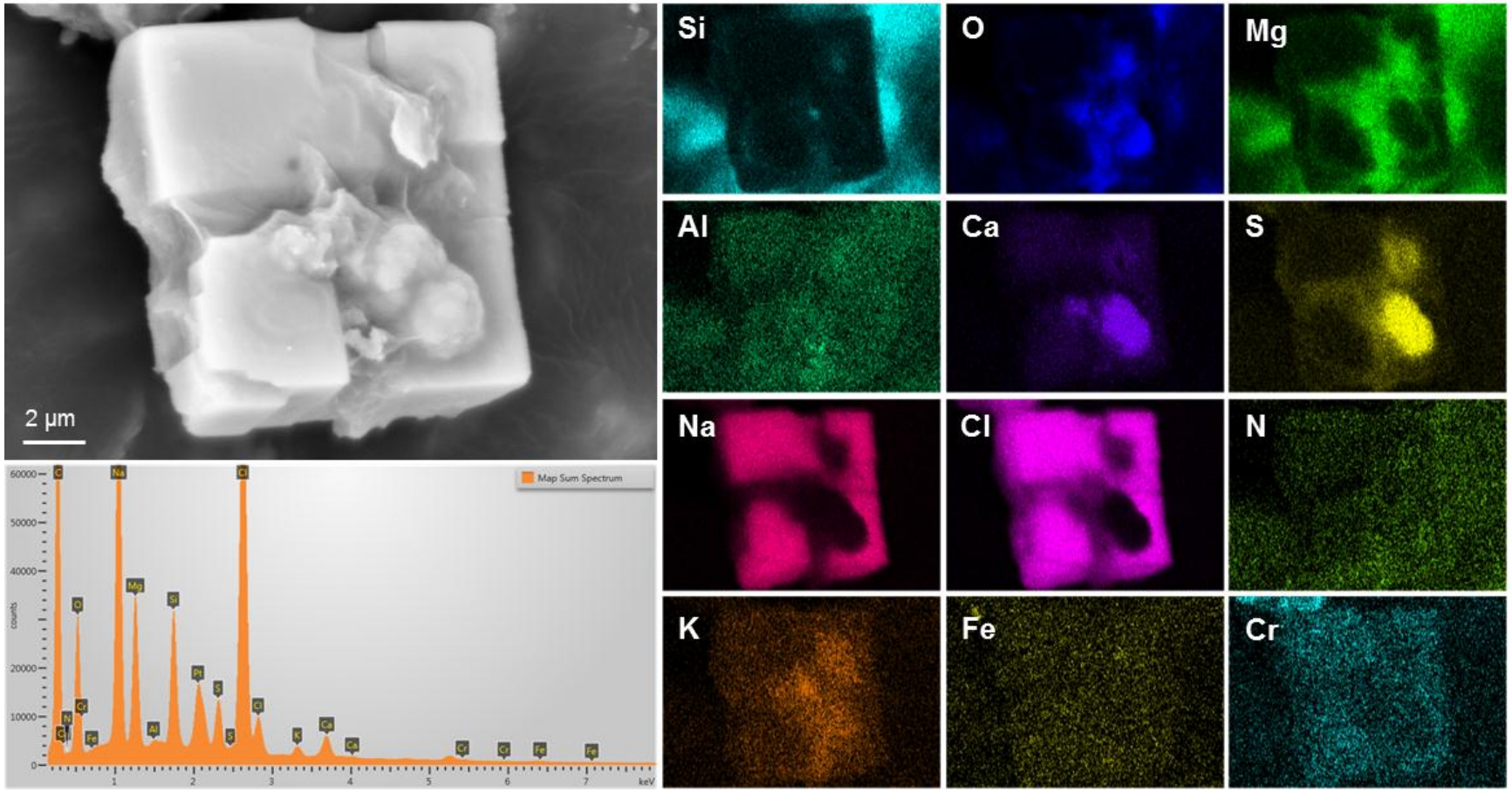

Sample: 170-004
Map I

Notes: Abundant dust on an abraded edge, consisting dominantly of aluminosilicates and sea-salt aggregates.

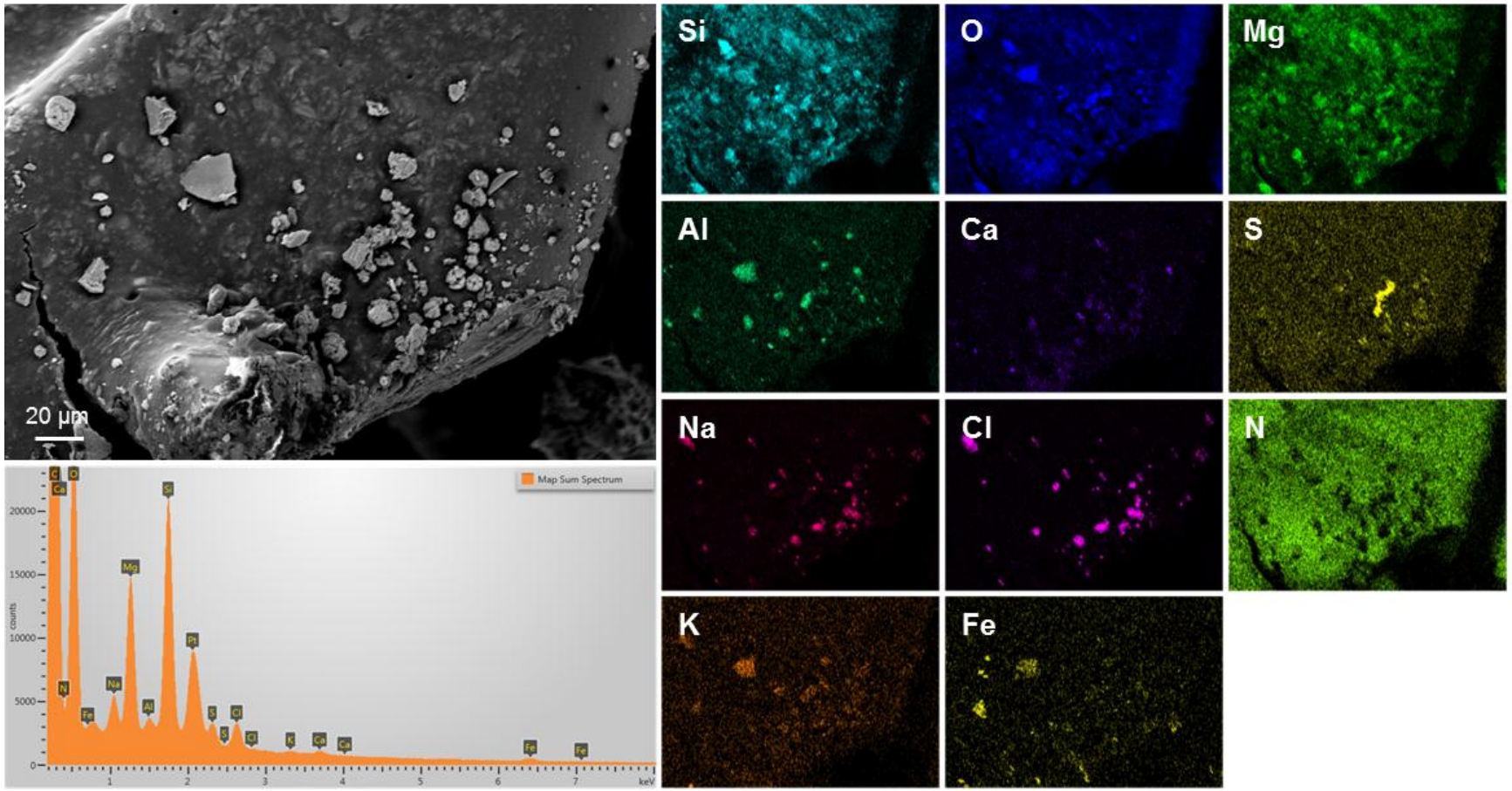

Sample: 170-005

Notes: Overview image of pad sample 170-005, showing the very light dust load.

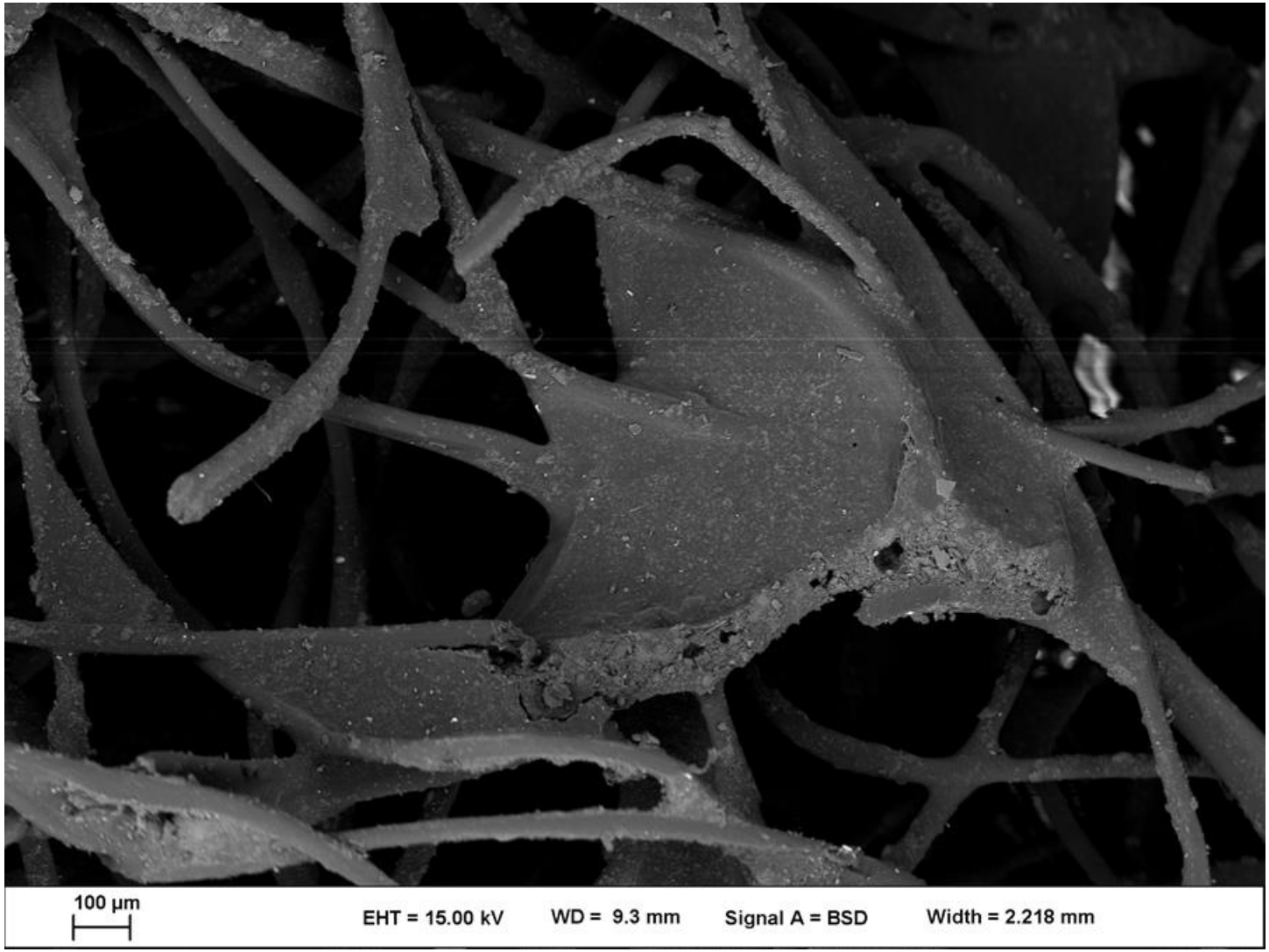

Sample: 170-005
Map A

Notes. The two elongated features are unidentified. They appeared as blade-like crystals initially, but rapidly changed in the electron beam, elongating by a factor of 3 or more. Compositionally, they contain K, O, N, C (not shown), and Ca.

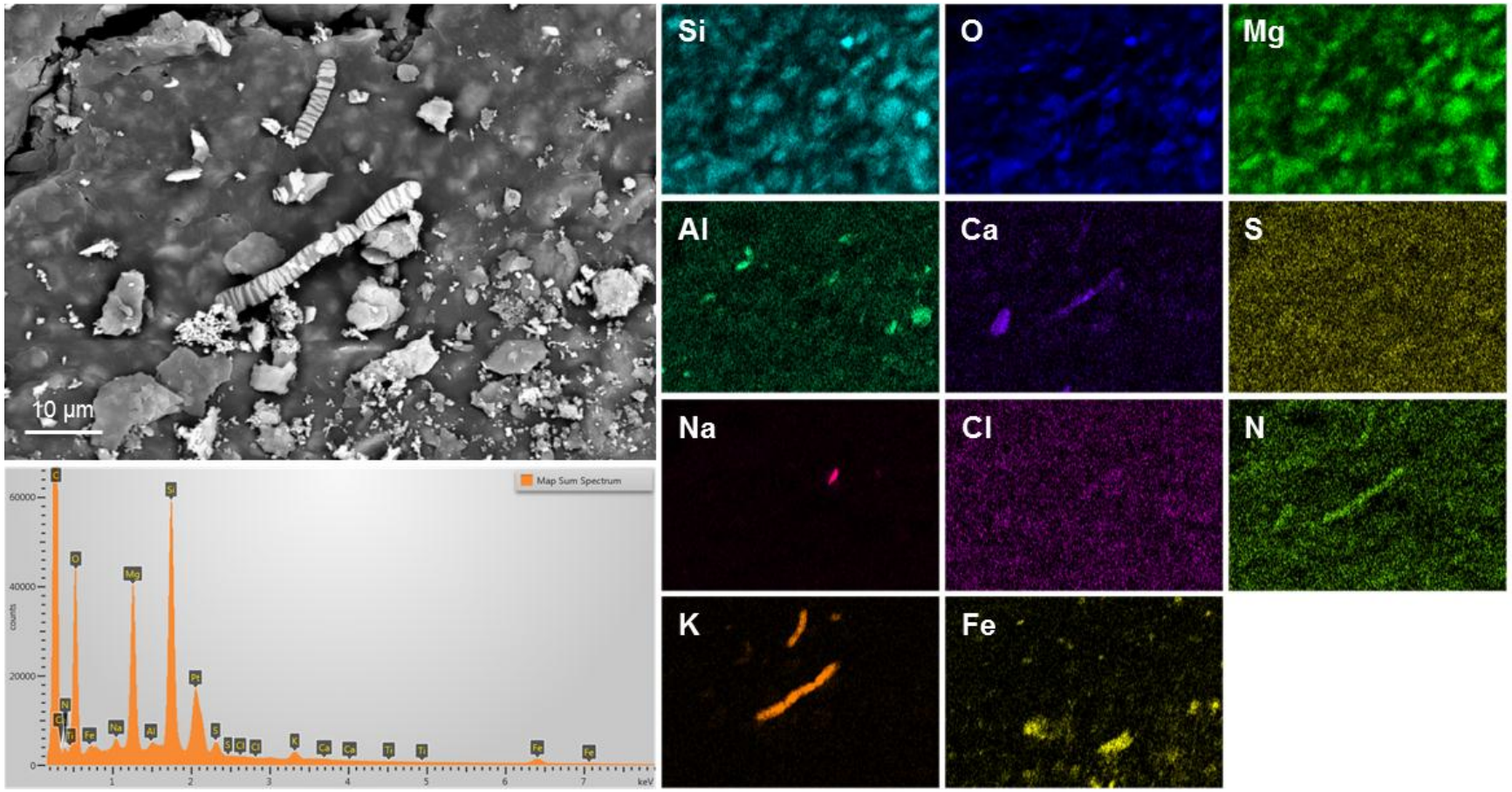

Sample: 170-005
Map B

Notes: Close-up of sea-salt aggregate consisting of NaCl cubes with Mg-SO_4 and minor Ca and K.

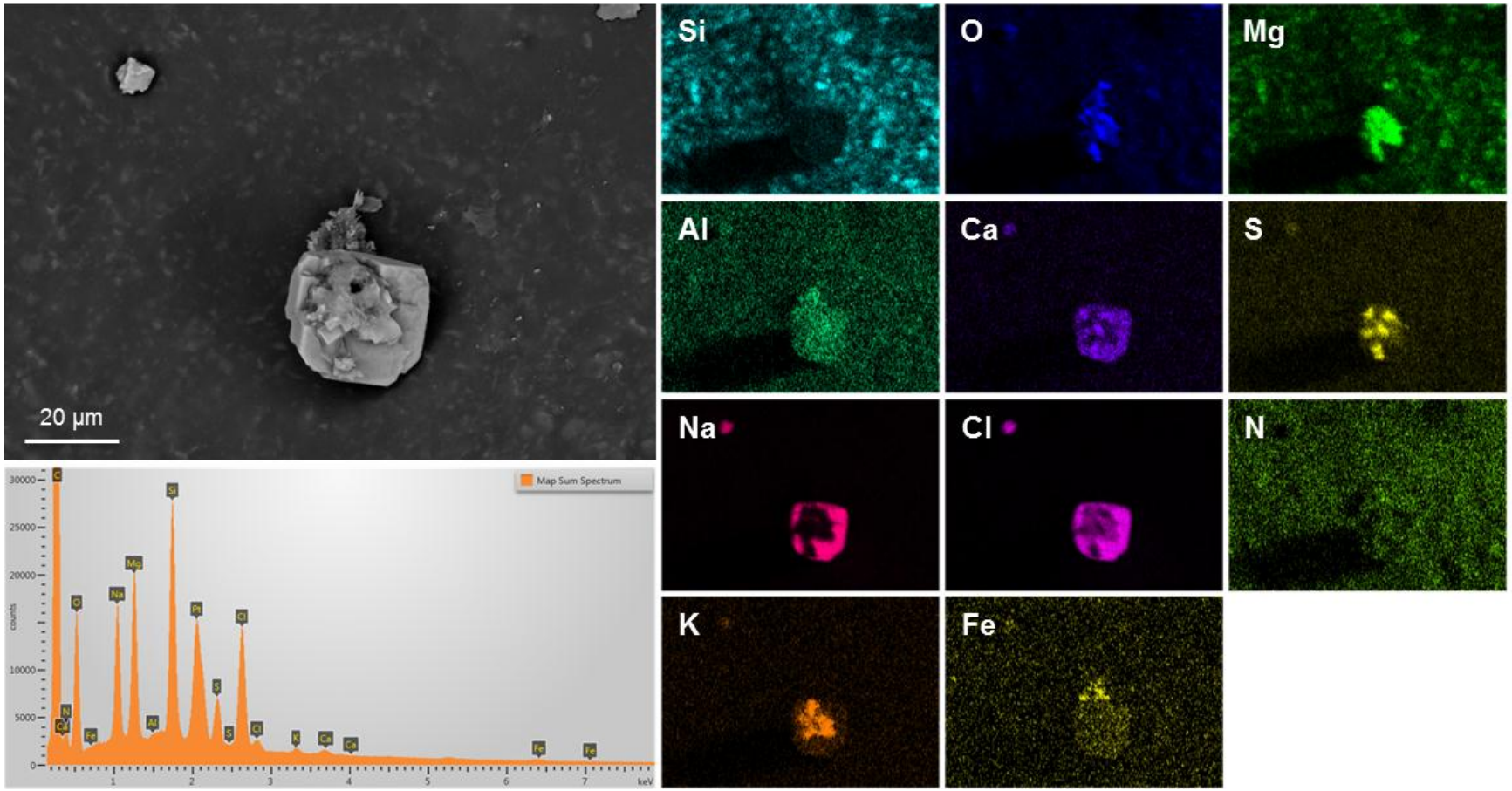

Sample: 170-005
Map C

Notes: Close-up of sea-salt aggregate consisting of a NaCl cube with sheaf-like Mg-SO_4 and minor Ca and K.

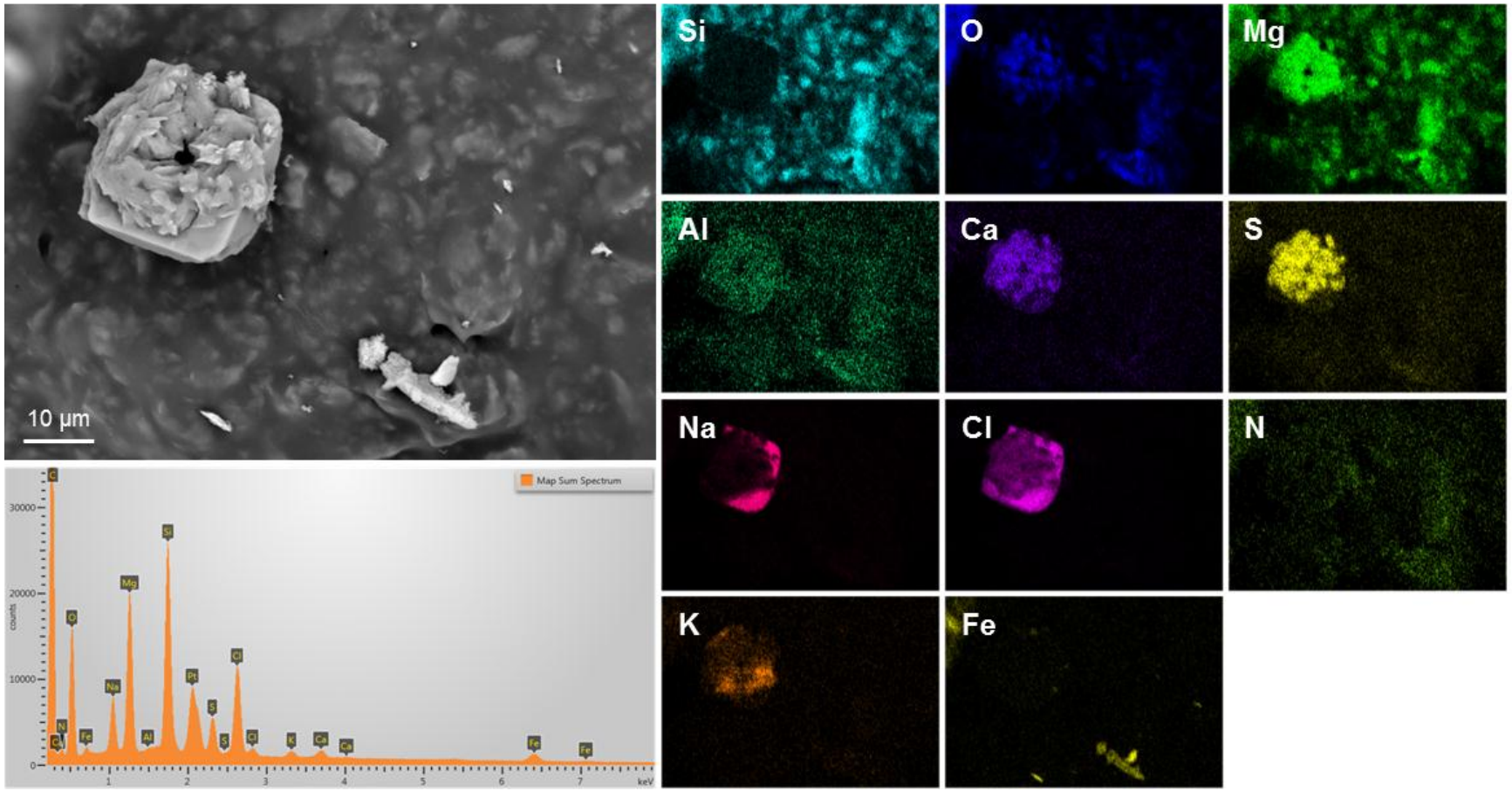

Sample: 170-005
Map D

Notes: Dust on an abraded edge, consisting dominantly of aluminosilicates and two large sea-salt aggregates.

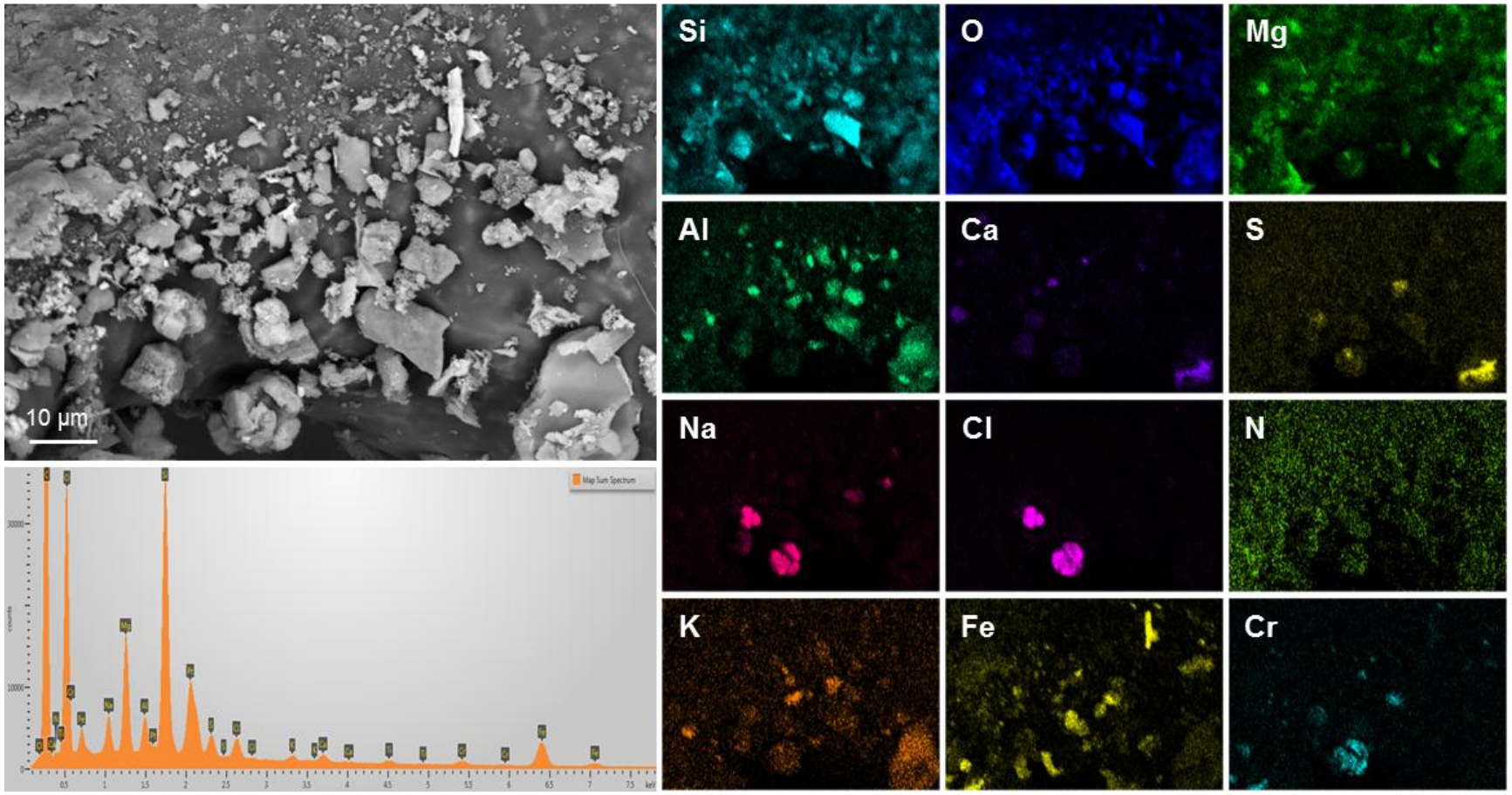

Sample: 170-006

Notes: Overview image of pad sample 170-006, showing the very light dust load.

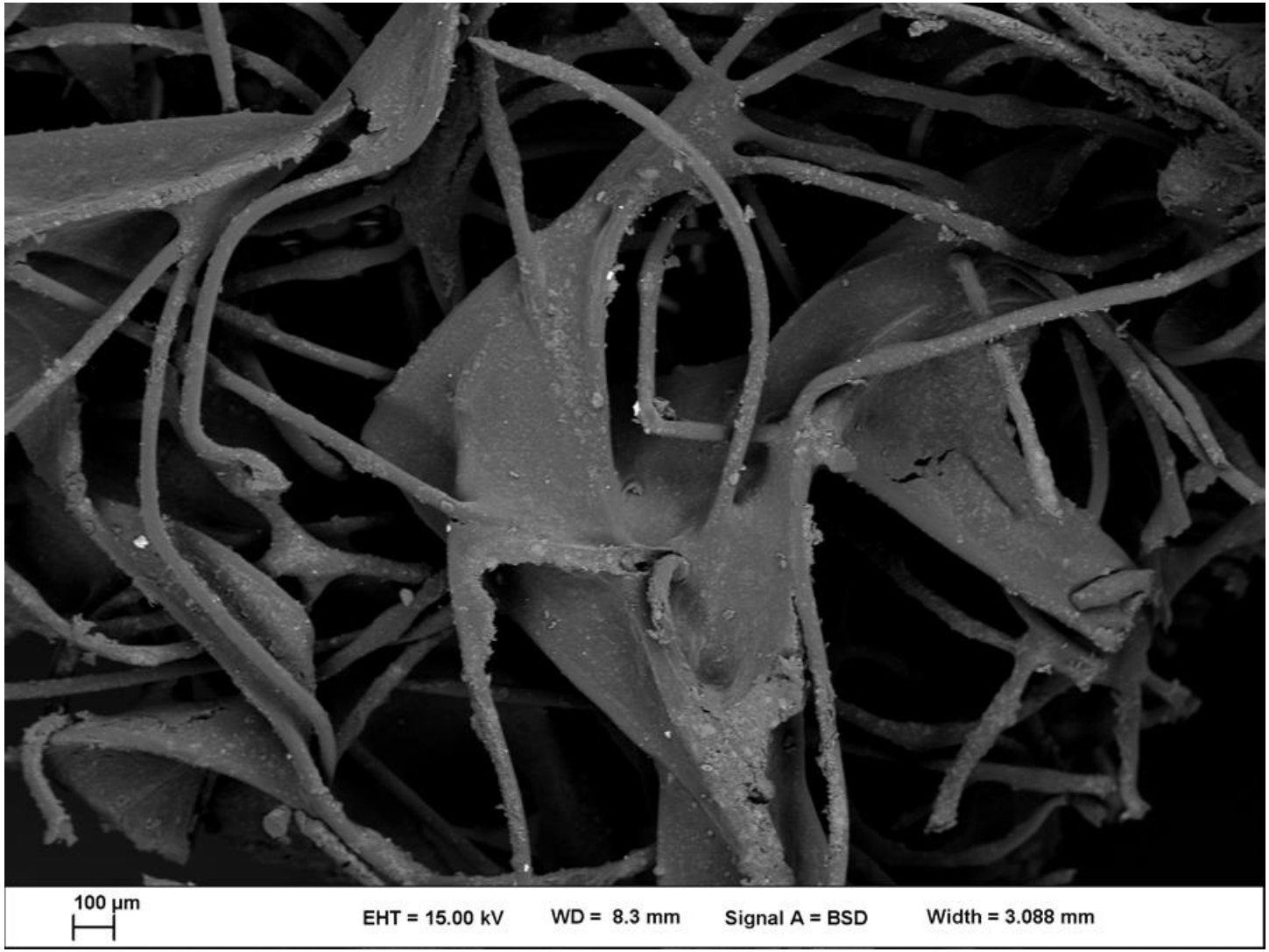

Sample: 170-006
Map A

Notes: Most particles are talc, liberated by abrasion of the pad. Sparse dust is dominantly stainless steel particles. A few grains of NaCl are present.

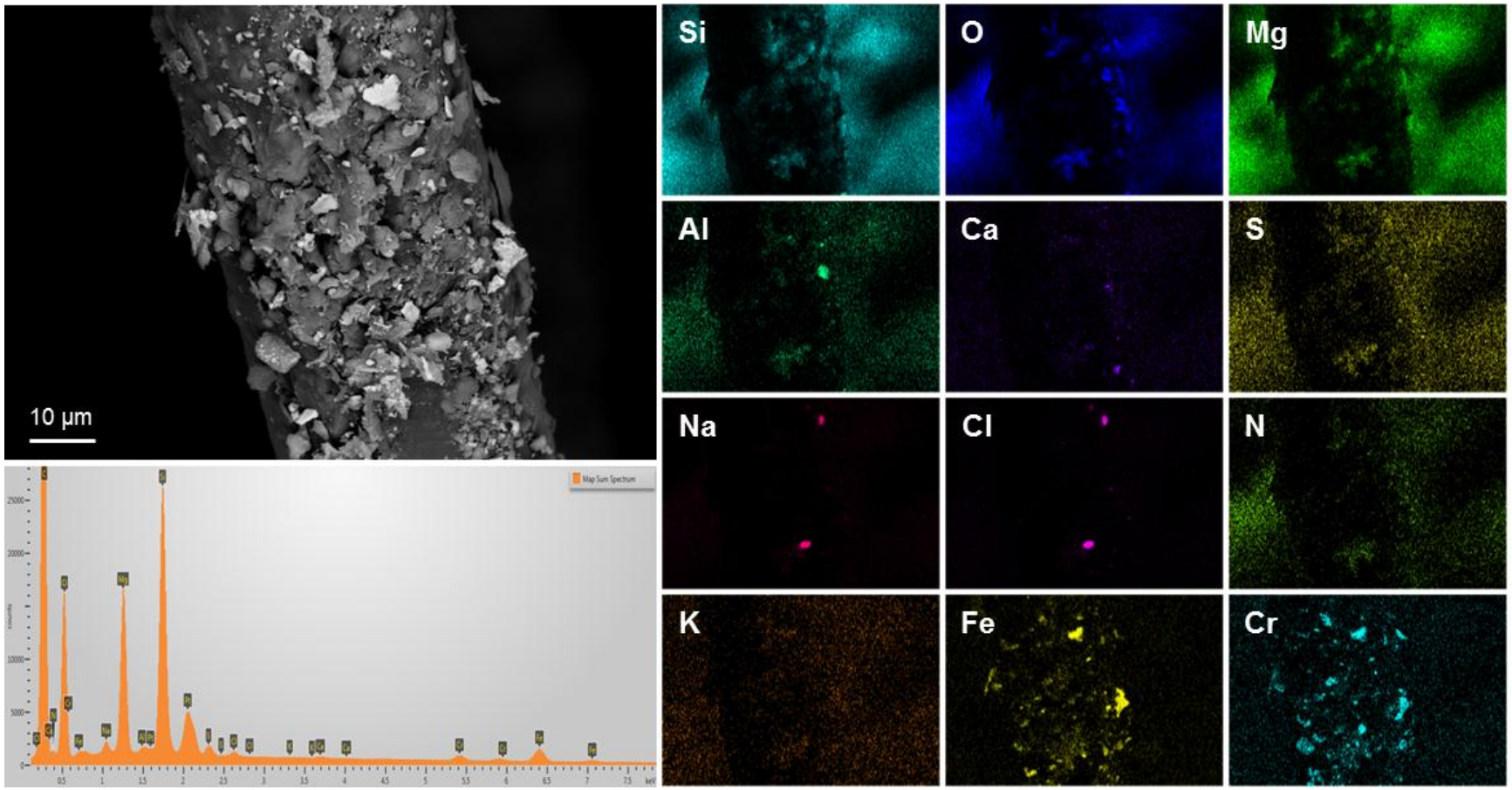

APPENDIX B: XRF DATA

XRF data for the Hope Creek and Diablo Canyon dust samples are discussed in Section 3.0, and a subset of the results is presented. This appendix contains the complete suite of analyses collected for these samples, allowing the reader to better evaluate the representativeness of the results provided in Section 3.0.

Sample: Pad Blank

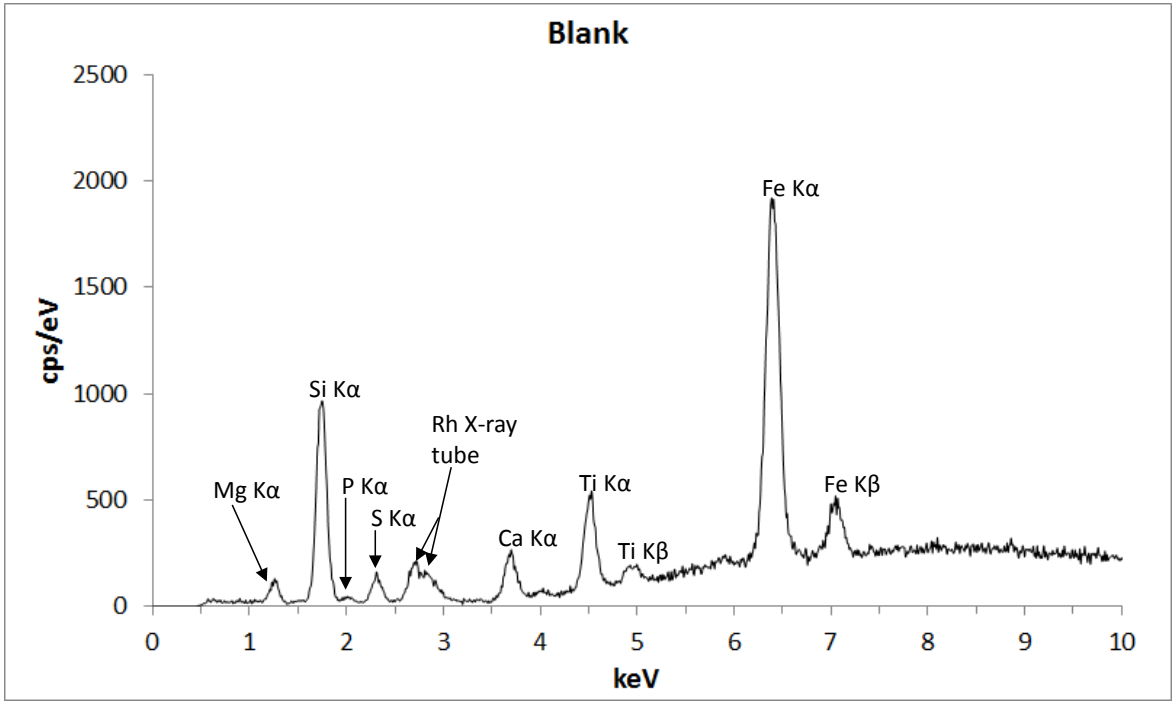

Below is the elemental map for Fe

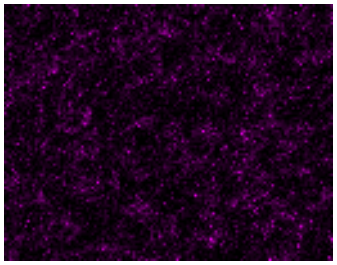

Vision Quant Results: **Blank**				
Total Area Spc from ROI Map		12:53 PM		10-Feb-14
Elem:	Net	Wt%	At%	I-Error%
MgK	1.57	29.42	35.12	3.79
AlK	0.2	1.2	1.29	18.91
SiK	15.88	47	48.58	1.02
P K	0.45	1.77	1.66	10.07
S K	2.06	4.06	3.68	3.32
K K	0.18	0.22	0.17	25.03
CaK	4.25	3.5	2.54	2.25
TiK	8.81	3.67	2.23	1.62
CrK	0.27	0.08	0.04	43.76
MnK	1.12	0.28	0.15	12.39
FeK	38.9	8.46	4.4	0.73
NiK	0.53	0.11	0.06	30.79
ZnK	0.81	0.17	0.07	21.53
ZrK	0.23	0.05	0.02	36.82

Sample: Hope Creek 144-001

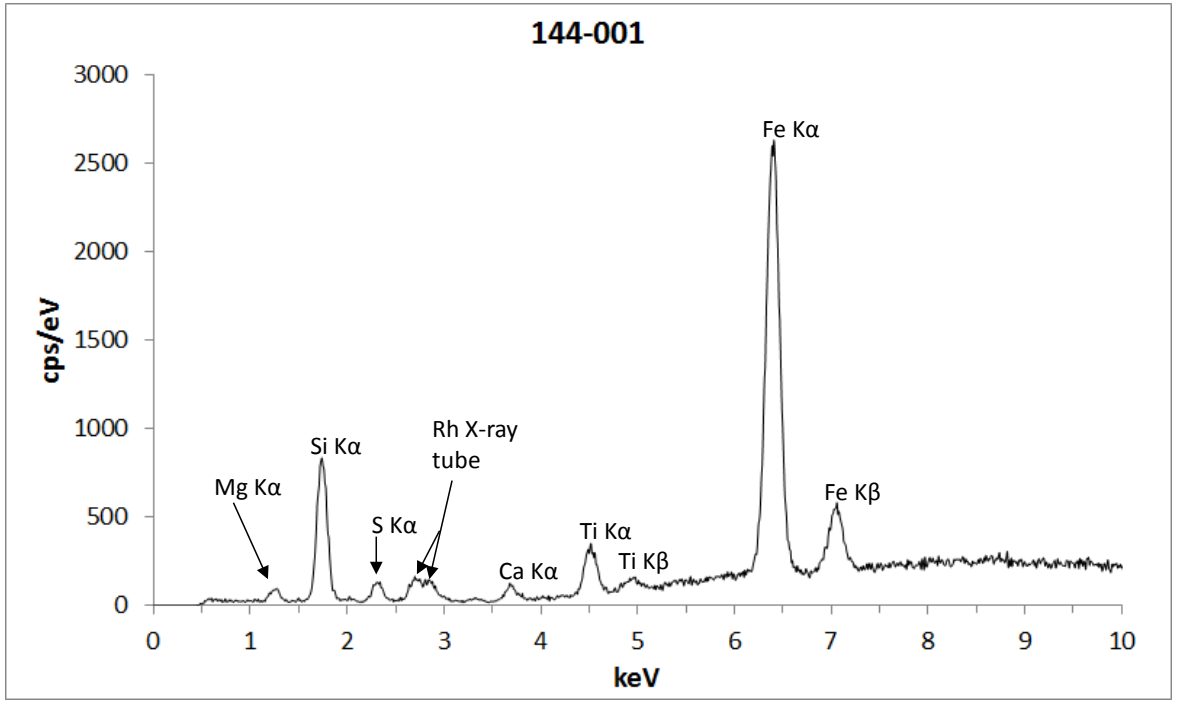

This shows higher concentrations of Fe compared to **Blank** (right-side table).

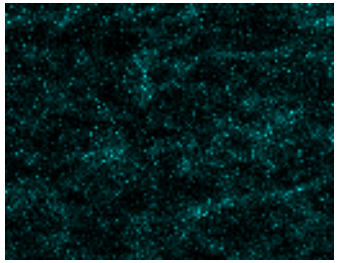

Vision Quant Results: 144-001				
Total Area Spc from ROI Map		5:04 PM		10-Feb-14
Elem:	Net	Wt%	At%	I-Error%
MgK	1.14	26.55	32.66	5.12
AlK	0.12	0.86	0.95	34
SiK	13.39	44.67	47.58	1.12
P K	0.34	1.48	1.43	13.53
S K	1.96	4.26	3.97	3.48
ClK	1.35	2.9	2.45	4.57
K K	0.36	0.52	0.4	13.14
CaK	1.59	1.5	1.12	4.34
TiK	5.63	2.57	1.6	2.11
CrK	0.58	0.18	0.1	18.58
MnK	0.64	0.18	0.1	19.26
FeK	55.67	13.83	7.41	0.58
NiK	0.39	0.11	0.05	38.51
ZnK	1.27	0.34	0.15	13.35
ZrK	0.27	0.08	0.03	36.12

Vision Quant Results: **Blank**				
Total Area Spc from ROI Map		12:53 PM		10-Feb-14
Elem:	Net	Wt%	At%	I-Error%
MgK	1.57	29.42	35.12	3.79
AlK	0.2	1.2	1.29	18.91
SiK	15.88	47	48.58	1.02
P K	0.45	1.77	1.66	10.07
S K	2.06	4.06	3.68	3.32
K K	0.18	0.22	0.17	25.03
CaK	4.25	3.5	2.54	2.25
TiK	8.81	3.67	2.23	1.62
CrK	0.27	0.08	0.04	43.76
MnK	1.12	0.28	0.15	12.39
FeK	38.9	8.46	4.4	0.73
NiK	0.53	0.11	0.06	30.79
ZnK	0.81	0.17	0.07	21.53
ZrK	0.23	0.05	0.02	36.82

Sample: Hope Creek 144-001 with Blank subtracted

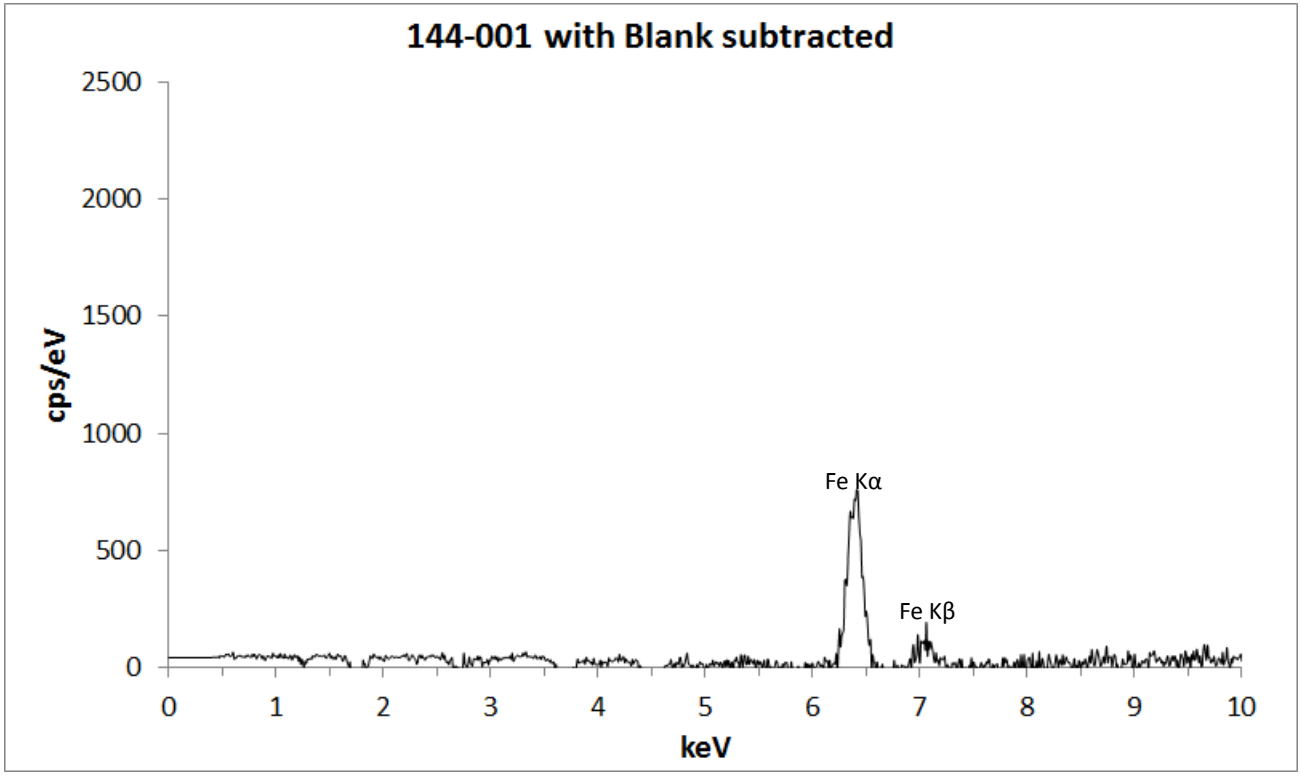

Sample: Hope Creek 144-002

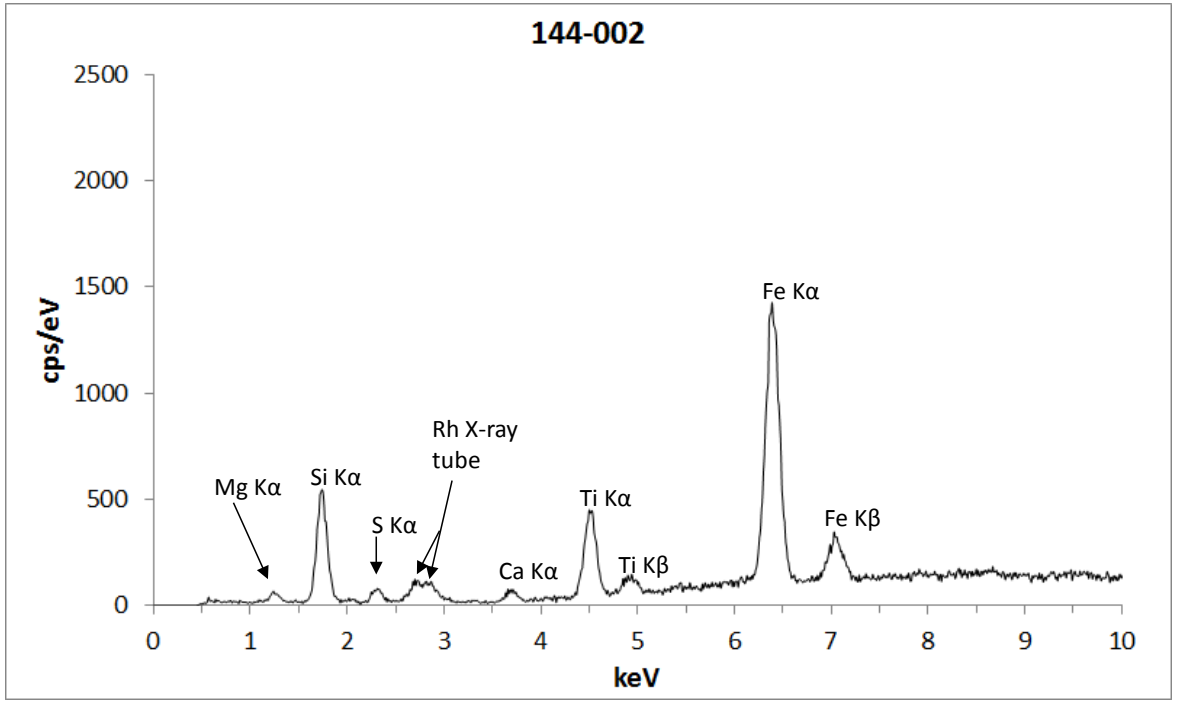

This shows higher concentrations of Fe compared to **Blank** (right-side table).

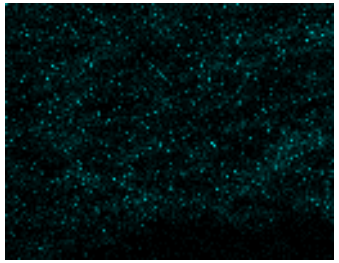

Vision Quant Results: 144-002				
Total Area Spc from ROI Map		1:05 PM		11-Feb-14
Elem:	Net	Wt%	At%	I-Error%
MgK	0.73	26.18	32.39	6.35
AlK	0.08	0.87	0.97	41.13
SiK	8.59	43.74	46.84	1.4
P K	0.26	1.76	1.7	14.48
S K	1.14	3.77	3.54	4.71
ClK	0.95	3.1	2.63	5.43
K K	0.14	0.3	0.23	27.27
CaK	1.01	1.45	1.09	5.58
TiK	8.22	5.84	3.66	1.55
CrK	0.4	0.21	0.12	21.39
MnK	0.4	0.18	0.1	24.16
FeK	29.79	11.94	6.43	0.8
NiK	0.27	0.12	0.06	42.89
ZnK	1.02	0.42	0.19	12.73
ZrK	0.3	0.14	0.04	24.06

Vision Quant Results: **Blank**				
Total Area Spc from ROI Map		12:53 PM		10-Feb-14
Elem:	Net	Wt%	At%	I-Error%
MgK	1.57	29.42	35.12	3.79
AlK	0.2	1.2	1.29	18.91
SiK	15.88	47	48.58	1.02
P K	0.45	1.77	1.66	10.07
S K	2.06	4.06	3.68	3.32
K K	0.18	0.22	0.17	25.03
CaK	4.25	3.5	2.54	2.25
TiK	8.81	3.67	2.23	1.62
CrK	0.27	0.08	0.04	43.76
MnK	1.12	0.28	0.15	12.39
FeK	38.9	8.46	4.4	0.73
NiK	0.53	0.11	0.06	30.79
ZnK	0.81	0.17	0.07	21.53
ZrK	0.23	0.05	0.02	36.82

Sample: Hope Creek 144-002 with Blank subtracted

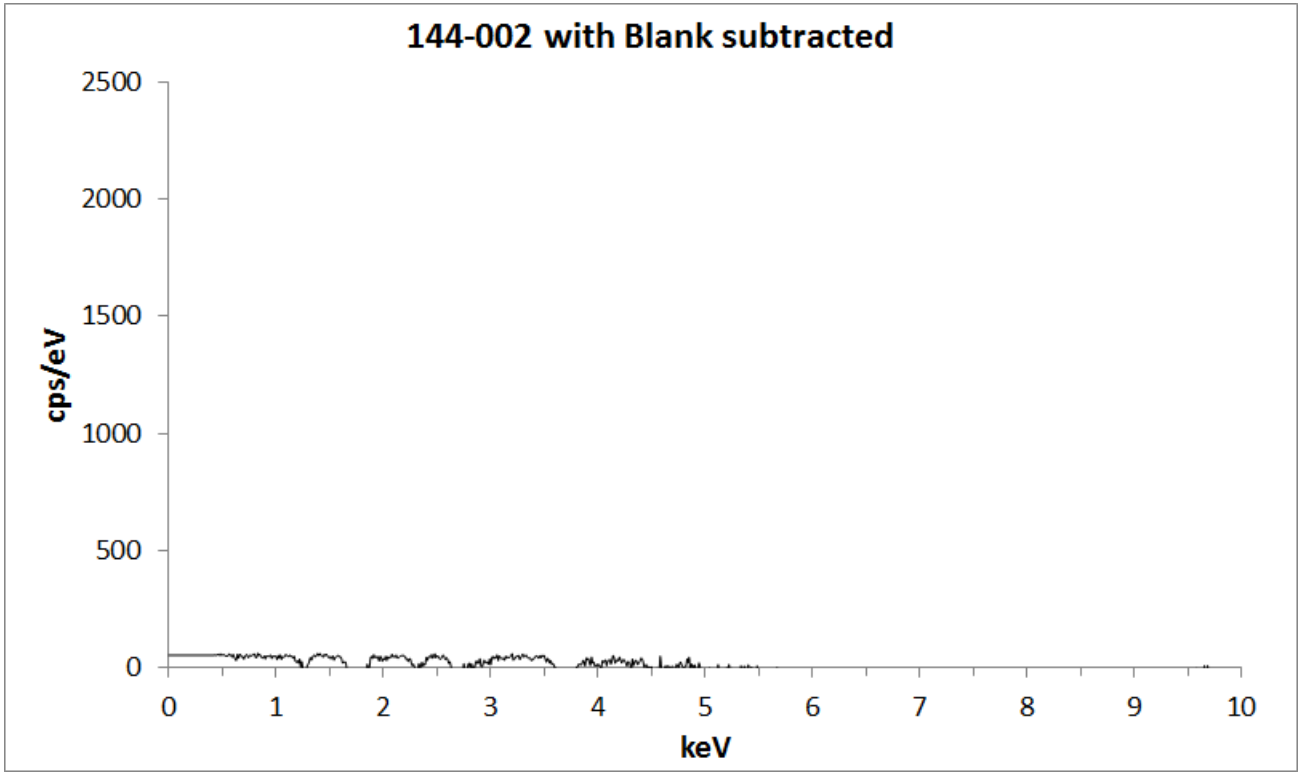

Sample: Hope Creek 144-005

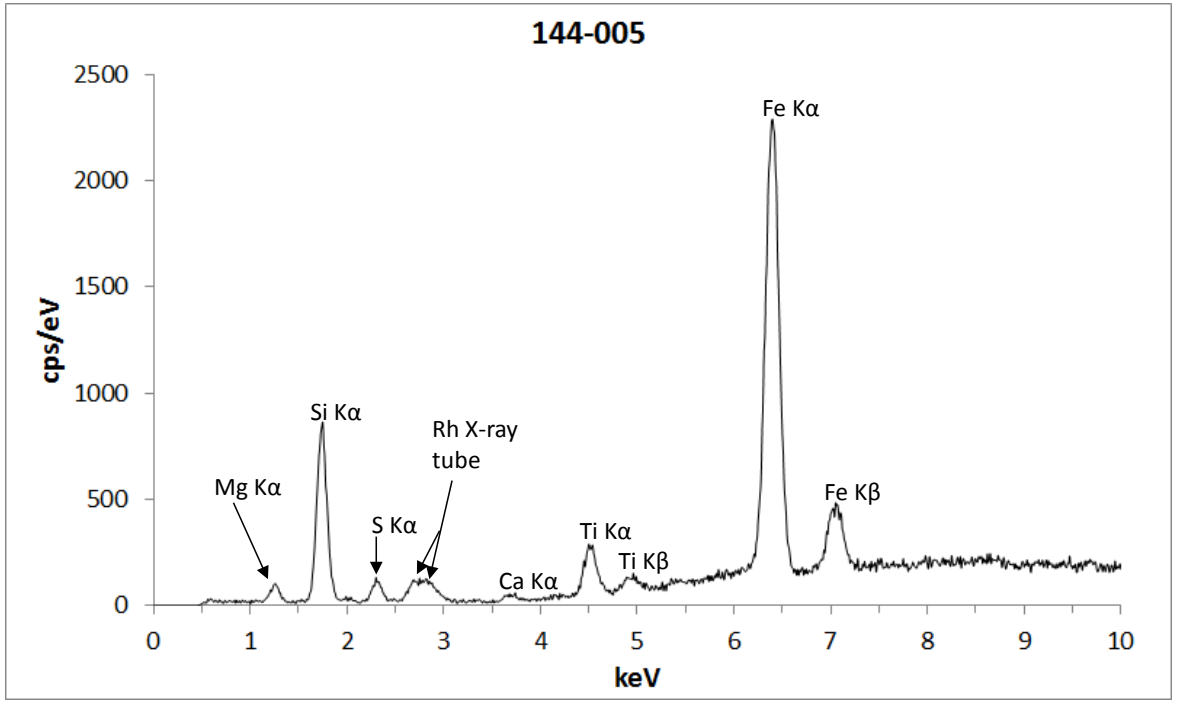

This shows higher concentrations of Fe compared to **Blank** (right-side table).

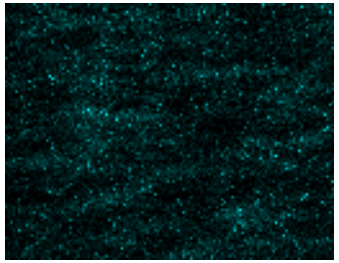

Vision Quant Results: 144-005				
Total Area Spc from ROI Map		2:04 PM		11-Feb-14
Elem:	Net	Wt%	At%	I-Error%
MgK	1.27	29	34.98	4.35
AlK	0.1	0.72	0.79	34.75
SiK	13.4	46.39	48.44	1.11
P K	0.32	1.46	1.39	12.82
S K	1.71	3.9	3.57	3.66
ClK	1.14	2.57	2.13	4.88
K K	0.17	0.25	0.19	23.98
CaK	0.62	0.6	0.44	8.46
TiK	4.8	2.2	1.35	2.26
CrK	0.54	0.17	0.09	18.27
MnK	0.64	0.17	0.09	17.98
FeK	49.14	12	6.3	0.61
NiK	0.56	0.15	0.07	24.74
ZnK	1.26	0.32	0.14	12.11
ZrK	0.3	0.08	0.03	26.5

Vision Quant Results: **Blank**				
Total Area Spc from ROI Map		12:53 PM		10-Feb-14
Elem:	Net	Wt%	At%	I-Error%
MgK	1.57	29.42	35.12	3.79
AlK	0.2	1.2	1.29	18.91
SiK	15.88	47	48.58	1.02
P K	0.45	1.77	1.66	10.07
S K	2.06	4.06	3.68	3.32
K K	0.18	0.22	0.17	25.03
CaK	4.25	3.5	2.54	2.25
TiK	8.81	3.67	2.23	1.62
CrK	0.27	0.08	0.04	43.76
MnK	1.12	0.28	0.15	12.39
FeK	38.9	8.46	4.4	0.73
NiK	0.53	0.11	0.06	30.79
ZnK	0.81	0.17	0.07	21.53
ZrK	0.23	0.05	0.02	36.82

Sample: Hope Creek 144-005 with Blank subtracted

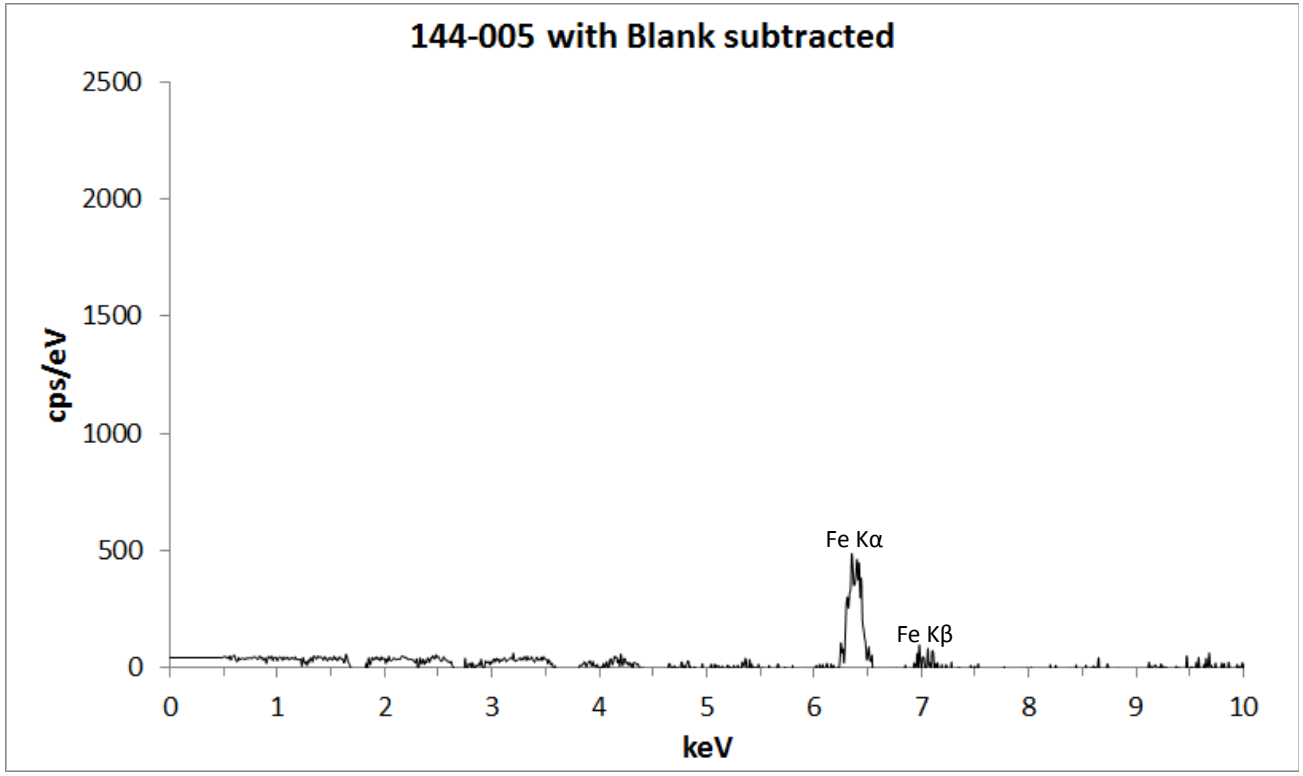

Sample: Hope Creek 144-006

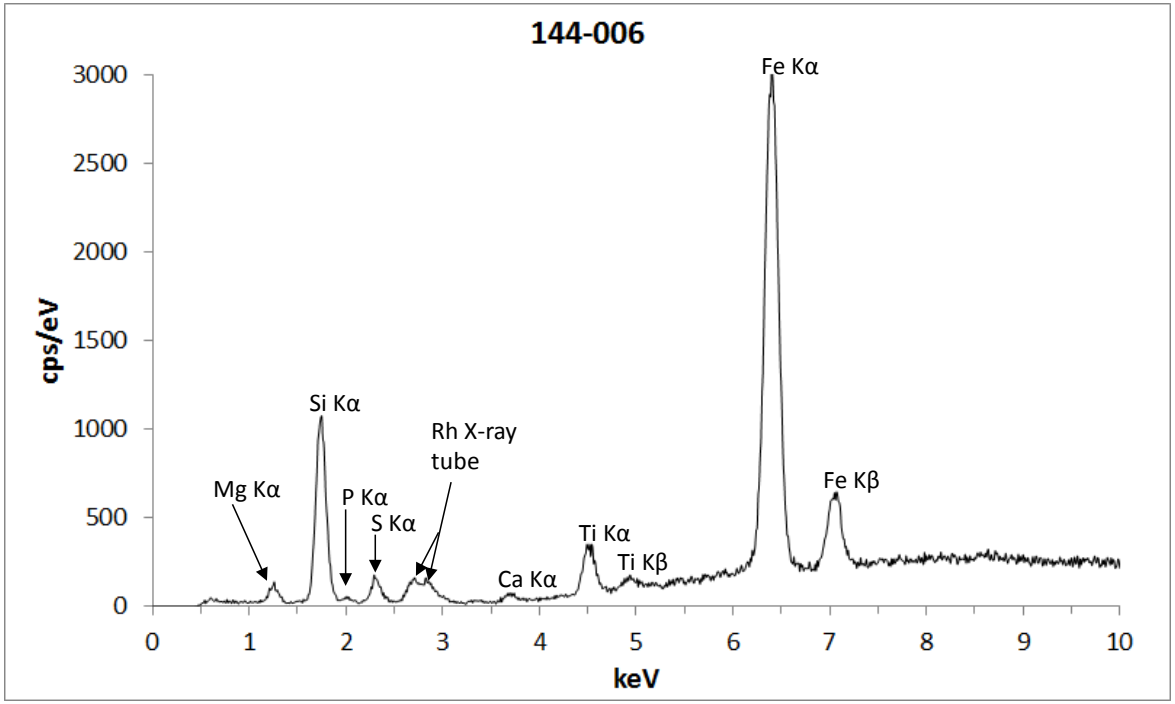

This shows higher concentrations of Fe compared to **Blank** (right-side table).

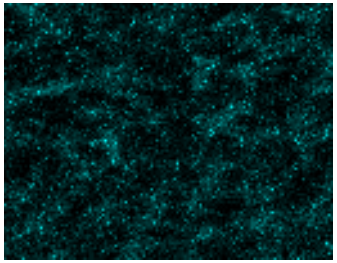

Vision Quant Results: 144-006				
Total Area Spc from ROI Map		6:00 PM		10-Feb-14
Elem:	Net	Wt%	At%	I-Error%
MgK	1.54	27.72	33.65	3.94
AlK	0.17	0.96	1.05	22.61
SiK	17.13	46.06	48.41	0.98
P K	0.51	1.81	1.72	9.33
S K	2.29	4.08	3.76	3.09
ClK	1.56	2.74	2.28	3.99
K K	0.27	0.32	0.24	15.93
CaK	0.85	0.65	0.48	6.93
TiK	5.83	2.1	1.29	2.07
CrK	0.73	0.18	0.1	14.99
MnK	0.98	0.21	0.11	12.91
FeK	65.04	12.52	6.62	0.53
NiK	0.82	0.17	0.09	19.35
ZnK	1.78	0.36	0.16	9.87
ZrK	0.57	0.13	0.04	16.85

Vision Quant Results: **Blank**				
Total Area Spc from ROI Map		12:53 PM		10-Feb-14
Elem:	Net	Wt%	At%	I-Error%
MgK	1.57	29.42	35.12	3.79
AlK	0.2	1.2	1.29	18.91
SiK	15.88	47	48.58	1.02
P K	0.45	1.77	1.66	10.07
S K	2.06	4.06	3.68	3.32
K K	0.18	0.22	0.17	25.03
CaK	4.25	3.5	2.54	2.25
TiK	8.81	3.67	2.23	1.62
CrK	0.27	0.08	0.04	43.76
MnK	1.12	0.28	0.15	12.39
FeK	38.9	8.46	4.4	0.73
NiK	0.53	0.11	0.06	30.79
ZnK	0.81	0.17	0.07	21.53
ZrK	0.23	0.05	0.02	36.82

Sample: Hope Creek 144-006 with Blank subtracted

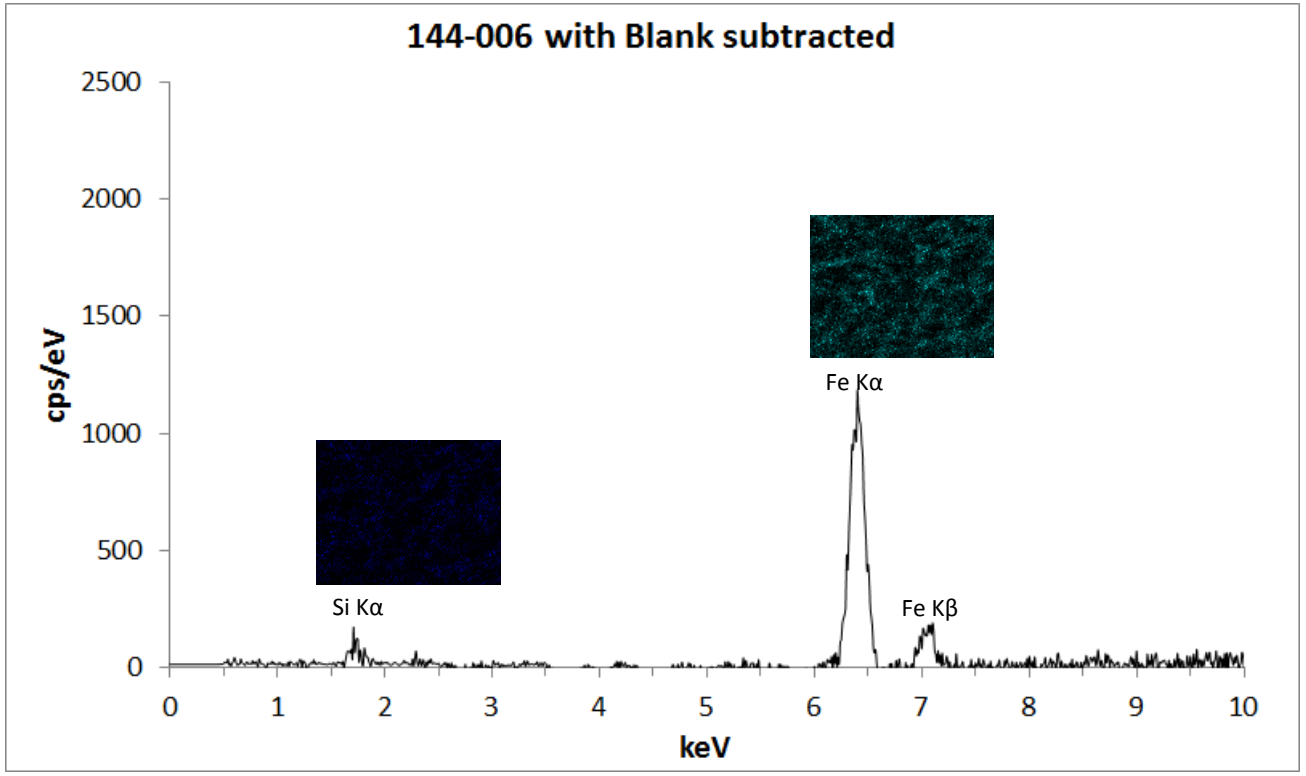

Sample: Hope Creek 144-007

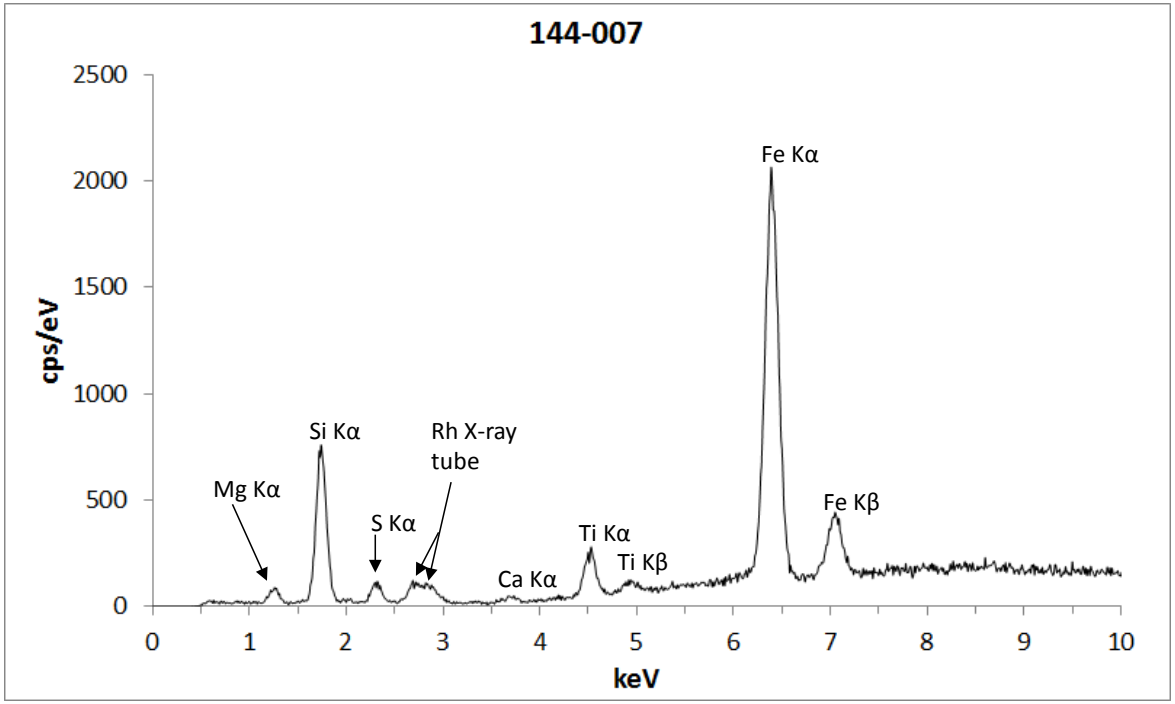

This shows higher concentrations of Fe compared to **Blank** (right-side table).

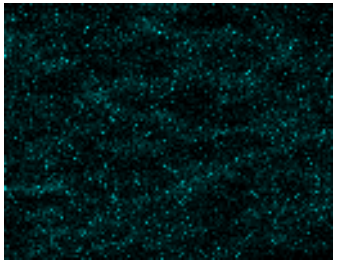

Vision Quant Results: 144-007				
Total Area Spc from ROI Map		3:02 PM		11-Feb-14
Elem:	Net	Wt%	At%	I-Error%
MgK	1.09	28.33	34.17	4.8
AlK	0.12	1	1.08	29.01
SiK	11.9	46.95	49.01	1.18
P K	0.24	1.27	1.2	17.11
S K	1.59	4.18	3.82	3.88
ClK	1.02	2.65	2.19	5.27
K K	0.14	0.24	0.18	26.53
CaK	0.55	0.61	0.45	8.96
TiK	4.2	2.22	1.36	2.45
CrK	0.25	0.09	0.05	36.34
MnK	0.33	0.1	0.05	32.25
FeK	42.29	11.84	6.22	0.66
NiK	0.31	0.09	0.05	41.02
ZnK	1.01	0.29	0.13	14.22
ZrK	0.4	0.13	0.04	19.74

Vision Quant Results: **Blank**				
Total Area Spc from ROI Map		12:53 PM		10-Feb-14
Elem:	Net	Wt%	At%	I-Error%
MgK	1.57	29.42	35.12	3.79
AlK	0.2	1.2	1.29	18.91
SiK	15.88	47	48.58	1.02
P K	0.45	1.77	1.66	10.07
S K	2.06	4.06	3.68	3.32
K K	0.18	0.22	0.17	25.03
CaK	4.25	3.5	2.54	2.25
TiK	8.81	3.67	2.23	1.62
CrK	0.27	0.08	0.04	43.76
MnK	1.12	0.28	0.15	12.39
FeK	38.9	8.46	4.4	0.73
NiK	0.53	0.11	0.06	30.79
ZnK	0.81	0.17	0.07	21.53
ZrK	0.23	0.05	0.02	36.82

Sample: Hope Creek 144-007 with Blank subtracted

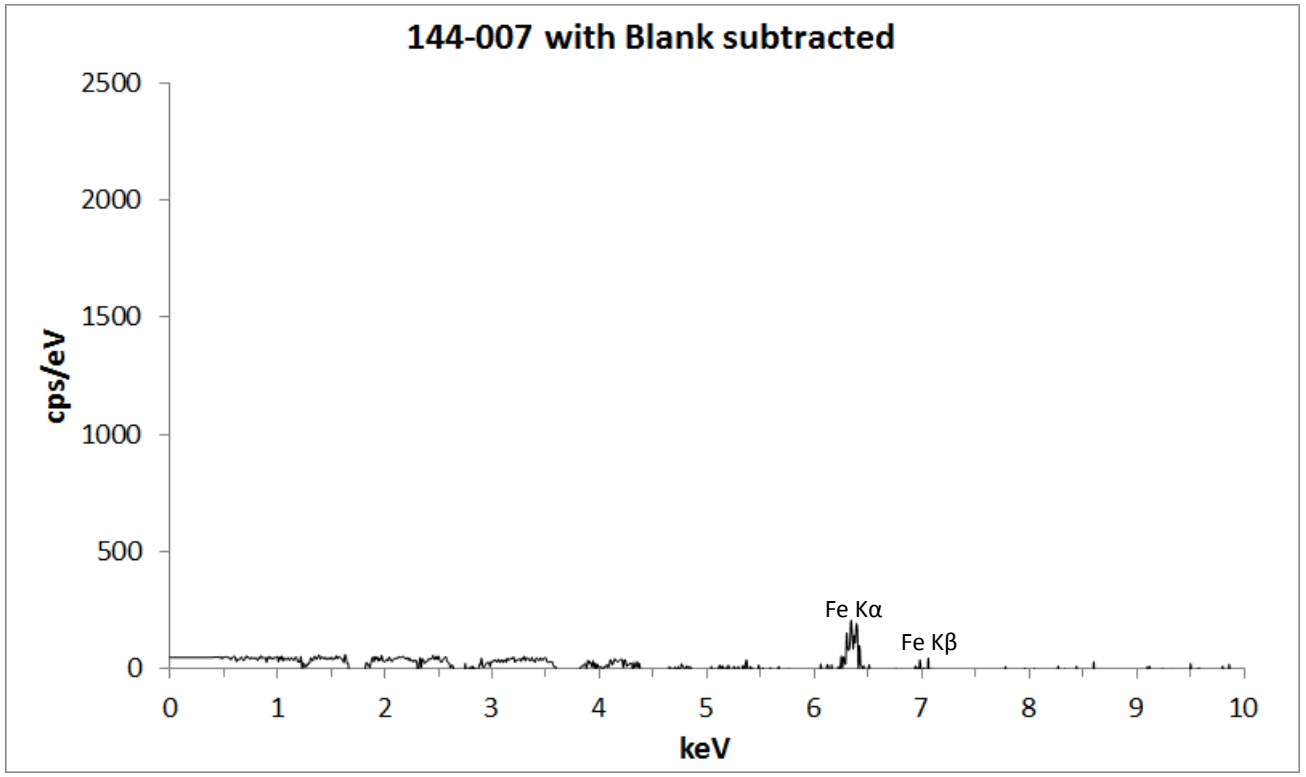

Sample: Hope Creek 144-011

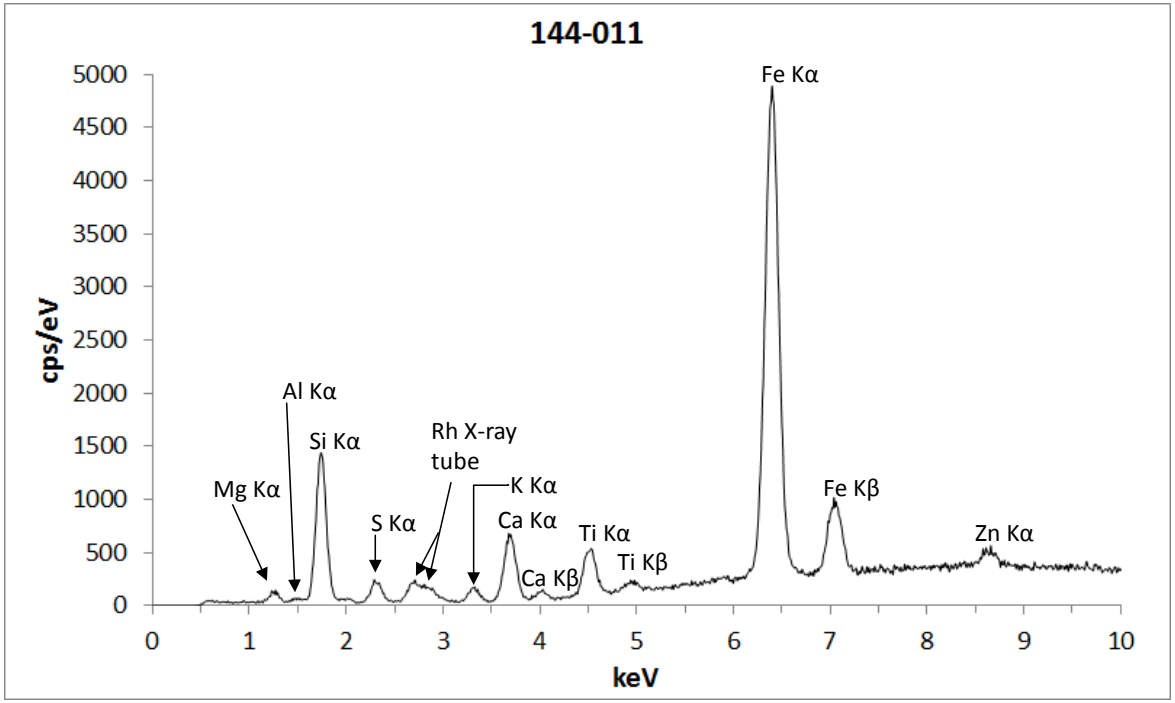

This shows higher concentrations of Fe compared to **Blank** (right-side table).

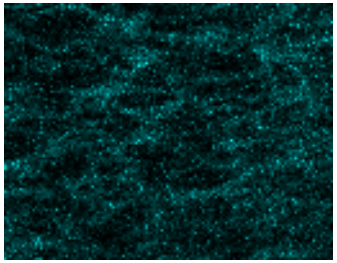

Vision Quant Results: 144-011				
Total Area Spc from ROI Map		9:48 AM		11-Feb-14
Elem:	Net	Wt%	At%	I-Error%
MgK	1.6	21.5	27.41	4.15
AlK	0.71	2.53	2.91	7.77
SiK	23.15	40.97	45.22	0.84
P K	0.72	1.63	1.63	7.69
S K	3.56	3.99	3.86	2.45
ClK	2.16	2.39	2.09	3.48
K K	2.39	1.79	1.42	3.39
CaK	11.97	6.09	4.71	1.25
TiK	9.37	2.51	1.62	1.6
CrK	0.51	0.09	0.06	24.93
MnK	1.34	0.22	0.12	11.19
FeK	104.41	15.21	8.44	0.41
NiK	1.04	0.17	0.09	17.9
ZnK	5.1	0.8	0.38	4.27
ZrK	0.55	0.1	0.03	21.14

Vision Quant Results: **Blank**				
Total Area Spc from ROI Map		12:53 PM		10-Feb-14
Elem:	Net	Wt%	At%	I-Error%
MgK	1.57	29.42	35.12	3.79
AlK	0.2	1.2	1.29	18.91
SiK	15.88	47	48.58	1.02
P K	0.45	1.77	1.66	10.07
S K	2.06	4.06	3.68	3.32
K K	0.18	0.22	0.17	25.03
CaK	4.25	3.5	2.54	2.25
TiK	8.81	3.67	2.23	1.62
CrK	0.27	0.08	0.04	43.76
MnK	1.12	0.28	0.15	12.39
FeK	38.9	8.46	4.4	0.73
NiK	0.53	0.11	0.06	30.79
ZnK	0.81	0.17	0.07	21.53
ZrK	0.23	0.05	0.02	36.82

Sample: Hope Creek 144-011 with Blank subtracted

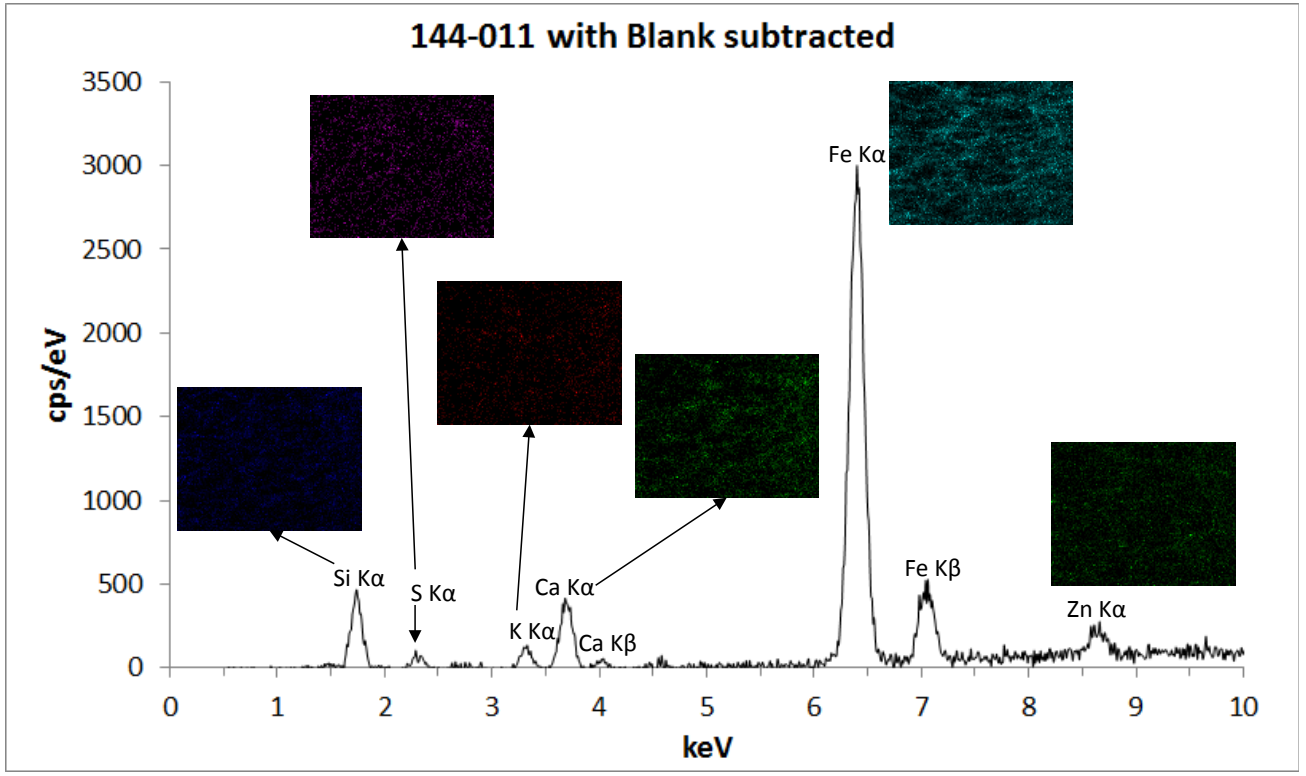

Sample: Hope Creek 144-012

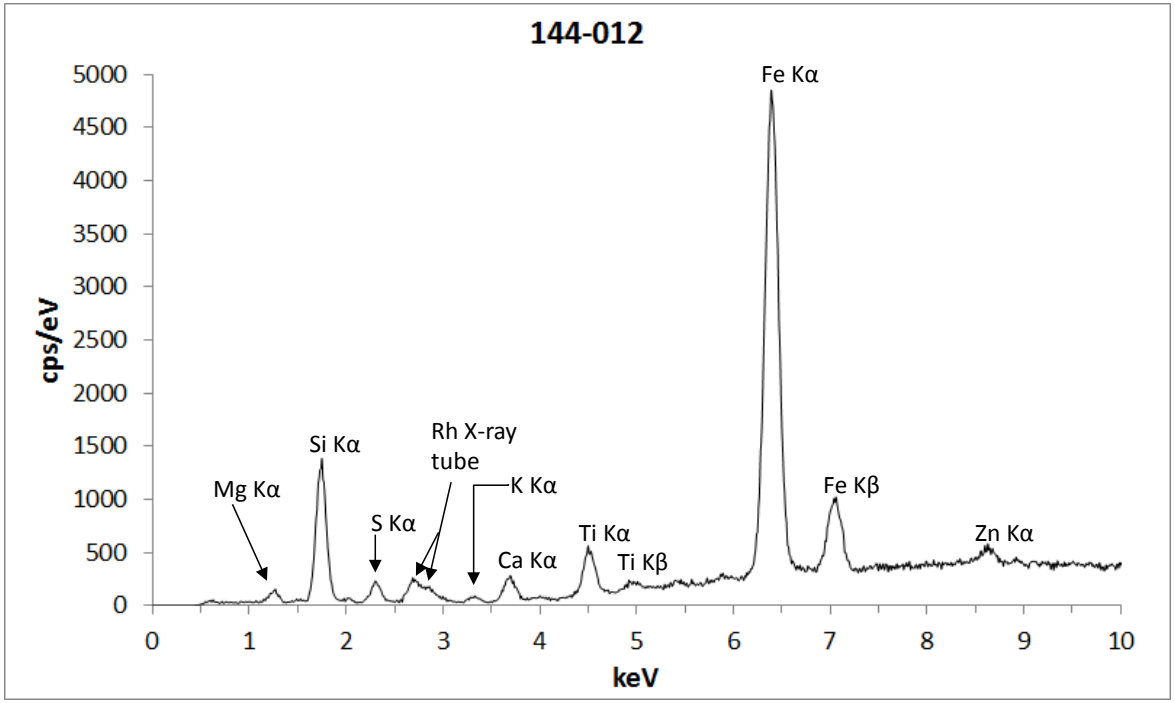

This shows higher concentrations of Fe compared to **Blank** (right-side table).

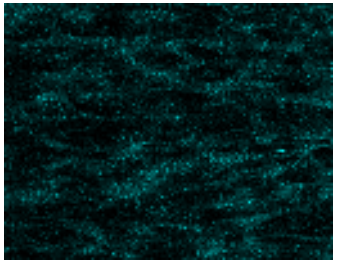

Vision Quant Results: 144-012				
Total Area Spc from ROI Map		11:55 AM		11-Feb-14
Elem:	Net	Wt%	At%	I-Error%
MgK	1.75	24.81	31.09	3.87
AlK	0.47	1.89	2.14	10.78
SiK	21.41	42.03	45.6	0.88
P K	0.65	1.63	1.6	8.49
S K	3.22	4	3.81	2.61
ClK	2.4	2.95	2.53	3.2
K K	1.01	0.84	0.65	6.23
CaK	4.47	2.43	1.85	2.25
TiK	9.04	2.43	1.54	1.61
CrK	1.46	0.27	0.16	9.02
MnK	1.54	0.25	0.14	9.87
FeK	103.43	15.34	8.37	0.42
NiK	1.16	0.19	0.1	16.62
ZnK	4.94	0.81	0.38	4.53
ZrK	0.71	0.13	0.04	17.37

Vision Quant Results: **Blank**				
Total Area Spc from ROI Map		12:53 PM		10-Feb-14
Elem:	Net	Wt%	At%	I-Error%
MgK	1.57	29.42	35.12	3.79
AlK	0.2	1.2	1.29	18.91
SiK	15.88	47	48.58	1.02
P K	0.45	1.77	1.66	10.07
S K	2.06	4.06	3.68	3.32
K K	0.18	0.22	0.17	25.03
CaK	4.25	3.5	2.54	2.25
TiK	8.81	3.67	2.23	1.62
CrK	0.27	0.08	0.04	43.76
MnK	1.12	0.28	0.15	12.39
FeK	38.9	8.46	4.4	0.73
NiK	0.53	0.11	0.06	30.79
ZnK	0.81	0.17	0.07	21.53
ZrK	0.23	0.05	0.02	36.82

Sample: Hope Creek 144-012 with Blank subtracted

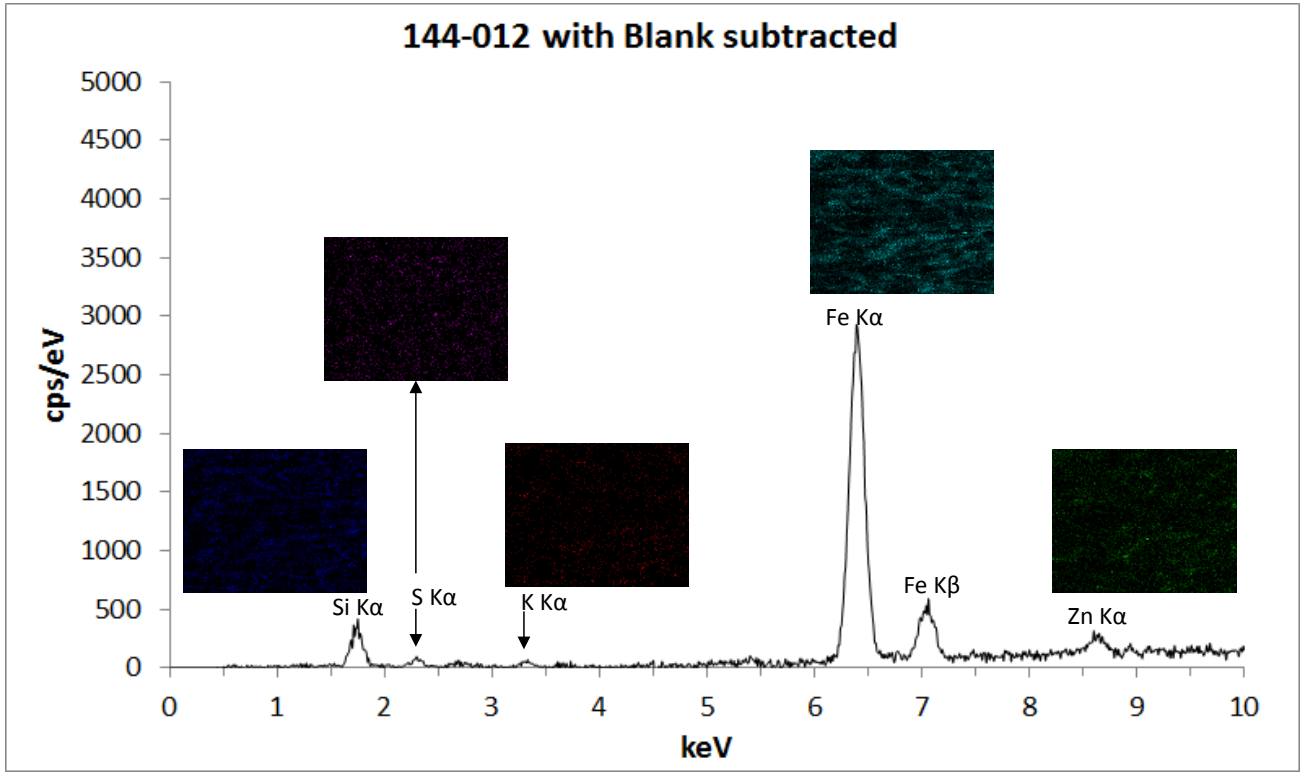

Sample: Hope Creek 145-001

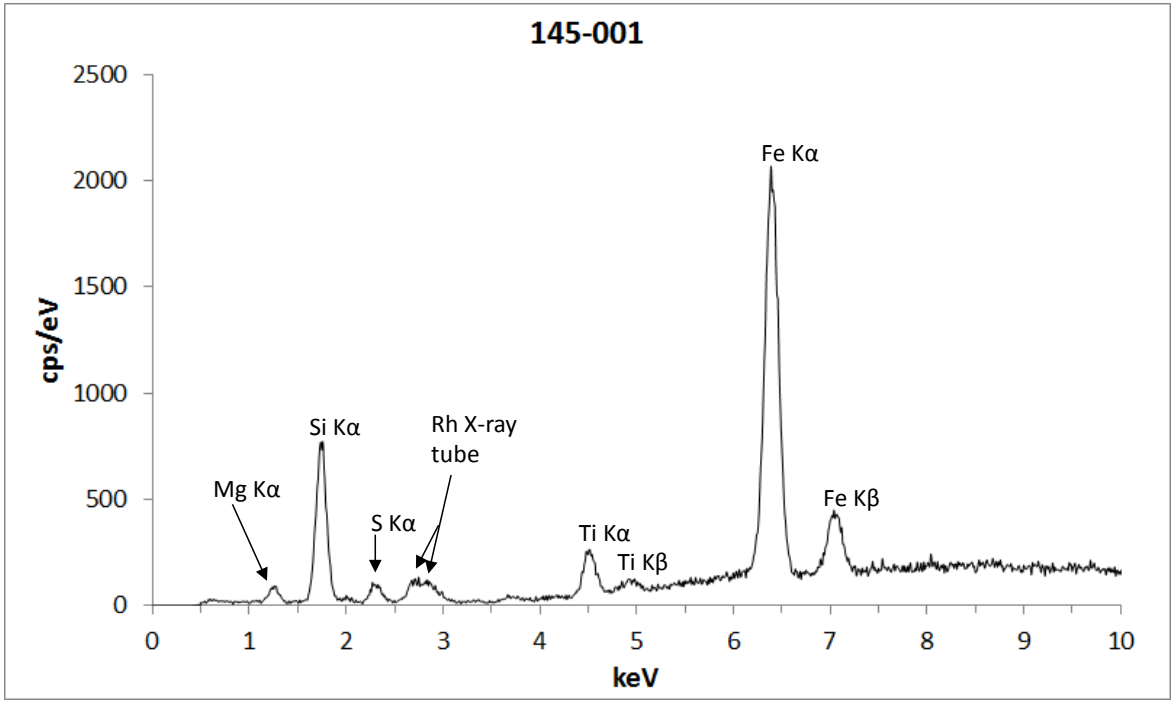

This shows higher concentrations of Fe compared to **Blank** (right-side table).

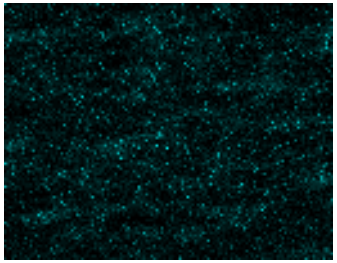

Vision Quant Results: 145-001				
Total Area Spc from ROI Map		4:01 PM		11-Feb-14
Elem:	Net	Wt%	At%	I-Error%
MgK	1.15	28.62	34.47	4.63
AlK	0.09	0.73	0.79	36.62
SiK	12.37	47	48.99	1.16
P K	0.32	1.65	1.56	12.66
S K	1.53	3.87	3.53	3.91
ClK	1.1	2.74	2.26	4.95
K K	0.17	0.28	0.21	22.38
CaK	0.49	0.53	0.39	9.95
TiK	4.35	2.22	1.36	2.39
CrK	0.24	0.08	0.05	39.17
MnK	0.52	0.16	0.08	21.38
FeK	43.2	11.64	6.1	0.66
NiK	0.45	0.13	0.06	29.95
ZnK	0.95	0.26	0.12	15.43
ZrK	0.31	0.09	0.03	25.62

Vision Quant Results: **Blank**				
Total Area Spc from ROI Map		12:53 PM		10-Feb-14
Elem:	Net	Wt%	At%	I-Error%
MgK	1.57	29.42	35.12	3.79
AlK	0.2	1.2	1.29	18.91
SiK	15.88	47	48.58	1.02
P K	0.45	1.77	1.66	10.07
S K	2.06	4.06	3.68	3.32
K K	0.18	0.22	0.17	25.03
CaK	4.25	3.5	2.54	2.25
TiK	8.81	3.67	2.23	1.62
CrK	0.27	0.08	0.04	43.76
MnK	1.12	0.28	0.15	12.39
FeK	38.9	8.46	4.4	0.73
NiK	0.53	0.11	0.06	30.79
ZnK	0.81	0.17	0.07	21.53
ZrK	0.23	0.05	0.02	36.82

Sample: Hope Creek 145-001 with Blank subtracted

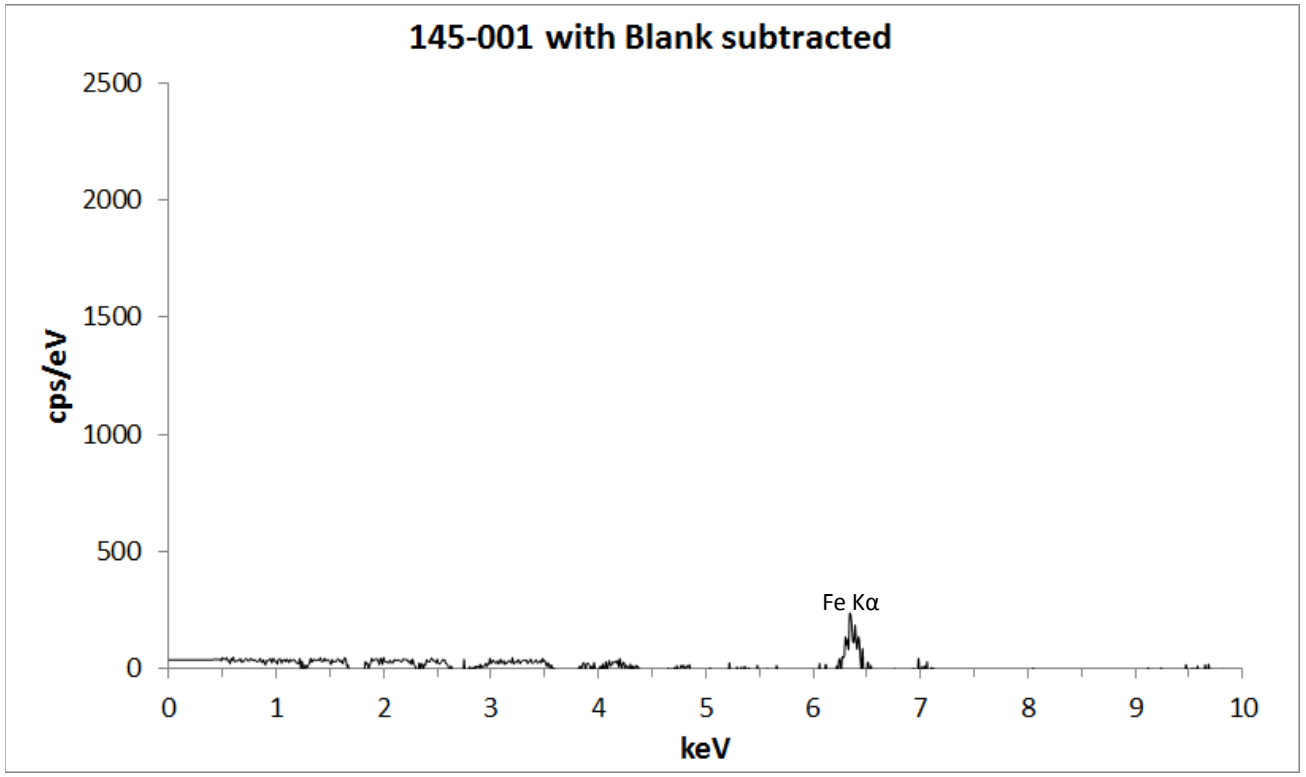

Sample: Hope Creek 145-003

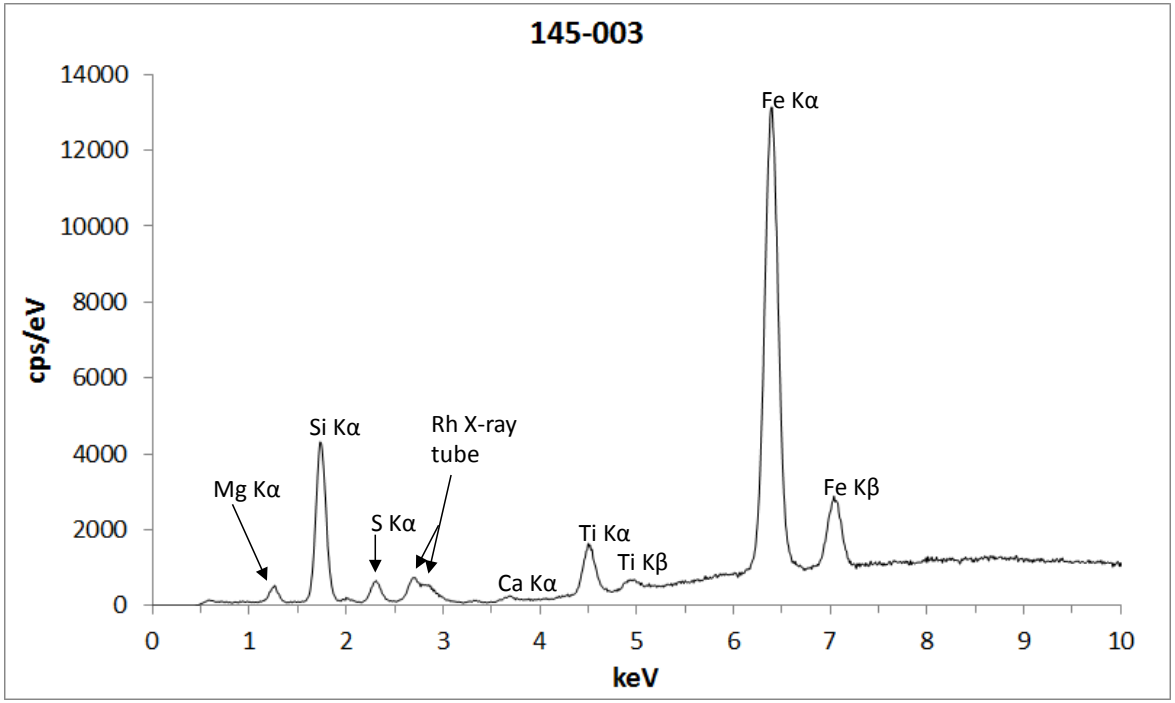

This shows higher concentrations of Fe compared to **Blank** (right-side table).

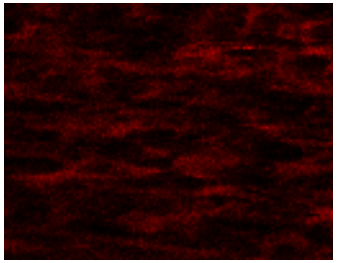

Vision Quant Results: 145-003				
Total Area Spc from ROI Map		6:01 PM		11-Feb-14
Elem:	Net	Wt%	At%	I-Error%
MgK	1.56	30.34	37.01	1.99
AlK	0.1	0.55	0.61	19.8
SiK	17.16	44.27	46.75	0.49
P K	0.42	1.30	1.25	5.68
S K	2.41	3.71	3.44	1.52
ClK	0.07	0.11	0.08	31.48
K K	0.2	0.26	0.20	11.11
CaK	0.65	0.56	0.42	4.47
TiK	6.74	2.80	1.74	0.95
CrK	0.41	0.12	0.06	13.81
MnK	0.98	0.25	0.13	6.89
FeK	69.45	15.22	8.08	0.26
NiK	0.6	0.14	0.07	14
ZnK	1.3	0.29	0.13	7.19
ZrK	0.36	0.08	0.03	14.4

Vision Quant Results: **Blank**				
Total Area Spc from ROI Map		12:53 PM		10-Feb-14
Elem:	Net	Wt%	At%	I-Error%
MgK	1.57	29.42	35.12	3.79
AlK	0.2	1.2	1.29	18.91
SiK	15.88	47	48.58	1.02
P K	0.45	1.77	1.66	10.07
S K	2.06	4.06	3.68	3.32
K K	0.18	0.22	0.17	25.03
CaK	4.25	3.5	2.54	2.25
TiK	8.81	3.67	2.23	1.62
CrK	0.27	0.08	0.04	43.76
MnK	1.12	0.28	0.15	12.39
FeK	38.9	8.46	4.4	0.73
NiK	0.53	0.11	0.06	30.79
ZnK	0.81	0.17	0.07	21.53
ZrK	0.23	0.05	0.02	36.82

Sample: Hope Creek 145-003 with Blank subtracted

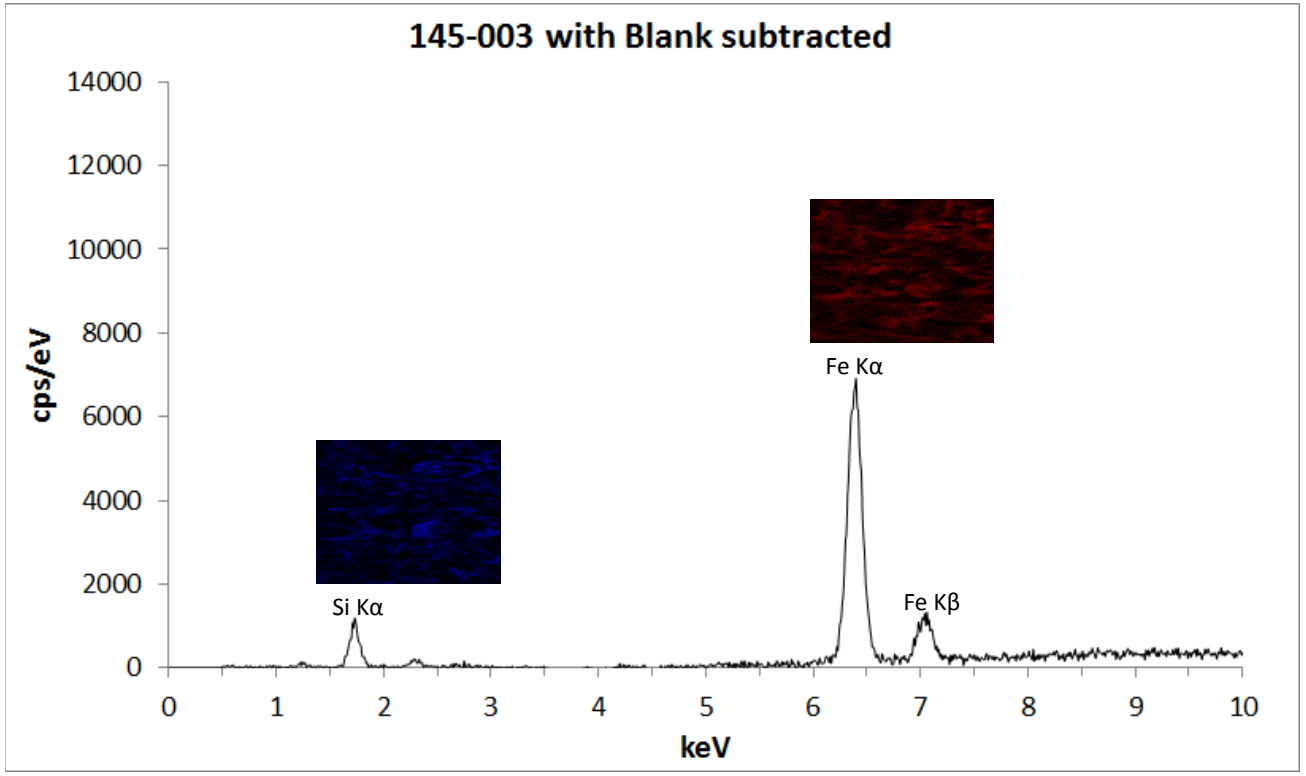

Sample: Hope Creek 145-004

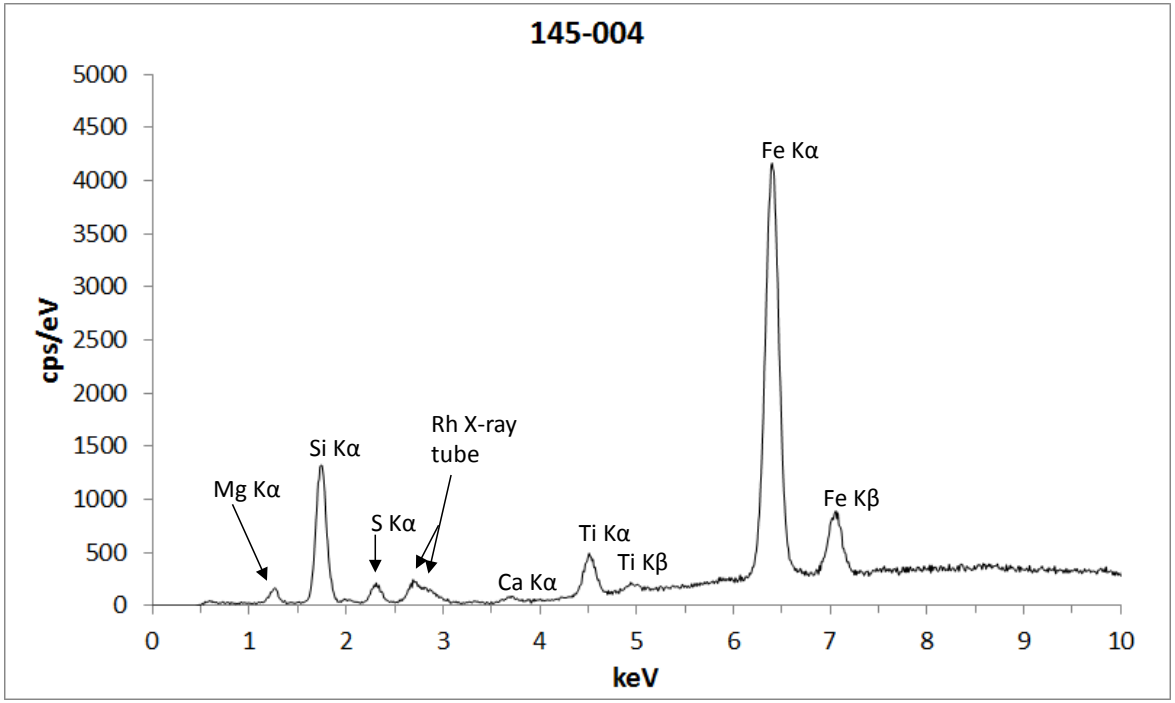

This shows higher concentrations of Fe compared to **Blank** (right-side table).

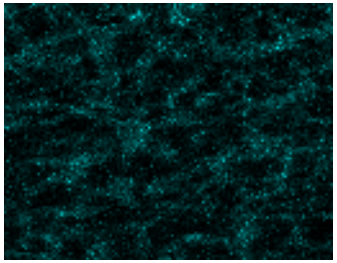

Vision Quant Results: 145-004				
Total Area Spc from ROI Map		6:55 PM		10-Feb-14
Elem:	Net	Wt%	At%	I-Error%
MgK	2.04	28.48	34.66	3.34
AlK	0.16	0.68	0.74	27
SiK	21.66	44.93	47.34	0.87
P K	0.57	1.55	1.48	9.15
S K	3.07	4.14	3.82	2.65
ClK	2.21	2.94	2.45	3.27
K K	0.35	0.31	0.24	13.49
CaK	1.1	0.63	0.47	5.84
TiK	8.08	2.22	1.37	1.73
CrK	0.6	0.11	0.06	20.75
MnK	1.25	0.21	0.11	11.75
FeK	89.28	13.19	6.99	0.45
NiK	1.07	0.17	0.09	17
ZnK	2.16	0.34	0.15	9.27
ZrK	0.57	0.1	0.03	18.01

Vision Quant Results: **Blank**				
Total Area Spc from ROI Map		12:53 PM		10-Feb-14
Elem:	Net	Wt%	At%	I-Error%
MgK	1.57	29.42	35.12	3.79
AlK	0.2	1.2	1.29	18.91
SiK	15.88	47	48.58	1.02
P K	0.45	1.77	1.66	10.07
S K	2.06	4.06	3.68	3.32
K K	0.18	0.22	0.17	25.03
CaK	4.25	3.5	2.54	2.25
TiK	8.81	3.67	2.23	1.62
CrK	0.27	0.08	0.04	43.76
MnK	1.12	0.28	0.15	12.39
FeK	38.9	8.46	4.4	0.73
NiK	0.53	0.11	0.06	30.79
ZnK	0.81	0.17	0.07	21.53
ZrK	0.23	0.05	0.02	36.82

Sample: Hope Creek 145-004 with Blank subtracted

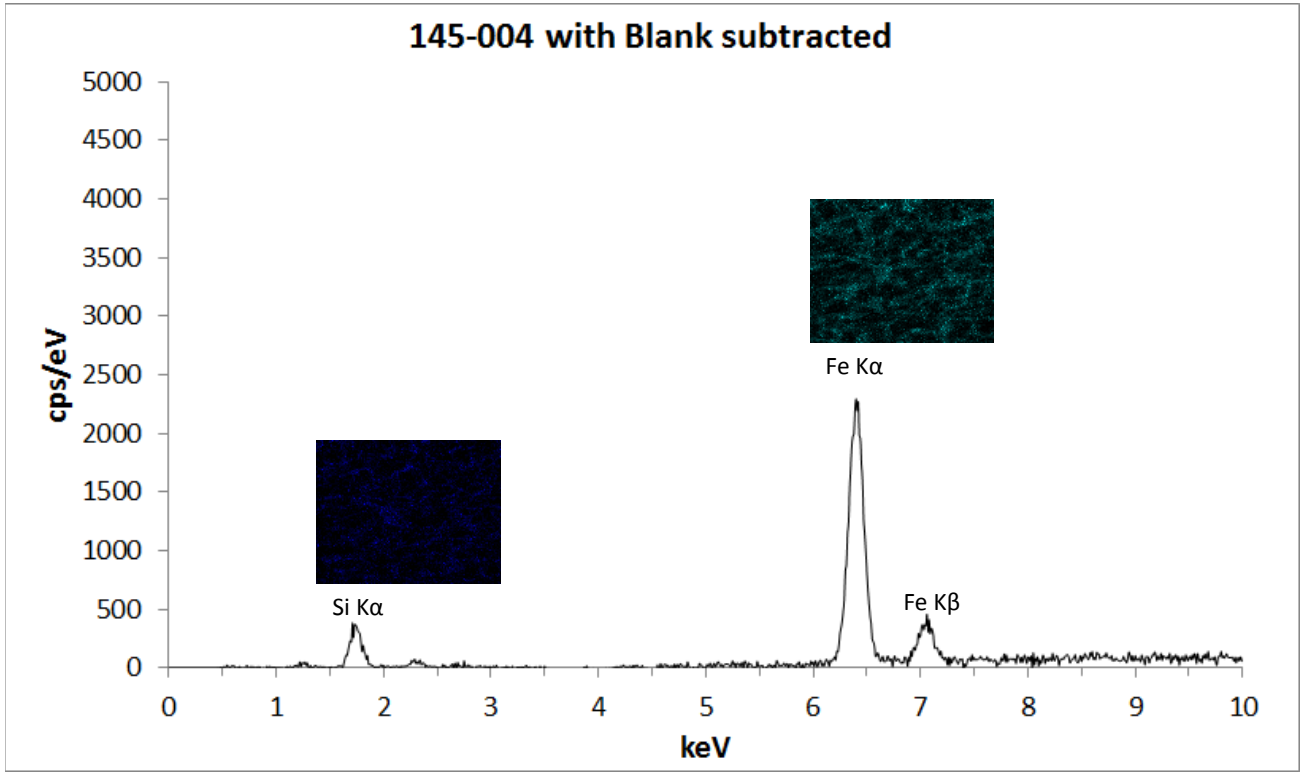

Sample: Hope Creek 145-005

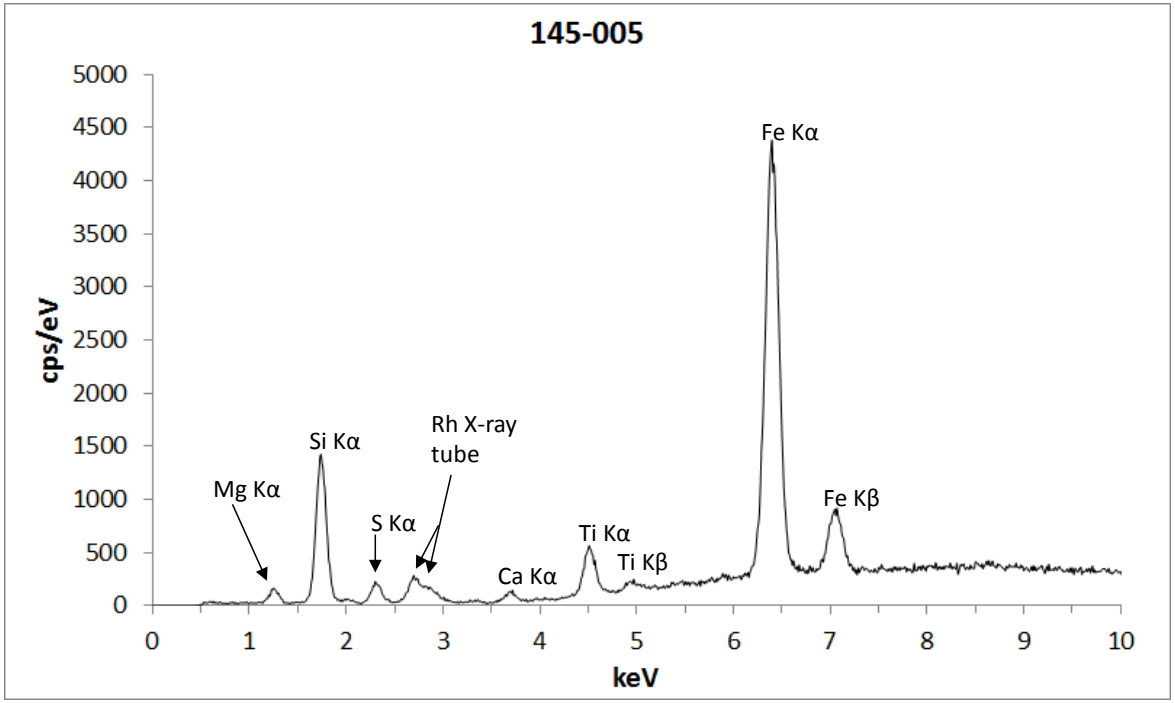

This shows higher concentrations of Fe compared to **Blank** (right-side table).

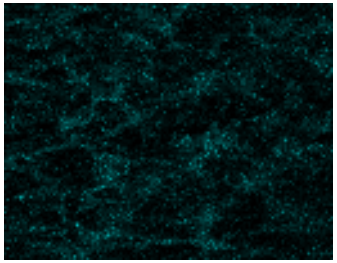

Vision Quant Results: 145-005				
Total Area Spc from ROI Map		7:51 PM		10-Feb-14
Elem:	Net	Wt%	At%	I-Error%
MgK	2.09	27.79	33.96	3.28
AlK	0.21	0.84	0.93	20.27
SiK	22.67	44.34	46.9	0.85
P K	0.68	1.74	1.67	7.58
S K	3.29	4.18	3.88	2.51
ClK	2.53	3.18	2.66	2.99
K K	0.47	0.4	0.3	10.77
CaK	1.8	0.99	0.73	4.15
TiK	9.33	2.46	1.52	1.59
CrK	1.07	0.19	0.11	12.34
MnK	1.23	0.19	0.11	12.33
FeK	92.1	13.1	6.97	0.45
NiK	1	0.15	0.08	18.76
ZnK	2.36	0.36	0.16	8.62
ZrK	0.55	0.09	0.03	18.58

Vision Quant Results: **Blank**				
Total Area Spc from ROI Map		12:53 PM		10-Feb-14
Elem:	Net	Wt%	At%	I-Error%
MgK	1.57	29.42	35.12	3.79
AlK	0.2	1.2	1.29	18.91
SiK	15.88	47	48.58	1.02
P K	0.45	1.77	1.66	10.07
S K	2.06	4.06	3.68	3.32
K K	0.18	0.22	0.17	25.03
CaK	4.25	3.5	2.54	2.25
TiK	8.81	3.67	2.23	1.62
CrK	0.27	0.08	0.04	43.76
MnK	1.12	0.28	0.15	12.39
FeK	38.9	8.46	4.4	0.73
NiK	0.53	0.11	0.06	30.79
ZnK	0.81	0.17	0.07	21.53
ZrK	0.23	0.05	0.02	36.82

Sample: Hope Creek 145-005 with Blank subtracted

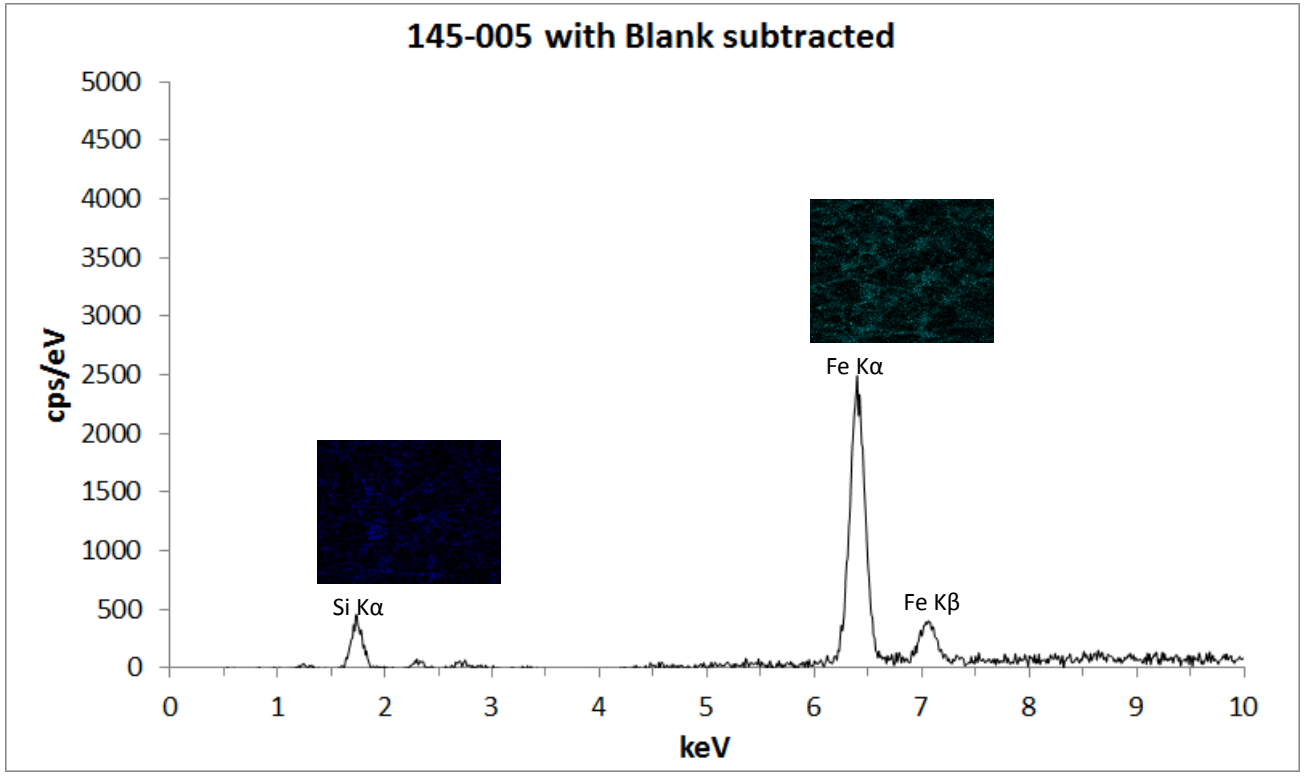

Sample: Hope Creek 145-012

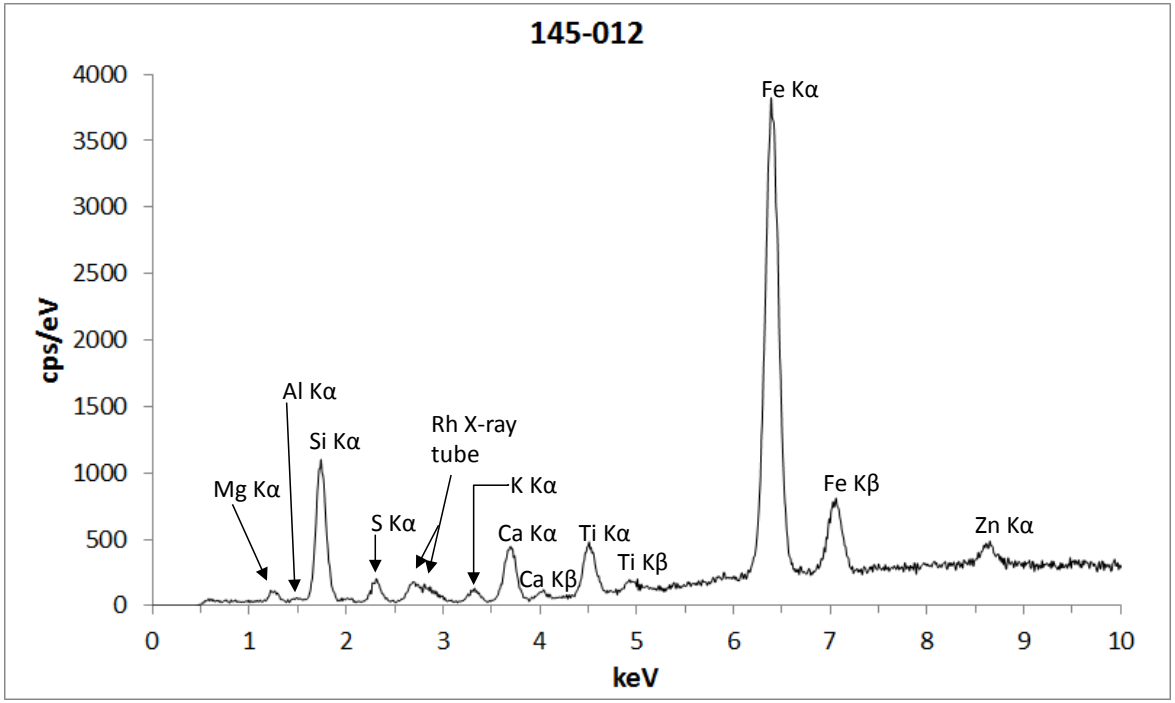

This shows higher concentrations of Fe compared to **Blank** (right-side table).

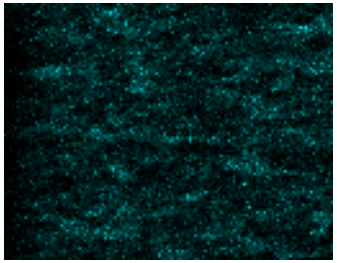

Vision Quant Results: 145-012				
Total Area Spc from ROI Map		10:47 AM		11-Feb-14
Elem:	Net	Wt%	At%	I-Error%
MgK	1.33	23.24	29.52	4.71
AlK	0.5	2.39	2.74	10.26
SiK	17.08	40.15	44.14	0.99
P K	0.48	1.41	1.41	10.86
S K	2.7	3.94	3.8	2.91
ClK	1.67	2.42	2.11	4.08
K K	1.66	1.62	1.28	4.19
CaK	7.95	5.23	4.03	1.57
TiK	7.89	2.7	1.74	1.73
CrK	0.62	0.14	0.09	18.14
MnK	1.37	0.29	0.16	9.8
FeK	80.84	15.14	8.37	0.47
NiK	0.89	0.18	0.1	19.08
ZnK	4.97	1.01	0.48	4.06
ZrK	0.56	0.13	0.04	20.9

Vision Quant Results: **Blank**				
Total Area Spc from ROI Map		12:53 PM		10-Feb-14
Elem:	Net	Wt%	At%	I-Error%
MgK	1.57	29.42	35.12	3.79
AlK	0.2	1.2	1.29	18.91
SiK	15.88	47	48.58	1.02
P K	0.45	1.77	1.66	10.07
S K	2.06	4.06	3.68	3.32
K K	0.18	0.22	0.17	25.03
CaK	4.25	3.5	2.54	2.25
TiK	8.81	3.67	2.23	1.62
CrK	0.27	0.08	0.04	43.76
MnK	1.12	0.28	0.15	12.39
FeK	38.9	8.46	4.4	0.73
NiK	0.53	0.11	0.06	30.79
ZnK	0.81	0.17	0.07	21.53
ZrK	0.23	0.05	0.02	36.82

Sample: Hope Creek 145-012 with Blank subtracted

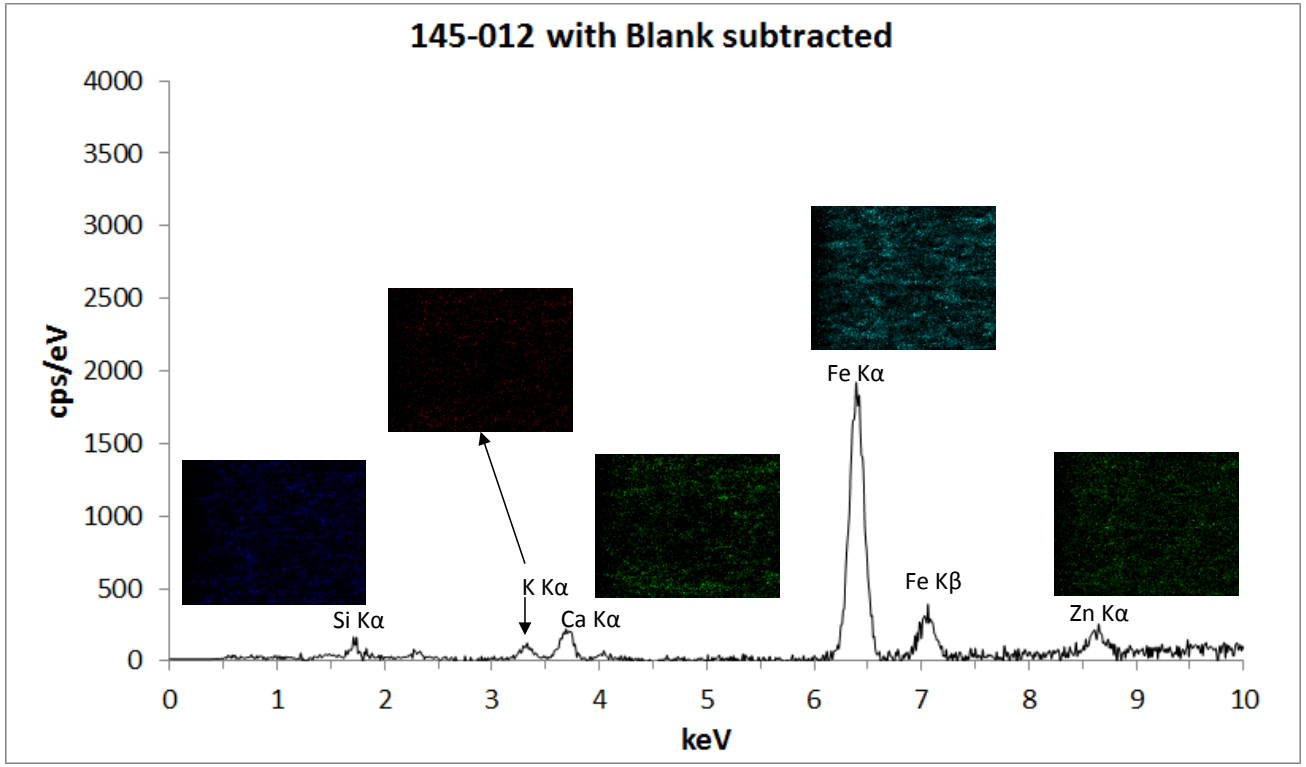

Sample: Diablo Canyon 123-001

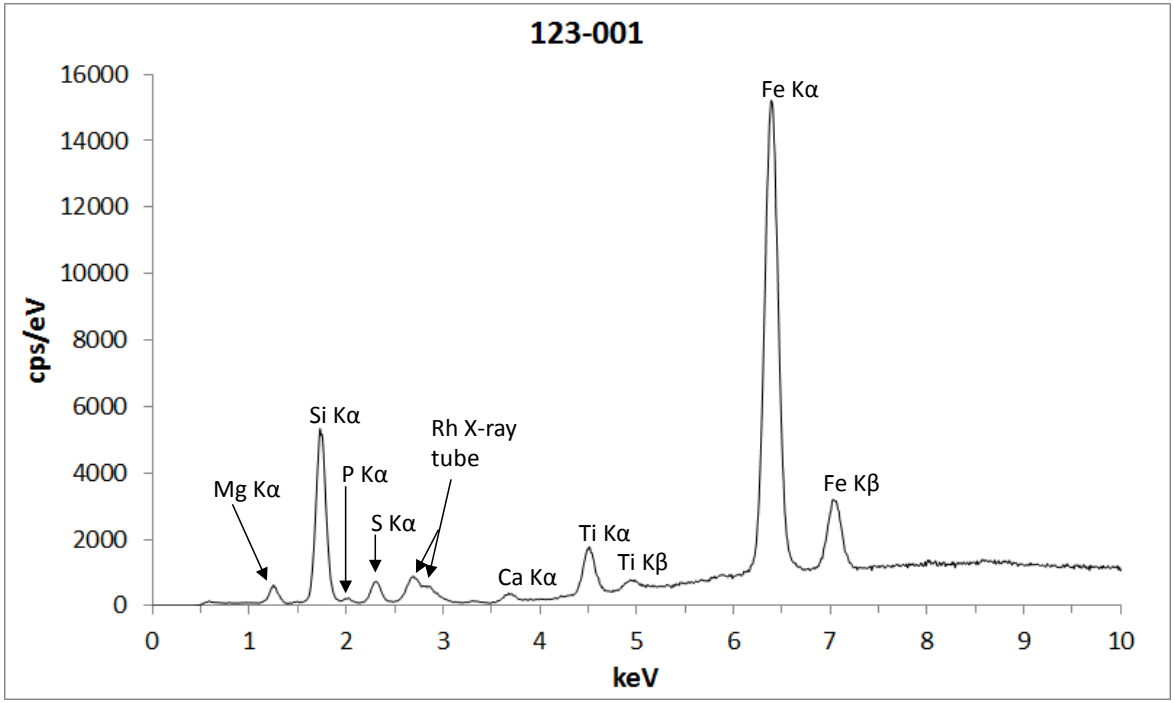

This shows higher concentrations of Fe compared to **Blank** (right-side table).

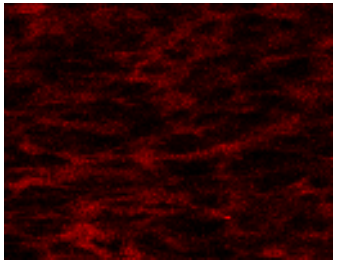

Vision Quant Results: 123-001				
Total Area Spc from ROI Map		7:05 PM		11-Feb-14
Elem:	Net	Wt%	At%	I-Error%
MgK	1.93	30.28	36.81	1.69
AlK	0.18	0.79	0.86	10.95
SiK	21.05	44.41	46.73	0.44
P K	0.55	1.41	1.35	4.4
S K	2.77	3.51	3.23	1.38
ClK	0.56	0.70	0.59	4.43
K K	0.25	0.27	0.20	8.93
CaK	1.25	0.90	0.66	2.63
TiK	7.29	2.50	1.54	0.92
CrK	0.39	0.09	0.05	15.17
MnK	1.12	0.22	0.13	6.31
FeK	81.15	14.50	7.67	0.24
NiK	0.57	0.10	0.05	15.4
ZnK	1.53	0.28	0.13	6.22
ZrK	0.25	0.05	0.01	20

Vision Quant Results: **Blank**				
Total Area Spc from ROI Map		12:53 PM		10-Feb-14
Elem:	Net	Wt%	At%	I-Error%
MgK	1.57	29.42	35.12	3.79
AlK	0.2	1.2	1.29	18.91
SiK	15.88	47	48.58	1.02
P K	0.45	1.77	1.66	10.07
S K	2.06	4.06	3.68	3.32
K K	0.18	0.22	0.17	25.03
CaK	4.25	3.5	2.54	2.25
TiK	8.81	3.67	2.23	1.62
CrK	0.27	0.08	0.04	43.76
MnK	1.12	0.28	0.15	12.39
FeK	38.9	8.46	4.4	0.73
NiK	0.53	0.11	0.06	30.79
ZnK	0.81	0.17	0.07	21.53
ZrK	0.23	0.05	0.02	36.82

Sample: Diablo Canyon 123-001 with Blank subtracted

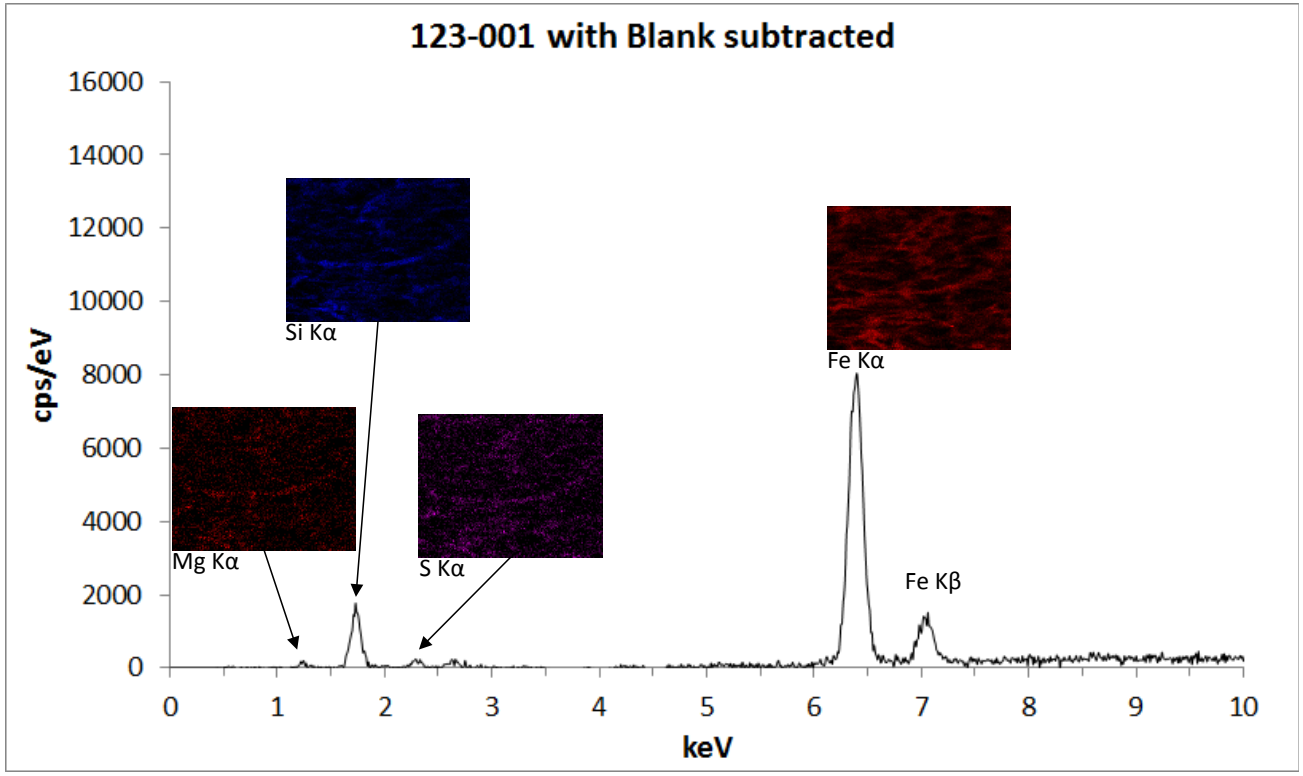

Sample: Diablo Canyon 123-006

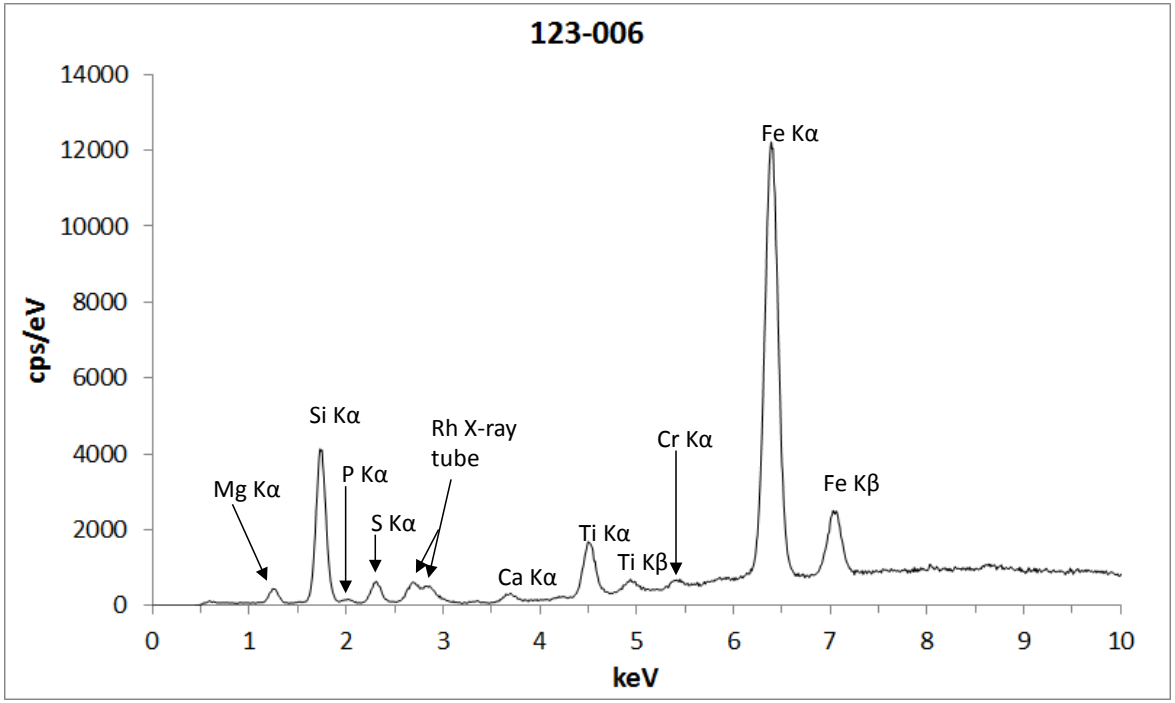

This shows higher concentrations of Fe compared to **Blank** (right-side table).

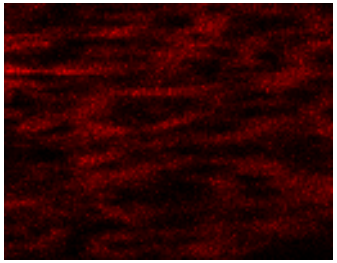

Vision Quant Results: 123-006				
Total Area Spc from ROI Map		8:09 PM		11-Feb-14
Elem:	Net	Wt%	At%	I-Error%
MgK	1.43	29.18	35.81	2.05
AlK	0.1	0.57	0.64	18.29
SiK	16.33	44.07	46.82	0.5
P K	0.4	1.33	1.28	5.49
S K	2.37	3.86	3.60	1.5
ClK	0.26	0.42	0.35	7.95
K K	0.19	0.26	0.20	10.62
CaK	1.1	0.98	0.73	2.79
TiK	7.3	3.15	1.96	0.88
CrK	1.26	0.37	0.21	4.43
MnK	0.96	0.25	0.14	6.43
FeK	65.15	15.00	8.01	0.26
NiK	0.65	0.16	0.08	11.79
ZnK	1.42	0.33	0.16	5.89
ZrK	0.23	0.06	0.02	18.62

Vision Quant Results: **Blank**				
Total Area Spc from ROI Map		12:53 PM		10-Feb-14
Elem:	Net	Wt%	At%	I-Error%
MgK	1.57	29.42	35.12	3.79
AlK	0.2	1.2	1.29	18.91
SiK	15.88	47	48.58	1.02
P K	0.45	1.77	1.66	10.07
S K	2.06	4.06	3.68	3.32
K K	0.18	0.22	0.17	25.03
CaK	4.25	3.5	2.54	2.25
TiK	8.81	3.67	2.23	1.62
CrK	0.27	0.08	0.04	43.76
MnK	1.12	0.28	0.15	12.39
FeK	38.9	8.46	4.4	0.73
NiK	0.53	0.11	0.06	30.79
ZnK	0.81	0.17	0.07	21.53
ZrK	0.23	0.05	0.02	36.82

Sample: Diablo Canyon 123-006 with Blank subtracted

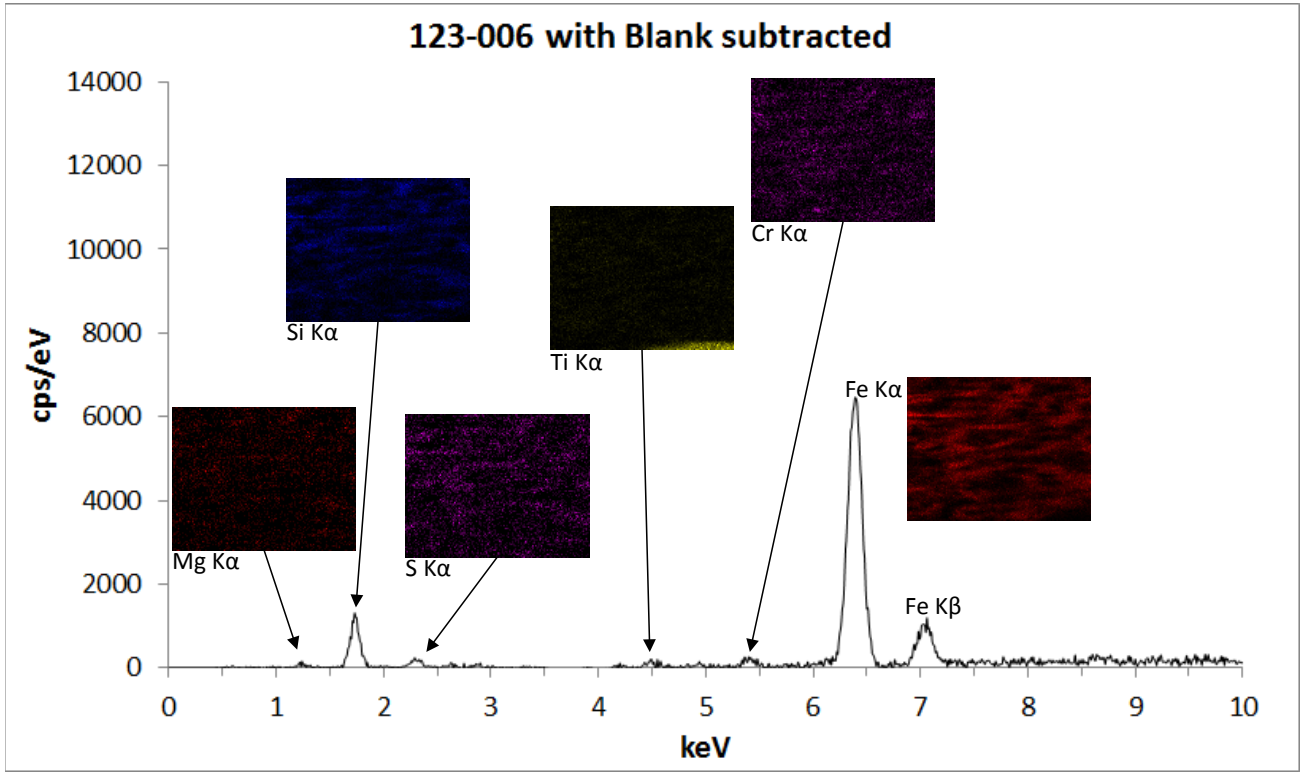

Sample: Diablo Canyon 123-007

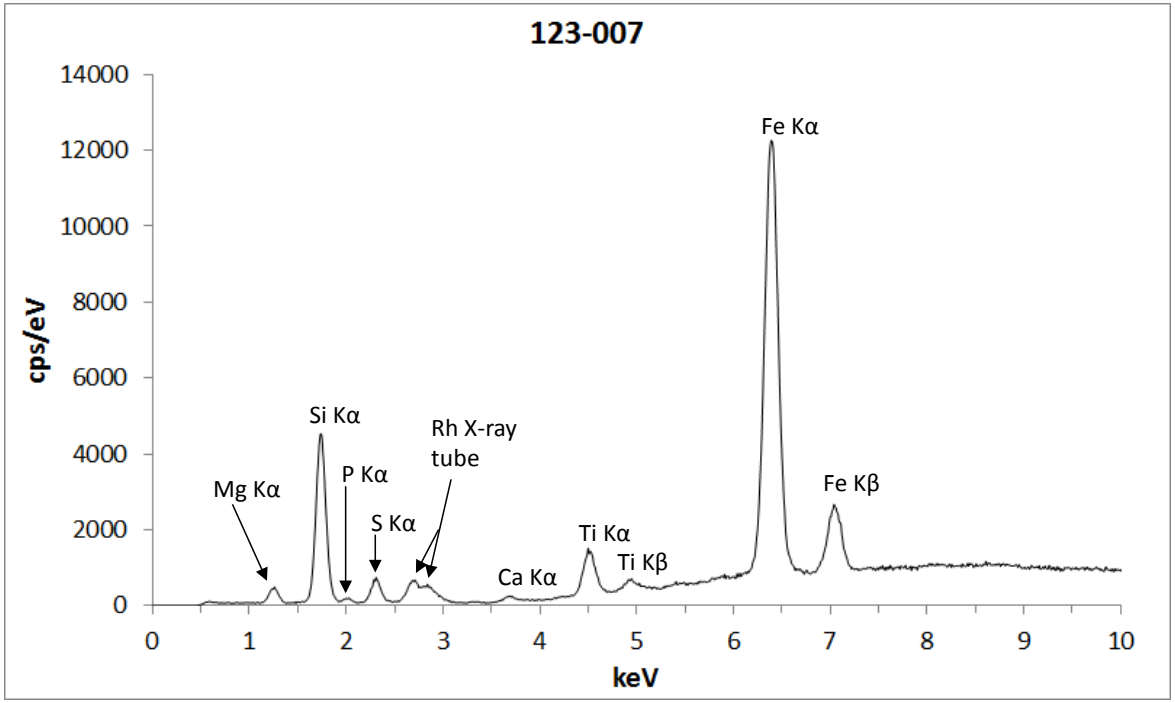

This shows higher concentrations of Fe compared to **Blank** (right-side table).

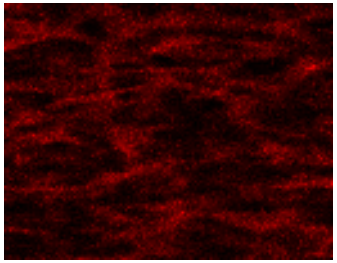

Vision Quant Results: 123-007				
Total Area Spc from ROI Map		9:12 PM		11-Feb-14
Elem:	Net	Wt%	At%	I-Error%
MgK	1.55	29.53	35.88	1.93
AlK	0.11	0.60	0.66	16.51
SiK	17.79	45.51	47.85	0.48
P K	0.47	1.48	1.41	4.9
S K	2.6	4.06	3.74	1.42
ClK	0.27	0.41	0.34	7.88
K K	0.15	0.20	0.15	13.48
CaK	0.73	0.63	0.47	3.9
TiK	6.13	2.53	1.56	1
CrK	0.63	0.17	0.10	8.78
MnK	0.97	0.23	0.13	6.63
FeK	65.7	14.18	7.50	0.26
NiK	0.7	0.15	0.07	11.45
ZnK	1.19	0.25	0.11	7.27
ZrK	0.24	0.06	0.02	18.45

Vision Quant Results: **Blank**				
Total Area Spc from ROI Map		12:53 PM		10-Feb-14
Elem:	Net	Wt%	At%	I-Error%
MgK	1.57	29.42	35.12	3.79
AlK	0.2	1.2	1.29	18.91
SiK	15.88	47	48.58	1.02
P K	0.45	1.77	1.66	10.07
S K	2.06	4.06	3.68	3.32
K K	0.18	0.22	0.17	25.03
CaK	4.25	3.5	2.54	2.25
TiK	8.81	3.67	2.23	1.62
CrK	0.27	0.08	0.04	43.76
MnK	1.12	0.28	0.15	12.39
FeK	38.9	8.46	4.4	0.73
NiK	0.53	0.11	0.06	30.79
ZnK	0.81	0.17	0.07	21.53
ZrK	0.23	0.05	0.02	36.82

Sample: Diablo Canyon 123-007 with Blank subtracted

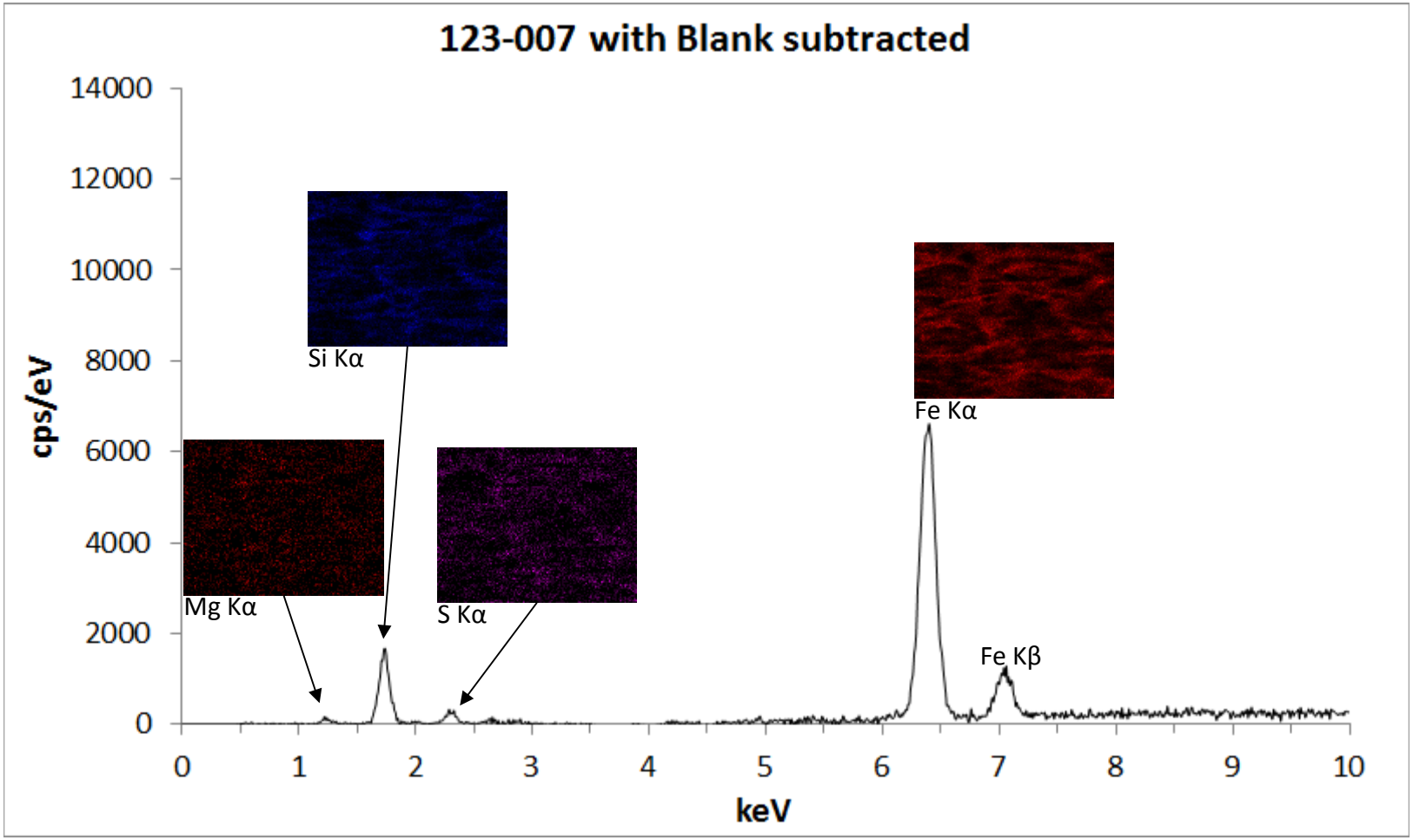

Sample: Diablo Canyon 123-008

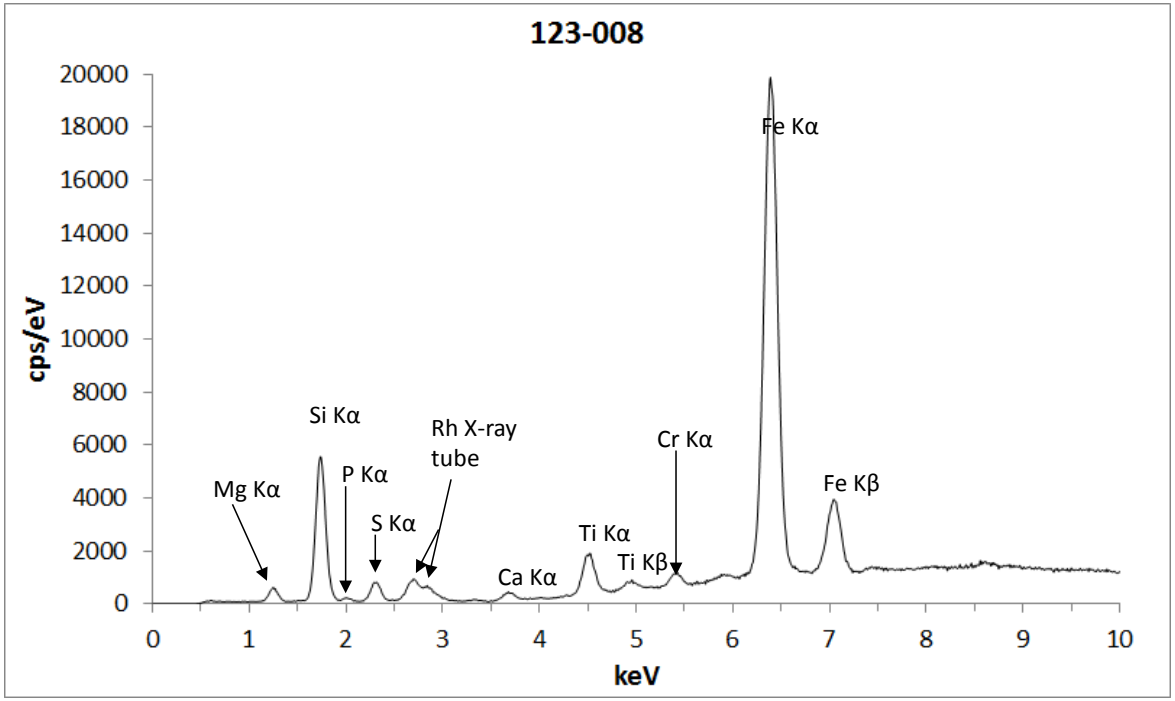

This shows higher concentrations of Fe compared to **Blank** (right-side table).

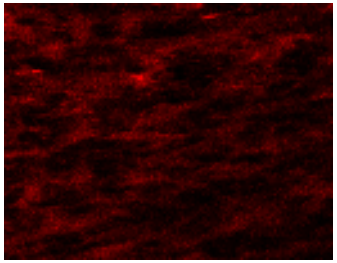

Vision Quant Results: 123-008				
Total Area Spc from ROI Map		10:16 PM		11-Feb-14
Elem:	Net	Wt%	At%	I-Error%
MgK	1.93	28.97	35.99	1.74
AlK	0.14	0.57	0.63	15.24
SiK	21.95	42.53	45.73	0.43
P K	0.5	1.17	1.14	5
S K	3.15	3.58	3.38	1.3
ClK	0.36	0.40	0.34	6.84
K K	0.27	0.25	0.20	8.8
CaK	1.53	0.97	0.73	2.33
TiK	8.09	2.47	1.56	0.87
CrK	2.74	0.57	0.33	2.53
MnK	1.45	0.27	0.15	5.15
FeK	106.31	17.58	9.51	0.2
NiK	1.3	0.23	0.11	7.11
ZnK	2.3	0.40	0.19	4.38
ZrK	0.22	0.05	0.01	22.95

Vision Quant Results: **Blank**				
Total Area Spc from ROI Map		12:53 PM		10-Feb-14
Elem:	Net	Wt%	At%	I-Error%
MgK	1.57	29.42	35.12	3.79
AlK	0.2	1.2	1.29	18.91
SiK	15.88	47	48.58	1.02
P K	0.45	1.77	1.66	10.07
S K	2.06	4.06	3.68	3.32
K K	0.18	0.22	0.17	25.03
CaK	4.25	3.5	2.54	2.25
TiK	8.81	3.67	2.23	1.62
CrK	0.27	0.08	0.04	43.76
MnK	1.12	0.28	0.15	12.39
FeK	38.9	8.46	4.4	0.73
NiK	0.53	0.11	0.06	30.79
ZnK	0.81	0.17	0.07	21.53
ZrK	0.23	0.05	0.02	36.82

Sample: Diablo Canyon 123-008 with Blank subtracted

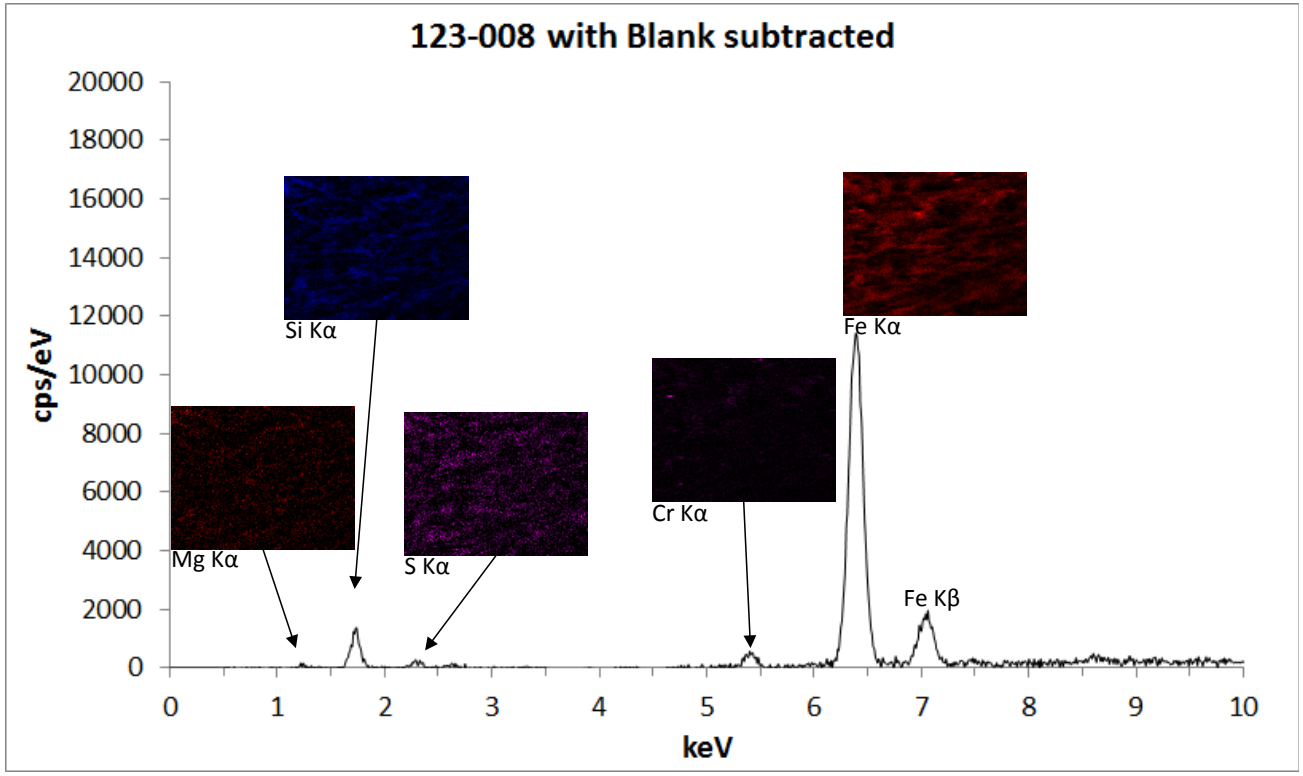

Sample: Diablo Canyon 123-009

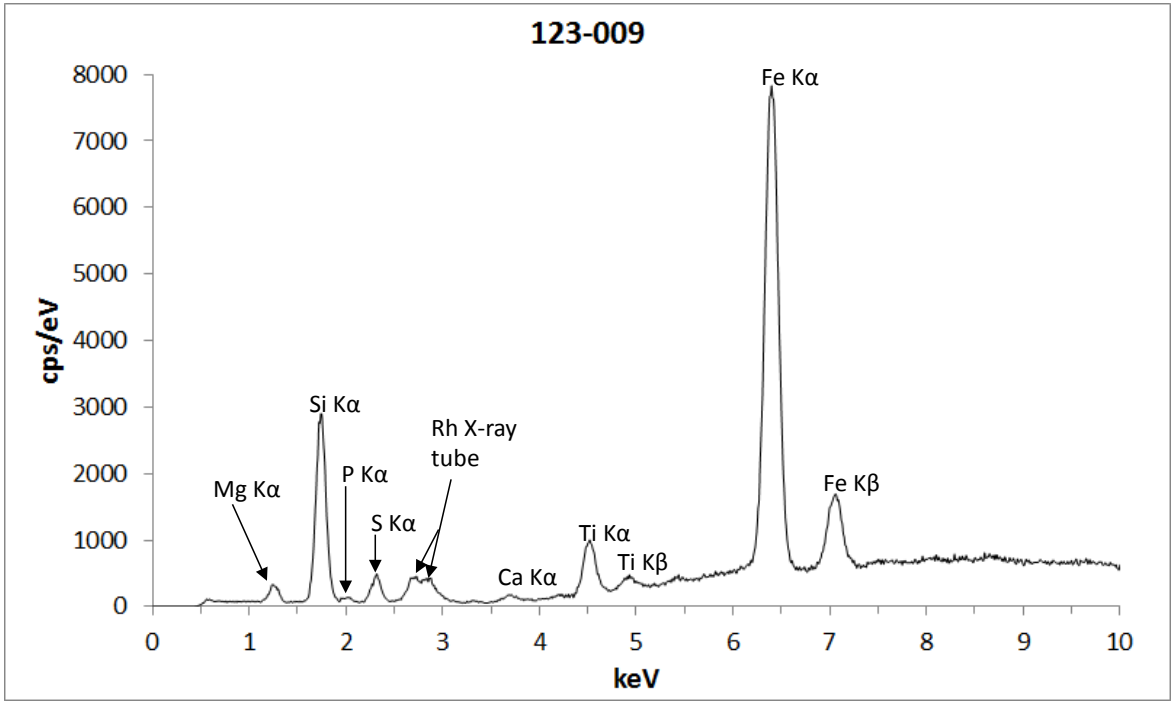

This shows higher concentrations of Fe compared to **Blank** (right-side table).

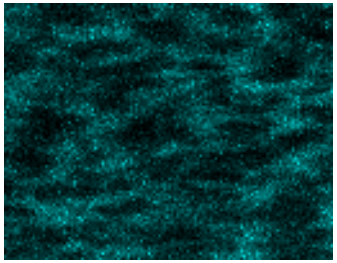

Vision Quant Results: 123-009				
Total Area Spc from ROI Map		9:47 AM		12-Feb-14
Elem:	Net	Wt%	At%	I-Error%
MgK	1.02	27.74	33.67	2.53
AlK	0.06	0.53	0.58	26.85
SiK	11.46	46.20	48.53	0.6
P K	0.33	1.76	1.68	6.2
S K	1.66	4.45	4.09	1.84
ClK	1.12	2.98	2.48	2.39
K K	0.13	0.22	0.17	14.29
CaK	0.51	0.59	0.43	4.68
TiK	4.17	2.27	1.40	1.22
CrK	0.6	0.22	0.13	7.74
MnK	0.62	0.20	0.11	8.53
FeK	42.16	12.31	6.50	0.33
NiK	0.56	0.18	0.09	11.49
ZnK	0.98	0.30	0.13	7.23
ZrK	0.15	0.05	0.02	25.45

Vision Quant Results: **Blank**				
Total Area Spc from ROI Map		12:53 PM		10-Feb-14
Elem:	Net	Wt%	At%	I-Error%
MgK	1.57	29.42	35.12	3.79
AlK	0.2	1.2	1.29	18.91
SiK	15.88	47	48.58	1.02
P K	0.45	1.77	1.66	10.07
S K	2.06	4.06	3.68	3.32
K K	0.18	0.22	0.17	25.03
CaK	4.25	3.5	2.54	2.25
TiK	8.81	3.67	2.23	1.62
CrK	0.27	0.08	0.04	43.76
MnK	1.12	0.28	0.15	12.39
FeK	38.9	8.46	4.4	0.73
NiK	0.53	0.11	0.06	30.79
ZnK	0.81	0.17	0.07	21.53
ZrK	0.23	0.05	0.02	36.82

Sample: Diablo Canyon 123-009 with Blank subtracted

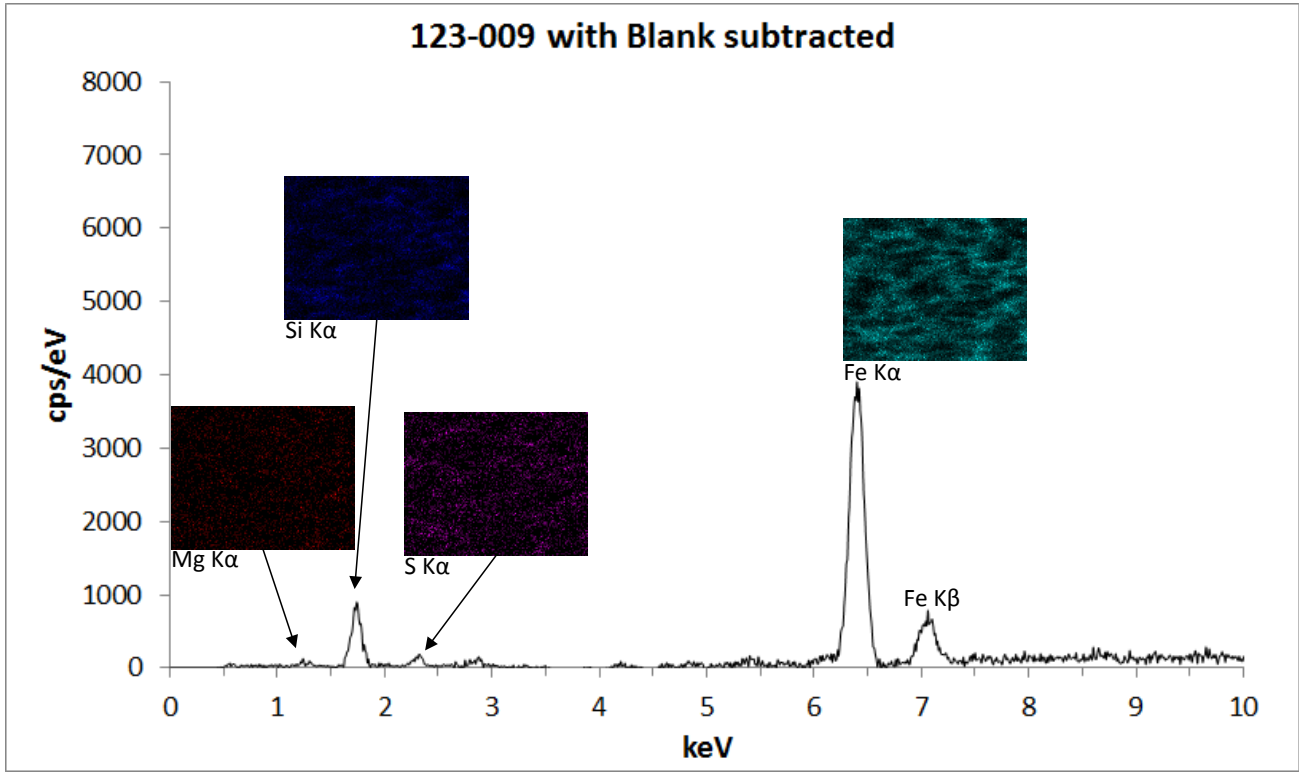

Sample: Diablo Canyon 123-011

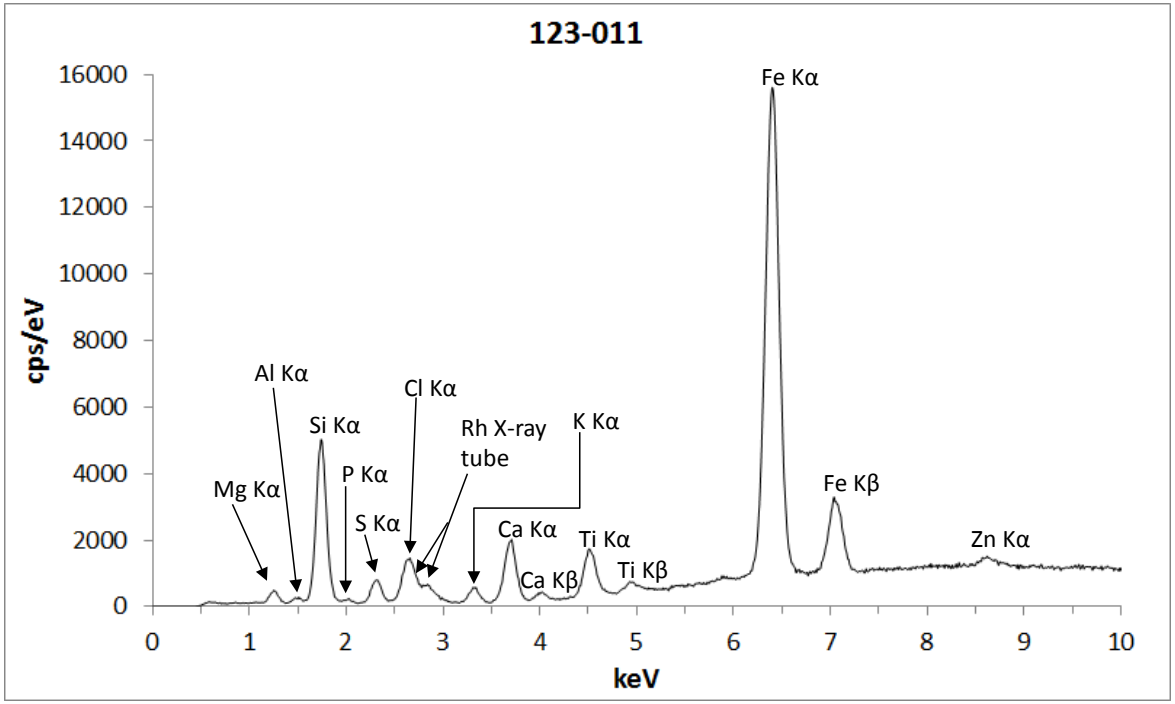

This shows higher concentrations of Fe compared to **Blank** (right-side table).

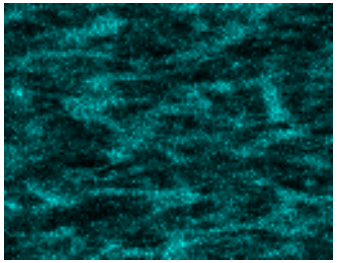

Vision Quant Results: 123-011				
Total Area Spc from ROI Map		5:57 PM		12-Feb-14
Elem:	Net	Wt%	At%	I-Error%
MgK	1.44	21.30	27.08	2.16
AlK	0.68	2.71	3.11	3.85
SiK	19.89	39.33	43.29	0.46
P K	0.47	1.18	1.18	5.41
S K	3.04	3.77	3.64	1.34
ClK	6.1	7.60	6.62	0.88
K K	1.97	1.77	1.40	1.86
CaK	8.68	5.26	4.05	0.74
TiK	7.18	2.24	1.45	0.92
CrK	0.43	0.09	0.05	13.57
MnK	1.14	0.21	0.12	5.97
FeK	83.69	13.94	7.72	0.23
NiK	0.63	0.11	0.06	13.5
ZnK	2.6	0.45	0.21	3.7
ZrK	0.21	0.04	0.01	24.84

Vision Quant Results: **Blank**				
Total Area Spc from ROI Map		12:53 PM		10-Feb-14
Elem:	Net	Wt%	At%	I-Error%
MgK	1.57	29.42	35.12	3.79
AlK	0.2	1.2	1.29	18.91
SiK	15.88	47	48.58	1.02
P K	0.45	1.77	1.66	10.07
S K	2.06	4.06	3.68	3.32
K K	0.18	0.22	0.17	25.03
CaK	4.25	3.5	2.54	2.25
TiK	8.81	3.67	2.23	1.62
CrK	0.27	0.08	0.04	43.76
MnK	1.12	0.28	0.15	12.39
FeK	38.9	8.46	4.4	0.73
NiK	0.53	0.11	0.06	30.79
ZnK	0.81	0.17	0.07	21.53
ZrK	0.23	0.05	0.02	36.82

Sample: Diablo Canyon 123-011 with Blank subtracted

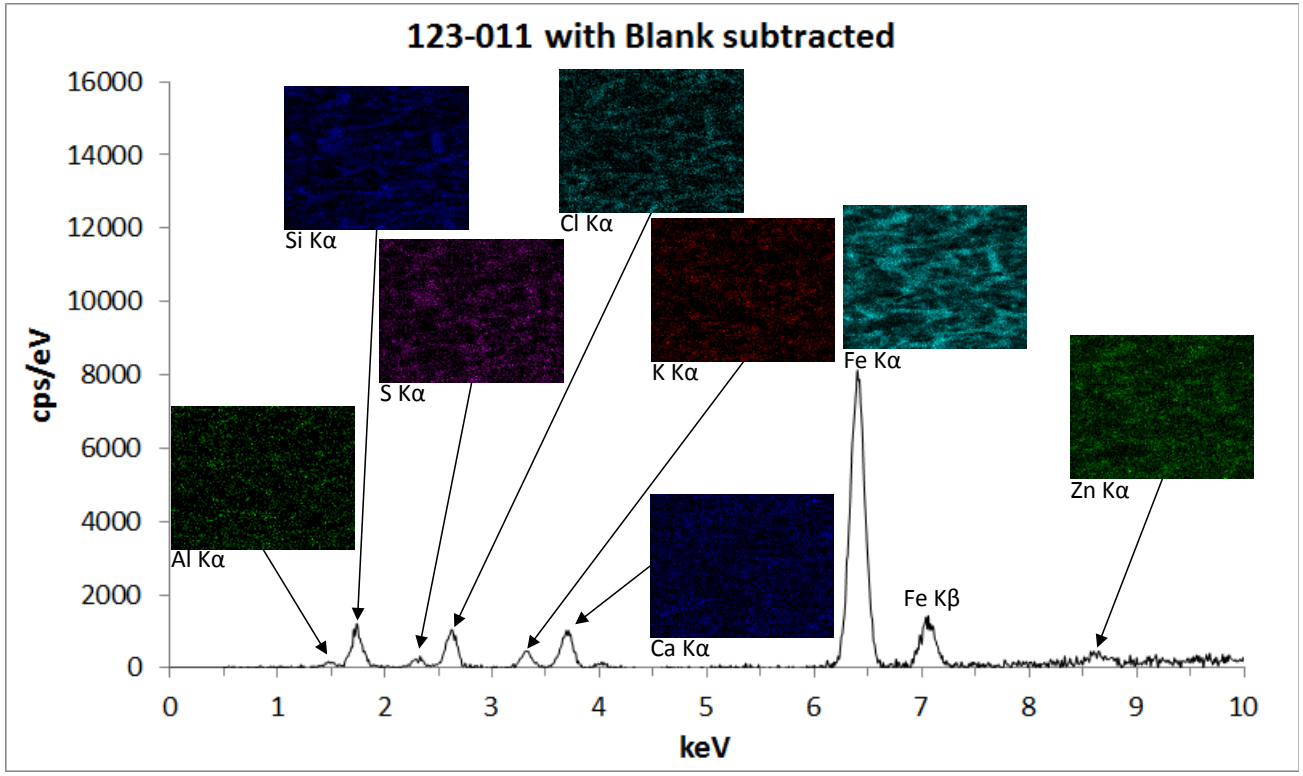

Sample: Diablo Canyon 123-012

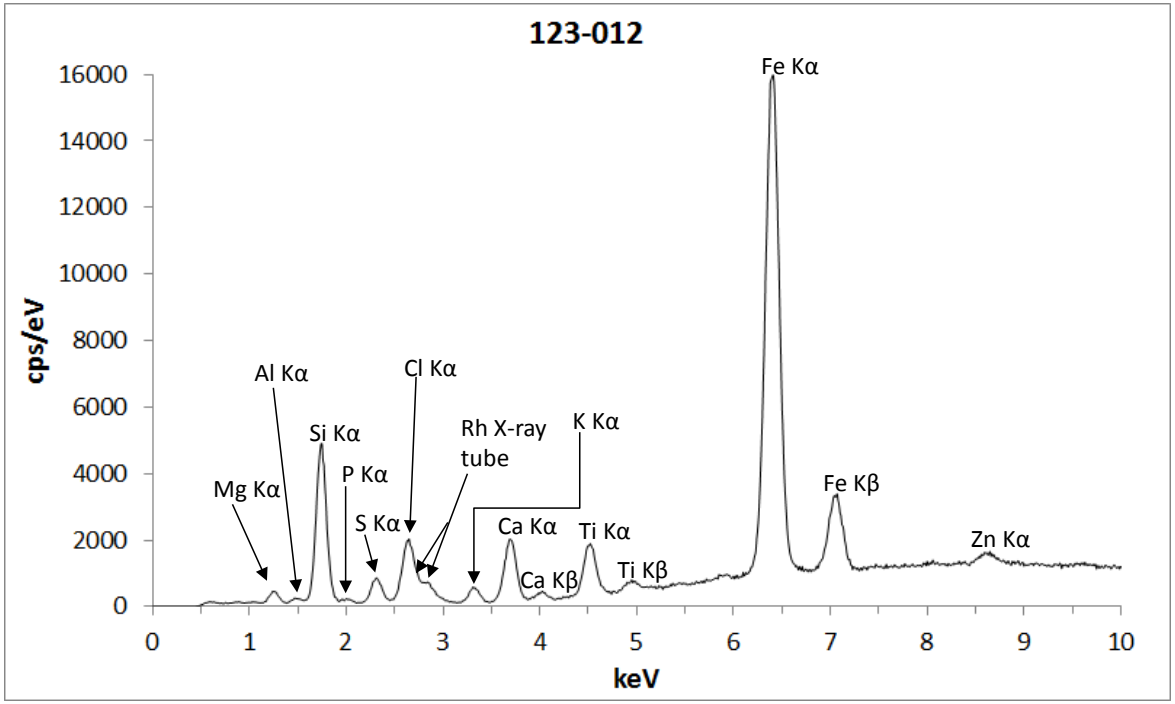

This shows higher concentrations of Fe compared to **Blank** (right-side table).

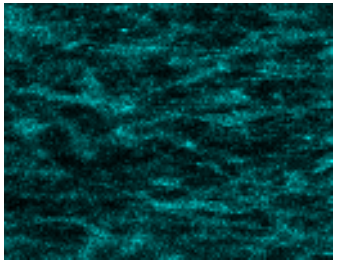

Vision Quant Results: 123-012				
Total Area Spc from ROI Map		6:58 PM		12-Feb-14
Elem:	Net	Wt%	At%	I-Error%
MgK	1.36	20.14	25.97	2.29
AlK	0.62	2.40	2.79	4.25
SiK	19.38	37.01	41.31	0.46
P K	0.5	1.18	1.20	5.3
S K	3.27	3.84	3.76	1.3
ClK	8.5	10.15	8.97	0.73
K K	2.02	1.80	1.44	1.85
CaK	9.02	5.42	4.24	0.73
TiK	8.09	2.51	1.64	0.86
CrK	0.57	0.12	0.07	10.63
MnK	1.2	0.22	0.13	5.91
FeK	86.61	14.48	8.13	0.23
NiK	0.68	0.12	0.07	12.95
ZnK	3.11	0.55	0.26	3.21
ZrK	0.25	0.05	0.02	21.1

Vision Quant Results: **Blank**				
Total Area Spc from ROI Map		12:53 PM		10-Feb-14
Elem:	Net	Wt%	At%	I-Error%
MgK	1.57	29.42	35.12	3.79
AlK	0.2	1.2	1.29	18.91
SiK	15.88	47	48.58	1.02
P K	0.45	1.77	1.66	10.07
S K	2.06	4.06	3.68	3.32
K K	0.18	0.22	0.17	25.03
CaK	4.25	3.5	2.54	2.25
TiK	8.81	3.67	2.23	1.62
CrK	0.27	0.08	0.04	43.76
MnK	1.12	0.28	0.15	12.39
FeK	38.9	8.46	4.4	0.73
NiK	0.53	0.11	0.06	30.79
ZnK	0.81	0.17	0.07	21.53
ZrK	0.23	0.05	0.02	36.82

Sample: Diablo Canyon 123-012 with Blank subtracted

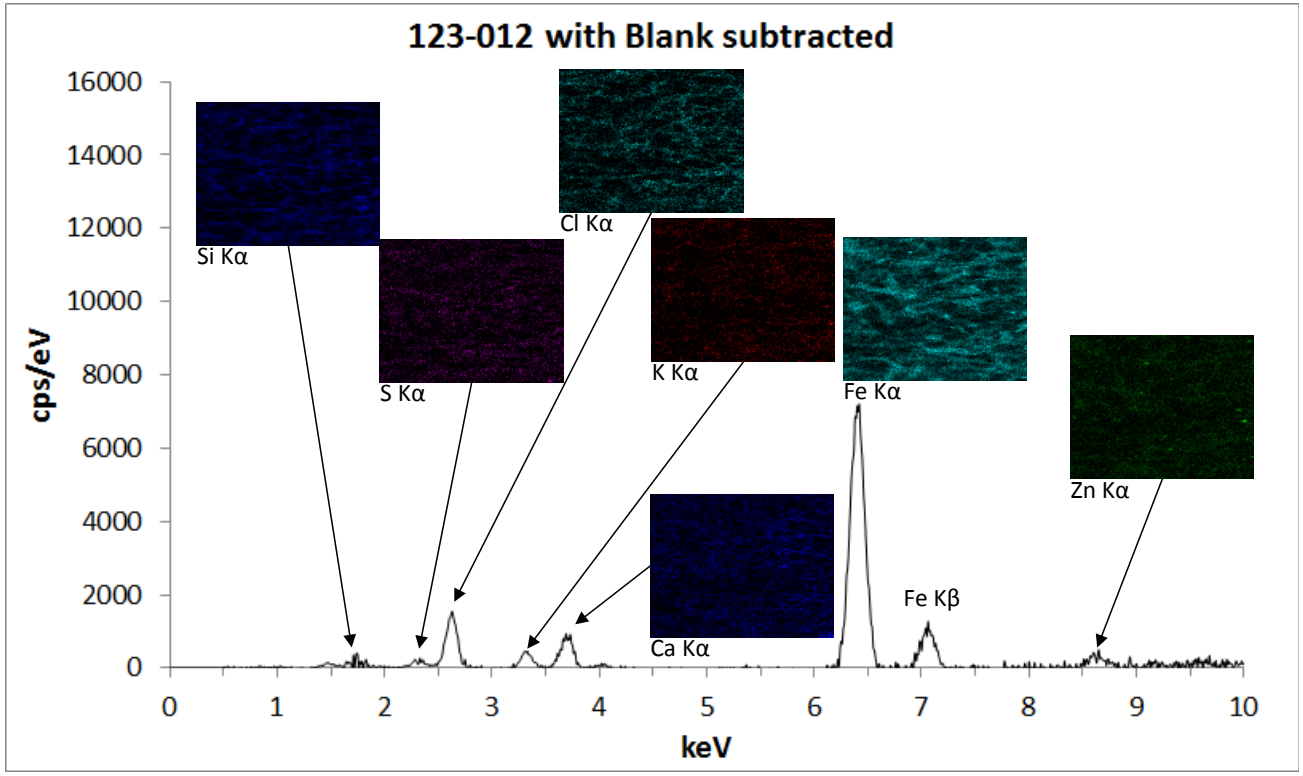

Sample: Diablo Canyon 170-001

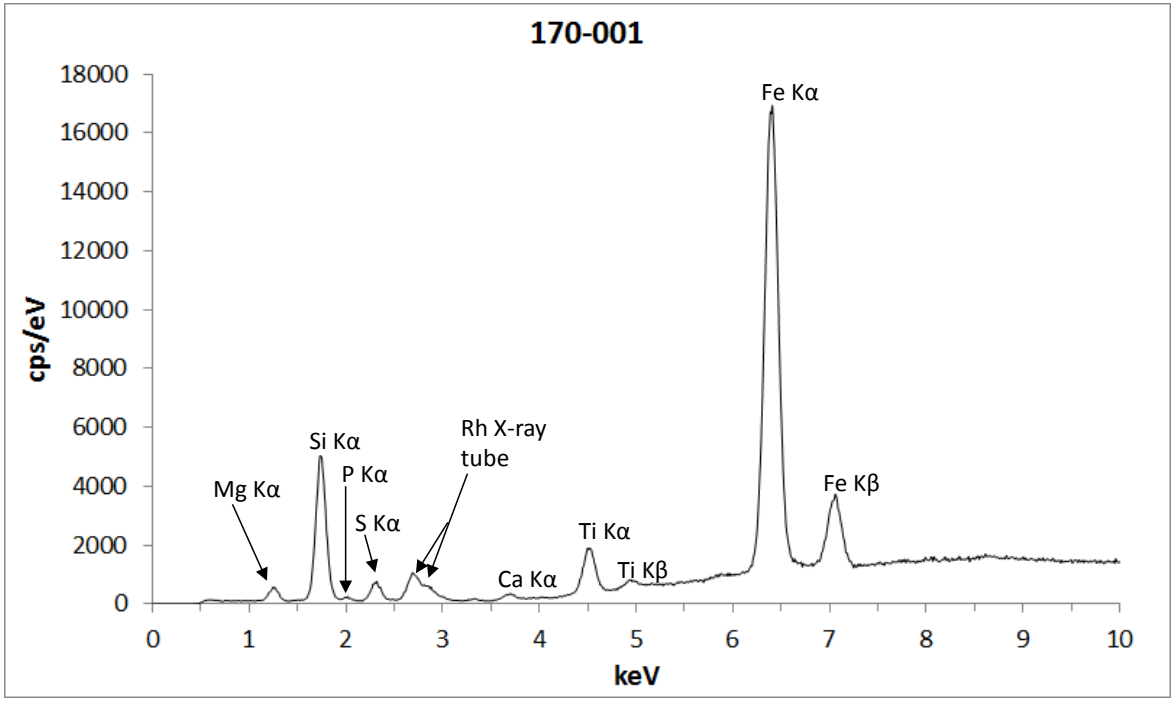

This shows higher concentrations of Fe compared to **Blank** (right-side table).

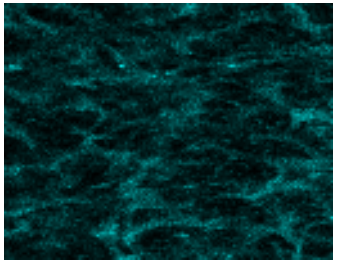

Vision Quant Results: 170-001				
Total Area Spc from ROI Map		4:56 PM		12-Feb-14
Elem:	Net	Wt%	At%	I-Error%
MgK	1.76	27.26	33.53	1.9
AlK	0.15	0.67	0.75	15.16
SiK	19.9	44.35	47.22	0.46
P K	0.49	1.42	1.38	5.25
S K	2.71	3.90	3.63	1.45
ClK	2.56	3.65	3.08	1.5
K K	0.3	0.29	0.22	8.26
CaK	1.03	0.64	0.48	3.21
TiK	8.14	2.41	1.50	0.86
CrK	0.45	0.09	0.05	13.87
MnK	1.08	0.19	0.11	6.88
FeK	90.4	14.66	7.85	0.23
NiK	0.57	0.10	0.05	16.52
ZnK	1.88	0.33	0.15	5.6
ZrK	0.17	0.03	0.01	33.27

Vision Quant Results: **Blank**				
Total Area Spc from ROI Map		12:53 PM		10-Feb-14
Elem:	Net	Wt%	At%	I-Error%
MgK	1.57	29.42	35.12	3.79
AlK	0.2	1.2	1.29	18.91
SiK	15.88	47	48.58	1.02
P K	0.45	1.77	1.66	10.07
S K	2.06	4.06	3.68	3.32
K K	0.18	0.22	0.17	25.03
CaK	4.25	3.5	2.54	2.25
TiK	8.81	3.67	2.23	1.62
CrK	0.27	0.08	0.04	43.76
MnK	1.12	0.28	0.15	12.39
FeK	38.9	8.46	4.4	0.73
NiK	0.53	0.11	0.06	30.79
ZnK	0.81	0.17	0.07	21.53
ZrK	0.23	0.05	0.02	36.82

Sample: Diablo Canyon 170-001 with Blank subtracted

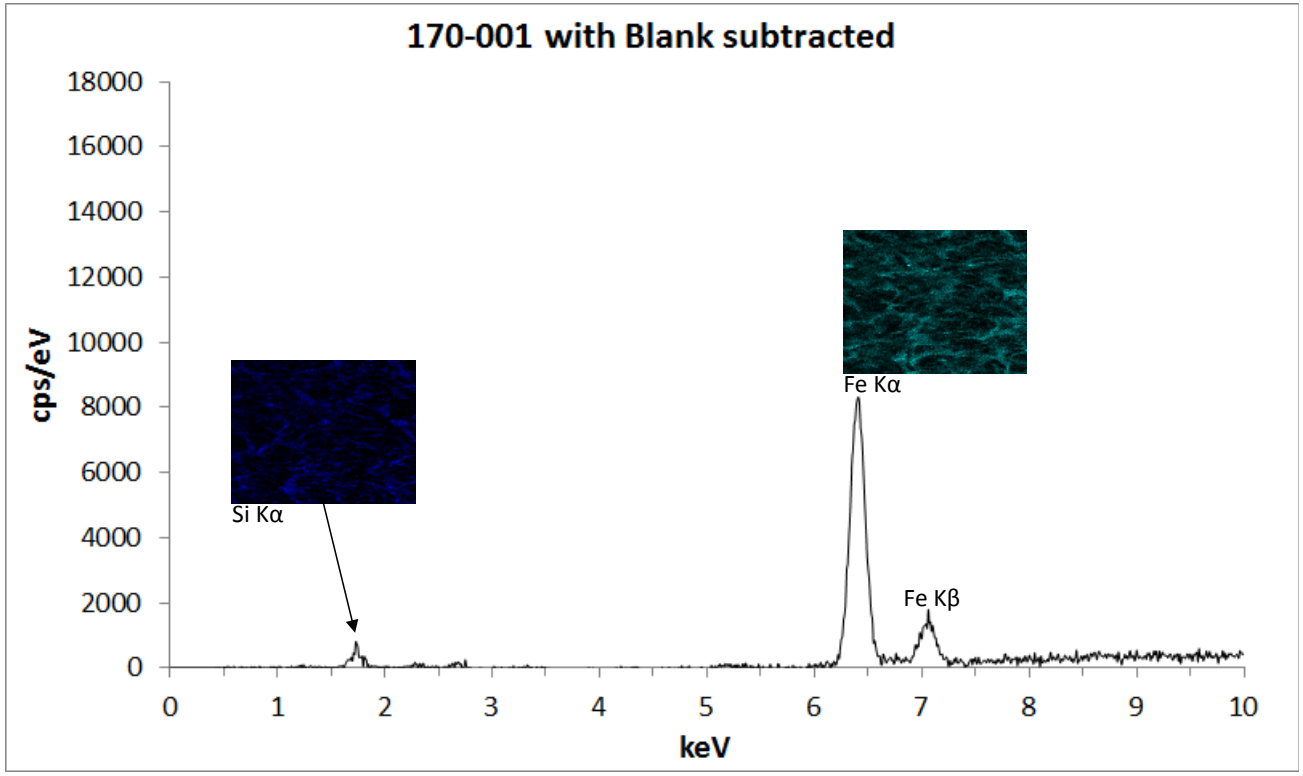

Sample: Diablo Canyon 170-003

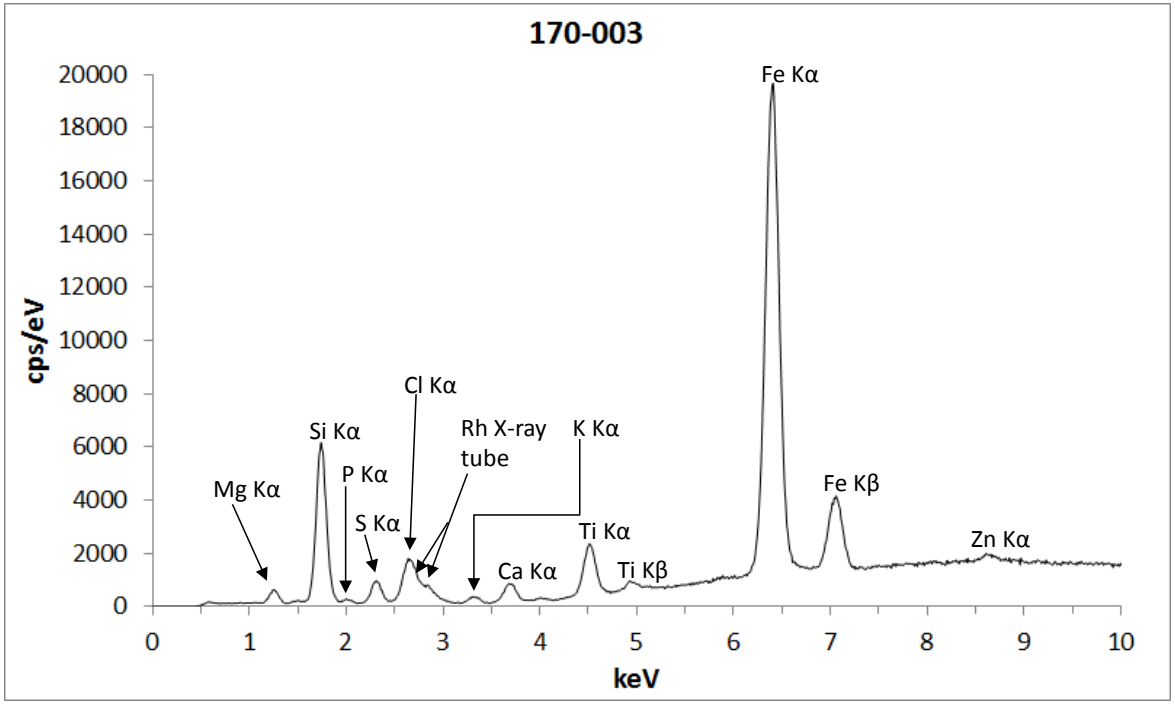

This shows higher concentrations of Fe compared to **Blank** (right-side table).

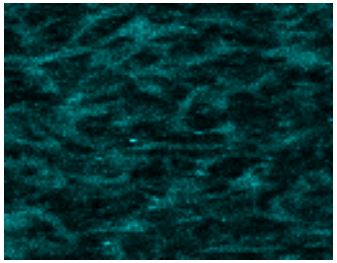

Vision Quant Results: 170-003				
Total Area Spc from ROI Map		7:58 PM		12-Feb-14
Elem:	Net	Wt%	At%	I-Error%
MgK	1.92	23.80	29.82	1.84
AlK	0.42	1.48	1.67	6.12
SiK	24.29	41.40	44.90	0.41
P K	0.58	1.26	1.24	4.9
S K	3.62	3.93	3.74	1.24
ClK	7.35	8.03	6.90	0.8
K K	1.12	0.87	0.68	2.96
CaK	3.45	1.77	1.35	1.37
TiK	10.09	2.52	1.60	0.76
CrK	0.38	0.06	0.04	17.52
MnK	1.1	0.17	0.09	7.08
FeK	104.83	14.13	7.71	0.21
NiK	0.65	0.10	0.05	15.24
ZnK	2.99	0.43	0.20	3.75
ZrK	0.25	0.04	0.01	24.22

Vision Quant Results: **Blank**				
Total Area Spc from ROI Map		12:53 PM		10-Feb-14
Elem:	Net	Wt%	At%	I-Error%
MgK	1.57	29.42	35.12	3.79
AlK	0.2	1.2	1.29	18.91
SiK	15.88	47	48.58	1.02
P K	0.45	1.77	1.66	10.07
S K	2.06	4.06	3.68	3.32
K K	0.18	0.22	0.17	25.03
CaK	4.25	3.5	2.54	2.25
TiK	8.81	3.67	2.23	1.62
CrK	0.27	0.08	0.04	43.76
MnK	1.12	0.28	0.15	12.39
FeK	38.9	8.46	4.4	0.73
NiK	0.53	0.11	0.06	30.79
ZnK	0.81	0.17	0.07	21.53
ZrK	0.23	0.05	0.02	36.82

Sample: Diablo Canyon 170-003 with Blank subtracted

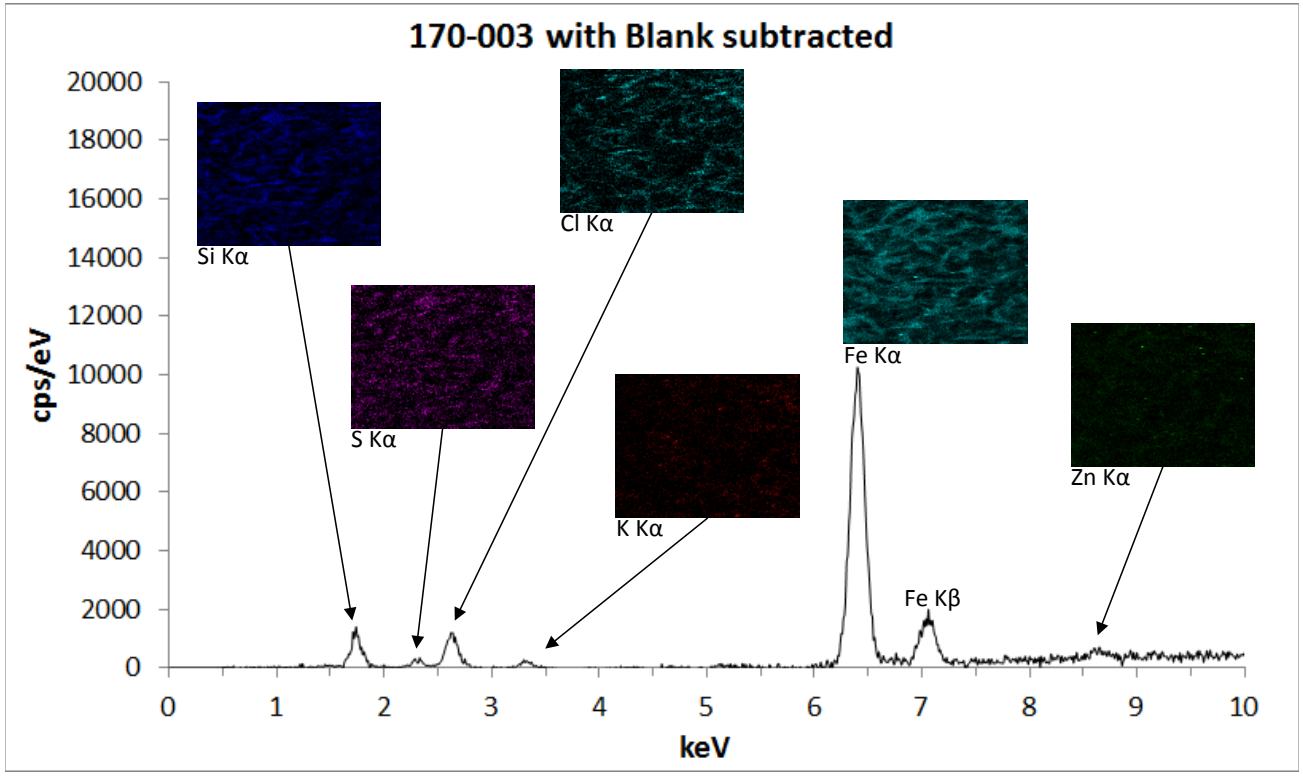

Sample: Diablo Canyon 170-004

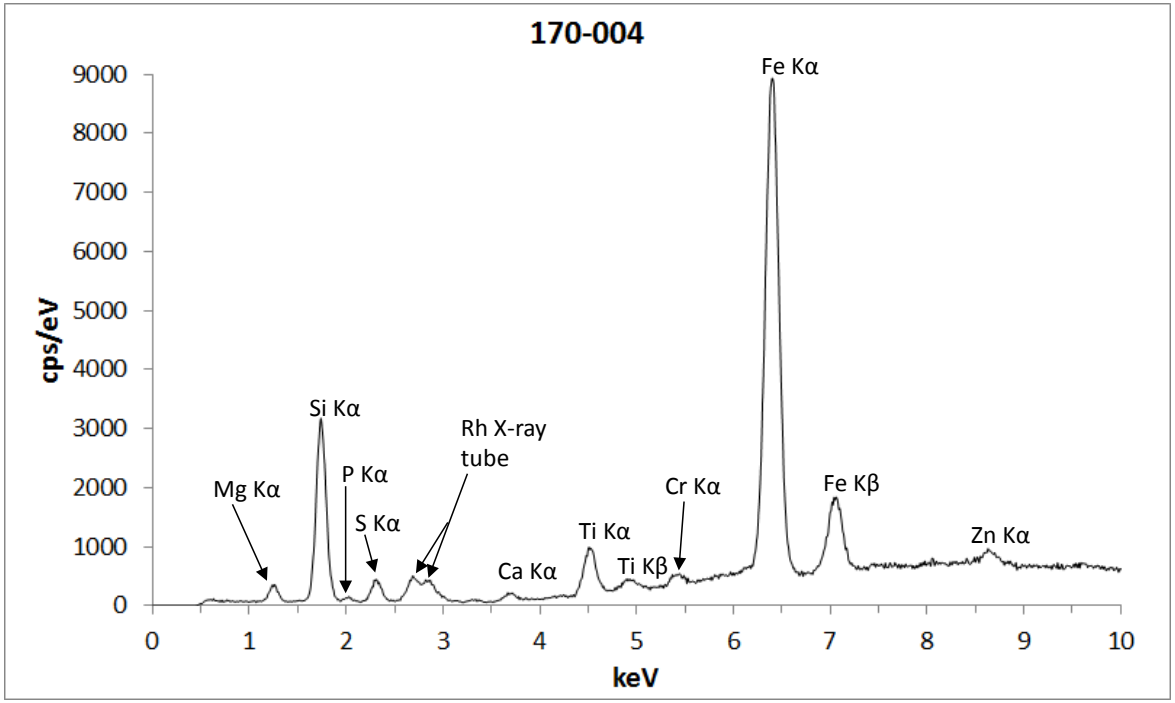

This shows higher concentrations of Fe compared to **Blank** (right-side table).

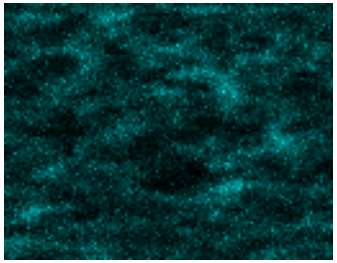

Vision Quant Results: 170-004				
Total Area Spc from ROI Map		10:52 AM		12-Feb-14
Elem:	Net	Wt%	At%	I-Error%
MgK	1.06	27.27	33.31	2.5
AlK	0.07	0.56	0.62	24.51
SiK	12.32	46.21	48.86	0.58
P K	0.28	1.41	1.35	7.19
S K	1.58	3.90	3.61	1.92
ClK	1.25	3.06	2.57	2.23
K K	0.18	0.30	0.23	10.45
CaK	0.63	0.66	0.49	4.1
TiK	4.07	2.05	1.27	1.24
CrK	1.15	0.39	0.22	4.23
MnK	0.7	0.21	0.11	7.52
FeK	48.05	13.05	6.94	0.31
NiK	0.7	0.21	0.11	9.3
ZnK	2.14	0.62	0.28	3.46
ZrK	0.27	0.09	0.03	14.03

Vision Quant Results: **Blank**				
Total Area Spc from ROI Map		12:53 PM		10-Feb-14
Elem:	Net	Wt%	At%	I-Error%
MgK	1.57	29.42	35.12	3.79
AlK	0.2	1.2	1.29	18.91
SiK	15.88	47	48.58	1.02
P K	0.45	1.77	1.66	10.07
S K	2.06	4.06	3.68	3.32
K K	0.18	0.22	0.17	25.03
CaK	4.25	3.5	2.54	2.25
TiK	8.81	3.67	2.23	1.62
CrK	0.27	0.08	0.04	43.76
MnK	1.12	0.28	0.15	12.39
FeK	38.9	8.46	4.4	0.73
NiK	0.53	0.11	0.06	30.79
ZnK	0.81	0.17	0.07	21.53
ZrK	0.23	0.05	0.02	36.82

Sample: Diablo Canyon 170-004 with Blank subtracted

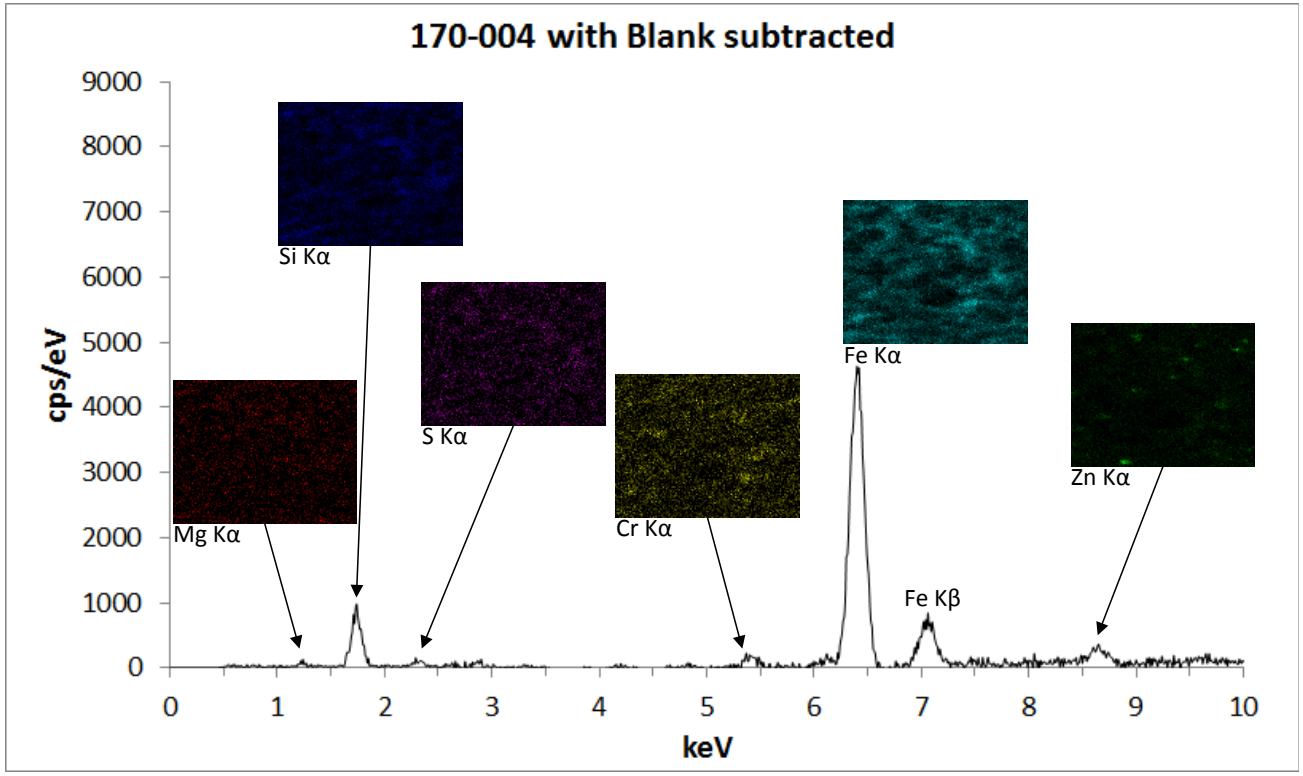

Sample: Diablo Canyon 170-005

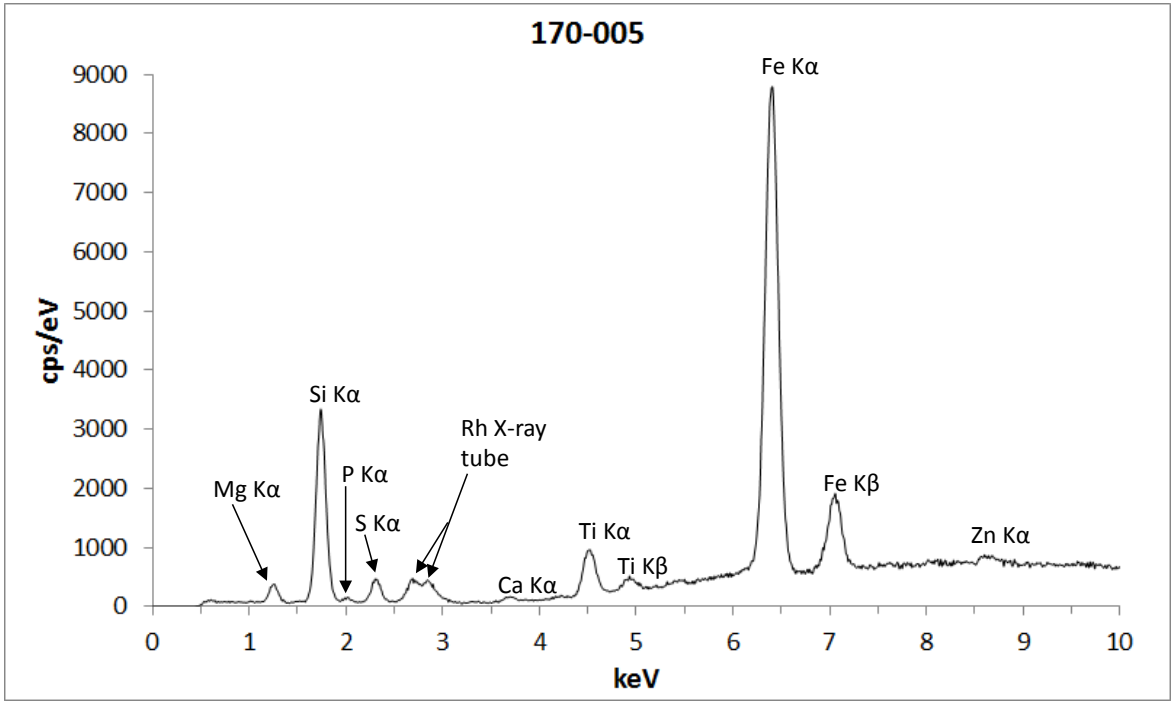

This shows higher concentrations of Fe compared to **Blank** (right-side table).

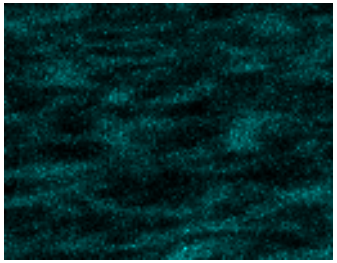

Vision Quant Results: 170-005				
Total Area Spc from ROI Map		11:56 AM		12-Feb-14
Elem:	Net	Wt%	At%	I-Error%
MgK	1.17	28.25	34.11	2.3
AlK	0.11	0.83	0.90	15.93
SiK	12.84	46.84	48.96	0.57
P K	0.32	1.57	1.48	6.41
S K	1.66	4.01	3.68	1.85
ClK	1.22	2.91	2.41	2.27
K K	0.11	0.18	0.13	16.45
CaK	0.43	0.44	0.32	5.6
TiK	4.06	1.98	1.21	1.25
CrK	0.59	0.19	0.11	7.95
MnK	0.64	0.18	0.10	8.35
FeK	46.66	12.06	6.34	0.31
NiK	0.43	0.12	0.06	15.51
ZnK	1.36	0.37	0.17	5.42
ZrK	0.21	0.06	0.02	19.01

Vision Quant Results: **Blank**				
Total Area Spc from ROI Map		12:53 PM		10-Feb-14
Elem:	Net	Wt%	At%	I-Error%
MgK	1.57	29.42	35.12	3.79
AlK	0.2	1.2	1.29	18.91
SiK	15.88	47	48.58	1.02
P K	0.45	1.77	1.66	10.07
S K	2.06	4.06	3.68	3.32
K K	0.18	0.22	0.17	25.03
CaK	4.25	3.5	2.54	2.25
TiK	8.81	3.67	2.23	1.62
CrK	0.27	0.08	0.04	43.76
MnK	1.12	0.28	0.15	12.39
FeK	38.9	8.46	4.4	0.73
NiK	0.53	0.11	0.06	30.79
ZnK	0.81	0.17	0.07	21.53
ZrK	0.23	0.05	0.02	36.82

Sample: Diablo Canyon 170-005 with Blank subtracted

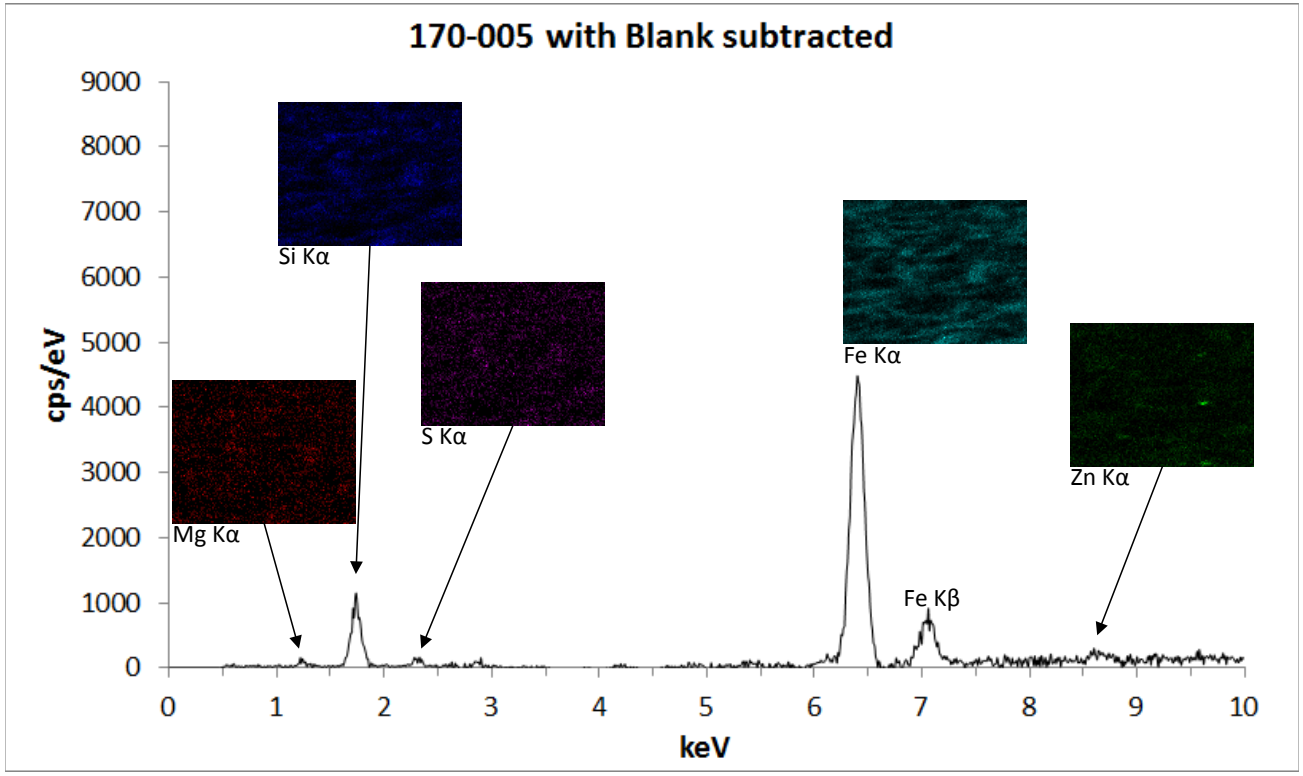

Sample: Diablo Canyon 170-006

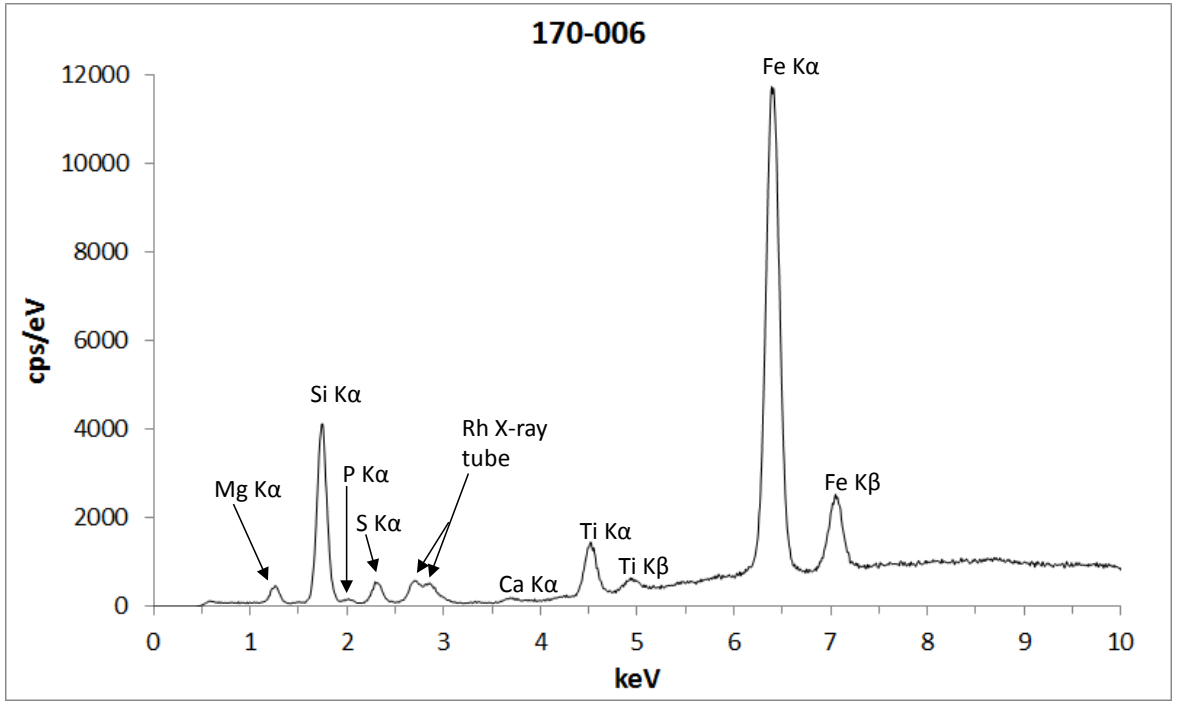

This shows higher concentrations of Fe compared to **Blank** (right-side table).

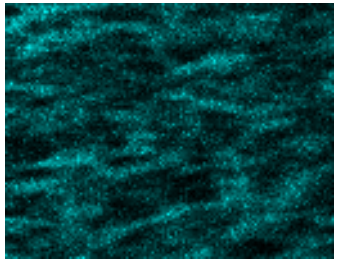

Vision Quant Results: 170-006				
Total Area Spc from ROI Map		12:59 PM		12-Feb-14
Elem:	Net	Wt%	At%	I-Error%
MgK	1.49	28.65	34.68	2
AlK	0.11	0.65	0.70	17.29
SiK	16.08	46.40	48.62	0.51
P K	0.39	1.50	1.42	5.71
S K	2.03	3.85	3.54	1.67
ClK	1.36	2.55	2.11	2.18
K K	0.11	0.13	0.10	18.91
CaK	0.48	0.38	0.28	5.53
TiK	6.02	2.28	1.40	1
CrK	0.45	0.12	0.07	11.74
MnK	0.8	0.18	0.10	7.76
FeK	63.11	12.86	6.78	0.27
NiK	0.56	0.13	0.06	13.7
ZnK	1.26	0.27	0.12	6.76
ZrK	0.23	0.05	0.02	19.86

Vision Quant Results: **Blank**				
Total Area Spc from ROI Map		12:53 PM		10-Feb-14
Elem:	Net	Wt%	At%	I-Error%
MgK	1.57	29.42	35.12	3.79
AlK	0.2	1.2	1.29	18.91
SiK	15.88	47	48.58	1.02
P K	0.45	1.77	1.66	10.07
S K	2.06	4.06	3.68	3.32
K K	0.18	0.22	0.17	25.03
CaK	4.25	3.5	2.54	2.25
TiK	8.81	3.67	2.23	1.62
CrK	0.27	0.08	0.04	43.76
MnK	1.12	0.28	0.15	12.39
FeK	38.9	8.46	4.4	0.73
NiK	0.53	0.11	0.06	30.79
ZnK	0.81	0.17	0.07	21.53
ZrK	0.23	0.05	0.02	36.82

Sample: Diablo Canyon 170-006 with Blank subtracted

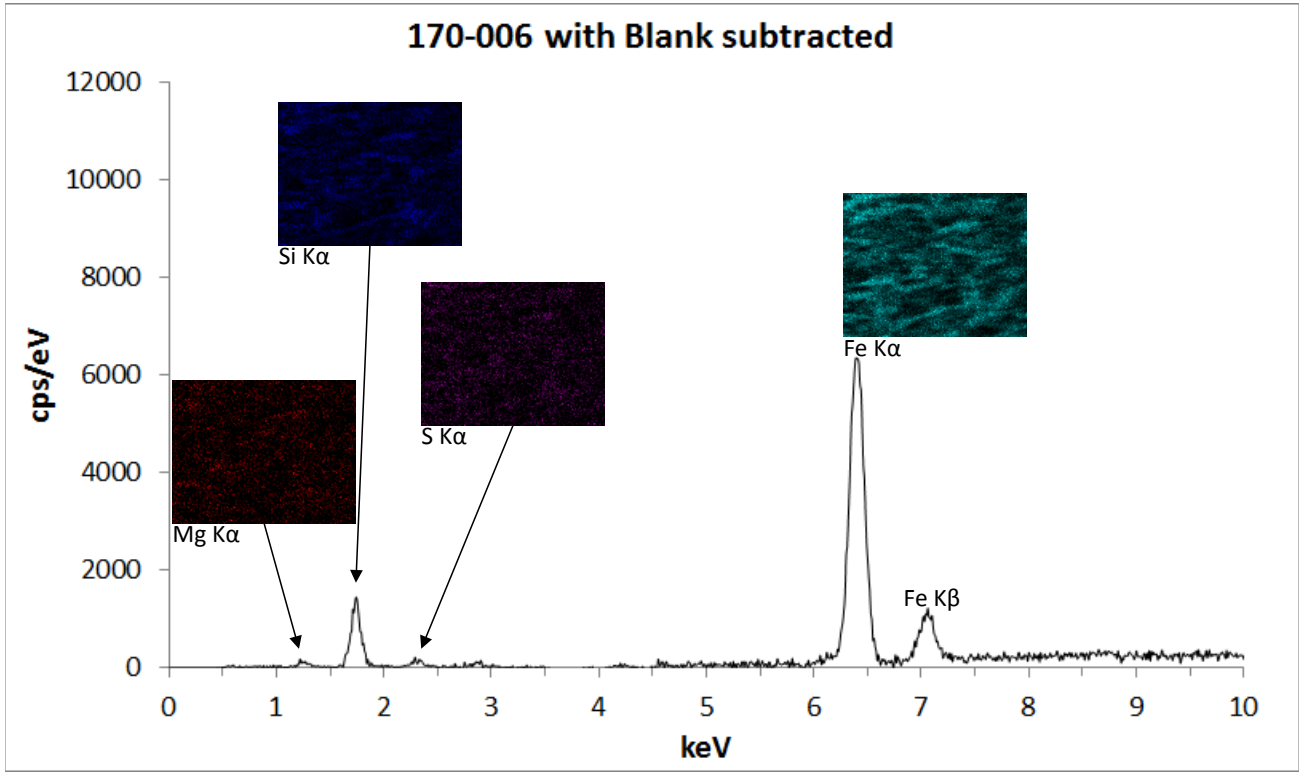

Distribution

1 Keith Waldrop (electronic copy)
Used Fuel and HLW Management Program
Electric Power Research Institute
1300 West WT Harris Blvd.
Charlotte, NC 28262

1 John Kessler (electronic copy)
Manager, Used Fuel and HLW Management Program
Electric Power Research Institute
1300 West WT Harris Blvd.
Charlotte, NC 28262

1 Shannon Chu (electronic copy)
Senior Technical Leader, Spent Fuel and High Level Waste
Electric Power Research Institute
3420 Hillview Avenue.
Palo Alto, CA 94304

1 Ned Larson (electronic copy)
M/S NSF 165, Room B119
U.S. Department of Energy
232 Energy Way
North Las Vegas, NV 89030

1	MS0115	OFA/NFE Agreements	10012
1	MS0736	P. Swift	6220 (electronic copy)
1	MS0747	K. Sorenson	6223 (electronic copy)
1	MS0779	S. Saltzstein	6225 (electronic copy)
1	MS0899	Technical Library	9536 (electronic copy)


Sandia National Laboratories